Vladimir L. Bychkov
Gennady V. Golubkov
Anatoly I. Nikitin
Editors

PHYSICS OF EARTH AND SPACE ENVIRONMENTS

The Atmosphere and Ionosphere

Dynamics, Processes and Monitoring

Springer

The Atmosphere and Ionosphere

Physics of Earth and Space Environments

The series *Physics of Earth and Space Environments* is devoted to monograph texts dealing with all aspects of atmospheric, hydrospheric and space science research and advanced teaching. The presentations will be both qualitative as well as quantitative, with strong emphasis on the underlying (geo)physical sciences. Of particular interest are

- contributions which relate fundamental research in the aforementioned fields to present and developing environmental issues viewed broadly
- concise accounts of newly emerging important topics that are embedded in a broader framework in order to provide quick but readable access of new material to a larger audience

The books forming this collection will be of importance for graduate students and active researchers alike.

For other titles published in the series, go to
www.springer.com/series/5117

Vladimir L. Bychkov • Gennady V. Golubkov •
Anatoly I. Nikitin
Editors

The Atmosphere and Ionosphere

Dynamics, Processes and Monitoring

With 59 Figures and 8 Tables

Springer

Editors
Dr. Vladimir L. Bychkov
Lomonosov Moscow State University
Fac. Physics
Leninskie Gory 1
Moscow
Russia 119991
bychvl@orc.ru

Prof. Gennady V. Golubkov
Russian Academy of Sciences
Semenov Inst. Chemical
Physics
Kosygina St. 4
Moscow
Russia 117977
golubkov@chph.ras.ru

Dr. Anatoly I. Nikitin
Russian Academy of Sciences
Inst. Energy Problems of Chemical
Physics
Leninsky Prosp. 38, build. 2
Moscow, Russia 117829
anikitin@chph.ras.ru

ISSN 1610-1677 e-ISSN 1865-0678
ISBN 978-90-481-3211-9 e-ISBN 978-90-481-3212-6
DOI 10.1007/978-90-481-3212-6
Springer Dordrecht Heidelberg London New York

Library of Congress Control Number: 2010927479

Cover design: eStudio Calamar S.L., F. Steinen-Broo, Pau/Girona, Spain

Printed on acid-free paper

Springer is part of Springer Science+Business Media (www.springer.com)

Abstract

The first part of the book is devoted to the modern methods for calculating the energy eigenvalues of Rydberg atoms A^{**} and molecules XY^{**} perturbed by neutral particles of a medium and to the results of studying the interaction processes with them. Interest in this study is caused by numerous applications in plasma chemistry, aeronomy, and astrophysics.

The second part of the book is devoted to the atmospheric aerosol – one of the most important factors affecting the Earth climatic and weather conditions. The study of the mechanisms of formation and evolution of atmospheric aerosols is of primary importance for predictions of the climatic changes on our planet. Special attention is given to the last achievements in theory of particle formation and their subsequent growth.

The third part of the book is devoted to numerous phenomena occurred in the mesosphere, ionosphere and the magnetosphere of the Earth caused by the sources located in the lower atmosphere and on the ground. Effects produced by lightning activity and by ground-based transmitters operated in high frequency and very low frequency ranges are described.

The fourth part of the book is devoted to modern methods of earthquake prediction. First section contains first results of special satellite "COMPASS 2" destined for detection of seism-electromagnetic effects. A whistler group in higher-order guided mode was recorded. Probably it was propagating between two layers, caused by onion-like structure of in homogeneities in the plasmasphere. Extremely low and very low frequency effects observed over seism-active regions by the satellite "INTERCOSMOS-24" are considered.

The achievements of the basic researches of the upper atmosphere and ionosphere processes with the mathematical modeling methods are briefly presented in the fifth part of the book. The mathematical problem of the model atmosphere/ionosphere description and existing global theoretical model of environment and results of the investigations with their using are considered.

The last part of the book is devoted to ball lightning investigations. Researches historical review is presented. They consist of gathering and data processing of observations, experiments on reproduction of long-lived shining formations in electric discharges, and theoretical models. Detailed descriptions of three high-energy ball lightning models are presented.

About Editors

Vladimir L. Bychkov is a leading researcher of the physical department of Lomonosov Moscow state university; he is also head of a laboratory of Moscow Radiotechnical Institute, Russian Academy of Sciences. He received MS degree in theoretical physics from the University of Peoples Friendship, Moscow, Russia, a Ph.D. in plasma physics and chemistry from Kurchatov Institute of Nuclear Energy, and Doctor of Sciences degree from Moscow Regional State University. He has 35 years of experience in plasma physics researches, namely, in the physics of elementary processes, gas discharges, electron-beam plasmas, plasma chemistry, and ball lightning. He is head of the Russian Committee on ball lightning, vice president of the International Committee on Ball Lightning, and a member of Moscow Physical Society.

Anatoly I. Nikitin is a principal researcher of Institute for Energy Problems of Chemical Physics, Russian Academy of Sciences, Moscow, Russia. He received a MS degree in physics from the Lomonosov Moscow state university, a Ph.D. in radiophysics from Lebedev Physical Institute, Russian Academy of Sciences, Moscow and Doctor of Sciences degree from Karpov Institute of Physical Chemistry, Moscow. He has 50 years of experience in quantum electronics (masers, lasers) researches, chemical physics, selective by isotopes chemical reactions, plasma physics, laser chemistry, and ball lightning. He is Secretary of the International Committee on Ball Lightning and a member of the Moscow Physical Society.

Gennady V. Golubkov is a leading scientist of Semenov Institute of Chemical Physics, Moscow, Russian Academy of Sciences. He received MS degree in theoretical and nuclear physics from Moscow Engineering Physical Institute, Moscow, Russia, Ph.D. in chemical physics in Semenov Institute of Chemical Physics, and Doctor of Sciences degree in chemical physics from the Semenov Institute of Chemical Physics. He has 40 years of experience in the quantum scattering theory, the theory of atom-molecular processes and elementary chemical reactions, chemical physics of atmosphere, and of low temperature plasma. He is the author of a monograph “Rydberg states of atoms and molecules and the elementary processes

with their participation" (2001). Golubkov is a Member of the Bureau of Moscow and National Russian Physical Society, Actual member of New York Academy of Sciences, Member of International Committee on Theoretical Chemistry, and Chair of International Advisory Committee of International Conference "Atmosphere, ionosphere, Safety" (Kaliningrad, Russia, 2008).

Introduction

From July 7 to 12, 2008 in Zelenogradsk, a cosy resort on the bank of the Baltic Sea near Kaliningrad in Russia, the 1st International Conference "Atmosphere, Ionosphere, Safety (AIS-2008)" has been carried out. The State Russian University of I. Kant, Semenov Institute of chemical physics of the Russian Academy of Sciences, Pushkov Institute of terrestrial magnetism and radio-waves propagation of the Russian Academy of Sciences, and Russian Committee on Ball Lightning (BL) have acted as organizers of the conference. Financial support was made by Russian Fund of Fundamental Research Project N. 08-03-06041 and European Office of Aerospace Research and Development Grant award FA8655-08-1-5052.

The International conference "Atmosphere, Ionosphere, Safety" (AIS-2008) was devoted to (i) the analysis of the atmosphere–ionosphere response on natural and man-made processes, the reasons of occurrence of the various accompanying geophysical phenomena, and an estimation of possible consequences of their influence on the person and technological systems; (ii) the study of the monitoring possibility and search of the ways for the risk level decrease. Discussion of the physical and chemical processes accompanying the observable geophysical phenomena was undertaken.

One can see from a list of the Conference sections that questions of safety took only rather modest place, so main topics of the Conference became discussion of processes taking place in the atmosphere, ionosphere and methods of monitoring these processes.

At carrying out of the Conference besides plenary sessions, five sections worked in parallel: (A) Dynamics of atmospheric aerosols; (D) dynamics of an ionosphere and atmosphere – their communication through an ionosphere; (E) elementary processes in the upper atmosphere and the ionosphere; (P) the electromagnetic and optical phenomena in atmosphere, including long-lived and plasma objects and ball lightning; and (S) information systems of environment monitoring and prevention of incidents. At the Conference, nine plenary reports, 65 reports on sections and 40 poster reports have been presented.

The analysis of reactions in system "atmosphere–ionosphere" and influences of natural and technogenic processes on them was the basic question brought for

discussion of conference participants. In this connection, considerable attention has been given to the study of reasons and cases of the various geophysical and atmospheric phenomena display, an estimation of their influence on people and technological systems, development of systems of monitoring, and decrease in risk of negative influence of natural processes on mankind ability to live.

The physical and chemical phenomena proceeding in the upper atmosphere and ionosphere occur in the conditions and the scales that are not available in usual laboratories. Moreover, it is possible to create such nonequilibrium conditions to study the response of an environment on the external perturbations, the realization of which is difficult on the earth in general. All atmospheric layers interact among themselves by means of various physical and chemical processes, forming the complex system subject to influences of flashes on the Sun, earthquakes on the Earth, man-caused catastrophes, etc. The primary goal of theoretical and experimental researches consists in revealing interrelations of dynamics of various atmospheric layers, parameters of the atmosphere and ionosphere, an establishment of a role of various physical factors, in studying, understanding, and, finally, forecasting of dynamics of the environment in development of external perturbations. Research of these phenomena is impossible without the deep analysis of features of interaction of participating particles and also a detailed study of the elementary chemical processes occurring here. The trustworthy information is necessary for their solution about reactionary ability of the excited particles, about activation efficiency of various freedom degrees of interacting reagents that requires development of absolutely new techniques of measurements. In turn, it leads to the necessity of improving the existing theory that would not only qualitatively but also quantitatively explain observable laws. The last puts forward not trivial problems which at first sight seem in general insoluble for theorists. Overcoming of difficulties arising here is probably possible only within the limits of essentially new theoretical approaches different from traditional methods of quantum chemistry, though substantially using its achievements. Now we have extensive data on an electronic structure of atoms and molecules and about dynamics of their interaction. Sometimes, it is reliable to calculate cross sections and rates of elementary chemical processes because in most cases (and especially with participation of the electronically excited fragments), we do not have any trustworthy information about features of these particles interaction acts.

One of the most reliable and effective enough tools for their studying is fast molecular beams. This area of science has intensively developed since last 20 years, thanks to its numerous practical applications – from space programs to problems of ecology and chemical technology. Advantage of fast beams is connected first of all with the possibility of carrying out the reagents relative speeds variation measurements in a wide range – from thermal to high ($\propto 10^{10}$–10^{11} m/c). Thus, in crossed (or combined) beams, the recording resolution of counter particles relative energy can reach $\propto 10^{-3}$ eV that opens possibility of a detailed study of elementary chemical processes (including determination of endothermic reaction threshold, a role of initial excitation for the reaction rate and course, etc.).

One of the major processes taking place in the Earth upper atmosphere is dissociative recombination (DR) of slow electrons and molecular ions. Researchers who study

ionized states have to solve problems relating to various fields of physics. Many of these problems are associated with the microscopic properties of plasma, that is, with states of atomic and molecular species and with the elementary processes involving them. These properties depend substantially on the presence of positively charged molecular ions, since reactions involving these species even at low concentrations can lead to a noticeable increase in the rate of the volume charge disappearance in decaying plasma. The latter is accompanied, as a rule, by the formation of excited atomic fragments followed by light emission. Thus, the recombination of electrons and ions determining the ionization structure of the plasma and the recombination spectrum, in turn, provides the necessary information on the physical conditions in the medium in which the emitting species are located. However, the measurement of partial cross-sections of recombination using the cross beam technique is complex due to the fact that for beams, there are no reliable methods for detecting the initial and final states of the recombining system. Therefore, the observed cross-sections are averaged over the energy distribution in electron beams and over vibrational and rotational states, which hampers the direct comparison of experimental and theoretical results. Recently, results of new experiments where DR was studied in storage rings were obtained. The measurements undertaken in the presence of external laser radiation can also play an important role and allow control of a reaction course.

Atmospheric aerosols – particles suspended in air – play an extremely important role in the "metabolism" of the atmosphere. Despite their very low mass concentrations and extremely small sizes they remain active agents in the atmospheric chemical cycles and in the energy transfer in the atmosphere. The small sizes of the aerosol particles (comparable to the molecular mean free path) make their physics and chemistry quite unusual. To answer the questions, where are these particle from? What are the mechanisms of their interaction with the atmospheric air and the Sun radiation? How do they affect the weather condition and what is their role in the climate changes?, etc., this is a far from complete list of the aerosol problems. Part of this book devoted to aerosols intoduces the readers to the area of these problems.

As an essentially new method of elementary physical and chemical processes, research can be done by carrying out laboratory measurements to circumterraneous space with the use of techniques of active (radiating) influence and space complexes. In these conditions (when the measuring device is placed in the reacting environment), there are no difficulties with vacuum of the high resolution, no foreign impurity, and so on.

The indicated problems are of interest for a wide range of the investigators working in various areas of science and techniques. At the same time, it is necessary to carry out the additional researches that are connected with the high human activity in the atmosphere–ionosphere system, leading to occurrence of new risks. They concern an active development of the manned and uninhabited orbital systems, aircrafts (using height of an average atmosphere), new kinds of communication, long-distance transmission circuits, etc. Non-stationary atmosphere–ionosphere system is the subject of powerful natural affects. Its bottom level is disturbed by earthquakes, volcanic eruptions, typhoons, thunderstorms, etc. From above, it is influenced by the geomagnetic storms. As a result of these processes such disturbing

factors, as powerful atmospheric perturbations, electric currents, electromagnetic radiations in the various spectrum ranges, the plasma and optical disturbances, an accelerated particles, the increased level of radioactivity, and changing of ionic and molecular components are realized. Besides, the microwave radiation of highly excited particles of the ionosphere accompanying the processes of solar activity increase and the appearance of magnetic storms impacts mankind negatively. Its spectrum, apparently, is completely defined by the neutral ionosphere components. The knowledge of the influencing factor origination allows to use them for disaster monitoring and to create the corresponding techniques on this base.

For low atmosphere, investigation of thunderstorm activity represents substantial scientific and practical interest, in particular, such an uninvestigated phenomenon is ball lightning. One can say that the nature of usual linear lightning is understood to some extent and there are means of surface objects protection; however, the same cannot be said about ball lightning. This state cannot be considered as acceptable since in a number of cases destructions caused by the ball lightning are as serious as those caused by the linear lightning and sometimes results of its impact are unpredictable (ruination of aircraft, explosions in industrial objects). Besides, investigation of ball lightning is interesting from the point of view of physics and power, nature at its example demonstrates a possibility of high-energy density concentration and storing.

During AIS-2008 conference the tenth jubilee Symposium on Ball Lightning was carried out at the electromagnetic and optical phenomena in the atmosphere section. It was an occasion to make the review of Ball Lightning (BL) researches history and, in particular, the work analysis for last 20 years. It can be seen that these years were the time of active researches of a BL problem. Data banks of BL observations collected and replenished; experiments on obtaining and research of long-lived shining formations were carried out, works on creation and check of BL models were conducted. Unfortunately, this activity has yet not brought notable results. The reason for failure, apparently, is implied in the fact that we could not choose "the main link" in properties BL and as a result have incorrectly chosen ways of its experimental modeling. In the field of BL observation data collection there was some saturation: new data practically add nothing to a "portrait" of an average BL which for some reason yet has not helped to create adequate model of this phenomenon. But there is a shortage of information on rare BL properties: its high energy manifestation, capability to penetrate through subjects (glass, composite materials) connection with other geophysical events. Likely time has come to pass to the publication of full descriptions of BL observations. Quite probably, among them, there can be data that can become the "key" opening its secrets. Time has come to seriously consider data file of UFO observations as among them more than half of objects possess properties of BL. It is necessary to realize, that BL science is the interdisciplinary science requiring participation of experts, working in various areas of physics, chemistry, power, synergetic, biology and psychology.

V.L. Bychkov
G.V. Golubkov
A.I. Nikitin

Contents

Contributors

L. Bodnar Bl-electronics, Solimar, Hungary, ble@axelero.hu

V.L. Bychkov M.V. Lomonosov Moscow State University, Moscow, Russia

V.M. Chmyrev Institute of Physics of the Earth, Russian Academy of Sciences, 10, Bolshaya Gruzinskaya Str., Moscow, 123995 Russia

G.C. Dijkhuis Department of Mathematics and Informatics, Eindhoven University of Technology, P.O Box 513, 5600 MB Eindhoven, The Netherlands

C. Ferencz Space Research Groupe, Eotwös University, Budapest, Hungary, spacegr@sas.elte.hu

G.V. Golubkov Semenov Institute of Chemical Physics, Russian Academy of Sciences, Moscow, Russia

M.G. Golubkov Semenov Institute of Chemical Physics, Russian Academy of Sciences, Moscow, Russia

G.K. Ivanov Semenov Institute of Chemical Physics, Russian Academy of Sciences, Moscow, Russia

O.V. Kapustina Pushkov Institute of Terrestrial Magnetism, Ionosphere and Radio Wave Propagation, Russian Academy of Sciences, IZMIRAN, Troitsk, Moscow region, 142190 Russia, yumikh@izmiran.ru

I.V. Karpov West Department IZMIRAN, Russian Academy of Sciences, Kaliningrad, Russia

V.V. Khegay Pushkov Institute of Terrestrial Magnetism, Ionosphere and Radio Wave Propagation, Russian Academy of Sciences, IZMIRAN, Troitsk, Moscow region, 142190 Russia, ikir@ikir.kamchatka.ru

V.E. Korepanov Center of Cosmic Investigations of NASU and NCAU, Naukova 5, Lviv, 79000 Ukraine, vakor@isr.lviv.ua

L.P. Korsunova Pushkov Institute of Terrestrial Magnetism, Ionosphere and Radio Wave Propagation, Russian Academy of Sciences, IZMIRAN, Troitsk, Moscow region, 142190 Russia, yumikh@izmiran.ru

V.D. Kuznetsov Pushkov Institute of Terrestrial Magnetism, Ionosphere and Radio Wave Propagation, Russian Academy of Sciences, IZMIRAN, Troitsk, Moscow region, 142190 Russia, kvd@izmiran.ru

A.A. Lushnikov Karpov Institute of Physical Chemistry, Moscow, Russia

Yu.S. Lyubovtseva Geophysical Center of Russian Academy of Sciences, Moscow, Russia

Yu.M. Mikhailov Pushkov Institute of Terrestrial Magnetism, Ionosphere and Radio Wave Propagation, Russian Academy of Sciences, IZMIRAN, Troitsk, Moscow region, 142190 Russia, yumikh@izmiran.ru

G.A. Mikhailova Pushkov Institute of Terrestrial Magnetism, Ionosphere and Radio Wave Propagation, Russian Academy of Sciences, IZMIRAN, Troitsk, Moscow region, 142190 Russia, yumikh@izmiran.ru

A.I. Nikitin Institute for Energy Problems of Chemical Physics, Russian Academy of Sciences, Moscow, Russia

S.E. Smirnov Institute of Cosmophysical Research and Radio Wave Propagation Far-East Branch of Russian Academy of Sciences, IKIR, Paratunka, Kamchatka region, 68300 Russia, ikir@ikir.kamchatka.ru

V.M. Sorokin Pushkov Institute of Terrestrial Magnetism, Ionosphere and Radio Wave Propagation, Russian Academy of Sciences, IZMIRAN, Troitsk, Moscow Region, 142190 Russia

V.A. Zagaynov Karpov Institute of Physical Chemistry, Moscow, Russia

Chapter 1
Rydberg States of Atoms and Molecules in a Field of Neutral Particles

G.V. Golubkov, M.G. Golubkov, and G.K. Ivanov

Abstract This book is devoted to the modern methods of calculating the energy eigenvalues of Rydberg atoms A^{**} and molecules XY^{**} perturbed by neutral particles of a medium and to the results of studying the interaction processes with them. Numerous applications in plasma chemistry, aeronomy, and astrophysics have contributed to conducting this study. These methods are based on the use of integral variant of the theory utilizing Green's function approach. Because of the closeness to the continuum boundary, these energies cannot be properly described in terms of the standard quantum chemistry. When the radius of electronic cloud of excited states is large enough (i.e., $R_c = 2n^2 \gg 1$, where n is the principal quantum number), they cannot be regarded as isolated even in the case of a rarefied gas. The spectral distortion is the strongest when the number N of perturbing neutral particles falling into this region exceeds unity. This chapter is divided into four main parts.

In the first part, the generalized method of finite-radius potential (FRP) is discussed. This method self-consistently takes into account the short- and long-range interactions in the two-center system under consideration. It adequately describes the scattering of a weakly bound electron by the ion core and a perturbing atom with nonzero angular momenta l and L with respect to these centers, thereby allowing the theory to be extended to the intermediate (on the order of and less than electron wavelength $\lambda \propto n$) interatomic distances R. As an application of the theory, the detailed analysis is performed for the behavior of the potential energy surfaces (PESs) of a system composed of a highly excited atom $A^{**}(n, l)$ and a neutral atom B with the filled electronic shell. It is demonstrated that the inclusion of nonzero momentum L for the $e^- - B$ scattering results in the additional splitting of the PES into the separate groups of interacting terms classified by the projection m of electronic angular momentum l on the quasimolecular axis. At distances $R \gg n$, the FRP method exactly transforms to the zero-radius pseudopotential

G.V. Golubkov (✉)
Semenov Institute of Chemical Physics, Moscow, Russia

V.L. Bychkov et al. (eds.), *The Atmosphere and Ionosphere,*
Physics of Earth and Space Environments,
DOI 10.1007/978-90-481-3212-6_1,

(ZRP) model and, correspondingly, to the asymptotic theory in which the PESs acquire a simple analytic form. It turns out that, at large values $n \gg 1$, the ZRP method is valid up to the distances $R \sim n$.

In the second part, the specific features of the diabatic and adiabatic PESs are discussed by taking into account the dissociative, covalent, and ion configurations. The potentialities and disadvantages of the existing ab initio approaches are analyzed. The matching method is suggested, which allows a unique self-consistent picture devoid of the above-mentioned disadvantages to be obtained for the terms. As an illustration, the potential curves are calculated for the $nl\,(^{2s+1}\Lambda)$ states of the $Na^{**} + He$ quasimolecule (n, l, and Λ are the principal quantum number, angular momentum, and its projection on the molecular axis, respectively, and S is the spin of the system), and a detailed comparison with the computational results of other authors is carried out.

In the third part, the possible applications of the theory to the shock ionization, excitation, and quenching processes are discussed for the Rydberg states (RSs). Among these are also the simplest dissociation, exchange, and charge exchange reactions. They can be schematically represented as

$$XY^{**} + M \rightarrow XY^{**} + M, \tag{1.1a}$$

$$XY^{**} + M \rightarrow X + Y^{*} + M, \tag{1.1b}$$

$$XY^{**} + M \rightarrow XM + Y^{*}, \tag{1.1c}$$

$$XY^{**} + M \rightarrow XY^{+} + e^{-} + M, \tag{1.1d}$$

$$XY^{**} + M \rightarrow XY^{+} + M^{-} \tag{1.1e}$$

The interaction of XY^{**} with a neutral particle M includes the interactions with both ion and a weakly bound electron. The former is characterized by small impact parameters, whereas the latter has large impact parameters. As a result, the total scattering cross-sections can appreciably exceed the gas-kinetic values. The material is presented in terms of the PES of the $XY^{**} + M$ system followed by the description of the dynamics of processes (1.1a–e) within the framework of the integral variant of the multichannel quantum defect (MQD) theory using the renormalized Lippmann–Shwinger equation technique. Such a formulation of the MQD theory allows one to obtain a convenient representation for Green's function of a highly excited molecule, which opens up wide possibilities for various applications.

In the fourth part, the many-center perturbation of the atomic Rydberg states is analyzed for the situation wherein two (or more) perturbing neutral centers fall inside the electronic cloud. The behavior of Rydberg atom in a dense medium is considered with allowance for the influence of finite number N of the neutral particles chaotically distributed in its volume. The stochastic approach is proposed for the solution to this problem.

Keywords Atom−molecular processes · Elementary chemical reactions

1.1 Introduction

The Rydberg states (RSs) are situated near the continuum boundary and are characterized by the presence of a weakly bound electron with the orbit size on the order of n^2. These states are prone to the strong influence of, practically, any external action: constant electric and magnetic fields [1], laser radiation [2], and the surrounding medium [3] (including gas, liquid, or solid). This is important for the study of the processes occurring in the upper atmosphere, in low-temperature plasma and gaseous laser systems, for the study of the quantum size effects in nanostructures, reactions involving excited particles at solid surfaces, etc. Researchers are interested in these phenomena owing to the development of the fundamentally new experimental methods and their possible applications. Among these are the photoelectron spectroscopy of superslow electrons [4–7], storage rings [8–11], and scanning tunnel spectroscopy [12–14].

The spectral distortion in Rydberg atom A^{**} by the ground-state neutral atom B is the simplest situation modeling the presence of the surrounding medium. The corresponding influence is assumed to be bordered by the sphere of radius R^*, which exceeds the classical radius $R_{cl} = 2n^2$ by several wavelengths $\lambda \sim n$. The region $r > 2\,n^2$ is classically forbidden for electron. Next, in the order of complexity are quantum systems including N perturbing atoms in the sphere of radius R^*, with $N \geq 2$.

Because of the difference in masses of electron and particles A^+ and B, the energy-exchange processes in the $A^{**} - B$ collisions are unlikely. For this reason, the investigation of the collisional dynamics, as a rule, is preceded by the calculation of the potential energy surface (PES) of a united system with the aim of revealing those regions of mutual particle arrangement, where the corresponding terms quasicross or draw close together. If the electron wavelength λ changes only slightly on the scale of the effective interaction region ρ_0 with the neutral particle,

$$\rho_0 \frac{\mathrm{d}\lambda}{\mathrm{d}r} \ll \lambda \quad \text{or} \quad \frac{\rho_0}{(kR)^2} \ll \lambda$$

(k is the classical electron momentum), then the $e^- - B$ interaction can be described in terms of the free scattering approach.

The properties of PES and the dynamics of collisional processes in the simplest ($N = 1$) system are described in many publications, which are discussed in detail in [15]. In most works, the approaches based on the information about the free-electron scattering by the independent fragments are used, namely by the ion core and atom B. Among the most elaborated approaches is the asymptotic treatment, which is valid at sufficiently large interatomic distances $R \sim n^2$, where the main theoretical results can be represented in a simple analytic form. An important fact is that the wave functions and the corresponding Green's functions describing electron behavior in the field of ion A^+ are well known.

On the other hand, this circumstance serves as a necessary base for developing the theory of electronic structure for nanoclusters with ordered or disordered structure, where the characteristic interparticle distances are of few angstroms. This is also true for the electron-excited states of atoms and molecules adsorbed at the solid surface. The use of the theory of multiple scattering for the solution of the problem on perturbation of highly excited atomic states by the system of chaotically or orderly arranged interaction centers within the framework of asymptotic approach was considered in [15, 16].

For the two-center axially symmetric system "Rydberg atom $A^{**}(nl)$ – atom B", this problem was solved using the generalized zero-radius pseudopotential (ZRP) model [17] for the electron S-scattering by the perturbing atom B at a sufficiently large n. Taking into account the long-range interaction at "intermediate" distances, R brings about the redetermination of the potential scattering length for $e^- - B$ and the removal of the degeneracy of Rydberg levels with respect to the projections m of electronic angular momentum l on the quasimolecular axis. An important part is played by the centrifugal potential, which reduces the number of degenerate Coulomb states by forming covalent terms and violates the quasiclassical description used for the electron motion in the asymptotic theory [18–20].

At small values of the principal quantum number n, one should include higher harmonics to describe electron scattering by the perturbing center. In [21], the method of constructing one-center operators for the $e^- - B$ scattering was developed, allowing the calculation of the PESs for the Rydberg atom $A^{**}(n)$ – atom B system at intermediate distances between atoms and for small values of n. The method is based on the use of finite-radius potential (FRP) including nonzero harmonics of the scattered electron and consistently takes into account the short-range and long-range interactions of particles at these distances. At large values, $n \gg 1$, the ZRP results are reproduced in a natural way, and, at distances, $R > n$, they exactly transform into the asymptotic theory. As an illustration, the terms were calculated for the $\mathrm{Na}^{**}(nlm) + \mathrm{He}$ system, and comparison with the existing data was carried out.

Thereupon, a systematic analysis of the strong nonadiabatic coupling between the molecular Rydberg states in the collisional processes was carried out. We discuss the main structural features of the vibronic PESs describing the interaction of highly excited atoms and molecules with neutral particles. The asymptotic method given here is an alternative to the traditional quantum chemical calculations. It does not use the variational principle, while the PES of the system is determined on the basis of the algebraic equations containing information on the free-electron motion in the field of isolated fragments (of ion and neutral particle). The asymptotic theory deals with the scattering **T** and **K** matrices, which are fundamental characteristics in the quantum collision theory, even as the parameters appearing in it can be directly associated with the experimentally observed electron-scattering amplitudes (or phases) by ions, atoms, and molecules. The unique feature of the asymptotic method is that it allows the multisheet PES to be represented in a simple analytic form including the whole diversity of merging points and quasicrossing regions responsible for the nonadiabatic transitions in the system.

The objects considered in our work also possess remarkable properties. The terms split-off from the group of orbitally degenerate states of Rydberg atom X^* or molecule XY^{**} demonstrate anomalous behavior. These terms are virtually independent of the nature of Rydberg particle (if the perturbation is produced by molecule M, the dependence on its orientation also vanishes). An important property of these (valence) configurations is that they are capable of autoionization owing to the escape to continuum as the interacting fragments approach each other. The weakly bound states can also form in the valence configurations of Rydberg complexes. The mechanism of their formation is caused by the Ramsauer effect in the elastic electron scattering from particle M. They arise due to the presence of shallow, though rather wide, hollows in the potential curve, where the weakly bound states can exist in the Rydberg complex (of the $X^{**}B$ or $XY^{**}B$ type) at large distances from the ion core.

New features appear in the processes involving Rydberg molecules XY^{**}. They are caused by the strong nonadiabatic coupling between the states, i.e., by the fact that each Rydberg $nlNv$ – state (with small l) is a superposition of, at least, two (or greater, if the rotation is taken into account) series closely spaced in v. This gives rise to a sharp (resonance) n dependence of the cross-sections for the elementary processes (even after averaging over the relative velocities of colliding particles), which is particularly important in the analysis of kinetic phenomena under non-equilibrium conditions.

1.2 Spectral Structure of the $A^{**} - B$ System

A highly excited atom $A^{**}(nlm)$ is electrically neutral and represents an A^+ surrounded by the extended electronic cloud whose sizes $R \approx n^2$ appreciably exceed the sizes of the unexcited atom. Here, l and m are, respectively, the angular momentum of the Rydberg electron and the projection of angular momentum on a certain axis, which can naturally be directed along the vector $\mathbf{R}$ connecting the centers of gravity of particles A^{**} and B in the $A^{**} - B$ system. The binding energy of this electron is considerably lower than the atomic ionization potential I_0,

$$E_n = -\frac{1}{2n^2}, \quad |E_n| \ll I_0 \tag{1.2}$$

(hereafter, atomic units are used, i.e., $\hbar = e = m_e = 1$). At large $n^2 \gg 1$, a certain electronic angular momentum l^* exists, which, owing to the presence of centrifugal barrier, separates the states strongly and weakly penetrating into the ion core (in most atoms, $l^* = 3$). The states with small angular momenta $l < l^*$ strongly interact with the ion core and contain quantum defects μ_l that give rise to the shift Δ_{nl} of Rydberg levels from the Coulomb levels E_n; i.e.,

$$E_{nl} = -\frac{1}{2(n-\mu_l)^2} = E_n + \Delta_{nl}, \quad \Delta_{nl} \cong \frac{\mu_l}{n^3}. \tag{1.3}$$

The remaining levels $l \geq l^*$ are orbitally degenerate Coulomb states (with $\mu_l = 0$), because quantum defects decrease as $\mu_l \propto l^{-5}$ with increasing l [22]. The large sizes and multitude of energy-degenerate states are the characteristic features of the system under consideration. Since the atom B occupies a small part of volume in which electron moves, we will assume that the effective radius ρ_0 of the $e^- - B$ interaction is smaller than the electron wavelength,

$$\rho_0 < \lambda \propto \sqrt{R}. \tag{1.4}$$

In essence, condition (1.3) implies the transition to the intermediate distances,

$$1 \ll R \ll n^2, \tag{1.5}$$

where (as also in the asymptotic region $R \propto n^2$) electron moves with the total energy $|E_{nl}| \ll 1$ in a combined field

$$U(R) = -\frac{1}{r} + \frac{l(l+1)}{2r^2},$$

of the Coulomb and centrifugal potentials free from ion core.

Since the strong interaction V_{e^-B} of electron and atom B is concentrated near the point R inside the region of radius ρ_0, the wave function $\Phi_s^{(R)}(\mathbf{r})$ of the Rydberg atom A^{**} changes only weakly on this scale. It is normalized to unity and has the form [3]

$$\Phi_s^{(R)}(\mathbf{r}) = R_{vl}^{(R)}(r)\, Y_{lm}(\mathbf{r}/r), \tag{1.6}$$

where $\mathbf{r}$ is the coordinate of the weakly bound electron, $s = \{vlm\}$, $\nu = 1/\sqrt{-2E}$ is the effective principal quantum number, and $Y_{lm}(\mathbf{r}/r)$ is the spherical harmonic [23]. The radial part is defined by

$$R_{vl}^{(R)}(r) = \frac{W_{\nu,l+1/2}\,(2r/\nu)}{r\nu\,[\Gamma(\nu - l)\,\Gamma(\nu + l + 1)\,]^{1/2}} \tag{1.7}$$

(here, $\Gamma(x)$ is the gamma-function and $W_{\nu,l+1/2}\,(2r/\nu)$ is the Whittaker function [24]). Note that for the integer values $\nu = n$, function (1.7) exactly coincides with the Coulomb wave function.

The solution to the problem is based on the formalism of the reconstructed Lippmann–Shwinger equations for the level-shift operator [15]

$$\boldsymbol{\tau} = \mathbf{K}_{e^-B}\,(\mathbf{G}_{A^{**}} - \mathbf{G}_0)\,\boldsymbol{\tau}, \tag{1.8}$$

where, after the separation of Green's function of Rydberg atom A^{**} into the strongly and weakly energy-dependent parts,

$$\mathbf{G}_{A^{**}}(\mathbf{r},\mathbf{r}',E)=\pi\nu^{3}(E)\sum_{lm}\left|\Phi^{(R)}_{\nu lm}(\mathbf{r})\right\rangle\left\langle\Phi^{(R)}_{\nu lm}(\mathbf{r}')\right|\cot\pi\left(\nu(E)+\mu_{l}\right)+\mathbf{G}_{0}(\mathbf{r},\mathbf{r}') \tag{1.9}$$

the scattering matrix $\mathbf{K}_{e^{-}B}$, which is defined for the kinetic energy of Rydberg electron and exactly takes into account all the specific features of the $e^{-}-B$ interaction in the states entering into the function $\mathbf{G}_0$, is introduced into the theory. Formally, this operator satisfies the integral equation

$$\mathbf{K}_{e^{-}B}=\mathbf{V}_{e^{-}B}+\mathbf{V}_{e^{-}B}\mathbf{G}_{0}\,\mathbf{K}_{e^{-}B},$$

where $\mathbf{V}_{e^{-}B}$ is the operator for the $e^{-}-B$ interaction. The determination of the $\mathbf{K}_{e^{-}B}$ matrix is generally a challenge, because the action of operator $\mathbf{V}_{e^{-}B}$ can extend to a rather wide region, where no unique analytic representation can be obtained for the electron-perturbing particle potential. At the same time, the region of strong interaction, where the explicit representation is necessary for the function $\mathbf{G}_0$, and the region of a comparably weak interaction, where this function is not needed at all, can always be found in the interaction potentials between an electron and the neutral particles (atoms or molecules much smaller than the Rydberg atoms). Then, according to the definition of Green's function $\mathbf{G}_0$, the $\mathbf{K}_{e^{-}B}$-matrix elements must be expressed through the characteristics of the electron scattering from atom B.

At small distances $\rho\ll R$ from the perturbing atom, where the interaction $\mathbf{V}_{e^{-}B}$ is the strongest, Green's function $\mathbf{G}_0$ is chosen as follows [15]:

$$\mathbf{G}_{0}(\mathbf{r},\mathbf{r}')=\mathbf{g}_{0}(\mathbf{r},\mathbf{r}')=-\frac{1}{2\pi|\,\mathbf{r}-\mathbf{r}'\,|}\begin{cases}\cos p_{e}(R)\,|\,\mathbf{r}-\mathbf{r}'\,|, & |E|<1/R,\\ \exp[-\alpha_{e}(R)\,|\,\mathbf{r}-\mathbf{r}'\,|], & |E|>1/R,\end{cases} \tag{1.10}$$

where $p_e(R)=[2(E+1/R)]^{1/2}$ is the classical electron momentum at distance R for energies $|E|<1/R$, whereas the quantity $\alpha_e(R)$ is, correspondingly, determined for $|E|>1/R$ and equals $\alpha_e(R)=[-2(E+1/R)]^{1/2}$.

Owing to the level degeneracy at $l\geq l^{*}$ (see comment to formula (1.3)), the pole part of Green's function (1.9) is separated into two parts. The first includes the terms with $\mu_l\neq 0$, which correspond to the nondegenerate states with $l<l^{*}$. The second part (with $l\geq l^{*}$) contains the terms with $\mu_l=0$. From the condition that the determinant of the system of equations (1.8) must be zero and using Eqs. (1.9) and (1.10) to write system (1.8) in the form

$$\boldsymbol{\tau}=\mathbf{K}_{e^{-}B}\left[\sum_{l<l^{*},m}\left|\varphi^{(R)}_{\nu lm}\right\rangle\left\langle\varphi^{(R)}_{\nu lm}\right|\cot\pi\left(\nu+\mu_{l}\right)+\cot\pi\nu\sum_{l\geq l^{*},m}\left|\varphi^{(R)}_{\nu lm}\right\rangle\left\langle\varphi^{(R)}_{\nu lm}\right|\right]\boldsymbol{\tau},$$
$$\varphi^{(R)}_{\nu lm}=\sqrt{\pi\nu^{3}}\,\Phi^{(R)}_{\nu lm,} \tag{1.11}$$

one obtains the PES of the combined system. The terms of the nondegenerate states relate to the Rydberg configuration, while the remaining terms will be referred to as covalent. When calculating the scattering $\mathbf{K}_{e^-B}$ matrix with allowance for the strong interaction, one can use the fact that the properties of function (1.11) and Green's function of free electron are close and, hence, use the characteristics of the $e^- - B$ scattering observed in the beam experiments, at which point one can also include perturbatively the long-range interaction. This greatly simplifies the procedure of determining the corresponding matrix elements.

1.3 Finite-Radius Pseudopotential

The simplest method for the introduction of finite-radius pseudopotential into the theory under condition (1.4) is proposed in [25]. The scattering amplitude is a function of three variables: momenta $\mathbf{p}_e$, $\mathbf{p}'_e$, and the electron kinetic energy ε. It is related to the $\mathbf{K}^{(0)}_{e^-B}$-scattering operator by the expression

$$F(\mathbf{p}_e, \mathbf{p}'_e, \varepsilon) = -\frac{1}{2\pi} \left\langle \mathrm{e}^{i\mathbf{p}'_e(\mathbf{r}-\mathbf{R})} \middle| \mathbf{K}^{(0)}_{e^-B} \middle| \mathrm{e}^{i\mathbf{p}_e(\mathbf{r}-\mathbf{R})} \right\rangle \tag{1.12}$$

or, in the representation of LM harmonics (where L is the electronic angular momentum with respect to atom B, and M is its projection on the direction of vector $\mathbf{R}$),

$$\begin{aligned} F(\mathbf{p}_e, \mathbf{p}'_e, \varepsilon) &= \sum_L (2l+1)\, F_L(p_e, p'_e, \varepsilon)\, P_L(\cos\Theta) \\ &= -4\pi \sum_{LM} \langle LM|\, \mathbf{K}^{(0)}_{e^-B} |LM\rangle\, Y_{LM}(\mathbf{p}_e/p_e)\, Y^*_{LM}(\mathbf{p}'_e/p'_e), \end{aligned} \tag{1.13}$$

where the wave functions $|LM\rangle$ are

$$|LM\rangle = \sqrt{2}\, j_L(p_e\rho)\, Y_{LM}(\boldsymbol{\rho}/\rho) \tag{1.14}$$

$j_L(x)$ is the L-order Bessel spherical function of the first kind, Θ is the angle between the vectors $\mathbf{p}_e$ and $\mathbf{p}'_e$, and $\boldsymbol{\rho} = \mathbf{r} - \mathbf{R}$. The observed scattering cross-sections or amplitudes correspond to functions (1.12) and (1.13) determined at the energy surface, i.e., under the condition

$$\varepsilon = \frac{p_e^2}{2} = \frac{p'^2_e}{2} > 0. \tag{1.15}$$

Under condition (1.3), matrix elements (1.13) for slow electrons can be brought to the separable form ($k_0^2 = 2\varepsilon$),

$$K_{L,L}^{(0)} = -2\pi \left(\frac{p'_e}{k_0}\right)^L f_L^{(0)}(\varepsilon) \left(\frac{p_e}{k_0}\right)^L. \tag{1.16}$$

Here, $f_L^{(0)}(\varepsilon)$ is the free-electron elastic scattering amplitude, which is determined by [26]

$$f_L^{(0)}(\varepsilon) = \frac{k_0^{2L}}{\kappa_L + c_L^{(1)}\varepsilon + c_L^{(2)}\varepsilon^2 + \cdots + ik_0^{2L+1}}. \tag{1.17}$$

The expansion coefficients $c_L^{(s)}$ in Eq. (1.17) determine specific features of the low-energy electron scattering and depend on the structure of potential created by the perturbing particle. According to Eq. (1.17), an electron in the $e^- - B$ system can be bound at negative energies ε in the states with $L \geq 1$, whereas, at positive energies, the quasistationary (resonance) levels can form.

The $\mathbf{K}_{e^-B}^{(0)}$ operator can be represented in the following form [25]:

$$\begin{aligned} \mathbf{K}_{e^-B}^{(0)} &= \sum_L \mathbf{K}_L^{(0)}, \\ \mathbf{K}_L^{(0)} &= -8\pi^2 \left|2\varepsilon\right|^{-L} f_L^{(0)}(\varepsilon) \sum_M \mathbf{d}_{LM}(\mathbf{r})\, \mathbf{d}_{LM}^*(\mathbf{r}')\ \delta(\mathbf{r} - \mathbf{R})\ , \end{aligned} \tag{1.18}$$

where the quantity

$$\mathbf{d}_{LM}(\mathbf{r}) = Y_{LM}(\mathbf{k}/k)\,(-i\,\nabla_{\mathbf{r}})^L.$$

Then, the scattering-matrix elements in Eq. (1.18) are written as

$$K_{nlm,\,nl'm}^{(0)} = -8\pi^2 \sum_{LM} \left|2\varepsilon\right|^{-L} f_L^{(0)}(\varepsilon) \left(\mathbf{d}_{LM} \Phi_{vlm}^{(R)}\right) \left(\mathbf{d}_{LM}^* \, \Phi^{*(R)}_{vl'm}\right). \tag{1.19}$$

The action of the operator $\mathbf{d}_{LM}$ on the wave function $\Phi_{vlm}^{(R)}(\mathbf{r})$ amounts to the multiplication of the latter by $(4\pi)^{-1/2}$ at $L = 0$ and (at $L \geq 1$) its differentiation at the point R. The scattering amplitude $f_L^{(0)}(\varepsilon)$ takes the form

$$f_L^{(0)}(\varepsilon) = \begin{cases} g_L^{-1}(\varepsilon), & r, r' < |2\varepsilon|^{-1}, \\ \left[g_L(\varepsilon) - \sqrt{-2\varepsilon}\right]^{-1}, & r, r' > |2\varepsilon|^{-1}, \end{cases} \tag{1.20}$$

where $g_L(\varepsilon)$ is the integral function of ε; its expansion in powers of ε is

$$(2\varepsilon)^L g_L(\varepsilon) = C_L^{(0)} + C_L^{(1)}\varepsilon + \cdots. \tag{1.21}$$

The inclusion of the states with $L \geq 1$ perturbs the states with the nonzero projections of electronic angular momentum m on the direction of vector $\mathbf{R}$.

The effective $e^- - B$ interaction can be represented as the sum of two terms

$$V_{e^-B}(\boldsymbol{\rho}, \mathbf{R}) = V^{(0)}_{e^-B}(\rho) + U_{A^+e^-B}(\boldsymbol{\rho}, \mathbf{R}), \tag{1.22}$$

where the strong $V^{(0)}_{e^-B}$ interaction is concentrated inside a bounded region $\rho \leq \rho_0$, where the wave functions of Rydberg electron change only weakly. Here, $\boldsymbol{\rho}$ and $\mathbf{R}$ are the radius vectors of particles e^- and A^+, measured from the center of gravity of the perturbing atom B. The long-range portion of the force field $U_{A^+e^-B}$ contains all polarization terms (including the polarization of atom B by electron) and can be taken into account perturbatively. For the ground S state and the states of atom B with the zero electronic orbital moment, the potential $U_{A^+e^-B}$ describes, in the case of LS-coupling, the interaction with two oppositely charged particles. It has the form [27]

$$U_{A^+e^-B}(\boldsymbol{\rho}, \mathbf{R}) = -\frac{\beta}{2}\left(\frac{\boldsymbol{\rho}}{\rho^3} - \frac{\mathbf{R}}{R^3}\right)^2 = -\frac{\beta}{2\rho^4} - \frac{\beta}{2R^4} + \Delta U_{A^+e^-B}(\boldsymbol{\rho}, \mathbf{R}), \tag{1.23}$$

$$\Delta U_{A^+e^-B}(\boldsymbol{\rho}, \mathbf{R}) = \frac{\beta \boldsymbol{\rho}\,\mathbf{R}}{(\rho R)^3},$$

where β is the static polarizability of atom B.

The uncertainty in the separation of $V_{e^-B}(\boldsymbol{\rho}, \mathbf{R})$ into the short-range and long-range parts in Eq. (1.22) using the theory of perturbation for the interaction $U_{A^+e^-B}$ can be eliminated under the following conditions:

$$(\beta\,|E|, \beta/R^2) \ll 1, \quad \beta/\rho_0^2 < 1. \tag{1.24}$$

As a result, the scattering $\mathbf{K}_{e^-B}$ matrix takes the form

$$\mathbf{K}_{e^-B}(\boldsymbol{\rho}, \mathbf{R}) = \sum_L \mathbf{K}^{(0)}_L(\boldsymbol{\rho}, \mathbf{R}) + U(\boldsymbol{\rho}, \mathbf{R}), \tag{1.25}$$

where the partial operators $\mathbf{K}^{(0)}_L(\boldsymbol{\rho}, \mathbf{R})$ are given by Eq. (1.18), and the long-range part is $U(\boldsymbol{\rho}, \mathbf{R}) = \left[U_{A^+e^-B}(\boldsymbol{\rho}, \mathbf{R}) + \frac{\beta}{2R^4}\right]\eta(\rho - \rho_0)$, where $\eta(x)$ is the Heaviside function. The corresponding matrix elements are written as

$$K_{nlm,n'l'm} = \left\langle \Phi^{(R)}_{nlm} \middle| \sum_L \mathbf{K}^{(0)}_L(\boldsymbol{\rho}, \mathbf{R}) \middle| \Phi^{(R)}_{n'l'm} \right\rangle + \left\langle \Phi^{(R)}_{nlm} \middle| U \middle| \Phi^{(R)}_{n'l'm} \right\rangle. \tag{1.26}$$

(here, only elements with the specified value of projection m are nonzero). The first term corresponding to $L = 0$ in Eq. (1.26) is equal to

$$\left\langle \Phi^{(R)}_{nlm} \middle| \mathbf{K}^{(0)}_0(\boldsymbol{\rho}, \mathbf{R}) \middle| \Phi^{(R)}_{n'l'm} \right\rangle = 2\pi a_0 \Phi^{(R)}_{nlm}(\mathbf{R})\,\Phi^{(R)}_{n'l'm}(\mathbf{R}), \tag{1.27}$$

where $a_0 = -1/\kappa_0$ is the scattering length in the arbitrarily introduced short-range part of potential (1.22). Because the electron wave functions $\Phi_{vlm}^{(R)}$ change only weakly on the ρ_0 scale, the integral for the polarization term $-\frac{\beta}{2\rho^4}$ in potential (1.23) is equal to $-2\pi(\beta/\rho_0)\,\Phi_{vlm}^{(R)}(\mathbf{R})\,\Phi_{vl'm}^{(R)}(\mathbf{R})$. This allows one to introduce the quantity $a = a_0 - \beta/\rho_0$ into Eq. (1.26) (at small k_0, it exactly coincides with the observed scattering length [27]) and recast matrix elements $K_{nlm,n'l'm}$ as

$$K_{nlm,n'l'm}(\mathbf{R}) = 2\pi a\,\Phi_{vlm}^{(R)}(\mathbf{R})\,\Phi_{v'l'm}^{(R)}(\mathbf{R})\,\delta_{m0} + \Delta K_{nlm,n'l'm}(\mathbf{R}), \tag{1.28}$$

where

$$\Delta K_{n\,l\,m,n'l'm}(\mathbf{R}) = \left\langle \Phi_{vlm}^{(R)} \middle| U(\boldsymbol{\rho},\mathbf{R}) \middle| \Phi_{v'l'm}^{(R)} \right\rangle + \left\langle \Phi_{vlm}^{(R)} \middle| \sum_{L\geq 1} \mathbf{K}_L^{(0)}(\boldsymbol{\rho},\mathbf{R}) \middle| \Phi_{v'l'm}^{(R)} \right\rangle. \tag{1.29}$$

Note that, to an accuracy of terms $\propto \beta/\rho_0^2 \ll a$, this result does not depend on ρ_0, so that the uncertainty in its choice vanishes [17]. In the quasiclassical conditions of electron motion (at $R \propto n^2$), expression (1.28) takes the form

$$K_{nlm,n'l'm}(\mathbf{R}) = -2\pi\, f_0^{(0)}\,\Phi_{vlm}^{(R)^*}(\mathbf{R})\,\Phi_{v'l'm}^{(R)}(\mathbf{R})\delta_{m0} + \left\langle \Phi_{vlm}^{(R)} \middle| U(\boldsymbol{\rho},\mathbf{R}) \middle| \Phi_{v'l'm}^{(R)} \right\rangle, \tag{1.30}$$

where the amplitude $f_0^{(0)}(\varepsilon) \cong -(a + \pi\beta p_e/3)$ depends on energy and, for the negative values of scattering length a, demonstrates the Ramsauer effect [28].

Since, at small values of k_0, the amplitude is $f_L^{(0)}(\varepsilon) \cong \frac{\delta_L^{(0)}}{k_0} \propto k_0^{2L}$ [26], the combination entering into Eq. (1.19) is written for $L \geq 1$, according to Eqs. (1.20) and (1.21), as

$$|2\varepsilon|^{-L} f_L(\varepsilon) \cong \frac{1}{C_L^{(0)}} - \frac{C_L^{(1)}}{\left(C_L^{(0)}\right)^2}\varepsilon, \tag{1.31}$$

where the coefficient $C_L^{(0)}$ is related to the scattering phase $\delta_L^{(0)}$ by the expression $\delta_L^{(0)} \cong k_0^{2L+1}/C_L^{(0)}$. The constant $C_L^{(1)}$ is found from the energy dependence of phase $\delta_L^{(0)}(\varepsilon)$. The corrections to the scattering amplitudes $f_L^{(0)}(\varepsilon)$ in the presence of long-range interaction (1.23) are contained in the second term $\Delta K_{nlm,n'l'm}$ in expression (1.28). In the asymptotic region of distances, $R \propto n^2$, they are proportional to βk_0, i.e., $\varepsilon^{1/2}$ [27].

The mutual influence of the Rydberg and covalent states is significant only in the vicinities of the points of possible mutual approach or term quasicrossings. According to Eq. (1.11), the equation in this case takes the following form:

$$\left[E - U_{vlm}^{(R)}(R)\right]\left[E - U_{v'Lm}^{(c)}(R)\right] = K_{nlm,n'l'm}^2(R), \tag{1.32}$$

i.e., only states with the same projections can interact with each other. As a result, one has for the Rydberg $U^{(R)}_{vlm}$ and covalent $U^{(c)}_{v'Lm}$ terms

$$
\begin{aligned}
U^{(R)}_{vlm}(R) &= -\frac{1}{2(n-\mu_l)^2} + \left[2\pi a \left|\Phi^{(R)}_{vlm}(\mathbf{R})\right|^2 \delta_{m0} + \Delta K_{nlm,nl'm}(R)\right] - \frac{\beta}{2R^4}, \\
U^{(c)}_{vlm}(R) &= -\frac{1}{2[n-\mu_{nLm}(R)]^2} - \frac{\beta}{2R^4}, \\
\mu_{nLm}(R) &= -\frac{1}{\pi}\arctan\left[\pi v^3 K_{nLm,nLm}(R)\right],
\end{aligned}
\tag{1.33}
$$

where the elements $\Delta K_{nlm,nlm}$ are specified by expression (1.28), and the quantity $K_{nLm,nLm}(R)$ is

$$
K_{nLm,nLm}(R) = \sum_{l' \geq l^*} \left[2\pi a \Phi^{(R)^*}_{vlm}(\mathbf{R}) \Phi^{(R)}_{vl'm}(\mathbf{R}) \delta_{m0} + \Delta K_{nlm,nlm}(R)\right]. \tag{1.34}
$$

The interaction between these terms is determined by

$$
\Delta_{nlm,n'Lm} = 2\left|K_{nlm,n'Lm}\right| \cos^2 \pi v(E), \tag{1.35}
$$

where

$$
K_{nlm,n'Lm}(R) = \sum_{l' \geq l^*} \left[2\pi a \Phi^{(R)^*}_{vlm}(\mathbf{R}) \Phi^{(R)}_{v'l'm}(\mathbf{R}) \delta_{m0} + \Delta K_{nlm,n'l'm}(R)\right]. \tag{1.36}
$$

One can see that the quantum defect $\mu_{nL}(R)$ induced in the covalent term by the field of perturbing atom B is noticeably different from the corresponding expression $\mu_L = ap_e$, which is obtained in the asymptotic theory at $R \propto n^2$ [15].

The interaction between Rydberg terms is defined by

$$
\Delta_{nlm,n'l'm} = 2\left|K_{nlm,n'l'm}\right| \cos^2 \pi v(E). \tag{1.37}
$$

Owing to the axial symmetry of the problem, only the states with different values of angular momentum l and fixed projections m on the quasimolecular axis can interact with each other. At some points (at energy E^*_c and distance R^*_c), the Rydberg terms can quasicross.

The covalent terms are found from the system of equations

$$
\boldsymbol{\tau} = \mathbf{K}_{e^-B} \pi v^3 \cot \pi v \sum_{l \geq l^*} \left|\Phi^{(R)}_{vlm}\right\rangle \left\langle \Phi^{(R)}_{vlm}\right| \boldsymbol{\tau}, \tag{1.38}
$$

The unambiguous solution to this equation is found from

$$
Det\left|\delta_{ll'} \tan \pi v(E) - \pi n^3 K_{nlm,nl'm}\right| = 0. \tag{1.39}
$$

In the case of $L = 0$ corresponding to the ZRP model, the nondiagonal elements are separable

$$K^{(0)\,2}_{nlm,\,nl'm} = K^{(0)}_{nlm,\,nlm} K^{(0)}_{nl'm,\,nl'm}, \tag{1.40}$$

for which reason only one degenerate covalent term splits off from the Coulomb levels [25].

According to Eq. (1.39), the inclusion of higher harmonics ($L \geq 1$) in the ZRP method should give rise to the branches containing N split-out covalent terms at intermediate distances ($R \propto n$), each representing the l-mixed groups of states for a given value m. This occurs because the separability of nondiagonal elements $K_{nlm,nl'm}$ is broken because of the last term $\left\langle \Phi^{(R)}_{vlm} \middle| \sum_{L\geq 1} \mathbf{K}^{(0)}_L(\boldsymbol{\rho}, \mathbf{R}) \middle| \Phi^{(R)}_{vl'm} \right\rangle$ in Eq. (1.28). Since all states, except $m = 0$, are doubly degenerate with respect to the $\pm m$ values, the total number of split-out covalent terms $N = \frac{1}{2}(n - l^*)(n + 2l^* - 2)$ depends on the principal quantum number.

In the case of $n = 4$, there are four noninteracting covalent terms with angular momentum l^* and projections m = 0–3. For the next value $n = 5$, one has nine states. They represent a group of four independent pairs (mixed with respect to $l = 3, 4$ for each of m = 0–3) of terms and one isolated term (with $l = m = 4$). In the case of $n = 6$, 15 terms appear, among which there are 4 independent triads (l = 3–5; m = 0–3) of interacting terms, 1 interacting pair ($l = 4, 5$; $m = 4$), and 1 isolated term with $l = m = 5$. For $n = 7$, their number is 22, and they include four independent groups of four interacting terms (l = 3–6; $m = 4$), one triad (l = 4–6; $m = 4$), one pair ($l = 5, 6$; $m = 5$) of interacting terms, and one state with $l = m = 6$, etc. Note also that, among each of the interacting groups containing $(n - l^*)$ states classified by the projection m, only the two first groups of states with $m = 0$ and $m = 1$ are subjected to the strongest action. It is precisely these groups that are of chief interest, because the remaining states are weakly perturbed and, hence, are close to the Coulomb states. The shift of the terms with $m = 1$ decreases rapidly with increasing distance R between centers, because the corresponding matrix elements behave as $\langle nl1|\,\mathbf{K}^{(0)}_1|nl1\rangle = \propto R^2_{vl}(R)/R^2$, whereas the elements $\langle nl0|\,\mathbf{K}^{(0)}_1|nl0\rangle = \propto R^2_{vl}(R)/R$ decrease more slowly. For this reason, at distances $R \geq n$, where a smooth transition to the ZRP model occurs, the Σ states are perturbed most strongly.

1.4 PES of the A^* – B System at Large Interatomic Distances

Taking large distances into consideration, the necessity arises of revealing the correlation between the PES of the $A^{**} - B$ system at intermediate distances and the corresponding terms in the asymptotic region $R \propto n^2$, where the role of centrifugal barrier is insignificant and electron motion can be described using the quasiclassical approximation in the plane-wave representation. For the Rydberg states

corresponding to small values $l < l^*$, no such problem exists. It arises for the PESs of the covalent states ($l \geq l^*,\ m$), because their number in Eq. (1.38) noticeably increases with a decrease in R.

The plane-wave expansion of the Rydberg wave functions $\Phi_{vlm}^{(R)}$ at $l < l^*$ in the asymptotic region of electron motion is written as [15]

$$|nlm\rangle = \Phi_{vlm}^{(R)}(\mathbf{r}) = \sum_{L} \sqrt{2\pi\,(2L+1)}\; Z_{vl}^{(L)}(R)\; Y_{lm}(\mathbf{r}/r)\; |LM\rangle\, \delta_{M0}. \tag{1.41}$$

Here, L and M are, respectively, the electron angular momentum relative to the atom B and its projection on the direction of vector $\mathbf{R}$ and $Z_{vl}^{(L)}(R)$ are the periodic functions of the form

$$Z_{vl}^{(L)}(R) = (-1)^k \frac{2}{R} (2\pi p_e v^3)^{-1/2} \left\{ \begin{array}{ll} \sin\ S_{vl(R)}^{(L)}, & (L = 2k) \\ \cos S_{vl(R)}^{(L)}, & (L = 2k+1) \end{array} \right\}, \tag{1.42}$$

where $S_{vl}^{(L)}(R)$ is the corresponding quasiclassical phase.

Inasmuch as in the vicinity of perturbing atom at $|\,\mathbf{r} - \mathbf{R}\,|, |\,\mathbf{r}' - \mathbf{R}\,| \ll R$, the Coulomb Green's function for the degenerate states with $l \geq l^*$ has in the quasiclassical approximation a simple form with respect to the angular variables [21],

$$\pi v^3 \cot \pi v \sum_{l>l^*,\,m} \left| \Phi_{vlm}^{(R)} \right\rangle \left\langle \Phi_{vlm}^{(R)} \right| \cong \frac{\sin p_e(R)\,|\,\mathbf{r} - \mathbf{r}'\,|}{2\,\pi\,|\,\mathbf{r} - \mathbf{r}'\,|} \cot \pi v = p_e(R)\ \cot \pi v \sum_{LM} |\,LM\,\rangle\ \langle\,LM\,|, \tag{1.43}$$

the matrix elements $\langle LM|\ \mathbf{K}_{e^-B}|nlm\rangle$ and $\langle nlm|\ \mathbf{K}_{e^-B}|nlm\rangle$ appear in the asymptotic theory. They are expressed through the diagonal (in M) elements $\langle LM|\ \mathbf{K}_{e^-B}|L'M\rangle$ and are determined by

$$\begin{aligned} \langle LM\ |\,\mathbf{K}_{e^-B}|\ nlm\rangle &= \sum_{L'} \sqrt{2\pi\,(2L'+1)} \\ &\quad \times\ Z_{vl}^{(L')}(R)\, Y_{lm}(\mathbf{R}/R)\ \langle LM|\ \mathbf{K}_{e^-B}|L'M\rangle\, \delta_{M0}\,, \\ \langle\, nlm\ |\mathbf{K}_{e^-B}|\ nlm\rangle &= 2\pi \sum_{L,L'} \sqrt{(2L+1)\,(2L'+1)} \\ &\quad \times\ Z_{vl}^{(L)}(R)\ Z_{vl}^{(L')}(R)\,|\,Y_{lm}(\mathbf{R}/R)\,|^2\ \langle LM|\,\mathbf{K}_{e^-B}|L'M\rangle\, \delta_{M0}\,. \end{aligned} \tag{1.44}$$

Since the functions $Y_{lm}(\mathbf{R}/R)$ are nonzero only for $m = 0$, matrix elements (1.44) are, in fact, the superposition of two waves propagating along the vector $\mathbf{R}$. Inasmuch as the electron scattering in this case is determined by the angular momentum L relative to the perturbing atom B, the orbitally degenerate (in $l \geq l^*$)

covalent term splits into the individual L components corresponding to $m = 0$. The presence of the term $\frac{\beta\boldsymbol{\rho}\mathbf{R}}{(\rho R)^3}$ in the potential $\Delta U_{A^+e^-B}$ leads to an additional mixing of the states with $\Delta L = \pm 1$. Because of this, the summation over L' in (1.44) includes only three terms $(L\,,\ L \pm 1)$.

In this representation, the matrix elements $\langle LM \,|\, \mathbf{K}_{e^-B} \,|\, L'M\rangle$ can be conveniently written as

$$\langle LM \,|\, \mathbf{K}_{e^-B} | \, L'M\rangle = \langle LM \,|\, \tilde{\mathbf{K}}^{(0)}_{e^-B} \,|\, LM\rangle + \langle LM \,|\, \Delta U | L'M\rangle, \tag{1.45}$$

where the operator $\tilde{\mathbf{K}}^{(0)}_{e^-B}$ includes, in the outer region, the polarization interaction of electron with atom B; i.e.,

$$\tilde{\mathbf{K}}^{(0)}_{e^-B}(\rho, \mathbf{R}) = \mathbf{K}^{(0)}_{e^-B}(\rho, \mathbf{R}) - \frac{\beta}{2\rho^4}\ \eta(\rho - \rho_0),$$

whereas the long-range potential ΔU, by analogy with Eq. (1.25), is determined as

$$\Delta U(\rho, \mathbf{R}) = [\,\Delta U_{A^+e^-B}(\rho, \mathbf{R})]\ \eta(\rho - \rho_0).$$

In this case, the diagonal matrix elements $\langle LM \,|\, \tilde{\mathbf{K}}^{(0)}_{e^-B} \,|\, LM\rangle$ are independent of M (because of the spherical symmetry of interaction) and can be expressed through the observed characteristics of the potential $e^- - B$-scattering: scattering length a and polarizability β [18]

$$\begin{aligned} \tilde{K}^{(0)}_{0,0} &= a + \frac{\pi\beta\, p_e}{3} + \frac{4}{3} a\beta\, p_e^2 \ln p_e + \cdots, \\ \tilde{K}^{(0)}_{L,L} &= a\delta_{L0} - \frac{\pi\beta\, p_e}{(2L-1)(2L+1)\,(2L+3)} + \cdots. \end{aligned} \tag{1.46}$$

Since ΔU is the effective electric dipole interaction with the moment $D = \beta\,/R^2$, the nondiagonal (in L) elements $\langle LM \,|\, \Delta U \,|\, L'M\rangle$ in Eq. (1.44) can be represented in the form

$$\langle LM \,|\, \Delta U | \, L'M\rangle = \sqrt{\frac{2L'+1}{2L+1}}\ (\,1L'0\,M \,|\, LM\,)\ (\,1L'0\,0 \,|\ L0\,)\, P_{LL'}(R, n), \tag{1.47}$$

where

$$P_{LL'}\,(R, n) = \frac{\beta}{p_e R^2}\ \left[\ \int\limits_0^{2n^2 p_e} j_L(x) j_{L'}(x)\ \mathrm{d}x\ \right].$$

For the sufficiently large values of n such that $n^2 p_e \gg 1$, the upper limit can be turned to infinity ∞ to obtain the simple expression

$$\langle LM|\,\Delta U|L'M\rangle = \frac{\beta}{R^2 p_e}\begin{cases} \dfrac{1}{\sqrt{(2L+1)\,(2L+3)}}\left[1-\dfrac{M^2}{(L+1)^2}\right]^{1/2}, & L'=L+1, \\ \dfrac{1}{\sqrt{(2L-1)\,(2L+1)}}\left[1-\dfrac{M^2}{L^2}\right]^{1/2}, & L'=L-1. \end{cases} \tag{1.48}$$

In as much as the elements $\tilde{K}^{(0)}_{L,L}$ rapidly decrease with increasing L, one can self-restrict to the particular calculations of the two-channel situation $L=0$ and 1. Then, the covalent terms are determined from the system of equations

$$\tau_{LM,l} = p_e \cot \pi\nu \sum_{L'=0,1} K_{LM,L'M}\,\tau_{L'M,\,l}, \tag{1.49}$$

whose solution describes two pairs of states classified by the effective angular momentum $\tilde{L}$ and $|M|=0,1$. It has the following form:

$$U^{(0)}_{\tilde{L}M} = -\frac{1}{2\nu^{(0)2}_{\tilde{L}M}(R)} - \frac{\beta}{2R^4}, \qquad \nu^{(0)}_{\tilde{L}M}(R) = n - \mu^{(0)}_{\tilde{L}M}(R), \tag{1.50}$$

where the quantum defects induced by the field of atom B for the levels with $M=0$ are determined by

$$\mu^{(0)}_{\tilde{L}M}(R) = \frac{1}{\pi}\,\arctan\left\{\frac{p_e}{2}\left[K^{(0)}_{00,00} + K^{(0)}_{10,10}\,\cdot \right.\right. \\ \left.\left. \pm\sqrt{\left(K^{(0)}_{00,00} - K^{(0)}_{10,10}\right)^2 + 4\left(K^{(0)}_{10,00}\right)^2}\right]\right\} \tag{1.51}$$

(state with $\tilde{L}=0$ corresponds to the sign "+", and with $\tilde{L}=1$, to the sign "−"). For the states with $L=1$ and $|M|=1$, the matrix elements $K^{(0)}_{1M,00}=0$, so that

$$\mu^{(0)}_{\tilde{L}=1\,M=1}(R) = \frac{1}{\pi}\arctan\,(p_e K^{(0)}_{10,10}). \tag{1.52}$$

Since $K^{(0)}_{00,00} \gg K^{(0)}_{10,10}, K^{(0)}_{10,00}$ at $R \gg n^2$, only one term with

$$\mu^{(0)}_{\tilde{L}=1\,M=0}(R) = \frac{1}{\pi}\,\arctan\,(p_e K^{(0)}_{00,00}).$$

stands out, in fact, in the group of degenerate states. The other terms tend to the unperturbed Coulomb levels.

1.5 Exchange Interaction Between the Rydberg States in the $A^{**} - A$ System

We now turn to a quasimolecule consisting of the identical atoms A^{**} and A. For definiteness, we assume that the electronic shell of the ion residue is filled and the atom A is in the ground state $^2S_{1/2}$ with one valence electron (as, e.g., in alkali metal atoms). In this case, one can also use the approximation of LS coupling. Let us denote the sets of quantum numbers for Rydberg atom $A^{**}(q_1)$ and atom $A(q_2)$ in the ground state by

$$q_1 = (n_1 l_1 m_1;\ s_1 = 1/2, \sigma_1 = \pm 1/2) \text{ and}$$
$$q_2 = (n_2, l_2 = m_2 = 0\,;\, s_2 = 1/2, \sigma_2 = \pm 1/2).$$

Here, an additional symmetry arises caused by the reflection about the plane perpendicular to the molecular axis and passing through its midpoint. Since the Hamiltonian of the system does not change as a result of electron reflection about this plane, the quasimolecular states are divided into even (g) and odd (u) states, and their wave functions do not change or change sign on electron reflection. According to the general rules [26], the total wave functions of the odd and even states with the given total spin $\mathbf{S} = \mathbf{s}_1 + \mathbf{s}_2$ and its projection $\sigma = \sigma_1 + \sigma_2$ on the chosen direction are written (without the normalization factor) as

$$\begin{aligned}\Psi_{g,u}^{(S\sigma)} = \sum_{\sigma_1+\sigma_2} &(s_1 0 \sigma_1 0\,|\,s_1\sigma_1)\,(s_2 0 \sigma_2 0\,|\,s_2\sigma_2)\,(s_1\, s_2\, \sigma_1\, \sigma_2\,|\,S\sigma)\\ &\times \Big\{\big[\Psi(1a^{**}, 2b)\chi_{s_1\sigma_1}(1)\chi_{s_2\sigma_2}(2) - \Psi(2\,a^{**}, 1b)\chi_{s_1\sigma_1}(2)\chi_{s_2\sigma_2}(1)\big]\\ &\pm \big[\Psi(2a, 1b^{**})\chi_{s_1\sigma_1}(1)\chi_{s_2\sigma_2}(2) - \Psi(1a, 2b^{**})\chi_{s_2\sigma_2}(1)\chi_{s_1\sigma_1}(2)\big]\Big\}.\end{aligned}$$

The indices 1 and 2 label the valence electrons, $\Psi(1a^{**}, 2b)$ and $\Psi(2a^{**}, 1b)$ are the coordinate parts of the two-electron wave functions corresponding to the location of these electrons near the corresponding atom (for simplicity, atoms A^{**} and A are denoted by a and b), $\chi_{s\sigma}$ is the electron spin function, and $(j_1\, j_2\, m_1\, m_2\,|\,JM)$ are the vector composition coefficients [23]. Note that the expression in braces contains two terms enclosed in square brackets, of which the first accounts for the electron exchange and the second additionally includes the electron transfer between centers. After simple mathematics, this expression can be written in the form

$$\begin{aligned}\Psi_{g,u}^{(S\sigma)} = \frac{1}{2}\sum_{\sigma_1+\sigma_2} &(s_1\, s_2\, \sigma_1\, \sigma_2\,|\,S\sigma)\\ &\times \Big\{\Big[\Psi(1a^{**}, 2b) + (-1)^S\,\Psi(2a, 1b^{**})\Big]\,\chi_{s_1\sigma_1}(1)\,\chi_{s_2\sigma_2}(2)\\ &- \Big[\Psi(1a, 2b^{**}) + (-1)^S\,\Psi(2\,a^{**}, 1b)\Big]\,\chi_{s_1\sigma_1}(2)\,\chi_{s_2\sigma_2}(1)\Big\}.\end{aligned}$$

Owing to the electron identity and symmetry about the plane passing through the midpoint of the quasimolecular axis, one has the following representation for the total normalized wave functions $\Psi_{g,u}^{(S\sigma)}$ of the noninteracting system [29]:

$$\Psi_{g(u),n_1l_1m_1,n_2}^{(S\sigma)}(\mathbf{r},\boldsymbol{\rho}) = \Phi_{n_1l_1m_1,n_2}^{(g,u)}(\mathbf{r},\boldsymbol{\rho})\,\chi_{S\sigma}^{(\mp)} = A_{g,u}\left[\Phi_{n_1l_1m_1}^{(R)}(\mathbf{r})\,\Phi_{n_2}(\boldsymbol{\rho}) \pm \Phi_{n_1l_1m_1}^{(R)}(\boldsymbol{\rho})\,\Phi_{n_2}(\mathbf{r})\right]\chi_{S\sigma}^{(\mp)}, \tag{1.53}$$

where the even (g) and odd (u) functions have the signs ($\pm$), $\Phi_{n_1l_1m_1}^{(R)}$ and Φ_{n_2} are the wave functions of the excited atom A^{**} and A, respectively, and $\mathbf{r}$ and $\boldsymbol{\rho}$ are the electron coordinates measured from the centers of these atoms. The normalization factors $A_{g,u}$ are found from the condition $\int d\mathbf{r}d\boldsymbol{\rho}\left[\Phi_{n_1l_1m_1,n_2}^{(g,u)}(\mathbf{r},\boldsymbol{\rho})\right]^2 = 1$; they are equal to

$$A_{g,u} = \frac{1}{\sqrt{2\,(1 \pm S_{12}^2)}}, \tag{1.54}$$

where S_{12} is the overlap integral

$$S_{12} = \int d\mathbf{r}\,\Phi_{n_1l_1m_1}^{(R)}\Phi_{n_2}. \tag{1.55}$$

The normalized spin functions $\chi_{S\sigma}^{(\pm)}$ are

$$\chi_{S\sigma}^{(\pm)} = \frac{1}{2}\sum_{\sigma_1+\sigma_2}(s_1\,s_2\,\sigma_1\,\sigma_2\,|\,S\sigma) \times\left[\chi_{s_1\sigma_1}(1)\chi_{s_2\sigma_2}(2) \pm \chi_{s_2\sigma_2}(1)\chi_{s_1\sigma_1}(2)\right]. \tag{1.56}$$

The even (g) and odd (u) wave functions $\Psi_{g,u}^{(S\sigma)}$ are antisymmetric about the electron and spin permutation and correspond to $S = 0,\ 1$ and $\sigma = 0,\ \pm 1$. Since spin functions (1.56) are mutually orthogonal, the elements of the $e^- - A$ scattering $\mathbf{K}_{e^-A}$ matrix determined, by analogy with Eq. (1.18), satisfy the relation

$$\left\langle \Psi_{g(u)}^{(S\sigma)}\right|\mathbf{K}_{e^-A}\left|\Psi_{g(u)}^{(S\sigma)}\right\rangle = K_{g(u),g(u)}^{(S)}\delta_{SS'}\delta_{\sigma\sigma'}. \tag{1.57}$$

They are nonzero only for the transitions between the states with the same parity and independent of σ. For this reason, to determine the PES of the system, one can restrict oneself to the consideration of the situation with $\sigma = 0$. After insertion of Eq. (1.57) into the initial equation for the level-shift operator, the perturbed diabatic Rydberg terms $n_1l_1m_1$ can be determined from the homogeneous system [29]

$$\langle g(u)|\,\boldsymbol{\tau}|g(u)\rangle = \frac{K_{g(u),g(u)}^{(S)}}{E - E_{v_1l_1}}\,\langle g(u)|\,\boldsymbol{\tau}|g(u)\rangle, \tag{1.58}$$

whose nontrivial solution gives two (singlet g and triplet u) noninteracting perturbed Rydberg terms

$$U_{g,u}^{(S)}(R) = E_{v_1 l_1} + K_{g(u),g(u)}^{(S)} - \frac{\beta}{2R^4}, \tag{1.59}$$

split by

$$\Delta = K_{g,g}^{(0)} - K_{u,u}^{(1)}. \tag{1.60}$$

The matrix elements $K_{g(u),g(u)}^{(S)}$ entering in Eqs. (1.58) through (1.60) are written as

$$\begin{aligned}
&K_{g(u),g(u)}^{(S)}(R) \\
&= 2A_{g,u}^2 \left\langle \Phi_{n_1 l_1 m_1}^{(R)}(\mathbf{r})\, \Phi_{n_2}(\boldsymbol{\rho})\, \chi_{S0}^{(\mp)} \middle| \mathrm{K}_{e^-A} \middle| \chi_{S0}^{(\mp)}\, \Phi_{n_1 l_1 m_1}^{(R)}(\mathbf{r})\, \Phi_{n_2}(\boldsymbol{\rho}) \right\rangle \\
&\quad \pm 2A_{g,u}^2 \left\langle \Phi_{n_1 l_1 m_1}^{(R)}(\boldsymbol{\rho})\, \Phi_{n_2}(\mathbf{r})\, \chi_{S0}^{(\mp)} \middle| \mathbf{K}_{e^-A} \middle| \chi_{S0}^{(\mp)}\, \Phi_{n_1 l_1 m_1}^{(R)}(\mathbf{r})\, \Phi_{n_2}(\boldsymbol{\rho}) \right\rangle \\
&= 2A_{g,u}^2 \left[\left\langle \Phi_{n_1 l_1 m_1}^{(R)}\, \chi_{S0}^{(\mp)} \middle| \mathbf{K}_{e^-A} \middle| \chi_{S0}^{(\mp)}\, \Phi_{n_1 l_1 m_1}^{(R)} \right\rangle \right. \\
&\quad \left. \pm S_{12} \left\langle \Phi_{n_2}\, \chi_{S0}^{(\mp)} \middle| \mathbf{K}_{e^-A} \middle| \chi_{S0}^{(\mp)}\, \Phi_{n_1 l_1 m_1}^{(R)} \right\rangle \right].
\end{aligned} \tag{1.61}$$

The first term describes the level shift induced by the electron elastic scattering from the perturbing center, and the second term corresponds to the excitation transfer from one center to the other. According to Eq. (1.25), they take into account the contributions from the short- and long-range interactions. In contrast to the above-considered perturbation of atom A^{**} by a foreign atom B, the contribution of the short-range exchange interaction is determined through the singlet (a_+) and triplet (a_-) electron-elastic-scattering lengths, whereas the contribution of the long-range interaction depends on the total spin S. Note that, in the absence of the long-range interaction, expression (1.60) takes the form

$$\begin{aligned}
&\Delta_{n_1 l_1 m_1}^{(R)}(R) \\
&= 2\pi \left\{ \frac{a_+}{1 + S_{12}^2} \left[\left| \Phi_{n_1 l_1 m_1}^{(R)}(\mathbf{R}) \right|^2 + S_{12}\, \Phi_{n_1 l_1 m_1}^{(R)}(\mathbf{R})\, \Phi_{n_2}(\mathbf{R}) \right] \right. \\
&\quad \left. - \frac{a_-}{1 - S_{12}^2} \left[\left| \Phi_{n_1 l_1 m_1}^{(R)}(\mathbf{R}) \right|^2 - S_{12}\, \Phi_{n_1 l_1 m_1}^{(R)}(\mathbf{R})\, \Phi_{n_2}(\mathbf{R}) \right] \right\} \delta_{m_1 0}.
\end{aligned} \tag{1.62}$$

The interaction between the perturbed Rydberg states $n_1 l_1 m_1$ and $n_1' l_1' m_1$ is determined by the matrix element $\left\langle \Phi_{n_1 l_1 m_1, n_2}^{(g,u)}\, \chi_{S0}^{(\mp)} \middle| \mathbf{K} \middle| \chi_{S0}^{(\mp)}\, \Phi_{n_1' l_1' m_1, n_2}^{(g,u)} \right\rangle$ and is given by the expression

$$V^{(S)}_{n_1 l_1 m_1,\, n'_1 l'_1 m_1}(R) = \frac{\pi a_{\pm}}{\sqrt{(1 \pm S^2_{12})(1 \pm S^2_{12})}} \left\{ 2\,\Phi^{(R)}_{n_1 l_1 m_1}(\mathbf{R})\Phi^{(R)}_{n'_1 l'_1 m_1}(\mathbf{R}) \pm \Phi_{n_2}(\mathbf{R}) \left[S_{12}\,\Phi^{(R)}_{n'_1 l'_1 m_1}(\mathbf{R}) + S_{1'2}\,\Phi^{(R)}_{n_1 l_1 m_1}(\mathbf{R}) \right] \right\}. \quad (1.63)$$

1.6 Potential Curves for the Na(nl)** + He System

As a particular application of the theory, we analyze the PES of a quasimolecule composed of highly excited atom A^{**} and a neutral atom B with filled electronic shell. It is natural to restrict oneself to the simplest and well-documented system $\mathrm{Na}^{**}(nl) + \mathrm{He}$, because it attracts increased interest in researchers today. This is caused primarily by the discovery of brown dwarfs (BD) [30] and giant extrasolar planets (GEPs) [31], which have become the subject of intensive study in the last years [32, 33]. Brown dwarfs (BDs) are the substellar-mass objects in which the thermonuclear fusion reaction of hydrogen transformation into helium does not proceed. They substantially differ from Sun and planets of our solar system and have effective atmospheric temperature as high as thousands of degrees. As distinct from the main-sequence stars (which possess regions of radiation energy transfer), the heat-transfer processes in BDs proceed only through convection, thereby providing homogeneity of chemical composition in depth.[1] Photon fluxes from BDs are characterized by the optical wavelengths indicating the presence of alkali metal atoms in their atmosphere [34, 35]. Analogous situation occurs in the giant extrasolar planets (GEPs), although no radiation from them is observed directly. Theoretical estimates also suggest the predominance of the sodium and potassium resonance lines in the radiation spectra of GEPs [36, 37]. The atmospheres of these substellar-mass objects almost totally consist of the hydrogen molecules and helium atoms [32]. Owing to the collisions of alkali metal atoms with these particles, the observed profiles of resonance lines are noticeably broadened (more than by 100 nm, depending on the temperature and density of the medium). In addition, these profiles strongly deviate from the Lorentzian shape typical of an isolated atom. Such broadening and line profiles are observed in the BD spectra and can be the cause of the nontransparency of the GEP atmospheres [32, 36, 38–40].

[1] It is generally believed that, for the thermonuclear reactions to proceed, the stellar mass must be, at least, 80 times greater than the Jupiter mass (i.e., equal to about 0.08 of the Sun mass). The hypothesis of BDs as star-like objects (with masses from five to 75 Jupiter mass) was put forward in early 1960s of the twentieth century. It was assumed that the BD formation proceeds following the scenario analogous to the formation of other stars. However, the detection of BD is hampered by the fact that they virtually do not emit visible light. The most intense emission from them occurs in the IR range.

The profiles of these lines are usually calculated on the basis of the quantum mechanical description of collisional broadening and the available data on the potential curves and dipole transition moments. The properties of "satellites" are particularly informative, because they can arise at the line wings in the presence of singularities in the differences between adiabatic potentials. The satellite shapes are highly sensitive to the ambient temperature, whereas their positions and amplitudes are sensitive to the details of interaction potentials. Moreover, an algorithm allowing the temperature and pressure of the BD and GEP atmospheres to be reconstructed from the line shape is formulated in [41, 42]. This explains the increased interest of researchers in the correct theoretical calculations of the original potentials.

The shock broadening of the resonance $2s \rightarrow 2p$ line of lithium atom was studied in [42]. In [43], the collisional broadening of the sodium $3s \rightarrow 3p$ and potassium $4s \rightarrow 4p$ lines by helium atoms was considered and the emission and absorption coefficients on the red and blue wings were calculated. In addition to the determination of the temperature and density, the obtained results allowed one to develop the methods for the diagnostic of albedo and atmosphere composition of the objects of interest [44, 45]. The potential curves of the low-lying electron-excited states of the Na + He system were calculated in [46–51] using different numerical methods. The first one [46] is based on the semiempirical pseudopotential method that is widely used in atomic physics. The second [47] is the traditional quantum chemical LCAO method. The calculations in [48–50] were made using the standard MRD CI and MOLCAS programs. In [51], the terms of highly excited states of the $Na^{**}(nlm)$ + He system were calculated and a detailed comparison with the existing data was carried out.

In [52], the Hartree–Fock basis of cationic orbitals [53] was invoked to calculate the potential curves and dipole moments for the $4s \rightarrow 4p$ transition in the K + He system within the full ab initio approach and with the use of the multireference configuration interaction (MRCI) method and the MOLPRO program [54, 55]. In addition, the PESs of the $K + H_2$ system were constructed in [52] and the resonance wavelengths and dipole transition moments were calculated as functions of the total number of degrees of freedom, including the changes in the bond lengths and angles to determine the position of potassium atom relative to the axis of molecular hydrogen.[2]

Generally speaking, the medium-perturbed higher lying electronic states are also involved in the formation of the frequency profile at its wings (under the condition that $\Delta\omega \gg v/b_0$, where v is the relative velocity and b_0 is the Weisskopf radius [57]). It then follows that the correct calculations require additional analysis of the behavior of a set of potential curves, especially for the small impact parameters where the standard quantum approaches are inapplicable [15].

[2]Earlier, this system was studied in the work of Rossi and Pascale [56], where the PESs were calculated with allowance for two orientations of the molecular axis of H_2 about the atom K (the dependence of the dipole transition moments on the geometry was disregarded).

The perturbation of Rydberg terms is determined from the behavior of the diagonal matrix elements $K_{nlm,\,nlm}$. For instance, the l-dependent oscillatory structure of the terms in overbarrier region, according to [15], reproduces the specific features of electron wave function $\Phi_{vlm}^{(R)}(\mathbf{r})$ of Rydberg atom A^{**} and dies out with increasing R. With an increase in l, this structure becomes more pronounced. The effect of long-range interaction is determined by the element $\left\langle \Phi_{vlm}^{(R)} \middle| U \middle| \Phi_{vlm}^{(R)} \right\rangle$, the value of which is the most significant at the distances $R \leq n$. The azimuthal angular dependence of long-range potential (1.23) is responsible for the Π and Δ components of Rydberg terms, whose shifts from the isolated unperturbed levels decrease with increasing l, because the corresponding matrix elements satisfy condition $\left|K_{nl2,nl2}\right| < \left|K_{nl1,nl1}\right| < \left|K_{nl0,nl0}\right|$.

One should also expect the appearance of quasicrossing between the terms with different values of l and a fixed projection of angular momentum. This is caused by the fact that the states with different quantum defects behave differently in the near-barrier region.

Contrary to the interaction between the Rydberg terms (1.37), the interaction parameters between the Rydberg terms and covalent term (1.34) can be significantly greater. In the case of $L = 0$, only one term corresponding to the covalent nL state formed by the orbitally degenerate Coulomb states is split-off from the Coulomb terms and characterized by the isotropic electron S scattering from the perturbing atom. This state interacts only with those perturbed Rydberg states nlm, which have zero projection m, in line with the ZRP model.

The aforesaid is clearly demonstrated in Figs. 1.1 through 1.3 where the potential curves measured from the ground-state of the $Na^{**}(nl) + He$ system are presented. The dependences on the interatomic distance R were calculated by formulas (1.28) through (1.37) with account taken of the harmonics $L = 0$ and $L = 1$ in the matrix elements $K_{nlm,\,n'l'm}(\mathbf{R})$ with various n, l, and m. To this end, we used the data on elastic $e^- - He$ scattering [28] and the following expansion coefficients in (1.30)

$$C_1^{(0)} = 1.631, \quad C_1^{(1)} = 1.963. \tag{1.64}$$

For the quantum defects in the sodium s, p, and d states, we used the values

$$\mu_0 = 1.349, \quad \mu_1 = 0.857, \quad \mu_2 = 0.015, \tag{1.65}$$

which were found using the data reported in [58]. These figures demonstrate the adiabatic potential curves of the Rydberg $nl^2\Sigma^+$ states calculated for the quantum numbers $n = 4$–6 and $l = 0$–3 [51]. The computational results of other authors [46–50] are also presented. A comparison with them is of particular interest, because the accuracy of quantum chemical computations for such values is not too high [15]. One can see that our results [51] obtained for the component $n = 4$ of the term $4s^2\Sigma^+$ (Fig. 1.1a) are in accordance with the data reported in [46, 48], whereas the terms obtained in [35, 36] lie too low (this is typical of the MRD CI program used in those works). The next Rydberg terms $4p^2\Sigma^+$ and $4p^2\Pi$ are shown

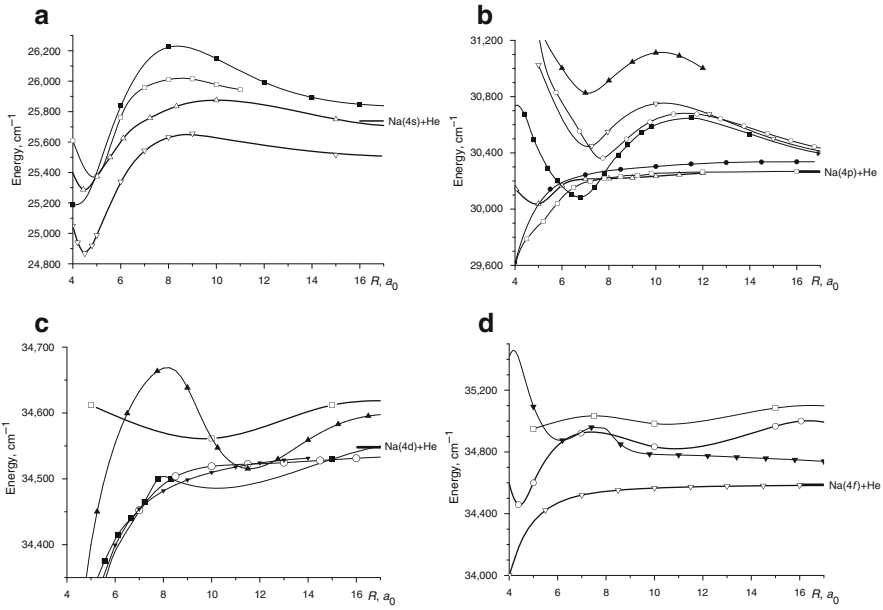

Fig. 1.1 Adiabatic terms of the Rydberg $4l\,^2\Sigma^+$ states in the Na + He quasimolecule for the angular momenta $l = 0$–3. Curves (**a**) relating to the $4s^2\Sigma^+$ state are the results of the following calculations: □ [46], Δ [48], ▽ [50], and ■ [51]. Curves (**b**) are for the $4p^2\Sigma^+$ and $4p^2\Pi$ states, first corresponding to the ▲ [46], ▽ [48], ■ [50], and O [51] terms, and the second, to the Δ [46], □ [50], and ● [51] terms. The potential curves (**c**) include the $4d^2\Lambda$ states, which are denoted as follows: ■ [47], □ [48], and ▲ [51] for the $4d\,^2\Sigma^+$ state, and O and ▼ [51] for the $4d\,^2\Pi$ and $4d\,^2\Delta$ states, respectively. The terms (**d**) are the results of the following calculations: □ [47], O [48], and ▼ [51] for the $4f\,^2\Sigma^+$ state, and ▽ [51] for the closely spaced $4f^2\Pi, \Delta, \Phi$ states. The horizontal line _____ denotes the dissociation limit corresponding to the energy of the separated atoms in the given states

in Fig. 1.1b. The term $4p^2\Sigma^+$ best agrees with the results [48, 50], and the $4p^2\Pi$ term is in accordance with the calculations performed in [46, 48]. The potential curves calculated by us for the $4d^2\Sigma^+$ and $4f^2\Sigma^+$ terms (Figs. 1.1c, d) [51] agree well with the data in [48] (the terms $4d,\ f^2\Pi$, $4d, f^2\Delta$, and $4f^2\Phi$ were calculated for the first time). In the case of $n = 5$, a good agreement for the term $5s^2\Sigma^+$ at intermediate distances (Fig. 1.2a) is achieved with the data in [46–48, 50]. At larger distances, the term calculated in [50] lies too high. The potential curve calculated for the $5p^2\Sigma^+$ term [51] (Fig. 1.2b) well reproduces the result [48]. The data reported in [47] are overstated, whereas the term $5p^2\Pi$ was not calculated previously. The term $6s\,^2\Sigma^+$is also in good agreement with [48] (Fig. 1.3).

It is worth noting that the results obtained in [51] are the most preferable, because the accuracy of calculations performed by the ZRP method [27] are controlled by the accuracy of determining scattering amplitudes (1.30), which are usually calculated independently or can be determined from the experiment. With an increase in n (due to the increase in the number of possible crossings), the

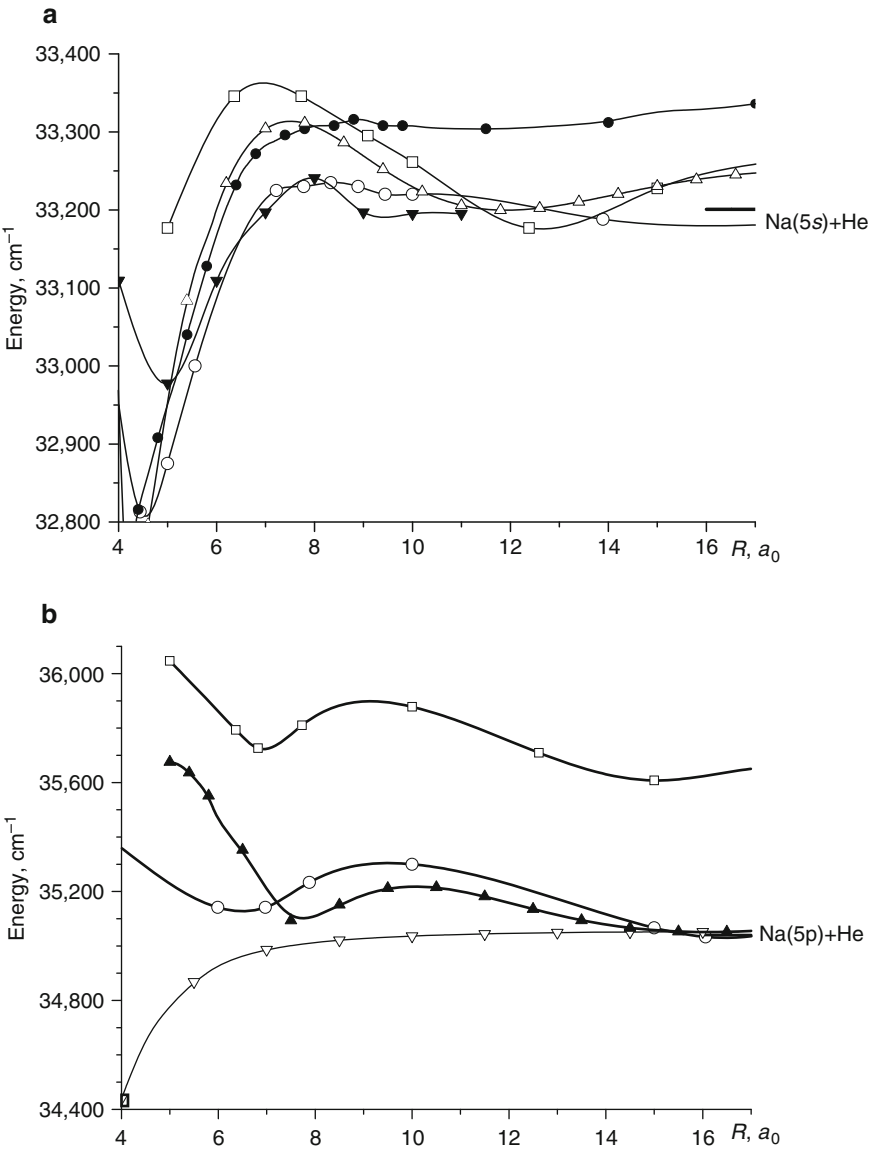

Fig. 1.2 Adiabatic terms of the Rydberg (**a**) $5s^2\Sigma^+$ and (**b**) $4p^2\Sigma^+$, Π states in the Na + He quasimolecule. Curves (**a**) are the results of the following calculations: ▼ [46], □ [47], O [48], ● [50], and Δ [51]. Curves (**b**) correspond to the □ [47], O [48], and ▲ [51] calculations for the $^2\Sigma^+$ state and ∇ [51] for the $^2\Pi$ state

classification of the adiabatic terms without preliminary construction of the diabatic picture becomes difficult. As to the quantum chemical programs used in [46–50], they are adapted only to the calculation of adiabatic terms. The advantage of the

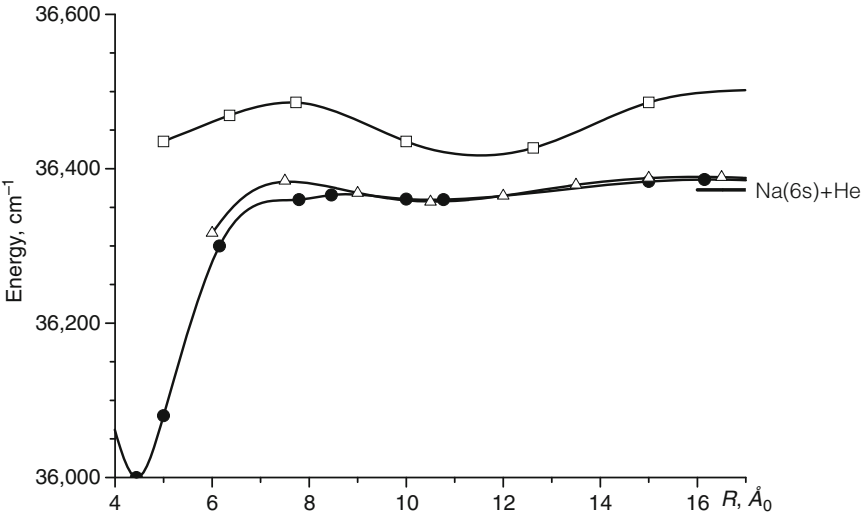

Fig. 1.3 Adiabatic terms of the Rydberg $6s\,^2\Sigma^+$ state in the Na + He molecule, calculated in [47] (□), [48] (●), and [51] (Δ)

method [27] is that it allows one to determine simultaneously the adiabatic and diabatic potential curves and determine the exact structure of adiabatic terms with all possible quasicrossings.

For the transitions to higher values, $n \geq 10$, the adiabatic description of PESs breaks down because of the appearance of many pseudocrossing points between the Rydberg and covalent terms. For this reason, it is difficult to classify the corresponding states, because, for each n, the degenerate in l covalent terms converge to the common limit $U^{(c)}_{vlm}(R_*) = -\frac{1}{2n^2}$ at the point $R_* = 2n^2$.

1.7 Relation to Quantum Chemistry – Matching Method

The quantum chemically calculated terms possess some disadvantages that restrict the accuracy of computations. First, they do not ensure proper asymptotics for the calculated PES energies of the separated atoms and, thereby, understate (or overstate) the potential energies at small interatomic distances. Second, these approaches disregard the orbitally degenerate states, which form starting at $n = 5$ and have quasicrossings with the Rydberg states. This hampers the correct determination of the adiabatic potential curves at intermediate distances (on the order of the Rydberg electron wavelength). However, they give proper coordinate dependences for the potential curves in the region of small and intermediate interatomic distances, though do not provide exact agreement with the energy scale. Hence, the necessity arises of developing a fundamentally new computational procedure free of the indicated disadvantages.

The approach [27] gives the required solution, though it applies only in the region of intermediate and asymptotically large distances. This is so because the corresponding solutions are constructed on the basis of Rydberg functions centered on the ion core. Therefore, the problem amounts to the matching of the quantum chemical results with the results obtained within the framework of integral approach and to the construction of general consistent picture of terms. To solve this problem, the integral variant [27] needs modification. This amounts to the transformation of PES through the inclusion of the additional dissociative valence and ionic configurations into the theory. This procedure was partially accomplished in [51]. The inclusion of the dissociative and valence configurations is usually done by expanding the basis of eigenstates for the Green's operator $\mathbf{G}_{A^{**}}$ of the Rydberg atom A^{**} [3] entering in Eq. (1.8) for the level shift operator. The ionic configurations are introduced through the following renormalization of the scattering matrix:

$$\mathbf{K} = \mathbf{K}_{e^-B} + \mathbf{V}\frac{|\varphi_\mathrm{r}\rangle\langle\varphi_\mathrm{r}|}{E - E_\mathrm{r} + 1/R}\mathbf{V}. \tag{1.66}$$

Here, E is the total energy of the system, φ_r and E_r are, respectively, the wave functions and electron affinity in the ionic configuration A^+B^-, R is the interatomic distance, and $\mathbf{V}$ is the corresponding interaction. The poles of the second term determine the positions of the ionic terms

$$U^{(i)}(R) = E_\mathrm{r} - 1/R. \tag{1.67}$$

Note that if the resonance occurs at distances $E_\mathrm{r}>1/R$, the potential curve $U^{(i)}(R)$ passes into continuum and acquires the autoionization width. This result follows from the eigenvalue solution to the equation for the level shift operator. Then, the quantum chemical calculations are corrected through the direct coincidence with our results at those intermediate distances where there is no quasicrossings of the Rydberg and orbitally degenerate covalent terms. As the result, we obtain the required energy shift of the potential curve at small distances. Note that the PESs determined in this manner must exactly transform, at small internuclear distances, to the potential curves of the corresponding Rydberg molecules. We thus obtain a consistent structure of the adiabatic PESs that can be used to reproduce the full diabatic picture (including all quasicrossings) for the terms in the region where the intercenter coordinates change. The use of diabatic terms is necessary for the correct calculations of the quantum defects as functions of interatomic distances that enter into the definition of electronic matrix elements.

An important role belongs also to the ionic configuration that interacts with the Rydberg valent and dissociative states and gives rise to the additional quasicrossings between the diabatic terms. This result can be obtained by expanding the basis of Green's function entering into the main equation for the $\mathbf{T}$ matrix of multichannel scattering [3]

$$\mathbf{T} = \tilde{\mathbf{t}} + \tilde{\mathbf{t}}(\mathbf{G} - \tilde{\mathbf{G}}_0)\,\mathbf{T} - i\,\tilde{\mathbf{t}}\sum_\beta |\beta\rangle\langle\beta|\mathbf{T}, \tag{1.68}$$

where the difference $\mathbf{G} - \tilde{\mathbf{G}}_0$ is a portion of Green's operator containing poles corresponding to the discrete levels of the Coulomb center, and $|\beta\rangle$ are the wave functions of the dissociative configurations. In contrast to the operator $\mathbf{G}_0$, which includes the Rydberg $e^- + XY^+$ states (without poles corresponding to the discrete levels of the Coulomb center), dissociative $X + Y^*$, and discrete valence states, the operator $\tilde{\mathbf{G}}_0$ involves the states of ionic configuration, i.e.,

$$\tilde{\mathbf{G}}_0 = \mathbf{G}_0 + \frac{|\varphi_\mathrm{r}\rangle\langle\varphi_\mathrm{r}|}{E - E_\mathrm{r} + 1/R}. \tag{1.69}$$

After the renormalization, the reaction matrix $\tilde{\mathbf{t}}$ is written as

$$\tilde{\mathbf{t}} = \mathbf{t} + \tilde{\mathbf{V}} \frac{|\varphi_\mathrm{r}\rangle\langle\varphi_\mathrm{r}|}{E - E_\mathrm{r} + 1/R} \tilde{\mathbf{V}}, \tag{1.70}$$

where the matrix $\mathbf{t}$ is defined in [3], and the operator $\tilde{\mathbf{V}}$ also includes the interaction with the ionic configuration. The dependences on the internuclear distance for the electronic parts of the matrix elements corresponding to the configuration coupling between the Rydberg, valence, dissociative, and ionic terms can be determined from the difference between the adiabatic and diabatic potential curves in the vicinity of quasicrossings.

1.8 Interaction of Rydberg Molecules with Atoms and Molecules

The Rydberg states (RSs) of molecules (as well as atoms) can clearly be divided into the two groups: strongly and weakly interacting with the core. They differ in the electron angular momentum l, whose value characterizes the height of orbital barrier. The number of the states in the first group is smaller than in the latter, because the effective electron angular momentum l^* dividing these groups is small. For instance, in the two-atomic molecules (of the type H_2, N_2, NO, O_2, and CO) $l^* = 2$. In the case of weakly interacting states (with $l > l^*$), the level positions can be satisfactorily approximated by the expression

$$E_{nlq} = E_q - \frac{1}{2n^2},$$

and the levels themselves can be assumed to be purely coulombic for every fixed value of the index q characterizing the set of vibrational v and rotational N ionic states; i.e., $q = \{v, N\}$.

Let us consider the evolution of molecular spectrum with changing principal quantum number n. For the fixed interatomic distance R, the positions of Rydberg levels relative to the ionic term $U_i(R)$ is given by the formula

$$E_{n\lambda}(R) = -\frac{1}{2\ [n - \mu_{\lambda}(R)]^2},$$

where $\mu_{\lambda}(R)$ is the R-dependent diabatic quantum defect of the level and λ is the set of quantum numbers determining this state with inclusion of the internal degrees of freedom. Under the conditions of nonadiabatic motion, the set of levels is determined by the expression

$$E_{nlq} = E_q - \frac{1}{2\ [n - \mu_{lq}(n)\ ]^2},$$

which describes the Rydberg series with different ionization limits that, similar to atomic series, differ from each other by the energy E_q of ionic core excitation. In the spectral regions where the period of electron rotation is comparable with the periods of core vibration or rotation, the energy levels of Rydberg molecule (referred to as rovibronic levels) demonstrate the irregular dependence on n [1, 3].

The next important feature of the spectrum of highly excited molecules is that, along with the Rydberg states (i.e., one-electron configuration $e^{-}XY^{+}$), the states mixed with other (non-Rydberg) valent configurations of molecule can be formed. Among these are, first, the quasistationary states forming the additional set of resonance levels in the $XY^{+} + e^{-}$ system and, second, the dissociative states having a continuous spectrum of nuclear motion. The dissociative states lead to the decay of a Rydberg molecule into atomic fragments.

The nonadiabatic coupling of the channels (in the excited states of the nuclear subsystem) and the configuration interaction induce broadening that is determined by the contribution from the autoionization states and, generally, is a nonmonotonic function of energy. Under certain conditions, the autodecay widths of some levels can turn to zero (for the interference-stabilized level). These states in continuum are the most interesting in atomic and molecular physics and are the subject of wide subject of wide interest in the literature (see. e.g., [59–63]).

The experimental investigations of the highly excited Rydberg molecules (with the principal quantum numbers $n \geq 10$) have been carried out over 20 years. The results of these studies, including the developed and elaborated methods, are reported in detail in the Freund's review in [1], where the history of this problem is given and extensive literature is presented.

1.8.1 General Equations of the Theory

The quasimolecules $XY^{**} + A$ and $XY^{**} + M$, where atom A or molecule M are in the ground electronic state, have the same PES configurations as in the above-considered simpler systems $X^{**} + A$ and $XY^{**} + M$. To obtain them, one should determine explicitly the Green's function for the $e^{-} + XY^{+}$ system. The inelastic

transitions induced in an ion XY^+ by electron renders this problem multichannel, because the states with total energy are formed owing to the interaction (and interference mixing) of the states corresponding to the different channels q of entrain excitation

$$E = \varepsilon_q + E_q, \tag{1.71}$$

where q is the set of vibrational v and rotational N quantum numbers $q = \{v, N\}$ of the ion, E_q is the ion excitation energy, and ε_q is the electron energy measured from the spectrum boundary in a given channel. The presence of a nonadiabatic coupling between motion channels fundamentally distinguishes Rydberg molecules from atoms and imparts to them a number of unique features. Among these are, e.g., irregular dependence of the quantum defects on the level number n [1, 3] and of their near-threshold absorption spectra on the frequency of incident light [64], the presence of bound states on the continuum background [61], the stroboscopic effect [65–67], etc. The nonadiabatic interaction gives rise also to the interesting physical phenomena consisting of a strong (resonance) dependence of the inelastic-transition cross-sections, ionization cross-sections, and charge-transfer cross-sections for highly excited molecules XY^{**} on the principal quantum number [68, 69].

Let us consider the method of constructing Green's function of a Rydberg molecule in more detail. With this aim, it is convenient, following [70], to use the Dyson equation

$$\mathbf{G_V} = \mathbf{G} + \mathbf{GTG}. \tag{1.72}$$

The operator $\mathbf{G}$ (without interaction $\mathbf{V}$ between an electron and ion core) represents a convolution of the Coulomb Green's function $\mathbf{G}_q^{(c)}$ and Green's function of the nuclear subsystem,

$$\mathbf{G}(E) = \sum_q |\, q\rangle\, \mathbf{G}_q^{(c)}(E - E_q)\, \langle q|, \tag{1.73}$$

where $|q\rangle$ are the corresponding wave functions of the nuclear subsystem of XY^+, and $\mathbf{G}_q^{(c)}$ is Green's operator of electron in the Coulomb field. Inasmuch as the main contribution to the matrix elements of the $\mathbf{T}$ operator comes from the region of small r satisfying condition $r\left|\varepsilon_q\right| \ll 1$, Green's function can be expressed through the matrix element of the operator $\mathbf{T}$ and represented in the following form [70]:

$$\mathbf{G}_{(v)}(E) = \mathbf{G}(E) + \sum_{ll',\, qq';\, JM} (-1)^{l+l'} \frac{\pi\left(v_q v_{q'}\right)^{3/2}}{\sin \pi v_q \sin \pi \mathrm{v}_{q'}} \left| l_q JM\right\rangle T^{(J)}_{lq,\, l'q'}(E) \left\langle l'q' JM \right| \tag{1.74}$$

In this equation, the operator $\mathbf{G}$ is determined by the first term of expression (1.72), and the basis functions are defined by

$$|lqJM\rangle = Q_{lqE}(r)\, \chi^J_v(\xi)\, \phi_i(\mathbf{x})\, \Phi^{JM}_{lN}(\hat{r}, \hat{R}), \tag{1.75}$$

where Q_{lqE} coincides with radial function (1.7), $\varphi_i(\mathbf{x})$ is the ionic electron wave function, $\{\mathbf{x}\}$ is the set of coordinates of inner electrons, $\chi_v^J(\xi)$ is the ionic vibrational wave function, ξ is the internuclear distance, and ν_q is the effective principal quantum number, $\nu_q(\varepsilon) = (-2\varepsilon_q)^{-1/2}$, where $\varepsilon_q = E_q - E$. The total angular function $\Phi_{lN}^{JM}(\hat{r}, \hat{R})$ of the system is determined in the representation with the total angular momentum J, its projection M, nuclear rotational motion N, and, in the case of LS coupling (e.g., for the state of XY^+), has the form [71]

$$\Phi_{lN}^{JM}(\hat{r}, \hat{R}) = \sum_m Y_{lm}(\hat{r})\, Y_{N,M-m}(\hat{R})(lN\, mM - m\,|JM), \tag{1.76}$$

($\hat{r}$ and $\hat{R}$ are the corresponding angular variables).

For the subsequent consideration, it is important to separate the radial Green's function $G_{lq}^{(c)}(r, r'; \varepsilon)$ into the parts strongly and weakly depending on energy [72, 73]:

$$G_{lq}^{(c)}(r,\, r';\, \varepsilon) = \cot \pi\nu_q(\varepsilon)\, \left|\varphi_{lq\varepsilon}(r)\right\rangle \left\langle\varphi_{lq\varepsilon}(r')\right| + g_{lq}^{(c)}(r,\, r';\, \varepsilon). \tag{1.77}$$

The first term in (1.77) reproduces positions $\nu_q(\varepsilon) = (-2\varepsilon_q)^{-1/2}$ of the Coulomb levels at $\varepsilon < 0$; it is expressed through the Coulomb wave functions regular at zero point and is normalized as

$$\left\langle \phi_{lq}\varepsilon(r) \,\middle|\, \phi_{lq\varepsilon'}(r)\right\rangle = \pi\delta(\varepsilon - \varepsilon'). \tag{1.78}$$

The elements of $\mathbf{T}$ matrix in (1.74) are determined from the integral equation [3]

$$\mathbf{T} = \mathbf{t} + \mathbf{t}\sum_q |lqJM\rangle\langle lqJM|\ \cot \pi\nu_q \mathbf{T}, \tag{1.79}$$

where the reaction matrix $\mathbf{t}$ describes the electron scattering by the ion core (for all open Rydberg channels the functions $\cot \pi\nu_q = -i$). Owing to the separable nuclear structure (i.e., the factorable dependence on the variables r, R and r', R'), integral equation (1.79) reduces to a system of linear algebraic equations for the elements of collisional $\mathbf{T}$-matrix. Under condition $B\, n^3 \ll 1$ (where B is the ion rotational constant), which encompasses a broad spectral range for the majority of molecules, the Rydberg states can be described within the framework of adiabatic approximation. To transfer to the adiabatic basis, one should pass to the molecular-axis-fixed coordinate system, in which the absolute value of the projection of electronic angular momentum onto the molecular axis is fixed. On this basis, the states of a two-atomic molecule are classified by the values of J and Λ; i.e., the electronic angular momentum l is generally not conserved. The basis functions in the Rydberg states (taking into account the vibrational and rotational motions) are [74]

$$|JM\rho\Lambda v,\ \pm\rangle = \sum_l a_{\rho\Lambda}^{J\,l} |JMl\Lambda v,\ \pm\rangle, \tag{1.80}$$

where ρ is the quantum number characterizing the effective electronic angular momentum in the Rydberg configuration with allowance for the mixing of states l. The coefficients $a_{\rho\Lambda}^{Jl}$ are normalized to unity and assumed to be known.

In the adiabatic basis, the elements of reaction matrix $\mathbf{t}$ are diagonal in the indices ρ and Λ and expressed through the adiabatic quantum defects of the levels

$$t_{\rho\Lambda,\,\rho'\Lambda'}\,(\xi^{+}) = -\tan\pi\mu_{\rho\Lambda}(\xi^{+})\delta_{\rho,\,\rho'}\,\delta_{\Lambda,\,\Lambda'}. \tag{1.81}$$

Because the diabatic (1.80) and channel (1.76) bases are related by the unitary transformation, the following relationship is true for the elements $t^{J}_{lNv,\,l'N''v'}$ inducing vibrational–rotational transitions in XY^{+}[74]:

$$t^{J}_{lNv,\,l'N'v'} = -\sum_{\rho\,\Lambda} a^{Jl}_{\rho\,\Lambda}\,U^{Jl}_{N\,\Lambda}\,\left\langle\,\chi^{J}_{v}\,\middle|\,\tan\,\pi\,\mu_{\rho\,\Lambda}\,(\xi^{+})\,\middle|\,\chi^{J}_{v'}\,\right\rangle a^{Jl'}_{\rho\,\Lambda}\,U^{Jl'}_{N\,\Lambda}, \tag{1.82}$$

where $U^{Jl}_{\Lambda N}$ is the Fano rotation submatrix [71] with elements

$$U^{Jl}_{N\Lambda} = \langle lN \mid l\Lambda\rangle = (-1)^{J+\Lambda-N}(2-\delta_{\Lambda 0})^{1/2}(lJ\Lambda\,-\,\Lambda|N0). \tag{1.83}$$

The nondiagonal matrix elements are generally smaller than the diagonal elements by the ratio of the amplitude of zero-point vibrations a_0 to the interatomic distance. For this reason, the strong vibronic coupling is significant, as a rule, only for a pair of energetically close states.

Of the greatest interest for the problem under consideration is the coordinate region $(\,|\,\mathbf{r}-\mathbf{R}\,|,\;|\,\mathbf{r}'-\mathbf{R}\,|\,) \ll R$ near the perturbing atom. For the states with $l \ll v_q^{2/3}$, the direction of electron momentum at the point R coincides with the direction of vector $\mathbf{R}$. Physically, this situation is the most important, because the interaction with ion core noticeably distorts only the states with small l. Also, our strongest assumption is that the perturbing particle is in the classical region of electron motion.

In the quasiclassical conditions, it is convenient to use the rotationally adiabatic approximation and consider it, similar to the translation, as the motion of a representative point along the set of vibronic PESs corresponding to different vibrational states of the molecule. In this case, expression (1.74) takes the form

$$\begin{aligned}\mathbf{G_V} = \mathbf{g}_0 &\\ &+\sum_{LK,\,L'K',\,vv'}\left|\,\chi_v(\,\xi^{+})\,j_L(\,p_v\rho)\,Y_{LK}(\hat{\rho})\rangle\,\right\rangle\left\langle\,\chi_v(\,\xi'^{+})\,j_{L'}(\,p_v\rho')\,Y_{L'K'}(\hat{\rho}')\right| \\ &\times\;(\,p_v\cot\pi v_v\,\delta_{LK,\,L'K'}\,\delta_{vv'} + \alpha^{(J)}_{Llv,\,L'l'v'}\,\delta_{K0}\,\delta_{K'0}),\end{aligned} \tag{1.84}$$

where $\hat{\rho}$ is the set of angles specifying the direction of vector $\boldsymbol{\rho}$ relative to $\mathbf{R}$. The matrix $\alpha^{(J)}_{Llv,\,L'l'v'}$ is defined by

$$\alpha^{(J)}_{Llv,L'l'v'}(\mathbf{R}) = 2\pi^2 \sum_{l\Lambda} \frac{(v_v v_v)^{3/2}}{\sin \pi v_v \sin \pi v_{v'}} [(2L+1)(2L'+1)]^{1/2} \times T^{(J)}_{l\Lambda v,\,l'\Lambda' v'} \tilde{\phi}^{(l)}_{LvE}(R)\, \tilde{\phi}^{(l')}_{L'v'E}(R)\, Y_{l\Lambda}(\hat{R})\, Y^{*}_{l'\Lambda'}(\hat{R}), \qquad (1.85)$$

The electron wave functions are

$$\tilde{\phi}^{(l)}_{LqE}(R) = \begin{cases} Q_{lqE}(R, v_q), & L = 2p; \\ Q_{lqE}(R, v - 1/2), & L = 2p+1 \\ \qquad (p = 0, 1, 2, \ldots) \end{cases} \qquad (1.86)$$

(for the even and odd values of L, they differ in the phase shift by $\pi/2$). Correspondingly, the function $\mathbf{g}_0$ is

$$\mathbf{g}_0 = -\sum_v \chi_v(\xi^+) \frac{\cos p_v |\,\boldsymbol{\rho} - \boldsymbol{\rho}'\,|}{2\pi\,|\,\boldsymbol{\rho} - \boldsymbol{\rho}'\,|} \chi_v(\xi'^+). \qquad (1.87)$$

According to Eq. (1.84), the function $\mathbf{G} - \mathbf{g}_0$ is the sum of terms, each demonstrating the factorable dependence on the variables $\mathbf{r}, \mathbf{r}'$ and ξ, ξ'. Under these conditions, the integral equations for the level-shift operator $\boldsymbol{\tau}$ describing the eigenvalue spectrum of the system $XY^{**} + M$ reduce to the algebraic equations. The operator form of these equations is written as

$$\boldsymbol{\tau} = \tilde{\mathbf{K}}(\mathbf{G}_v - \mathbf{g}_0)\,\boldsymbol{\tau}. \qquad (1.88)$$

The operator $\tilde{\mathbf{K}}$ corresponds to energy $\tilde{\varepsilon}_q = p_q^2/2$ in the motion channel q.

1.8.2 *Perturbation of the Rydberg Series in a Homoatomic Molecule X_2 by the Field of Neutral Particle*

Let us consider a system $X_2^{**}(nl\Lambda) + M$ with energy $|E| \ll 1$, in which the total energy E at a fixed distance between the particles X_2^+ and M is equal to the binding energy of Rydberg electron in the ground vibrational state of the ion (here, the electronic angular momentum l is a good quantum number). The ion core perturbs the states with a small electronic angular momentum l relative to the Coulomb center ($l = 0$, 1, and 2). The field of perturbing particle, in turn, influences only those superpositions of the Coulomb states that have small values of electronic angular momentum L relative to the particle. These two groups of heterocenter terms that are characteristic of a purely Coulomb center will be briefly called l and L terms.

The substitution of Eq. (1.84) into Eq. (1.88) reduces the homogeneous integral equation with degenerate kernel to the following system of algebraic equations [70]:

$$\tau^{LK}_{v,ss'} = \sum_{s''} \tilde{K}_{Lv,ss''} \times \left[p_{vs''} \cot \pi\nu_{vs''} \tau^{LK}_{v,s''s'} + \delta_{K0} \sum_{L'v'} \alpha_{Lvs'',L'v's''} \tau^{L'K}_{v',s''s'} \right]. \tag{1.89}$$

The index s labels the vibrational states of molecule M with the excitation energy E_s, and the quantities p_{vs} and ν_{vs} are defined by

$$p_{vs} = \left[\frac{2}{R} - \frac{1}{\nu^2_{vs}} \right]^{1/2}, \quad \nu_{vs} = [2(E_v + E_s - E)]^{-1/2}.$$

The system of equations (1.89) describes all the possible types of vibronic PESs for the $X_2^{**}(nl\Lambda) + M$ system with inclusion of the nonadiabatic coupling between the electronic and vibrational motions. Note that the shift of Coulomb levels, as a result of the joint effect of the perturbing particle M and the ion core, is the most efficient for $K = 0$. It is this case that holds the greatest interest. For the nonzero K, the condition for unambiguous solution to the homogeneous system of equations determines the set of Coulomb terms that are split by the field of particle M and do not interact with the ion core.

There are two main mechanisms of the electron interaction with atoms and molecules: direct and resonance. The direct mechanism (potential or background scattering) is described in the adiabatic approximation

$$\tilde{K}^{(0)}_{Lv,ss'} = -\frac{1}{p_{vs}} \langle s| \tan \delta_{vs}(\tilde{\varepsilon}_{vs}) |s'\rangle, \tag{1.90}$$

where δ_{vs} is the electron elastic-scattering phase determined for energy $\tilde{\varepsilon}_{vs} = p^2_{vs}/2$ at the point where particle M is situated. Since the vibrational coupling is weak, the terms nondiagonal in s are small when compared with the diagonal terms, i.e., the interaction between vibronic terms is appreciable only in the vicinity of their quasicrossings.

For the resonance mechanism of interaction between electron and the perturbing particle, the scattering operator has the form

$$\tilde{\mathbf{K}} = \tilde{\mathbf{K}}^{(0)} + \sum_{vs^-} \mathbf{V} \frac{\left|\varphi^{(r)}_{vs^-}\right\rangle \left\langle\varphi^{(r)}_{vs^-}\right|}{E' - (E_r + E_{s^-} + E_v)} \mathbf{V}. \tag{1.91}$$

Here, $E' = E + 1/R$ and $|\varphi_{vs^-}^{(r)}\rangle$ are the total wave functions of the (v, s^-) state in the ionic configuration $X_2^+M^-$, and E_r is the resonance energy. The poles of the second term in Eq. (1.91) define the positions

$$U_{vs^-}^{(i)}(R) = E_r + E_{s^-} + E_v - 1/R, \tag{1.92}$$

of different vibrational v and s^- states in terms of ionic configuration. Note that the $\tilde{\mathbf{K}}$ operator is the same for both the positive and negative energies. The solution to the above equations provides the full picture of the interaction between Rydberg molecule and neutral particle.

By neglecting the anharmonic interaction in molecule M and taking into account that the residues of the second term in Eq. (1.89) are appreciably smaller (by $\sim n^2$ times) than those of the first term, one obtains the following equation giving the unambiguous solution of the energy eigenvalues:

$$1 - p_{vs}\tilde{K}_{Lvs}\, ctg\pi\nu_{vs} - \tilde{K}_{Lvs}\,\alpha_{Lsv,Lvs}(\mathbf{R}) = 0, \tag{1.93}$$

The solution to this equation points to the fact that there are two groups of vibronic terms of the combined system $XY^{**}M$. The first group is composed of the Rydberg **R**-independent l terms

$$U_{n_v l\Lambda s}^{(R)} = E_v + E_s - \frac{1}{2(n_v - \mu_{l\Lambda v})^2}, \tag{1.94}$$

($\mu_{l\Lambda v}$ is the quantum defect of the $l\Lambda v$-series), whose positions are determined by the poles of the electron–ion core scattering matrix **T**. The second group includes covalent terms L that are split off from the Coulomb terms by the field of perturbing particle.

$$U_{n_{vs}}^{(L)}(R) = E_v + E_s - \frac{1}{2\left\{n_{vs} + \frac{1}{\pi}\arctan\left[p_{vs}(R)\,\tilde{K}_{Lvs}^{(0)}(R)\right]\right\}^2}, \tag{1.95}$$

where n_{vs} corresponds to the principal quantum number of the nearest Coulomb level at the classical turning point ($R_{vs}^* \approx 2n_{vs}^2$) determined from the condition $p_{vs} = 0$.

1.8.3 Interaction with the Covalent Term

The collisions between particles X_2^{**} and A induce nonadiabatic transitions between the Rydberg l terms and the covalent L terms in the vicinity of their quasicrossings. The greatest contribution to the inelastic vibronic–transition cross-sections comes

from the vicinities of the quasicrossing points $R^{(c)}_{n_{v'}}$ between the Rydberg $n_{v'}l$ and covalent n_vL terms corresponding to different vibrational states of the ion. It can be shown that Eq. (1.93) in its vicinity takes the form

$$\left(E - U^{(L)}_{n_v}\right)\left(E - U^{(R)}_{n_{v'}l\Lambda}\right) = V^2_{n_vL,\,n_{v'}l}. \tag{1.96}$$

The interaction between these states is given by the expression

$$V^2_{n_vL,\,n_{v'}l} = \frac{B_{l\Lambda Lv} p_v \tilde{K}^2_{Lv} \cos^2 \pi\nu_v}{\pi \nu_v^3} f^{(l)}_{n_v n_{v'}}, \tag{1.97}$$

where the multiplier

$$f^{(l)}_{n_v n_{v'}} = \frac{\left(t^{(\Lambda)}_{lv,\,lv'}\right)^2}{\lambda\left(\tan \nu_v - t^{(\Lambda)}_{lv,\,lv}\right)^2 + \left(t^{(\Lambda)}_{lv,\,lv'}\right)^2}, \qquad \lambda = \left(\frac{\nu_{v'}}{\nu_v}\right)^3 \frac{\cos \pi\nu_v}{\cos \pi\nu_{v'}} \tag{1.98}$$

is defined as a nonadiabatic mixing factor.

On the background of continuum, the terms of quasimolecule $X_2^{**}A$ are described by Eq. (1.93) with the formal substitution $\tan \pi\nu_{v'} = i$ corresponding to the autoionization. The solution to this equation gives the following expression for the covalent term:

$$U^{(L)}_{n_v}(\mathbf{R}) = E_v - \frac{1}{2n_v^2} + \frac{p_v(R)\,\tilde{K}_{Lv}(R)}{\pi \nu_v^3} - i\,\frac{\Gamma_{n_vL}(\mathbf{R})}{2}, \tag{1.99}$$

where $\Gamma_{n_vL}(\mathbf{R})$ is the autoionization width whose explicit form is given in [64].

1.8.4 Interaction with the Ionic Term

Using expression (1.91), one can determine from Eq. (1.93) the interaction between the Rydberg molecular $X_2^{**}(v')\,M(s=0)$ and ionic $X_2^{+}(v)M^{-}(s^{-})$ configurations [69],

$$V^{\,2}_{i\nu s^-,\,n_{v'}l\Lambda} = 4\pi^2 \left| A^{(s^-)}_{L\Lambda^-} \right|^2 \left| \Phi_{\varepsilon_v\, l\Lambda}(\mathbf{R})\, Y_{L\Lambda^-}(\hat{\Omega}) \right|^2 f^{(l)}_{n_v n_{v'}}\, q_{0s^-}. \tag{1.100}$$

Here, $A^{(s^-)}_{L\Lambda^-}$ is the coefficient characterizing the asymptotic expression

$$\phi^{(-)}_{L\Lambda^-} = \frac{A^{(s^-)}_{L\Lambda^-}}{\rho}\, \exp(-\alpha^{(i)}_{s^-}\,\rho\,)$$

for the normalized electron radial wave function in the negative ion, Λ^- is the projection L of the electronic angular momentum on the axis of molecule M, $\alpha_{s^-}^{(i)} = [-2\,(E_{\rm r} + E_{s^-}\,)\,]^{-1/2}$ and $\Phi_{\varepsilon_v l\Lambda}(\mathbf{R})$ are the functions normalized to unity and coinciding, at energy $\varepsilon' = -1/2n^2$, with the electron wave functions in the field of Coulomb center, $\hat{\Omega}$ are the angular variables characterizing the orientation of molecule M relative to vector $\mathbf{R}$, $f_{n_v n_{v'}}^{(l)}$ is the nonadiabatic mixing factor (1.98), and $q_{\,0\,s^-} = \langle\, 0\,|s^-\rangle^2$ is the Frank–Condon factor. The interaction of the covalent $n_v L$-term with the term $X_2^+(v)\,M^-(s^-)$ of ionic configuration on the continuum background is expressed, according to Eq. (1.89), through the full autonization width of the resonance level s^- [75]; i.e.,

$$V^{\,2}_{i v s^-,\, n_{v'} L} = \frac{1}{2\,\pi v_{v'}^3}\;\Gamma_{s^-}\;q_{0 s^-}. \tag{1.101}$$

1.9 Dynamical Models in the Theory of Collisional Transitions Between Rydberg States

The dynamical models used in the description of the processes involving Rydberg atoms are described in detail in the review of Hickman, Olson, and Pascale in [1]. For this reason, we will not discuss here all possible theoretical approaches and concentrate only on those, which are used more frequently and efficiently. Among these is primarily the impulse approximation [76, 77], in which the transition matrix elements $nlm \to n'l'm'$ with a given momentum transfer $\mathbf{Q}$ are calculated by the formula

$$A\;(\,k, nlm \to k - Q,\, n'l'm'\,) = \int \Phi^*_{n'l'm'}\,(\,k - Q\,) f_e\,\Phi_{nlm}(\,k\,)\,\mathrm{d}k. \tag{1.102}$$

Here, the amplitude f_e of the $e^- - A$ scattering can be calculated using the low-energy approximation suggested by O'Malley [78–80]. As a rule, this approximation is restricted to the first terms of expansion

$$f_e = -a - \frac{4\,\pi}{3}\beta Q. \tag{1.103}$$

The formulas of Born approximation are described by the standard way using the effective potential $V(r,R)$ chosen in such a way that it describes the real characteristics of the $e^- - B$ scattering [1].

Both approaches are, in essence, equivalent. Their limitation is associated with the fact that they do not take into account a change in the mutual arrangement of the terms between which transition occurs. However, the regions of mutual approach or

quasicrossing terms combined in the collisional transitions play the decisive role in some cases.

The study performed above directly points to this fact. For example, when studying the direct transitions between the *nlm* and *nL*0 groups of states, the distortions in the group of *nL*0-terms should be taken into account explicitly. Along with this, the interaction between these groups of states can be treated perturbatively, because, when moving along a given trajectory, the transition probability W is low enough ($W \ll 1$).

In the approximation of linear trajectories, W is calculated by the following formula [1]:

$$W = \left| \int_{-\infty}^{\infty} \mathrm{d}t \; V_{if}(R(t)) \exp(i\Delta E_{nl,nL}(t') \, \mathrm{d}t') \right|^2, \tag{1.104}$$

where $R = \sqrt{b^2 + V_c^2 t^2}$, b is the impact parameter, $V_{if}(R(t))$ is the effective interaction between the states of interest.

In the method of perturbed stationary states, the impulse and Born approximations correspond to the assumption that energies E_i and E_f are independent of time t. The inclusion of the dependence $\Delta E(t)$ corresponds to the perturbation theory in the distorted wave method. In addition, the fact is also taken into account that, as a result of the interaction induced between the state $l < l^*$ and a large group of states $l > l^*$ by the external particle A, its m components become mixed (in the case of molecule XY^{**}, the same is true for the M components of the total angular momentum J).

It should be emphasized that the calculations utilizing information on the PES reveal term quasicrossings and regions of the spatially localized transitions for which

$$V_c \left| F_{if} \right|^{-1} \leq R^2 \tag{1.105}$$

(F_{if} is the difference in the forces acting along the particle trajectory from the crossing terms i and f), so that the collisional processes can be described by the Landau–Zener method. Under condition (1.105), the Landau–Zener formula is obtained from Eq. (1.104) in the approximation of two coupled states. A more complex situation arises for the case of multiple term crossings. However, the exactly solvable models in the theory of nonadiabatic transitions [81–83] show that, in many cases, a rather simple and reliable estimate of cross-sections can be obtained in the approximation of independent Landau–Zener transitions at the term-crossing points, which are characterized by the parameter

$$\eta = \frac{2\pi \left| V_{if} \right|^2}{\left| F_{if} \right| V_c}. \tag{1.106}$$

Therefore, the use of the data on PES of the system $X^{**} + M$ represents new step in the study of collisional processes involving highly excited atoms.

Formula (1.104) (including the $\Delta E(t)$ dependence) and the model of independent Landau–Zener transitions are used below in the calculations of the l-mixing, charge transfer, and atomic ionization processes. The l-mixing process can be regarded as a dynamic transition from the states with fixed value of l (for $l < l^*$) to a group of states with $l > l^*$.

As an example, we refer to the $l$mixing process for the Rydberg states of atom $Na^{**}(nl)$ in slow collisions with atom Xe; i.e.,

$$Na^{**}(l \le l^*) + Xe \rightarrow Na^{**}(l > l^*) + Xe, \tag{1.107}$$

and compare the computational results [84] with the experiment and the data of other approximate approaches [85]. The corresponding dependences are presented in Fig. 1.4. The calculation was carried out for the relative velocity $V_c = 2 \times 10^{-4}$ of the colliding particles (which corresponds to the temperature $T_c \propto 300$ K) and parameters $\mu_d = 0.015$, $a = -6.0$, and $\beta = 27.06$, taken from [86]. The black circles on the right wing correspond to room temperature $T_c = 300$ K [87]. On the left wing of the curve, white circles are the results obtained in [88] for the temperature $T_c = 430$ K.

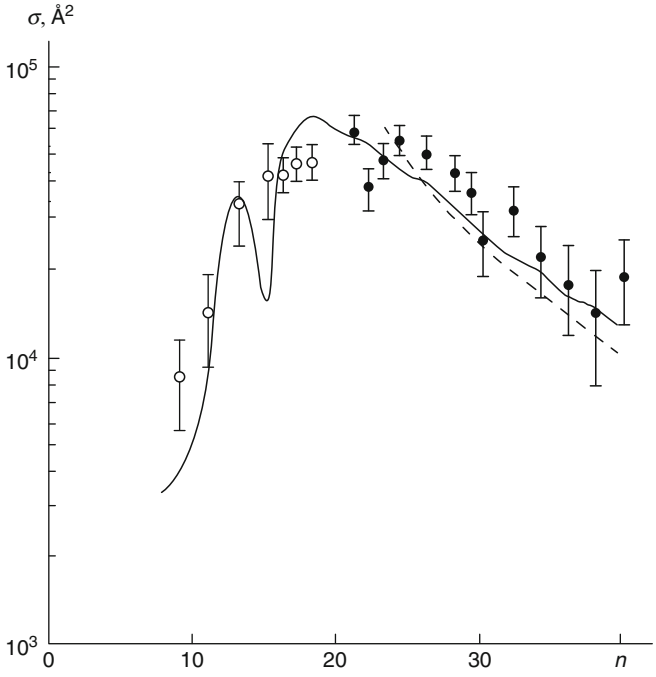

Fig. 1.4 l-Mixing cross-section for the Rydberg states of atom Na^{**} in the collisions with atoms Xe as a function of the principal quantum number n

The fact that the cross-section increases at small n is explained by the increase in a scale factor of $\sim n^4$, which is proportional to the square of a geometric size of the Rydberg particle, whereas the decrease is explained by the fact that $\Delta E_{nl,nL}$ weakly depends on R at large n, although becomes small. In the limit $n \to \infty$, the cross-section of process (1.107) transforms to the known result [89]

$$\sigma_{nlL} = 2\pi \frac{a^2}{n^3 V_c^2}, \tag{1.108}$$

which is well reproduced in the impulse and Born approximations [1].

As a next example, we consider the ionization process of Rydberg atom A^{**} in the collision with a diatomic molecule M possessing autodecaying state M^-. The specific feature of the terms (denoted below by the index i) correlating with this state at $R \to \infty$ is that they intersect continuum boundary at the point $R_r = |E_r|^{-1}$. The ionization can be regarded as being completed if the characteristic residence time of the system in continuum is much longer than the half-life of ion M^-; i.e.,

$$\Gamma_i (R_i^2 - b^2)^{1/2} V_c^{-1} \gg 1. \tag{1.109}$$

The transition to the ionic state can occur both at the approach stage and at the stage of flying apart. One can show that the second stage is more efficient. The characteristic ionization cross-sections at thermal velocity are on the order of the gas-kinetic cross-sections. This is confirmed by the dependence of ionization cross-section on the principal quantum number for the reaction (Fig. 1.5)

$$H^{**}(n_0) + N_2(s=0) \to H^+ N_2^-(s^- = 1) \to H^+ + e^- + N_2(s=0), \tag{1.110}$$

At low electron energies, the $e^- + H_2$ system has a resonance corresponding to the autodecaying Σ_u-state ($L = 1$, $M = 0$). To describe the $X^* + H_2$ processes associated with the occupation of this H_2^- state, one can set $E_r = 1.7$ eV and $\Gamma = 0.5$ eV (with these parameters, the theory reproduces well the experiment on the ionization of atoms K from the ground state by molecules H_2 [90]). Table 1.1

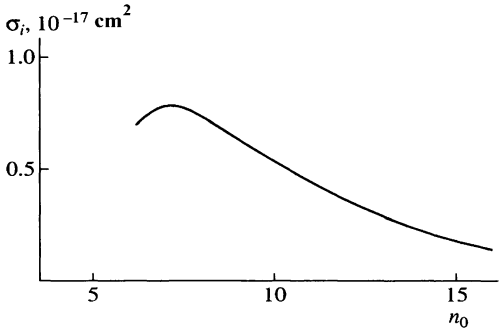

Fig. 1.5 Ionization cross-section as a function of the principal quantum number n, as calculated by the harpoon mechanism for atom H

Table 1.1 Recommended parameters for the description of charge transfer in the $H^{**} + N_2$ system [75][a]

s^-	0	1	2	3	4	5
Γ_{0s^-}	1.1	2.3	2.4	1.7	0.9	0.4
Γ_{1s^-}	2.3	1.3	0.01	0.7	1.6	1.5
$R^{(s)}$	11.8	10.7	9.8	9.0	8.3	7.7

[a] Partial widths are given in units of 10^{-3}au

reports the recommended parameters for process (1.110). These parameters were calculated using the analytical model [91], which reproduces well the resonance $e^- + N_2$ scattering ("shape" resonance in the $^2\Pi_g$-state with the resonance energy $E_r = 2.3$ eV). The dependence of partial cross-section shown in Fig. 1.5 was calculated in [75] using parameters taken from Table 1.1 for the relative velocity of colliding particles $V_c = 1.32 \times 10^{-3}$ au. This function has a typical bell-shaped form with the maximal cross-section equal to 0.8×10^{-17} cm^2 at $n_0 = 7$. With increasing n_0, the cross-section decreases as $\sim 1/n_0^3$.

1.10 Ionization and Vibronic Transitions in Slow Collisions of Highly Excited Molecules with Neutral Particles

The expressions presented above for the interaction of the terms belonging to different states of the Rydberg atoms and molecules allow one to calculate the processes specific to these systems. The modern optical methods of electronic excitation of atoms and molecules, in conjunction with various methods of the collision theory and ionization by an electric field [92, 93], as well as with the methods of microwave multiphoton ionization allow the generation of atomic and molecular beams in the state with close values of n, the same n, and even in the individual Stark states [1]. In this connection, the question of how the cross-sections of elementary processes (or reactions) depend on the energy of a high-resolution initial excitation has great significance.

1.10.1 Probability and Cross-Section of the Collisional Ionization

When describing this process, it suffices to restrict oneself to the two-channel vibronic basis and use (as in the analogous problem of Rydberg ionization due to the perturbation introduced by the term intersecting continuum boundary [72]) the model of independent Landau–Zener transitions in a system with many term crossings [81]. In the approximation of linear trajectories, this problem can be solved analytically.

For the given impact parameter b, the ionization probability is given by

$$W^{(i)}_{n_1 n_0}(b) = p_{n_1 n_0}(b) q_{n_1 n_0+1}(b)[\,1 - S\,(b)], \tag{1.111}$$

where $p_{n_1 n_0}(b)$ is the probability of the first nonadiabatic transition from the Rydberg $n_0 l$ to the covalent $n_1 L$-term, and $q_{n_1 n_0+1}(b)$ is the probability to pass to continuum at the point $R^*_{n_1}$ along the diabatic $n_1 L$ term. The quantity S has a meaning of the probability that the atom remains on the covalent term as the representative point moves in the region of distances $R \le R^*_{n_1}$, where the term is autoionizing and determined by expression (1.99). The resulting ionization cross-section takes the form

$$\sigma^{(i)}_{n_0}\,(V_c) = \pi\,(R^*_{n_1})^2 P^{(i)}_{10}\,(V_c), \tag{1.112}$$

where

$$P^{(i)}_{10}\,(V_c) = 2\int_0^1 x\left[1 - \exp\Big(-\frac{A}{V_c}\,(1-x^2)^{-1/2}\Big)\right] \times \exp\left[-\frac{Q}{V_c}\,(1-x^2)^{-1/2}\right](1 - S(x))\mathrm{d}x, \quad x = b\,/R^{(c)}_{n_0}\,. \tag{1.113}$$

The quantities A and Q are associated, respectively, with the probability of the first Landau–Zener transition from the original term to the covalent $n_1 L$-term ($\sim A/V_c$) and the probability to remain on the original term ($\sim\exp(-Q/V_c)$). The corresponding expressions for these quantities are given in [82].

In the case that the strong nonadiabatic mixing of the Rydberg $n_0\,l$- and $n_1\,l$-states (i.e., the corresponding energy levels are close to each other) occurs near some point E_r, $A(n_0)$ and $Q(n_0)$ depend essentially on n_0 in the vicinity of this point. With an increase in n_0, $A(n_0)$ increases sharply, whereas $Q(n_0)$ decreases. As a result, the cross-sectional peak becomes asymmetric with respect to E_r.

If the initial energy E_{n_0} of the Rydberg molecule is lower than E_r, the efficient vibrational excitation occurs owing to the transition from the covalent $n_1 L$-term to the Rydberg $n_1 l$-term. This brings about sharp increase in the cross-section near the point E_{n_0}, because the function $A(n_0)$ increases, thanks to the strong mixing of the $n_0 l$- and $n_1 l$-states. In this case, along with the sharp peaks, the ionization cross-section (1.112) contains oscillations caused by the fact that the quasiclassical phase Φ depends on n_0. Such oscillations of the broadening cross-sections as a result of quenching Rydberg states of alkali atoms in the rubidium atmosphere were studied in [94] and reported in [75].

If an atom has the negative scattering length ($a < 0$), these two features are supplemented by the appearance of a sharp dip in the cross-section, which is caused

by the Ramsauer effect (i.e., turning to zero of the corresponding element in the scattering $\tilde{\mathbf{K}}$-matrix [68]).

1.10.2 Vibronic Transitions in the XY^{**} + A System

Let us now turn to the inelastic $XY^{**} - A$ collisions accompanied by the one-quantum vibrational excitation. The vibronic transitions to the covalent n_1L-states occurring with a change in the electronic angular momentum ($l' \neq l,\ l' \leq (n_1 - 1)$)

$$XY^{**}(n_0, l, v' = 0) + A \rightarrow XY^{**}(n_0, l' \gg 1, v = 1) + A, \tag{1.114}$$

and the transitions to the n_1l-states with the conservation of the angular momentum

$$XY^{**}(n_0, l, v' = 0) + A \rightarrow XY^{**}(n_1, l, v = 1) + A. \tag{1.115}$$

are of greatest interest.

In contrast to the ionization process, the inelastic vibronic transitions $(n_0\,, v = 0) \rightarrow (n_1\,, v = 1)$ proceed as a result of two passages of the representative point through the regions where the Rydberg and covalent terms meet quasicross. Since the corresponding transition probabilities are low, the total cross-sections of the indicated processes are combined additively from the individual cross-sections, each corresponding to the one-shot capture by the n_1L-state (accordingly, on the approach or flying apart). Besides, in contrast to Eq. (1.114), one should include in this case an additional factor describing the probability to escape from the n_1L-term in the vicinity of $E = E_r$.

One should set off two regions corresponding to different values of n_1 in the energy dependence of cross-sections. In the first region, the n_1L-terms lie near the continuum boundary and intersect it at the $R^*_{n_1}$ points (Fig. 1.6a). For this reason, one must take into account the possibility for autoionization in this region.

In the second region (Fig. 1.6b), the covalent term lies in the discrete spectrum ($E < 0$). In this case, the cross-section of the inelastic transitions has the form [68]

$$\sigma_{01} = 2\pi (R^{(c)}_{n_0})^2 \left[E_3\left(\frac{\bar{Q}(n_0)}{V_c} \right) - E_3\left(\frac{\bar{Q}(n_0) + A(n_0)}{V_c} \right) \right]. \tag{1.116}$$

($E_n(x)$ is the integral exponential function). In this case, the ratio of the maximal cross-section to the cross-section in the plateau region is

$$\sigma_{01}(E = E_r)/\sigma_{01}(E \neq E_r) \gg 1. \tag{1.117}$$

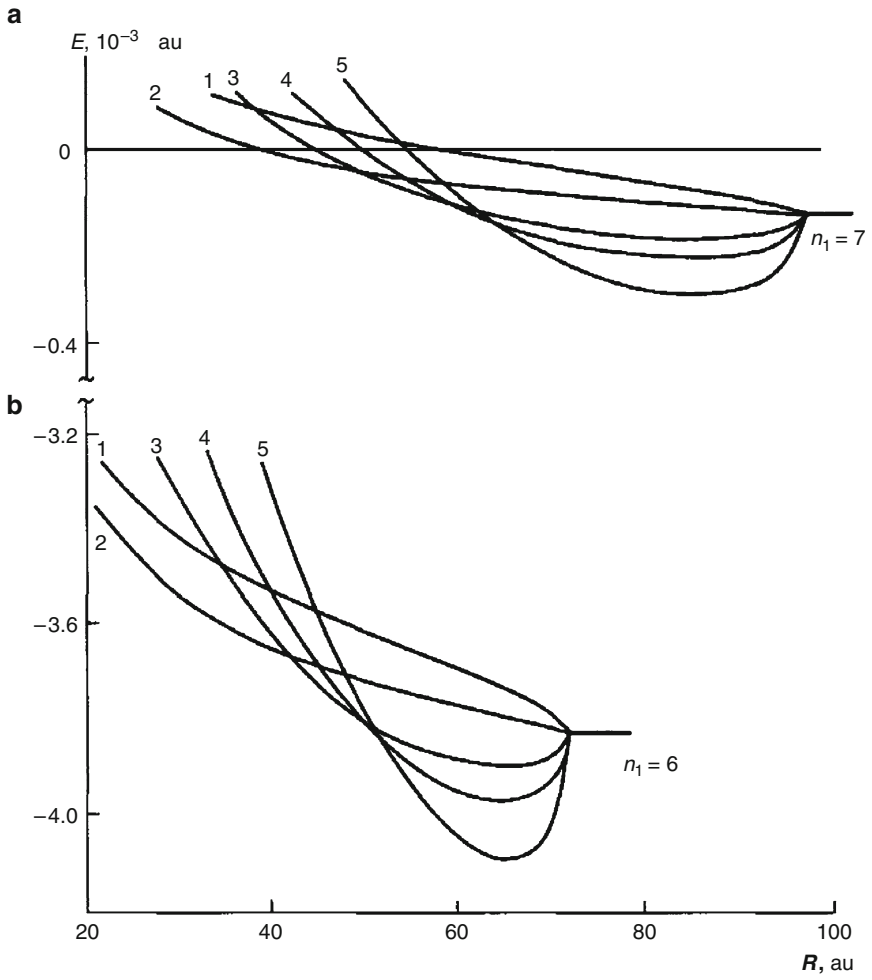

Fig. 1.6 The terms of the $N_2^{**} + A$ $\{A = \text{He}(1), \text{Ne}(2), \text{Ar}(3), \text{Kr}(4), \text{Xe}(5)\}$ system classified for $n_1 = 7$ and $n_1 = 6$ by the type of scattering ($L = 0$) from the perturbing center. The order in which the n_1L – terms are arranged is numbered for He through Xe [68]

Thus, the cross-sections of the inelastic vibronic transitions (by analogy with ionization) must demonstrate "resonance" structure in the dependence of $\sigma_{01}(n_0)$ on the initial principal quantum number. Another feature is associated with the fact that the cross-section increases in the vicinity of the $E_{n_0} = \omega - 1/2n_1^2$ level (where the matrix element K_{L1} turns to zero for $a < 0$) owing to the Ramsauer effect [68].

Note also that the cross-sections calculated for processes (1.114), (1.115) using the impulse approximation with the hydrogen-like distribution of electron density [95] coincide at $l = 0$ with the well-known classical expression [96], which has limited area of application $V_c \gg 1/n_0$.

1.10.3 Interaction of the N_2^{**} Molecules with the Noble Gas Atoms

Let us use the collisional ionization and inelastic $(n_0, v = 0) \rightarrow (n_1, v = 1)$ vibronic transitions to illustrate the theory by the example of the system

$$N_2^{**}(n_0 > 40,\ \ d\sigma_g) + A \rightarrow N_2^{+} + A + e^{-}, \tag{1.118a}$$

$$N_2^{**}(n_0 > 40,\ \ d\sigma_g) + A \rightarrow N_2^{**}(n_1 = 7,\ l \gg 1) + A, \tag{1.118b}$$

$$N_2^{**}(n_0 > 40, d\sigma_g) + A \rightarrow N_2^{**}(n_1 = 7, d\sigma_g) + A, \tag{1.118c}$$

(where $A = \{\text{He, Ne, Ar, Kr, Xe}\}$), whose covalent n_1L-terms intersect the continuum boundary (Fig. 1.6a). For the energy $E_r = -1.148 \times 10^{-4}$ corresponding to $n_r = 66$, the system is characterized by the strong nonadiabatic mixing of the vibronic Rydberg $d\sigma_g$-states $(v = 0)$ and $(v = 1)$. Figures 1.7 and 1.8 show the dependence of the cross-sections for processes (1.118a–c) on the initial quantum number n_0 calculated in [68] by formulas (1.112, 1.113). The cross-sections are characterized by the presence of sharp maxima covering a small group of Rydberg states. As expected, the obtained curves are asymmetric about the position of level $n_r = 66$.

Another common property of processes (1.118a–c) is the interference suppression of the cross-sections at the values of n_0 corresponding approximately to the condition $\sin \Phi(n_0) = 0$. For example, the first interference minima for He atom are situated at the points $n_0 = 80$ and 147. For Ne, in which the covalent n_1L-term is the smoothest, three oscillations are observed, respectively, at $n_0 = 65$, 77, and 114. Since the first interference minimum is situated close to the level $n_r = 66$, processes (1.118a and b) are only partially suppressed.

The characteristic feature of the interaction with the Ar, Kr, and Xe atoms (possessing the negative scattering length) consists in the manifestation of the Ramsauer effect and the resulting decrease in the cross-sections in the vicinity of the $n_0 = 59$ level. Similar effect should also be observed in the inelastic collisions of Rydberg atoms X^{**} with atoms [1]. However, as distinct from the atomic systems, where the Ramsauer minima are rather smooth, narrow localized dips form in these systems (Fig. 1.8). This is caused by the fact that the cross-sections of the processes reproduce the characteristic features in energy dependence of the $\tilde{\mathbf{K}}$-matrix, rather than its averaged characteristics (as in the case of collisions proceeding by the impulse mechanism [1]).

For all inert gases (except Xe), ionization cross-section (1.118a) is smaller than the inelastic-transition cross-section. For the Xe atom (where the ionization process is rather efficient), they are comparable. In the region of $n_1 = 6$ (Fig. 1.6b), the vibronic transitions to the covalent n_1L-state with the participation of the Rydberg $n_0 d\delta_g$ series should be the most efficient. In this case, the states with $n_0 \sim (n_r = 12)$ should also be strongly nonadiabatically mixed and, as a result, demonstrate

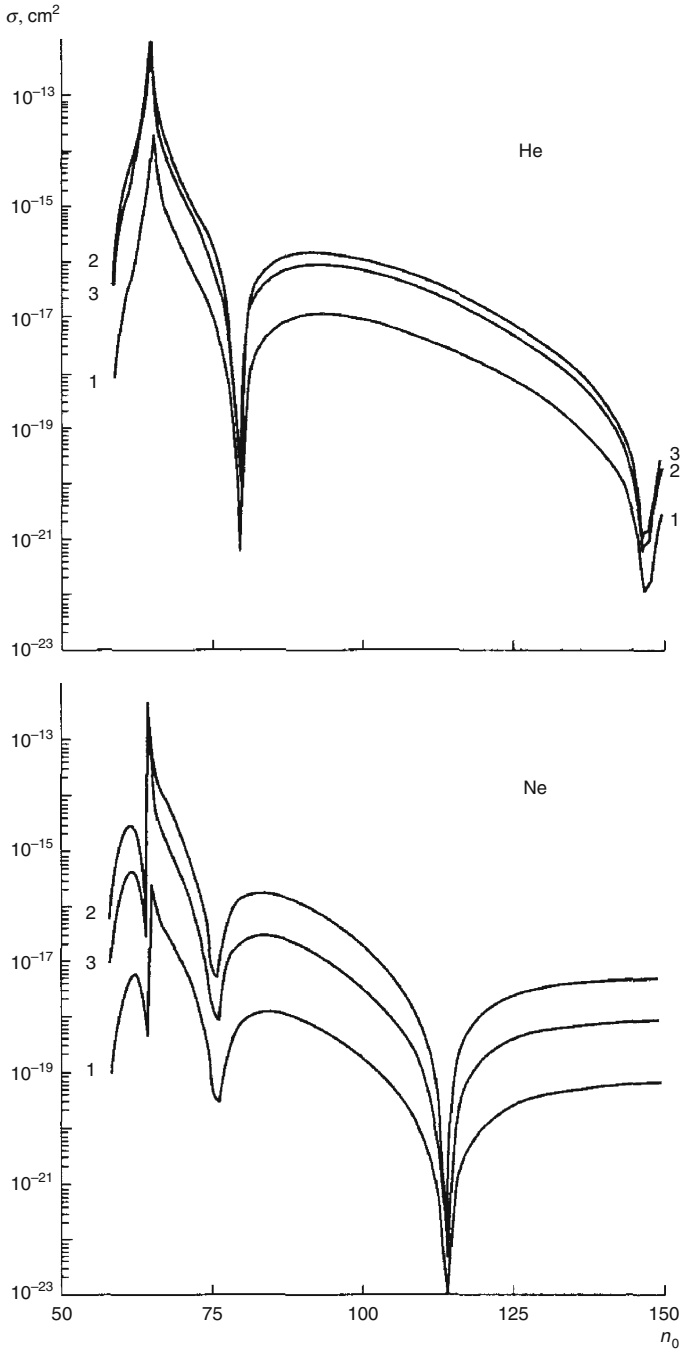

Fig. 1.7 Cross-sections of collisional ionization (1) and vibronic $v = 0 \rightarrow v = 1$ transitions (2) with and (3) without a change of the electronic angular momentum in the system $N_2^{**}(n_0, \delta_g, v = 0) + A\,(A = \{\text{He and Ne}\})$. Calculations were carried out in [68] for the relative velocity $V_c = 2 \times 10^{-4}$ au

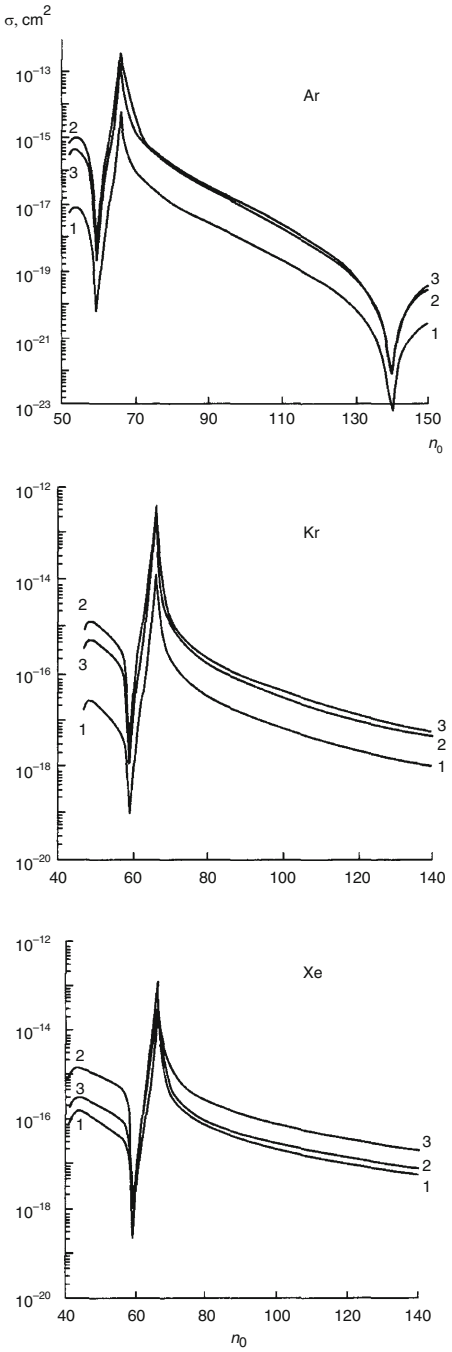

Fig. 1.8 Cross-sections of collisional ionization (1) and vibronic $v = 0 \rightarrow v = 1$ transitions (2) with and (3) without a change in the electronic angular momentum in the system $N_2^{**}(n_0, \delta_g, v = 0) + A(A = \{\text{He and Ne}\})$. Calculations were carried out in [68] for the relative velocity $V_c = 2 \times 10^{-4}$ au

Table 1.2 Cross-sections of the inelastic $(n_0, v = 0) \rightarrow (n_1, v = 1)$ transitions with a change in the electronic angular momentum in the collisions of $N_2^{**}(n_0 d\sigma_g, v = 0)$ molecules with noble gas atoms

n_0	$\sigma_{01}(n_0), 10^{-16}$ cm^2				
	He	Ne	Ar	Kr	Xe
12	466.0	22.8	108.0	6.18	84.0
13	0.58	2.39	0.92	4.38	1.41
14	0.04	0.11	0.51	0.58	0.02
15	0.04	0.61	0.03	0.03	–

The cross-sections are calculated for the relative velocity $V_c = 10^{-3}$ au

appreciably increased cross-sections. The results of calculation performed with the adiabatic quantum defect [97, 98]

$$\mu_{d\pi g}(\xi_e^+) = -0.11 + 0.166(\xi - \xi_e^+),$$

are presented in Table 1.2. Note that the cross-sections calculated near $n_r = 12$ are two orders of magnitude larger than the gas-kinetic sections.

1.11 Dynamics of the Charge-Exchange Reaction in the $X_2^{**} + A$ System

As in the case of ionization processes (including the inelastic vibronic transitions), the admixed $(v = 1)$ state in the charge-exchange reaction can be more active than the original $(v = 0)$ state. This is caused by the fact that the admixed state is characterized by a higher transparency of the tunnel barrier. The charge-exchange process induced by the movement of interacting particles with the relative velocity V_c is a dynamic transition of the representative point from the Rydberg to the ionic $XY^+ + M^-$ term. This process can proceed both at the particle approach stage and at the stage of flying apart. The probability $R_{vv'}^{(s)}$ that the transition occurs in the vicinity of the term-crossing point is described by the Landau–Zener formula [26]. In the conditions under consideration, this probability is low, because the region in which electron moves is wide and because it must overcome potential barrier (Fig. 1.9). For this reason, the subsequent transitions from the ionic term to the covalent states, as well as the transitions in continuum with the deactivation of vibrational excitation in the XY^+ ion can be ignored. Then the charge-exchange cross-section can be calculated by formula [69]

$$\sigma_{vv'}^{(ss^-)} = 4\pi^2 (R_{vv'}^{(s)})^4 \frac{V_{is^-v,n_{v'}l\Lambda}^2}{V_c}, \tag{1.119}$$

here $V_{is^-v,n_{v'}l\Lambda}$ stands for the interaction of the Rydberg and ionic configurations (100) at the point $R_{vv'}^{(s)}$. In the case that a group of states $E_{n_1 l}$ of the initial Rydberg

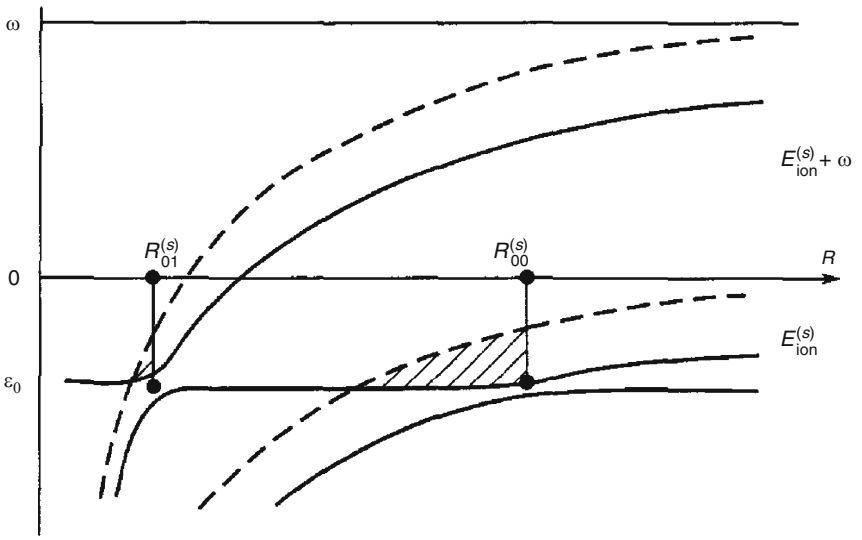

Fig. 1.9 Schematics of the adiabatic terms of the system $XY^{**} + M$. Boundaries of the regions classically allowed for the electron motion with $v' = 0$ and 1 are shown by the *dashed lines*. The subbarrier region transitions are *dashed*

series ($v = 0$) is involved in the interaction with the level $E_{n_0 l}$ of the series ($v = 1$), the dependence of the nonadiabatic mixing factor on n_0 assumes the resonance character:

$$f^{(l)}_{n_1 n_0} = \frac{t^2_{10}}{\pi^2 \frac{(v_0 v_1)^3}{(\cos \pi v_0 \cos \pi v_1)^2} \left(E_{n_0 l} - E_{n_1 l}\right)^2 + t^2_{10}}. \tag{1.120}$$

1.11.1 Charge Exchange in the Reaction of N_2^{**} with the Molecules NO and O_2

In the case of charge exchange on the NO molecule, the ratio $\sigma(v = 1)/\sigma(v = 0)$ is much greater that unity starting at $n_0 > 10$. The NO molecule is known to possess a low electron affinity $E_r = -0.024$ eV [99], whereas the molecular term of NO^- is stable only in the state with $s^- = 0$. The calculation of the reaction

$$N_2^{**}(v' = 0) + NO\,(s = 0) \rightarrow N_2^+(v = 1) + NO^-(s^- = 0), \tag{1.121}$$

(performed for the $n_0 p\pi_u$ and $n_0 d\delta_g$-series using the data from [3]) clearly reflects the irregular character of the dependence of the charge-exchange cross-sections (1.121) from the $n_0 p\pi_u$ and $n_0 d\delta_g$ states of the nitrogen molecule on the level

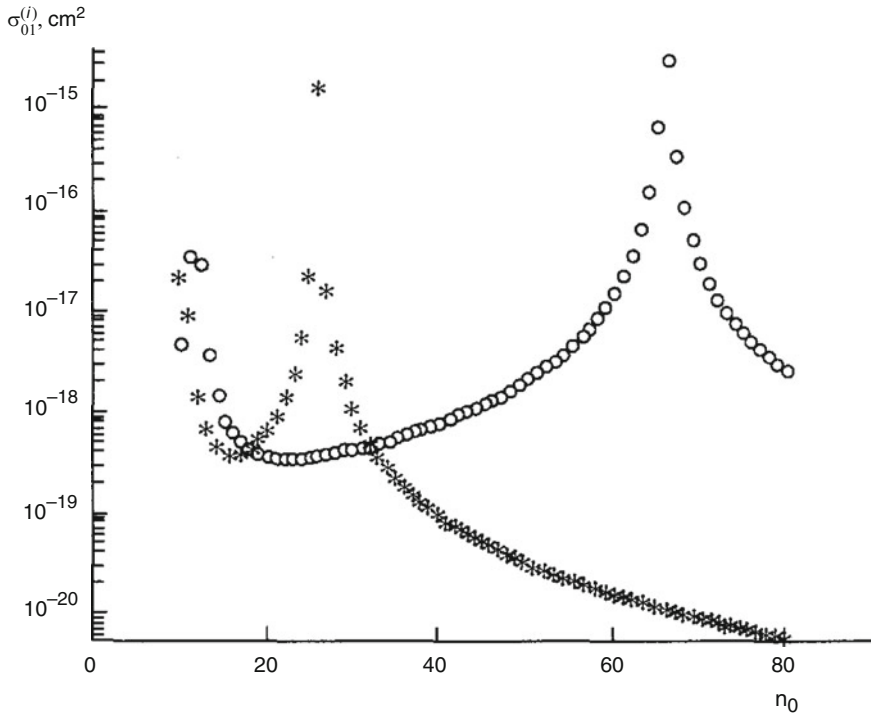

Fig. 1.10 The plot charge exchange cross-section $N_2^{**}(n_0 l\Lambda) + O_2 \rightarrow N_2^+ + O_2^-$ as a function of the initial principal quantum number n_0 for the Rydberg series $p\pi_u$ (1) and $d\delta_g$ (2). Calculations were carried out in [100] for the relative velocity $V_c = 4 \times 10^{-4}$ au

number n_0, as is seen from the presence of sharp splashes whose positions depend on the initial state of a highly excited molecule (Fig. 1.10). As a further application of the theory, we present the computational results obtained for the reaction [100]

$$N_2^{**}(v' = 0) + O_2\,(s = 0) \rightarrow N_2^+(v = 1) + O_2^-(s^- = 3), \tag{1.122}$$

playing an important role in the upper and middle Earth atmosphere. The electron affinity of oxygen molecule is $E_r = 0.44$eV [101]. Because of this, the negative ion $O_2^-(^2\pi_g)$ has four ($s^- = 0-3$) stable vibrational states lying below the ground-state ($X\,^3\Sigma_g^-$) energy of O_2. The computational results obtained for the charge-exchange reaction cross-sections (1.122) are given in Figs. 1.11 and 1.12 for various Rydberg $l\Lambda$ series. These results clearly demonstrate that the dependence of cross-sections on n_0 has irregular character and demonstrates a noticeable increase for $l \geq 1$ as Λ increases. For $n_0 < 20$, all the above-mentioned series contain the regions of a strong nonadiabatic coupling. The resonance splashes in the region of large principal quantum numbers ($n_0 > 20$) are the sharpest. This occurs for $n_0 p\pi_u$ and $n_0 d\delta_g$

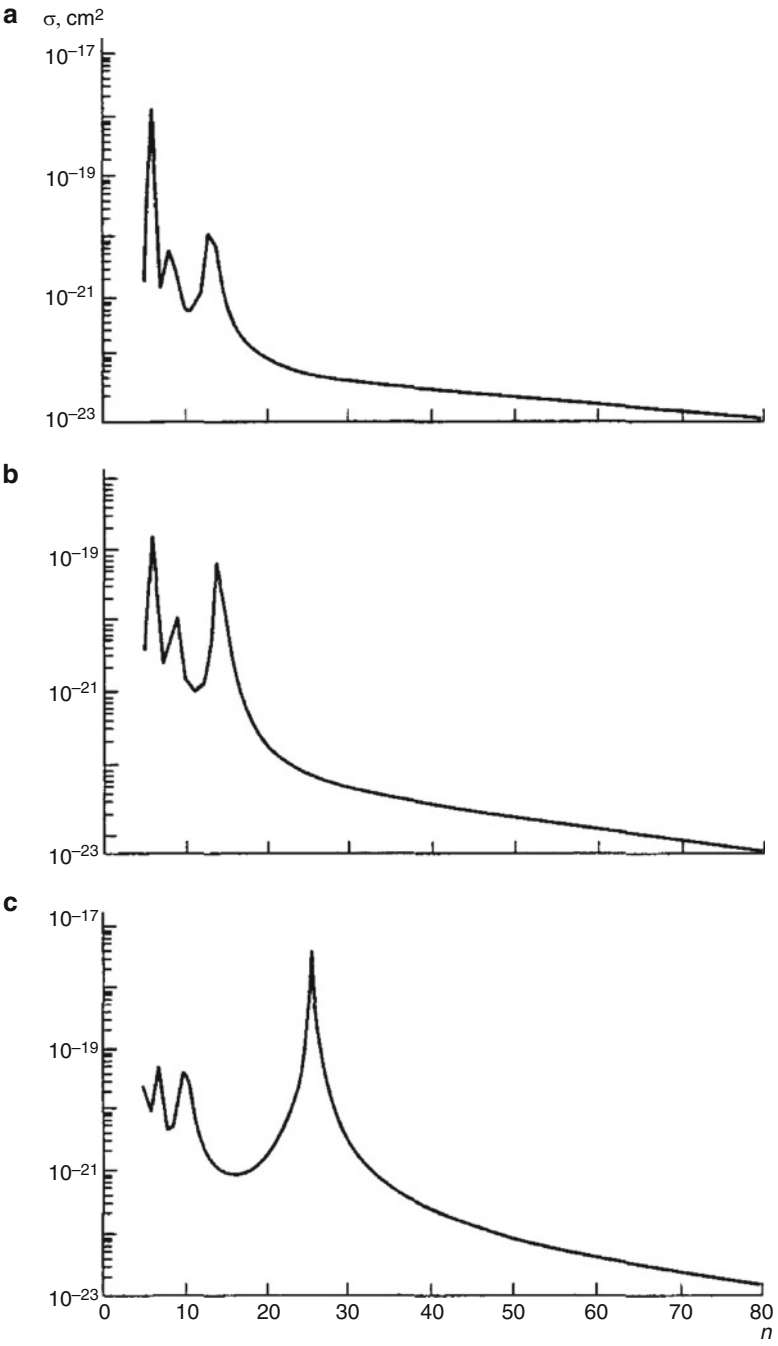

Fig. 1.11 The plot charge exchange cross-section $N_2^{**}(n_0 l\Lambda) + O_2 \rightarrow N_2^+ + O_2^-$ as a function of the initial principal quantum number n_0 for the Rydberg $s\sigma_g(\mathbf{a})$, $p\sigma_u(\mathbf{b})$, and $p\pi_u(\mathbf{c})$ series. Calculations were carried out in [100] for the relative velocity $V_c = 1.2 \times 10^{-3}$ au

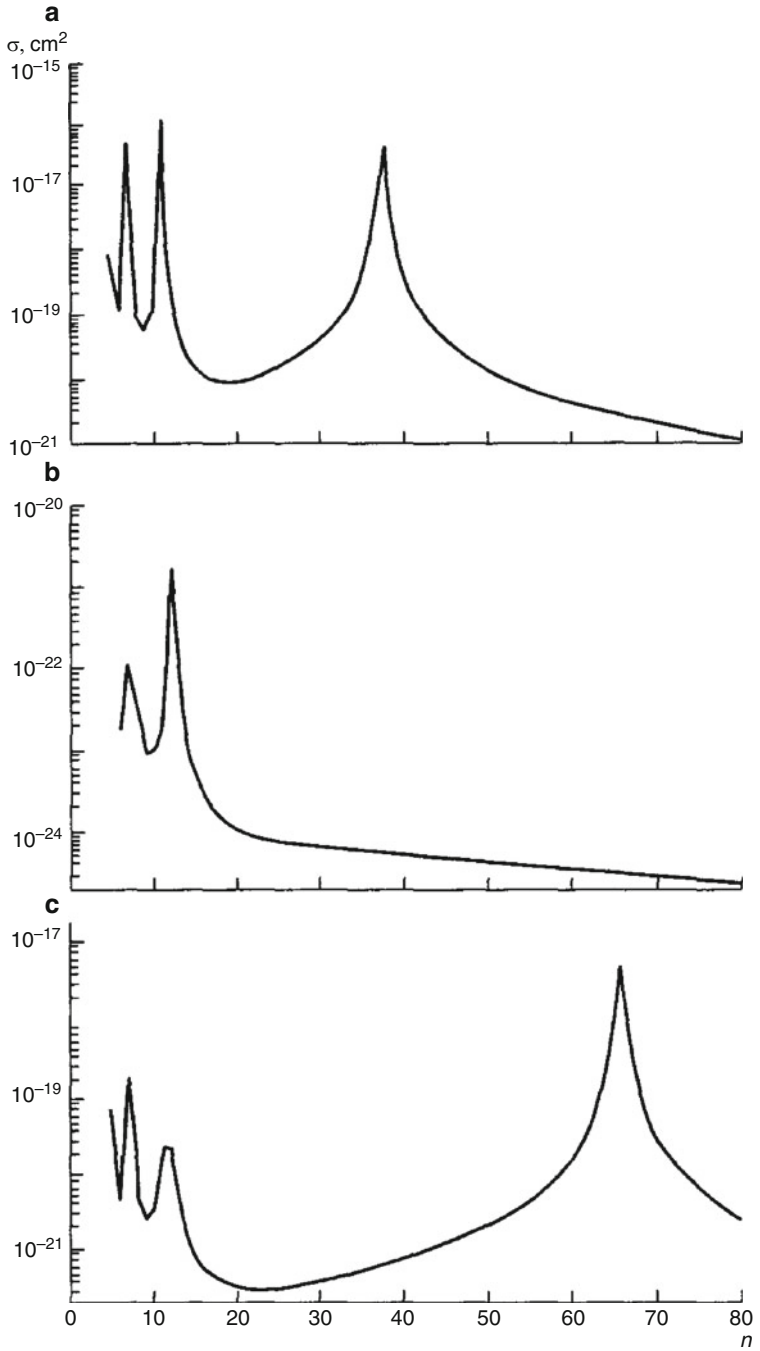

Fig. 1.12 The plot charge exchange cross-section $N_2^{**}(n_0 l\Lambda) + O_2 \rightarrow N_2^+ + O_2^-$ as a function of the initial principal quantum number n_0 for the Rydberg $d\sigma_g(\mathbf{a})$, $d\pi_g(\mathbf{b})$, and $d\delta_g(\mathbf{c})$ series. Calculations were carried out in [100] for the relative velocity $V_c = 1.2 \times 10^{-3}$ au

series, where the resonances are formed with the participation of the groups of states and the strong vibronic-coupling effect is the most pronounced. For the $n_0 p\pi_u$-series, the resonance occurs at $n_0 = 26$, and for the $n_0 d\delta_g$-series, at $n_0 = 66$. The corresponding cross-sections at these points are equal to 4.0×10^{-18} and 4.8×10^{-18}cm^2.

1.12 Nonadiabatic Effects in the *l*-Mixing Processes

The nonadiabatic electron–rotation coupling affects the PES structure of a quasi-molecule consisting of the interacting two-atomic Rydberg molecule and a neutral particle A (A is the noble gas atom), and to a great extent determines the character of the processes proceeding in these systems. The role of rotational nonadiabatic coupling in the collisional transitions is as yet poorly known. Here, we discuss it in detail by the example of l-mixing process, i.e., of a change in the angular momentum l of Rydberg electron in slow collision with the perturbing neutral particle B [83]. This process constantly draws the attention of researchers, because its cross-section reaches $\sigma \sim 10^{-12} - 10^{-11}$ cm^2 in the range $n \sim 10 - 40$ of the principal quantum number.

In [84], the cross-sections of the elastic and inelastic transitions in a hydrogen molecule excited to the Rydberg $np0(^1\Sigma_u^+)$ and $np2(^1\Pi_u)$ series of the optical $R(0)$-branch characterized by the strong nonadiabatic coupling with rotation were calculated. According to the composition rules, the nuclear angular momentum N takes in this case the values 0 and 2. It is known that, as regards the ion rotational motion, the Rydberg spectrum of hydrogen molecule can be divided in the three characteristic regions: adiabatic, nonadiabatic, and essentially nonadiabatic.

The first corresponds to the situation in which the period of nuclear rotation is much longer than the characteristic rotation period of a weakly bound electron (i.e., $Bn^3 \ll 1$), so that the projection Λ of electronic angular momentum l on the molecular axis is conserved (Hund's case "b" coupling [102]). As the principal quantum number n increases, the regular level arrangement breaks down and the spectrum structure becomes more complicated [103]. In the majority of states, the electron–vibration coupling becomes much less pronounced; i.e., the spectrum reproduces the v-repetitive system of terms shifted relative to each other by the energy of vibrational quantum ω. For this reason, the analysis of the nonadiabatic effects can be divided in two steps. At the first step, one should consider the nonadiabatic electron–rotation coupling and eliminate the vibrational motion (by fixing the interatomic distance in the equilibrium internuclear position R_e^+). At the second step (if necessary), one can include electron–vibration interaction. Here, we restrict ourselves only to the first step and study the processes in a fixed vibrational state (e.g., $v = 0$).

For the operator equation determining the PES of the $XY^{**} + A$ system and the interaction between the different groups of states, one has in this case [70]

$$\boldsymbol{\tau} = \sum_{l \le l^*, N} \tilde{K}_N \frac{\left|\Psi_{lN}^{JM}\right\rangle \left\langle \Psi_{lN}^{JM}\right|}{E - E_{nlN}^{J}} \boldsymbol{\tau} + \sum_{N, M_L} \tilde{K}_N p_N \cot \pi \nu_N \left| Y_{N M_L}\right\rangle \left\langle Y_{N M_L}\right| \boldsymbol{\tau} \tag{1.123}$$

(M_L is the projection of the nuclear angular momentum N on the direction of radius vector $\mathbf{R}$). The quantity $\tilde{K}_N(R)$ is the diagonal element of the $\mathbf{K}$-matrix describing the free-electron elastic scattering from particle A in the state with orbital moment $L = 0$. This element coincides, to an accuracy of sign and the terms quadratic in p_N, with the S-scattering amplitude determined at energy $\varepsilon_N = p_N^2/2$. Formula (1.123) contains the total wave functions (with regard to the influence of core and strong nonadiabatic electron–rotation coupling effects) of the H_2 molecule for the $np0$ and $np2$ series, which represent the following superpositions [67]:

$$\Psi_{lN}^{JM}(\mathbf{r}, \mathbf{x}, \mathbf{R}) = \sum_{N'} C_{NN'}(E_{nlN'}) Q_{lN'}(r) \phi_i(\mathbf{x}) \Phi_{lN'}^{JM}(\hat{r}, \hat{R}), \tag{1.124}$$

where $C_{NN'}$ are the corresponding expansion coefficients, ϕ_i is the electron wave function of the H_2^+ ion, and the functions Q_{lN} and Φ_{lN}^{JM} are given by expressions (1.75) and (1.77).

The l-mixing process is defined as a dynamic transition from the m-mixed groups of states with a fixed value of l (for $l \le l^*$) to the strongly m- and l-mixed groups of states with $l > l^*$. Note that the angular dependence of the wave function of Rydberg electron is weak for the transitions from the states with $l \le l^*$ and has no effect on the dynamics of the process. The dependences of the quantum defects on the number n and the quasiclassical oscillations of radial wave functions are more significant.

Analysis of the specific features of the l-mixing cross-sections can be carried out using the quasi-elastic transitions as an example,

$$H_2^{**}(npN) + \mathrm{Xe} \rightarrow H_2^{**}(n_L L N_L) + \mathrm{Xe}\ , \tag{1.125}$$

where N_L takes the values 0 or 2. Indeed, for $n \ge 10$, this process proceeds with a small (when compared with the energy of rotational excitation) change $\Delta E_{nlN} \propto \mu_{N_L}/v_{N_L}^3$ in the total energy of Rydberg molecule. At low relative energies of the colliding particles, $E_c \ge 6B$, only one component of the initial rovibronic state is actually involved in this process. Recall also that the Rydberg npN-series of the optical $R(0)$-branch in the H_2^{**} molecule are not autodecaying and possess, in the spectral range of interest, radiative lifetimes ($\tau_{\mathrm{rad}} \sim 10^{-6}$ s) considerably longer than the characteristic collision times ($\tau \sim 10^{-11}$ s).

One of the most characteristic features of the H_2^{**} molecule is that it can demonstrate the stroboscopic effect [66, 67] if the separate groups of states, whose classification corresponds to the adiabatic representation, form in the spectrum. In the classical limit [65], it allows for a simple interpretation: the molecular

axis assumes the same orientation in a sequence of interaction events between the Rydberg electron and ion core. This effect appears if ν_0 and ν_2 satisfy the simple relation: $\nu_2 = \nu_0 - k$ $(k = 1, 2, ...)$. In this case, the adiabatic quantum defects $\mu_\sigma = 0.191$ and $\mu_\pi = -0.078$ are the roots of the secular equation

$$D = (\tan \pi\nu_0 - t_{00})\,(\tan \pi\nu_2 - t_{22}) - t_{02}^2 = 0, \tag{1.126}$$

describing the spectrum of highly excited molecular states [67]. This has a simple physical meaning and signifies that, when scattering from the ion core, the Rydberg electron passes to new phase trajectory without changing its phase. Since the quantities ν_0 and ν_2 satisfy the relation $-\frac{1}{2\nu_0^2} = 6B - \frac{1}{2\nu_2^2}$, this situation, as noted earlier, can be realized under the condition $6Bn^2 \ll 1$ and $6Bn^3 \approx k$. In the hydrogen molecule, this spectral region is situated in the $10 \leq n \leq 30$ interval.

The rotational nonadiabatic coupling in the $npN \rightarrow n_L L N_L$ transitions should manifest itself through the dependence of quantum defects $\mu_N(n)$ on the level number, because $\Delta E(t)$ in Eq. (1.73) strongly depends on n. As to the transitions with a change in the ion rotational state in the $np(0)$ and $n'p(2)$ series, the latter should be markedly different if the principal quantum numbers n and n' for the next closely spaced pairs $np(0) \rightarrow n_L L, N_L = 2$ or $n'p\,(2) \rightarrow n_L L, N_L = 0$ also strongly differ from each other. In the first case, the term L split out from the group of orbitally degenerate states plays a significant part; for instance, the transitions following the term-quasicrossing mechanism become possible at $n' \ll n$. In contrast, the distortions in the term L can be disregarded at $n' \gg n$ in the second case. This is clearly demonstrated in Figs. 1.13 through 1.16, where the l-mixing

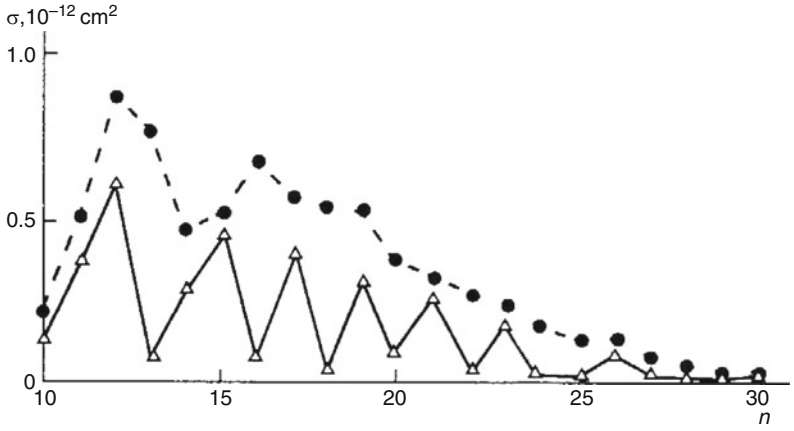

Fig. 1.13 Dependence of the $H_2^{**}(np, N = 0) + Xe \rightarrow H_2^{**}(n_L L\,, N_L = 0) + Xe$ cross-section on the initial principal quantum number n. *Dotted line* (●) denotes the cross-section of quasi-elastic $np\sigma \rightarrow n_L L$ transition calculated in the rotation adiabatic approximation [84], *solid line* (△) represents the calculation results with rotation coupling taken into account [70]

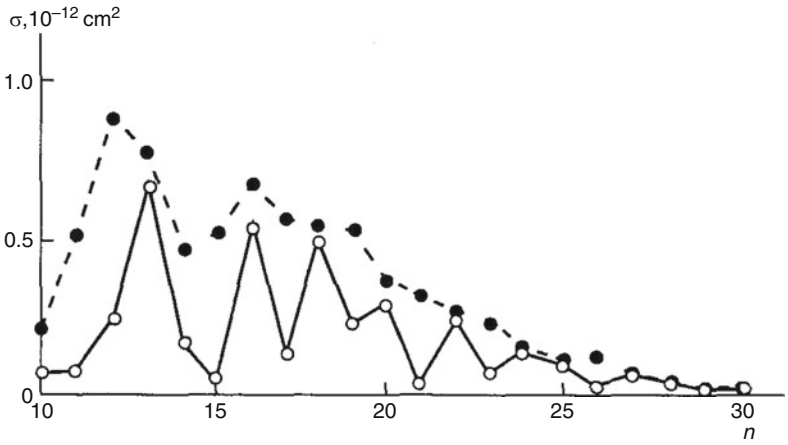

Fig. 1.14 Dependence of the $H_2^{**}(np, N = 0) + Xe \rightarrow H_2^{**}(n_L L, N_L = 2) + Xe$ cross-section on the initial principal quantum number n. *Dotted line* (●) denotes the cross-section of quasi-elastic $np\sigma \rightarrow n_L L$ transition calculated in the rotation adiabatic approximation [84], *solid line* (○) represents the calculation results with rotation coupling taken into account [70]

cross-sections are shown as functions of the initial principal quantum number n for the following quasi-elastic transitions [70]:

$$np(0) \rightarrow \begin{cases} n_L L, N_L = 0 \\ n_L L, N_L = 2 \end{cases}. \tag{1.127}$$

They were calculated for the relative velocity $V_c = 9 \times 10^{-4}$ with the parameters taken from [66]. As expected, the sharp nonmonotonic dependence on n is the most characteristic feature of these cross-sections. The envelope of the cross-sections has a typical bell-shaped form with a maximum of $\propto 10^{-12}$ cm^2. For comparison, the curves calculated previously in the rotationally adiabatic approximation for the np_σ- and np_π-states correlating at $n \geq 10$ with the $np0$- and $np2$-series are also shown in these figures [84].

1.13 Many-Center Perturbation of the Atomic Rydberg States

We now turn to the interaction of a Rydberg atom A^{**} with the system of particles situated near or inside this atom. To describe the spectrum in a rarefied gas, one can restrict oneself to the perturbation introduced by only one particle [15, 27]. In a denser medium, one must solve the problem of the influence of a force field produced by the finite number N of neutral particles falling within the volume of a highly excited atom. The dependence of N on the principal quantum number n and

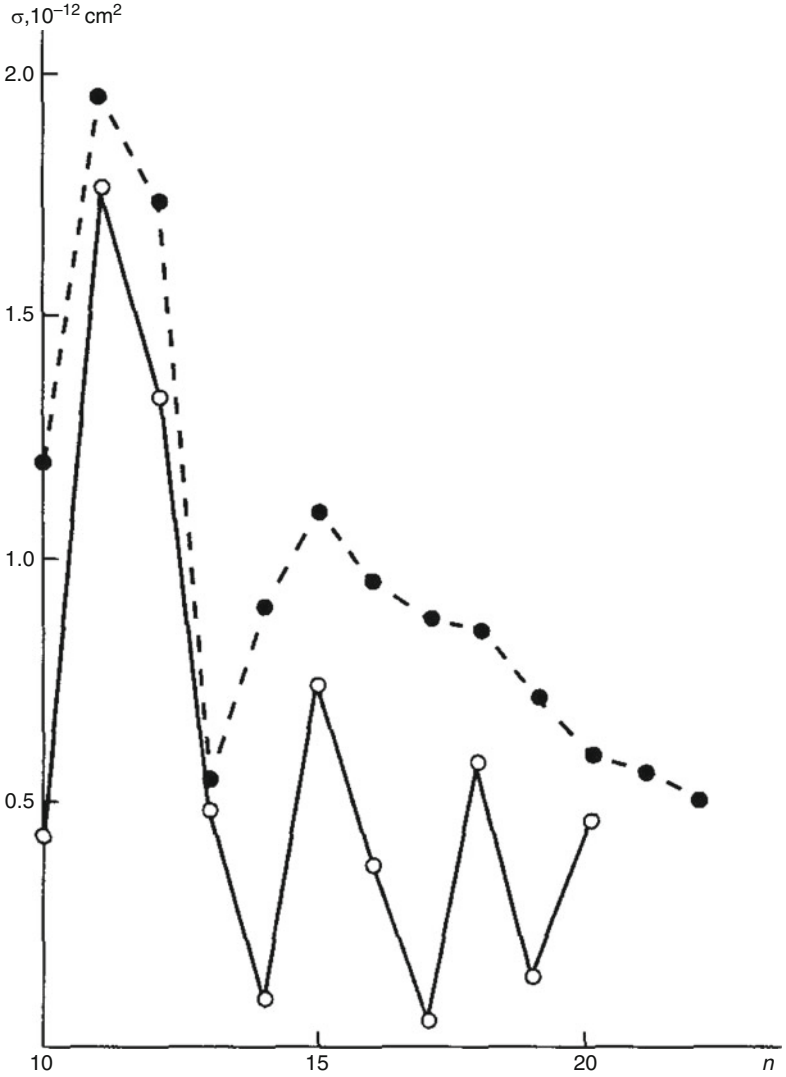

Fig. 1.15 Dependence of the $H_2^{**}(np, N = 2) + Xe \rightarrow H_2^{**}(n_L L, N_L = 0) + Xe$ cross-section on the initial principal quantum number n. *Dotted line* (●) denotes the cross-section of quasi-elastic $np\sigma \rightarrow n_L L$ transition calculated in the rotation adiabatic approximation [84], *solid line* (○) represents the calculation results with rotation coupling taken into account [70]

concentration c of medium in unit volume is presented in Table 1.3 (a concentration of 10^{17} cm^{-3} in the Earth atmosphere corresponds to the altitude ∼40 km, and 10^{13} cm^{-3} is attained at ∼100 km).

Since these particles are well separated in space, the electron scattering by each s center does not correlate with the others. For this reason, the results obtained

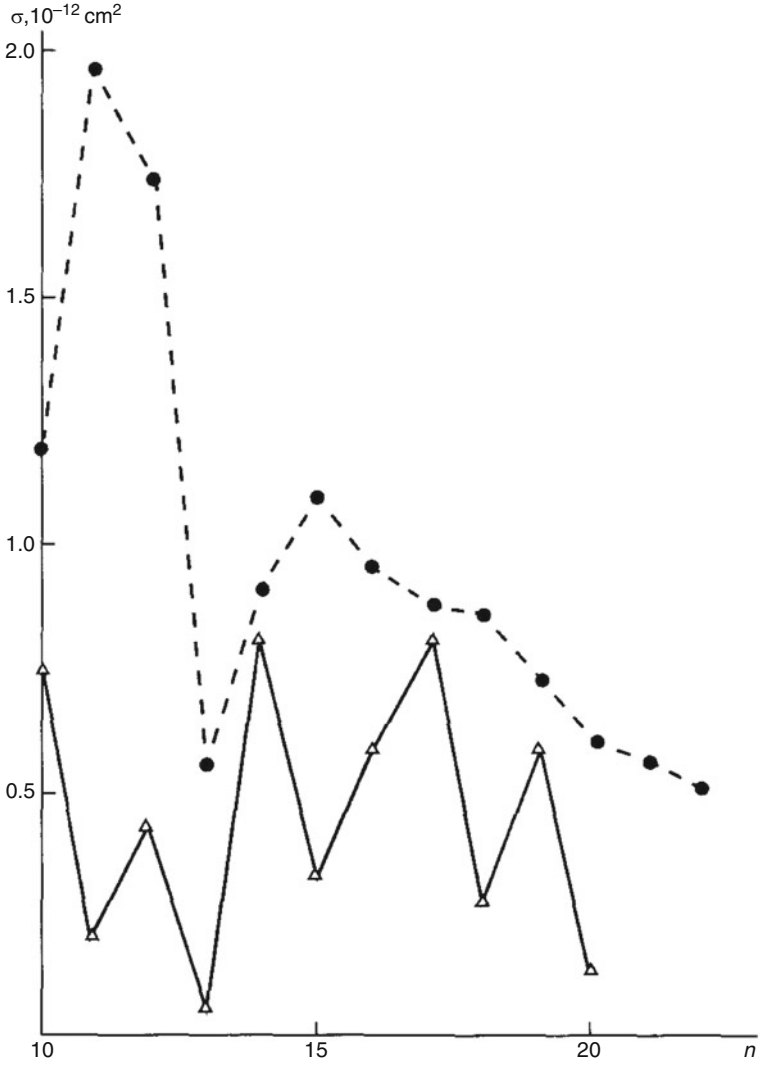

Fig. 1.16 Dependence of the $H_2^{**}(np, N = 2) + Xe \rightarrow H_2^{**}(n_L L\,, N_L = 2) + Xe$ cross-section on the initial principal quantum number n. *Dotted line* (●) denotes the cross-section of quasi-elastic $np\sigma \rightarrow n_L L$ transition calculated in the rotation adiabatic approximation [84], *solid line* (△) represents the calculation results with rotation coupling taken into account [70]

above for the one-center electron scattering from one neutral particle B can easily be extended to the many-center systems situated in the region of its action. Then, assuming that the electron interaction with these N centers is additive, i.e.,

$$U(\mathbf{r}) = \sum_{s}^{N} U(\mathbf{r} - \mathbf{R}_s),$$

Table 1.3 N as a function of the principal quantum number n and concentration c

c (cm^{-3})	10^{13}		10^{14}		10^{15}		10^{16}		10^{17}	
n	45	60	30	40	20	27	15	18	10	13
N	1	5	1	5	1	5	1	5	1	5

one can get equations of the multiple-scattering theory, in which the solutions of many-center problems reduce to the solution of the systems of algebraic equations containing the one-center scattering operators $\mathbf{K}_s = \mathbf{K}^{(0)}_{e^-B_s}$.

In studying the general properties of such systems, it is convenient to restrict oneself first to the study of a few-center situation, in which, on the one hand, the interparticle correlations inherent in the complex systems are strictly taken into account and, on the other hand, the characteristic features of energetic structure containing a set of groups of levels are also allowed for. The presence of many scattering centers placed outside or inside the atom A^{**} breaks the axial and azimuthal symmetry of interaction (when compared with the simplest two-center system). The appearance of many l and m components of the Rydberg levels must introduce certain changes also in the electronic structure of the system, as a result of which the processes of electronic transitions between the Rydberg atom and neutral cluster, as well as the autoionization processes of various kinds can become efficient.

The corresponding system of equations for the level-shift operator takes the form [27]

$$\boldsymbol{\tau} = \mathbf{T}(\mathbf{G}_{A^{**}} - \mathbf{G}_0)\,\boldsymbol{\tau}, \tag{1.128}$$

$\mathbf{T} = \sum_s \mathbf{T}_s$, where $\mathbf{T}_s$ is the operator for electron scattering from the s center. This operator takes into account the rescattering from other centers and satisfies the following equation:

$$\mathbf{T}_s = \mathbf{t}_s + \mathbf{t}_s \sum_{s' \neq s} \mathbf{G}_0(\mathbf{R}_s, \mathbf{R}_{s'})\,\mathbf{T}_{s'}. \tag{1.129}$$

The function $\mathbf{G}_0$ in Eq. (1.129) is defined in Eq. (1.10) as a function of the positions of vectors $\mathbf{R}_s, \mathbf{R}_{s'}$ relative to the ion A^+, with the momentum p_e being taken at the point $R = \frac{1}{2}|\mathbf{R}_1 + \mathbf{R}_2|$. For instance, in a system of two scattering centers,

$$\mathbf{T}_1 + \mathbf{T}_2 = \frac{1}{D}\left[\mathbf{t}_1 + \mathbf{t}_2 + \overleftarrow{\mathbf{t}}_1 \mathbf{G}_0(\mathbf{R}_1, \mathbf{R}_2)\,\vec{\mathbf{t}}_2 + \overleftarrow{\mathbf{t}}_2\,\mathbf{G}_0(\mathbf{R}_2, \mathbf{R}_1)\,\vec{\mathbf{t}}_1\right], \tag{1.130}$$

where

$$D(\mathbf{R}_1, \mathbf{R}_2) = 1 - t_1 t_2 G_0^2(\mathbf{R}_1, \mathbf{R}_2) \tag{1.131}$$

is the determinant of the two-center system. The arrowed operators in Eq. (1.130) are defined as

$$\langle\Phi(\mathbf{r})|\ \overleftarrow{\mathbf{t}}_s = t_s\,\Phi(\mathbf{R}_s)$$

and similarly for the operator acting toward the right. The contribution from the combination $\mathbf{t}_1\mathbf{t}_2$ is zero, because these operators act on different centers. For definiteness, we will assume that the matrices $\mathbf{t}_s$ of electron scattering from the s center correspond to the S-scattering ($L = 0$). Note that, according to Eq. (1.10), the operator $\mathbf{t}_s$ corresponds to the scattering $\mathbf{K}$-matrix [3], which depends only on the scattering length in the ZRP model; i.e., $t_s = 2\pi/\kappa_s = 2\pi a_s$. If $R_s > 1/|E|$, t_s is replaced by $t_s = 2\pi/(\kappa_s - \alpha_s)$, where $\alpha_s = \sqrt{-2\,(E + 1/R_s)}$. Inasmuch as, under certain conditions, determinant (1.131) can turn to zero, we consider this situation in more detail.

If the centers 1 are identical and situated in the classically allowed region of electron motion, one has for determinant (1.131) [27]

$$D(\mathbf{R}_1, \mathbf{R}_2) = \left[1 - \frac{a\cos p_e(R)|\mathbf{R}_1 - \mathbf{R}_2|}{|\mathbf{R}_1 - \mathbf{R}_2|}\right]\left[1 + \frac{a\cos p_e(R)|\mathbf{R}_1 - \mathbf{R}_2|}{|\mathbf{R}_1 - \mathbf{R}_2|}\right], \quad (1.132)$$

where

$$R = \frac{1}{2}|\mathbf{R}_1 + \mathbf{R}_2| \gg 1.$$

Note that near this pole, representation (1.130) is separable,

$$\mathbf{T}_1 + \mathbf{T}_2 = \frac{1}{D}\left(\frac{\overleftarrow{\mathbf{t}_1}}{\sqrt{|t_1|}} + \frac{\overleftarrow{\mathbf{t}_2}}{\sqrt{|t_2|}}\right)\left(\frac{\vec{\mathbf{t}}_1}{\sqrt{|t_1|}} + \frac{\vec{\mathbf{t}}_2}{\sqrt{|t_2|}}\right), \quad (1.133)$$

which greatly simplifies further analysis. The roots of equation obtained from the condition that the right-hand side of Eq. (1.129) turns to zero is denoted by $U_{\mathrm{r}}(R)$. These roots depend parametrically on the ratio $\eta = d/a$. If the centers are situated on a sphere of radius $R < 1/|E|$ around the atom A^{**} and the distance d between them is small, i.e., $1 < d = |\mathbf{R}_1 - \mathbf{R}_2| < |a| < R \propto n$, the solution to this equation is written as

$$U_r(R) = -\frac{1}{R} + E_{\mathrm{r}}, \quad E_{\mathrm{r}} = \frac{1}{2}\left[\frac{1}{d}\ \arccos\left(\frac{d}{|a|}\right)\right]^2, \quad (1.134)$$

where the position E_{r} of the resonance level does not depend on the sign of scattering length a. Consequently, the electron scattering from two centers with momentum $p_e = d^{-1}\arccos\,(d/|a|\,)$ is accompanied by the formation of a quasi-bound state near which the electron density is strongly redistributed. For small

values of the argument, $p_e d \ll 1$, the position of this term in the region $R<1/|E|$ is given by the expression

$$E_{\mathrm{r}} = \frac{1}{d}\left(\frac{1}{d} - \frac{1}{|a|}\right). \tag{1.135}$$

Note also that, under the more rigid condition $R = \frac{1}{2}|\mathbf{R}_1 + \mathbf{R}_2| \gg |a|$, this situation appears also in the case where the scattering centers are arranged arbitrarily. Clearly, the energy spectrum is expected to be strongly rearranged near the regions $U_r(R) \approx -\frac{1}{2n^2}$ at a given n. Inasmuch as term (1.133) corresponds to the electron localization at these two centers, there is full analogy with the ionic configuration in the region $E > -1/R$, where, on passing to continuum with an increase in R, it can become the autoionizing state of the system.

The terms of the ionic configuration $A^+ - (2B)^-$ can also form in the classically forbidden region $R > 1/|E|$. The equation determining their position takes the form

$$D = \left[1 - \frac{\mathrm{e}^{-\alpha_e d}}{(\kappa - \alpha_e)\, d}\right]\left[1 + \frac{\mathrm{e}^{-\alpha_e d}}{(\kappa - \alpha_e)\, d}\right] = 0$$

and, in the general case, has two solutions $E_{\mathrm{r}}^{(1)}$ and $E_{\mathrm{r}}^{(2)}$. It also follows from this equation that its solutions must turn to zero at the turning point $\alpha_e = 0$ where $d = |a|$. Since the Rydberg wave functions $\Phi_{vl0}^{(R)}(\mathbf{R})$ decrease exponentially at $R > 1/|E|$, it is natural to restrict oneself to the consideration of the small values of $\alpha_e d$. Under these conditions, the first solution $E_{\mathrm{r}}^{(1)}$ coincides with expression (1.135), and the second is

$$E_{\mathrm{r}}^{(2)} = -\frac{1}{8}\left(\frac{1}{d} + \frac{1}{a}\right)^2. \tag{1.136}$$

The solutions $E_{\mathrm{r}}^{(1)}$ and $E_{\mathrm{r}}^{(2)}$ can exist simultaneously only in the case of $0 < a < d$, whereas, at $1 < d < |a|$, there is only one solution $E_{\mathrm{r}}^{(2)}$. Note that the case $|a| = d$, where ionic terms (1.134 through 1.136) merge with the Coulomb potential, corresponds to the formation of a virtual state with the zero binding energy. One more feature arises under the condition $\kappa = \alpha_e$. At this point, $D \to \infty$ and scattering $\mathbf{T}$ operator (1.133) turns to zero; i.e., a "transparency window" appears in the forbidden region and the initial state is not perturbed at the distances $R = \frac{\nu_l |a|}{\sqrt{a^2 - \nu_l^2}} > 2n^2$ for a given energy E_{vl} of the Rydberg level. Such a situation must take place at $\nu_l \propto |a|$, which corresponds to the small values of the principal quantum number n. This result is not surprising and is well known in the quantum mechanics [104]. In the subsequent analysis of the term behavior in the vicinities of the corresponding quasicrossings, this particular case can be eliminated. It is significant that, for a given arrangement of the scattering centers relative to ion A^+, the transition from the classically allowed region of electron motion

(corresponding to the large values of n) to the forbidden region (with small n) should be accompanied by a change in the sign of electron affinity in the ionic configurations. In addition, these and the nearest lying Rydberg terms must be strongly perturbed in the range $U_{vlm}^{(R)}(R) < U_{\mathrm{r}}(R) < U_{v+1,lm}^{(R)}(R)$, resulting in a change in their wave functions and in the corresponding electron densities inside the volume of Rydberg atom. It is natural that these effects become more pronounced with the increasing number of scattering centers.

Therefore, three main groups of states formed by the families of one-center scattering harmonics with the nonzero angular momenta ($L \neq 0$) can simultaneously exist in the systems containing $N \geq 2$ scattering centers. The stationary states (with energies $|E| < 1/R$) relate to the first group and the ionic states (with energies $0 < |U_{\mathrm{r}}| < 1/R$) strongly interacting with the Rydberg configurations relate to the second group. Finally, the third group includes the autoionizing states with negative electron affinity, which should be observed at sufficiently large n.

1.14 Conclusions

In this book, the methods and results of systematic studies on the interaction of Rydberg atoms and molecules with individual neutral particles (atoms or molecules) are considered. To determine PES of the systems under consideration at intermediate distances $R \propto n$, it is necessary to take into account the interaction between a positively charged ion and atom B by introducing the operators for scattering from each of them and then express their matrix elements through the characteristics of electron elastic scattering without recourse to the quasiclassical approximation.

Inasmuch as the electron momentum in the $e^- - B$ interaction is not conserved in the system of three particles, it is required to define the scattering $\mathbf{K}$ operator outside of the energy surface. This problem can be solved on the following two counts. First, the scattering amplitude at the short-range portion of the potential of $e^- - B$ interaction is factorized because of the behavior of the Bessel function at small distances from the perturbing center. Second, there is a small parameter – the ratio of electron mass to the reduced mass of the particles A^+ and B. Inclusion of the long-range interaction at intermediate distances R gives rise to the azimuthal dependence of the effective interaction. For this reason, the states of an $A^{**}B$ quasimolecule become dependent on the projection of electronic angular momentum m about A^+ on the axis connecting the interacting centers. Because of the axial symmetry of interaction, these projections are integrals of motion, so that the states with different values of m do not mix.

The study of a two-center system possessing axial symmetry shows that the inclusion of long-range interaction (1.23) leads to the redefinition of the potential $e^- - B$-scattering length and to the appearance of an additional term describing the electrostatic interaction in Eq. (1.33). This term allows for the polarization of atom B in the field of ion A^+ and for the effective electrodipolar interaction of atom with

electron. At the intermediate distances R, the role of the latter proves to be greater than that in the asymptotic region. At these distances, the centrifugal potential also plays an important role. Its influence amounts to a drastic decrease in the number of degenerate Coulomb states forming covalent term and to the breaking of the quasiclassical description used in the asymptotic approach to the electron motion, thereby bringing about a more severe distortion of the Rydberg states by virtue of the increase in electron density at the intermediate distances. In the construction of covalent terms, the asymptotic theory can be used only for $R \geq n$. At the intermediate distances R between centers, this inequality greatly restricts the area of its applicability; i.e., this theory becomes valid only for small n. For such values of the principal quantum number, the quasiclassical electron momentum p_e is small and the S-scattering approximation is valid. However, with a decrease in n, the momentum increases, and one must also consider higher harmonics when describing the electron scattering from atom B.

The additional features arise in PESs for the processes involving Rydberg molecules XY^{**}. They are caused by the strong nonadiabatic coupling between the electron and nuclear motions, i.e., by the fact that each Rydberg $nlNv$-state (for small l) is a superposition of at least two closely spaced v series (which can be more in number if the rotation is taken into account). As a result, the processes become dependent on the principal quantum number n (even after averaging over the relative velocities of the colliding particles). This is particularly important in the analysis of the kinetic phenomena under nonequilibrium conditions.

We have discussed the main structural features of the vibronic PESs describing the interaction of highly excited atoms and molecules with neutral particles. The asymptotic method presented in this review is an alternative to the traditional quantum mechanical approaches. We do not use the variational principle and determine PES of the system from the algebraic equations containing information on the free-electron motion in the field of isolated fragments (of ion and neutral particle). The theory operates with the scattering $\mathbf{T}$ and $\mathbf{K}$ matrices, which are the fundamental characteristics in the quantum theory of scattering, whereas the parameters appearing in it can be directly related to the experimentally observed amplitudes (or phases) of electron scattering from ions, atoms, and molecules. The unique feature of the asymptotic method is that it allows many-sheet PES to be represented in a simple analytic form with the whole diversity of the regions of mutual approach and quasicrossings that are responsible for the nonadiabatic transitions in the system.

The objects considered in this work possess remarkable properties. The terms split out from the group of orbitally degenerate states of the Rydberg atom X^* or molecule XY^{**} demonstrate anomalous behavior. In reality, these terms do not depend on the nature of Rydberg particle (as well as on the orientation of the perturbing molecule M). An important feature of such (valence) configurations is that they are capable of autoionization after the term passes to continuum as a result of the mutual approach of interacting fragments. Moreover, weakly bound states caused by the Ramsauer effect in the elastic electron scattering from the perturbing particle can form in the Rydberg complexes. They represent shallow,

though rather wide, potential wells that are responsible for the existence of weakly bound states of the Rydberg complex (of the $X^{**}B$ or $XY^{**}B$ type) at large distances from the ion core.

Next, the perturbations of the atomic Rydberg states in the field of chaotically arranged neutral particles have been analyzed. The interaction with them splits levels into a group of sublevels corresponding to the different values of the angular momentum l of weakly bound electron and of its projection m onto the axis connecting the positive ion and the center of gravity of the particles falling into the electronic cloud of the Rydberg atom. This gives rise to a complex energy structure containing many pseudocrossings. These electronic states can change in the presence of a regular structure in the arrangement of the centers. Because of the numerous mutual approaches and term quasicrossings of different groups of states, the processes of electron transfer between different centers become rather active. This opens up new spectroscopic possibilities in the study of physical properties of the nanoclusters composed of atoms with a rather complex electronic structure.

Acknowledgment This work was supported by Russian Foundation for Basic Research, project N. 10-03-00737.

References

1. Stebbings, R., Dunning, F. (eds.): Rydberg States of Atoms and Molecules. Cambridge University Press, Cambridge (1983)
2. Golubkov, G.V., Ivanov, G.K.: Dynamic behavior of highly excited molecular states in the strong monochromatic laser fields. Russ. Chem. Bull. **43**(3), 327–345 (1994)
3. Golubkov, G.V., Ivanov, G.K.: Rydberg States of Atoms and Molecules and Elementary Processes with Their Participation. URRS, Moscow (2001)
4. Fielding, H.H., Softley, T.P., Merkt, F.: Photoionisation and ZEKE photoelectron spectroscopy of Ar, H_2 and CO_2 using a coherent XUV laser source. Chem. Phys. **155**, 257–265 (1991)
5. Muller-Dethlefs, K., Schlag, E.W.: High-resolution zero kinetic energy (ZEKE) photoelectron spectroscopy of molecular systems. Annu. Rev. Phys. Chem. **42**, 109–136 (1991)
6. Merkt, F., Softley, T.P.: Final-state interactions in the zero-kinetic-energy-photoelectron spectrum of H_2. J. Chem. Phys. **96**, 4149–4156 (1992)
7. Merkt, F., Fielding, H.H., Softley, T.P.: Electric field effects on zero-kinetic-energy photoelectron spectra: an explanation of observed trends. Chem. Phys. Lett. **202**, 153–160 (1993)
8. Larsson, M., Carlson, M., Danared, H., et al.: Vibrational cooling of D_2^+ in an ion storage ring as revealed by dissociative recombination measurements. J. Phys. **B27**, 1397–1406 (1994)
9. Larsson, M., Broström, L., Carlson, M., et al.: Dissociative recombination of H_2^+ studied in CRYRING. Phys. Scr. **51**, 354–358 (1995)
10. Tanabe, T., Katayama, I., Kamegaya, H., et al.: Dissociative recombination of HD^+ with an ultracold electron beam in a cooler ring. Phys. Rev. Lett. **75**, 1066–1069 (1995)
11. Schneider, I.F., Stromholm, C., Carata, L., et al.: Rotational effects in HD^+ dissociative recombination: theoretical study of resonant mechanisms and comparison with ion storage ring experiments. J. Phys. **B30**, 2687–2706 (1997)
12. Balashov, E.M., Dalidchik, F.I.: Current peculiarities of scanning tunneling microscope close by the collective state excitation thresholds of low-sized regular structures. Khim. Fiz. **23**(6), 38–42 (2004)

13. Grishin, M.V., Dalidchik, F.I., Kovalevsky, S.A., Kovytin, A.V.: Atomic and electronic structure of the surface nanoscaled graphite systems. Khim. Fiz. **23**(7), 83–90 (2004)
14. Balashov, E.M., Dalidchik, F.I., Shub, B.R.: Structure and electronic characteristics of imperfective oxides and nano-oxides. Khim. Fiz. **27**(12), 10–27 (2008)
15. Golubkov, G.V., Ivanov, G.K.: Rydberg atoms and molecules in the medium of neutral particles. Khim. Fiz. **22**(10), 25–86 (2003)
16. Ivanov, G.K., Bodneva, V.L., Golubkov, G.V.: Perturbation of highly excited atomic states by a system of chaotically and orderly arranged interaction centers. Chem. Phys. Rep. **19** (10), 1797–1809 (2001)
17. Golubkov, G.V., Golubkov, M.G., Ivanov, G.K.: Perturbation of Rydberg atom A^{**} states by neutral particles at intermediate distances. Khim. Fiz. **24**(5), 3–13 (2005)
18. Ivanov, G.K.: Perturbation of the degenerate atom states by the neutral particles. Opt. Spectrosc. **43**, 1044–1049 (1977)
19. Ivanov, G.K.: Interaction between atoms in the electron-excited quasimolecules. Teor. Eksp. Khim. **15**(6), 644–650 (1979)
20. Golubkov, G.V., Ivanov, G.K.: Transitions between Rydberg states of diatomic molecules in slow collisions with atoms. Z. Phys. **A319**, 17–23 (1984)
21. Ivanov, G.K.: Perturbation of the single-electron atom states by the field of diatomic molecule. Teor. Eksp. Khim. **10**, 303–309 (1974)
22. Freeman, R., Kleppner, D.: Core polarization and quantum defects in high-angular-momentum states of alkali atoms. Phys. Rev. **A14**, 1614–1619 (1976)
23. Davydov, A.S.: Atomic Nucleus Theory. Fizmatgiz, Moscow (1958)
24. Bateman, H., Erdélyi, A.: Higher Transcendental Functions, vol. I. McGraw-Hill, New York (1953)
25. Ivanov, G.K.: Finite-radius potential approximation for the atomic systems. Teor. Eksp. Khim. **10**, 450–455 (1974)
26. Landau, L.D., Lifshitz, E.M.: Quantum Mechanics. Nonrelativistic Theory. Pergamon, Oxford (1978)
27. Golubkov, G.V., Golubkov, M.G., Ivanov, G.K.: Highly excited electronic states of nanoscaled systems. Khim. Fiz. **24**(9), 3–18 (2005)
28. Drukarev, G.F., Collisions of Electrons with Atoms and Molecules, Nauka, Moscow (1978); Plenum, New York (1987)
29. Golubkov, G.V.: Exchange interaction of highly excited atom A^{**} with non-excited atom A at intermediate distances. Khim. Fiz. **25**(2), 3–14 (2006)
30. Oppenheimer, B.R., Kulkarni, S.R., Matthews, K., et al.: Infrared spectrum of the cool Brown Dwarf Gl 229B. Science **270**, 1478–1479 (1995)
31. Mayor, M., Queloz, D.: A Jupiter-mass companion to a solar-type star. Nature **378**, 355–359 (1995)
32. Burrows, A., Hubbard, W.B., Lunine, J.I., et al.: The theory of brown dwarfs and extrasolar giant planets. Rev. Mod. Phys. **73**, 719–765 (2001)
33. Christova, M., Allard, N.F., Kielkopf, J.F.: New line profiles of sodium and potassium perturbed by helium for brown dwarf and very cool white dwarf stars. In: Gigosos, M.A., Gonzalez, M.A. (eds.) Spectral Line Shapes, vol. 15; XIX ICSLS. Valladolid. Spain, pp. 308–310. Melville, New York (2008)
34. Burrows, A., Burgasser, A.J., Kirkpatrik, J.D., et al.: Theoretical spectral models of T dwarfs at short wavelengths and their comparison with data. Astrophys. J. **573**, 394–417 (2002)
35. Burgasser, A.J., Kirkpatrik, J.D., Liebert, J., et al.: The spectra of T dwarfs. II. Red optical data. Astrophys. J. **594**, 510–524 (2003)
36. Seager, S., Sasselov, D.D.: Theoretical transmission spectra during extrasolar giant planet transits. Astrophys. J. **537**, 916–921 (2000)
37. Brown, T.M.: Transmission spectra as diagnostics of extrasolar giant planet atmospheres. Astrophys. J. **553**, 1006–1026 (2001)
38. Jayawardhana, R.: Unraveling brown dwarf origins. Science **303**, 322–323 (2004)

39. Lodders, K.: Brown dwarfs–faint at heart, rich in chemistry. Science **303**, 323–324 (2004)
40. Burrows, A.: A theoretical look at the direct detection of giant planets outside the solar system. Nature **433**, 261–268 (2005)
41. Chung, H.-K., Kirby, K., Babb, J.F.: Theoretical study of the absorption spectra of the sodium dimer. Phys. Rev. **A63**, 032516 (2001)
42. Zhu, C., Babb, J.F., Dalgarno, A.: Theoretical study of pressure broadening of lithium resonance lines by helium atoms. Phys. Rev. **A71**, 052710 (2005)
43. Zhu, C., Babb, J.F., Dalgarno, A.: Theoretical study of sodium and potassium resonance lines pressure broadened by helium atoms. Phys. Rev. **A73**, 012506 (2006)
44. Allard, N.F., Allard, F., Hauschildt, P.H., et al.: A new model for brown dwarf spectra including accurate unified line shape theory for the Na I and K I resonance line profiles. Astron. Astrophys. **411**, L473–L476 (2003)
45. Burrows, A., Volobuyev, M.: Calculations of the far-wing line profiles of sodium and potassium in the atmospheres of substellar-mass objects. Astrophys. J. **583**, 985–995 (2003)
46. Pascale, J.: Use of *l*-dependent pseudopotentials in the study of alkali-metal-atom–He systems. The adiabatic molecular potentials. Phys. Rev. **A28**, 632–644 (1983)
47. Kumar, A., Lane, N.F., Kimura, M.: Quenching of low-lying Rydberg states of Na colliding with ground-state He: a semiclassical approach. Phys. Rev. **A39**, 1020–1028 (1989)
48. Geum, N., Jeung, G.H.: Undulating potential curves of the Rydberg states of NaHe. Chem. Phys. Lett. **333**(9), 314–318 (2001)
49. Theodorakopoulos, C., Petsalskis, I.D.: Potential energy curves and radiative lifetimes of Rydberg states of NaHe. J. Phys. **B26**, 4367–4380 (1993)
50. Buenker, R.J., Liebermann, H.P.: Private communications (2008)
51. Golubkov, G.V., Golubkov, M.G., Ivanov G.K.: Rydberg atom A^{**} in a field of neutral atom B. In: Gigosos, M.A., Gonzalez, M.A. (eds.) Spectral Line Shapes, vol. 15; XIX ICSLS, Valladolid, Spain, pp. 140–142. Melville, New York (2008)
52. Santra, R., Kirby, K.: *Ab initio* configuration-interaction investigation of optical transitions in K+He and K+H_2. J. Chem. Phys. **123**, 214309 (2005)
53. Szabo, A., Ostlund, N.S.: Modern Quantum Chemistry. Dover, Mineola, New York (1966)
54. Werner, H.-J., Knowles, P.J.: An efficient internally contracted multiconfiguration – reference configuration interaction method. J. Chem. Phys. **89**, 5803–5814 (1988)
55. Knowles, P.J., Werner, H.-J.: An efficient method for the evaluation of coupling coefficients in configuration interaction calculations. Chem. Phys. Lett. **145**, 514–522 (1988)
56. Rossi, F., Pascale, J.: Pseudopotential molecular-structure calculations for alkali-metal-atom–H_2 systems. Phys. Rev. **A32**, 2657–2669 (1985)
57. Sobel'man, I.I.: Introduction to the Theory of Atomic Spectra. Fizmatgiz, Moscow (1963)
58. Golubkov, G.V., Golubkov, M.G.: Potential energies of the Na**-He quasi-molecule. Khim. Fiz. **29**(3), 1–13 (2010)
59. Aymar, M., Camus, P.: Multichannel quantum-defect analysis of the bound even-parity spectrum of neutrale barium. Phys. Rev. **A28**, 850–857 (1983)
60. Aymar, M.: Stabilisation of 5dnd autoionising states of barium by destructive interference effects between ionising channels. J. Phys. **B18**, L768–L770 (1985)
61. Frederich, H., Wintgen, P.: Interfering resonances and bound states in the continuum. Phys. Rev. **A32**, 3231–3242 (1985)
62. Connerade, J.P., Lane, A.M.: Vanishing points of particle widths of resonances: an atomic parallel of a well known nuclear phenomenon. J. Phys. **B18**, L605–L610 (1985)
63. Golubkov, G.V., Ivanov, G.K.: Interaction of auto-decayed states in molecule photodissociation processes. IL Nuovo Cimento **12D**(1), 1–20 (1990)
64. Balashov, E.M., Golubkov, G.V., Ivanov, G.K.: Radiative transitions between Rydberg states of molecules. Sov. Phys. JETP. **59**(6), 1188–1194 (1984)
65. Labastie, P., Bardass, M.S., Tribollet, B., et al.: Stroboscopic effect between electronic and nuclear motion in highly excited molecular Rydberg states. Phys. Rev. Lett. **52**, 1681–1684 (1984)

66. Bodrov, A.E., Dalidchik, F.I.: Stroboscopic effect in the spectra of highly excited states of Rydberg molecules. Khim. Fiz. **8**(7), 876–882 (1989)
67. Golubkov, G.V., Ivanov, G.K., Balashov, E.M.: Manifestation of nonadiabatic electron-rotational coupling in radiative transitions between Rydberg states of the H_2 molecule. Opt. Spectrosc. **80**(1), 33–40 (1996)
68. Balashov, E.M., Golubkov, G.V., Ivanov, G.K.: Strong irregular excitation-energy dependence of the inelastic transitions and collisional ionization cross-sections of highly excited molecules. JETP **76**(2), 200–209 (1993)
69. Ivanov, G.K., Golubkov, G.V., Balashov, E.M.: Role of non-adiabatic mixing of the vibronic states of highly excited molecules with neutral particles. Dokl. Akad. Nauk, SSSR. **323**, 311–315 (1992)
70. Golubkov, G.K., Ivanov, G.K.: Nonadiabatic effects in Rydberg molecular states and their manifestation in collision processes. Chem. Phys. Rep. **19**(3), 549–571 (2001)
71. Fano, U.: Quantum defect theory of *l*-uncoupling in H_2 as an example of channel-interaction treatment. Phys. Rev. **A2**(2), 353–365 (1970)
72. Demkov, Yu.N., Komarov, I.V.: Ionization under slow collisions of two atoms. Sov. Phys. JETP **23**, 189–196 (1966)
73. Presnyakov, L.P., Urnov, A.M.: Excitation of the multicharged ions by electron impact. Sov. Phys. JETP **41**, 31–35 (1975)
74. Golubkov, M.G., Golubkov, G.V., Ivanov, G.K.: Low-temperature dissociative recombination of electrons with H_2^+, HD^+ and D_2^+ molecular ions. J. Phys. **B30**, 5511–5534 (1997)
75. Golubkov, G.V., Ivanov, G.K.: Ionization and vibronic transitions under slow collisions of highly excited atoms with molecules. Sov. Phys. Tech. Phys. **35**, 401–410 (1990)
76. Demkov, Yu.N., Rudakov, V.S.: Method of the partial waves for a nonspherical scatterer. Sov. Phys. JETP **32**(60), 1103–109 (1971)
77. Beigman, I.L., Lebedev, V.S.: Collision theory of Rydberg atoms with neutral and charged particles. Phys. Rep. **250**, 95–328 (1995)
78. O'Malley, T.F., Spruch, L., Rosenberg, L.: Low-energy scattering charged particle by polarizable system. Phys. Rev. **125**, 1300–1306 (1962)
79. O'Malley, T.F.: Exstrapolation of electron-rare gas atom cross-sections to zero energy. Phys. Rev. **130**, 1020–1025 (1963)
80. O'Malley, T.F.: Low-energy expansion of the scattering amplitude for long-range quadrupole potentials. Phys. Rev. **134**, 1188–1197 (1963)
81. Demkov, Yu.N., Osherov, V.I.: Stationary and time-dependent quantum problems solved by the contour integral method. Sov. Phys. JETP **26**, 916–923 (1968)
82. Nikitin, E.E., Umanskii, S.Ya.: Theory of Slow Atomic Collisions. Springer Verlag, Berlin, Heidelberg/New York/Tokyo (1984)
83. Demkov, Yu.N., Golubkov, G.V.: Adiabatic approximation in time-dependent problems of quantum mechanics. Khim. Fiz. **22**(10), 7–24 (2003)
84. Golubkov, G.V., Ivanov, G.K., Balashov, E.M., Golubkov, M.G.: *l* mixing and dissociation of Rydberg molecules accompanying slow collisions with inert-gas atoms, JETP **87**(1), 56–63 (1998)
85. Petitjean, L., Gounand, F.: Simple analytical formulas for collisional *l*-mixing, *n*-changing and ionization of Rydberg atoms with neutral particles at thermal energy. Phys. Rev. **A30**, 2946–2957 (1984)
86. Radtsig, A.A., Smirnov, B.M.: Handbook of Atomic and Molecular Physics. Atomizdat, Moscow (1980)
87. Chapelet, M.J., Boulmer, J., Gauthier, J.C., et al.: Collisional angular momentum mixing of very high (#) Rydberg d-states of Na by Ar, Kr and Xe. J. Phys. **B15**, 3455–3467 (1982)
88. Kachru, R., Gallagher, T.F., Gounand, F., et al.: Collisional angular-momentum mixing of Na Rydberg states with Xe. Phys. Rev. **A27**, 795–804 (1983)
89. Omont, A.: Theory of collisions of atoms with neutral particles. J. Phys. **38**, 1343–1359 (1977)

90. Ivanov, G.K.: Transfer of electron in atomic collisions. Opt. Spectrosc. **37**, 636–642 (1974)
91. Golubkov, G.V., Dalidchik, F.I., Ivanov, G.K.: Vibrational excitation of molecules under resonant scattering by electrons. Sov. Phys. JETP **46**(2), 230–238 (1977)
92. Merkt, F., Fielding, H.H., Softley, T.P.: Electric field effects on zero-kinetic-energy photoelectron spectra an explanation of observed trends. Chem. Phys. Lett. **202**, 153–160 (1993)
93. Merkt, F., Schmutz, H.: Very high resolution spectroscopy of high Rydberg states. J. Chem. Phys. **108**, 10033–10039 (1998)
94. Borodin, V.M., Kazansky, A.K.: Mechanism of the oscillation origin widths for the alkali-metal atom Rydberg states. JETP **70**, 252–262 (1990)
95. Bethe, H.A., Salpeter, E.E.: Quantum Mechanics of One and Two-electron Atoms. Springer-Verlag, Berlin (1957)
96. Smirnov, B.M.: Physics of Weakly Ionized Gases. Mir, Moscow (1985)
97. Duzy, C., Berry, R.S.: Autoionization of N_2. J. Chem. Phys. **64**, 2431–2436 (1976)
98. Cremaschi, P.A.: A theoretical study of the Rydberg states of N_2 obtained from excitations of valence $3\sigma_g$ $1\pi_u$, $2\sigma_u$ levels. Chem. Phys. **109**, 117–124 (1976)
99. Schulz, G.J.: Resonanses in electron impacts on atoms. Rev. Mod. Phys. **45**, 378–422 (1973)
100. Golubkov, G.K., Ivanov, G.K., Balashov, E.M.: Interactions of the highly excited atoms and molecules with neutral particles. Features of the potential energy surfaces and the charge exchange processes. Chem. Phys. Rep. **14**(8), 1104–1127 (1995)
101. Parlant, G., Fiquet-Fayard, F.: The O2-П2g resonance. J. Phys. **B9**, 1617–1628 (1976)
102. Herzberg, G., Jungen, Ch: Rydberg series and ionization potential of the H_2 molecule. J. Mol. Spectrosc. **41**, 425–486 (1972)
103. Golubkov, G.V., Ivanov, G.K.: Rydberg states of molecules. JETP **53**, 674–683 (1981)
104. Galitskii, V.M., Karnakov, B.M., Kogan, V.I.: Problems on the Quantum Mechanics. URSS, Moscow (2001)

Chapter 2
Formation of Aerosols in the Atmosphere

A.A. Lushnikov, V.A. Zagaynov, and Yu.S. Lyubovtseva

Abstract Atmospheric aerosol is one of the most important factors affecting the Earth's climatic and weather conditions. The study of the mechanisms of formation and evolution of atmospheric aerosols is of primary importance for predictions of the climatic changes on our planet. We hope that this short overview of the modern state of art in aerosol science will be of use to all those who are involved to the study of atmospheric processes that form the Earth's climate. We introduce the readers to the basics of physical chemistry of aerosols. Special attention is given to the latest achievements in the theory of particle formation and their subsequent growth.

Keywords Aerosols · Nucleation · Condensation · Growth

2.1 Introduction

Atmospheric aerosols and trace gases affect considerably the global characteristics of the Earth's atmosphere [1–7]. The point is that these components play a decisive direct and indirect role in the energy balance of the atmosphere. In particular, the aerosols define the cloudiness of the sky: cloud formation is impossible without cloud condensation nuclei [8]. Submicron atmospheric aerosol particles play the role of such nuclei [4,6,7].

On the other hand, the aerosols are of primary importance in the atmospheric chemical processes. It is enough to recall the ozone holes, not mentioning other atmospheric chemical cycles, where aerosols participate either as catalysts or as an

A.A. Lushnikov (✉)
Karpov Institute of Physical Chemistry, Moscow, Russia

V.L. Bychkov et al. (eds.), *The Atmosphere and Ionosphere,*
Physics of Earth and Space Environments,
DOI 10.1007/978-90-481-3212-6_2,

active reactant. Therefore, it is of interest to know the mechanisms of particle formation in the atmosphere [1,3,6,7].

Attempts to answer questions such as, where are the aerosol particles from? what structure do they have? and what is their chemical composition? appeared already more than one and half century ago (see [9–11]). Up to now no definite answers have been found. Aerosol particles are even less studied objects than the elementary particles and quarks. The reasons for such a situation are clear. The small sizes of aerosol particles do not allow them to be watched through optical microscopes. Normally, the sizes of particles that are especially interesting for investigations do not exceed 100 nm, i.e., these particles are much smaller than the wavelength of visible light. Next, they are transparent (and thus invisible) in UV light and x-rays. The atmospheric aerosol particles immediately evaporate under the electronic beam in electron microscopes. The mass spectrometry is also practically powerless in the study of tiniest atmospheric aerosols, because the samples contain very small quantities of the aerosol substance, and it is impossible to come to some definite conclusions on the chemical composition of the particles [12]. Next, the atmospheric aerosols do appear under well-defined conditions. The point is that the atmosphere is a stochastic medium and it is very difficult (better to say, impossible) to control all the parameters governing intra-atmospheric physicochemical processes.

The submicron atmospheric aerosols were the most popular object for the study since 3 decades ago. The reason for the interest to this item is clear. These very particles are optically active. They play the crucial role in cloud formation. On the other hand, these particles have their predecessors. At present the standard aerosol instruments permit to detect the particles of nanometer sizes [12–15]. It occurs, however, that this limit is not enough for answering all questions concerning the mechanisms of gas-to-particle conversion.

The goal of this short overview is to introduce the outside reader to the circle of problems related to the particle formation and growth in the atmosphere.

2.2 Classification of Aerosols

The aerosols are divided into two classes: primary aerosols and secondary aerosols, according to the mechanisms of their origination. The primary aerosol particles result, for example, from fragmentation processes or combustion and appear in the carrier gas as already well-shaped objects. Of course, their shape can change because of a number of physicochemical processes like humidification, gas–particle reactions, coagulation, etc. Secondary aerosol particles appear in the carrier gas from “nothing” as a result of gas-to-particle conversion. For example, such aerosols regularly form in the Earth’s atmosphere and play a key role in the number of global processes like formation of clouds. They serve as the centers for heterogeneous nucleation of water vapor [8]. No aerosols – no clouds, so one can imagine how our planet would look without the secondary aerosol particles.

Primary and secondary aerosols are characterized with the size, shape, and chemical contents of aerosol particles. As for the shape, one normally assumes that the particles are spheres. Of course, this assumption is an idealization necessary for the simplification of mathematical problems related to the behavior of aerosol particles. There are many aerosols comprising the irregularly shaped particles. The nonsphericity of particles creates a heap of problems. There exist also agglomerates of particles which in some cases reveal the fractal properties.

There are a number of classifications of particles with respect to their sizes. For example, if the particles are much smaller than the molecular mean free path, they are referred to as fine particles. This size ranges from 1 to 10 nm at normal conditions. But from the point of view of aerosol optics these particles are not small if the light wave length is comparable with their size. This is the reason why such very convenient and commonly accepted classifications cannot compete with natural classifications based on the comparison of the particle size with a characteristic size that comes up each time one solves a concrete physical problem.

The particle size distributions play the central role in physics and chemistry of aerosol, although a direct observation of the distributions is possible only in principle. Practically what we really observe is just a response of an instrument to a given particle size distribution,

$$P(x) = \int_0^\infty R(x,a) f(a) \mathrm{d}a. \tag{2.1}$$

Here $f(a)$ is the particle size distribution (normally a is the particle radius), $P(x)$ is the reading of the instrument measuring the property x of the aerosol, and $R(x,a)$ is referred to as the linear response function of the instrument. For example, $P(x)$ can be the optical signal from an aerosol particle in the sensitive volume of an optical particle counter, the penetration of the aerosol through the diffusion battery (in this case x is the length of the battery), or something else. The function $f(a)$ is normalized to unity,

$$\int_0^\infty f(a) \mathrm{d}a = 1. \tag{2.2}$$

Although the particle size distribution is an elusive characteristic of the aerosol, it is convenient to introduce it because it unifies all properties of aerosols.

In many cases the distribution function can be found on solving the general dynamic equation governing the time evolution of the particle size distribution can be found theoretically [1], but the methods for analyzing this equation are not yet reliable, not mentioning the information on the coefficients entering this equation. This is the reason why the phenomenological distributions are so widespread.

There is a commonly accepted collection of particle size distributions. It includes:

The lognormal distribution [1,3,16],

$$f_{\mathrm{L}}(a) = \frac{1}{\sqrt{2\,\pi}\, a_s \ln\sigma} \exp\left(-\frac{1}{2\ln^2\sigma}\ln^2\frac{a}{a_{\mathrm{s}}}\right). \tag{2.3}$$

Here a is the particle radius. This distribution depends on two parameters: a_{s} and σ where a_{s} is the characteristic particle radius and σ is the width of the distribution. Equation (2.3) is the famous lognormal distribution. It is important to emphasize that it is not derived from a theoretical consideration. Rather, it is introduced "by hands" for different set of the parameters.

Another size distribution (the generalized gamma-distribution) is given by the formula:

$$f_{\mathrm{G}}(a) = \frac{1}{\Gamma(k/j)}\left(\frac{a}{a_{\mathrm{s}}}\right)^k \exp\left[-\left(\frac{a}{a_{\mathrm{s}}}\right)^j\right]. \tag{2.4}$$

Here $\Gamma(x)$ is the Euler gamma-function. The distribution $f_{\mathrm{G}}(a)$ depends on three parameters, a_{s}, k, and j [1,3,17].

2.3 Nucleation Scenarios

Nucleation is responsible for production of the tiniest particles due to gas-to-particle conversion [18–21]. Condensable vapors cannot exist in the vapor phase under certain conditions; normally when the vapor pressure exceeds the saturation value that, in turn, depends on the temperature. Statistical mechanics predicts the phase transition in these cases, but it does not answer the question, how does the transition go on. For example, the vapor can condense either on the walls of the vessel containing the gas–vapor mixture, or on foreign aerosol particles suspended in the carrier gas, or form the particles itself without any help from other external factors. The latter case is referred to as spontaneous nucleation. There are some principal difficulties in the theoretical description of the nucleation process. We will try to elucidate the nature of these difficulties and outline the ways for avoiding them.

Although everybody saw how a kettle boils producing visible vapor from its nose, the quantitative measurements on the nucleation are very far from being simple. The point is that respective nucleation theories are applicable for steady-state and very clean (no foreign condensation nuclei) conditions. To provide such conditions is not an easy task.

Already for many decades there exists an irreconcilable conflict between the theoretical predictions and the experimental data on the spontaneous nucleation of vapors. The reason for this is quite clear: the problem itself is far from being simple

either theoretically or experimentally. This opinion is commonly recognized and shared by most of the researchers investigating the nucleation of vapors (and not only vapors). After the brain storm of 60th and 70th (everybody remember the hot battles around the Lothe–Pound correction) the development of our knowledge on the nature of this remarkable phenomenon returned to a quiet stream. Although the necessity in a correct and reliable Nucleation Theory had been emphasized many times by very diverse leaders of Physics of Aerosols and Physics of Clouds, nobody yet died because of the absence of such a theory. Decades elapsed, but as it was many years ago the new generations of scientists continue to investigate the properties and the content of critical embrii, investigate the details of the particle formation under different specific conditions, and seek for the interpretable nucleation events in the atmosphere. Of course, the situation with the experiment and especially with theory principally changed. First of all, it became possible to model the nucleation processes on computers that allowed for performing very complicated and quite informative numerical experiments. And still the nature of the discrepancies remains unclear.

The diversity of the results of nucleation measurements makes us to think that there could exist a number of principally different scenarios of the nucleation processes. This section introduces the readers to some of them.

2.3.1 Thermodynamically Controlled Nucleation

Statistical physics predicts that after a long time under nucleation conditions a one droplet + nucleating gas will occur in the thermodynamic equilibrium [22–24]. The mass of the droplet is $\propto V$ (here V is the total volume of the system), i.e., it is infinitely large. The starting point for the thermodynamic consideration is the Gibbs distribution

$$W \propto \exp\left[\frac{H(p,q)}{kT}\right], \tag{2.5}$$

where p, q are generalized moments and coordinates respectively, k is the Boltzmann constant, and T is the temperature in K. The Hamiltonian H possesses the property of the translation invariance, which means that all correlation functions depend on the differences of respective spatial variables. The density is thus independent of the coordinates. This fact is somewhat strange in view of existence of the macroscopic droplet. The latter should possess a boundary (interface) that should locate somewhere. On the other hand, the distribution (2.5) predicts the spatially uniform density, i.e., it does not see the interface. Next, the pair correlation function should distinguish the molecules in the gas and liquid phases. No conflict, however, arises, for the distribution function does not specify the location of the interface. The droplet is simply spread over the coordinate space. If we fix the

location of the interface, then the translation invariance is broken (this step is equivalent to adding an external force field depending on coordinates). Pay attention, that in doing so we introduce (by hands) a new information in the system thus changing its entropy.

The first attempts to describe the nucleation process based on the thermodynamic theory of fluctuations (see [24] and references therein). The idea was (and is) quite clear and transparent: the molecules of a condensing vapor should occur in a volume, where the intermolecular interaction is sufficiently strong to keep them together. In order to find the probability to form such a cluster (critical or supercritical embryo), it is necessary to find the free energy of the cluster and exponentiate it. The problem is just how to find this free energy. It is quite natural to assume that this free energy is identical to the free energy of a liquid (solid) droplet of the condensing substance. This assumption is not so bad for large droplets, but if the embryo is small, the doubts in the validity of such approach can arise. Of course, it is possible to try to find the free energy starting with the microprinciples, that is, to calculate the free energy of the cluster by solving the respective classical or quantum mechanical problem.

It is commonly accepted to express the nucleation rate in terms of the probability for the critical embryo to exist and a kinetic factor describing the flux of nucleating vapor toward the growing embryo,

$$J = Z_c \exp\left(-\frac{G}{kT}\right). \tag{2.6}$$

Here Z_c is the flux of vapor.

The values of central interest are the formation energy G and the size of the critical embryo. There exist numerous models of critical embryo beginning with the macroscopic (droplet) model describing the energetics of the critical embryo in terms of macroscopic characteristics (surface tension, bulk density) and ending with entirely microscopic models that use the pair intermolecular potential for evaluating the partition functions of the embryo.

This scenario will be referred to as "thermodynamically controlled nucleation", for it assumes setting a thermodynamic equilibrium inside the embrii. Many nucleation processes (but not all) are thermodynamically controlled. The flux of nucleating vapor to the growing embryo is reported in refs [25–30].

2.3.2 *Kinetically Controlled Nucleation*

It is very difficult to imagine that a very slow thermodynamically controlled nucleation scenario can realize in the atmosphere. More likely is another scenario that assumes the formation of the critical embryo after one successful collision of two vapor molecules. In this case a dimer forms. This dimer can grow and cast to a

trimer etc., once the latter is stable. The formation of the dimer requires the presence of a third body that takes away the excess of energy appearing after the formation of the bound state of two molecules. The nucleation rate in this case is proportional to the second power of the vapor concentration. This scenario has been recently investigated in detail in ref. [25]. It has been shown that only the bound states of the dimer contribute to the growth process, which means that a thermodynamic equilibrium is never attained in this case. The states in the continuous spectrum have a short lifetime and thus should be ignored in the kinetic consideration of the process.

The kinetic approach allows one to assume that the supercritical embryo can form via the formation of mixed clusters comprising the molecules of the condensing vapor and the molecules of the carrier gas. When such a cluster grows and reaches a thermodynamically controllable size, the molecules of the carrier gas are lost (they evaporate back from the droplet). The mixed states of the growing embryo are apparently non-equilibrium and thus cannot be predicted within the scopes of the thermodynamically controlled scenario. As far as we know, nobody yet tried to consider such a type of nucleation. Meanwhile, the existing experiments sometimes display the dependence of the nucleation rate on the pressure of the carrier gas.

The kinetics of the particle formation–growth process is described by the Szillard–Farcas scheme which assumes that the vapor molecules can join to (or escape from) by one until the growing particle reaches the critical mass. This kinetic scenario produces a well-known chain of equations for the concentrations of growing particles. This set of equations can be solved in the steady-state limit and gives the expression for the nucleation rate in terms of the evaporation and condensation efficiencies. If one assumes the Principle of Detailed Balance to be applicable under nucleation conditions, then the evaporation efficiencies could be expressed in terms of the equilibrium concentrations and condensation efficiencies. Then the Szillard–Farcas scheme leads to the well-known expression for the nucleation rate. The kinetic approach denies this step. Now it has become evident that the secondary atmospheric aerosols in most cases form according to the kinetic scenario.

2.3.3 Fluctuation-Controlled Nucleation

Even very strongly supersaturated vapors consist of independent (noninteracting) molecules (the interaction time is much shorter than the free flight time). The nucleation rate, however, in such vapors is extremely high. Moderately supersaturated vapor, in principle, always contains very highly supersaturated areas that are formed due to the density fluctuations. The nucleation process within these areas goes very quickly, so the rate of nucleation is limited by the rate of formation of the fluctuation areas. Therefore the details of the nucleation process inside these highly supersaturated areas are not important, it goes instantly. Here we return to the

ancient idea on the role of fluctuations in the nucleation process. But in contrast to the classical thermodynamic approach we consider the fluctuation areas wherein the molecules do not (yet) interact. The vapor density is sufficient for creating high supersaturation, but it consists of noninteracting molecules. It is clear that such a scenario can be described by the scheme

$$1 + 1 + 1 + \cdots + 1 \rightarrow g^*$$

and the rate of the process is proportional to the vapor concentration to the power $g*$ This very type of nucleation has been introduced and investigated in ref. [26]. It is important to emphasize that the formation of particles by nucleation alone cannot be observed directly. The point is that the nucleation process is accompanied by coagulation, and the latter process is also very swift. So just formed (by nucleation) particles coagulate, and we observe only the final result of this process. This means that the observed nucleation rate is much slower than that predicted by the nucleation theory alone.

2.3.4 Ion-Induced Nucleation

Although the role of ions in the formation of aerosols has been understood long ago, the ion-induced nucleation in the atmosphere has become popular only now after the papers [27–29]. Cosmic rays are known to produce ions that serve as active centers on which the aerosol particles can form. These charged clusters then evolve forming neutral and charged aerosol particles. The rate of formation of such particles has been shown to be enough for accounting for the rate of aerosol particle formation observed in rural regions. In this presentation we discuss the role of an additional mechanism of the particle charging, the aerosol photo effect. It is commonly believed that the thresholds of photo effect are too high for the photoelectrons from the aerosol particles to play any role in the evolution of the atmospheric aerosols. Indeed, normally the photo effect thresholds correspond to the wave lengths of the order of 250 nm. The ozone layer cuts off these photons in the lower atmosphere. But there exists another mechanism of photoionization: (the two-quantum photoeffect) that which assumes simultaneous absorption of two photons. The wavelengths of these photons correspond to green light, where the Sun's radiation spectrum is a maximum. Of course, the efficiency of the two-quantum photo effect is by $\propto 100$ times smaller than the single-quantum photo effect, but still it is enough to produce the photoelectrons in noticeable quantity. In order to investigate the role of the photo effect we apply a simple kinetic model that describes the formation of aerosols and includes all charging mechanisms. The photoeffect is shown to produce the overcharging of the smallest particles, that is, the total charge of the smallest fraction is always negative.

2.4 Kinetics of Nucleation

Everyone knows what is going on when a vapor is supersaturated. Very many tiny particles are formed. These particles then grow and are lost somewhere, let us say, because of sedimentation or some other reasons. It is clear that this picture does not bear on any thermodynamics and requires a kinetic description. The whole process can be described by the scheme

$$\text{Independent vapor molecules} \rightarrow \text{collective of tiny droplets}$$

The droplets are, however, not quite independent. They grow by consuming the vapor molecules and thus interact via vapor (condensation).

The Szillard–Farcas scheme assumes that nucleation goes along the route [1,3],

$$(g) + 1 \leftrightarrow (g + 1). \tag{2.7}$$

The rates of the forward and backward processes are assumed to be known.

In the case of kinetically controlled nucleation the chain of reactions remains unchanged. The reaction rates, however, are controlled by the kinetic processes in the carrier gas. For example, the dimerization requires triple collisions, where one of the participants is a carrier gas molecule. Of course, a dimer decay never occurs without a collision with a third body.

In principle, the mixed embrii can arise. For instance, the dimer can form as follows:

$$1 + 1' \rightarrow (1 + 1'),\ (1 + 1') + 1 \rightarrow (2) + 1' \tag{2.8}$$

The idea is clear. Very tiny embrii may consist of a mixture of the vapor and the carrier gas molecules. At later stages of the nucleation process the carrier gas molecules escape the growing embrii.

2.4.1 The Szillard–Farcas Scheme

The Szillard–Farcas scheme assumes the rates of the elementary processes $g \pm 1 \leftrightarrow (g \pm 1)$ to be known. Although this scheme is widely known [1–3,30], we refresh some central moments of the derivation of the expression for the nucleation rate. Respective kinetics obeys the following set of equations

$$J_{g-1}(C) = J_g(C) \tag{2.9}$$

with J_g being the total rates of jumps from the state $g - 1$ to g

$$J_g = J = \alpha_{g-1} C c_{g-1} - \beta_g c_g. \tag{2.10}$$

The notation is standard and is explained in detail elsewhere. The nucleation rate J is independent of g if the steady state is assumed.

Equation (2.10) is a set of linear algebraic equations with respect to population concentrations c_g. The boundary condition (particles disappear on reaching a large size) allows one to resolve the set and to find

$$J(C) = J_2 \frac{1}{1 + x_2 + x_2 x_3 + \cdots}. \tag{2.11}$$

Here $J_2\,(C)$ is the rate of dimerization.

$$J_2(C) = \frac{1}{2}\ \alpha_1\, C^2. \tag{2.12}$$

The notation C stands for the monomer concentration. This value is specially introduced instead of the supersaturation

$$x_g = \frac{\beta_g}{\alpha_{g-1} C}. \tag{2.13}$$

The nucleation rate $J(C)$ is thus expressed in terms of C, α_g , and β_g. The concentration C can be measured (in principle). The situation with $\alpha_g$and β_g is much less clear.

2.4.2 Condensation and Evaporation

From the first sight the evaporation is a very simple process and is as follows:

$$\alpha_g = v_{\mathrm{T}} \sigma_{\mathrm{c}} \tag{2.14}$$

with v_{T} being the thermal velocity (depends on g via the particle mass) and σ_{c} is the capture cross-section. The condensation is always an inelastic process. The dynamics of the collision process is far from simple. For example, the dimerization requires the presence of the third body (usually a molecule of the carrier gas). For larger particles the energy excess can be transferred to the internal degree of freedom.

The force fields like van der Waals forces or particle charge can affect the value of the capture cross section. In the simplest case cross-section equals $\sigma_{\mathrm{c}} = \pi a^2$. The situation with β is more complex [31]. A molecule of vapor should escape from the particle. The picture looks as if the molecule diffuses inside a self-consistent field created by other interacting molecules. Its energy fluctuates and it can escape reaching the interface (if it has an energy excess enough for over-jumping the

potential barrier). In principle, it is possible to find the evaporation rate by considering this or that model of interacting molecules.

However, very few researchers risked to apply this straightforward approach. Most of them prefer to apply the principle of detailed balance. The idea is an attempt to express the evaporation rate in terms of the condensation rate. It is assumed that the conditions exist when a droplet of mass g is in thermodynamic equilibrium with the surrounding vapor–gas mixture. If yes, then

$$\alpha_{g-1} C c_{g-1}^0 = \beta_g c_g^0. \tag{2.15}$$

This condition means that we can fit the temperature and the vapor concentration in such a way that this condition fulfills. Actually this condition is just the application of the method of variable constants. Indeed, such choice of c_g^0 makes $J = 0$. This step is typical for the method of variable constants. The solution to Eq. (2.10) is sought as a sum of the solution to the homogeneous equation ($J = 0$) + particular solution of inhomogeneous equation ($J > 0$). On the other hand, Eq. (2.15) reminds the condition of the equilibrium which permits one statistical mechanics for calculating the concentration c_g^0. But the equilibrium under the nucleation conditions is impossible. Here we wish to emphasize that the introduction of c_g^0 is just the formal trick for solving the set of equations (2.10).

2.4.3 Nucleation via Dimers

It is possible to imagine a different (and even opposite) scheme: very few vapor molecules are grouped into a stable cluster whose life time is not related to the contact with the carrier gas. In order to understand what we want to say, let us consider a "dimer-controlled nucleation". The dimers (serving as critical embrii) form by *three* molecular reactions. Once occurred in the bound state the dimer cannot leave it without colliding with a carrier gas molecule. The difference between such microscopic critical embryo and the commonly accepted critical embrii is seen from the first sight: nothing happens inside the embryo giving rise to its decay. Of course, the dimer is distributed over its energy states, but this distribution is controlled by the kinetics of the three body collisions between vapor molecules and a molecule of the carrier gas [25]. Not all dimers can serve as the critical embrii.

The rate of kinetically controlled nucleation is expressed as follows:

$$J = A c^{g^*}.$$

Here again g^* is the mass of the critical embryo. Very close to this scheme is "quasi-chemical nucleation" where a couple of substances can form a stable molecule. This type of nucleation is known and quite widespread. For example, the sulfuric oxides

can form stable compounds with water molecules. These compounds have a tendency to agglomerate and form rather stable clusters of several molecules. These clusters can serve as critical embrii for a nucleation process. In this case the binding energy of such embrii exceeds the thermal energy. The excess of energy should be somehow taken away. The radiation processes or further multiple collisions can serve to this end. The kinetics of such a nucleation process can be very complicated and related to numerous specific factors.

2.5 Growth by Condensation

The role of particle condensational growth and evaporation is extremely important for the particle size spectra formation. These very mechanisms are responsible for appearance of climatically active aerosols (of sizes 100–1,000 nm) in the atmosphere. It is commonly accepted to consider three regimes of the particle growth: the free-molecule regime, the continuous regime, and the transition regime. Each regime is characterized by the Knudsen number (Kn) – by the ratio of the molecular mean free path to the particle size. Large Knudsen's number corresponds to the free-molecule regime, that is, the molecules of the carrier gas do not prevent the condensable molecules to approach the target particle. In this case the efficiency α of the molecule trapping is limited by the total particle surface area. The exact result looks as follows [1,3]:

$$\alpha = \pi a^2 v_{\mathrm{T}}, \tag{2.16}$$

where a is the particle radius and v_{T} is its thermal velocity. The condensational efficiency is introduced as follows

$$j = \alpha\,(n_\infty - n_{\mathrm{e}}), \tag{2.17}$$

where n_∞ and n_{e} are the concentrations of the condensable vapor far away from the particle and over its surface, respectively. The notation j stands for the vapor flux toward the particle. Most frequently n_{e} is the equilibrium vapor concentration over the particle surface. If, however, the processes of evaporation or condensation are very fast then this concentration is different from its equilibrium value and should be found after solving the diffusion-reaction equation inside the particle This situation is typical for the fast evaporation.

The expression for the condensational efficiency in the continuous regime is also very simple [1,3,9]

$$\alpha = 4\,\pi D\,a. \tag{2.18}$$

Here D is the diffusivity of the condensing molecules. In this case the condensational efficiency is proportional to the particle size.

In order to find the condensational efficiency in the transition regime a more sophisticated approach should apply. In this case the full solution of the Boltzmann kinetic equation should be found. It is impossible to do analytically. Therefore, already long ago there appeared the semiempirical versions of the expressions for α [1,2,13] that reproduced the respective limiting expressions and described the experimental data on the transition regime.

The first simplest theories applied the continuous models of condensation (the particle radius a much exceeds the condensing molecule mean free path l). Such models were not able to describe very small particles with sizes less than the l [9]. It was quite natural therefore to try to attack the problem starting with the free-molecule limit, that is, to consider a collisionless motion of condensing molecules. Respective expressions for the condensational efficiencies had been derived and can be found in refs. [1–3]. The important step directed to the reconciliation of these two limiting cases was done by Fuchs [9] who invented the flux-matching theory.

The flux-matching theories are well adapted for studying the behavior of aerosol particles in the transition regime. Although these theories mostly did not have a firm theoretical basis, they successfully served for systematizing numerous experiments on the growth of aerosol particles and until now these theories remain rather effective and are very practical tools for studying the kinetics of aerosol particles in the transition regime (see [9,32]). On the other hand, these theories are always semi-empirical, that is, they contain a parameter that should be taken from somewhere else, not from the theory itself.

We introduce the reader to the ideology of the flux-matching theories by considering the condensation of a nonvolatile vapor onto the surface of an aerosol particle. The central idea of the flux-matching procedure is a hybridization of the diffusion and the free-molecule approaches. The concentration profile of a condensing vapor far away from the particle is described by the diffusion equation. This profile coincides with the real one down to the distances of the order of the vapor molecule mean free path. A limiting sphere is then introduced inside with which the free-molecule kinetics governs the vapor transport. The concentration profile in the free-molecule zone is considered to be flat. The equality of the fluxes in both the zones and the continuity of the concentration profile at the surface of the limiting sphere define the flux and the reactant concentration at the particle surface. The third parameter, the radius of the limiting sphere, cannot be found from such a consideration.

Hence, we apply a more sophisticated scheme [33]. We also introduce a limiting sphere outside of which the density profile of condensing vapor can be described by the diffusion equation. But inside the limiting sphere we solve the collisionless Boltzmann equation subject to a given boundary condition at the particle surface and put an additional condition: the vapor concentration at the surface of the limiting sphere coincides with that found from the solution of the diffusion equation. Even in the absence of any potential created by the particle the vapor profile in the free-molecule zone depends on the radial coordinate, because the particle surface adsorbs all incoming molecules. We thus gain the possibility to call for the continuity of the first derivatives of the profile on both sides of the limiting

sphere. This additional condition defines the radius of the limiting sphere [13]. The respective expression for the condensational efficiency has a serious advantage over the formulas used before. The point is that the final result is expressed in terms of the diffusivity and the thermal velocity of the condensable molecules, rather than in terms of the mean free path. The final result is,

$$\alpha = \frac{2\,\pi a^2 v_{\mathrm{T}}}{1+\sqrt{1+\left(\frac{a\,v_{\mathrm{T}}}{2D}\right)^2}}. \tag{2.19}$$

The extension of this formula to the case of an arbitrary external potential is,

$$\alpha\,(a) = \frac{\alpha\,(a,R)\,\mathrm{e}^{-U(R)/kT}}{1+\alpha\,(a,R)\mathrm{e}^{-U(R)/kT}\int\limits_R^\infty \mathrm{e}^{U(r)/kT}\,\frac{\mathrm{d}r}{4\pi r^2}}. \tag{2.20}$$

This formula widely applies for calculation of the charging efficiency.

Charged particles play a notable role in the processes of tiny particles formation. The nucleation process in the presence of ions goes much easier. The particle growth also becomes faster because bipolar charges on particles accelerate the coagulation. The study of atmospheric charged particles began a century ago [35–48]. First simplest theories were grounded on the use of the diffusion equation and applied to the particles of large sizes, much exceeding the ion mean free path in air. Such models were not able to describe the charging of smaller particles, with the sizes of order or less than the ion mean free path. Latest attempts to attack the particle charging problem applied the free-molecule approximation, that is, the collisionless motion of ion was considered as the charge transport mechanism. Respective expressions for the charging efficiencies were reported in refs. [33,34]. However, as was shown in ref. [34] the free-molecule regime does not realize even at normal conditions and arbitrary small particles. The point is that in the case of charged particles another characteristic length comes up. It is the Coulomb length $l_{\mathrm{c}} = q\,Q\,e^2/kT$. Even at the particle charges equal to unity this length is equal to 60 nm, i.e., it is comparable with the mean free path of ions. This fact means that the ion–molecular collisions are of importance at the distances where the Coulomb energy of the charge particle is comparable with the thermal energy kT. Hence, the criterion of validity of the free-molecule regime $l >> l_{\mathrm{c}}$ fulfils only at very low air pressure, i.e., in upper layers of the atmosphere. Next, the bound states of ions in the Coulomb or the image potentials are also of importance for bipolar charging processes. The point is that an ion can occupy a bound state only on colliding with the carrier gas molecule. The diffusion model assumes that all bound states are occupied. In the free-molecule model all these states are empty. On the other hand, it is clear that both the models have nothing common with the reality. The ions

cannot lose a very large energy and occur very deep in the potential well. This fact creates huge difficulties because it is necessary to solve the collision task in an external field.

2.6 Uptake of Trace Gases by the Aerosol Particles

Trace gases are commonly recognized to react actively with the aerosol component of the Earth's atmosphere [3,49–59]. Substantial changes to the atmospheric chemical cycles due to the presence of aerosol particles in the atmosphere make us look more attentively at the nature of the processes stipulated by the activity of atmospheric aerosols (see, e.g., [3]). The process of the gas–particle interaction is usually a first-order chemical reaction going along the route:

$$X + AP \rightarrow (APX), \tag{2.21}$$

where X, AP, and (APX) stand respectively for a reactant molecule, an aerosol particle and the final product resulting from the reaction Eq. (2.21).

As an example we refer to ozone, which is a key substance for our atmospheric system since it protects the living systems on our planet against the Sun's UV radiation. However, since the discovery of the ozone hole in the mid-1970s (details, last achievements, and references see in [3]) , it has been well established that ozone is subject to periodical large depletion events at the poles and to continuous decay in the global stratosphere. These trends are initiated by the presence of halogenated radicals that are produced by a cycle of photochemical processes. The amplitudes of ozone level variations are also driven by heterochemical reactions occurring on the surfaces of polar stratosphere clouds which transform stable reservoir molecules into radical precursors.

Yet some important aspects of aerosol heterochemistry are not so well studied (see, however, [60–64]). Among them is the interconnection between uptake and mass accommodation efficiencies [61]. Still there exist discrepancies between the results because of different understanding of the meaning of uptake coefficient. The whole issue of *Journal of Aerosol Science* 32(7) (2001) is entirely devoted to the problems of gas–aerosol interaction in the atmosphere.

In the following paragraphs we wish to outline our point of view. Let a particle of the radius a initially containing N_B molecules of a substance B be embedded to the atmosphere containing a reactant A. The reactant A is assumed to be able to dissolve in the host particle material and to react with B. The particle will begin to absorb A and will do this until the pressure of A over the particle surface will be enough for blocking the diffusion process. Our task is to find the consumption rate of the reactant A as a function of time. Next, we focus on sufficiently small particles whose size is comparable to or less than the mean free path of the reactant

molecules in the carrier gas. The mass transfer of such particles is known to depend strongly on the dynamics of the interaction between incident molecules and the particle surface. In particular, the value of the probability β for a molecule to stick to the particle surface is suspected to strongly affect the uptake kinetics. The question "how?" has not yet found a full resolution.

Below we are trying to answer this question starting with a simple analysis of the boundary condition to the kinetic equation for the molecules of a reactant A.

Let an aerosol particle be put in the atmosphere containing a reacting gas admixture A. The molecules of A are assumed to react with a guest reactant B dissolved in a host material of the particle (in principle, B. itself can be the host material). The reactant A is assumed to react with the reactant A along the route:

$$\mathrm{A} + \mathrm{B} \rightarrow \mathrm{C} \tag{2.22}$$

The particle initially containing no molecules of A begins to consume those crossing the particle–carrier gas interface. Our goal is to investigate the kinetics of this process.

Our basic integral principle asserts:

$$\text{Flux of A from outside} \;=\; \text{total consumption of A inside} \tag{2.23}$$

We consider four stages of the uptake process:

1. The diffusion of A toward the particle
2. Crossing the particle–air interface
3. Diffusion-reaction process inside the particle
4. Accumulation of nonreacted A-molecules in the particle

Balancing the fluxes gives the equation for the uptake rate.

In principle, the consideration of the uptake requires a solution of the time-dependent transport problem. Here we give some order-of-magnitude estimations allowing for a correct statement of the problem in realistic conditions of the Earth's atmosphere. Our idea is to get rid of the non-stationarity wherever it is possible. Below we use the notation D_X $(X = \mathrm{A}, \mathrm{B})$, $D_{g\mathrm{A}}$ for the diffusivity of the reactant molecules inside the particle and in the gas phase respectively.

The characteristic time of the non-stationarity in the gas phase is estimated as $\tau \propto a^2/D$. This time is extremely short. For $D = 0.1$ cm^2/s and $a = 1{,}000$ nm

$\tau \propto 10^{-7}$s. So the transport in the gas phase can be considered in the steady-state limit. The diffusion process in the liquid phase is much slower. Its characteristic time is $\tau \propto 10^{-3}$s for micron particles and $D_X \approx 10^{-5}$ cm^2/s.

The time for the chemical reaction of A molecules in the liquid phase is estimated as $\tau_{\mathrm{A}} \propto \kappa n_{\mathrm{B}}$ where κ is the binary reaction rate constant for the reaction given by Eq. (2.22). The maximal value of $\kappa \propto D_X a_m \propto 10^{-13}$cm^2/s for the molecule radius $a_m \propto 10^{-8}$cm. The book [3] cites the values within the interval $\kappa = 10^{-11} - 10^{-18}$cm^3/s.

The estimate of the characteristic of time τ_A depends on the value of n_B. If the gaseous reactant reacts with the host material, the characteristic reaction times are very short $\tau \propto 10^{-9}$s for diffusion controlled reactions and much longer for other types of chemical processes (up to seconds or even minutes).

The characteristic transport times should be compared to the characteristic times of substantial chemical changes inside the particle that are stipulated by the flux of A from outside. These times are of the order of $\tau_{changes} \propto 1/j_A$, where j_A is the total flux of *A*-molecules trapped by the particle. This is the characteristic time for one molecule of A to attach to the particle surface. Actually this time depends on the sticking probability β and can reach 10 s.

These estimates show (see also [3]) that all the characteristic times for the transient processes inside and outside the particle are much shorter than the characteristic time for the particle to change its chemical composition due to uptake. This means that a quasi-steady-state approximation can be used for the description of very slow changing parameters such as the total number of molecules inside the particle or its size. Fast transport processes establish instantly the steady-state concentration profiles.

Let us first consider condensation of *A*-molecules onto a spherical particle of *B*-liquid. In the gas phase the distribution function f_A of *A*-molecules over coordinates and velocities satisfies the Maxwell boundary condition [11],

$$f_A{}^- = (1-\beta) f_A{}^+ + \frac{\beta}{2\pi} n_{A\,e}, \tag{2.24}$$

where β is the sticking probability, $f_A{}^-$ is the velocity distribution function of molecules flying outward the particle, $f_A{}^+$ is the same for molecules flying towards the particle surface, and n_{Ae} is the equilibrium concentration of A-molecules over the particle surface. The first term on the right of this equation describes the mirror rebound of A-molecules from the particle surface. The second term gives the density of the accommodated and then emitted from the surface molecules of A. The coefficient $1/2\ \pi$ reflects the fact that the molecules fly only in the outward direction. At $f^+ = f^- = n_e/2\ \pi$ (full thermodynamic equilibrium) Eq. (2.24) satisfies automatically. The total flux of A is expressed as

$$j_A = \alpha(a)\,(n_{A\,\infty} - n_{A\,e}). \tag{2.25}$$

Here $n_{A\,\infty}$ is the concentration of A far away from the particle.

The solution of the kinetic equation defines the concrete form of the dependence of the condensational efficiency $\alpha(a)$ on the particle radius and β. The form of the second multiplier is universal and in neither way is related to any approximation.

Now we are returning to uptake. In this case the inward flux inside the particles makes concentration $n^+{}_A$ of outflying particles lower than $n_{A\,e}$. The boundary condition Eq. (2.24) is replaced by

$$f_A{}^- = (1-\beta) f_A{}^+ + \frac{\beta}{2\pi} n_A{}^+ \tag{2.26}$$

with the value of the reactant concentration $n_{\mathrm{A}}{}^{+}$ being determined from balancing the fluxes. This is the principal point of our further consideration. This equation differs from Eq. (2.24) by replacement $n_{\mathrm{A\,e}} \to n_{\mathrm{A}}{}^{+}$. Hence, the flux of $n_{\mathrm{A\,e}}$ toward the particle looks as follows:

$$j_{\mathrm{A}} = \alpha(a)\left(n_{\mathrm{A\,e}} - \frac{n_{\mathrm{A}}{}^{+}}{\beta}\right). \tag{2.27}$$

Instead of solving the kinetic equation, we apply any semi-empirical formula for $\alpha(a)$. For example, the Fuchs–Sutugin formula

$$\alpha\ (a) = \frac{\alpha_{\mathrm{fm}}(a)}{1 + \beta S\,(Kn)}, \tag{2.28}$$

where

$$\alpha_{\mathrm{fm}}(a)\beta = \ \pi\, v_{\mathrm{T}}\, a^2 \tag{2.29}$$

is the condensational efficiency in the free-molecule regime and

$$S(x) = \frac{3}{4x} - \frac{0.466}{x+1}, \tag{2.30}$$

$$n^{*}{}_{\mathrm{A}} = H\, n_{\mathrm{A}}{}^{+}, \tag{2.31}$$

where H is the dimensionless Henri constant defined as

$$H = \frac{H_{\mathrm{s}} RT}{0.981 \times 10^9} \tag{2.32}$$

Here H_{s} is the Henri constant (in units mol/a, see the definition in [3]). At $T = 300$ K

$$H = 26.4 H_{\mathrm{s}}. \tag{2.33}$$

We demonstrate the application of the above scheme for the case of complete mixing the reactants inside the particle, that is, we assume that the reactant concentration profiles are independent of coordinates. Then the following set of equations describes the evolution of the particle chemical composition,

$$\frac{\mathrm{d}N_{\mathrm{A}}}{\mathrm{d}\,t} = \alpha(a)\,(n_{\mathrm{A}\,\infty} - \frac{N_{\mathrm{A}}}{HV}) - \frac{\kappa}{V} N_{\mathrm{A}} N_{\mathrm{B}}, \tag{2.34}$$

$$\frac{\mathrm{d}N_{\mathrm{B}}}{\mathrm{d}t} = -\frac{\kappa}{V} N_{\mathrm{A}} N_{\mathrm{B}}, \tag{2.35}$$

$$V(t) = v_a N_{\mathrm{A}} + v_b N_{\mathrm{B}} + v_c N_{\mathrm{C}}, \tag{2.36}$$

where v_x is the molecular volume of each component $(x = a, b, c)$.

2.7 Nucleation Bursts in the Atmosphere

Regular production of nonvolatile species of anthropogenic or natural origin in the atmosphere eventually leads to their nucleation, formation of tiny aerosol particles, and their subsequent growth. Thus formed aerosol is able to inhibit the nucleation process because of condensation of nonvolatile substances onto the surfaces of newly born particle surfaces. This process is referred to as the nucleation burst [1].

The dynamics of atmospheric nucleation bursts possesses its own specifics, in particular, the particle production and growth is suppressed mainly by preexisting aerosols rather than freshly formed particles of nucleation mode [12]. In many cases the nucleation bursts have heterogeneous nature. The smallest (undetectable) particles accumulated during nighttime begin to grow at daytime because of sunlight-driven photochemical cycles producing low volatile (but not nucleating) substances that are able to activate the aerosol particles [65]. Stable sulfate clusters [66–72] can serve as heterogeneous embryos provoking the nucleation bursts.

The nucleation bursts were regularly observed in the atmospheric conditions and were shown to serve as an essential source of cloud condensation nuclei [12,73–77].

Now it becomes more and more evident that the nucleation bursts in the atmosphere can contribute substantially to the cloud condensation nuclei production and can thus affect the climate and weather conditions on our planet (see e.g., [3,6,7] and references therein). Existing at present time opinion connects the nucleation bursts with additional production of nonvolatile substances that can then nucleate producing new aerosol particles, and/or condense onto the surfaces of newly born particles, foreign aerosols, or on atmospheric ions. The production of nonvolatile substances, in turn, demands some special conditions to be fulfilled imposed on the emission rates of volatile organics from vegetation, current chemical content of the atmosphere, rates of stirring, and exchange processes between lower and upper atmospheric layers, presence of foreign aerosols (accumulation mode, first of all) serving as condensational sinks for trace gases and the coagulation sinks for the particles of the nucleation mode, the interactions with air masses from contaminated or clean regions [12,68,77]. Such a plethora of very diverse factors most of which have a stochastic nature prevents direct attacks on this effect. A huge amount of field measurements of nucleation bursts dynamics appeared during the last decade (see [12,68,77] and extensive citation therein).

The attempts of modeling this important and still enigmatic process also appeared rather long ago. All models (with no exception) start from a commonly accepted point of view that the chemical reactions of trace gases are responsible for the formation of nonvolatile precursors which then give life to subnano- and nanoparticles in the atmosphere. In turn, these particles are considered as active participants of the atmospheric chemical cycles leading to the particle formation. Hence, any model of nucleation bursts included (and includes) coupled chemical and aerosol blocks. This coupling leads to strong nonlinearities which means that all intra-atmospheric chemical processes (not all of which are, in addition, firmly established)

are described by a set of nonlinear equations. In addition, there is no assurance that we know all the participants of the chemical cycles leading to the production of low volatile gas constituents that then convert to the tiniest aerosol particles.

Our main idea is to decouple the aerosol and chemical parts of the particle formation process and to consider here only the aerosol part of the problem. We thus introduce the concentrations of nonvolatile substances responsible for the particle growth and the rate of embryo production as external parameters whose values can be found either from measurements or calculated independently, once the input concentrations of reactants and the pathways leading to the formation of these nonvolatile substances are known. Next, introducing the embryo production rate allows us to avoid a rather slippery problem of the mechanisms responsible for embryos formation. Since neither the pathways nor the mechanisms of production of condensable trace gases and the embryos of condense phase are well established so far, our semiempirical approach is well approved. Moreover, if we risk to begin from the basic principles, we need to introduce too many empirical (fitting) parameters.

Aerosol particles throughout the entire size range beginning with the smallest ones (with the sizes of order 1 nm in diameter) and ending with sufficiently large particles (submicron and micron ones) are shaped by some well-established mechanisms.

They are condensation and coagulation. Little is known, however, on atmospheric nucleation. This is the reason why this very important process together with self-coagulation is introduced here as an external source of the particles of the smallest sizes. The final productivity of the source is introduced as a fitting parameter whose value is controlled by these two processes simultaneously and is thus always lower than the productivity of the nucleation mechanism alone. Next, coagulation produces the particles distributed over a size interval, rather than monodisperse ones of a critical size (like in the case of nucleation alone). The productivity should be introduced as a function of the particle size and time, respectively. In principle, the size dependence of the source can be found theoretically, but it is better to refuse this idea and to introduce it as the product of a lognormal function and a time-dependent total production rate.

The condensational growth depends on the concentrations of condensable vapors, with the condensational efficiencies being known functions of the particle size. The concentrations of condensable trace gases are introduced as known functions. They can also be calculated, once all reactions responsible for conversion of volatile trace gases to low volatile ones and respective reaction rates are known (+ stoichiometry of the reactions + initial concentrations of all participants and many other unpleasant things). Of course, nothing like this is known and there is no chance to get this information in the near future.

The losses of particles are caused mainly by preexisting submicron and micron particles. There are also other types of losses: deposition of particles onto leaves of trees, soil losses, scavenging by deposits, and mists. Here the term ‘loss’ is introduced as a sink of small particles on preexisting submicron and micron aerosol particles.

Self-coagulation of particles with sizes exceeding 3 nm in diameter is entirely ignored in the model. Many authors estimated the characteristic times of the self-coagulation process and found them to exceed 10^4 s. In what follows we ignore this process. On the contrary, the intermode coagulation (the deposition of newly born particles onto preexisting aerosols) is of great importance and must be taken into account.

Now it is easy to answer the question why the linear model is able to describe the nucleation bursts in the atmosphere. The nucleation mode does not affect the surrounding atmosphere whose chemical state is defined by other numerous external factors. For example, the lifetimes of trace gases and the particles of nucleation mode depend on the concentration and the size distribution of preexisting aerosol particles.

The mechanisms of particle growth (condensation and coagulation) are well established for the whole size interval of interest. This is the reason why the model for the description of atmospheric particles is based on the continuity equation

$$\frac{\partial n}{\partial t} + \dot{a}\frac{\partial n}{\partial a} + \lambda n = J. \tag{2.37}$$

Here $n = n\,(a, t)$ is the particle size distribution, $\dot{a}$ is the rate of particle growth

$$\dot{a} = \alpha\, C(t) = \frac{v_{\mathrm{T}}\, V_0\, C(t)}{4}, \tag{2.38}$$

where v_{T} is the thermal velocity of condensing molecules, V_0 is the volume of the single molecule, and $C = C(t)$ is the number concentration of condensing molecules in air. The value λ is the coagulation sink (a fitting parameter), $J = J(a, t) = j(t)f(a)$ is the productivity of the stable embrii source. The function $f(a)$ describes the size distribution of the newly born particles.

At this stage it is especially important to emphasize that the coagulation sink is created mainly by foreign aerosols with the sizes of order 1,000 nm. Then the continuity equation (2.20) becomes linear. We removed all the sources of nonlinearity which arises from the nucleation term and the coagulation sink (the concentration of condensing gases are considered to be known functions of time). Next, we ignore the intra-mode coagulation. Equation (2.20) is the first-order partial differential equation, whose solution can be presented in the form:

$$n(a, t) = n_0(a, t) + n_J(a, t), \tag{2.39}$$

where $n_0(a, t)$ is the general solution of the homogeneous equation and $n_J(a, t)$ is a particular solution of the inhomogeneous equation. The full spectrum in the form of Eq. (2.39) allows one to classify the scenarios of nucleation bursts.

Scenario 1. At the initial moment of time (night time) the nucleation mode is entirely absent. At sunrise the trace gases appear that are able to nucleate. They

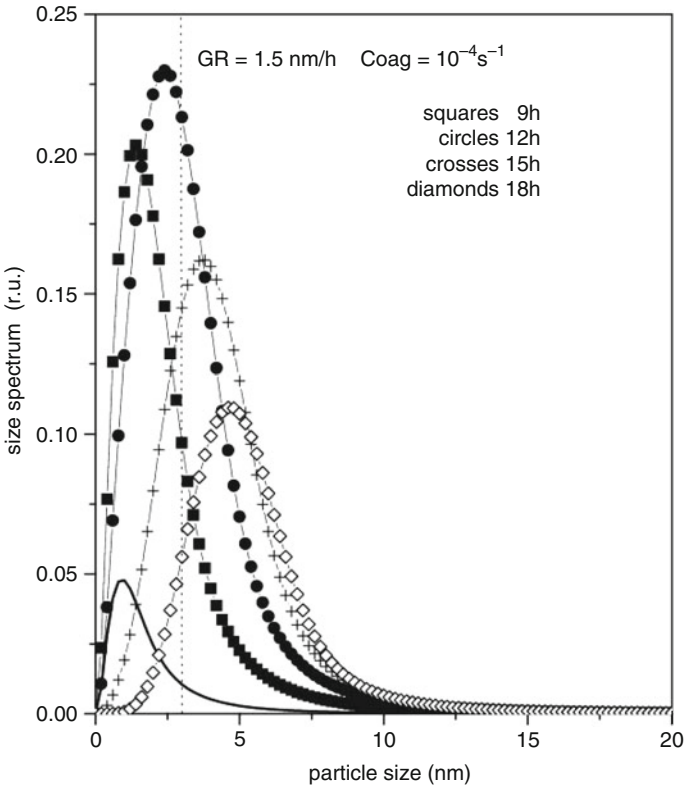

Fig. 2.1 The evolution of size distributions typical for summer periods is shown. Source produces the particles of the nucleation mode. The sinks are seen not to prevent the particle growth up to sizes 10 nm. This situation is typical for boreal regions of Finland and Siberia in summer period

form the particles growing further by condensing low volatile trace gases that cannot form the aerosol particles themselves. An example of such situation is shown in Fig. 2.1. It is seen that if the coagulation sinks are sufficiently large the particles larger 3 nm do not appear at all (see Fig. 2.2). It is important to stress that there is no well-distinguishable peak in the particle size distribution.

Scenario 2. Nucleation does not occur at all, but the smallest particles formed during nighttime are still present in the atmosphere. Then these particles begin to grow as soon as condensable gases appear after the sunrise. These particles can pass the threshold 3 nm in diameter and become detectable. In this case the peak in the particle distribution is well expressed. The picture of the nucleation burst is shown in Fig. 2.3.

Scenario 3. The running mode can appear after a new, more clean air mass comes to the observation point.

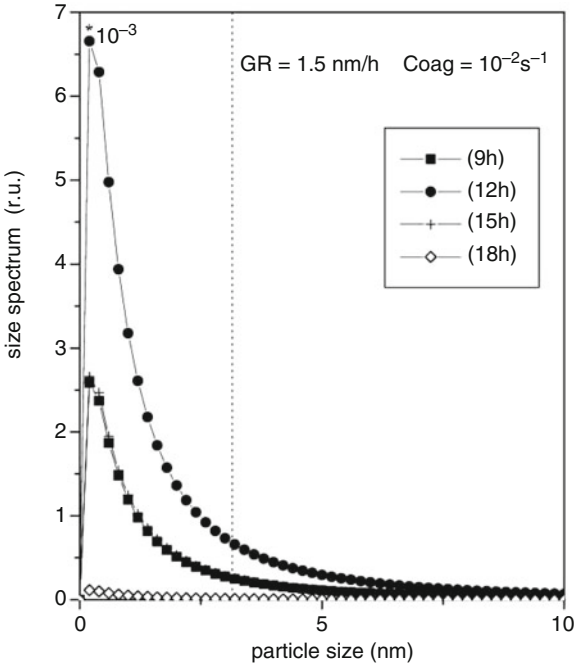

Fig. 2.2 In winter time the rate of particle formation is low. The sinks suppress the particle growth and they do not reach up to detectable sizes

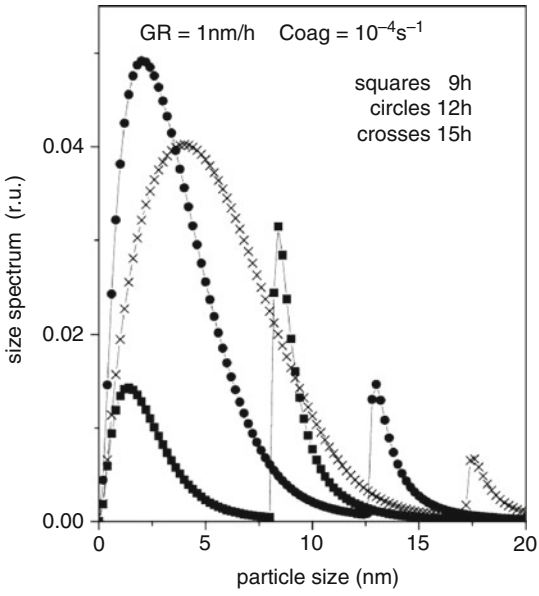

Fig. 2.3 If the particle formation precedes the condensational growth (e.g., small particles were born at nighttime due to dark reactions), then a well distinguishable peak appears at daytime

2.8 Concluding Remarks

We have presented a short overview of existing data on the processes of aerosol formation in the atmosphere. Our conclusions are as follows:

1. Although there is not full clarity in theory of gas-to-particle conversion, the productivity of the nucleation process can be introduced as a fitting parameter to the equation describing the atmospheric aerosol particle formation and growth.
2. The mechanism of the condensational growth is clear and can be described theoretically. Very often we do not know the participants of this process therefore their concentrations should be introduced as parameters or calculated from the respective chemical block.
3. Extremely important achievement is the theoretical description of the condensation growth of mixed particles. Now we know how to include the accommodation coefficient to the expression for the condensational efficiency of mixed particles.
4. At sufficiently short times (of order of 24 h) the intra-mode coagulation processes do not play an essential role. The inter-mode coagulation can be included into the coagulation sinks and be considered as a fitting parameter of the formation-growth models.

References

1. Friedlander, S.K.: Smokes, Haze, Mist. Wiley, New York/London (2000)
2. Hidy, J.M., Brock, J.R.: The dynamics of aerocolloidal systems. Pergamon, Oxford (1970)
3. Seinfeld, J.H., Pandis, S.N.: Atmospheric Chemistry and Physics. Wiley, New York (1998)
4. Taylor, F.W.: The greenhouse effect and climate change revisited. Rep. Prog. Phys. **65**, 1 (2002)
5. Graedel, T.E., Crutzen, P.J.: The changing atmosphere. Sci. Am. **261**, 58 (1989)
6. Charlson, R.J., Schwartz, S.E., Hales, J.M., Cess, R.D., Coslkey Jr., J.A., Hansen, J.E., Hofmann, D.J.: Climate forcing by anthropogenic aerosols. Science **255**, 423 (1992)
7. Charlson, R.J., Heitzenberg, R.L.: Aerosol forcing of climate. Wiley, New York (1995)
8. Pruppacher, H.R., Klett, J.D.: Microphysics of clouds and precipitation. Reidel, Dordrecht, The Netherlands (1991)
9. Fuchs, N.A.: Mechanics of aerosols. Pergamon, New York (2002)
10. Reist, P.C.: Introduction to aerosol science. Macmillan, New York (1984)
11. Williams, M.M.R., Loyalka, S.K.: Aerosol science, theory and practice. Pergamon, Oxford (1991)
12. Kulmala, M., Vehkmäki, H., Petäjä, T., Dal Maso, M., Lauri, A., Kerminen, V.-M., Birmili, W., McMurry, P.H.: Formation and growth rates of ultrafine atmospheric particles: a review of observations. J. Aerosol Sci. **35**, 143–176 (2004)
13. Alpin, K.L., Harrison, R.G.: A computer controlled Gerdien atmospheric ion counter. Rev. Sci. Instrum. **71**, 3037 (2000)
14. Eisele, F.L., Hanson, D.R.: First measurements of prenucleation molecular clusters. J. Phys. Chem. **104**, 830–836 (2000)

15. Gamera-Castano, M., de la Mora, F.: A condensation nucleus counter (CNC) sensitive to singly charged sub-nanometer particles. J. Aerosol Sci **31**, 757 (2000)
16. Aitchison, J., Brown, J.A.: The lognormal distribution function. Cambridge University Press, Cambridge (1957)
17. Deirmenjian, D.: Electromagnetic scattering on spherical polidispersions. Elsevier, New York (1969)
18. Abraham, F.F.: Homogeneous nucleation theory. Academic, New York (1974)
19. Kaschiev, D.: Nucleation: Basic principles and application. Butterworth, Heinemann (2000)
20. Laaksonen, A., Talanquer, V., Oxtoby, D.W.: Nucleation: measurements, theory, and atmospheric applications. Annu. Rev. Phys. Chem. **46**, 189 (1995)
21. Anisimov, M.A.: Nucleation: theory and experiment. Russ. Chem. Rev. **72**, 591 (2003)
22. Hill, T.: Statistical mechanics. Principles and selected applications. McGraw-Hill, New York (1956)
23. Gross, D.H.E.: Microcanonical thermodynamics. World Scientific, Singapore (2001)
24. Landau, L.D., Lifshits, E.M.: Statistical physics. Nauka, Moscow (1998)
25. Lushnikov, A.A., Kulmala, M.: Dimer in nucleating vapor. Phys. Rev. **E58**, 3157 (1998)
26. Lushnikov, A.A., Kulmala, M.: Nucleation controlled formation and growth of disperse particles. Phys. Rev. Lett. **81**, 5165 (1998)
27. Castleman Jr., A.W., Holland, P.M., Keesee, R.G.: The properties of ion clusters and their relationship to heteromolecular nucleation. J. Chem. Phys. **68**, 1760 (1978)
28. Yu, F., Turco, R.P.: From molecular clusters to nanoparticles: role of ambient ionization in tropospheric aerosol formation. J. Geophys. Res. **106**, 4797–4814 (2001)
29. Svensmark, H.: Influence of cosmic rays on Earth's climate. Phys. Rev. Lett. **81**, 5027 (1998)
30. Reiss, H., Tabahzade, A., Talbot, J.: Molecular theory of vapor phase nucleation: the physically consistent cluster. J. Chem. Phys. **92**, 1266 (1990)
31. Ford, I.J., Harris, S.A.: Molecular cluster decay viewed as escape from a potential of mean force. J. Chem. Phys. **120**, 4428 (2004)
32. Fuchs, N.A., Sutugin, A.G.: High–dispersed aerosols. In: Hidy, G.M., Brock, J.R. (eds.) Topics in current aerosol research, vol. 2, pp. 1–60, Pergamon, Oxford (1971)
33. Lushnikov, A.A., Kulmala, M.: Flux–matching theory of particle charging. Phys. Rev. **E70**, 046413 (2004)
34. Lushnikov, A.A., Kulmala, M.: Charging of aerosol particles in the near free-molecule regime. Eur. Phys. J. **D29**, 345 (2004)
35. Arnold, F.: Multi-ion complexes in the stratosphere – implication for trace gases and aerosols. Nature **284**, 610 (1980)
36. Arnold, F., Stilp, T., Busen, R., Shauman, U.: Jet engine exhaust chemi-ion measurements: implication for gaseous SO_2 and H_2SO_4. Atmos. Environ. **32**, 3073 (1998)
37. Castleman Jr., A.V.: Nucleation and molecular clustering about ions. Adv. Colloid Interface Sci. **10**, 73 (1979)
38. Horrak, U., Salm, J., Tammet, H.: Burst of intermediate ions in atmospheric air. J. Geophys. Res. **103**, 13909 (1998)
39. Karher, B., Yu, F., Schroeder, F.P., Turco, R.P.: Ultrafine aerosol particles in aircraft plumes: analysis of growth mechanisms. Geophys. Res. Lett. **25**, 2793 (1998)
40. Raes, F., Augustin, J., Vandingenen, R.: The role of ion induced aerosol formation in the lower atmosphere. J. Aerosol Sci. **17**, 466 (1986)
41. Turco, R.P., Zhao, J.-X., Yu, F.: A new source of tropospheric aerosols: ion–ion recombination. Geophys. Res. Lett. **25**, 635 (1998)
42. Yu, F., Turco, R.P.: The role of ions in the formation and evolution of particles in aircraft plumes. Geophys. Res. Lett. **24**, 1927 (1997)
43. Yu, F., Turco, R.P.: Ultrafine aerosol formation via ion-mediated nucleation. Geophys. Res. Lett. **27**, 883 (2000)
44. Yu, F., Turco, R.P.: On the contribution of lightning to ultrafine aerosol formation. Geophys. Res. Lett. **27**, 1453 (2000)

45. Lushnikov, A.A., Kulmala, M.: A kinetic theory of particle charging in the free-molecule regime. J. Aerosol Sci. **39**, 1069 (2005)
46. Marlow, W.H.: Derivation of the aerosol collision rates for singular attractive contact potentials. J. Chem. Phys. **73**, 6284 (1980)
47. Pui, D.Y.H., Fruin, S., McMurry, P.H.: Unipolar charging of fine particles. Aerosol Sci Technol. **8**, 173 (1988)
48. Hoppel, W.A. Frick, G.M.: Ion-aerosol attachment coefficients and the steady-state charge distribution on aerosols in a bipolar ion environment. Aerosol Sci. Technol. **5**, 1 (1986)
49. Friedlander, S.K.: Dynamics of aerosol formation by chemical reactions. Ann. N Y Acad. Sci. **354**, 1 (1983)
50. Prastinis, S.E., Friedlander, S.K., Pearlstein, A.J.: Aerosol reactor theory: stability and dynamics of a continuous stirred tank aerosol reactor. AiChE J. **32**, 177 (1986)
51. McGraw, R., Marlow, W.H.: The multistate kinetics of nucleation in the presence of an aerosol. J. Chem. Phys. **78**, 2542 (1983)
52. McMurry, P.H., Wilson, J.C.: Growth laws for formation of secondary ambient aerosols: implication for chemical conversion mechanisms. Atmos. Environ. **16**, 121 (1982)
53. Lushnikov, A.A., Kulmala, M.: Source enhanced condensation in monocomponent disperse systems. Phys. Rev. **E52**, 1658 (1995)
54. Lushnikov, A.A., Kulmala, M., Arstila, H., Zapadinskii, E.L.: Source enhanced condensation of a single component vapor in the transition regime. J. Aerosol Sci. **27**, 853 (1996)
55. Pratsinis, S.E.: Simultaneous nucleation, condensation and coagulation in aerosol reactors. J. Colloid Interface Sci. **124**, 416 (1988)
56. Jacobson, M.Z., Turko, R.P.: Simulating condensational growth, evaporation and coagulation of aerosols using a combined moving and stationary size grid. Aerosol Sci. Technol. **22**, 73 (1995)
57. Tsang, T.H., Rao, A.: Comparison of different numerical schemes for condensational growth of aerosols. Aerosol Sci. Technol. **9**, 133 (1988)
58. Warren, D.R., Seinfeld, J.H.: Simulation of aerosol size distribution evolution in systems with simultaneous nucleation, condensation and coagulation. Aerosol Sci. Technol. **4**, 31 (1985)
59. Aikin, A.C., Pesnel, W.D.: Uptake coefficient of charged aerosols – implication for atmospheric chemistry. Geophys. Res. Lett. **25**, 1309 (1998)
60. Davis, E.J.: Transport phenomena with single aerosol particle. Aerosol Sci. Technol. **2**, 121 (1983)
61. Davidovits, P., Hu, J.H., Worsnop, D.R., Zahnister, M.S., Kolb, C.E.: Entry of gas molecules into liquids. Faraday Discuss. **100**, 65 (1995)
62. Li, W., Davis, E.J.: Aerosol evaporation in the transition regime. Aerosol Sci. Technol. **25**, 11 (1995)
63. Natanson, G.M., Davidovits, P., Worsnop, D.R., Kolb, C.E.: Dynamics and kinetics at the gas–liquid interface. J. Phys. Chem. **100**, 13007 (1996)
64. Shi, B., Seinfeld, J.H.: On mass transport limitation to the rate of reaction of gases in liquid droplets. Atmos. Environ. **25A**, 2371 (1991)
65. Aalto, P., Hammeri, K., Becker, S., Weber, R., Salm, J., Mäkelä, J.M., Hoell, C., O'Dowd, C., Karlsson, H., Hansson, H.-C., Väkevä, M., Buzorius, G., Kulmala, M.: Physical haracterization of aerosol particles during nucleation events. Tellus **53B**, 344 (2001)
66. Arey, J., Atkinson, R., Aschmann, S.M.: Product study of gas-phase reactions of monoterpenes with the OH radical in the presence of NO_x. J. Geophys. Res. **96**, 18539 (1990)
67. Juozaitis, A., Trakumas, S., Girgzdiene, D., Girgzdis, A., Sopauskiene, D., Ulevicius, V.: Investigation of gas-to-particle conversion in the atmosphere. Atmos. Res. **41**, 445 (1996)
68. Boy, M., Kulmala, M.: Nucleation events on the continental boundary layer: influence of physical and meteorological parameters. Atmos. Chem. Phys. **2**, 1 (2002)
69. Lushnikov, A.A., Kulmala, M.: Foreign aerosols in nucleating vapor. J. Aerosol Sci. **31**, 651 (2000)

70. Lushnikov, A.A., Kulmala, M.: Nucleation burst in a coagulating system. Phys. Rev. **E62**, 4932 (2000)
71. Lushnikov, A.A., Kulmala, M.: Kinetics of nucleation controlled formation and condensational growth of disperse particles. Phys. Rev. **E63**, 061109 (2001)
72. Griffin, R., Cocker, D.R., Flagan, R., Seinfeld, J.H.: Organic aerosol formation from the oxidation of biogenic hydrocarbons. J. Geophys. Res. **104**, 3555 (1999)
73. Hoffmann, Th, Odum, J., Bowman, F., Collins, D., Klockow, D., Flagan, R., Seinfeld, J.: Formation of organic aerosols from the oxidation of biogenic hydrocarbons. J. Atmos. Chem. **26**, 189 (1997)
74. Kerminen, V.-M., Virkkula, A., Hillamo, R., Wexler, A.S., Kulmala, M.: Secondary organics and atmospheric cloud condensation nuclei production. J. Geophys. Res. **105**, 9255 (2000)
75. Korhonen, H., Lehtinen, K., Kulmala, M.: Multicomponent aerosol dynamic model UHMA: model development and validation. Atmos. Chem. Phys. Discuss. **22**, 471 (2004)
76. Kulmala, M., Pirjola, L., Mäkelä, J.M.: Stable sulfate clusters as a source of new atmospheric particles. Nature **404**, 66 (2000)
77. Lyubovtseva, YuS, Sogacheva, L., Dal-Maso, M., Bonn, B., Keronen, P., Kulmala, M.: Seasonal variations of trace gases, meteorological parameters, and formation of aerosols in boreal forests. Boreal Env. Res. **10**, 493 (2005)

Chapter 3
Atmosphere–Ionosphere Electrodynamic Coupling

V.M. Sorokin and V.M. Chmyrev

Abstract Numerous phenomena that occur in the mesosphere, ionosphere, and the magnetosphere of the Earth are caused by the sources located in the lower atmosphere and on the ground. We describe the effects produced by lightning activity and by ground-based transmitters operated in high frequency (HF) and very low frequency (VLF) ranges. Among these phenomena are the ionosphere heating and the formation of plasma density inhomogeneities, the excitation of gamma ray bursts and atmospheric emissions in different spectral bands, the generation of ULF/ELF/VLF electromagnetic waves and plasma turbulence in the ionosphere, the stimulation of radiation belt electron precipitations and the acceleration of ions in the upper ionosphere. The most interesting results of experimental and theoretical studies of these phenomena are discussed below. The ionosphere is subject to the action of the conductive electric current flowing in the atmosphere–ionosphere circuit. We present a physical model of DC electric field and current formation in this circuit. The key element of this model is an external current, which is formed with the occurrence of convective upward transport of charged aerosols and their gravitational sedimentation in the atmosphere. An increase in the level of atmospheric radioactivity results in the appearance of additional ionization and change of electrical conductivity. Variation of conductivity and external current in the lower atmosphere leads to perturbation of the electric current flowing in the global atmosphere–ionosphere circuit and to the associated DC electric field perturbation both on the Earth's surface and in the ionosphere. Description of these processes and some results of the electric field and current calculations are presented below. The seismic-induced electric field perturbations produce noticeable effects in the ionosphere by generating the electromagnetic field and plasma disturbances. We describe the generation mechanisms of such experimentally observed effects as excitation of plasma density inhomogeneities, field-aligned

V.M. Sorokin (✉)
Pushkov Institute of Terrestrial Magnetism, Ionosphere and Radio Wave Propagation, Russian Academy of Sciences, IZMIRAN, Troitsk, Moscow Region 142190, Russia

V.L. Bychkov et al. (eds.), *The Atmosphere and Ionosphere*,
Physics of Earth and Space Environments,
DOI 10.1007/978-90-481-3212-6_3,

currents, and ULF/ELF emissions and the modification of electron and ion altitude profiles in the upper ionosphere. The electrodynamic model of the ionosphere modification under the influence of some natural and man-made processes in the atmosphere is also discussed. The model is based on the satellite and ground measurements of electromagnetic field and plasma perturbations and on the data on atmospheric radioactivity and soil gas injection into the atmosphere.

Keywords Electromagnetic field · Plasma disturbances · Upper ionosphere · Atmosphere

3.1 Introduction

This chapter presents a review of the most interesting results of experimental and theoretical studies of the electromagnetic field and plasma disturbances in the ionosphere, which are initiated by different natural sources in the atmosphere and on the ground, and of the technogenic disturbances connected with human activity. A chain of interconnected processes in the lithosphere–atmosphere–ionosphere interaction system causes the ionosphere to react on such phenomena as earthquakes, volcano eruptions, typhoons, lightning discharges, high power explosions, functioning of powerful sources of electromagnetic radiation, etc. Due to such coupling, the ionosphere appears to be a sensitive indicator of the many processes occurring on the ground and in the near-Earth atmosphere. Apparently, this factor defines growing interest to investigation of the atmosphere–ionosphere interaction.

A fundamental role in the energy transfer from the atmosphere to the ionosphere belongs to thunderstorms. Large quasi-electrostatic fields in the mesosphere and the lower ionosphere connected with cloud-to-ground lightning discharges and intense electromagnetic pulses of ∼20 GW peak power generated by lightning current cause significant ionospheric disturbances because of the heating and acceleration of electrons, production of ionization, optical emissions, gamma ray bursts, etc.

Other powerful mechanism of lightning influence on the ionosphere is connected with additional ionization and formation of ionospheric inhomogeneities that are caused by the radiation belt electron precipitation due to the pitch-angle scattering of trapped particles in the magnetosphere by whistler mode waves from lightning.

Technogenic effects in the ionosphere also became a subject of intense experimental and theoretical studies. Significant attention is devoted to controlled influence on the ionosphere aimed at generating the desired ionospheric response dependent on the parameters of influence. In this connection, one can mention the generation of ultra low frequency (ULF)/extra low frequency (ELF) waves in a process of ionosphere heating by the radiation of powerful high frequency (HF) transmitters [1–4], the formation of artificial very low frequency (VLF) ducts and other types of inhomogeneities [5–7], the acceleration of ions and the excitation of atmospheric emissions in different spectral bands [8–11], etc. One can note the

transition into an active phase of the investigation of VLF wave impact on the high-energy particle distributions in the Earth's radiation belt including the experiments that use powerful VLF transmitter onboard spacecraft [12,13].

Since physical mechanisms for transfer of perturbations into the ionosphere from the abovementioned natural and artificial sources in many cases are similar, we thought it reasonable to discuss both types of influence (natural and man-made) in a frame of one paper. Such phenomena as the effects of ballistic rocket launches and of explosions of different kinds on the ionosphere stand by itself. These effects are of a different physical nature, and, therefore, their consideration lies beyond the scope of this chapter.

Among the numerous natural sources influencing the ionosphere, the most important role is thought to be played by earthquakes. An importance is defined by the potential of using the ionosphere as a sensitive indicator of earthquake preparation processes and possible tool for the short-term earthquake forecasting in future. Such potentiality is based on numerous ground and satellite observations of seismic-related phenomena occurring in the atmosphere and the ionosphere of the Earth several days or weeks before earthquake. Some results of these observations are reviewed in refs. [14–17]. Though the number of publications devoted to seismic effects on the ionosphere is huge, there is no more or less complicated understanding of cause–effect relations between the phenomena involved in the ionosphere responding to the seismic processes. Because of the insufficient experimental base and a lack of reliable statistical data on the ionospheric precursors to earthquakes, currently, there is no tangible ground to use ionospheric phenomena for sure earthquake forecasting. Nevertheless, a noticeable progress comes to pass in accumulating and analyzing the data from satellite and ground-based observations and in theoretical modeling of interconnected processes in the lithosphere–atmosphere–ionosphere system. Significant contribution is done from the Demeter satellite research program (see, e.g. [18–20]). A comprehensive model of the lower atmosphere and the ionosphere coupling was developed in ref. [21].

We can suppose that the earthquake effects in the ionosphere arise as a result of simultaneous actions of various factors, such as acoustic waves, electric fields, electromagnetic radiation, chemically active substances, etc. Since seismic activity is accompanied by the enhanced injection of soil aerosols into the atmosphere, an important role in the formation of these factors is played by aerosol fluxes, which influence the electric conductivity and generate external electric currents in the lower atmosphere [22]. Experimental evidences of earthquake-related enhancement in the injection of soil aerosols into the atmosphere, the increase in concentration of some gases (e.g., H_2, CO_2, and CH_4) by several orders of magnitude in seismically active zone, and the increase in atmospheric radioactivity associated with such radioactive elements as radon, radium, uranium, thorium, and actinium and their decay products on the eve of earthquake are presented in refs. [23–28]. Effects of strong atmospheric processes associated with typhoons on the electric field and plasma density fluctuations in the ionosphere were reported in refs. [29, 30].

Satellite measurements carried out during last 2 decades (see, e.g., [18, 20, 31, 32] confirmed the existence of low frequency emissions associated with earthquakes,

which was first reported by [33]. Comparison of the ground-based observations and the satellite measurements of ELF waves performed during different seismic events showed the similarity of the observed emissions; the only difference was in the wave intensity in the ionosphere and on the ground [34]. The negative experimental findings in [35] were connected with the use of incorrect method for data reduction: short events ($\leq$ 5 s), such as single or a small number of spherics or whistlers were not classified as disturbances and were hence not considered. At the same time, the ELF precursors to earthquakes could be associated with thunderstorm electromagnetic pulses propagated in the Earth–ionosphere waveguide and scattered into the ionosphere by plasma inhomogeneities formed in the lower ionosphere over the seismic zone before an earthquake [36]. The duration of such pulses is much less than 2 s, and the maximum power is concentrated at frequencies below $\sim$500 Hz.

DC electric field perturbations can play a key role in a coupling between the lower atmosphere and the ionosphere [21]. Ground-based and satellite observations confirm an enhancement of the electric field both in the ionosphere and on the ground in a seismic zone before earthquakes [37–42].

Small-scale plasma irregularities and large-scale disturbances of electron and ion density profiles in the upper ionosphere over seismically active region were observed before earthquakes [28, 32, 43–46].

The formation of thermal anomalies in seismic zones several days before large magnitude earthquakes presents another pronounced effect that is well observable from satellites with the use of IR sensors [47–50]. In addition, we can mention the observations of anomalous airglow at 557.7 and 630 nm correlated with the growth of seismic activity [51].

Numerous theoretical models were suggested for explanation of separate phenomena stimulated in the atmosphere and the ionosphere by seismic activity. Reference [52] considered the generation and propagation of internal gravity waves and their effects on the ionosphere. The generation of ULF emissions by lithospheric sources and their possible penetration into the ionosphere was analyzed in refs. [53–55]. The formation of electric currents in the lithosphere and the propagation of the excited waves from the source region into the ionosphere were considered in refs. [56,57]. Possible acoustic effects on the ionosphere and the generation of geomagnetic pulsations were investigated in refs. [38, 58, 59] considered the conductivity and the electric field variations in the lower atmosphere that can be caused by increase in radon concentration connected with the growth of seismic activity. The enhanced injection of radon and metallic aerosols in the epicenter region and its influence on the ionosphere were discussed in ref. [28]. The mechanisms for the electric field penetration from the source region in the lithosphere into the ionosphere and related effects on the ionosphere were analyzed in refs. [60,61].

Electrodynamic model of the ionosphere response to seismic-related lower atmosphere disturbances is developed in ref. [22]. This model describes the complete chain of processes in the lithosphere–ionosphere coupled system, which starts from the injection of radioactive substances and charged aerosols into the atmosphere and the formation of external electric current. This current is responsible for

the enhancement of DC electric field and the subsequent development of acoustic-gravity wave (AGW) instability in the ionosphere. It results in the generation of conductivity inhomogeneities in the lower ionosphere, the formation of magnetic field-aligned currents and plasma density disturbances in the upper ionosphere stretched along geomagnetic field lines. Besides, the electric field increase leads to an additional Joule heating of the lower ionosphere, which results in an elevation of F-layer maximum, a decrease of electron density in the maximum of this layer, and a growth of light ion density in the upper ionosphere. Thus, this model connects disturbances of the electric field and the key ionosphere parameters with increase of atmospheric radioactivity and injection of charged aerosols into the ionosphere. Detailed consideration of all these processes is presented below.

3.2 Effects of Lightning and Powerful Ground-Based Transmitters on the Near-Earth Space

3.2.1 Lightning Effects on the Ionosphere and the Magnetosphere

Thunderstorms play a fundamental role in the energy transfer from the atmosphere to the ionosphere. At any given time, more than 2,000 thunderstorms are active over the globe, and on average, lightning strikes the Earth about 100 times per second [62]. Every cloud-to-ground lightning discharge transfers to the ground a charge of the order of ~300 C during several milliseconds, leading to the formation of large quasi-electrostatic fields in the mesosphere and the lower ionosphere over millisecond time scales [63]. These fields together with intense electromagnetic pulses of ~20 GW peak power generated by lightning current [64] cause significant disturbances in the lower ionosphere due to heating of the ambient electrons and acceleration of runaway electrons, producing ionization and optical emissions [63, 65–67].

Plasma inhomogeneities caused by high-energy electron precipitation from the Earth's radiation belt in a process of pitch-angle scattering of trapped particles by intense whistler mode waves from lightning discharges present other class of lightning-induced disturbances in the ionosphere. Troposphere–magnetosphere coupling of such kind has been many times confirmed in ground-based observations [68–70], balloon measurements [71], rocket experiments [72, 73], and satellite observations [74–76]. Theoretically, the mechanism of pitch-angle scattering and particle precipitation from the radiation belt by ducted whistlers in the magnetosphere is also well investigated (see, e.g. [77, 78] and references therein).

Experimental indication of strong electrodynamic coupling of thunderstorms to the mesosphere and the lower ionosphere includes such phenomena as fast lightning-induced perturbations of subionospheric VLF transmitter signals propagating over the thunderstorm areas [79–84], optical emissions associated with sprites [85–91] and blue jets [92], and airglow enhancements [93] connected with

short-term (<1 ms) "elves" emissions excited at 80–95 km altitudes before sprites [65, 88, 94]. Sprites clearly associated with intense lightning discharges [95] are correlated with fast perturbations of subionospherically propagating VLF signals [82], providing an evidence of interconnection of these phenomena. An important manifestation of strong upward energy pumping from thunderstorms was obtained from the observations of gamma-ray flashes of atmospheric origin [96] associated with lightning discharges [97] and of intense bursts of broadband VHF emissions [98].

The existing generation models of the abovementioned phenomena are based on heating of the ambient electrons by electromagnetic pulses from lightning discharges [65, 99–102] or by quasielectrostatic thundercloud electric fields [103–106], and on runaway electron acceleration processes [107–109].

First registration of optical emissions stimulated by lightning has been reported by Franz et al. in ref. [110]. Later, numerous observations of similar flashes of luminescence called sprites [111] have been performed from the ground [86, 90, 91], the aircraft [92, 111–113], and space-based platforms [89,114]. The main characteristics of sprites obtained from these measurements could be summarized as follows. This phenomenon is usually observed at 50–90 km altitudes over positive cloud-to-ground lightning discharge with peak current of the order of 100 kA or above. Transverse size of luminescence area is 5–50 km; sometimes containing structural elements with a cross section of ~2 km. Sprite arises 1.5–4 ms after lightning discharge and lasts for several milliseconds. The brightness of sprites was estimated to be 25–50 kR, for most intense events it was up to 100 kR. Maximum of intensity ranges between spectral bands 650–680 nm and 750–780 nm.

Blue jets present other type of luminescence occurring at altitudes below 50 km over thunderstorm clouds. They are observed as narrowly collimated light beams of blue color propagating upward from thunderclouds with velocity ~100 km/s up to 40–50 km altitudes, where they disappear. Blue jets in contrast to sprites are not accompanied by strong electromagnetic radiation in VLF range. Observations did not display direct connection with simultaneous cloud-to-ground lightning discharges [115]. Blue jet generation theory based on accumulating charges in thundercloud and subsequent breakdown ionization and upward propagation of ionization wave has been developed by Pasko et al. in ref. [105].

Electron heating in the lower ionosphere by the thundercloud's electric field can lead to enhancement of infrared radiation, particularly to intensification of CO_2 emission at 4.3 μm wave length [116]. Different electromagnetic emissions associated with thunderstorm activity have been observed onboard the Demeter satellite [117]. The effects of ion heating and generation of plasma turbulence in the ionosphere under the influence of lightning discharges were reported by Berthelier et al. in ref. [118] based on the Demeter data.

As mentioned above, one of important mechanisms of the troposphere–ionosphere–magnetosphere coupling is lightning-induced precipitation of high energy (>40 keV) electrons from the Earth's radiation belt into the ionosphere [76, 119, 120]. Comprehensive data of satellite observations of this phenomenon were reported by Voss et al. [76], who used the low orbital (170–280 km) S81-1

polar satellite measurements of electron and ion fluxes with energies 2–1,000 keV and 10–1,500 keV, respectively. These observations were accompanied by the ground wave measurements at Palmer station in Antarctica. Analysis of numerous precipitation events associated with lightning has shown that the time delay between causative spheric and appearance of first burst of precipitating particles registered on satellite increased with L-shell according to prediction of theory [78]. The global distribution of intense precipitations of such kind correlated with thunderstorm activity distribution and displayed maximum in the depletion zone of the electron radiation belt at $2 < L < 3$. The density of electron energy flux in lightning-induced precipitations was about $\sim 10^3$ erg·cm^{-2}·s^{-1} (10^{-4} J/(m^2 s)) and particles with an energy of 100–200 keV prevailed. The most recent experimental data on electron precipitations stimulated by lightning were obtained from the Demeter satellite [121]. Bursts of 100–300 keV electrons registered within 1s after an arrival of causative VLF pulses from lightning were observed.

3.2.2 *Effects of the Ionosphere Heating by Powerful HF Transmitters*

The first successful observations of the lower ionosphere heating by electromagnetic radiation from a powerful ground-based HF (3–30 MHz) transmitter were carried out in ref. [122]. They used the experimental HF transmitter in Platteville, Colorado, 50 MW effective isotropic-radiated power, as a heater and subionospheric VLF (20 kHz) and LF (60 kHz) probe signals for detecting lower ionosphere heating by measurements of amplitude and phase perturbations in these signals. Transmissions were made at 5.1 and 7.4 MHz to heat the midday *D*-region and the diameter of the heated region at the reflection height of probe waves ($\sim$70 km) was $\sim$25 km. The heating effect in this region was obtained from the amplitude perturbation $\sim$0.53% (0.046 dB) at 60 kHz and phase perturbation $\sim 0.3^\circ$ at a frequency of 20 kHz.

Later, subionospheric VLF probe waves were used to probe *D*-region heating in the experiments by Barr et al. in refs. [123, 124] with steerable heater in Tromso (Norway) operated at the frequency of 2.759 MHz; the maximum effective radiated power was 200 MW. VLF probe waves were from the 12.1 kHz Omega navigation transmitter in Aldra, Norway, and the 16.4 kHz JXN transmitter nearby Helgeland. The heated spot was located near the end of <500 km great circle paths from the transmitters and had a form of a 27 by 34 km ellipse at 80 km height since the heating wave beam was focused on the Omega probe wave path (38° from vertical). Amplitude and phase perturbations of sub-ionospheric signals were correspondingly $\sim$0.05 dB and 0.3° during the daytime heating and up to 6 dB and 50° at night.

The heating experiment with the use of 2.8 MHz HIPAS transmitter near Fairbanks, Alaska, and 23.4 kHz probe waves from NPM transmitter in Oahu received at Fort Yukon, Alaska has demonstrated the perturbations in NPM amplitudes of -0.2 to $+0.4$ dB simultaneous with heater modulation patterns [125].

Beginning practically from earlier experiments, the lower ionosphere heating by intense modulated HF radiation in the presence of natural ionospheric electric currents (auroral electrojet and middle latitude dynamo currents) was investigated as a possible tool for the generation of electromagnetic ULF/ELF/VLF waves [1, 4, 126–131]. The generation mechanism is relatively simple. Periodic heating of the ionosphere in the current region modulates the electrical conductivity in this region and consequently causes the modulation of natural electric current. This process forms giant radiating antenna at the altitudes of 60–100 km. The generation of ULF/ELF/VLF waves by such antennas is extensively studied with the use of special high-frequency (HF) heating facilities in Tromso (Norway), Arecibo (Puerto Rico), HIPAS (High-Power Auroral Stimulation), and HAARP (High-frequency Active Auroral Research Program) (Alaska) and SURA (Russia). The most interesting results of these studies are presented below.

HF heater in Tromso operated at the frequencies from 2.7 to 8.0 MHz. A successful generation of ELF/VLF waves was carried out with the use of amplitude modulation by rectangular pulses in the frequency range 0.2–6.5 kHz. Maximum amplitudes of generated waves ~1, 0.1, and 0.03 pT were registered at the distances of 20, 200, and 500 km from the HF transmitter correspondingly [124, 126]. Successful excitation of the Earth–ionosphere waveguide and reception of artificially generated ELF/VLF signals with amplitude ~10 fT at the distance ~2,000 km has been demonstrated in several transmissions [129].

Amplitude measurements at large distances were used to estimate the power of ELF/VLF radiation from the ionosphere. Far-zone ground-based measurements have shown the amplitudes corresponding to ~1 W dipole radiation source at the altitude of maximum modulation of Hall conductivity in the ionosphere [124]. However, the satellite measurements [2] over the same heating facility have given an estimate of ~30 W for the ionospheric ELF/VLF oscillator. Different source characteristics related to simultaneous ground and satellite measurements have been also obtained in ref. [132].

Several successful experiments on ELF/VLF wave generation were carried out in Arecibo (Puerto Rico) where a powerful HF transmitter has modulated a current of the equatorial electrojet. In these experiments, the heater frequency and the radiated power were 3 MHz and ~800 kW, respectively, and the modulation frequencies were in the range from 500 to 5,000 Hz [133]. The efficiency of ionospheric ELF/VLF wave generator depending on the polarization of HF heater radiation and its daily work cycle was investigated by Ferrano in ref. [127].

High-frequency heating facility HIPAS located near Fairbanks (Alaska) was successfully used for the modulation of auroral electrojet in the experiment [134], in which the generation of ULF/ELF waves (11–76 Hz) with amplitudes ~1 pT at the phase modulation of a heater radiation has been observed. Villasenor et al. [135] have investigated the dependence of ELF/VLF wave generation efficiency on the modulation schemes of HF transmitter including the amplitude rectangular pulse modulation, phase and two frequency modulations. It was shown that the amplitude pulse modulation is most effective. ELF/VLF waves generated with the use of HIPAS heating facility have been observed in space plasma in ref. [136]. In this paper, in

contrast to similar measurements over the Tromso station [132], good correspondence between the satellite and ground-based measurements was demonstrated.

Experiments on generation of ELF/VLF waves with HAARP heating facility were carried out with use of different frequencies and polarizations of HF radiation [137]. It was shown that the possibility existed to control the polarization of artificially generated ELF waves by changing the frequency and the polarization of the heater radiation [137]. Within the framework of this Program the Stanford University has carried out a series of successful experiments on the injection of artificially excited ELF/VLF waves into the upper ionosphere and the Earth–ionosphere waveguide. Platino et al. [138] have reported the Demeter satellite observations of ELF/VLF emissions generated by HAARP heater in the ionosphere. For three of four modulation frequencies the satellite and the ground-based measurements have shown the same results corresponding to radiated power of ionospheric source ~3–4 W. Multi-hop magnetospheric echo of ELF/VLF signals induced by the HF transmitter have been observed by Inan et al. [3]. These echoes displayed dispersion and amplification in equatorial region of the magnetosphere leading to generation of trigger emissions. ELF/VLF waves excited by the HAARP heating facility were also injected into the Earth–ionosphere waveguide. Moore et al. [4] have demonstrated unique results of observations of HAARP-induced ELF emissions at the distance ~4,400 km from the heater. Characteristics of these emissions conformed to 4–32 W power of ionospheric oscillator at the altitude 75–80 km [4]. Long-term program of the experiments with HAARP HF transmitter performed by Stanford University have shown that heating of the lower ionosphere by powerful amplitude modulated HF radiation could be an effective tool for generation of ELF and VLF waves with given properties practically at any geomagnetic conditions [139].

The formation of VLF ducts (magnetic field-aligned channels of enhanced ionization) in the upper ionosphere recently detected by the Demeter satellite presents other important effect of the ionosphere HF heating. Characteristics of these ducts and other types of plasma disturbances and wave emissions observed over the heating facilities were presented in [6, 7, 140, 141]. Typical size of ducts across geomagnetic field was ~40 km at the satellite altitude and the plasma density excess within a duct over background level was 20–30%. Temperature and plasma density fluctuations in the ionosphere over the heating area were about 10–15%.

3.2.3 Influence of Powerful VLF Transmitters on the Ionosphere and the Magnetosphere

3.2.3.1 Artificially Stimulated Particle Precipitation into the Ionosphere

First experimental confirmation of artificial stimulation of radiation belt electron precipitation was obtained in 1975 by Zhulin et al. [142] with use of powerful

ground-based VLF transmitter located in Arkhangelsk region (Russia). Diagnostics of electron precipitation was performed by special optical devices installed onboard the aircraft-laboratory Yak-40. This experiment has shown significant enhancement in intensity of atmospheric emission at 557.7 nm correlated with periodic VLF transmitter pulses. Pulsations of the emission intensity were up to 40 R. An estimate of precipitating electron energy flux with account of the experiment's geometry has given $\sim$0.13 erg/cm^2·s (1.3×10^{-4} J/m^{2}s) that corresponded to flux of electrons with energy $\sim$15 keV approximately 5×10^4 particles/cm^2·s and was a factor of 10 above the background level.

Direct measurements of artificially stimulated electron precipitations from the radiation belt were carried out onboard the S81-1 satellite with use of USA VLF transmitters NAA and NSS [143–145] and independently by the Aureol-3 satellite [146, 147]. Bursts of precipitating electrons were observed by S81-1 satellite 1–2 s after commencement of the transmitter pulses [143, 144]. Similar delay followed from the theoretical estimates [145]. The most recent results on the electron precipitations stimulated by ground VLF transmitter were reported by Sauvaud et al. [148] and Gamble et al. [13], based on the Demeter satellite data.

3.2.3.2 Effects of the Ionosphere Heating by Powerful VLF Transmitters

Experiments on artificial stimulation of radiation belt electron precipitation led to discovery of the effect of lower ionosphere heating by the radiation from ground-based VLF transmitters with use of probe VLF signals [149]. First experiments were performed with NAU transmitter in Puerto Rico. About $\sim$100 kW power at 28.5 kHz were radiated by pulses of 3 s duration and 5 s repetition period. Search for lower ionosphere perturbations was carried out using probe signals from several US VLF transmitters at the receiving stations in Arecibo (Puerto Rico) and Palmer (the Antarctic). Data analysis revealed the 5 s periodicity in a spectrum of amplitude envelope of probe signals from the NAA transmitter. Perturbations of amplitude with the modulation period of heating transmitter were in the range from -0.04 to $+0.12$ dB [149]. It is interesting to note that such disturbances caused by 100 kW NAU VLF transmitter coincided in the order of magnitude with the heating effect of the Tromso HF transmitter, the effective radiated power of which was 200 MW [150]. This seeming contradiction was resolved by Taranenko et al. [151] who showed that the amplitude disturbances of probe VLF wave in the Earth–ionosphere waveguide in both cases should be comparable in magnitude since VLF heating is maximum at the reflection heights of subionospheric signals in *D*-region, and consequently the heating effect on the probe wave amplitude should be strongest there.

A series of purposeful experiments on VLF heating of the lower ionosphere was performed by Stanford University in the period from 1987 to 1992 [149]. In the experiment of 1992, the amplitude and phase perturbations of probe signals at 21.4 kHz from NSS transmitter in Annapolis (Maryland) were registered in Gander (Newfoundland). Investigated were the effects of ionosphere heating by the NAA

transmitter in Cutler (Maine) operating at 24 kHz. For monitoring measurements, the station in Gander received the NLK (24.8 kHz) and the NAU (28.5 kHz) signals whose great circle paths did not pass through the ionosphic region heated by the NAA transmitter. The ionosphere heating effect was found in 41 of 53 episodes of NAA transmitter "ON/OFF". The amplitude and phase perturbations of probe signals lie in the ranges from −0.11 to +0.84 dB and from 0 to −5.3°, respectively [152, 153]. In a similar experiment with the NLK transmitter as a heater, the observed perturbations of probe wave amplitude on the NPM (Hawaii) – Saskatoon (Saskatchewan) propagation path ranged from 0.3 to 1.6 dB [152, 153].

Strong ionospheric disturbances in the zone of powerful VLF transmitter NWC (Australia) were observed from the Demeter satellite [5]. Significant enhancement of electron temperature and fluctuations of electron and ion densities were recorded together with intensification of HF and ELF electrostatic waves. Dimension of the perturbation zone in the ionosphere at the satellite altitude (∼700 km) was about 800 km along the orbit, the position of center of this zone corresponded to L-shell of the NWC transmitter ($L = 1.41$).

Thus numerous experiments show that intense VLF waves from different sources influence on the lower ionosphere and therefore on the characteristics of radio wave propagation sensible to changes in the ionosphere parameters.

Three-dimensional (3D) theoretical modeling of the lower ionosphere heating by VLF transmitter radiation was carried out by Rodriguez and Inan [153] and Rodriguez [152]. The heated area in the ionosphere has a form of a spot with a radius of ∼150 km at the level half of the perturbation maximum. Position of maximum is slightly shifted to pole from the position of heater. For transmitters with radiated power ∼1,000 kW the electron temperature in maximum of heating (∼87 km) exceeds the undisturbed level approximately threefold.

3.2.3.3 Acceleration of Ionospheric Ions

Effect of acceleration of ions in the ionosphere under influence of radiation from ground-based VLF transmitter was first observed onboard the Aureol-3 satellite [8]. The observations were made in the zone of Arkhangelsk VLF transmitter (64° 24′N, 41° 32′E, $L = 4$), which radiated ∼300 kW power at the carrier frequency 19.1 kHz with amplitude modulation by periodic pulses (8 s ON–8 s OFF). The satellite instrumentation set provided measurements of ion distributions for $M = 1$–32 atomic mass units at energies from 0.01 to 3.5 keV/charge and pitch-angles 85° and 145° combined with analysis of electromagnetic fields in the frequency range from 10 Hz to 20 kHz.

The observations showed that a mid-latitude increase in H^+, He^+ and O^+ ion fluxes, of about an order of magnitude above the background level, at the energies 250–330 eV and pitch-angles 85° and 145° occurred in the zone, in which the transmitter signals were detected. Such quasi-transverse and upward ion fluxes with magnitude up to 10^6–10^7 $cm^{-2}{\cdot}s^{-1}{\cdot}sr^{-1}{\cdot}keV^{-1}$ were observed in five passages of the Aureol-3 satellite

over the zone of Arkhangelsk VLF transmitter. It is significant that the upward (145°) ion fluxes directed from the ionosphere into the magnetosphere were of the same order of magnitude as the quasi-transverse (85°) ion fluxes. Simultaneously with anomalous ions the VLF emission at the frequencies ~4.5 kHz well correlated with the transmitter pulses have been observed. These frequencies were close to local low hybrid resonance frequency. Let us note that the measurements were carried out in the conditions of low geomagnetic activity ($D_{st} = -10$), therefore the zone of natural auroral precipitations lied in higher latitudes.

From the discussed Aureol-3 data Dzhordzhio et al. [8] have concluded that intense electromagnetic waves radiated by ground VLF transmitter could stimulate acceleration up to 300 eV energy and injection into the magnetosphere of ionospheric O^+, He^+ , H^+ ions combined with excitation of ELF/VLF noises.

Due to high phase velocity of whistler mode waves, their interaction with supra thermal (<1 keV) ions in the ionosphere is not effective. For explanation of these experimental results, it seems reasonable to consider a two-step process – nonlinear conversion of whistler waves from the transmitter into other plasma modes and the subsequent interaction of these secondary waves with ionospheric ions. Mechanisms for transformation of waves and acceleration of ions are considered below.

Continuation of active experiments on the influence of VLF transmission on ion distributions and ELF/VLF emissions in the ionosphere has been performed by Chmyrev et al. [10]. These experiments were carried out onboard the COSMOS-1809 satellite using a Arkhangelsk VLF transmitter operated at frequencies 15 and 19.1 kHz in the same regime as above (300 kW radiated power, pulse modulation: 8 s ON–8 s OFF). The satellite was operating on the near circular orbit with altitude ~960 km and inclination 82.5°. Eight episodes of the transmitter operation were carried out during the satellite passages over the transmitter zone. Distance in longitude between the satellite trajectory and the transmitter location in these episodes was ≤30°.

Figure 3.1 shows the distribution of low-energy ion fluxes in the ionosphere over the transmitter zone obtained on the satellite orbit 1376, which was nearest to the transmitter. Each of the four panels in Fig. 3.2, which corresponds to different energy channels of electrostatic analyzer SF-3M, presents the ion fluxes for pitch-angles $\alpha = 5–40°$, 50–85°, 95–130°, 140–175°. In this episode, the transmission started at 20.30 UT when COSMOS-1809 crossed the L-shell of the transmitter ($L = 4$).

It is seen from Fig. 3.1 that effective heating of ions occurred in the ionosphere over the transmitter zone, where the flux of ions with energy 28–74 eV increased from the background level of 10^3 $cm^{-2}{\cdot}s^{-1}{\cdot}sr^{-1}{\cdot}keV^{-1}$ up to $(2–4){\cdot}10^4$ $cm^{-2}{\cdot}s^{-1}{\cdot}sr^{-1}{\cdot}keV^{-1}$ during the time smaller or of the order of 1 min. An important peculiarity of the particle distributions in Fig. 3.1 is that the downward ion fluxes were the strongest and the particles with higher energy appeared later (at higher L-shells). For precipitation and quasi-transverse fluxes, it means that particles accumulate energy at larger length or at higher altitudes along the line of magnetic field above the satellite. The characteristic transverse scale of the acceleration zone, as estimated from 28 eV ion distribution, is ~200 km at the satellite altitude ($h \approx 960$ km). The analysis

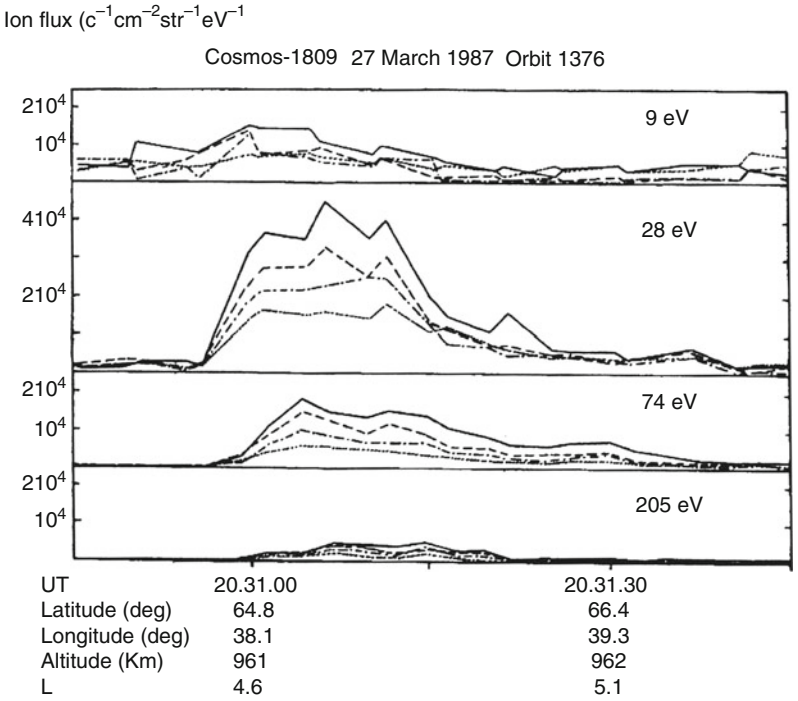

Fig. 3.1 Distribution of low energy ion fluxes along the orbit 1376 of COSMOS-1809 satellite over the Arkhangelsk VLF transmitter zone for energies ~ 9, 28, 74, and 205 eV and pitch-angles 5–40° (——), 50–85° (– – –) , 95–130° (– · –), and 140–175° (· · ·)

of energy spectrum of ions for all pitch-angles showed that the enhancement of ion fluxes in the transmitter zone took place in the range from 10 to 200 eV with maximum at 20–70 eV.

3.2.3.4 Parametric Excitation of ELF Waves in the Upper Ionosphere

Enhancement of intensity (stimulation) of ELF noises correlated with VLF transmissions was observed on three passages of COSMOS-1809 over the transmitter zone where the discussed above ion acceleration occurred [10]. Stimulated ELF emissions were found very near the transmitter (within $\pm 5°$ in longitudes and $\pm 3°$ in latitudes) in the region of maximum intensity of the transmitter signals. The spectral density of noises at the lower part ($f < 400$ Hz) of the device frequency range increased during the transmitter pulses 2–3 times above the undisturbed level observed in pauses between the pulses. A maximum of induced ELF wave intensity appeared to be at 140–180 Hz.

Spectra of VLF transmitter signals during the observation of stimulated ELF emissions at all three orbits was found to be broadened; the characteristic broadening was $\Delta f \sim \pm$ (200–400 Hz). This value corresponds to the frequency band of ELF emissions correlated with VLF transmitter pulses.

Let us note that the effect of spectral broadening of VLF signals in the ionosphere and the magnetosphere of the Earth were numerously observed from satellites and on the ground [154–157]. Titova et al. [156] interpreted this effect in terms of VLF signal scattering by low-frequency plasma turbulence (in particular the ion-cyclotron one) in the ionosphere below and/or near the satellite. At such scattering process the observed electrostatic ELF emissions were not correlated with the transmitter signals and the broadening effect took place for all transmitters independently on their power [156].

In the experiment [10] such scattering of VLF signals was also observed; ELF emissions in these cases were not correlated with transmitter pulses and the spectrum-broadening effect was registered for all VLF transmitters (independently on power) observed on satellite at the frequencies below 20 kHz. However, besides the scattering by ionospheric turbulence, the nonlinear VLF wave interaction process occurred in the experiment [10], which resulted in the generation of ELF waves and depended on the intensity of pump wave. Such conclusion was made based on the correlation between the observed ELF emissions and the transmitter signals and also from the fact that spectrum broadening in such events has been observed only for powerful signals. The latter followed from the comparison of simultaneously observed signals of the Arkhangelsk VLF transmitter (radiated power ~300 kW) at 19.1 kHz with signals from the OMEGA transmitter in Norway (radiated power ~10 kW) at 10.2 kHz.

The measurements of wave intensity in separate spectral channels showed that the propagation of a strong electromagnetic wave from a VLF transmitter through the ionosphere was accompanied by the generation of rather intense (~8 $\mu V/m \cdot Hz^{1/2}$) secondary emissions in the electric field at frequencies ~140 Hz. This emission was well correlated with the transmitter signals, while other spectral channels did not indicate any reaction on the transmitter operation. However, magnetic component of the emission at 140 Hz did not exceed the level of noise (~0.3 $pT/Hz^{1/2}$). The filter bandwidth in a channel 140 Hz of the spectrum analyzer was ~20 Hz. The ratio of magnetic-to-electric field components for the transmitter signals was $N = B/E \approx 18$ that corresponded to the refraction index of the whistler mode wave.

Thus, the presented experimental results confirm the generation of ELF waves and acceleration of ionospheric ions under the influence of strong VLF transmissions. Before considering physical mechanisms for such influence, let us resume the main characteristics of the observed phenomena:

- The excitation of ELF emissions correlating with Arkhangelsk VLF transmitter signals was observed in the frequency range 70–400 Hz with maximum intensity ~8 $\mu V/m \cdot Hz^{1/2}$ at frequencies 140–180 Hz.
- Simultaneously, with the generation of ELF emissions, the spectral broadening $\Delta f = \pm$ (200–400 Hz) was observed in Arkhangelsk transmitter signals while

broadening of weaker signals from the OMEGA transmitter in the same zone was not found.

- The enhancement of ion flux in the transmitter zone took place in the range of energies from 10 to 200 eV; maximum of flux intensity $\sim(2–4)\cdot10^4$ $cm^{-2}\cdot s^{-1}\cdot sr^{-1}\cdot eV^{-1}$ was observed at 20–70 eV.
- Accelerated ion fluxes were anisotropic; the highest anisotropy was observed at ~28 eV.

As we mentioned the interaction of low energy ($\leq$1 keV) ions with whistler waves at the transmitter frequencies and in ELF range is not effective due to high phase velocities of these waves in the ionosphere. Therefore, it was reasonable to suppose that suprathermal ions were accelerated by one of the ion branches of plasma waves, which could be excited due to parametric instability of intense whistler mode waves. In the frequency range 70–400 Hz, it could be electrostatic ion-cyclotron waves, ion-acoustic, and electromagnetic ion-cyclotron waves, the generation of which has been considered in many papers (see, e.g. [158, 159]). The highest growth rates are realized in a process of decay interaction of whistler with low frequency plasma wave and ion-cyclotron wave. Detailed analysis of the ion wave modes generation by decay instability of quasimonochromatic whistler waves with account of several types of ions and variations of ion composition with altitude in the ionosphere has been performed by Chmyrev et al. [160]. Effectiveness of decay process with participation of electromagnetic ion-cyclotron waves in the ionosphere is substantially higher than with electrostatic waves due to strong linear attenuation of latter [159]. Electromagnetic ion-cyclotron waves present one of the most effective sources of ion acceleration in the upper ionosphere [161]. With account of these circumstances Taranenko and Chmyrev [159] and Chmyrev et al. [160] suggested the following scheme for explanation of the above-discussed experimental results. Intense whistler mode wave from the ground VLF transmitter decays in the upper ionosphere on other whistler propagating near the resonance cone and highly oblique left-polarized electromagnetic ion-cyclotron wave. The ion waves propagating upward in the region of decreasing geomagnetic field will be effectively absorbed by ions providing their acceleration. This mechanism is similar to [161] with the difference that in [161] the electromagnetic ion-cyclotron waves are excited due to instability of precipitating auroral electrons while in [159, 160] – due to parametric instability of intense whistler waves. Analysis of growth rates γ_1 and frequencies ω_3 of electromagnetic ion-cyclotron waves for this process showed that excitation was possible only for waves with large transverse components of wave vectors [159]. The corresponding frequency range $\omega_3 \approx$ 100–350 Hz calculated for altitudes below 2,000 km was in agreement with the data on generation of ELF emissions and VLF wave spectra broadening. Maximum growth rate was $\gamma_1 \approx$ 2–3 s^{-1} at the amplitude of pump wave ~10 mV/m [159].

Let us consider now the interaction of parametrically excited electromagnetic ion-cyclotron waves with ions [10]. Dispersion equation for these waves as known can be written as follows:

$$\omega_3 = k_{||3} v_A (1 - {\omega_3}^2/{\omega_{Bi}}^2)(1 + \kappa^2)^{-1/2}, \ \kappa = ck_{\perp 3}/\omega_{pe}, \tag{3.1}$$

where $k_{\|3}$, $k_{\perp 3}$ are longitudinal and transverse components of wave vector, ω_{Bi} is cyclotron frequency of ions, v_{A} is Alfven velocity, c and ω_{pe} are light velocity and electron plasma frequency. Resonance energy of ions interacting with wave (3.1) at first cyclotron resonance is defined as

$$W_{//\mathrm{res}} = \frac{Mv_{//\mathrm{res}}^2}{2} = \frac{Mv_{\mathrm{A}}^2}{2}\left(1 - \frac{\omega_3^2}{\omega_{\mathrm{Bi}}^2}\right)\left(\frac{\omega_{Bi}}{\omega_3} - 1\right)^2 (1+\kappa^2)^{-1}, \tag{3.2}$$

where $v_{//\mathrm{res}} = (\omega_{\mathrm{Bi}} - \omega_3)/k_{//3}$, M is ion mass, $v_{//\mathrm{res}}$ and $k_{//3}$ are oppositely directed. Let us estimate $W_{//\mathrm{res}}$ for H^+ ions in the ionosphere at altitudes ~2,000 km, where $v_{\mathrm{A}} \approx 10^8$ cm/s. At $\kappa = 3$, which corresponds to maximum growth rate we find $W_{//\mathrm{res}} = 1.3$ eV for frequency $\omega_3/\omega_{\mathrm{Bi}} = 0.9$ and $W_{//\mathrm{res}} = 12.5$eV for frequency $\omega_3/\omega_{\mathrm{Bi}} = 0.8$.

Following ref. [161], let us estimate an effectiveness of resonance heating of ions in the conditions of the above-considered experiment [10]. We assume that some part of the geomagnetic field tube is filled by electromagnetic ion-cyclotron waves, born in the decay process, with a sufficient wide-frequency band so that in every part of the trajectory in an inhomogeneous magnetic field, the particle could find the wave, which satisfies the condition of local cyclotron resonance and therefore experiences continuous acceleration along the trajectory. The transverse energy increment of resonance ion can be written as

$$\Delta W_{\perp} = \frac{M(\Delta V_{\perp})^2}{2} = \frac{e^2 E_{\perp 3}^2}{2M}(\Delta t)^2,$$

where e and M are particle charge and mass, $E_{\perp 3}$ is transverse component of wave electric field, Δt is a time of particle being in resonance with wave. In the vicinity of resonance frequency, one may assume ${E_{\perp 3}}^2 = P(f)\Delta f$, where $P(f)$ is a spectral density of the emission and Δf is the frequency bandwidth. For the wide band wave packet, it is possible to believe the resonance time Δt to be equal to the characteristic time of phase correlation in the packet, that is, $\Delta t \sim (\Delta f)^{-1}$. Then, for the energy growth rate, we obtain [161]

$$\frac{\mathrm{d}W_{\perp}}{\mathrm{d}t} == \frac{e^2 P(f)}{2M}. \tag{3.3}$$

The movement of a particle in an inhomogeneous magnetic field $B_0(s)$ in approximation of a leading center with an account of Eq. (3.3), neglecting the geomagnetic field-aligned electric field, is described by the following equations [161]:

$$\frac{\mathrm{d}W_{\perp}}{\mathrm{d}t} = W_{\perp} v_{//} B_0^{-1} \mathrm{d}B_0/\mathrm{d}s + e^2 P(f,s)/2M, M\frac{\mathrm{d}v_{//}}{\mathrm{d}t} = -W_{\perp} B_0^{-1} \mathrm{d}B_0/\mathrm{d}s, \tag{3.4}$$

where $v_{//}$ is longitudinal velocity of particle, $W_{\perp}$ is transverse energy, and ds is an element of length. For dipole magnetic field, Eq. (3.4) has a form

$$v_{//}\frac{2dW_{\perp}}{2d\varphi} = v_{//}W_{\perp}\frac{3\ \sin\varphi(3+5\ \sin^2\varphi)}{\cos\varphi(1+3\ \sin^2\varphi)} + \frac{e^2P(f,\varphi)}{2M}LR_0\cos\varphi(1+3\ \sin^2\varphi)^{1/2},$$

$$Mv_{//}\frac{2dv_{//}}{2d\varphi} = -W_{\perp}\frac{3\ \sin\varphi(3+5\ \sin^2\varphi)}{\cos\varphi(1+3\ \sin^2\varphi)} \tag{3.5}$$

where φ is geomagnetic latitude, L is McIlwain parameter, and R_0 is the Earth's radius. When obtaining Eq. (3.5) we assumed $\mathrm{d}/\mathrm{d}t = v_{//}(\partial\varphi/\partial s)\mathrm{d}/\mathrm{d}\varphi$.

Numerical integration of Eq. (3.5) along the part of magnetic field line at $L = 4.64$, where ion acceleration took place was performed in [10]. Integration was carried out in the range of $\Delta\varphi$ from initial latitude φ_0 corresponding to altitude h at a given magnetic field line downward to final latitude $\varphi_1 = 61.3°$ corresponding to altitude 450 km. While calculating, it was assumed that electromagnetic ion-cyclotron waves were generated along a geomagnetic field line and that their intensity was constant ($\mathrm{d}P/\mathrm{d}\varphi = 0$) within $\Delta\varphi$. A resonant particle with initial parallel energy $W_{//0}$ in the point $\varphi = \varphi_o$ was moving downward. Calculations were made for H^+ ions with initial transverse energy $W_{\perp 0} = 0$ and initial parallel energies $W_{//0} = 12.5$ and 6.25 eV. Spectral density of electromagnetic ion-cyclotron waves was taken according to experimentally observed value $P = 8 \times 10^{-11}\ \mathrm{V^2\ m^{-2}Hz^{-1}}$. It was found that at this wave intensity, the particle energy increase could reach $\Delta W \approx 20$–30 eV in the interval $\Delta\varphi = 3$–$5°$, which corresponds to interval of heights $\Delta h \approx 1{,}400$–$2{,}300$ km on a given magnetic field line. Pitch-angle, with which the particle comes to satellite at the altitude ~1,000 km, depends on the altitude (or latitude $\Delta\varphi$) and on initial parallel energy, from which this particle starts acceleration. The particles accelerated at altitudes below satellite and the accelerated particles came from above and turned back in mirror points below 1,000 km provide some upward flux corresponding to pitch-angles $\alpha > \pi/2$. All these characteristics are in agreement with the experiments.

So this modeling shows that the mechanism of ion acceleration by electromagnetic ion-cyclotron waves generated by parametric instability of strong VLF waves in the ionosphere is sufficiently effective to explain existing experimental data.

The VLF transmitter described in ref. [8] started to work several hours before satellite arrival in the transmitter zone, and there was enough time for pumping the accelerated particles into the wide range of geomagnetic field tubes (life time of such accelerated particles is $\sim 10^4$ s). Experimental data from COSMOS-1809 collected at orbit 1376 allow to analyze the development of ion acceleration process in time and in altitudes along geomagnetic field lines since the transmitter located at $L = 4$ was switched on at 20.30 UT, when the satellite was practically on the same L-shell ($L = 3.9$). Thus, the accelerated ions whose velocities exceed the velocity of satellite could reach the satellite only at higher L-shells moving to it from the acceleration region, while the magnetic field tube is not completely filled by

accelerated particles. Note that the lower energy (10–200 eV) accelerated ions measured by COSMOS-1809 could be observed in a wider range of latitudes than 250–330 eV analyzed in ref. [8]. On the whole, the presented results of ion measurements onboard the COSMOS-1809 satellite do not contradict the AUREOL-3 observations [8].

Though the scientific instruments onboard the COSMOS – 1809 did not analyze mass distribution of ions, we can assume that anomalous ion fluxes observed at orbit 1376 have been accelerated in the upper ionosphere at altitudes below several thousand kilometers. At the same effectiveness and location of acceleration mechanism, the O^+ ion needs by a factor of 4 longer time to reach the satellite altitude than the H^+ ion. With account of the discussed data this means that the oxygen ions could be observed by satellite only from narrower range of altitudes near the satellite trajectory (or significantly later when satellite was far away from the transmitter). Moving downward from the acceleration region at the sufficient parallel velocity the H^+ ions started at several thousand kilometers and the O^+ ions from the lower altitudes could be able to "run down" the satellite on ascending orbit at $L > L_{\Pi}$, where L_{Π} is the transmitter L-shell.

So the presented materials can be considered as experimental evidence of the acceleration processes in the upper ionosphere initiated by electromagnetic radiation from the powerful VLF transmitter. As a confirmation of this thesis, we can mention the observation of 630 nm [OI] and H_β atmospheric emissions from the "Intercosmos-Bulgaria 1300" satellite, which demonstrated the possibility of stimulation (or intensification) of these emissions due to forming the fluxes of accelerated ions and suprathermal electrons under the influence of intense VLF waves [9].

3.2.3.5 Artificial Stimulation of Geomagnetic Pulsations

In 1975 Frazer-Smith and Cole from Stanford University first paid attention on the fact that powerful ground-based VLF transmitters influenced on the generation regime of geomagnetic pulsations [162]. They have shown that the occurrence rate and the intensity of Pc-1 oscillations increased when the VLF transmitter located near the registration site operated.

Beginning from 1975 the Institute of Terrestrial Magnetism, Ionosphere and Radio Wave Propagation of Russian Academy of Sciences (IZMIRAN) has carried out a series of active experiments on the ionosphere modification by electromagnetic radiation from VLF transmitters. Below we consider the results of these experiments related to artificial stimulation of geomagnetic pulsations.

First of these experiments called "Juliana" has been carried out in February 1975 with use of Arkhangelsk VLF transmitter operated for this experiment at the frequency 12.5 kHz in the mode of amplitude pulse modulation, 15 s ON–15 s OFF. Module magnetic measurements were carried out at IZMIRAN expedition base ~200 km away from the transmitter. Data reduction of the magnetic records with use of the epoch superposition method revealed an excitation of the magnetic field oscillations with the repetition period (30 s) of the transmitter signals and with amplitude ~16 nT

[163]. In pauses between the transmissions, no regular 30 s oscillations were observed. This observation was the first direct experimental evidence of artificial generation of geomagnetic pulsations under influence of VLF transmitter on the ionosphere and the magnetosphere.

The experiments of 1987 were also carried out with use of Arkhangelsk VLF transmitter. The radiated power was 300 kW, the carrier frequencies were 15 and 19.1 kHz, and the modulation regimes were 2 s ON–2 s OFF, 8 s ON–8 s OFF, and 50 s ON–10 s OFF. Measurements of geomagnetic pulsations were performed at Lekhta station in Karelia (Russia) and at Oulu, Kevo, and Sodankyla stations in Finland. In these experiments the ground-based geomagnetic observations were accompanied by the measurements of ELF/VLF waves and particle fluxes onboard the COSMOS-1809 satellite.

Figure 3.2 shows one of the episodes of artificial stimulation of geomagnetic oscillations [164]. In this episode the transmitter was operating in the modulation regime 8/8 during the night time in quiet geomagnetic conditions. Presented are the wave forms of *D*-component of geomagnetic pulsations recorded in Lekhta in two frequency channels (LF: 0.005–1.0 Hz and HF: 0.1–1.0 Hz) and the spectrogram of *H*-component of geomagnetic pulsations observed in Kevo. The bar near 21.00 UT in the lower part of Fig. 3.2 indicates the time interval when transmitter was active.

It is seen from Fig. 3.2 that the pulsation bursts of *Pi*-1 and *Pi*-2 types have appeared 10–15 min after beginning of transmitter operation and terminated approximately 15 min after transmitter switching off. Maximum amplitudes were ~0.1 nT (HF channel) and ~4 nT (LF channel) [164].

We already discussed the COSMOS-1809 satellite data on 9–205 eV ions observed over the transmitter zone during this episode (see Fig. 3.1). When the ground

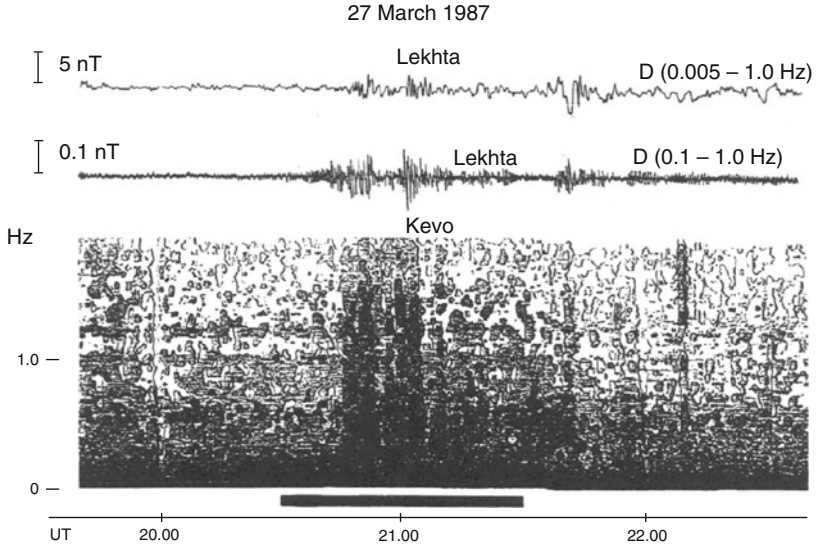

Fig. 3.2 Wave forms of the magnetic field oscillations (*D* – component) at Lekhta station and the spectrogram of geomagnetic oscillations (*H* – component) observed at Kevo station 27 March 1987

multistation measurements indicated the generation of geomagnetic oscillations, the satellite observed significant enhancement of ion fluxes with energies 9–205 eV in narrow zone $\leq 3^\circ$ above transmitter, the maximum $\sim 4 \times 10^4$ cm^{-2}s^{-1}sr^{-1}eV^{-1} was at 20–70 eV [10]. This combination of simultaneous ground and satellite observations has given a base for assumption that the generation of *Pi*-1 and *Pi*-2 geomagnetic pulsations in this case was stimulated by the VLF transmitter [164].

The characteristic time delay between the commencement of VLF transmission and the appearance of stimulated magnetic oscillations was about 10–15 min. Owing to such conjunction in observations of geomagnetic pulsations and accelerated ions it was natural to conclude that transmitter influence on the generation of magnetic oscillations was performed by means of artificially accelerated ionospheric ions carried into the magnetosphere.

VLF transmitter-induced formation of conic ion distributions and transfer of accelerated ionospheric ions (O^+, He^+, and H^+) into the magnetosphere was observed from the AUREOL-3 satellite [8] as we already discussed.

The considered experimental data have been used for the development of theoretical model of artificially stimulated geomagnetic oscillations [160, 164]. According to this model transverse acceleration of ions takes place in the upper ionosphere below 2,000 km, where the intensities of injected VLF waves and of parametrically excited ELF emissions are sufficiently high, while the generation (amplification) of geomagnetic oscillations by accelerated ions occurs in the magnetosphere (mainly in the near equator region), where the magnetic field and plasma spatial gradients are small. The time delay between the commencement of VLF wave injection and the appearance of geomagnetic pulsations is about the time needed for accelerated ions to fill up the magnetic field tube in the acceleration zone. The estimates made in refs. [160, 164] have shown that the ion fluxes observed in the discussed experiments could provide the amplification of oblique Alfven waves in the magnetosphere near $L \approx 4$ with exponential growth rate ~ 0.2 s^{-1} for frequencies ~ 5 Hz and ~ 0.05 s^{-1} for frequencies ~ 0.5 Hz. At such growth rates the stimulation of geomagnetic pulsations could be provided at the time scale of the order of several minutes.

3.3 Electric Current and Field Perturbation in the Atmosphere–Ionosphere Circuit

3.3.1 Equations Describing the Electric Potential in the Ionosphere

The below-considered electrodynamic model of electromagnetic and plasma precursors to earthquake was formulated in refs. [21, 165] to explain some of the observed phenomena by the electric field enhancement in the ionosphere over a seismically active zone. The idea of such explanations arose from the observations

of anomalous DC electric fields ~10 mV/m in the low-latitude ionosphere over a region shortly before an earthquake [45]. An existence of seismic-related electric fields and their possible role in the lithosphere–ionosphere coupling were discussed in refs. [38, 43, 166, 167]. The main conclusion made in these papers was that to excite more or less significant (≥1 mV/m) electric field in the ionosphere, the vertical component of long-term DC electric field on the Earth's surface should be ~1–10 kV/m in the area ~100 km. Such fields at the time scale about several days have never been observed. Vershinin et al. [42] reported the observation of short-time (1–2 h) bursts of the localized vertical electric field ~500 V/m 8–10 h before an earthquake. According to Buchachenko et al. [15], the meaningful ionospheric precursors should exist at least for several days. The long-time electric field variations observed before earthquakes have a magnitude ~100 V/m or less [42]. So for proper modelling, we should find the mechanism providing the generation of ~10 mV/m electric field in the ionosphere at slow variations of the vertical electric field near the Earth's surface with magnitude ~100 V/m or below.

Such mechanism based on the electric field perturbation by the conductivity currents in the atmosphere and the ionosphere was suggested in refs. [30, 168]. Their source was an external electric current generated by the injection of charged aerosols into the atmosphere with soil gases, the upward transfer of these aerosols, and their gravitational sedimentation with charge relaxation. Evidently the time scales of the external current generation and the injection of soil gases into the atmosphere should be similar.

Let us consider the generation of the electric field perturbation by an external current $\mathbf{j_e}$ in the Earth–ionosphere layer. We will find a system of equations that determine the potential φ of the electric field perturbation $\mathbf{E} = -\nabla \cdot \varphi$. Let us introduce Cartesian coordinates $(x, y, z)$with the z-axis directed vertically upward. The homogeneous magnetic field $\mathbf{B}$ is directed at epy angle of α with respect to the x-axis. The $z = 0$ plane coincides with the ideally conducting Earth's surface. We assume that the electric field potential is zero on this plane, $\phi|_{z=0} = 0$. The layer $0 < z < z_1$ is the atmosphere, whose conductivity $\sigma(z)$ depends on the altitude z. The $z = z_1$ plane coincides with the thin conducting ionosphere characterized by the integral conductivity tensor with the components Σ_P, Σ_H (the Pedersen and Hall conductivities, respectively). According to refs. [30, 168], for slow processes with characteristic times $t \gg 1/\sigma$, the distribution of the horizontal electric field components in the ionosphere is derived by the equations:

$$
\begin{aligned}
E_x(x,y) &= \frac{1}{4\pi\Sigma_P} \int_{-\infty}^{\infty} \int_{-\infty}^{\infty} K_x(x-x', y-y')\, j_1(x', y')\, \mathrm{d}x'\, \mathrm{d}y';\\
E_y(x,y) &= \frac{1}{4\pi\Sigma_P} \int_{-\infty}^{\infty} \int_{-\infty}^{\infty} K_y(x-x', y-y')\, j_1(x', y')\, \mathrm{d}x'\, \mathrm{d}y';\\
K_x(x,y) &= \frac{x \sin^3 \alpha}{x^2 \sin^2 \alpha + y^2}; \quad K_y(x,y) = \frac{y \sin \alpha}{x^2 \sin^2 \alpha + y^2}.
\end{aligned}
\tag{3.6}
$$

Equations (3.6) are used to calculate the spatial electric field distribution in the ionosphere.

3.3.2 Electric Field Limitation on the Earth's Surface

As mentioned above, the long-time (∼ several days) variations of the electric field on the ground do not exceed ∼100 V/m. Such limitation can be connected with the feedback between the vertical electric field perturbation and the causative external electric current near the Earth's surface [30]. The feedback is provided by the potential barrier at the Earth–atmosphere boundary that controls the upward moving of charged aerosol particles through this boundary. The movement occurs owing to viscosity of soil gases injected into the atmosphere. For instance, if a positively charged particle emerges from the Earth into the atmosphere, the Earth's surface gets charged negatively, and the electric field that appears, which is directed downward, impedes particle emergence to the surface. At the same time, this field stimulates the emergence of negatively charged particles onto the surface.

The vertical electric field component in the atmosphere $E_z = -\partial\varphi/\partial z$ is defined by the following equation [30]:

$$E_z(\mathbf{r},z) = \frac{1}{\sigma(z)}\left[j_1(\mathbf{r}) - j_e(\mathbf{r},z)\right]; \quad j_1(\mathbf{r}) = \int_0^{z_1} \frac{j_e(\mathbf{r},z)}{\sigma(z)}\mathrm{d}z \Big/ \int_0^{z_1} \frac{\mathrm{d}z}{\sigma(z)}. \tag{3.7}$$

We assume that an external current is formed as a result of the injection of positively (j_p) and negatively (j_n) charged soil aerosols into the atmosphere,

$$j_e(x,y,z) = j_p(x,y)s_p(z) - j_n(x,y)s_n(z); \quad s_p(z=0) = s_n(z=0) = 1.$$

The $s_p(z)$ and $s_n(z)$ functions describe the altitude distribution of external currents. Substituting the above equality into Eq. (3.7) yields an equation for the vertical electric field component on the Earth's surface, namely,

$$\begin{aligned} E_{z0}(x,y) &= \frac{1}{\sigma_0}\left[j_1(x,y) - j_p(x,y) + j_n(x,y)\right]; \\ j_1(x,y) &= \frac{1}{\rho}\left[j_p(x,y)k_p - j_n(x,y)k_n\right]. \\ E_{z0}(x,y) &= E_z(x,y,z=0); \quad \sigma_0 = \sigma(z=0); \\ k_{p,n} &= \int_0^{z_1} \mathrm{d}z \frac{s_{p,n}(z)}{\sigma(z)}; \quad \rho = \int_0^{z_1} \frac{\mathrm{d}z}{\sigma(z)} \end{aligned} \tag{3.8}$$

External currents of positively and negatively charged aerosols depend on the vertical electric field component on the Earth's surface as required by the feedback mechanism,

$$j_{\mathrm{p}}(x,y) = j_{\mathrm{p0}}(x,y) f\left(E_{z0}(x,y)/E_{\mathrm{cp}}\right); \quad j_{\mathrm{n}}(x,y) = j_{\mathrm{n0}}(x,y) f(-E_{z0}(x,y)/E_{\mathrm{cn}}),$$

where $j_{\mathrm{p0}}(x,y)$, $j_{\mathrm{n0}}(x,y)$ are determined by the intensity of charged aerosols injection in the absence of an electric field. When the negative field reaches some critical value E_{cp}, it blocks the flow of positively charged particles. Accordingly, a positive field blocks the flow of negatively charged particles. The critical field can be estimated in the order of magnitude from the balance equation for viscous, gravity, and electrostatic forces,

$$E_{\mathrm{cp}} = (6\ \pi\eta R_{\mathrm{p}} V - m_{\mathrm{p}} g)/eZ_{\mathrm{p}}; \quad E_{\mathrm{cn}} = (6\ \pi\eta R_{\mathrm{n}} V - m_{\mathrm{n}} g)/eZ_{\mathrm{n}},$$

where η is the viscosity of air, V is the velocity of upward movement of soil gases in earth, $R_{\mathrm{p,n}}$ is the aerosol particle radius, $m_{\mathrm{p,n}} = (4/3)\ \pi R_{\mathrm{p,n}}^3 \mu$ is the particle mass, and μ is the particle density. The viscous force of soil gases that rise in the Earth acts on a particle upward. The gravity force is directed downward. The electrostatic force, which appears as a result of the emergence of a positively charged particle onto the surface, is directed downward. For simplicity, we assume that positively and negatively charged aerosols have equal sizes and masses, $E_{\mathrm{cp}} = E_{\mathrm{cn}} = E_{\mathrm{c}}$. To perform calculations, let us specify the functional dependence f on the electric field as $f = \sqrt{1 + E_{z0}/E_{\mathrm{c}}}$. Using this dependence in Eq. (3.8) yields

$$E_{z0}(x,y) = \frac{1}{\sigma_0}\left[j_{\mathrm{p0}}(x,y)\left(\frac{k_{\mathrm{p}}}{\rho} - 1\right)\sqrt{1 + \frac{E_{z0}(x,y)}{E_{\mathrm{c}}}} - j_{\mathrm{n0}}(x,y)\left(\frac{k_{\mathrm{n}}}{\rho} - 1\right)\sqrt{1 - \frac{E_{z0}(x,y)}{E_{\mathrm{c}}}}\right]. \tag{3.9}$$

Given j_{p0}, j_{n0}, this equation allows us to calculate the vertical electric field component on the Earth's surface. After solving Eq. (3.9), we can determine the horizontal distribution of the conductivity current flowing from the atmosphere into the ionosphere. It follows from Eqs. (3.8) and (3.9) that

$$j_1(x,y) = \frac{1}{\rho}\left[j_{\mathrm{p0}}(x,y)\sqrt{1 + \frac{E_{z0}(x,y)}{E_{\mathrm{c}}}}k_{\mathrm{p}} - j_{\mathrm{n0}}(x,y)\sqrt{1 - \frac{E_{z0}(x,y)}{E_{\mathrm{c}}}}k_{\mathrm{n}}\right]. \tag{3.10}$$

Let us assume $\eta = 1.72 \times 10^{-7}$ kg/(cm·s), $V = 10^{-4}$ m/s, $R = 5 \times 10^{-7}$ m, $\mu = 1.5 \times 10^3$ kg/m^3, and $Z = 100$. Then the estimates of the critical field give $E_{\mathrm{c}} = 450$ V/m and $\sigma_0 E_{\mathrm{c}} = 10$ pA/m^2. It means that the vertical electric field on the Earth's surface cannot exceed the value $E_{\mathrm{zm}} = 90$ V/m.

3.3.3 Mechanisms of External Electric Current Generation in the Lower Atmosphere

Various mechanisms can be responsible for the formation of external currents in the near-ground atmospheric layer [169, 170]. One of the most effective mechanisms is associated with intensification of charged soil aerosol injection into the atmosphere or with changes in meteorological conditions at a stable altitude distribution of aerosols. It was experimentally shown [23–27] that, several days before an earthquake, the concentration of metal ion-containing soil aerosols in the atmosphere increases by one or two orders of magnitude. The quasi-stationary aerosol distribution is formed as a result of turbulent upward transfer and gravitational sedimentation. Turbulent transfer occurs due to two main reasons. First is connected with vertical gradient of horizontal wind velocity and transformation of wind kinetic energy into the energy of turbulent pulsations. Second is caused by the thermal instability of the atmosphere arising when negative temperature gradient exceeds its adiabatic gradient. Turbulent vortices transfer aerosols from the altitudes, where their concentration N is high to the altitudes of a lower concentration. Equilibrium is attained when the vertical flux of aerosols is balanced by their gravitational sedimentation at the rate w.

For describing the dynamics of particles determined by stochastic differential equations we will use the probability distribution function $f(q,z,t)$ of aerosols, which has the meaning of a probability that a particle has the charge q at the time t and the altitude z [21]. If transport coefficient K weakly depends on the altitude, the kinetic equation for the $f(q,z,t)$ distribution function takes the form [21]:

$$\frac{\partial f}{\partial t} - w\frac{\partial f}{\partial z} - 4\ \pi\sigma(z)\frac{\partial}{\partial q}(qf) = K\frac{\partial^2 f}{\partial z^2}.$$

The space–time distributions of aerosol concentration, $N(z,t)$, their electric charge density, $\rho_e(z,t)$, and the density of external current connected with their motion, $j_e(z,t)$, can be written in terms of the moments of the $f(q,z,t)$ distribution function. The equation for the moments has a form

$$\frac{\partial N}{\partial t} - w\frac{\partial N}{\partial z} = K\frac{\partial^2 N}{\partial z^2};\quad \frac{\partial \rho_e}{\partial t} + 4\ \pi\sigma(z)\rho_e = -\frac{\partial j_e}{\partial z}.$$

The last equality describes the density of external charge and current in a conducting medium. Changes in the number of external charges in a distinguished volume are determined by two processes. First, this is electromotive force-induced transfer through the surface that bounds this volume. Secondly, there is a decrease in the external charge caused by its relaxation in the environment with conductivity σ. For instance, if the total flux of external charges through the surface binding the volume becomes zero $\nabla \cdot \mathbf{j}_e = 0$, the number of these charges in the volume decreases according to the law $\rho_e \sim \exp(-4\pi\sigma t)$. The relaxation time is $\sim 1/4\pi\sigma$.

If the process is fairly fast ($t \ll 1/4\pi\sigma$), charges fail to relax, and the continuity condition takes the form $\partial\rho_e/\partial t + \nabla \cdot \mathbf{j}_e = 0$. Otherwise, if external charges are formed at a low rate ($t \gg 1/4\pi\sigma$), the external charge density is connected with the external current as $4\pi\sigma\rho_e + \nabla \cdot \mathbf{j}_e = 0$. This equality means that, in the stationary state, the disappearance of external charges in the volume due to relaxation is balanced by their transfer through the boundary surface. We assume that the characteristic time of the processes under consideration is longer than the relaxation time $1/4\ \pi\sigma$. Equation for the altitude distribution of external current in the quasi-stationary approximation can be found from the above consideration in the following form:

$$\frac{\partial}{\partial z}\left[\frac{1}{4\pi\sigma(z)}\frac{\partial j_e(z,t)}{\partial z}\right] + \frac{w}{4\pi\sigma(z)K}\frac{\partial j_e(z,t)}{\partial z} - \frac{j_e(z,t)}{K} = 0.$$

An influence of variations in conductivity and radioactivity in the lower atmosphere on DC electric field over a seismic region was investigated by Sorokin et al. [171]. This effect is associated with the occurrence of ionization source due to seismic-related emanation of radon and other radioactive elements into the atmosphere. The natural radioactivity of the lower atmosphere is mainly associated with such elements as radon, radium, thorium, actinium, and their decay products. Radioactive elements enter the atmosphere together with soil gas, and then they are transferred by the air streams upwards up to the altitude of a few kilometers. An increase in the level of atmospheric radioactivity, for example, prior to an earthquake, leads to an increase in the ion production rate q. The number density of light ions and the mean charge of aerosols are determined by recombination of ions and their adhesion to aerosols at given ionization sources. The vertical distribution of ion production rate is formed as a result of atmospheric absorption of gamma radiation and alpha particles from the decay of radioactive elements in the atmosphere. The total ion production rate in the lower atmosphere is formed by two sources – the cosmic rays and the atmospheric radioactivity. To calculate the external current and the atmosphere conductivity, it is necessary to find an equilibrium ion number density depending on the ion formation rate. The equilibrium value of ion number density is defined by their recombination in the air and adhesion to aerosols. The perturbations of conductivity and external electric current as a function of altitude have been calculated from the following equations [171]:

$$H_{p,n}\frac{d}{dz}\left(\frac{1}{\sigma}\frac{dj_{p,n}}{dz}\right) + \frac{1}{\sigma}\frac{dj_{p,n}}{dz} - \frac{j_{p,n}}{2\varepsilon_0 v_{p,n}} = 0; \quad \sigma = 2e\mu n,$$

$$n = \sqrt{N^2 + n_0^2} - N; \quad N = \frac{e\mu}{4\varepsilon_0\alpha}\left(\frac{N_p}{\lambda_p} + \frac{N_n}{\lambda_n}\right); \quad n_0 = \sqrt{\frac{q}{\alpha}}$$

where $\sigma = 2e\mu n$ is the atmospheric conductivity, n_0 is the ion number density in the clean atmosphere without aerosols, $N_{p,n}$ are the positive and negative aerosol number densities, α is the recombination constant, and μ is the light ion mobility in the atmosphere. Rapid growth of the conductivity occurs in the near surface layer.

At altitudes up to 6 km, the conductivity increases with the growth of the radioactivity level. The aerosol number density increase leads to decrease of conductivity due to loss of the light ions caused by their adhesion to aerosols. The calculations showed significant current densities at the altitude up to 12–14 km with maximum at 1–2 km. External current decreases with growth of atmospheric radioactivity.

3.3.4 Results of the Electric Field Calculation

Let us consider the electric field generation by external currents associated with the charged aerosol dynamics in the lower atmosphere. We accept the large-scale axially symmetrical external current distribution. Such distribution corresponds to vertical transport of aqueous aerosols in typhoon regions [30]. The horizontal electric field component in the ionosphere $E_r(r,\varphi) = \sqrt{E_x^2 + E_y^2}$ is calculated for various $\varphi = \arctan(y/x)$ angles, $\varphi = 0$ and corresponds to the magnetic meridian plane. The external current is induced by vertical atmospheric convection, which acts as an electrostatic generator. Air moving upward transfers small positively charged particles, whereas gravitational sedimentation transfers negative charges downward. The index of charge separation in unit cloud volume is $dQ/dt \approx 1$ C/km^{3}min $\approx 10^{-11}$ C/m^{3}s. Perhaps, the vertical convective movements in typhoon regions are characterized by smaller indices; their values are not exactly known. We assume that, at altitudes of $z_0 = 10$ km, the mean charge separation index is of $\sim 4 \times 10^{-12}$ C/m^3 s. The estimates then give the current density $j_{e0} \sim (dQ/dt)z_0 \sim 4 \times 10^{-6}$ A/m^2. It was found that the electric field component in the magnetic meridian plane is much smaller than the component in the perpendicular plane. The distribution substantially depends on the field tilt angle α. The spatial field structure has two maxima with a very small component in the magnetic meridian plane (in the center of a typhoon) for small ($<20°$) field tilt angle [30].

Seismic and volcanic activities initiate the enhanced injection of charged aerosols with soil gases into the atmosphere. These aerosol fluxes as we discussed above generate the external electric currents and related electric field perturbations. Sorokin et al. [168] have calculated the structure of such perturbations for the seismic event with axially symmetric horizontal distribution of external currents $\sim$100 km in radius. Figure 3.3 presents the distributions of a vertical component of the electric field on the Earth's surface and of the horizontal electric field component in the ionosphere. It is seen from this figure that the ionospheric field can reach the values up to 10 mV/m, whereas the vertical field component on the Earth's surface does not exceed 100 V/m. This is good illustration of the feedback mechanism for limitation of the ground electric field considered in Section 3.3.2.

The field in the ionosphere reaches a maximum at the edge of an area covered by an external current. The vertical electric field enhancement on the Earth's surface occurs in the region, which is approximately three times larger than the horizontal scale of the external current. Within this region, the field virtually does not vary with distance.

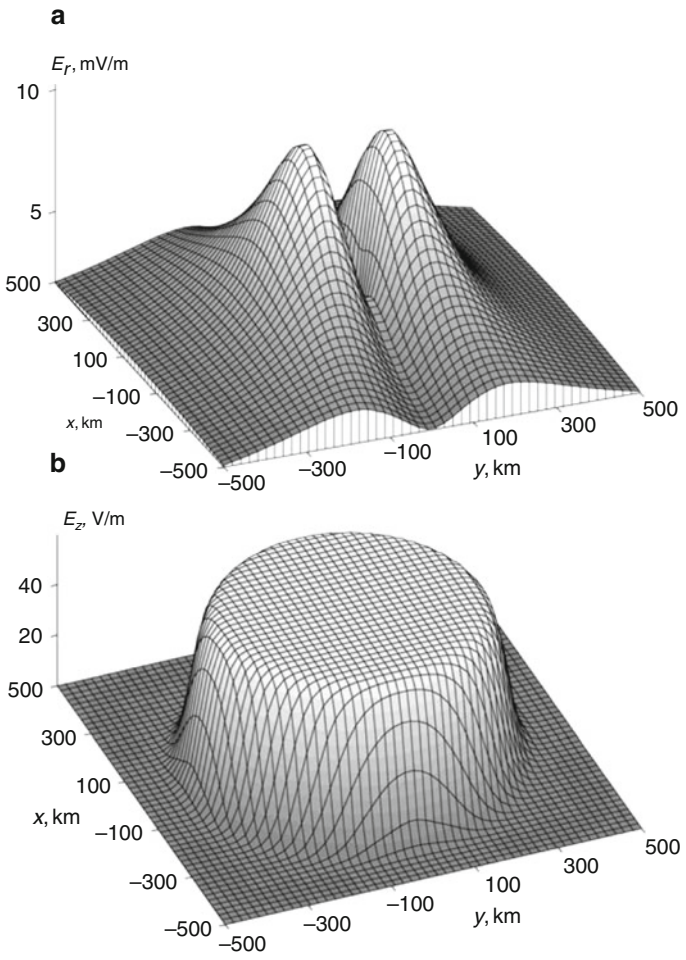

Fig. 3.3 Spatial distributions of the (**a**) horizontal electric field component in the ionosphere and (**b**) vertical field component on the Earth's surface

3.4 Plasma and Electromagnetic Effects of Seismic-Related Electric Field in the Ionosphere

3.4.1 Instability of Acoustic-Gravity Waves and the Formation of Horizontal Conductivity Inhomogeneities in the Lower Ionosphere

Growth of the electric field leads to the instability of acoustic-gravity waves in the ionosphere [172, 173]. The instability is connected with the transformation of Joule heat of the ionosphere currents into the wave energy. According to [174], the

ionosphere can be treated as a continuous medium with tensor conductivity in the low-frequency approximation. The propagation of acoustic-gravity waves in this medium is accompanied by the perturbation of conductivity and, therefore, of currents. Under certain conditions, these perturbations are sufficiently strong for Joule heat of the perturbed currents to increase an amplitude of acoustic-gravity waves. The source of energy for this instability is the electromotive force of external electric field. Field energy transforms into the energy of waves without disturbing the heat balance of the medium. Let us analyze the stability of acoustic-gravity waves in the presence of an external electric field on the assumption that the magnetic field B is directed along the z-axis, and the electric field E, along the x-axis. We shall use the equations of motion, continuity, conservation, and ideal gas state in the gravitational field g. The gas is characterized by the velocity v, density ρ, pressure p, and temperature T. We shall also use the Ohm's law for the current density j in the ionosphere.

Let us consider the horizontal propagation of a plane wave along the x-axis in a homogeneous medium, when the free fall acceleration can be neglected. We assume that the unknown values depend on the coordinates and time as $\exp(-i\omega t + ikx)$. The dispersion equation then takes the form [172]:

$$k^2 = \frac{\omega(\omega + i\omega_m)[\omega + i(\omega_m - \omega_2)]}{a^2[\omega + (\omega_m + \omega_1)]};$$
$$\omega_1 = (2\alpha + 1)(\gamma - 1)\sigma_{P0}E^2/2a^2\rho_0; \quad \omega_2 = \gamma(\gamma - 1)\sigma_{P0}E^2/2a^2\rho_0;$$
$$\omega_m = \sigma_{P0}B^2/c^2\rho_0; \quad a^2 = \gamma RT_0$$

where γ is the ratio between the specific heat capacities, R is the universal gas constant, and σ_{P0} is the Pedersen conductivity of the unperturbed ionosphere. The α coefficient characterizes the ratio between the relative changes in density of ions and gas density in the wave. The time dependence of perturbation is defined by complex frequencies. If $\omega = \omega' + i\Gamma$, where $\Gamma \ll \omega'$, one obtains $\omega' = ak$ and $\Gamma = -(\omega_m - \omega_1 - \omega_2)/2$. If $\omega_m > \omega_1 + \omega_2$, then $\Gamma < 0$, and the wave turns damp. At $\omega_1 = \omega_2 = 0$, the damping of the wave is determined by the parameter $\omega_m = \sigma_{P0}B^2/c^2\rho_0$, which characterizes induction deceleration. If $\omega_m < \omega_1 + \omega_2$, we have $\Gamma > 0$, that corresponds to instability. The equality $\omega_m = \omega_1 + \omega_2$ defines the critical field value,

$$E_k = \frac{aB}{c}\sqrt{\frac{2}{(\gamma - 1)(2\alpha + \gamma + 1)}}.$$

If the field is lower than critical, the initial perturbation fades out, and if it is higher, the wave amplification occurs. Estimation gives E_k=(7 − 8)mV/m. For the estimates we used a = 3×10^2m/s; B = 0.3Oe; c = 3×10^8m/s; $\gamma = 1.4$; $\alpha = 2$.

Let us consider the horizontal propagation of an acoustic-gravity wave (AGW) along the x-axis on the assumption that $\partial/\partial z = 0$. The dispersion equation then takes the form [172]:

$$\left(\frac{ak}{\omega}\right)^2 = \frac{(\omega + i\omega_m)\left\{\omega^2[\omega + i(\omega_m - \omega_2)] - (\omega + i\omega_m)\omega_a^2 + i\omega_2\omega_3^2\right\}}{\omega\left\{\omega^2[\omega + i(\omega_m + \omega_1)] - (\omega + i\omega_m)\omega_g^2\right\}},$$

where $\omega_a^2 = \gamma g/4H$ is the boundary acoustic frequency, $\omega_g^2 = (\gamma - 1)g/\gamma H$ is the Brunt–Vaisala frequency, and $\omega_3^2 = \omega_a^2(2\alpha + 3)/\gamma$. Let us introduce the complex refractive index $n + i\kappa = ka/\omega$. The $n = n(\omega)$ and $\kappa = \kappa(\omega)$ dependences have been calculated from this equation in the vicinity of ω_g. It appeared that the absorption coefficient is negative and has a maximum at the frequencies $\omega \sim \omega_g$. This means the instability regime, which provides the exponential growth of acoustic-gravity waves at $\omega \sim \omega_g$ and produces the periodic plasma structure. Along with density and pressure oscillations, the conductivity oscillations occur in the wave. Thus the AGW instability leads to formation of periodic horizontal inhomogeneities of the ionosphere conductivity with the characteristic scale $l \sim \lambda/2$, where λ is the wavelength at $\omega \sim \omega_g$, where the AGW growth rate is maximum. At these frequencies, the refractive index $n(\omega_g)$ reaches a maximum and the phase velocity becomes less than the velocity of sound, $v_g = a/n(\omega_g) < a$. The horizontal inhomogeneity scale is

$$l = \lambda/2 = \pi v_g/\omega_g = \pi a/\omega_g n(\omega_g). \tag{3.11}$$

Thus the enhancement of DC electric field causes the instability of acoustic-gravity waves and generation of horizontal conductivity inhomogenities in the lower ionosphere.

3.4.2 *The Formation of Longitudinal Currents and Plasma Inhomogeneities in the Upper Ionosphere and the Magnetosphere*

Horizontal conductivity inhomogeneities in the lower ionosphere change the structure of the electric fields and form the magnetic field-aligned plasma layers in the upper ionosphere [172, 173, 175]. A high conductivity along magnetic field lines results in electric field propagation into the upper ionosphere and the magnetosphere. This causes the formation of an electric circuit, which includes the longitudinal currents in the magnetosphere that transfer the electric field along geomagnetic field lines and the transverse closure currents provided by Pedersen conductivity in the ionosphere. Note that the longitudinal currents are carried by electrons, whereas ions are transverse current carriers. Therefore, the electric field propagation along geomagnetic field lines and the formation of closure currents should be accompanied by local changes in plasma density. Thus, the alternation of ionospheric E-layer conductivity in the presence of an external electric field results

in the appearance of a polarization electric field. The upward propagation of this field causes the changes in plasma density structure in the upper ionosphere. Let us estimate this effect.

Although an acoustic-gravity wave propagates along the x-axis, the conductivity inhomogeneities associated with AGW instability are extended along the y-axis. We assume that the electric field $\mathbf{E}_0$ lies in the (x, y) plane and the magnetic field $\mathbf{B}$ is directed along the z-axis. When a conductivity inhomogeneity with the amplitude $\Delta\sigma_{P,H}$ moves in the E-layer of the ionosphere as an isolated band of width $l \sim \lambda/2$ extending along the y-axis, the plasma inhomogeneity extending along the magnetic field is formed in the upper ionosphere [176]. The band moves along the x-axis with the AGW velocity $v_g = a/n(\omega_g, \omega_1)$. The magnetosphere is characterized by the Alfven velocity v_a or wave integral conductivity $\Sigma_w = c^2/4\pi v_a$. The formation of the conducting band in E-layer results in the occurrence of a polarization electric field $\Delta\mathbf{E}$, which is transferred along geomagnetic field lines into the upper ionosphere and changes the plasma density in this region. The relative magnitude of this change can be found from the equation [172]

$$\frac{N}{N_0} = \frac{1 + D_1 - v_g/v_{ex}}{1 + D_2 - v_g/v_{ex}};$$

$$D_1 = \frac{v_i E_{x0}}{\omega_i E_{y0}}; \quad D_2 = \frac{v_i}{\omega_i} \frac{(\Sigma_{P0} + \Sigma_w)E_{x0} + (\Sigma_H - \Sigma_{H0})E_{y0}}{(\Sigma_P + \Sigma_w)E_{y0}},$$

where N and N_0 are the equilibrium densities of ions inside and outside the band, $v_{ex} = -cE_{y0}/B$ is the particle drift velocity, v_g is the horizontal velocity of band movement along the x-axis, Σ_P and Σ_H are the integral conductivities of the lower ionosphere, and v_i is the ion collisions frequency. We assume that the electric field is directed along the x-axis ($E_{y0} = 0$). The equality $\Sigma_P = \Sigma_w$ holds to a fairly high accuracy in the ionosphere. If $\Delta\Sigma_P/\Sigma_{P0} = \Delta\sigma_P/\sigma_{P0}$ and $v_i cE_{x0}/\omega_i v_g B \ll 1$, the change in plasma density $\Delta N = N - N_0$ can be estimated from the equation

$$\frac{\Delta N}{N_0} = \frac{\Delta\sigma_P v_i cE_{x0}}{\sigma_{P0}\omega_i v_g B(2 + \Delta\sigma_P/\sigma_{P0})} \approx \frac{v_i cn(\omega_g)E_{x0}}{2\omega_i aB}.$$

The altitude dependence of $\Delta N/N_0$ is described by the function $v_i = v_i(z)$. Thus the appearance of horizontal inhomogeneities in the lower ionosphere conductivity results in the formation of plasma layers extended along the geomagnetic field. The transverse size of these layers coincides with the scale of horizontal spatial structure of conductivity.

3.4.3 Electromagnetic Perturbations in ULF/ELF Ranges

As mentioned above, satellite data on intensification of extremely low-frequency (ELF) radiation over earthquake region were reported repeatedly. Several

mechanisms of the generation of such radiation have been discussed during the past years (e.g., see [177]). Calculations showed that these mechanisms produced much weaker effects than those observed experimentally over the spectral range covering several hundred hertz. A new mechanism based on the transformation of atmospheric ELF noise on the small-scale inhomogeneities in the ionosphere was proposed by [36]. This pulse electromagnetic noise is generated by lightning and always exists in the Earth–ionosphere waveguide. The excitation of small-scale plasma inhomogeneities in the ionosphere before earthquake was experimentally confirmed [32] and explained by AGW instability in the presence of an overcritical DC electric field [172, 173].

Let us consider the mechanism suggested by Borisov et al. [36]. The lowest eigenmode of subionosphere waveguide (the TM mode) has the weakest attenuation at frequencies below 1 kHz and can therefore propagate through large distances. Because of the high conductivity of the Earth near the surface, the electric field of this mode is directed vertically. A horizontal electric field component appears as the altitude increases. Its value approaches the amplitude of the vertical component over the spectral range 100–1,000 Hz at altitudes of 115–120 km, at which the conductivity of the ionosphere is maximum. Horizontal components of the electric field pulses from lightning discharges induce polarization currents on the conductivity inhomogeneities. The radiation from these currents, which depends on frequency, propagates in a whistler mode upward into the upper ionosphere and the magnetosphere. Satellite should observe this radiation at the same geomagnetic field lines where plasma density inhomogenities are observed. The spectral characteristics and the intensity of this radiation were found to be near the experimentally observed values [32].

Generation of small-scale plasma density irregularities in the ionosphere over seismic zone, and the effects of these irregularities upon characteristics of very low-frequency transmitter signals propagated through these disturbances and then registered onboard a satellite were analyzed in [178]. The main effect is in observable spectral broadening of signals. The calculations showed two characteristic spatial scales of plasma density irregularities across the magnetic field. The first is 4–40 km, which has been confirmed by satellite observations, and the second is of the order or less than 100 m [18]. These smaller-size irregularities produce noticeable effect in very low-frequency signal spectral broadening, which is most pronounced when the transmitter frequency is above, but close to the local low-hybrid resonance frequency in the region where the small scale irregularities are present, which in turn sets the requirement that the transmitter frequency be in the range from 10 to 20 kHz. This corresponds to operational band of most VLF transmitters. For the 100 m irregularities, we get the spectral broadening $\sim$100 Hz that can easily be registered by simple very low-frequency receiver onboard a satellite, provided the transmitter power is high enough. This effect together with the direct satellite measurements of plasma density variations can be used as an effective tool for diagnostics of seismic-related ionospheric disturbances and therefore considered as a possible ionospheric precursor to earthquake.

The observations of ultra low-frequency electromagnetic noises in the vicinity of a forthcoming earthquake area were reported in several papers

(e.g., see [177, 179–181]). In particular, Frazer-Smith in ref. [179] have observed ULF oscillations in the frequency band 0.01–5 Hz approximately 10 days before a strong earthquake at a distance ∼50 km from the epicentre. Fitterman [56], Molchanov et al. [55], and Pilipenko et al. [57] considered a source of this phenomenon to be located in the lithosphere. An alternative ionospheric mechanism for the generation of ULF magnetic field oscillations based on excitation of gyrotropic waves (GW) was presented in refs. [182, 183].

Gyrotropic waves earlier observed by Sorokin and Fedorovich [59] propagate within a thin layer of the lower ionosphere in low and medium latitudes with weak attenuation at phase velocities from tens to hundreds of kilometers per second.

Some geophysical effects related to the generation and propagation of GW in the horizontally homogeneous ionosphere were considered in refs. [184, 185]. A comprehensive theory of these waves in the mid-latitude ionosphere was developed by Sorokin and Pokhotelov [186].

Let us consider the generation mechanism for gyrotropic waves suggested in ref. [183] where the key role, as for ELF radiation, belongs to ionospheric inhomogeneities. This mechanism involves the generation of GW in the lower ionosphere by the interaction of electromagnetic noises with periodic horizontal inhomogeneities of electrical conductivity excited by the acoustic-gravity wave instability in the presence of an overcritical DC electric field. Polarization current excited on such periodic structure forms the distributed source of gyrotropic waves with horizontal spatial scale ∼10 km. These waves propagated along the ionospheric E-layer produce the magnetic field oscillations that can be observed on the ground in the frequency band ∼1–10 Hz.

The ground-based measurements yielded the detection of discrete narrow-band spectra of ULF magnetic field oscillations during seismic enhancements, volcanic eruptions, and space shuttle launches and landing [187]. It was found that the spectrum maxima in these oscillations are located at separate frequencies of ∼2, 6, 11, and 17 Hz. An attempt to explain such discrete structure in terms of gyrotropic waves was undertaken by Sorokin and Hayakawa [188] who have analyzed the generation and propagation of GW in the conducting layer of a finite thickness in the lower ionosphere in the presence of conductivity inhomogeneities. Discrete spectrum containing several lines was obtained; the position of lines depended on the thickness of the layer with Hall conductivity. The width of those spectral lines was defined by width of a spatial spectrum of ionosphere irregularities and the ratio between Pedersen and Hall conductivities. The attenuation was determined by Pedersen conductivity and a number of frequency lines depended on the dimension of source region. For instance, if conductivity irregularities with a size of ∼80 km in horizontal direction are distributed within the ionospheric region over seismic area, then the spectrum of excited pulsations consists of six spectral lines in the frequency range 1–30 Hz. Amplitude of magnetic oscillations is defined by the intensity of ionosphere irregularities, their spatial structure, and by the wave attenuation.

Irregularities of the ionosphere conductivity can influence on the propagation of ULF waves excited in the magnetosphere through the ionosphere. In ref. [189],

Sorokin et al. have shown that such irregularities could produce the screening effect on the geomagnetic pulsations penetrating through the ionosphere and decrease the amplitude of the oscillations observed on the Earth's surface. This effect should take place during night time and be more significant for higher frequencies [189].

3.4.4 *Perturbation of the Ionosphere*

The heat flux emitted by a thin conducting layer of the ionosphere in the horizontal electric field is $\sim(10^{-4} \sim 10^{-3})$ W/m^2. One of the main sources of the ionosphere heating is short-wave solar radiation ($\lambda < 102.6$ nm). The supply of heat caused by the absorption of this radiation at altitudes above 100 km is approximately several, $10^{-3}\mathrm{W}/\mathrm{m}^2$. Depending on the solar cycle, it changes several times in either direction. An estimate made in ref. [190] shows that the Joule heat of ionospheric currents over the earthquake preparation region constitutes a substantial fraction of the total heat balance of the ionosphere. Evidently this source of heat has determining action on the state of the ionosphere. Heating the ionosphere by currents increases the scale of altitude distribution of ionospheric components and, therefore, the altitude profile of $F2$ layer. Apart from the other possible mechanisms, this heating mechanism should contribute to the observed ionosphere response on the earthquake preparation processes [190]. The ionosphere is isothermal at altitudes exceeding 200 km, and there is a positive temperature gradient over the altitude range 100–200 km. Owing to heat conductivity, the presence of the temperature gradient generates a heat flux directed downward. The Joule heat source is localized in the lower ionosphere at 120–150 km. The upper ionosphere heating can then occur only if gases move in the vertical direction. Changes in the altitude distribution of ionization in the ionosphere at a given spatial inhomogeneity of the electric field on the ground were considered in ref. [191]. They assumed that the ionosphere modification was caused by plasma drift.

An increase of the electric field and current in the lower ionosphere over a seismic region leads to additional release of Joule heat that produces additional vertical flux of neutral particles and changes the ionosphere temperature [190]. Such mechanism of effecting the formation of F2 layer is realized through collisions between ions and neutral particles and an increase in the vertical scale of their altitude distribution. The modelling of seismic-related modification of the ionosphere F region performed by Sorokin and Chmyrev [190] with use of some simplifying assumptions [192] showed that heat release in the lower ionosphere increases the height of F layer maximum and decreases the concentration of electrons at this height. The altitude profiles of ion densities are also modified towards the increase in density above F layer maximum.

Along with the rearrangement of the altitude profile of plasma density in the upper ionosphere above a seismically active region, the formation of sporadic layers in the lower ionosphere has been observed [193, 194]. The critical frequency

of the sporadic E layer, f_0E_s, reached 8 $\sim$ 9 MHz in daytime. This value corresponds to a number density of electrons $\sim 10^6$ cm^{-3}. High-altitude rocket measurements in the medium-latitude ionosphere showed that electron number density in the sporadic layer was 2×10^5 cm^{-3}, and the electric field in this layer reached 10 mV/m [195]. A model of the formation of an anomalous sporadic E layer based on the effect of atmospheric electric current flowing into the ionosphere was considered in ref. [196]. This current initiates the occurrence of a longitudinal current, which flows from the ionosphere into the magnetosphere, and transverse closure current, which flows in the conducting ionosphere layer. The atmospheric current transfers ions into the ionosphere, and the longitudinal current, which balances electric charge, transfers electrons into the ionosphere. As a result, plasma density in the lower ionosphere increases [196]. The presence of metal ions in the lower ionosphere causes the appearance of a thin ($\sim$3 km) layer of enhanced electron concentration when electric current flows into the ionosphere. This layer could be recorded as a sporadic E layer.

3.4.5 Electrodynamic Model of the Atmosphere and the Ionosphere Coupling

According to the electrodynamic model [21], an enhancement of a DC electric field in the ionosphere can be caused by an increase in conductivity of the lower atmosphere due to the intense outbursts of radioactive substance from a seismic source at the preparatory stage of earthquake. Such outbursts were repeatedly observed several days or weeks before earthquake. The time dependence of radon concentration in soil gases and in natural water was investigated by Virk and Singh [25]. An intense radon burst was registered approximately a week before the earthquake. The concentration of radon then increased by factors of 2.5 and above 1.5 in gases and water, respectively. Measurements were taken at a distance of 300 km from the epicenter. According to ref. [26], the concentration of radon increased approximately fourfold 5 days prior to an earthquake. The statistical analysis of the data obtained during 3 years of observations for about 300 micro earthquakes ($M < 4$) in south-east Germany shows that 75% of the earthquakes were preceded by a substantial increase in the concentration of radon. It can be suggested that, simultaneously with radon, other radioactive elements are injected into the atmosphere. In addition, such injections should not necessarily be related to radon. The seismic-related increase in the concentration of soil aerosols containing metal ions in the atmosphere was reported in several papers (e.g., see [23, 43].

According to the considered model [21] these injection processes are responsible for the formation of external currents and enhancement of electrical conductivity in the lower atmosphere that causes an increase in the electric field in the ionosphere, as it is shown in Fig. 3.4.

Such approach finds support in the data obtained in [197] after the Chernobyl accident. It was found that intense injections of radioactive substances into the atmosphere were accompanied by changes in the phase and amplitude of VLF signals along the propagation path crossing the accident area. The VLF signal alternations were connected with the localized lower ionosphere perturbation, which could be caused by the electric field growth in this region [198].

According to modeling [21], changes in the electrophysical parameters of the lower atmosphere lead to amplification of the electric field in the ionosphere and stimulate several effects observed experimentally. As an example, we can mention the satellite observations reported in refs. [32, 40]. The data on ULF magnetic field oscillations over the frequency range (1–8) Hz and on the vertical DC electric field component obtained onboard the "Intercosmos-Bulgaria 1300" satellite 15 min before the earthquake of 01.12.1982 were discussed in ref. [40]. An increase in the electric field $\sim$ (3–7) mV/m and the appearance of ULF magnetic field oscillations with an amplitude of 3 nT were observed in two regions: above the epicenter and in the magnetically conjugated zone. COSMOS-1809 satellite measurements over Spitak earthquake region showed that intense ELF radiation was generated over the longitude range $\leq 6^\circ$ and latitude range $2\sim4^\circ$ about the epicenter [32]. The intensity of radiation was about 10 pT at the frequencies $\sim$140 Hz (in the band

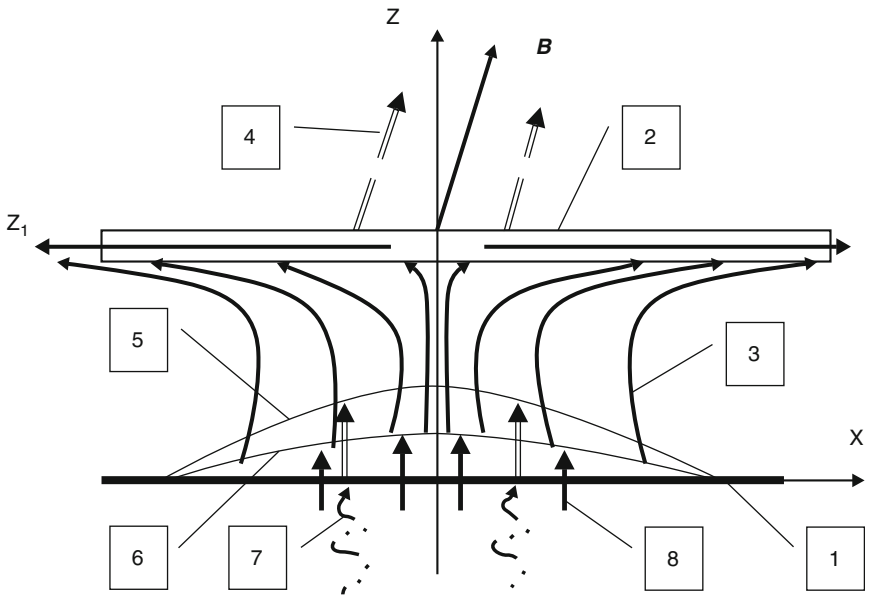

Fig. 3.4 Scheme of the model used for calculations of electric field in the atmosphere–ionosphere circuit. 1 – Earth's surface, 2 – ionosphere, 3 – conducting current in the atmosphere and the ionosphere, 4 – field aligned current, 5 – zone of upward convection of charged aerosols and external electric current formation, 6 – zone of perturbation of atmospheric conductivity induced by radioactive elements emanation, 7 – charged aerosols moving upward with soil gases, 8 – radioactive elements emanation

~25 Hz) and about 3 pT at 450 Hz(in the band ~75 Hz). In the same region, small-scale (4–10 km along the orbit) plasma density inhomogeneities with the relative amplitude (3~7)% were observed. An existence of plasma density perturbations above seismically active regions was confirmed in ref. [45].

As discussed, an increase in the ionosphere electric field above the earthquake preparation region results in the instability of acoustic-gravity waves [172, 173]. The development of this instability is accompanied by the generation of horizontal inhomogeneities in the ionosphere conductivity, whose interaction with the electric field in the ionosphere works as a source for the radiation of guided Alfven waves into the magnetosphere. These waves form the field-aligned electric currents and plasma layers extended along the geomagnetic field. The transverse spatial size of these layers coincides with the scale of the horizontal spatial structure of conductivity. Let us consider numerical estimates. At an altitude of ~1,000 km, the summed frequency of ion collisions with ions and molecules is $\nu_i \sim 0.5\ s^{-1}$ [199], and the gyrofrequency of ions is $\omega_i \sim 30\ s^{-1}$. For the velocity of sound $a = 3 \times 10^2 m/c$, perturbed electric field value $E \approx 9 mV/m$, refractive index $n \approx (1 \sim 10$ and $\omega_g \approx 2 \times 10^{-2} s^{-1}$, we obtain:

$$l = \pi a/\omega_g n(\omega_g) \approx (4 \sim 40)\ \text{km}; \quad \Delta N/N \approx (1.6 \sim 16)\%.$$

When a satellite moving at the velocity $v_s \approx 8$ km/s crosses plasma inhomogeneities of horizontal scale $l \approx (4 \sim 40)$ km, plasma density fluctuations with the period $\Delta t = l/v_s = \pi a/v_s\ \omega_g n(\omega_g) \approx (0.4 \sim 4)$ s should be observed. Since these inhomogeneities are formed by field-aligned currents, geomagnetic oscillations with the same period should be recorded when satellite crosses these currents. Their amplitude is found to be $b \sim 5$ nT. This estimate is in agreement with the satellite measurements. A scheme of such measurements is illustrated by Fig. 3.5.

Geomagnetic oscillations observed on the Earth's surface before earthquakes are interpreted in frame of the discussed model [21] in terms of gyrotropic waves (GW). These waves are connected with polarization currents associated with the horizontal inhomogeneities of conductivity and their interaction with the background electric field.

This interaction generates GW, which propagate in the horizontal direction and form geomagnetic oscillations in ULF range on the Earth's surface [182, 183]. The normalized spectrum of geomagnetic oscillations has the intensity maximum ~40% of the unperturbed (background) value and lies in ULF range. The spectral maximum frequency decreases as the horizontal scale of inhomogeneities increase. The amplitude of perturbation decreases with a distance from epicenter due to attenuation of gyrotropic waves.

According to a mechanism of electromagnetic ELF precursors to earthquakes [36], the enhanced ELF emission in the upper ionosphere arises when pulsed electromagnetic radiation from lightning discharges propagating in the Earth–ionosphere waveguide is scattered by lower ionosphere conductivity inhomogeneities over earthquake region. Intensities of lightning-induced whistler mode waves in the upper ionosphere vary substantially depending on lightning activity. The modeling

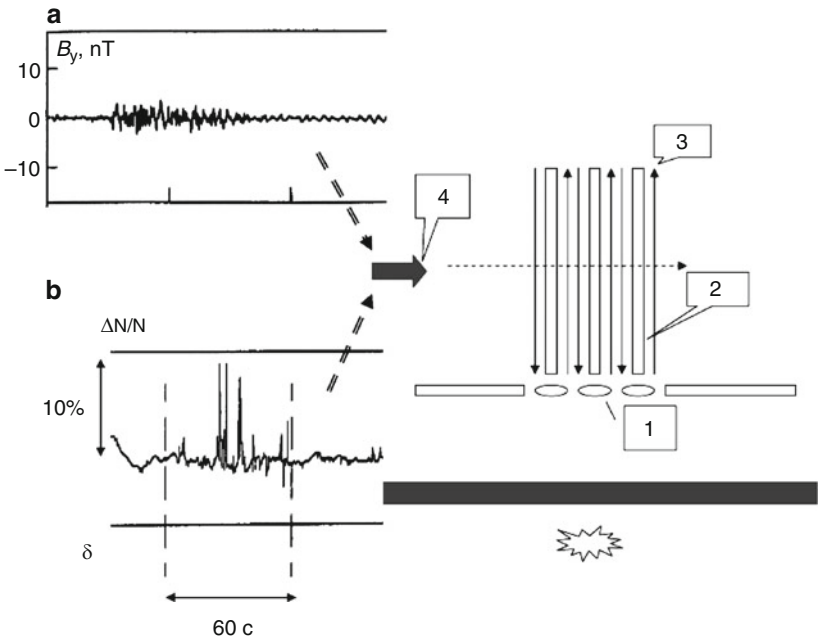

Fig. 3.5 Scheme of satellite observations of (**a**) ultralow-frequency geomagnetic field oscillations and (**b**) plasma density inhomogeneities. 1 – Horizontal ionosphere conductivity inhomogeneities, 2 – plasma density inhomogeneities stretched along the geomagnetic field, 3 – field aligned electric currents, and 4 – satellite

yields the maximum of magnetic field amplitude of ELF emission borne in this scattering process of the order of $b \approx (1 \sim 2)$ pT over the frequency range $(200 \sim 500)$ Hz. These characteristics are in agreement with the experimental data [31, 32, 200].

The estimates of the characteristic transverse size (∼10 km) and the magnitude of plasma layer density inhomogeneities obtained earlier have allowed to suppose that small-scale plasma structures excited this way could play a role of ducts or waveguides that canalized whistler mode waves along the geomagnetic field [201]. An appearance of such structures in the ionosphere above the epicenter region could increase the probability of the emergence of magnetospheric whistlers into the Earth–ionosphere waveguide and change the dispersion characteristics of signals recorded on the Earth's surface. An influence of seismic activity on the parameters of magnetospheric whistlers was reported in ref. [202]. The statistical analysis carried out demonstrated the unusual changes in mid-latitude whistler characteristics, such as an increase in the dispersion and the occurrence rate, associated with enhancement of seismic activity. Hayakawa et al. [202] discussed the possible mechanisms of such influence. In particular, they considered the seismic effect on the wave trapping in duct (or excitation of duct) at its entrance and the enhanced occurrence of ducts in the ionosphere disturbed by the acoustic or internal gravity

waves generated by earthquakes. This idea was experimentally confirmed by satellite observations of small-scale plasma density irregularities and correlated ELF emissions over the seismic zone [32].

At the preparatory stage of earthquake, large-scale changes in the ionosphere parameters were observed several days before the main seismic shock using the topside ionosphere sounding from the INTERCOSMOS-19 satellite [43]. It was shown that the altitude of F2 layer maximum increased from approximately 280 to 360 km, and the maximum electron density decreased from 3×10^5 to 10^5 cm^{-3} 1 day before the earthquake.

It was shown in Section 3.4.4 that an enhancement of the electric field and related release of Joule heat in the lower ionosphere increased the temperature and the upward mass flux in the upper ionosphere. This modifies the diffusion process that forms ionospheric F layer and changes its characteristics [190]. Let us estimate the energy flux and the temperature variation in the ionosphere caused by electric field enhancement. Assuming that the heat flux produced by solar radiation is $q_0 = 10^{-3}\mathrm{W}/\mathrm{m}^2$, and the integral Pedersen conductivity and the ionosphere electric field value to be equal to $\Sigma_\mathrm{P} \approx 10\ \Omega^{-1}$ and $E_0 \approx 3\mathrm{mV}/\mathrm{m}$, respectively, we obtain the heat flux $q = 10^{-3}\mathrm{W}/\mathrm{m}^2$. Such a flux will heat the ionosphere up to the temperature $T \approx 1,400$ K. If above the region of preparing earthquake the electric field was increased by the quantity ~6 mV/m, as observed in ref. [40], it results in the thermal flux $q = 2\ \times 10^{-3}\mathrm{W}/\mathrm{m}^2$and in the ionosphere temperature growth up to $T \approx 2{,}100$ K. This in turn leads to an elevation of the F-layer and a decrease of the maximum electron and ion densities in the layer [190] as it was observed from the INTERCOSMOS-19 satellite [43].

The other observable characteristics of the seismic-related ionosphere disturbances are ion composition and the density of the light ions. It was shown that in a near-earthquake zone during the earthquake preparation processes the H^+ and He^+ ion densities in the ionosphere increased by about a factor of 3 [44]. The modeling [190] has shown that the relative increase of the ion density (including the light ions) at altitudes 700–1,000 km could be six- to eightfold at the electric field enhancement in the ionosphere by the quantity ~6 mV/m.

In conclusion, we note that the electrodynamic model of the atmosphere and the ionosphere coupling [21] is applicable to the interpretation of some effects produced in the ionosphere by tropical storms and typhoons [29, 30, 203, 204].

3.5 Conclusions

Experimental studies and theoretical modeling show that the ionosphere is influenced by many processes, which are developed on the ground, in the lower atmosphere and in the stratosphere. This influence provides the ionosphere response to such phenomena as earthquakes, volcano eruptions, typhoons, some types of technogenic disasters, etc. The mechanisms of influencing include a set of rather complicated chemical, electrophysical, hydrodynamic and electromagnetic processes in the

atmosphere that accompany the development of these phenomena. The most comprehensive model of the atmosphere and the ionosphere coupling [21], which is presented above describes the complete causal-sequence chain of seismic-induced processes beginning from modification of the lower atmosphere state to excitation of the plasma density variations, the geomagnetic field-aligned currents and ULF/ELF emissions in the ionosphere, an elevation of the F-layer maximum, a decrease of electron density in the maximum of this layer, and a growth of light ion density in the upper ionosphere. The lower atmosphere modification is produced by the injection and turbulent transfer of charged aerosols and radioactive substances, which lead to the formation of external electric current in the atmosphere, changes in the Earth–-ionosphere electric circuit, an enhancement of DC electric field in the lower ionosphere, and related development of acoustic-gravity wave instability responsible for generation of the plasma density and electric conductivity inhomogeneities. The scattering of electromagnetic radiation from lightning by these inhomogeneities produces additional ELF wave flux observed over an earthquake area in the upper ionosphere together with plasma density irregularities.

Two other noticeable effects of the lower ionosphere modification by DC electric field enhancement are the amplitude and phase perturbations of subionospheric VLF signals and the generation of narrow band gyrotropic waves that can be observed on the Earth surface as ULF geomagnetic oscillations.

An intensified inflow of atmospheric conductivity current into the ionosphere changes the plasma density distribution in the lower ionosphere and causes the formation of an anomalous sporadic E-layer.

Let us note that the considered model is applicable to interpretation of some effects produced on the ionosphere by intense atmospheric disturbances connected with tropical storms, typhoons, etc.

In spite of definite progress in experimental studies of man-made and natural effects on the ionosphere, there is significant gap in the understanding of an origin and interconnection of many processes involved in the lithosphere–atmosphere–ionosphere coupling. The way of filing this gap is the development and implementation of long-term international research program based on coordinated observations from the ground networks, aviation, and satellite platforms of all the processes occurred in different layers of near-Earth space in association with catastrophic natural phenomena such as earthquakes, volcano eruptions, typhoons, etc.

References

1. Getmantsev, C.G., Zuikov, N.A., Kotik, D.S., Mironenko, L.F., Mityakov, N.A., Rapoport, V.O., Sazonov, Y.A., Trakhtengerts, V.Y., Eidman, V.Y.: Combination frequencies in the interaction between high-power short-wave radiation and ionospheric plasma. JETP Lett. **20**, 101–112 (1974)
2. James, H., Inan, U.S., Rietveld, M.T.: Observation on the DE-1 spacecraft of ELF/VLF waves generated by an ionospheric heater. J. Geophys. Res. **95**, 12187 (1990)

3. Inan, U.S., Golkowski, M., Carpenter, D.L., Reddell, N., Moore, R.C., Bell, T.F., Paschal, E., Kossey, P., Kennedy, E., Meth, S.Z.: Multi-hop whistler-mode ELF/VLF signals and triggered emissions excited by the HAARP HF heater. Geophys. Res. Lett. **31**, L24805 (2004)
4. Moore, R.C., Inan, U.S., Bell, T.F., Kennedy, E.J.: ELF waves generated by modulated HF heating of the auroral electrojet and observed at a ground distance of 4400 km. J. Geophys. Res. **112**, A05309 (2007). doi:10.1029/2006JA012063
5. Parrot, M., Sauvaud, J.A., Berthelier, J.J., Lebreton, J.P.: First in-situ observations of strong ionospheric perturbations generated by powerful VLF transmitter. Geophys. Res. Lett. **34**, L11111 (2007). doi:10.1029/2007GL029368
6. Frolov, V., Rapoport, V., Komrakov, G., Belov, A., Markov, G., Parrot, M., Rauch, J., Mishin, E.: Density ducts formed by heating the Earth's ionosphere with high-power HF transmitter. JETP Lett. **88**, 790–794 (2008)
7. Milikh, G.M., Papadopoulos, K., Shroff, H., Chang, C.L., Wallace, T., Mishin, E.V., Parrot, M., Berthelier, J.J.: Formation of artificial ionospheric ducts. Geophys. Res. Lett. **35**, L17104 (2008). doi:10.1029/2008GL034630
8. Dzhordzhio, N.V., Mogilevskii, M.M., Chmyrev, V.M., Kovrazhkin, R.A., Molchanov, O.A., Galperin, YuI, Boske, J.M., Roche, J.L.: Acceleration of ions in the plasma environment of the Earth by the radiation from a low-frequency transmitter on the ground. JETP Lett. **46**, 405–409 (1987)
9. Chmyrev, V.M., Kuzmin, A.K., Lazarev, V.I., Isaev, N.V., Bilichenko, S.V., Taranenko, YuN, Teltsov, M.V., Teodosiev, D.K.: Correlation of stable red arcs and H_β emissions with ion fluxes, electric fields and VLF radiation. Geom. Aeron. **28**, 813–819 (1988)
10. Chmyrev, V.M., Mogilevsky, M.M., Molchanov, O.A., Sobolev, Ya.P., Titova, E.E., Yakhnina, T.A., Suncheleev, R.N., Gladyshev, V.A., Baranets, N.V., Dzhordzhio, N.V., Galperin, Yu.I., Streltsov, A.V.: Parametric excitation of ELF waves and acceleration of ions at the injection of strong VLF waves into the ionosphere. Kosmich. Issled. **27**, 248–257 (1989)
11. Bernhardt, P.A., Scales, W.A., Grach, S.M., Keroshtin, A.N., Kotik, D.S., Polyakov, S.M.: Excitation of artificial airglow by high-power radio waves from "SURA" ionospheric heating facility. Geophys. Res. Lett. **18**(8), 1477–1480 (1991)
12. Cohen, D., Weiber, J., King, J., Kemper, S., Stephens, S., Davis, L., Spanjer, G., Winter, J., Adler, A., Easley, S., Tolliver, M., Guarnieri, J.: The SSTE-4: DSX flight experiment: design of a low-cost, R&D space mission with responsive enabling technologies. Paper N.2005-3004, AIAA 3rd Responsive Space Conference 2005, Los Angeles, CA (2005)
13. Gamble, R.J., Rodger, C.J., Clivlend, M.A., Sauvaud, J.-A., Thomson, N.R., Stewart, S.L., McCornick, R.J., Parrot, M., Berthelier, L.-J.: Radiation belt precipitation by manmade VLF transmission. J. Geophys. Res. (2008). doi:10.1029/2008JA013369
14. Molchanov, O.A.: Wave and plasma phenomena inside the ionosphere and the magnetosphere associated with earthquakes. In: Stone, W.R. (ed.) Review of Radio Science 1990–1992, pp. 591–600. Oxford University Press, New York (1993)
15. Buchachenko, A.L., Oraevskii, V.N., Pokhotelov, O.A., Sorokin, V.M., Strakhov, V.N., Chmyrev, V.M.: Ionospheric precursors to earthquakes. Phys.-Usp. **39**, 959–965 (1996)
16. Varotsos, P.: A review and analysis of electromagnetic precursory phenomena. Acta Geophys. Pol. **49**, 1–42 (2001)
17. Hayakawa, M., Molchanov, O.: Seismo-Electromagnetics (Lithosphere–Atmosphere–Ionosphere Coupling), pp. 1–477. Terrapub, Tokyo (2002)
18. Parrot, M., Berthelier, J.J., Lebreton, J.P., Sauvaud, J.A., Santolik, O., Blecki, J.: Examples of unusual ionospheric observations made by the DEMETER satellite over seismic regions. Phys. Chem. Earth **31**, 486–495 (2006)
19. Parrot, M., Berthelier, J.J., Lebreton, J.P., Treumann, R., Rauch, J.L.: DEMETER observation of EM emissions related to thunderstorms. Space Sci. Rev. **137**, 511519 (2008). doi: 10.1007/s11214-008-9347-y

20. Bhattacharya, S., Sarkar, S., Gwal, A.K., Parrot, M.: Satellite and ground-based ULF/ELF emissions observed before Gujarat earthquake in March 2006. Curr. Sci. **93**, 41–46 (2006)
21. Sorokin, V.M., Chmyrev, V.M., Yaschenko, A.K.: Electrodynamic model of the lower atmosphere and the ionosphere coupling. J. Atmos. Solar-Terr. Phys. **63**, 1681–1691 (2001)
22. Sorokin, V.M.: Plasma and electromagnetic effects in the ionosphere related to the dynamic of charged aerosols in the lower atmosphere. Russ. J. Phys. Chem. **1**, 138–170 (2007)
23. Alekseev, V.A., Alekseeva, N.G.: Investigation of metal transfer in the biosphere during gaseous emission in zones of tectonic activity using methods of nuclear physics. Nucl. Geophys. **6**, 99–105 (1992)
24. Voitov, G.I., Dobrovolsky, I.P.: Chemical and isotope – carbonic instability of the soil gases in the seismic regions. Izvestiya AN SSSR. Fizika Zemli **3**, 20–27 (1994)
25. Virk, H.S., Singh, B.: Radon recording of Uttarkashi earthquake. Geophys. Res. Lett. **21**, 737–741 (1994)
26. Heincke, J., Koch, U., Martinelli, G.: CO_2 and Radon measurements in the Vogtland area (Germany) – a contribution to earthquake prediction research. Geophys. Res. Lett. **22**, 774–779 (1995)
27. Igarashi, G., Saeki, T., Takahata, N., Sano, Y., Sumikawa, K., Tasaka, S., Sasaki, Y., Takahashi, M.: Groundwater radon anomaly before the Kobe earthquake. Science **269**, 60–61 (1995)
28. Pulinets, S.A., Alekseev, V.A., Legenka, A.D., Khegai, V.V.: Radon and metallic aerosols emanation before strong earthquakes and their role in atmosphere and ionosphere modification. Adv. Space Res. **20**, 2173–2176 (1997)
29. Isaev, N.V., Sorokin, V.M., Chmyrev, V.M., Serebryakova, O.N., Ovcharenko, O.Ya.: Electric field enhancement in the ionosphere above tropical storm region. In.: Hayakawa, M., Molchanov, O.A. (eds.) Seismo electromagnetics: litosphere–atmosphere–ionosphere coupling, pp. 313–315. Terrapub, Tokyo (2002)
30. Sorokin, V.M., Isaev, N.V., Yaschenko, A.K, Chmyrev, V.M., Hayakawa, M.: Strong DC electric field formation in the low latitude ionosphere over typhoons. J. Atmos. Solar-Terr. Phys. **67**, 1269–1279 (2005)
31. Serebryakova, O.N., Bilichenko, S.V., Chmyrev, V.M., Parrot, M., Rauch, J.L., Lefeuvre, F., Pokhotelov, O.A.: Electromagnetic ELF radiation from earthquake regions as observed by low-altitude satellites. Geophys. Res. Lett. **19**, 91–94 (1992)
32. Chmyrev, V.M., Isaev, N.V., Serebryakova, O.N., Sorokin, V.M., Sobolev, Ya.P.: Small-scale plasma inhomogeneities and correlated ELF emissions in the ionosphere over an earthquake region. J. Atmos. Solar-Terr. Phys. **59**, 967–973 (1997)
33. Gokhberg, M.B., Morgunov, V.A., Yoshino, T., Tomizawa, I.: Experimental measurements of electromagnetic emissions possibly related to earthquake in Japan. J. Geophys. Res. **87**, 7824–7828 (1982)
34. Koons, H.C., Roeder, J.L.: A comparison of ULF/ELF measurements associated with earthquakes. In: Hayakawa, M. (ed.) Atmospheric and ionospheric electromagnetic phenomena associated with earthquakes, pp. 171–175. Terrapub, Tokyo (1999)
35. Henderson, T.R., Sonwalkar, V.S., Helliwell, R.A., Inan, U.S., Fraser-Smith, A.C.: A Search for ELF/VLF emissions induced by earthquakes as observed in the ionosphere by the DE-2 satellite. J. Geophys. Res. **98**, 9503–9511 (1993)
36. Borisov, N., Chmyrev, V., Rybachek, S.: A new ionospheric mechanism of electromagnetic ELF precursors to earthquakes. J. Atmos. Solar-Terr. Phys. **63**, 3–10 (2001)
37. Kondo, G.: The variation of the atmospheric electric field at the time of earthquake. Memoirs of the Kakioka Magnetic Observatory, Kakioka. Japan **13**, 17–23 (1968)
38. Pierce, E.T.: Atmospheric electricity and earthquake prediction. Geophys. Res. Lett. **3**, 185–188 (1976)
39. Hao, J.: The anomalous of atmospheric electric field at the ground level and earthquakes. Acta Seismol. Sinica. **10**, 207–211 (1988)

40. Chmyrev, V.M., Isaev, N.V., Bilichenko, S.V., Stanev, G.A.: Observation by space-borne detectors of electric fields and hydromagnetic waves in the ionosphere over on earthquake center. Phys. Earth Planet. Inter. **57**, 110–114 (1989)
41. Tate, J., Daily, W.: Evidence of electro-seismic phenomena. Phys. Earth Planet. Inter. **57**, 1–9 (1989)
42. Vershinin, E.F., Buzevich, A.V., Yumoto, K., Saita, K., Tanaka, Y.: Correlations of seismic activity with electromagnetic emissions and variations in Kamchatka region. In: Hayakawa, M. (ed.) Atmospheric and ionospheric electromagnetic phenomena associated with earthquakes, pp. 513–518. Terrapub, Tokyo (1999)
43. Pulinets, S.A., Legenka, A.D. Alekseev, V.A.: Pre-earthquakes effects and their possible mechanisms. Dusty and dirty plasmas, noise and chaos in space and in the laboratory, pp. 545–557. Plenum Publishing, New York (1994)
44. Boskova, J., Smilauer, I., Triska, P., Kudela, K.: Anomalous behaviour of plasma parameters as observed by the Intercosmos-24 satellite prior to the Iranian earthquake of 20 June 1990. Studia Geophys. Geodet. **8**, 213–220 (1994)
45. Afonin, V.V., Molchanov, O.A., Kodama, T., Hayakawa, M., Akentieva, O.A.: Statistical study of ionospheric plasma response to seismic activity: search for reliable result from satellite observations. In: Hayakawa, M. (ed.) Atmospheric and ionospheric electromagnetic phenomena associated with earthquakes, pp. 597–617. Terra Scientific Publishing Company (TERRAPUB), Tokyo (1999)
46. Pulinets, S.A., Legenka, A.D.: Spatial-temporal characteristics of the large scale disturbances of electron concentration observed in the *F*-region of the ionosphere before strong earthquake. Cosmic Res. **41**, 221–229 (2003)
47. Tronin, A.A.: Satellite thermal survey application for earthquake prediction. In.: Hayakawa, M. (ed.) Atmospheric and ionospheric electromagnetic phenomena associated with earthquakes, pp. 717–723. Terrapub, Tokyo (1999)
48. Tronin, A.A., Hayakawa, M., Molchanov, O.A.: Thermal IR satellite data application for earthquake research in Japan and China. J. Geodyn. **33**, 519–534 (2002)
49. Qiang, Z.J., Dian, C.G., Li, L.Z.: Satellite thermal infrared precursors of two moderate-strong earthquakes in Japan and impending earthquake prediction. In: Hayakawa, M. (ed.) Atmospheric and ionospheric electromagnetic phenomena associated with earthquakes, pp. 747–745. Terrapub, Tokyo (1999)
50. Tramutoli, V., Di Bello, G., Pergova, N., Piscitalli, S.: Robust satellite techniques for remote sensing of seismically active areas. Ann. Geofis. **44**, 295–312 (2001)
51. Toroshelidze, T.I., Fishkova, L.M.: Analyzes of the middle and upper atmosphere luminescence before earthquakes. DAN SSSR, Fizika Zemli. **302**, 313–319 (1986)
52. Gokhberg, M.B., Nekrasov, A.K., Shalimov, S.L.: On influence of the unstable injection of green gases to the ionosphere in seismic region. Izvestiya AN SSSR, Fizika Zemli. **8**, 52–60 (1996)
53. Draganov, A.B., Inan, U.S., Taranenko, YuN: ULF magnetic signatures at the earth surface due to ground water flow: a possible precursor to earthquakes. Geophys. Res. Lett. **18**, 1127–1131 (1991)
54. Surkov, V., Pilipenko, V.: The physics of pre-seismic electromagnetic ULF signals. In: Hayakawa, M. (ed.) Atmospheric and ionospheric electromagnetic phenomena associated with earthquakes, pp. 357–363. Terrapub, Tokyo (1999)
55. Molchanov, O.A., Hayakawa, M., Rafalsky, V.A.: Penetration characteristics of electromagnetic emissions from an underground seismic source into the atmosphere, ionosphere, and magnetosphere. J. Geophys. Res. **100**, 1691–1712 (1995)
56. Fitterman, D.V.: Theory of electrokinetic–magnetic anomalies in a faulted half-space. J. Geophys. Res. **84**, 6031–6040 (1979)
57. Pilipenko, V.A., Fedorov, E.N., Yagova, N.V., Yumoto, K.: Attempt to detect ULF electromagnetic activity preceding earthquake. In: Hayakawa, M. (ed.) Atmospheric and

ionospheric electromagnetic phenomena associated with earthquakes, pp. 203–214. Terrapub, Tokyo (1999)
58. Alperovich, L.S., Gokhberg, M.B., Sorokin, V.M., Fedorovich, G.V.: On generation of the geomagnetic variations by acoustic oscillation occurring at the time of earthquakes. Izvestiya AN SSSR, Fizika Zemli **3**, 58–68 (1979)
59. Sorokin, V.M., Fedorovich, G.V.: Propagation of the short periodic waves in the ionosphere. Izvestiya VUZov, Radiofizika. **25**, 495–507 (1982)
60. Grimalsky, V.V., Hayakawa, M., Ivchenko, V.N., Rapoport, YuG, ZAdoroznii, V.I.: Penetration of an electrostatic field from the lithosphere into the ionosphere and its effect on the D-region before earthquakes. J. Atmos. Solar-Terr. Phys. **65**, 391–407 (2003)
61. Rapoport, Y., Grimalsky, V., Hayakawa, M., Ivchenko, V., Juarez, R.D., Koshevaya, S., Gotynyan, O.: Change of ionospheric plasma parameters under the influence of electric field which has lithospheric origin and due to radon emanation. Phys. Chem. Earth **29**, 579–587 (2004)
62. Volland, H.: Atmospheric electrodynamics. Springer, New York (1984)
63. Pasko, V.P.: Dynamic coupling of quasi-electrostatic thundercloud fields to the mesosphere and lower ionosphere: sprites and jets. Ph.D. thesis, Stanford University, Stanford, CA (1996)
64. Uman, M.A.: The lightning discharge. Academic, Orlando, FL (1987)
65. Inan, U.S., Sampson, W.A., Taranenko, Y.N.: Space-time structure of lower ionospheric optical flashes and ionization changes produced by lightning EMP. Geophys. Res. Lett. **23**, 133–138 (1996)
66. Roussel-Dupre, R.A., Gurevich, A.V., Tunnell, T., Milikh, G.M.: Kinetic theory of runaway air breakdown. Phys. Rev. E **49**, 2257–2269 (1994)
67. Bell, T.F., Pasko, V.P., Inan, U.S.: Runaway electrons as a source of Red Sprites in the mesosphere. Geophys. Res. Lett. **22**, 2127–2135 (1995)
68. Helliwell, R.A., Katsufrakis, J.P., Trimpi, M.L.: Whistler-induced amplitude perturbation in VLF propagation. J. Geophys. Res. **78**, 4679–4688 (1973)
69. Carpenter, D.L., Inan, U.S., Trimpi, M.L., Helliwell, R.A., Katsufrakis, J.P.: Perturbations of subionospheric LF and MF signals due to whistler-induced electron precipitation bursts. J. Geophys. Res. **89**, 9857–9867 (1984)
70. Burgess, W.C., Inan, U.S.: The role of ducted whistlers in the precipitation loss and equilibrium flux of radiation belt electrons. J. Geophys. Res. **98**, 15643–15650 (1993)
71. Rosenberg, T.J., Helliwell, R.A., Katsufrakis, J.P.: Electron precipitation associated with discrete, very low frequency emissions. J. Geophys. Res. **76**, 8445–8456 (1971)
72. Rycroft, M.J.: Enhanced energetic electron intensities at 100 km altitude and a whistler propagation through the plasmasphere. Planet. Space Sci. **21**, 239–247 (1973)
73. Goldberg, R.J., Curtis, S.A., Barcus, J.R.: Detailed spectral structure of magnetospheric electron bursts precipitated by lightning. J. Geophys. Res. **92**, 2505–2512 (1987)
74. Voss, H.D., Imhof, W.L., Mobila, J., Gaines, E.E., Walt, M., Inan, U.S., Helliwell, R.A., Carpenter, D.L., Katsufrakis, J.P., Chang, H.C.: Lightning-induced electron precipitation. Nature **312**, 740–749 (1984)
75. Imhof, W.L., Voss, H.D., Walt, M., Gaines, E.E., Mobila, J., Datlove, D.W., Reagan, J.B.: Slot region electron precipitation by lightning. J. Geophys. Res. **91**, 8883–8892 (1986)
76. Voss, H.D., Walt, M., Imhof, W.L., Mobila, J., Inan, U.S.: Satellite observation of lightning-induced electron precipitation. J. Geophys. Res. **103**, 11725–11732 (1998)
77. Inan, U.S., Bell, T.F., Helliwell, R.A.: Nonlinear pitch angle scattering of energetic electrons by coherent VLF waves in the magnetosphere. J. Geophys. Res. **83**, 3235–3246 (1978)
78. Chang, H.C., Inan, U.S.: Lightning-induce energetic electron precipitation from the magnetosphere. J. Geophys. Res. **90**, 4531–4539 (1985)
79. Armstrong, W.C.: Recent advances from studies of the Trimpi effect. Antarctic J. **18**, 281–286 (1983)

80. Inan, U.S., Shafer, D.C., Yip, W.Y., Orville, R.E.: Subionospheric VLF signatures of nighttime *D*-region perturbations in the vicinity of lightning discharges. J. Geophys. Res. **93**, 11455–11467 (1988)
81. Inan, U.S., Rodriguez, J.V., Idone, V.P.: VLF signatures of lightning-induced heating and ionization of the nighttime D-region. Geophys. Res. Lett. **20**, 2355–2360 (1993)
82. Inan, U.S., Bell, T.F., Pasko, V.P., Sentman, D.D., Wescott, E.M., Lyons, W.A.: VLF signatures of ionospheric disturbances associated with sprites. Geophys. Res. Lett. **22**, 3461–3466 (1995)
83. Inan, U.S., Slingeland, A., Pasko, V.P., Rodriguez, J.: VLF signatures of mesospheric/lower ionospheric response to lightning discharges. J. Geophys. Res. **101**, 5219–5228 (1996)
84. Dowden, R.L., Adams, C.D.C., Brundell, J.B., Dowden, P.E.: Rapid onset, rapid decay (RORD), phase and amplitude perturbations of VLF subionospheric transmissions. J. Atmos. Terr. Phys. **56**, 1513–1521 (1994)
85. Sentman, D.D., Wescott, E.M.: Red sprites and blue jets: thunderstorm-excited optical emissions in the stratosphere, mesosphere and ionosphere. Phys. Plasmas **2**, 2514–2522 (1995)
86. Lyons, W.A.: Characteristics of luminous structures in the stratosphere above thunderstorms as imaged by low-light video. Geophys. Res. Lett. **21**, 875–881 (1994)
87. Lyons, W.A.: Low-light video observations of frequent luminous structures in the stratosphere above thunderstorms. Mon. Weather Rev. **122**, 1940–1950 (1995)
88. Lyons, W.A.: Sprite observations above the U.S. high plains in relation to their parent thunderstorm systems. J. Geophys. Res. **101**, 29641–29652 (1996)
89. Boeck, W.L., Vaughan, O.H., Blakeslee, R.J., Vonnegut, B., Brook, M., McKune, J.: Observation of lightning in the stratosphere. J. Geophys. Res. **100**, 1465–1472 (1995)
90. Rairden, R.L., Mende, S.B.: Time resolved sprite imagery. Geophys. Res. Lett. **22**, 3465–3469 (1995)
91. Winckler, J.R., Lyons, W.A., Nelson, T., Nemzek, R.J.: New high-resolution ground-based studies of cloud-ionosphere discharges over thunderstorms (CI or Sprites). J. Geophys. Res. **101**, 6997–7012 (1996)
92. Wescott, E.M., Sentman, D., Osborne, D., Hampton, D., Heavner, M.: Preliminary results from the Sprites94 aircraft campaign: 2. Blue jets. Geophys. Res. Lett. **22**, 1209–1213 (1995)
93. Boeck, W.L., Vaughan, O.H., Blakeslee, R.J., Vonnegut, B., Brook, M.: Lightning-induced brightening in the airglow layer. Geophys. Res. Lett. **19**, 99–103 (1992)
94. Fukunishi, H., Takahashi, Y., Kubota, M., Sakanoi, K., Inan, U.S., Lyons, W.A.: Lightning-induced transient luminous events in the lower ionosphere. Geophys. Res. Lett. **23**, 2157–2163 (1996)
95. Boccippio, D.J., Williams, E.R., Heckman, S.J., Lyons, W.A., Baker, I.T., Boldi, R.: Sprites, ELF transients, and positive ground strokes. Science **269**, 1088–1093 (1995)
96. Fishman, G.J., Bhat, P.N., Mallozzi, R., Horack, J.M., Koshut, T., Kouveliotou, C., Pendleton, G.N., Meegan, C.A., Wilson, R.B., Paciesas, W.S., Goodman, S.J., Christian, H.J.: Discovery of intense gamma-ray flashes of atmospheric origin. Science **264**, 1313–1319 (1994)
97. Inan, U.S., Reising, S.C., Fishman, G.J., Horack, J.M.: On the association of terrestrial gamma-ray bursts with lightning discharges and sprites. Geophys. Res. Lett. **23**, 1017–1022 (1996)
98. Holden, D.N., Munson, C.P., Devenport, J.C.: Satellite observation of transionospheric pulse pairs. Geophys. Res. Lett. **22**, 889–893 (1995)
99. Taranenko, Y.N., Inan, U.S., Bell, T.F.: Interaction with the lower ionosphere of electromagnetic pulses from lightning: heating, attachment, and ionization. Geophys. Res. Lett. **20**, 1539–1545 (1993)
100. Taranenko, Y.N., Inan, U.S., Bell, T.F.: The interaction with the lower ionosphere of electromagnetic pulses from lightning: excitation of optical emissions. Geophys. Res. Lett. **20**, 2675–2680 (1993)

101. Milikh, G.M., Papadopoulos, K., Chang, C.L.: On the physics of high altitude lightning. Geophys. Res. Lett. **22**, 85–91 (1995)
102. Rowland, H.L., Fernsler, R.F., Huba, J.D., Bernhardt, P.A.: Lightning driven EMP in the upper atmosphere. Geophys. Res. Lett. **22**, 361–367 (1995)
103. Pasko, V.P., Inan, U.S., Taranenko, Y.N., Bell, T.F.: Heating, ionization and upward discharges in the mesosphere due to intense quasi-electrostatic thunderstorm fields. Geophys. Res. Lett. **22**, 365–370 (1995)
104. Pasko, V.P., Inan, U.S., Bell, T.F.: Sprites as luminous columns of ionization produced by quasi-electrostatic thunderstorm fields. Geophys. Res. Lett. **23**, 649–655 (1996)
105. Pasko, V.P., Inan, U.S., Bell, T.F.: Blue jets produced by quasi-electrostatic pre-discharge thunderstorm fields. Geophys. Res. Lett. **23**, 301–307 (1996)
106. Pasko, V.P., Inan, U.S., Bell, T.F., Taranenko, Y.N.: Sprites produced by quasi-electrostatic heating and ionization in the lower ionosphere. J. Geophys. Res. **102**, 4529–4539 (1997)
107. Roussel-Dupre, R.A., Gurevich, A.V.: On runaway breakdown and upward propagating discharges. J. Geophys. Res. **101**, 2297–2310 (1996)
108. Taranenko, Y.N., Roussel-Dupre, R.A.: High altitude discharges and gamma-ray flashes: a manifestation of runaway air breakdown. Geophys. Res. Lett. **23**, 571–576 (1996)
109. Lehtinen, N.G., Walt, M., Inan, U.S., Bell, T.F., Pasko, V.P.: X-ray emission produced by a relativistic beam of runaway electrons accelerated by quasi-electrostatic thundercloud fields. Geophys. Res. Lett. **23**, 2645–2652 (1996)
110. Franz, R.C., Nemzek, R.J., Winckler, J.R.: Television image of a large upward electric discharge above a thunderstorm system. Science **249**, 48–54 (1990)
111. Sentman, D.D., Wescott, E.M., Osborne, D.L., Hampton, D.L., Heavner, M.J.: Preliminary results from the Sprites94 campaign: red sprites. Geophys. Res. Lett. **22**, 1205–1211 (1995)
112. Sentman, D.D., Wescot, E.M.: Observation of upper atmosphere optical flashes recorded from an aircraft. Geophys. Res. Lett. **20**, 2857–2864 (1993)
113. Sentman, D.D., Wescott, E.M.: Red sprites and blue jets. Geophysical Institute Video Production, University of Alaska, Fairbanks (1994)
114. Vaughan, O.H., Blakeslee, R.J., Boeck, W.L., Vonnegut, B., Brook, M., McKune, J.: A cloud-to-space lightning as recorded by the space shuttle payload-bay TV cameras. Mon. Weather Rev. **120**, 1459–1465 (1992)
115. Wescott, E.M., Sentman, D.D, Heavner, M.J, Hampton, D.L.: Blue starters, discharges above an intense thunderstorm over Arkansas, July 1, 1994. In: Proceedings of the EOS Transactions. AGU, 1995 Fall Meeting, 76, F104 (1995)
116. Picard, R.H., Inan, U.S., Pasko, V.P., Winick, J.R., Wintersteiner, P.P.: Infrared glow above thunderstorms. Geophys. Res. Lett. **24**, 2635–2643 (1997)
117. Parrot, M., Berthelier, J.J., Lebreton, J.P., Treumann, R., Rauch, J.L.: DEMETER observation of EM emissions related to thunderstorms. Space Sci. Rev. **137**, 511–519 (2008). doi:10.1007/s11214-008-9347-y
118. Berthelier, J.J., Malingre, M., Pfaff, R., Seran, E., Pottelette, R., Lebreton, J.P., Parrot, M.: Lightning – induced plasma turbulence and ion heating in equatorial ionospheric depletion. Nat. Geosci. (2008). doi:10.1038/ngeo109
119. Inan, U.S., Carpenter, D.L.: Lightning-induced electron precipitation events observed at L 2.4 as phase and amplitude perturbations on subionospheric VLF signals. J. Geophys. Res. **92**, 3293–3299 (1987)
120. Clilverd, M.A., Rodger, C.J., Nunn, D.: Radiation belt electron precipitation fluxes associated with lightning. J. Geophys. Res. **109**, A12208 (2004). doi:10.1029/2004JA010644
121. Inan, U.S., Piddyachiy, D., Peter, W.B., Sauvaud, J.A., Parrot, M.: DEMETER satellite observation of lightning-induced electron precipitation. Geophys. Res. Lett. **34**, L07103 (2007). doi:10.1029/2006GL029238
122. Jones, T.B., Davis, K., Wieder, B.: Observation of *D*-region modifications at low and very low frequencies. Nature **238**, 33–37 (1972)

123. Barr, R., Rietveld, M.T., Kopka, H., Stubbe, P.: Effects of heated patch of auroral ionosphere on VLF radio wave propagation. Nature **309**, 534–538 (1984)
124. Barr, R., Rietveld, M.T., Kopka, H., Stubbe, P., Nielsen, E.: Extra-low-frequency radiation from the polar electrojet antenna. Nature **317**, 155160 (1985)
125. Bell, T.F., Inan, U.S., Danielson, M., Cummer, S.: VLF signatures of ionospheric heating by HIPAS. In: Goodmaned, J.M. (ed.) Proceedings of the 1993 Ionospheric Effects Symposium, pp. 622–628. SRI International, Arlington, VA (1993)
126. Stubbe, P., Kopka, H., Rietveld, M.T., Dowden, R.L.: ELF and VLF generation by modulated heating of the current carrying lower ionosphere. J. Atmos. Terr. Phys. **44**, 1123–1128 (1982)
127. Ferrano, A.J., Lee, H.S., Allshouse, R., Carroll, K., Lunnen, R., Collins, T.: Characteristics of ionospheric ELF radiation generated by HF heating. J. Atmos. Terr. Phys. **46**, 855–863 (1984)
128. Barr, R., Stubbe, P., Rietveld, M.T., Kopka, H.: ELF and VLF signals radiated by the "polar electrojet antenna": experimental results. J. Geophys. Res. **91**, 4451–4462 (1986)
129. Barr, R., Stubbe, P., Kopka, H.: Long-range detection of VLF radiation produced by heating the auroral electrojet. Radio Sci. **26**, 871–989 (1991)
130. Papadopoulos, K., Wallace, T., McCarrick, M., Milikh, G.M., Yang, X.: On the efficiency of ELF/VLF generation using HF heating of the auroral electrojet. Plasma Phys. Rep. **29**, 561–567 (2003)
131. Pashin, A.B., Mochalov, A.A., Bosinger, T., Rietveld, M.T.: Physics of auroral phenomena. In: Proceedings of the XXVI Annual Seminar, Apatity, pp. 111–114. Kola Science Centre, Russian Academy of Science (2003)
132. Kimura, I., Stubbe, P., Rietveld, M.T., Barr, R., Ishida, K., Kasahara, Y., Yagitani, S., Nagano, I.: Collaborative experimentsby Akebono satellite, Tromso ionospheric heater, and European incoherent scatter radar. Radio Sci. **29**, 23–29 (1994)
133. Ferrano, A.J., Lee, H.S., Allshouse, R., Carroll, K., Tomko, A.A., Kelly, F.J., Joiner, R.G.: VLF/ELF radiation from the ionospheric dynamo current system modulated by powerful HF signals. J. Atmos. Terr. Phys. **44**, 1113–1119 (1982)
134. McCarrick, M.J., Sentman, D.D., Wong, A.Y., Wuerker, R.F., Chouinard, B.: Excitation of ELF waves in the Schumann resonance range by modulated HF heating of the polar electrojet. Radio Sci. **25**, 1291–1298 (1990)
135. Villasenor, J., Wong, A.Y., Song, B., Pau, J., McCarrick, M., Sentman, D.: Comparison of ELF/VLF generation modes in the ionosphere by the HIPAS heater array. Radio Sci. **31**, 211–217 (1996)
136. Kimura, I., Wong, A., Chouinard, B., McCarrick, M., Okada, T.: Satellite and ground observations of HIPAS VLF modulation. Geophys. Res. Lett. **18**, 309–314 (1991)
137. Milikh, G.M., Papadopoulos, K., McCarrick, M., Preston, J.: ELF emissions generated by the HAARP HF-heater using varying frequencies and polarization. Izvestiya VUZov, Radiofizika **42**, 728–733 (1999)
138. Platino, M., Inan, U.S., Bell, T.F., Parrot, M., Kennedy, E.J.: DEMETER observations of ELF waves injected with the HAARP HF transmitter. Geophys. Res. Lett. **33**, L16101 (2006)
139. Moore, R.C.: ELF/VLF wave generation by modulated HF heating of the auroral electrojet. Ph.D. thesis, Stanford University, Stanford, CA (2007)
140. Rapoport, V.O., Frolov, V.L., Komrakov, G.P. Markov, G.A., Belov, A.S., Parrot, M., Rauch, J.L.: Some results of measuring the characteristics of electromagnetic and plasma disturbances stimulated in the outer ionosphere by high-power high-frequency radio emission from the "Sura" facility. Radiophys. Quantum Electron. **50**, 645–651 (2007)
141. Frolov, V., Komrakov, G., Rapoport, V., Ryzhov, N., Belov, A., Markov, G., Parrot, M., Rauch, J., Reitveld, M.: Phenomena observed by HF heating of middle – and high-latitude ionosphere and registered with DEMETER instruments. Geophys. Res. Abstracts **10**, EGU 2008-A-03872 (2008a)

142. Zhulin, I.A., Lyakhov, S.B., Majorov, A.D., Managadze, G.G., Mogilevsky, M.M., Chmyrev, V.M.: Artificially stimulated electron precipitation from the Earth's magnetosphere. Dokl. Akad. Nauk SSSR **230**, 1073–1077 (1976)
143. Imhof, W.L., Reagan, J.B., Voss, H.D., Gaines, E.E., Datlowe, D.W., Mobilia, J., Helliwell, R.A., Inan, U.S., Ratsufrakis, J.P.: Direct observation of radiation belt electrons precipitated by the controlled injection of VLF signals from a ground-based transmitter. Geophys. Res. Lett. **10**, 361–366 (1983)
144. Imhof, W.L., Reagan, J.B., Voss, H.D., Gaines, E.E., Datlowe, D.W., Mobilia, J., Helliwell, R.A., Inan, U.S., Ratsufrakis, J.P.: The modulated precipitation of radiation belt electrons by controlled signals from VLF transmitter. Geophys. Res. Lett. **10**, 615–620 (1983)
145. Inan, U.S., Chang, H.C., Helliwell, R.A., Imhof, W.L., Reagan, J.B., Walt, M.: Precipitation of radiation belt electrons by man-made waves: a comparison between theory and measurement. J. Geophys. Res. **90**, 359–370 (1985)
146. Kovrazhkin, R.A., Mogilevsky, M.M., Bosqued, J.-M., Galperin, Y.I., Dzhordzhio, N.V., Lisakov, Y.V., Molchanov, O.A., Reme, A.: Observation of particle precipitation from the ring-current zone stimulated by powerful ground-based VLF transmitter. JETP Lett. **38**, 397–402 (1983)
147. Kovrazhkin, R.A., Mogilevsky, M.M., Molchanov, O.A., Galperin, Y.I., Dzhordzhio, N.V., Lisakov, Y.V., Bosqued, J.-M., Reme, A.: Direct detection of the precipitation of ring current electrons and protons stimulated by artificial VLF emission. Geophys. Res. Lett. **11**, 705–709 (1984)
148. Sauvaud, J.-A., Maggiolo, R., Jacquey, C., Parrot, M., Berthelier, J.-J., Gamble, R.J.: Radiation belt electron precipitation due to VLF transmission. Satellite observations. Geophys. Res. Lett. **35**, L09101 (2008). doi:10.1029/2008GL033194
149. Inan, U.S., Rodriguez, J.V., Lev-Tov, S., Oh, J.: Ionospheric modification with a VLF transmitter. Geophys. Res. Lett. **19**, 2071–2077 (1992)
150. Barr, R., Rietveld, M.T., Stubbe, P., Kopka, H.: The diffraction of VLF radio waves by a patch of ionosphere illuminated by a powerful HF transmitter. J. Geophys. Res. **90**, 2861–2869 (1985)
151. Taranenko, Y.N., Inan, U.S., Bell, T.F.: VLF-HF heating of the lower ionosphere and ELF wave generation. Geophys. Res. Lett. **19**, 61–66 (1992)
152. Rodriguez, J.V.: Modification of the Earth's ionosphere by very-low-frequency transmitter. Ph.D. thesis, Stanford University, Stanford, CA (1994)
153. Rodriguez, J.V., Inan, U.S.: Electron density changes in the nighttime *D* region due to heating by very-low-frequency transmitter. Geophys. Res. Lett. **21**, 93–98 (1994)
154. Likhter, Ya.I., Molchanov, O.A., Chmyrev, V.M.: Modulation of spectrum and amplitude of low-frequency signal in the magnetosphere. JETP Lett. **14**, 325–327 (1971)
155. Bell, T.F., James, H.G., Inan, U.S., Katsufrakis, J.P.: The apparent spectral broadening of VLF transmitter signals during trans-ionospheric propagation. J. Geophys. Res. **88**, 4813–4818 (1983)
156. Titova, E.E., Di, V.I., Yurov, V.E., Raspopov, O.M., Trakhtengerts, V.Y., Jiricek, F., Triska, P.: Interaction between VLF waves and turbulent ionosphere. Geophys. Res. Lett. **11**, 323–327 (1984)
157. Bell, T.F., Inan, U.S., Lauben, D., Sonwalkar, V.S., Helliwell, R.A., Sobolev, YaP, Chmyrev, V.M., Gonzalez, S.: DE-1 and COSMOS-1809 observations of lower hybrid waves excited by VLF whistler mode waves. Geophys. Res. Lett. **21**, 653–656 (1994)
158. Taranenko, YuN, Chmyrev, V.M.: Interaction between whistler waves and ion-cyclotron waves in magnetospheric plasma. Radiophys. Quant. Electron. **29**, 373–376 (1986)
159. Taranenko, YuN, Chmyrev, V.M.: Parametric interaction of whistler and electromagnetic ion-cyclotron waves in ionospheric plasma. Geom. Aeron. **29**, 459–464 (1989)
160. Chmyrev, V.M., Draganov, A.B., Taranenko, YuN, Teodosiev, D.: Acceleration of particles in the upper ionosphere and the magnetosphere due to decay interactions of whistlers, part 1. Phys. Scr. **43**, 495–502 (1991)

161. Chang, T., Crew, G.B., Hershkowtz, N., Jasper, J.R., Retterer, J.M., Winningham, J.D.: Transverse acceleration of oxygen ions by electromagnetic ion cyclotron resonance with broad band left hand polarized waves. Geophys. Res. Lett. **13**, 636–640 (1986)
162. Frazer-Smith, A.C., Cole, C.A.: Initial observations of the artificial stimulation of ULF pulsations by pulsed VLF transmissions. Geophys. Res. Lett. **2**, 146–149 (1975)
163. Chmyrev, V.M., Roldugin, V.K., Zhulin, I.A., Mogilevsky, M.M., Di, V.I., Koshelevsky, V.K., Bushmarin, V.A., Raspopov, O.M.: Artificial injection of very low-frequency (VLF) waves into the ionosphere and the magnetosphere of the Earth. JETP Lett. **23**, 409–412 (1976)
164. Chmyrev, V.M., Taranenko, Yu.N, Kopytenko, Yu.A., Voronov, P.V., Draganov, A.B.: Observation of ULF pulsations correlated with transmission of VLF waves and amplification of ULF waves by O^+ ion conics in the equatorial magnetosphere. Paper presented at AGU Chapman Conference on auroral plasma dynamics, Minneapolis, MN, 21–25 Oct 1991
165. Sorokin, V.M., Chmyrev, V.M.: Electrodynamic model of ionospheric precursors of earthquakes and certain types of disasters. Geom. Aeron. **42**, 821–830 (2002)
166. Molchanov, O.A., Hayakawa, M.: VLF transmitter earthquake precursors influenced by a change in atmospheric electric field. In: Proceedings of 10th International Conference on Atmospheric Electricity, pp. 428–431. Osaka, Japan, 10–14 June 1996
167. Boyarchuk, K.A., Lomonosov, A.M, Pulinets, S.A., Hegai, V.V.: Variability of the Earth's atmospheric electric field and ion-aerosols kinetics in the troposphere. Studia Geophys. Geod. **42**, 197–206 (1998)
168. Sorokin, V.M., Chmyrev, V.M., Yaschenko, A.K.: Theoretical model of DC electric field formation in the ionosphere stimulated by seismic activity. J. Atmos. Solar-Terr. Phys. **67**, 1259–1268 (2005)
169. Sorokin, V.M., Yaschenko, A.K.: Perturbation of the conductivity and electric field in the Earth–ionosphere layer over preparing earthquake. Geom. Aeron. **39**, 100–106 (1999)
170. Sorokin, V., Yaschenko, A.: Electric field disturbance in the Earth–ionosphere layer. Adv. Space Res. **26**, 1219–1225 (2000)
171. Sorokin, V.M., Yaschenko, A.K., Hayakawa, M.: A perturbation of DC electric field caused by light ion adhesion to aerosols during the growth in seismic-related atmospheric radioactivity. Nat. Hazards Earth Syst. Sci. **7**, 155–163 (2007)
172. Sorokin, V.M., Chmyrev, V.M., Isaev, N.V.: A generation model of mall-scale geomagnetic field-aligned plasma inhomogeneities in the ionosphere. J. Atmos. Solar-Terr. Phys. **60**, 1331–1342 (1998)
173. Sorokin, V.M., Chmyrev, V.M.: On acoustic gravity waves instability by electric field in the ionosphere. Geom. Aeron. **39**, 38–45 (1999)
174. Piddington, J.H.: The transmission of geomagnetic disturbances through the atmosphere and interplanetary space. Geophys. J. **2**, 173–189 (1959)
175. Chmyrev, V.M., Sorokin, V.M., Pokhotelov, O.A.: Theory of small scale plasma density inhomogeneities and ULF/ELF magnetic field oscillations excited in the ionosphere prior to earthquakes. In: Hayakawa, M. (ed.) Atmospheric and Ionospheric Electromagnetic Phenomena Associated with Earthquakes, pp. 759–776. Terrapub, Tokyo (1999)
176. Lyatsky, V.B., Maltsev, YuP: Magnetosphere–Ionosphere Coupling. Nauka, Moscow (1983)
177. Molchanov, O.A., Mazhaeva, O.A., Golyavin, A.N., Hayakawa, M.: Observation by Intercosmos-24 satellite of ELF–VLF electromagnetic emissions associated with earthquakes. Ann. Geophys. **11**, 431–440 (1993)
178. Chmyrev, V.M., Sorokin, V.M., Shklyar, D.R.: VLF transmitter signals as a possible tool for detection of seismic effects on the ionosphere. J. Atmos. Solar-Terr. Phys. **70**, 2053–2060 (2008)
179. Frazer-Smith, A.C., Bernardi, A., McGill, P.R., Ladd, M.E., Helliwell, R.A., Villard Jr., O.G.: Low-frequency magnetic field measurements near epicentre of the MS 7.1 Loma Prieta earthquake. Geophys. Res. Lett. **17**, 1465–1468 (1990)

180. Kopytenko, Y.A., Matiashvili, T.G., Voronov, P.M., Kopytenko, E.A., Molchanov, O.A.: Detection of ultra-low-frequency emissions connected with the Spitak earthquake and its aftershock activity, based on geomagnetic pulsations data at Dusheti and Vardzia observatories. Phys. Earth Planet. Inter. **77**, 85–89 (1993)
181. Hayakawa, M., Kawate, R., Molchanov, O.A., Yumoto, K.: Results of ultra-low-frequency magnetic field measurements during the Guam earthquake of August 1993. Geophys. Res. Lett. **23**, 241–250 (1996)
182. Sorokin, V.M., Chmyrev, V.M., Yaschenko, A.K.: Ultra low frequency oscillations of magnetic field on the Earth's surface generated by irregularities of the ionosphere conductivity. Geom. Aeron. **41**, 327–331 (2001)
183. Sorokin, V.M., Chmyrev, V.M., Yaschenko, A.K.: Ionospheric generation mechanism of geomagnetic pulsations observed on the Earth's surface before earthquake. J. Atmos. Solar-Terr. Phys. **64**, 21–29 (2003)
184. Sorokin, V.M.: Wave processes in the ionosphere related to geomagnetic field. Izvestiya VUZov, Radiofizika. **31**, 1169–1179 (1988)
185. Sorokin, V.M., Yaschenko, A.K.: Propagation of the Pi2 pulsations in the low ionosphere. Geom. Aeron. **28**, 655–660 (1988)
186. Sorokin, V.M., Pokhotelov, O.A.: Gyrotropic waves in the mid-latitude ionosphere. J. Atmos. Solar-Terr. Phys. **67**, 921–930 (2005)
187. Rauscher, E.A., Van Bise, W.I.: The relationship of extremely low frequency electromagnetic and magnetic fields associated with seismic and volcanic natural activity and artificial ionospheric disturbances. In: Hayakawa, M. (ed.) Atmospheric and Ionospheric Electromagnetic Phenomena Associated with Earthquakes, pp. 459–487. Terrapub, Tokyo (1999)
188. Sorokin V. M., Hayakawa, M.: On the generation of narrow-banded ULF/ELF pulsations in the lower ionospheric conducting layer. J. Geophys. Res. **113**, A06306 (2008). doi:10.1029/2008JA013094
189. Sorokin, V.M., Fedorov, E.N., Schekotov, AYu, Molchanov, O.A., Hayakawa, M.: Depression of the ULF geomagnetic pulsation related to ionospheric irregularities. Ann. Geophys. **47**, 191–198 (2004)
190. Sorokin, V.M., Chmyrev, V.M.: Modification of the Ionosphere by Seismic Related Electric Field. In: Hayakawa, M. (ed.) Atmospheric and ionospheric electromagnetic phenomena associated with earthquakes, pp. 805–818. Terrapub, Tokyo (1999)
191. Kim, V.P., Khegay, V.V., Nikiforova, V.V.: On possible perturbation of the night ionosphere E region over large scale tectonic fault. Izvestiya RAN, Fizika Zemli. **7**, 35–39 (1995)
192. Bowhill, S.A.: The formation of the daytime peak of the ionospheric *F*2-layer. J. Atmos. Terr. Phys. **24**, 503–520 (1962)
193. Ondoh, T., Hayakawa, M.: Seismo discharge model of anomalous sporadic *E* ionization before great earthquakes. In.: Hayakawa, M., Molchanov, O.A. (eds.) Seismo electromagnetics: litosphere–atmosphere–ionosphere coupling, pp. 385-390. Terrapub, Tokyo (2002)
194. Ondoh, T.: Anomalous sporadic-*E* layers observed before M7.2 Hyogo-ken Nanbu earthquake; Terrestrial gas emanation model. Adv. Polar Upper Atmos. Res. **17**, 96–108 (2003)
195. Yokoyama, T., Yamamoto, M., Pfaff, R.F., Fukao, S., Iwagami, N.: SEEK-2 campaign measurement of the electric field in the E-region and its association with the QP echoes. In: Abstracts for the 112th SGEPSS Fall Meeting, pp. 12–13. University of Electro-Communications, Tokyo (2002)
196. Sorokin, V.M., Yaschenko, A.K., Hayakawa, M.: Formation mechanism of the lower ionosphere disturbances by the atmosphere electric current over a seismic region. J. Atmos. Solar-Terr. Phys. **68**, 1260–1268 (2006)
197. Fuks, I.M., Shubova, R.S.: Anomaly in ELF signals as response to the low atmosphere processes. Geom. Aeron. **34**, 130–134 (1995)
198. Martynenko, S.I., Fuks, I.M., Shubova, R.S.: Ionospheric electric-field influence on the parameters of VLF signals connected with nuclear accidents and earthquakes. J. Atmos. Electr. **15**, 259–269 (1996)

199. Schunk, R.W., Nagy, A.F.: Ionospheres of terrestrial planets. Rev. Geophys. Space Phys. **18**, 813–852 (1980)
200. Parrot, M.: Statistical study of ELF/VLF emissions recorded by a low-altitude satellite during seismic events. J. Geophys. Res. **99**, 23339–23347 (1994)
201. Sorokin, V.M., Chmyrev, V.M., Hayakawa, M.: The formation of ionosphere–magnetosphere ducts over the seismic zone. Planet. Space Sci. **48**, 175–182 (2000)
202. Hayakawa, M.T., Yoshino, T., Morgounov, V.A.: On the possible influence of seismic activity on the propagation of magnetospheric whistlers at low latitudes. Phys. Earth Planet. Inter. **77**, 97–102 (1993)
203. Sorokin, V.M., Cherny, G.P.: It is quite possible to monitor typhoons from outer space. Aerospace Courier. N. 3, pp. 84–87 (1999)
204. Isaev, N.V., Sorokin, V.M., Chmyrev, V.M., Serebryakova, O.N.: DC electric fields in the ionosphere related to sea storms and typhoons. Geom. Aeron. **42**, 670–676 (2002)

Chapter 4
"COMPASS 2" Satellite and Ground-Based Experiments

Yu.M. Mikhailov, V.D. Kuznetsov, C. Ferencz, L. Bodnar, V.E. Korepanov, G.A. Mikhailova, L.P. Korsunova, V.V. Khegay, S.E. Smirnov, and O.V. Kapustina

Abstract This review is devoted to modern methods of earthquake (EQ) prediction. Section 4.2 contains the first results of special satellite "COMPASS 2" destined for the detection of seism-electromagnetic (EM) effects. A whistler group in the higher-order guided mode was recorded. Probably it was propagating between two layers, caused by onion-like structure of inhomogeneities in the plasma sphere. In Section 4.3, ELF-VLF effects observed over seism-active regions by the satellite "INTERCOSMOS-24" are considered. It was revealed that the *D*-region conductivity decreases during the earthquake preparation at $Kp < 3$ and increases during geomagnetic disturbances. The seismic and geomagnetic effects are assumed to be attributable, respectively, to the increase in near-ground atmospheric conductivity caused by radon emanation during fissuring and to the precipitation of high-energy particles from the inner radiation belt. In Section 4.4, results of the earthquake precursor occurrence time analysis in quasi-static electric field of the surface atmosphere on the Kamchatka Peninsula are presented. The propagation velocity of the precursors and their occurrence time are estimated for different geophysical conditions. ULF-effects in magnetic fields as a result of aftershocks are considered. In Section 4.5, relation between precursors in quasistatic electric fields and in ionosphere parameters is analyzed. This relation reflects the processes of lithosphere–ionosphere interaction.

Keywords Satellite experiments · Ionosphere · Precursors · Earthquake prediction

Yu.M. Mikhailov (✉)
Pushkov Institute of Terrestrial Magnetism, Ionosphere and Radio Wave Propagation, Russian Academy of Science, IZMIRAN, Troitsk, Moscow region 142190, Russia
e-mail: yumikh@izmiran.ru

V.L. Bychkov et al. (eds.), *The Atmosphere and Ionosphere,*
Physics of Earth and Space Environments,
DOI 10.1007/978-90-481-3212-6_4, © Springer Science+Business Media B.V. 2010

4.1 Introduction

The basic principles of the search methodology of earthquake (EQ) predictions have been already formulated by Gufeld [1] by next propositions:

1. Proper choice of observation point and fixed parameters
2. Several extraction methods of key parameters
3. Some sign criterion as a combination of time sequences of key parameters
4. Cases of an extra low level of electromagnetic (EM) effects connected with EQ

At present, it is interesting to deal with special satellites, the main goal of which is to look for EQ-precursors (COMPASS-2, Demeter). They allow us to carry out a global control over the seismic situation under consideration. But some difficulty arises because of slow time-varying effects when preparing EQ. Further observation of these effects in the case of a quick satellite flight is rather complicated. To register precursors, it is necessary to understand their nature.

For this reason, the main attention in the present issue is paid to a velocity of EQ precursors. It has been shown that the same values of velocities (near 1 m/s) appear in different processes. But this immediately means that precursor registrations confirm real process under consideration.

4.2 Satellite Experiment "COMPASS 2"

4.2.1 Satellite Investigations

The "COMPASS 2" S/C (Fig. 4.1a) is a space platform consisting of a set of housekeeping systems including the science instrumentation. It was launched 24 May 2006 on orbit with parameters: apogee 534 km, perigee 402 km, inclination 78,89 degree.

The science instrumentation includes the following units:

- RFA (radio-frequency analyzer)
- Radiation and ultraviolet detector ("TATYANA") – (high energy particles)
- Total electron content (TEC) detector – GPS receivers for the ionosphere tomography
- NVK (low-frequency wave complex)
- Dual Frequency Radio Transmitter RBE-150/400 ("MAYAK").

Main characteristics of the satellite are

Average orbit power	25 W
Mass of the S/C	80 kg
Mass of the science payload	20 kg

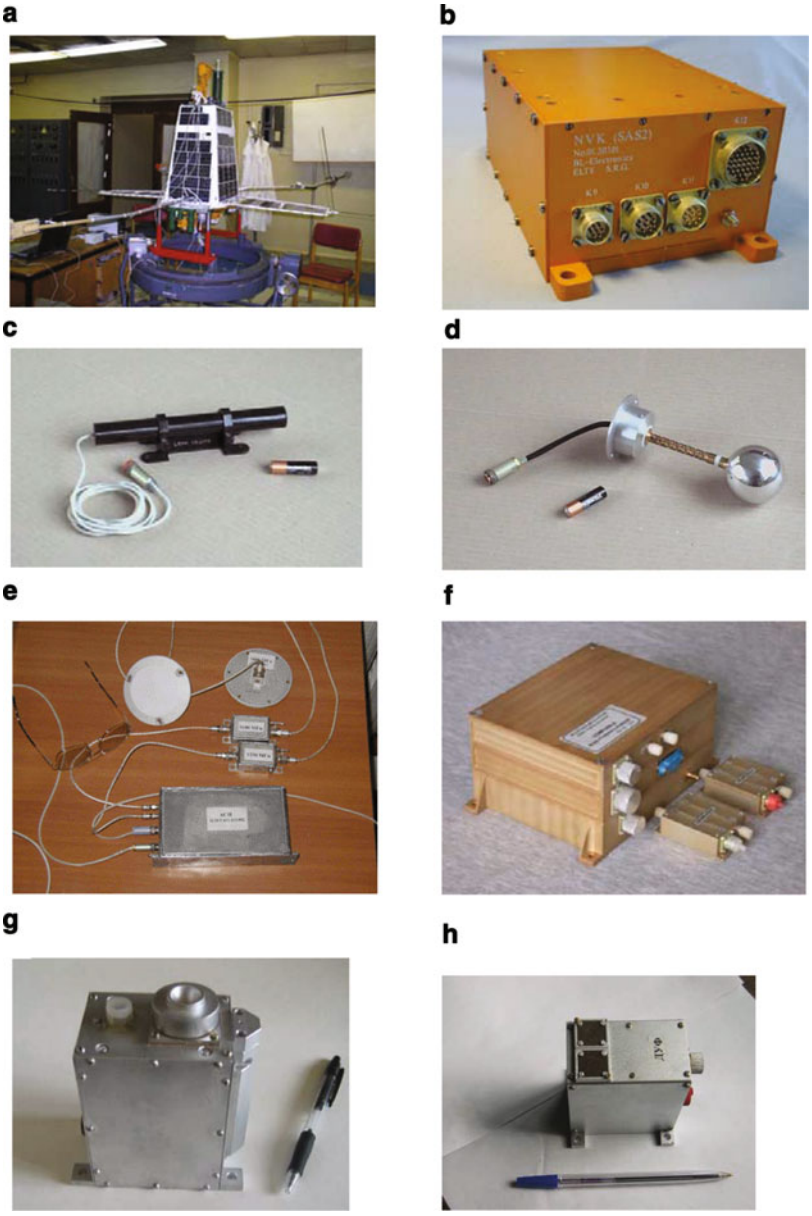

Fig. 4.1 (**a**) Satellite COMPASS 2; (**b**) Receiver SAS2 (NVK-complex); (**c**) magnetic sensor LEMI106 HS; (**d**) electric sensor LEMI502; (**e**) total electron content detector; (**f**) RFA-equipment; (**g**) block (TATYANA); (**h**) ultra violet emission detector

4.2.1.1 The Scientific Instrumentation

1. Total Electron Content Detector (IZMIRAN)

Total Electron Content (TEC) detector is designed for high-precision electron concentration distribution measurements (from the lower ionosphere to the satellite altitude) obtained by trans-ionospheric sounding using global navigation system (GPS) spacecraft (Fig. 4.1e).

Experiment aims are

Study of vertical structure of the ionosphere global distribution

Diagnostics of the active experiments in the ionospheric plasma, anthropogenic factors in the ionosphere, and effects caused by natural phenomena in the Earth's atmosphere, including seism-active and magnetic conjugation regions [8]

Main characteristics of the TEC device are

Registration of relative phase shifts of GPS signals at frequencies F1 = 1,250 MHz and F2 = 1,600 MHz

Registration of absolute code delay of the C/A signal, transmitted by GPS satellites at the frequency F1 = 1,250 MHz

Calculation of the location vector of the TEC device in PZ-90 or WGS-84 reference system

2. Dual Frequency Radio Transmitter RBE-150/400 ("MAYAK")

The onboard RBE-150/400 ("MAYAK") transmitter is designed for high-precision measurements of space–time distribution of the electron concentration structures above the sensitive regions, as predicted by the orbital transionosferic sounding (radio beacon method). It consists of two coherent transmitters at 150 and 400 MHz.

3. RFA (Radio Frequency Analyzer) IZMIRAN (Russia), CBK (Poland), IRF (Sweden)

The scientific objectives assigned to this device are the search for ionospheric precursors of the earthquakes as well as ionospheric phenomena caused by other natural and technogenic catastrophes. Its main functions are registering the electric component of plasma oscillation spectra in the 50 KHz–17.9 MHz frequency band and obtaining the electron density profiles along the orbit, including regions where strong earthquakes are expected (Fig. 4.1f).

4. Radiation and Ultraviolet Detector ("TATYANA")

TATYANA device was designed and manufactured by the Nuclear Physics institute (NIIYaF) of the Moscow State University (MSU). TATYANA's main purpose is to register radiation, cosmic rays, and ultraviolet emission coming from the Earth's atmosphere (Fig. 4.1g – radiation detector block, 4.1h – ultraviolet emission detector).

5. NVK (Low Frequency Wave complex)

The general scientific goals of the complete COMPASS mission are the study of the electromagnetic (EM) activity in the ionosphere concerning the seismic events, especially the existence of EM precursors of the earthquakes, the detailed investigation and monitoring of the electromagnetic environment of the Earth in the ULF–VLF bands, as well as the detailed characteristics of the lightning activity and whistler propagation and space weather-related tasks.

One of the main scientific experiments was the electromagnetic one performed with the help of advanced Signal Analyzer and Sampler (SAS2-K2), which used Ukrainian electromagnetic sensors: two spherical electric probes spaced at the distance of about 4 m producing one (differential) electric signal measured between these probes and one search coil magnetometer producing one magnetic signal, both operated in the ULF–VLF bands. The SAS2-K2 and the sensors worked perfectly, and a good balance of the efficient sensitivities of both electric and magnetic channels was revealed. It was also noted in the data that a very low noise of both sensors was obtained, according to the original specifications [2], which confirms good EM cleanliness of the satellite itself. The general view of SAS2-K2 for COMPASS-2 instrument is given in Fig. 4.1b. Inside the box of SAS2-K2 two identical SAS2 units were integrated operating in cold reserve mode to increase the reliability of the whole mission, as it is possible to see in the block diagram of the system.

The main characteristics of the SAS2 wave analyzer are the following:

1. Frequency range (search coil and the electric probes) from 1 Hz to 20 kHz
2. Search coil transfer function from 1 Hz to 1 kHz linear and from 1 kHz to 20 kHz flat
3. Electric sensor transfer function from 1 Hz to 20 kHz nearly flat (Fig. 4.1d)
4. Noise bands
5. Magnetic sensor of 10 Hz–2 $pT/Hz^{1/2}$, 100 Hz–0.2 $pT/Hz^{1/2}$, 1 kHz–0.03 $pT/Hz^{1/2}$, and 10 kHz–0.05 $pT/Hz^{1/2}$ (Fig. 4.1c)
6. Two electric probes of 10 Hz–40 $nV/Hz^{1/2}$ and 10 kHz–20 $nV/Hz^{1/2}$. The weight of the SAS2-K2 electronic unit is 470 g. The total weight of the system with sensors etc. is 1,260 g. The size of the electronic unit is $150 \times 70 \times 110$ mm^3. The power consumption is $\leq$3 W, including the sensors, by this, one electronic unit (the SAS2-A or the SAS2-B inside the SAS2-K2 box) is in a cold backup mode.

During the operation of the system it was possible using telemetry commands to select which of A or B unit is active inside the SAS2, the input gain of the input analog (ULF–VLF) amplifiers and the main operation mode and the parameters of the selected operation mode including the sampling rate of the registered signals. The maximum sampling rate was 43.2 kHz for each channel and the gain of input amplifiers was possible to change from -18 to $+$ 20 dB in three steps.

The SAS2 has three different memory modules beside the internal memory of the DSP. The first is the boot memory (128 KB EPROM) from which the operating

program is loaded after switch-on or power-on reset. The second is a 4 MB SRAM used for measurement data storage organized as circular buffer and telemetry buffer. The third is a 64 KB EPROM to set and store the actual parameters and reference spectrum of the measuring (operation) modes. Using this hardware and software possibilities the following SAS2 main operation modes are realized:

1. *Monitoring of the average EM noise spectra of both channels*. The averaging time can be set by commands from 1 s high-speed monitoring to 10-min long time averaging. This operation mode runs simultaneously with possibly two or three operation modes.
2. *Event detection*. After the processing of the signals coming simultaneously to both channels the processed signal (spectrum) of one selected channel is compared to a stored (and selected or modified by ground commands according to the actual onboard EM situation, etc.) reference signal (spectrum). If the recorded spectrum is higher than the reference one by one or more spectral lines (see more about these criteria given by Lichtenberger et al. [3]), it is accepted as a real event and valid trigger. Then, the system reads the recorded signal values stored in a circular buffer memory before a predefined time of the trigger signal and follows the trigger signal to another predefined time (e.g., 0.5 s before the trigger and 1 or 2 s after the trigger). If the registration of the detected electric and magnetic signals during this time period is finished, the whole record is rewritten to the telemetry buffer.
3. *Periodical, time-controlled data collection*. In this mode, the SAS2 detects and stores the incoming data of both channels with predefined sampling rate (normal "burst" mode) without triggering an event detection using a command controlled (predefined) registration time schedule list.

4.2.2 Experimental Results

Despite these difficulties related with submarine launch and short time of work, the satellite allows to receive interesting scientific results. We present a few results received by the instruments of the scientific complex and then in detail VLF-data.

Two-frequency receiver GPS – Glonass showed high quality of the definition of space–time parameters of the satellite. Continuing processing of information connected with reconstruction of the ionosphere profiles.

High-frequency receiver RFA registered dynamical spectrum in the frequency range from 0.3 to 18 MHz. In Fig. 4.2a local plasma resonances in frequency range from 12 to 14 MHz in conditions of high and low impedance of antennae are presented.

Radiation Detector "TATYANA" measured proton flows with energies 7–15 arrhythmic pulse number of the counter. Plato on curves shows penetration of energetic particles in the inner magnetosphere on open magnetic force lines up to altitudes near 400 km. The Earth in proton flows from South was shown in Fig. 4.2d. Pulses of ultraviolet emission 02.12.06 at 21.04.41 UT were also

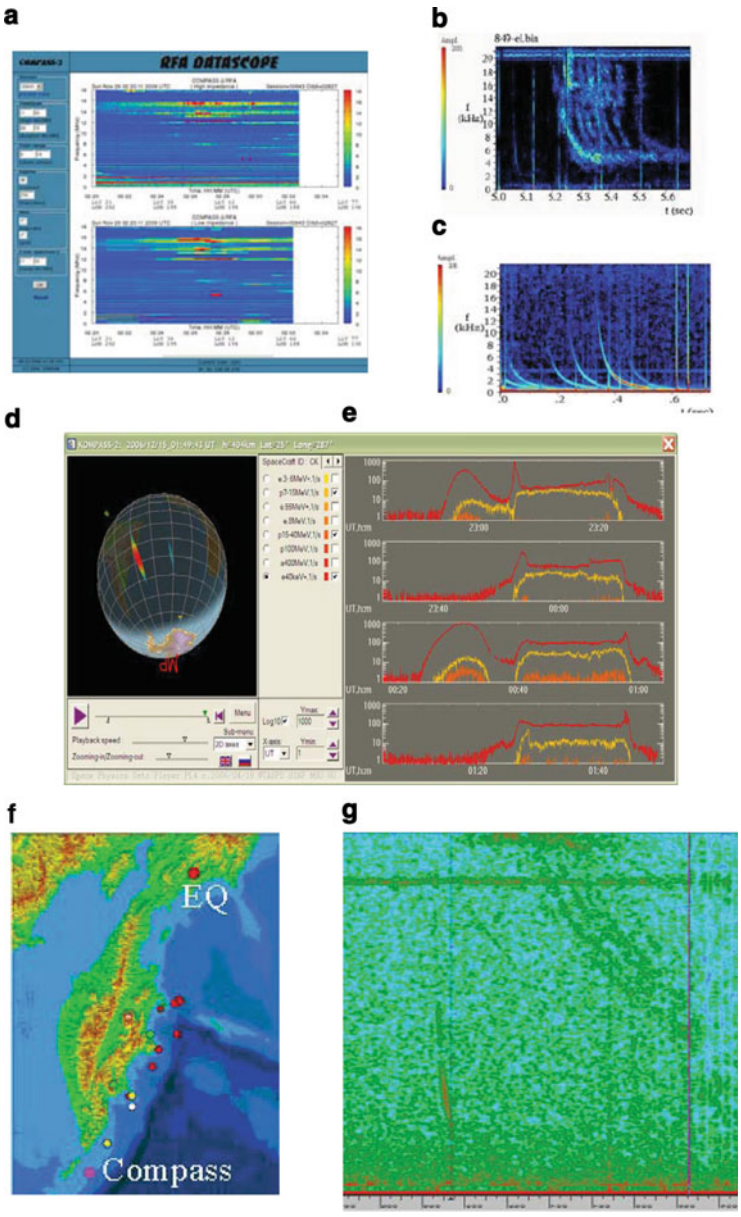

Fig. 4.2 (**a**) Local plasma Resonances over WS-America (RFA); (**b**) SpW (SAS2); (**c**) FDW (SAS2); (**d**) sight of Earth in proton flows; (**e**) proton flows 7–10 (red) and 15–40 MeV (yellow) over South Atlantic (altitude 400 km); (**f**) map of Kamchatka with EQ 28.02.07; (**g**) FDW and whistlers 27.02.07 at 21.35 UT (SAS2)

registered. This event is connected with the storm phenomena over Kenya at nighttime. Double pulses are connected with near-storm discharges (device DUF).

Low-Frequency Wave complex (NVK) registered electric and magnetic components of electromagnetic field in the range of frequencies from 1 Hz to 20 kHz. Frequently dispersed whistlers have been registered over Indonesia (Fig. 4.2b). The duration of signals equal to 200–400 ms, $D \sim 5$, frequency of maximum $\sim$ 2,500 Hz. Spiky Whistlers (SpW) phenomena was recorded on Demeter and COMPASS 2 the SAS2, 16.03.2007 (Fig. 4.2c). At 18.03.07 in 17.09.17 UT was detected a broadening of VLF-transmitter on frequency 12.0 kHz. The band of signals equals 200–400 Hz. The fluctuations of frequency have a time characteristic of about 0.05–0.13 that accords with dimensions of uncertainties about ~300–500 m. Now there is an actual problem – penetration of strong atmospheric on satellite altitudes. In times of flight over Central Europe, 11.02.07 10:02 UT satellite "COMPASS 2" registered strong noise burst in the frequency range from 500 to 2,500 Hz on the latitude of ~450 km [4]. An attempt was made to register a penetration of strong atmospheric signals, which can be considered as precursors of earthquakes. In Fig. 4.2h a dynamic spectrum of such a signal is represented; it was registered 27.02.07 at 21:35:49 UT over Kamchatka (Fig. 4.2g) before the earthquake. It is a frequently dispersed whistler with the dispersion rate of ~5.1/s^2. Later, a group of multipath whistlers with the dispersion rate of about 75.1/s^2 were noticed.

In the paper [5], analysis of an isolated whistler group with very low background received on "COMPASS 2" was presented. It confirms that every whistler has a special structure, that is, the spectrogram of these signals has no asymptote and zero asymptote; however, these signals were predicted by the theory of UWB propagation in waveguides filled with magnetized plasmas [6, 7] Using the theoretical model cited above it is possible to make a detailed comparison of computed and measured data. The form, spectrogram of computed (simulated) UWB signal and measured signals recorded on board of COMPASS 2 by SAS2 were nearly identical if simulated UWB signal propagates not in a tube, but between two layers (inside an onionskin-like structure) and it propagates in the third-order guided form (Fig. 4.3a). The correlation and similarity of these signals were very high.

Therefore, it is possibly to state, that SAS2 has recorded a whistler group, which propagated in the guided mode, probably between two layers of plasma inhomogeneities in the form of higher ($m = 3$) order guided mode. So, the new advanced EM analyzers on board electromagnetically very low-noise satellite has the capability to detect and identify VLF signals (whistlers) propagating in free space mode without guiding and in guided modes in waveguiding structures. The general shape of this recorded waveform (Fig. 4.3a, b) identifies its presence (tube-like or surface, i.e. onion-like etc.). In our case, there is evidence to confirm the existence of surface-like (onionskin-like) waveguide structure (Fig. 4.3c) in the magnetosphere; however, there was no evidence of a tube-like ("spaghetti-like") structure that appeared with rather high probability.

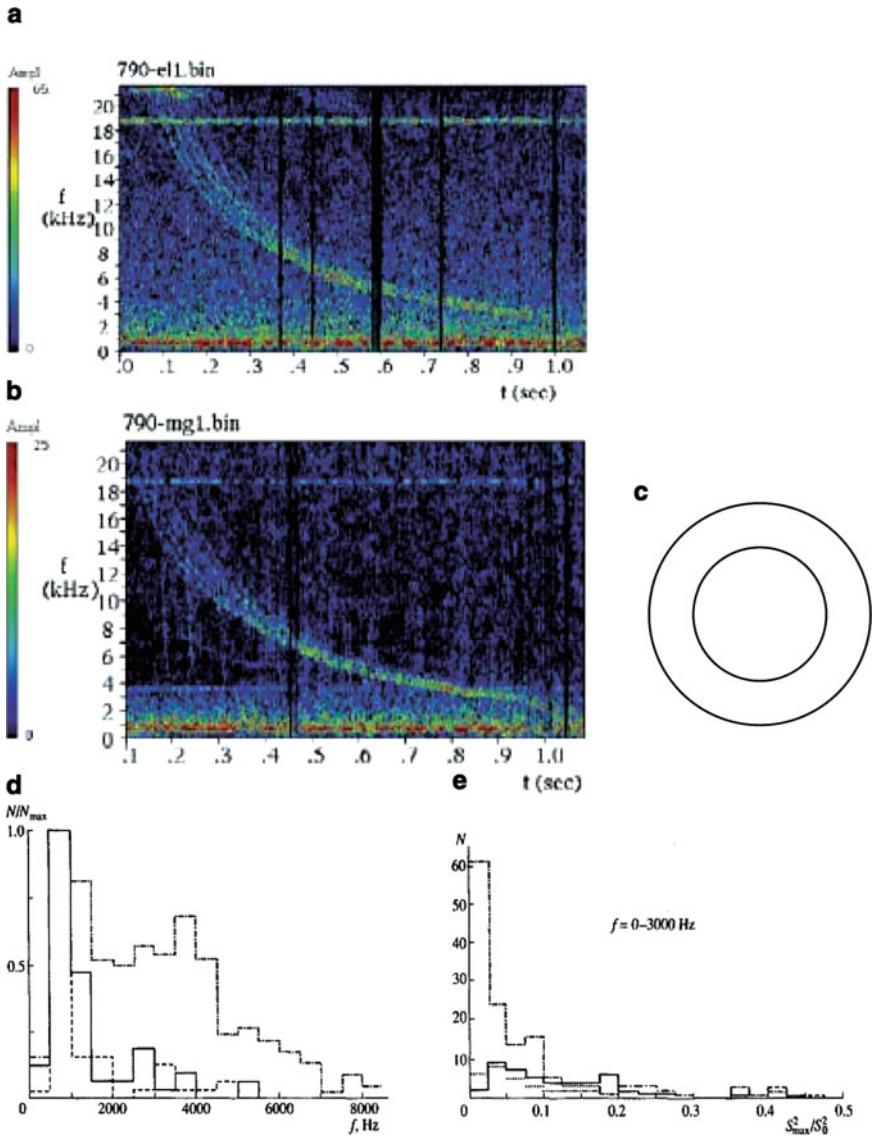

Fig. 4.3 (**a**) Sonogram of whistlers, electric component (SAS 2); (**b**) sonogram of whistlers magnetic component. At low frequencies curve $f(t)$ reaches zero in finite time; (**c**) onion-type waveguide model; (**d**) frequency histograms of maxima in the whistler spectrum, (**e**) its relative intensity at quiet conditions at $Kp < 3$ (*solid line*); at $Kp < 3$ but during the seismically active period (*dash-dotted line*); and at $Kp > 3$ in the absence of earthquakes (*dashed line*)

4.2.3 Conclusions

Data of devices RFA and "TATYANA" are under process. The satellite has high cleanliness that allows registering of very thin electromagnetic VLF-effects. Wave analyzer SAS2 has recorded a whistler group in the higher-order guided mode. The recorded whistlers propagated probably between two layers confirming the existence of an onionskin-like structure of inhomogeneities in the plasmasphere. These whistlers propagated probably in the form of a third-order guided mode between the boundary layers. These ideas, developed in ref. [5] have been confirmed by "COMPASS 2" data.

4.3 ELF and VLF Electromagnetic Background in Topside Ionosphere over Seismically Active Areas (Intercosmos-24 Satellite)

4.3.1 Introduction

This section is devoted to the continuation of our studies of the ionospheric *D*-region properties at the earthquake preparation phase on the basis of the observed "INTERCOSMOS-24" whistler spectra of broadband data, but using a large volume of experimental data. For comparison, we consider the amplitude spectra of whistlers during magnetically active and quiet periods in the absence of seismic activity.

4.3.2 Input Data and Processing Methods

We used broadband records of the electric component of the electromagnetic field received at the station of the Institute of Terrestrial Magnetism, Ionosphere, and Radio Wave Propagation ($\varphi \cong 55.5°$N, $\lambda \cong 37.3°$E) from "INTERCOSMOS-24" to study the response of the lower ionosphere to earthquakes. For this receiving station, the radio-visibility zone was extended from 25°N to 80°N in latitude and from 340°W to 80°E in longitudes; it included the two seismically most active areas; the Mediterranean Sea and the Caucasus with Iran. According to the catalog (NEIC), the epicenters of the earthquakes that occurred in 1990–1992 had the following limiting geographical coordinates: $\varphi_{max} = 45°$N, $\varphi_{min} = 34°$N and $\lambda = 10°$E–31°E ($L = 1.35$–1.85) for the first area; and $\varphi_{max} = 43°$ N, $\varphi_{min} = 27.5°$ N and $\lambda = 43.5°$E–58°E ($L = 1.3$–1.85) for the second area. For our data processing, we selected records taken in orbits whose latitudinal projection extended from 25 to 45°N, i.e., in the range of L shells 1.3–1.9. The data processing consisted of

the following steps. The signal tape records were first examined with an analog spectrum analyzer. Of the 250 satellite passes from October 1989 through June 1992, 75 append in the longitude sectors 10–30° and 45–60°E. For the subsequent digital data processing, we selected the most characteristic records on the following three conditions: in the absence of seismic and geomagnetic activity, at enhanced geomagnetic activity but in the absence of earthquakes, and during seismic activity but for $Kp < 3$ at daytime. By the analogy with ground-based observations of earthquake effects using whistlers, we choose the signal rate and the frequency and intensity of maxima in the spectra as the quantitative whistler parameters. We used the spectral density of a calibration sinusoidal signal of frequency 4 kHz and duration 2 s to quantitatively estimate the whistler intensity. This signal was fed to the input of the onboard broadband receiver every 8 min simultaneously with useful signals from the output of the antenna system. Next, we estimated the whistler's spectral density at a maximum of the spectrum (S_{max}).

To carry out a detailed digital data processing, the analog signals were read from the magnetic tape into a computer. A spectral-time analysis of the read signals was performed by the method of a sliding time "window" $\sim$ 25 ms in duration in the frequency range 70 Hz–4 kHz, which yielded a digital spectrogram, that is, with one dependence of $f(t)$. Concurrently, we estimated the spectral density of the maximum $S_{max}{}^2$ (f_{max}, t). Next, using the $f(t)$ curve near f_{max}, we estimated the dispersion D from two points on both sides of this frequency by assuming that the law $D = t/f$ was valid. For each whistler, we thus had t, f_{max}, S_{max}, and D, which, together with the satellite orbital data, give full information about the characteristics of the whistler and its position in space (φ, λ, h, L, and LT). We determined the signal rate from these data and the propagation path of the signal − whether it follows along a short path from the Earth–ionosphere waveguide or from the southern hemisphere − from the dispersion. The next processing step was to construct a statistical frequency distribution of maxima and the relative maximum spectral density in the whistler spectra for each satellite pass.

In addition, we calculated the terminator line at ground level and at heights of 60 and 100 km for all passes. The coordinates φ^* and λ^* of the conjugate regions [9] were estimated from φ and λ at the ends of the orbit projections in the latitudinal belt under consideration. The terminator curve at 60 and 100 km and the (φ, λ and φ^*, λ^* data were used to determine the sunrise and sunset times in the northern and southern hemispheres to estimate the illumination conditions for the whistler propagation path from the southern-hemisphere sources. For each satellite pass, there are also data on seismic and geomagnetic *(Kp* indices) activity.

Since the strongest seismic event, both in intensity and in duration, during the period 1990–1992 under consideration occurred in Iran from June 20 to 30, the greatest attention in our data analysis is given to this period. According to the data from seismic Catalog, there were six repeated shocks during this period with M_p in the range 4.8–6.1 and about 60 with $M_p < 4.8$.

4.3.3 Main Results

To study the behavior of the *D* region of the ionosphere during earthquake preparation and high magnetic activity, we selected 53 turns when the satellite passed a wide range of longitudes from −10 to 65°E, but mostly during the period that included the Iranian-earthquake events of 1990. Of them, ten turns were at $Kp < 3$ during the active seismic period, ten passes were at $Kp > 3$, and 33 passes were at $Kp < 3$ but in the absence of earthquakes. Since the damping coefficients of VLF waves for extraordinary polarization as they pass into the topside ionosphere from the Earth–ionosphere waveguide are at a maximum at $h \sim 60$–90 km and decrease by three orders of magnitude at $h \sim 1{,}000$ km [10], all the whistlers observed at $h \sim 700$–2,400 km were included in the data processing.

Quiet background, $Kp < 3$, no earthquakes. Fractional hop whistlers observed at morning and day local time, when the diurnal variation of thunderstorm activity and atmospheric interference near the ground exhibits a minimum, which is deeper than that in the morning, are of greatest interest in the analysis. These patterns of behavior showed up during satellite observations, when at $Kp < 3$ under seismically quiet conditions at heights up to 2,400 km fractional hop whistlers, irrespective of the longitude, were either completely unobservable or were observed very rarely (up to 4/min) and were less intense; only ELF components in the frequency band from 200 Hz to 2 kHz were present in their spectra. In the morning, ELF hisses were observed in all orbits in the frequency band 400–500 Hz. In addition, a secondary maximum was also observed in the spectrum of fractional hop whistlers over the Mediterranean Sea at maximum seasonal thunderstorm activity (May), but was of lower intensity than that for the first ELF. The whistler rate and intensity before the sunset increase compared to the morning and daytime.

Geomagnetic effects in the D *region.* To estimate the geomagnetic effects in the *D* region of the ionosphere in such low *L* shells ($1.4 < L < 2$), we considered two periods of high geomagnetic activity: May 19–21, 1990, and August 22–23, 1990, at $Kp \sim 5$–6. A data analysis for these periods revealed that exclusively fractional hop whistlers, whose amplitude spectra exhibited only ELF components with an upper cutoff frequency 0.7–1.5 kHz, that is, lower than in the signals under quiet-time conditions were observed. These signals had strongly diffuse traces on the $f(t)$ spectrograms. As the *Kp* index decreased, the whistler rate ($\sim$ 6–8/min) was essentially constant, but the ELF spectrum extended to higher frequencies (up to 2 kHz). For all passes, ELF hisses were observed in the band 300–400 Hz at $Kp > 3$ [16].

Seismic effects in the D *region.* We analyzed the whistler spectra for seven satellite passes over Western Iran from June 21 through 29, 1990; one pass over Southern Iran on November 6, 1990; one pass over the Mediterranean Sea on January 18, 1990; and one pass over Romania on May 29, 1990, during earthquake preparation *(*$Mp \sim 5$–6.1, $h \sim 3$ and 30 km). Our analysis of the whistler amplitude spectra revealed the following: first, the extension of the ELF spectra to higher

frequencies (up to 3 kHz) compared to the quiet background; second, the appearance of VLF spectral components; third, the observation of isolated fractional hop whistlers of anomalously high intensity $(S_{max})^2$ with a broad spectrum $\Delta F =$ 100–10,000 Hz without the minimum at frequencies of 2–3 kHz which is typical for the spectra of whistlers observed in the Earth–ionosphere waveguide; in the evening, these whistlers were accompanied by echo signals reflected in the southern hemisphere, suggesting that magnetospheric ducts are formed over seismically active areas at the earthquake preparation phase.

Figure 4.3d shows the frequency distributions of maxima in the spectra of fractional hop whistlers with a dispersion $D < 20$ normalized to the total number of maxima for three different geophysical conditions: quiet background ($\Sigma = 69$), geomagnetic activity ($\Sigma = 54$), and seismic activity ($\Sigma = 300$). Figure 4.3e shows the frequency distribution of the relative intensity of maxima for the same geophysical conditions. The following general trend clearly shows up both in the sample passes and in the histograms: the decrease in the upper cutoff frequency of the ELF spectra at $Kp > 3$ and its increase during the seismically active period compared to the quiet background values; the appearance of additional maxima at frequencies above 3 kHz during the seismically active periods. At the same time, there is no strong dependence of the whistler intensity on *D*-region conditions, and the number of whistlers during the seismically active period increases at the expense of weak signals (we excluded anomalously strong isolated whistlers when constructing the histograms).

4.3.4 Discussion

Our results show that fractional hop whistlers with dominating ELF components in their spectra are observed at daytime at heights 700–2,400 km in the absence of seismic and geomagnetic disturbances. VLF components are also observed in the spectra of daytime whistlers over the Mediterranean Sea at maximum thunderstorm activity, but they are weaker than the ELF components. This implies that at daytime, VLF waves undergo a stronger damping as they pass into the topside ionosphere than do ELF waves. This conclusion is consistent with the theoretical calculations [11], according to which the transmission coefficients of electromagnetic waves in the frequency range 1–30 kHz have their maximum at $f = 5$ kHz and change only slightly on both sides of this frequency. At the same time, the transmission coefficient at daytime is, first, an order of magnitude smaller than that at nighttime, and, second, being at a maximum at ~ 1 kHz (for a definite ionospheric model), it steadily decreases with frequency, for example, by a factor of 5 at $f \sim 15$ kHz. As the damping in the *D* region increases, this curve shifts to lower frequencies.

Based on the latter theoretical conclusion, we can qualitatively explain the amplitude spectra during seismically active and magnetically active periods. The shift of the upper cutoff frequency of the ELF components in the spectra of fractional hop whistlers to higher frequencies at the earthquake preparation

phase and the appearance of VLF components in their spectra suggest that the damping of these waves decreases as they pass into the topside ionosphere. With increasing geomagnetic activity, the upper cutoff frequency in the whistler ELF spectra steadily decreases and becomes lower than 1 kHz at $Kp \sim 6$. This suggests that the damping of ELF waves is enhanced as they pass into the topside ionosphere. It thus follows that the *D*-region of the ionosphere is modified by different agents during seismic and geomagnetic activity. During geomagnetic disturbances, high-energy electron beams, which produce additional ionization in the lower ionosphere, are the main agents responsible for the increase in the *D*-region conductivity. During the preparation of earthquakes, several hours before their active phase, an abrupt increase in the count rate of precipitating electrons from the inner radiation belt with energies 0.7–25 MeV [12] and 40–250 keV [13] was actually detected. Moreover, parameters of the seismogenic variations over the area of the Iranian earthquake in 1990 were estimated by using the Meteror-3 satellite counters of electrons with energy 0.7–25 MeV [14]. It turned out that the repeated shock of June 21 with $Mp \sim 6.1$ was preceded by an anomalous burst of particles 13 h before, while the repeated shocks with a smaller magnitude (June 21 and 22) were preceded by such a burst 2–4 h before. The appearance of these bursts did not coincide in time with the anomalous increase in intensity of the fractional hop whistlers observed from INTERCOSMOS-24, particularly during pass 3309 on June 21 [10]. These experimental facts suggest that the changes in *D*-region properties during the earthquake preparation are caused by an agent other than particles.

An attempt to explain the increase in the signal intensity of very-long-wave ground-based transmitters over the area of the preparing earthquake by the change in near-ground atmospheric conductivity due to the radioactive radiation associated with radon emanation during fissuring was first made by Martynenko [15]. According to their estimate, this causes the *D*-region electron density to increase only slightly and the frequency of their collisions with neutral particles to decrease appreciably. As a result, the lower-ionosphere conductivity decreases, as does the damping of VL waves as they propagate in the Earth–ionosphere waveguide and as they pass from the waveguide into the topside ionosphere.

4.3.5 Conclusion

An analysis of the amplitude spectra for the fractional hop whistlers observed from INTERCOSMOS-24 at daytime under various geophysical conditions has revealed the following [16]:

During a quiet period, in the absence of seismic and geomagnetic disturbances, the signal spectra exhibit mostly ELF components ($f_c < 3$ kHz) with its upper cutoff frequency $f_c \sim 1.5$ kHz. This result is consistent with theoretical views of the properties of ELF–VLF-wave passage into the topside ionosphere from the Earth–ionosphere waveguide.

With growing geomagnetic activity, the upper frequency of the ELF components shifts to lower frequencies (700–1,000 Hz), which, according to theoretical views, suggests that the damping of ELF waves enhances as they pass through the *D*-region of the ionosphere.

By contrast, during a seismically active period, in the earthquake preparation phase, the upper cutoff frequency of the ELF components in the whistler spectra shifts to higher frequencies (2.5–3 kHz), and VLF components emerge, that is, the damping of ELF and VLF decreases as they pass through the *D*-region.

Our analysis of the whistler amplitude spectra has allowed the seismic and geomagnetic effects in the region of the ionosphere to be clearly separated. They are related differently with wave damping, other words, *D*-region conductivity, they are attributing different physical agents which modify this on. The additional ionization in the *D*-region provided by the precipitation of high-energy particles from the inner radiation belt during geomagnetic disturbances does cause the damping of ELF and VLF waves to be enhanced, which is confirmed by experiment.

Other phenomena should be invoked, which allow a mechanism of the lithosphere–ionosphere interaction in its lowest part to be loped. There is no such mechanism so far. In this section, there was a hypothesis about the change of whistler characteristic as a result of lower ionosphere (*D*-layer) conductivity variations. But it is necessary to prove that these changes are related to lithosphere processes. It is a complicated problem. In Section 4.5, we will try to solve this problem experimentally with the help of ground-based measurements.

4.4 Quasi-static Electric and ULF Magnetic Fields on Kamchatka

4.4.1 Experimental Results

We analyzed earthquake precursors observed in various periods in the quasi-static electric field in the surface atmosphere on the Kamchatka Peninsula at the Institute of Cosmophysical Research and Radio Wave Propagation, RAS Fur East Division (Paratunka settlement; 52°58.3′N;158°14.9′E). Figure 4.4a, b illustrate two cases of the precursors occurrence before an earthquake.

A bay-like drop in the quasi-static field down to 300 V/m was observed before the earthquake of March 6, 1992 ($M = 6.1$) at the epicentral distance of 130 km, with the epicenter in the Avachinskii Bay and a source depth of 30 km (Fig. 4.4b) [17]. A similar decrease in the value of the quasi-static electric field was also observed before the earthquake of September 18, 1999 ($M = 6.0$; a source depth of 60 km) at the epicentral distance of 190 km (Fig. 4.4a) [18]. It is noteworthy that the precursors had similar shapes, but their premonitory times were different: 10 h in the first case and 29 h in the second. Assuming that the time difference depends on the precursor propagation velocity, we estimate the latter as $V = 0.87$ m/s [19].

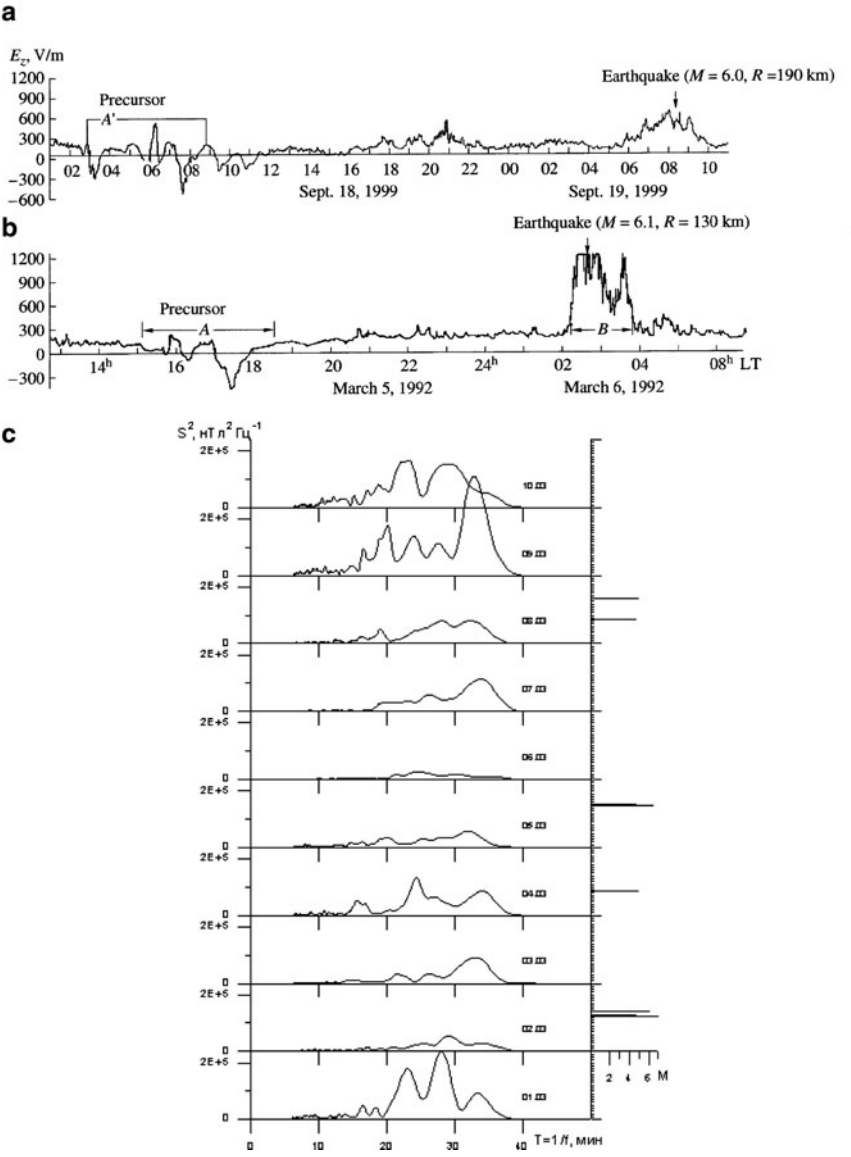

Fig. 4.4 Variations in the quasi-static electric field E_z from Kamchatca measurements in periods of nucleation and developments of the earthquakes 19.09.99 (**a**) and 06.03.92 (**b**). A and A′ are tentative earthquake precursors, and the interval B is the pulsation time of E_z in the neighborhood of an earthquake; (**c**) daily power spectra of horizontal component H for 01–10.03.92 in range of periods 6–40 min. Harmonics with periods 20 and 35 min are seen

In 1983, Zubkov, in his paper [20] informed that at earth current observations, the velocity of earthquake precursors is found to be about 0.3 mc^{-1}.

Korsunova and Khegai [21] analyzed occurrence times of earthquake precursors in the variations of critical frequencies of the ionospheric $F2$ layer in the seismically active Pacific Ocean region. For strong crustal earthquakes with sources shallower than 50 km, the precursor propagation velocity was found to be of the order of 1 m/s. It is unclear as to why these values coincide since the precursory effects were discovered in different parameters and different media. These questions will be considered in detail in Section 4.5.

Now we consider Fig. 4.4 in greater detail and analyze the seismic situation on the Kamchatka Peninsula at the beginning of March 1992. Two series of earthquakes occurred in this period: on March 2 and 5 (according the NEIC catalog).

Sequence of 2 March includes three shocks (12.29.39, 12.49.18, 14.07.59 UT) with deeps 38, 33, 34 km and magnitudes (6.9, 4.6, 6.0). Interval between shocks is near 20 min. Sequence of 5 March includes three such shocks (14.39, 15.14, 16.01 UT) with deeps (45, 33, 39 km) and magnitudes (6.4, 4.7, 4.4). The interval between shocks is near 40 min.

We analyzed by spectral method [18] a horizontal component of magnetic field. The results of data analysis obtained during 1–10 March (1992) are presented in Fig. 4.4c, where on the right-hand side of the vertical the time scale for this interval is given from the bottom upwards. Horizontal lines are concerned with EQ, whose magnitude exceeds 5. In doing so, the corresponding scale is at the bottom. Special attention here should be paid to some sequences consisting of two or three above-mentioned shocks for EQ 3.03.92 and 6.03.92. On horizontal lines one can see the daily spectra of the H-component of the magnetic field occurred at Petropalovsk-Kamchatsky's station in the case when the time period was varying from 6 to 40 min. It is interesting to note that the 35 min-harmonics could be roughly put in correspondence with the time interval between the shocks of EQ. These harmonics either appears most brightly or responds with some delay to the occurrence of EQ. Unfortunately it is difficult to evaluate correctly this delay in light of the small time interval of available data. Nevertheless from preliminary estimates one can conclude that this delay corresponds to the precursor propagation velocity of 1 m/s order.

4.4.2 Conclusions

The analysis of the properties of earthquake precursors in the quasi-static electric field of the surface atmosphere has led to the following conclusions:

- The precursor propagation velocities vary within the range of 0.87–1.8 m/s and depend on the focal depth.
- In electromagnetic signals, harmonics with equal periods of interval between foreshocks were found.

4.5 An Experimental Confirmation of the Relation Between Precursors of Earthquakes in Near-Earth Electric Fields and in Ionosphere Parameters

4.5.1 Introduction

Appearance of seism-ionosphere disturbances before/at earthquakes inspires a considerable interest for understanding of litho-, atmo-, ionosphere coupling, so for possibility of earthquake prediction. Two mechanisms of such coupling are discussed: electrodynamics and acoustic gravity wave (AGW) influence [22]. Thereby precursor effects are very different, having different duration and deviation from the background level; therefore, it is necessary in each occasion to choose available coupling mechanism. So, for interpretation of disturbances with periods $T \sim 1.5$–2.5 h in daily variations of $F2$ and E_s-layers frequency parameters, there is often a chosen hypothesis about the influence of those scales on ionosphere by AGW, increasing of activity which was observed during the seism-active periods [23].

However, in ref. [24], it was obtained that propagation of the ionospheric disturbances with $\tau = 2$–3 h, identified as medium-term precursors of earthquake, is realized with low velocities (4–8 km/h), compared with the earth core seismgenic disturbance velocities described in ref. [25]. Such velocities by two orders of magnitude are smaller than AGW velocities and therefore this hypothesis cannot serve as the satisfactory explanation of the observed ionospheric disturbances. On the other hand, the appearance of anomalously high E_s at $h = 120$–140 km in the period of the earthquakes preparation, which is the basic morphological sign during the identification of ionospheric precursors [24], corresponds to the model calculations, that consider the action of electric fields on the ionosphere [26, 27].

Simultaneous measurements of the electric field and ionosphere parameters can play an important role in the understanding of such coupling nature in the seism-active region. Such measurements are realized on geodynamic area in Paratunka village, Kamchatka region, at the Institute of Cosmophysical Research and Radio Wave Propagation of Far East Branch of Russian Academy of Science. The first results of simultaneous measurements of the vertical electric field component near the Earth's atmosphere and ionosphere parameters at EQ-preparation were published in ref. [28], where coupling between $F2$-variations and the electric field has been considered. However, in this paper only one ionosphere parameter – the critical frequency of $F2$-layer – was considered, and clear correlation between E_z- and $F2$-variations has not been obtained in the result of mask influence of earth magnetic field disturbances. Anomalies of electric field in the atmosphere, which may be considered as the precursors, and the velocity of their propagation have been discussed in ref. [29]. It was stated that virtual velocities of theirpropagation are equal to 1–3 km/h, that is, close to virtual velocities of ionosphere precursors propagation, according to ref. [24]. This fact correlates with this paper's purpose to find the coupling between the atmospheric electric fields and ionospheric

parameters in the periods of earthquake preparation. To find this coupling for search of ionosphere precursors, a new method was applied, which took into account the simultaneous measurements of E_s and $F2$ parameters. It used Paratunka ionosphere data ($\varphi = 52°58.3'$N; $\lambda = 158°14.9'$E) during February– March 1992, September–October 1999, and September–October 2002. During September–October 1999, full processing of ionosphere observations with sampling time of 30 min was made; for other months, there has been formed an hourly data of this station, obtained from archive of NOOAA's National Geophysical Data Center [31]. Processing the ionosphere data in more detail is necessary since the appearance of E_s in considered time intervals (equinox) is a rare event, and hence the existence of two sporadic formations is possible, which do not reveal in hourly data of the archive.

4.5.2 Method of the Analysis

In ref. [24], the ionospheric earthquake (IPE) precursors identification method proposed earlier in ref. [30] is tested. The main criterion for detecting precursors is to serve the appearance of an abnormally high-layer E_s with a duration (τ) of about 2 h in excess of 10 km or more background values of $h'E_s$.

Besides, only those events are taken into account, when increasing $h'E_s$ are accompanied by bursts in frequencies parameters of E_s and $F2$ of the same duration. This method allowed the detection of IPE for 33 strong EQ with $M \geq 6$ in Japan in the period from 1985 to 2001.

For Kamchatka weaker EQ are typical; therefore, weaker ionosphere effects of EQ premonitory are expected. It is connected with the fact that values of seism-ionosphere disturbances depend on a magnitude (M) of future EQ [30]. Nevertheless, the criteria of precursors determining proposed above were used for Kamchatka also. But in contrast to the cited work, average values on ten magneto-quiet days, which preceded earthquake were used as the background values of the ionospheric parameters. It is connected with the fact that at considered latitudes high influence of the magnetic disturbances on parameters of $F2$ layer is observed.

For the identification of the supposed IPE the instantaneous deviations values of the $h'E_s$, f_bE_s, f_oE_s, and f_oF2 from background values for each hour (and for half-an-hour interval for the selected periods of 1999) were calculated: $\Delta h'E_s = h'E_s - (h'E_s)_{mean}$, $\Delta f_bE_s = f_bE_s - (f_bE_s)_{mean}$, $\Delta f_oE_s = f_oEs - (f_oE_s)_{mean}$, $\Delta f_oF2 = f_oF2 - (f_oF2)_{mean}$. For the frequency parameters, we calculated the deviation relative values: $\Delta f_bE_s/(f_bE_s)_{mean}$, $\Delta f_oE_s/(f_oE_s)_{mean}$, and $\Delta f_oF2/(f_oF2)_{mean}$. The analysis was fulfilled from the moment of the earthquake to the time of the precursor appearance. All events, which coincided with higher mentioned signs, has been marked [24].

In Fig. 4.5a there are changes of base ionosphere parameters with sampling time 30 min and E_z-component of quasistatic electric field in preparing period of EQ 18.09.99 with $M = 6.0$. A distance from the epicenter to the observation point (R) equals to 190 km. The moment of earthquake is indicated by a dashed line arrow.

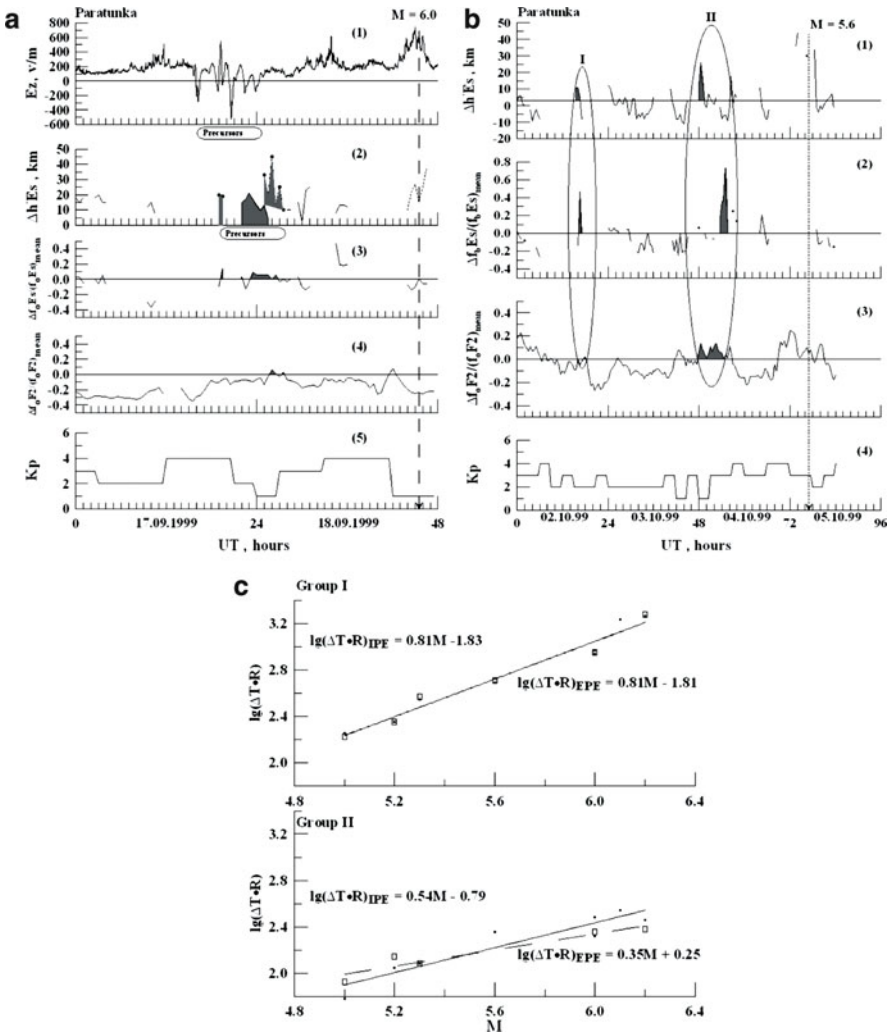

Fig. 4.5 (**a**) Changes of vertical electrical potential gradient (panel 1), ionosphere parameters (panels 2–4) and *K*p-index (panel 5) in preparing period of 18.09.1999 EQ; (**b**) variations of ionosphere parameters (panels 1–3) an *K*p-index (panel 4) in the period of preparing of EQ 05.10.1999. Different groups of supposed IPE have been marked by I and II; (**c**) the logarithm of the product of the lead-time (ΔT) up to the epicentral distance (R) in the dependence on the magnitude of earthquake (M) for two groups of assumed precursors of EQ and approximating lines (*solid line* – IPE, *dashed line* – EPE)

The time of electrical precursor appearance was defined on time registration of negative electric field bay shape curve at time E_z-variations, but IPE- on registration anomaly high E_s (type *h* – thick dotted line on Fig. 4.5a). Blackened bursts, corresponding to directed higher criteria, are presented as precursors. On lower panel there have been carried the variation of *Kp*-index at same time interval. It is

evident that the preparing of EQ 18.09.99 is accompanied by magnetic disturbances. That is why the positive deviation in the frequency parameters of E_s and $F2$ layers are very small, but their appearance in the same period of time as the anomalies in the E_z and $h'E_s$, and violation of the observed trend toward negative deviations in f_oF2 show their seismogenic nature.

However, when the data on E_s-layer are absent, the identification of IPE only with f_oF2 is very complicated; it is indicated in ref. [28].

Comparison of ionospheric parameters variations and E_z-component of electric field shows that precursor in electric field appeared few hours earlier than in ionosphere. Besides, a few hours earlier EQ are noticed bursts in E_s-parameters, which coincide with increasing of E_z.

Analysis of time ionosphere parameters variations in the absence of noticeable geomagnetic disturbances (when the average daily magnetic index $Ap \leq 17$ nT) shows that it was possible to select two groups (I, II) of E_s-parameters essential deviations, which satisfied to morphological signs of IPE-identification, defined in [24], distinguish on lead-time of EQ-moment, IPE of first and second orders on lead-time. It is illustrated by Fig. 4.5b, in which are given one half hours data, and two groups of IPE. It is evident that these groups differ not only in the earthquake lead-time (ΔT_{IPE}), but also the deviations values within groups and their duration.

The most deviations in the ionospheric parameters are noted in the second group for the E_s-layer. The duration of bursts and their numbers in the second group are greater than in group I, for which individual bursts are typical.

Quasistatic electric field variations at September–October 2002, presented in ref. [29] were compared with corresponding variations of E_s and F-layer calculated on hourly data. The onset of precursors and time interval from the moment of their appearance to the main shock (the lead-time for EPE, ΔT_{EPE}) was determined. Table 4.1 contains results of such a comparison and so EQ-parameters. Unfortunately, for March 1992 electric field data are absent, but for EQ 5.10.1999 precursors of II group were not identified (see dashes in Table 4.1).

By stars there are marked precursors, identified before in ref. [14] only by electric field measurements. For other events, there are identified bay-shape disturbances of electric field during day interval centered IPE relatively. Moment of appearance of such disturbance with maximum amplitude and ΔT are indicated in Table 4.1. It is seen that E_z anomalies appear before the appearance of ionospheric disturbances. Therefore one can suppose that appearance of two groups of different precursors corresponds to different phases of EQ preparing.

4.5.3 Results and Discussion

Results of analysis of the ionospheric parameters variations for before EQ periods (for 6 EQ) show that it is possible to select two groups of bursts with $\tau \sim 1$–2 h duration, which correspond to precursor signs, and, as a rule, are accompanied with specific "bay-shapes" in E_z electric component curves. Appearance of such bursts

Table 4.1 The characteristics of ionospheric and electric EQ-precursors

Date and time of EQ, UT	M	R, km	IPE		EPE	
			Date and time, UT	ΔT, days	Date and time, UT	ΔT, days
Group 1						
08.10.02 09 h 19 min	5.0	120	06.10.02 22 h	1.5	06.10.02 23 h	1.4
03.10.02 15 h 57 min	5.2	280	02.10.02 20 h	0.8	02.10.02 21 h	0.8*
20.10.02 01 h 35 min	5.3	110	16.10.02 22 h	3.2	16.10.02 15 h	3.4
05.10.99 05 h 02 min	5.6	190	02.10.99 15 h 30 min	2.6	02.10.99 12 h	2.7
02.03.92 14 h 08 min	6.0	160	25.02.92 19 h	5.8	–	–
18.09.99 21 h 29 min	6.0	190	14.09.99 07 h 30 min	4.6	14.09.99 06 h	4.7
05.03.92 14 h 39 min	6.1	130	21.02.92 10 h	13.2	–	–
16.10.02 10 h 12 min	6.2	160	04.10.02 20 h	11.6	04.10.02 14 h	11.8
Group 2						
08.10.02 09h 19m	5.0	120	07.10.02 20 h	0.5	07.10.02 17 h	0.7*
03.10.02 15 h 57 min	5.2	280	03.10.02 06 h	0.4	03.10.02 04 h	0.5
20.10.02 01 h 35 min	5.3	110	18.10.02 23 h	1.1	18.10.02 23 h	1.1*
05.10.99 05 h 02 min	5.6	190	04.10.99 00 h.	1.2	–	–
02.03.92 14 h 08 min	6.0	160	29.02.92 15 h	1.9	–	–
18.09.99 21 h 29 min	6.0	190	17.09.99 19 h	1.1	17.09.99 16 h 30 min	1.2*
05.03.92 14 h 39 min	6.1	130	02.03.92 22 h	2.7	–	–
16.10.02 10 h 12 min	6.2	160	14.10.02 14 h	1.8	14.10.02 22 h	1.5*

took place during daytime. The duration of the bursts into E_s for the second group, as a rule, has a duration $\tau \sim 1.5$–2 h, which is somewhat greater than that for the first group. The most considerable deviations in ionospheric parameters have groups with the short lead-time, which we signed as IPE for second group (II). As it follows from Table 4.1, for the same epicentral distances, the precursors in both groups appear earlier, if the value M of the subsequent earthquake is greater. This property is characteristic for those investigated by us before IPE [30]. However, the existence of two groups of IPE, which are distinguished not only by ΔT but also by the value of deflection, is detected by us for the first time. For E_z-component of electric field two groups of specific disturbances before EQ are selected, which differ by the value and lead-times. These times are given in Table 4.1, from which it follows that

E_z-disturbances were observed in the same days, when the IPE were noticed, although times of the E_z-bursts appearance were different from IPE. Depending on the time of appearance they are referred in the Table 4.1 as groups I or II, respectively.

The analysis of values of E_z-disturbances shows that in group II, there are predominated disturbances of E_z with negative swings and amplitudes ranging from −200 to −1,500 V/m. In group I deviations of E_z are small with alternate signs ±(150–300 V/m) bays shape disturbances with $\Delta\tau \sim$ 1–1.5 h. These differences in amplitudes and their durations are analogous to the earlier mentioned peculiarities of IPE for the same group. Therefore, one can suppose that appearance of two groups of different precursors (in EPE and IPE) corresponds to different phases of EQ preparation.

It is necessary to note that precursors of EQ in electric fields with long lead-time (3–26 days) for EQ with $M \cong 5.0$–6.4 have been observed in China [32] and also identified by us as precursors (IPE) of the first order. For Kamchatka EQ in E_z-variation, reliable precursors in the time interval of 1 day before EQ are selected [33, 34], which correspond to characteristics of IEP of the second order according to our classification. It is possible that this is connected with a circumstance that values of seismogenic anomalies in E_z of the second group usually by several times exceeds changes of E_z of the first group, so that they are undistinguished on the background of daily variations. The longest lead-times of EQ (2–3 and 6 months) were exposed in gradients and phase velocities ULF ($f = 0.03$–0.1) of geomagnetic disturbances before EQ with $M = 5.8$ and 6.4 in Japan for epicenter distances $R < 150$ km [35]. Though the nature of these anomalies may be other than those detected in the ionosphere and vertical gradient electrical potential, their appearance shows strong evidence for longer time of EQ preparation, including a few stages. Trends in the logarithm of the product of earthquake lead-time (ΔT) up to epicentral distance (R) depending on the earthquake magnitude (M) for both groups of the assumed precursors are shown in Fig. 4.5c (points – IPE, squares – EPE).

The approximating lines are carried out on the basis of the least squares method. For precursors of the first group next expressions are obtained:

$$\lg(\Delta T \cdot R)_{\mathrm{IPE}} = 0.81M - 1.83; \quad \lg(\Delta T \cdot R)_{\mathrm{EPE}} = 0.81M - 1.81 \tag{4.1}$$

For precursors of the second group, which are nearer to the moment of EQ we have:

$$\lg(\Delta T \cdot R)_{\mathrm{IPE}} = 0.54M - 0.79; \quad \lg(\Delta T \cdot R)_{\mathrm{EPE}} = 0.35M + 0.25 \tag{4.2}$$

It is seen from Fig. 4.5c that obtained empiric dependences are close especially for the first group. This confirms the relationship of Ez-anomalies seismogenic origin to the appearance of disturbances in the ionospheric parameters, which can be attributed to ionospheric precursors of earthquakes.

Besides that, formulae (4.1) are close to that, obtained in ref. [25]:

$$\lg(\Delta T \cdot R) = 0.72M - 0.72 \tag{4.3}$$

for precursors of EQ, propagating in the earth crust. This allows to establish a connection of them with the same phase of preparing EQ. The differences in the constant term in formulas (4.1)–(4.3) reflect, apparently, the structural special features of the earth's crust in the earthquake preparation zone.

As it was shown in ref. [24], on base (4.1), (4.2) it is possible to estimate the apparent velocities of disturbances from the seismic source in the atmosphere and the ionosphere. At propagation of disturbance from 100 to 200 km for $M = 6.0$ we obtained a velocity $V = (0.7–0.8)$ km/h for the first group: for the second group we obtained $V_{\mathrm{IPE}} = 3$ km/h; $V_{\mathrm{EPE}} = 3.7$ km/h. For the same magnitude of EQ and directed epicenter distances we have $V = 0.3$ km/h in accordance with ref. [24]. Comparison of obtained velocities shows that disturbances in ionosphere and E_z in the first group follow the border of preparing EQ region. The apparent velocities of the seism-genic disturbances propagation in group II practically coincide with the velocities of disturbances in the ionosphere according to the data of the stations of vertical sounding in Japan (4.4 ± 3.3) km/h [24] and with the obtained earlier velocities of EPE in ref. [29]. Close times of IPE and EPE appearance for simultaneous observations in the same point of observations, the correspondence of disturbance structure for two groups of precursors, and propagation's velocities of disturbances in the atmospheric electric fields and in the ionosphere are the experimental confirmation of the physical mechanism of seism–ionospheric interaction, based on the modification of near Earth surface quasi-electrostatic fields and their further action on the ionosphere [36]. As it follows from this model, the emanation of radioactive gases from the ground water and the earth's surface in the period of the earthquakes preparation is one of the important factors of impact on the surface quasi-electrostatic field.

It is possible to suppose that the region of exit of high radioactive gases follows the broadening border of EQ preparing zone on the earth's surface, formed by water arrival in microtransform fraction zone of the stress part of the earth's core. Indeed in many occasions few days before EQ an increase of radon concentration in waters and surface layers of earth at far distances from the epicenter (up to 450 km) was observed [37,38]. Next, tests of physical mechanism of lithosphere–ionosphere, proposed in ref. [36], require organization of complex experiments on simultaneous measurements in several points of radon and aerosols concentrations, atmospheric electrostatic fields, and ionosphere parameters. Geodynamic of Kamchatka region where seismic activity is high is in this respect most promising in Russia.

4.5.4 Conclusions

The fulfilled investigation allows us to make the following conclusions:

1. The empirical dependences which reflect the connection between the lead–time of EQ, the distance to the epicenter from the observation point and the

magnitude of earthquake are obtained. The similarity of these dependences for the IPE and EPE confirms their interrelation in the process of lithospheric–ionospheric interaction during the preparation of the earthquakes. As a rule EPE appear earlier than IPE.

2. In the Kamchatka region two groups of earthquake precursors in the ionosphere and in the near Earth surface electric fields with different lead–time of EQ (ΔT) from several hours to 2 weeks are selected. The amplitudes of precursors in the group, which is nearer up to the moment of the earthquake, are substantially greater.

Acknowledgments The authors thank Yu.Ya. Ruzhin, V.S. Dokukin, L.N. Leshenko, G.I. Druzhin, V.V. Bogdanov, O.E. Ferencz, D. Hamar, Ja. Lichtenberger, and P. Steibach for helpful discussions.

References

1. Gufeld, L.I.: Seismic process physical-chemistry aspects RSA, Academia of Cosmonavtics, IPE. Moscow, pp. 153 (2007)
2. Korepanov, V.E.: The modem trends in space electromagnetic instrumentation. Adv. Space Res. **32**(3), 401406 (2003). doi:10.l016/S0273-–1177(03)9020-8
3. Lichtenberger, J., Ferencz, O.E., Bodnar, L., Hamar, D., Steinbach, P.: Automatic whistler detector and analyzer system: Automatic whistler detector. J. Geoph. Res., **113**, A12201 (2008). doi:10.1029/2008JA013467
4. Mikhailov, Yu.M., Mikhailova, G.A., Kapustina, O.V., Druzhin, G.I., Smirnov, S.S., Ferencz, C.H., Lichtenberger, Ja., Bodnar, L., Korepanov, V.: E.: COMPASS 2 Satellite and ground base VLF-experiments. In: Abstracts. AIS-2008 "Atmosphere, Ionosphere, Safety", July 7–12, Kaliningrad, pp. 31 (2008)
5. Ferencz, O.E., Bodnar, L., Ferencz, C., Hamar, D., Lichtenberger, J., Steinbach, P., Korepanov, V., Mikhailova, G., Mikhailov, Yu, Kuznetsov, V.: Ducted whistlers propagating in higher order guided mode and recorded on board of COMPASS-2 satellite by the advanced signal Analyzer and Sampler SAS2. J. Geoph. Res. **114**, A003213 (2008). doi:1029/2008. JA013542, (2009)
6. Ferencz, O. E., Steinbach, P., Ferencz, C., Lichtenbcrger, J., Hamar, D., Berthelier, J.J., Lefeuvre, F., Parrot, M.: Full-wave modeling of long subionospheric propagation and fractional hop whistlers on electric field data of the DEMETFR satellite, paper presented at International Symposium on DEMETER, Cent. Nat. d'Etud, Spalialcs, Toulouse, France, 14–16 June (2006a)
7. Ferencz, O. E., Steinbach, P, Ferencz, C., Lichtenberger, J., Parrot, M., Lefeuvre, F.: UWB modeling of guided waves in anisotropic plasmas, paper presented at 2nd VERSIM Workshop 2006, Sodankyla Geophys. Obs., Sodunkyla, Finland (2006b)
8. Ruzhin, Yu.Ya., Zakharova, O.K.: Magnetic conjugation as a subject of investigation by the method of active experiments. Preprint N.23 (970), IZMIRAN, Moscow (1991)
9. Al'pert, Ya.L.: Radio-wave propagation and the ionosphere. Akad. Nauk SSSR, Moscow (1960)
10. Mikhailova, G.A., Golyavin, A.M., Mikhailov, Yu.M.: Dynamic spectra of VLF emissions in the topside ionosphere connected with Iranian earthquake of 21 June 1990 (The Intercosmos-24 Satellite). Geomag. Aeron. **31**(5), 801 (1991)
11. Aksenov, V.I.: On the origin of the electromagnetic waves of extremely low frequency through the ionospheric plasma. Radiotekhn. Elektron. **11**(6), 1030 (1966)

12. Aleshina, M.E., Voronov, S.A., Gal'per, A.M., et al.: On the relationship between the positions of seismic centers and regions of high-energy particle precipitations from the radiation belt. Kosmich. Issled. **30**(1), 79 (1992)
13. Gal'perin, Yu.L, Gladyshev, V.A., Georgio, N.V., et al.: Precipitation of energetic trapped particles in the magnetosphere over the epicenter of a preparing earthquake. Kosmich. Issled. **30**(1), 89 (1992)
14. Ginzburg, E.A., Malyshev, A.V., Proshkin, I.P., Pustovetov, V.P.: Correlation of strong earthquakes with variations of the radiation-belt particle flux. Geomag. Aeron. **34**(3), 60 (1994)
15. Martynenko, S.I., Fuks, I.M., Shubova, R.S.: Response of the lower ionosphere to variations in near-ground atmospheric conductivity. Geomagn. Aeron. **34**(2), 121 (1994)
16. Mikhailov, Yu.M., Mikhailova, G.A., Kapustina, O.V.: ELF and VLF Electromagnetic background in the topic ionosphere over seismically active areas. Geomag. Aeronom. **37**(4), 450–455 (1997)
17. Rulenko O.P., Ivanov, A.V**.,** Shumeiko, A.V. :A short-term atmospheric electric precursor of the Kamchatka earthquake of March 6, 1992 *(M* = 6.1). Dokl. Ross. Akad. Nauk. **326**(6), 980–982 (1992)
18. Mikhailov, Yu. M.: Seismoelectromagnetic signals before earthquakes on Kamchatka, solar-terrestrial bonds and electromagnetic precursors of earthquakes. In: Rep.4th International Meeting, Paratunka, Kamchatka region, pp. 398–402, Aug 2007
19. Mikhailov, Yu. M.: On the possible role of atmospheric waves in the formation of electromagnetic precursors of earthquakes. In: 2nd All-Russia Workshop on Electromagnetic Sounding of the Earth. November 28–30, 2005, Moscow. Tsentr Geoelektromagnit. Issled, pp. 91. IFZ RAN, Moscow (2005)
20. Zubkov, S.I.: About dependence time and radius of appearance of electrotelluric precursors from energy of earthquake. Phys. Earth. 5, 101–106 (1987) (in Russian)
21. Korsunova, L.P., Khegai, V.V.: Seismoionospheric effects of strong crustal earthquakes in the Pacific Region. Geomagn. Aeron. **45**(5), 706–711 (2005)
22. Sorokin, V.M., Chmyrev, V.M., Pohotelov, O.A., Liperovski, V.A.: Review of lithosphere-ionosphere relations at preparing of earthquake periods. In: Strachov, V.N., Liperovsky, V.A. (eds.) Short time prediction of catastrophe earthquakes by help of radiophysics ground-based-kosmic methods, pp.64–83. OIFZ RAS, Moscow (1998)
23. Husamiddinov, S.S.: Ionosphere Research Electrical and Magnetic Precursors of Earthquakes. In: Golovkov, V.P. (ed.) Tashkent FAS Uz SSR, pp. 90–111 (1983)
24. Korsunova, L.P., Hegai, V.V.: Analysis of seism-ionosphere disturbances on chain of Japan vertical sounding ionosphere station. Geom. Aeron. **48**(3), 407–415 (2008) (in Russian)
25. Sidorin, A.Ya.: Dependence of appearance time of earthquakes precursors of epicenter distance. Reports of RAS. **245**(4), 825–828 (1979)
26. Kim, V.P., Hegai, V.V.: About possibility of formation of metal ion layer in E-region of average-latitude of ionosphere before strong. Geom. Aeron. **33**(5), 114–119 (1993)
27. Sorokin, V.M., Yaschenko, A.K., Hayakawa, M.: Formation mechanism of the lower ionospheric disturbances by the atmospheric electric current over a seismic region. J. Atmos. Sol.-Terr. Phys. **68**(11), 1260–1268 (2006)
28. Mikhailov, Yu.M., Mikhailova, G.A., Kapustina, O.V., Depueva, A.X., Buzevich, A.V., Druzhin, G.I., Smirnov, S.E., Firstov, P.P.: Variation of different atmosphere and ionosphere parameters in periods of earthquake preparing on Kamchatka. Preliminary results. Geom. Aeron. **42**(6), 769–776 (2002)
29. Mikhailov, Yu.M.: On the properties of earthquake precursors in the electrostatic field of the surface atmosphere. Phys. Solid Earth. **43**(4), 336–339 (2007)
30. Korsunova, L.P., Khegai, V.V.: Medium-term ionospheric precursors to strong earthquakes Int. J. Geom. Aeron. **6**, GI3005 (2006). doi:10.1029/2005 GI000122
31. Solar-Geophysical Data. Coffey, H.E., Kroehl H. W. (eds.) Solar –Terrestrial Physics Divisions, NOAA, Boulder, CO (1999)

32. Hao, J., Tang, T., Li, D.: Progress in the research on atmospheric electric field anomaly as an index for short-impending prediction of earthquakes. J. Earthquake Prediction Res. **8**(3), 241–255 (2000)
33. Rulenko, O.P.: Short time precursor in near Earth atmosphere electricity. Vulcanol. Seismol. **4**, 57–68 (2000)
34. Smirnov, S.E.: Peculiarities of negative anomalies of electrical field at near Earth at Kamchatka. Geom. Aeron. **45**(2), 282–287 (2005)
35. Ismagilov, V.S., Kopytenko, Yu.A., Hattori, K., Hayakawa, M.: Use of gradients and phase velocities of ULF geomagnetic disturbances for definition point of source of future strong Earthquake. Geom. Aeron. **46**(3), 423–430 (2006)
36. Pulinets, S.A., Boyarchuk, K.A., Hegai, V.V., Kim, V.P., Lomonosov, A.M.: Quasielectrostatic model of atmosphere-thermosphere-ionosphere coupling. Adv. Space Res. **26**(8), 1209–1218 (2000)
37. Virk, H.S., Singh, B.: Radon recording of Uttarkashi earthquake. Geoph. Res. Lett. **21**(8), 737–740 (1994)
38. Steinitz, G., Vulkan, U., Lang, D.: Monitoring of the tectonically related radon flux in Israel. Isr. Geol. Surv. Curr. Res. **10**, 148–153 (1996)

Chapter 5
Mathematical Modeling of Dynamics Processes in the Upper Atmosphere and Ionosphere

I.V. Karpov and G.V. Golubkov

Abstract In this chapter, the achievements of the basic researches on the upper atmosphere and ionosphere processes with the mathematical modeling methods are briefly presented. The mathematical problem of the model atmosphere/ionosphere description, the existing global theoretical model of environment, and the results of the investigations as well as their applications have been considered. The numerical experiments using the theoretical models show that the results obtained through model calculations have a good relation with the experimental data on the quiet geophysical conditions. However, under perturbed conditions, the difference in the model results and observations can be more evident. The reasons for such difference can be attributed to the defects of the experimental data on the dynamics of the atmospheric perturbations sources, as well as the imperfection of the theoretical models. In particular, the experimental studies have observed an increase in the microwave radiation (MWR) flows from the upper atmosphere in the geomagnetic and solar-disturbed conditions. This work has focused on the increase in the MWR flows, which can be associated with the appearance of high-disturbed particles ($n > 10$) in the atmosphere. The correlation between the efficiencies of the chemical reactions and the participation of such particles is one of the directions of improvement of the theoretical models. Furthermore, the approaches to describe the chemistries of high-disturbed particles within the framework of theoretical atmosphere/ionosphere models also discussed.

Keywords Global theoretical models · Ionosphere perturbations · Precursors · Upper atmosphere

I.V. Karpov (✉)
West Department IZMIRAN, Kaliningrad, Russia

V.L. Bychkov et al. (eds.), *The Atmosphere and Ionosphere*,
Physics of Earth and Space Environments,
DOI 10.1007/978-90-481-3212-6_5,

5.1 Introduction

Currently, the application of mathematical modeling methods is the standard practice in the theoretical researches on the atmosphere and ionosphere structure and dynamics. Numerical models have been increasingly applied owing to the complexity of the physical and chemical processes determining the dynamics of the neutral and charged components of the upper atmosphere. The primary goals of theoretical researches with the application of numerical models include the creation of physical interpretation of the geophysical phenomena proceeding in a particular region of the atmosphere, research on the role of separate physical processes, study of the dynamic connections of the processes in the upper atmosphere and ionosphere along with the processes in the underlying atmospheric layers, as well as examination of the processes in the magnetosphere. In the review of the upper atmosphere and ionosphere, theoretical global models, systems of the equations describing their dynamics, some data on the achievements in modeling researches, and ways to achieve further perfection of the models are briefly discussed.

5.2 Global Numerical Models of the Upper Atmosphere and Ionosphere

The application of the three-dimensional models based on the hydrodynamic equations for neutral and charged components of the environment is necessary for the theoretical research on large-scale dynamic processes (scale of more than 1,000 km) in the upper atmosphere and ionosphere (heights of more than 100 km). A brief chronology of the global upper atmosphere and ionosphere modeling is given in [1]. Initially, the first global numerical models of the neutral components of the upper atmosphere (thermosphere) dynamics were elaborated in the 1980s [2–4]. The charged components' influence on thermosphere was taken into account by including the necessary data from the empirical ionosphere models or the simple theoretical ionosphere models. Further development of the upper atmosphere global models resulted in the creation of self-consistent models of the dynamics of the neutral and charged particles as well as the electric fields. The first numerical global model, GSM TIP, achieved such a self-consistent description [5]. Furthermore, the blocks of the ionosphere-parameters calculation [6–8] were included in the thermosphere models [2–4]. Subsequently, the blocks of calculation of electric fields were included in these advanced models, and were termed as TIME-GCM [9–11] and CTIP [7] models. The advanced version of model GSM TIP [5] – model UAM [12, 13] – was developed for high-latitude ionosphere modeling investigations as well as for a wide spectrum of researches comprising the empirical model data. All the above-mentioned models provided similar ionosphere–thermosphere description based on the equations for charged and neutral components of the upper atmosphere. Here, we consider the system of the equations as the model [5].

The system of the equations in a hydrostatics approximation for the basic neutral gas component of the thermosphere, namely, N_2,O_2,O, includes the following:

$$\frac{\partial n_n}{\partial t} + \nabla[n_n(\mathbf{V} + \mathbf{V}_{dn})] = Q_n - L_n, \tag{5.1}$$

$$\rho\left[\frac{\partial \mathbf{V}}{\partial t} + (\mathbf{V}\cdot\nabla)\mathbf{V} + 2\Omega\mathbf{V}\right] = -\nabla P - \sum_i \sum_n \mu_{ni} v_{ni} n_n(\mathbf{V} - \mathbf{V}_i) + \eta_n(\nabla^2\cdot\mathbf{V}),$$

$$\rho\, C_v \cdot \left[\frac{\partial T}{\partial t} + (\mathbf{V}\cdot\nabla)T\right] + P\nabla\mathbf{V} = \nabla(\lambda_n \nabla T) + \nabla\left(D_T\left(\nabla T + \frac{g}{C_p}\right)\right)$$

$$+ \eta_n\left[\frac{4}{3}[\nabla\times\mathbf{V}]^2 - (\nabla\mathbf{V})^2\right] + \sum_n n_n \sum_i \mu_{ni} v_{ni}(\mathbf{V}_i - \mathbf{V}_n)^2 + P_n^{uv}$$
$$+ P_n^c - P_L^r + P_n^T,$$

$$\frac{\partial \rho}{\partial t} + \nabla(\rho\,\mathbf{V}) = 0,\ P = \sum_n n_n k T,\ \rho = \sum_n m_n n_n,\ \frac{\partial P}{\partial r} = -\rho\, g,$$

$$V_{dn} = \sum_i D_{in}\left(\frac{\partial n_i}{\partial r} + \frac{n_i}{H_i} + \frac{n_i}{T}\cdot\frac{\partial T}{\partial r}\right) - D_T\left(\frac{\partial n_i}{\partial r} + \frac{n_i}{H} + \frac{n_i}{T}\cdot\frac{\partial T}{\partial r}\right)$$

In these equations, ρ, P, T are the density, pressure, and temperature of the neutral gas, respectively; n_n is the concentration of the gas components; $\mathbf{V}$ is the mean velocity of the neutral gas; V_{dn} is the diffusion velocity of the nth gas component; Ω is a vector of angular speed of rotation of the Earth; g is the acceleration of a gravity; μ_{ni} is the given weight for the nth neutral and ith ion component, equal to $m_n \cdot m_i/(m_n + m_i)$; v_{ni} is the ion–neutral collision frequency; $\mathbf{V}_i$ is a ith ion component velocity; η_n, λ_n are the viscosity and heat conductivity coefficients of the neutral gas, respectively; D_T, D_{ij} are the coefficients of turbulent and molecular diffusion, respectively; C_v, C_p are the thermal capacities of neutral gas at constant volume and pressure, respectively; P_n^{uv}, P_n^c, P_n^T are the heating of neutral gas from UV radiation of the Sun, corpuscular flaxes, and turbulent energy dissipation, respectively; $P_i^r -$ is the losses of energy owing to radiation; Q_n, L_n are the sources and losses of the gaseous component owing to photochemical reactions, respectively.

Equation (5.1) takes into account an exchange of the movement and energy in collisions with the charged particles. During the calculation of the characteristics, the charged components of the upper atmosphere are taken into account, to distinguish the dynamics of the field-aligned (atomic ions O^+, H^+, He^+ in the F-region of the ionosphere and in the plasmosphere) and non-field-aligned particles (molecular ions – O_2^+, N_2^+, NO^+ in the lower ionosphere).

The following are the equations for the molecular ions of the lower ionosphere:

$$\frac{\partial n\,(M^+)}{\partial t} = Q\,(M^+) - L\,(M^+) - \nabla\,(\,n(M^+)\,\mathbf{V}_i\,(M^+)), \tag{5.2}$$

$$(\,3n_i\,k/2)\;\frac{\partial T_i}{\partial t} = \sum_n n_n \sum_i \mu_{ni}\,\nu_{ni}(\mathbf{V}_i - \mathbf{V}_n)^2 + P^e_{i\,T} + P^n_{i\,T},$$

$$(\,3n_e\,k/2)\;\frac{\partial T_e}{\partial t} = P_{e\,q} + P^i_{e\,T} + P^n_{e\,T},$$

$$n_i\,m_i\,\mathbf{g} - \nabla\,(n_i\,k\,T_i) - \sum_n\;\mu_{\,ni}\,\nu_{\,ni}(\mathbf{V}_i - \mathbf{V}_n) + en_i\,\{\,\mathbf{E} + [\mathbf{V}_i \times \mathbf{B}]\} = 0,$$

Here, $n_e = n_i = n(M^+)$, and $\mathbf{E}$, $\mathbf{B}$ are the electric and magnetic fields, respectively.

The following are the equations for the description of the ionosphere parameters of F2-region and upper ionosphere:

$$\frac{D\,n_i}{Dt} + \nabla^{\parallel}\,(\,n_i\,\mathbf{V}_i^{\parallel}\,) = Q_i - L_i - n_i\,\nabla_{\perp}\,\mathbf{V}_i^{\perp}, \tag{5.3}$$

$$\begin{aligned}
&-2\,m_i\,n_i\,[\Omega \times \mathbf{V}_i]_i^{\parallel} = n_i\,m_i\,\mathbf{g}^{\parallel} - \nabla^{\parallel}p_i - \frac{n_i}{n_e}\nabla^{\parallel}P_e\\
&-\sum_j\,\mu_{ij}\nu_{ij}n_i\,(\,\mathbf{V}_i^{\parallel} - \mathbf{V}_j^{\parallel}\,) - \sum_n\,\mu_{in}\,\nu_{in}\,n_n\,(\,\mathbf{V}_i^{\parallel} - \mathbf{V}_n^{\parallel}\,)\\
&-\nabla(n_i\,k\,T_i) - \sum_n\,\mu_{ni}\,\nu_{ni}(\mathbf{V}_i - \mathbf{V}_n) + e\;n_i\,\{\,\mathbf{E} + [\mathbf{V}_i \times \mathbf{B}]\,\},
\end{aligned}$$

$$\begin{aligned}
&\frac{3}{2}n_{i,e}\,k\left(\frac{D\,T_{i,e}}{D\,t} + \mathbf{V}_{i,\,e}\,\nabla^{\parallel}\,T_{i,\,e}\right) + P_{i,\,e}\nabla^{\parallel}\mathbf{V}_{i,e} - \nabla^{\parallel}\,(\,\lambda_{\,i,\,e}\nabla^{\parallel}\,T_{i,\,e})\\
&\quad = P_{\,i,\,e,Q} - P_{\,i,\,e,L},\\
&\mathbf{V}_i^{\perp} = \mathbf{V}_e^{\perp} = \mathbf{E} \times \mathbf{B}/B^2,\;\mathbf{V}_i^{\parallel} = \sum_j\,n_j\,\mathbf{V}_j/n_e.
\end{aligned}$$

Here, $\parallel$ and $\perp$ are the components of the vectors along the direction and in the normal direction of the geomagnetic field, respectively (including the vector operator∇). The operator $\frac{D}{Dt} = \frac{\partial}{\partial t} + (\,\mathbf{V}^{\perp},\,\nabla\,)$ represents a full derivative on time along a trajectory of the electromagnetic drift, and Q_i, L_i are the gains and losses of ions, O^+, H^+, respectively, taking into account the photos and corpuscular ionization, ion–molecular reactions, and charge-exchange processes. The heating of the electronic gas P_{eQ} is considered as the nonlocal heating by the escaping photoelectrons.

The following is the equation for the calculation of the potential of the electric field:

$$\nabla\ [\hat{\sigma} \cdot (\nabla\varphi - \mathbf{V} \times \mathbf{B}\ ) - \mathbf{J}_m] = 0, \tag{5.4}$$

where $\hat{\sigma}$ is the ionosphere conductivity tensor, ϕ is the potential of a large-scale electric field, and $\mathbf{J}_m$ is the current along the geomagnetic field lines. Furthermore, as the sources of the electric field of the magnetosphere, the system of currents at the geomagnetic latitudes of 75° and 65° is set accordingly.

The equations (5.1–5.4) describe the dynamical interaction between the neutral and charged components of the upper atmosphere and ionosphere.

The solar radiations and corpuscular flaxes determining the chemical and ionization processes in the upper atmosphere can be chosen from the empirical models of the appropriate parameters. For example, the boundary conditions for the solution of equation (5.1) for the parameters of neutral particles can be set at the lower boundary thermosphere (in the model [5] at a height of 80 km) from the empirical models of the upper atmosphere [14–16].

At the upper boundary of the thermosphere (in the model [5] at a height of 526 km), the components of wind and temperature can be considered, with their vertical gradients assumed to be zero owing to dissipation, and by presuming that the gases are in diffusion balance.

In the model [5] equation for the atomic ions and the electric field integrated along the magnetic field lines and used as boundary conditions (at the base of the field lines) the results of integrating the equations for the molecular ions (5.2). In other models [6–8], the equation for ions are solved in a spherical system of coordinates, which assumes the choice of the upper boundary conditions at the fixed height of the top level of the integration region of the equations.

The equations for the neutral and charged particles of an atmosphere (5.1–5.4) are solved using finite-difference numerical methods on global spatial grids. The spatial grid scales in such models usually comprise some degrees of latitudes and longitudes. For example, in one model [6], the steps of integration have been considered as 5° along the latitudes and longitudes, and in another model [5], 5° and 15° were considered accordingly. It can be noted that in various versions of these models, the problems of numerical calculations in the grids with higher spatial resolution were solved [12, 13, 17]. The reduction in the steps of integration on spatial coordinates allows to precisely describe the changes in the sources of perturbations of the atmosphere and reaction of the atmospheric parameters in disturbed conditions.

Verification of such complex theoretical models was carried out by comparing the data on the parameters of global empirical models of the upper atmosphere and ionosphere [15–18]. The results of numerical calculations of global distributions of atmospheric and ionospheric parameters, calculated with the application of such theoretical models, have shown good consent with the data on empirical models, for the quiet and moderately disturbed geomagnetic conditions with average levels of solar activity. The results of electronic-concentration global distribution model

calculations for various seasons and levels of solar activity, calculated on model UAM [12], are shown in Figs. 5.1 and 5.2, and for comparison, the ionosphere data from the empirical model IRI [15] is presented.

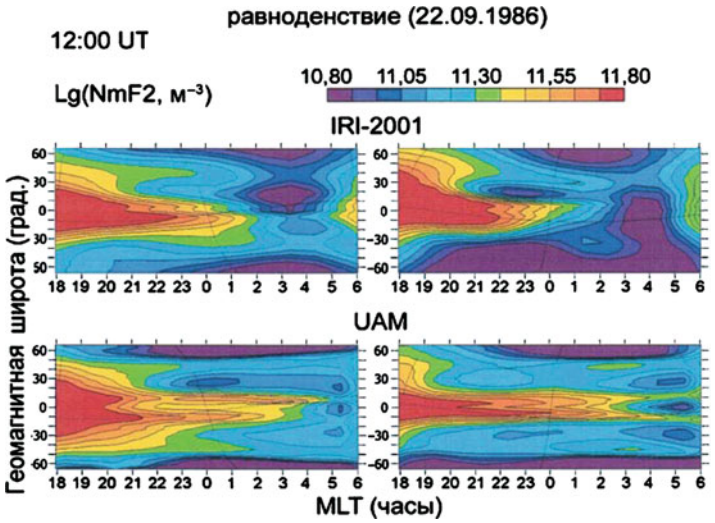

Fig. 5.1 Electron concentration in a maximum of F2-layer of ionosphere for equinox conditions and moments UT = 12 h (*left*) and UT = 18 h (*right*), obtained in empirical model IRI-2001 (*top*) and calculated in model UAM [12] (*below*)

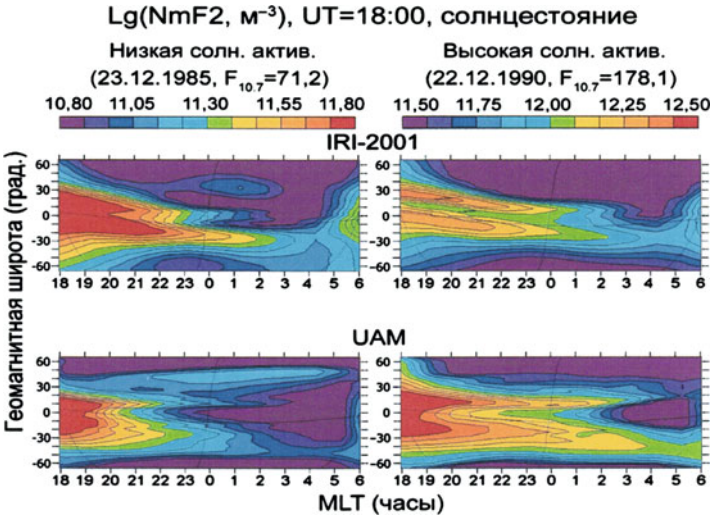

Fig. 5.2 Electron concentration in a maximum of F2-layer of ionosphere under conditions of a solstice and various levels of solar activity, obtained in empirical model IRI-2001 (*top*) and calculated in model UAM [12] (*below*)

Apparently, the theoretical model was found to reproduce all the basic morphological features of planetary distributions of the atmospheric and ionospheric parameters. Similar calculations of the parameters of the upper atmosphere and ionosphere were also carried out in researches with the application of the models TIME GCM, GSM TIP, and CTIP. These results show that complex global theoretical models adequately describe large-scale structure of the upper atmosphere and ionosphere, and can be successfully applied in studies on dynamic processes in a wide range of geophysical conditions.

5.3 Modeling Atmosphere and Ionosphere Perturbations

All atmospheric layers interact among themselves by means of various physical and chemical processes, forming the complex system subject to the influences of flashes on the Sun, earthquakes on the Earth, human activity, etc. A change in the environment's physical characteristics as a result of these influences is termed as perturbation. The primary goal of theoretical researches includes revealing the interrelations of various atmospheric layers' dynamics, parameters of the atmosphere and ionosphere, validation of various role factors, and studying, understanding, and finally, forecasting the dynamics of environment in the development of perturbations.

The complexity of modeling of the perturbation situations is determined by several factors. First, the usual system of upper atmospheric and ionospheric parameter observations does not allow for obtaining experimental data with the necessary spatial and temporal resolution. Besides, in the observations, separate parameters (e.g., either electron concentration in the wind or temperature is measured, etc.) and measurements indirectly associated with the characteristics of the parameters of the environment (e.g., intensity of radiation in various ranges of frequencies) are frequently carried out. However, the accuracy of empirical models in the description of the disturbed situations in an atmosphere and ionosphere is insufficient and does not allow for making exhaustive comparison with the theoretical researches.

Second, theoretical models have some limitations owing to the low spatial resolution of the equations' integration grids, as well as insufficient completeness of the energy transfer channel's perturbation description in the environment. Besides, boundary conditions in the numerical models and sources of perturbations are determined by the results of experimental researches. Thus, owing to the uncertainty of the experimental data, there exists an uncertainty as a result of theoretical modeling.

The general problems associated with developing models of the upper atmosphere and the accuracy of their comparison with experimental results have been formulated in an earlier work [19]. Nevertheless, mathematical modeling as the universal method of research on processes, even under conditions of insufficiency

of the experimental data for comparative analysis, allows for developing adequate interpretations of the observed physical phenomena.

5.4 Modeling Ionospheric Disturbances on the Geomagnetic Storms

The most complex physical phenomena of the upper atmosphere occur at high latitudes where the direct connection of the ionosphere and neutral atmosphere is possible through magnetosphere with the solar wind. The disturbances on the Sun and the changes in the solar-wind parameters as well as their associated interplanetary magnetic field result in significant perturbations in the upper-atmospheric condition. Development of atmospheric and ionospheric perturbations during such geophysical events influences various fields of activity of people and functioning of engineering. These circumstances determine the intensity of research on the influence of solar and geomagnetic activity on the characteristics of the parameters of environment. The complexity of the theoretical studies of such situations is determined by the diversity and dynamics of disturbing factors – change over time of the magnetic field components, perturbation of spectrum corpuscular precipitations and, therefore, complex and spatially heterogeneous reaction of atmospheric and ionospheric parameters [20, 21]. More accurate description of the structure of perturbation factors' dynamics requires higher accuracy of modeling, i.e., higher spatial and time resolution of the numerical model (e.g., the characteristic scale on latitudes is not 1,000 km as in middle latitudes, but 100 km or even less). The versions of models of the upper atmosphere in which calculations with high spatial resolution [12, 17] are realized were developed for this purpose. However, nowadays, the problems associated with reduction in the steps of integration of the equations of numerical models are not essential owing to the application of supercomputers in modeling researches. On the whole, the theoretical researches on disturbed geomagnetic situations in the upper atmosphere and ionosphere have allowed ofthe development of physically proven interpretations of the observed phenomena in experiments.

At the same time, numerical experiments have shown that an important setback for the adequate description of parameters of the upper atmosphere and ionosphere in theoretical models is the description of spatial and time variability of sources of perturbations [22–24]. Hence, in [23–26], it was shown that the account of dynamics of sources of geomagnetic perturbations, nonstationary behavior magnetospheric electric fields, and changes in the spectra and zones corpuscular precipitations allow for the more adequate description of the behavior of modeled parameters, with high conformity with the experimental data. Naturally, obtaining such observation data on the behavior of electric fields and corpuscular flaxes, necessary for inclusion in global numerical models, is impossible. In most cases, variability of these parameters is defined based on the observation of separate ground stations or satellites.

Hence, preparation of the data on perturbation factors characteristics for global models assumes development of methods of approximation of available given measurements. Owing to the insufficiency and separation of the experimental data, the spatial in such methods as well as the spatial and time characteristics of the sources of perturbations have essential uncertainty. Thus, further development of modeling researches assumes perfection of theoretical models by inclusion of the equations for magnetosphere dynamics in the modeling description. In this case, sources of perturbations of the magnetosphere–ionosphere–atmosphere system will be parameters of a solar wind and interplanetary magnetic field. Theoretical models in which blocks of calculation of magnetosphere parameters are included and executed calculations of distributions of parameters of the atmosphere and ionosphere are presented in [12, 13, 27–29]. It is obvious that such models are the most complete models describing large-scale structure and dynamics of a near-earth space.

Application of theoretical models to examine the atmospheric and ionospheric perturbations dynamics initiated by geomagnetic events has allowed of the development of the proven physical interpretations of the observable phenomena. Thus, it is necessary to note that the basic aim of these researches was to understand the physical processes that develop in the environment during geomagnetic perturbations.

However, at the height of the upper atmosphere and ionosphere, only a part of the solar radiation is absorbed. A significant part of this energy is absorbed in the underlying atmospheric layers. Absorption of solar radiation at the height of the middle atmosphere is an important energy source of the upper atmosphere, and it is taken into account in the theoretical models in the description of variations in the atmospheric parameters in the lower boundary of the modeling region, at the height of the upper mesosphere–lower thermosphere (70–90 km). Experimental researches have shown that the periods of geomagnetic perturbations are accompanied by perturbations of the parameters of the atmosphere at the height of lower thermosphere (70–110 km) [30–32], and the consequences of geomagnetic storms are revealed in the ionosphere perturbations for several days after the termination of geomagnetic perturbation [33, 34]. Thus, existential scales of these perturbations surpass those of the perturbations of the upper atmosphere and ionosphere initiated by geomagnetic storms. In lower thermosphere, perturbations of parameters define the changes in the characteristics of global tidal variations and changes in the daily average condition of the environment, while in the pretreated ionosphere, perturbations of the parameters are shown in the amplification of longitudinal and UT variations of the parameters.

Thus, changes in the characteristics of atmospheric parameters owing to geomagnetic perturbations can be observed in the upper atmosphere and ionosphere, as well as in the underlying atmospheric layers. From the perspective of the modeling researches, this indicates that in the field of the lower boundary conditions of the theoretical models [5, 7, 9, 13], the perturbations of the atmospheric parameters initiated by geomagnetic perturbations can be observed. Hence, to improve the accuracy of the description of the perturbation atmosphere during geomagnetic storm and the subsequent relaxation to quiet conditions, it is necessary to take into

account the changes in the atmospheric parameters on the lower boundary of numerical models. Till now, in modeling researches, the influence of geomagnetic perturbations on the boundary conditions in numerical models was not considered. Thus, the essential influence of variations in the atmospheric parameters on the lower boundary of the numerical models on large-scale dynamics of the upper atmosphere and ionosphere has been confirmed with detailed researches with the application of all the above-mentioned global models [32–35].

Obviously, the natural development of modeling researches on storm situations in the upper atmosphere should be accompanied by perfection of the theoretical models, by assuming the expansion of region of integration of the equations not only upward in the magnetosphere but also downward, including the underlying layers of the atmosphere.

5.5 Modeling of Interaction of Various Layers of the Atmosphere

The principal causes determining the necessity of expansion of area of integration of the equations in models of the upper atmosphere and ionosphere are connected as follows:

1. In experimental researches, it has been established that owing to the perturbations of solar and geomagnetic activity, there are perturbations of atmospheric parameters at the height of mesosphere, as well as perturbations of the upper atmosphere and ionosphere, which can proceed for a long time even after the geomagnetic storms have ceased. Besides, experimental researches have revealed wave variations of the parameters of ionosphere and upper atmosphere, with periods of more than a day [36, 37]. The occurrence of such variations in the upper atmosphere is thought to be due to the penetration of planetary waves from the lower and middle atmosphere in the upper atmosphere. Also, it is necessary to note that at the height of the upper atmosphere and ionosphere, the ionospheric and atmospheric parameters' perturbations are caused by the development of meteorological processes in troposphere and stratosphere [37].

2. Most part of the solar radiation is absorbed at the height of mesosphere and lower atmosphere. Photochemical and dynamic processes at these heights of atmosphere cause existential distributions of atmospheric parameters in the height of the lower boundaries of the existing theoretical models. It is natural to assume that the boundary conditions in the models on the heights of the lower atmosphere, where the characteristic times of processes is much higher than the corresponding magnitude in the upper atmosphere, thus eliminating the problem of choosing the boundary conditions in the lower thermosphere and rightly raise the possibility of integrating the equations for long periods. In such a statement of modeling research, sources of perturbations of environment will operate within the modeled region. The increase in the duration of integration of the equations of models is necessary

for studying the problem of penetration of perturbations from the lower atmospheric layers to the height of the upper atmosphere and ionosphere.

In fact, the requirement for the expansion of area of modeling researches is determined by an attempt to consider the most essential chemical and dynamic mechanisms of the atmosphere and ionosphere perturbations caused by absorption of solar energy within the framework of the theoretical model. Experiments with such a development of theoretical model were executed on the basis of models UAM and TIME-GSM [10, 13]. In [33], the results of the research on the processes of generation and distribution of planetary waves in thermosphere with the period of 2 days have been presented. As shown in the calculations, for the distribution of a planetary wave at the height of thermosphere, a very long duration (month) was found to be necessary. Experimental researches have shown that the time delay of occurrence of perturbations at the height of thermosphere, when compared with that of mesosphere, is much less. In this case, numerical experiment demonstrated an inefficiency of direct wave distribution of a planetary wave from the lower atmosphere up to the height of the thermosphere and ionosphere. In [38], modeling research with the application of model GSM TIP [5] was presented, in which the opportunity to generate large-scale perturbations in thermosphere owing to the vertical propagation of the short-scale (the period of waves studied was close to Brent–Vaisala period) internal gravitational waves (IGW) were located along a line of solar terminator, from mesosphere–lower thermosphere. These numerical experiments have shown efficiency of such channel of penetration of perturbations from the lower atmosphere to the upper atmosphere, and in another study [38], a variant, without taking into account the perturbations from short-scale IGW (Fig. 5.3a), has been shown along with the indignations from IGW in the field of solar terminator (Fig. 5.3b). As can be observed from Fig. 5.3, the short-scale IGW influences the formation of circumpolar vortex at the height of ~140–160 km under polar night conditions. Similar modeling researches will help to perform complex physical processes, providing penetration of perturbations from lower to upper atmosphere.

For a long time, the modeling of the dynamics of the lower and middle atmosphere was an independent scientific problem. The important purpose of such researches was to study a difficult and complex photochemical and dynamic processes initiated by the absorption of solar radiation. Currently, numerical global mesosphere models that take into account the chemistry and dynamics [39,40] have been realized. One of the limitations of the mesosphere–lower thermosphere modeling is the description of the upper boundary conditions, which is the height of ~150 km; in such region, the account of ionospheric influence on the dynamics of environment is necessary. As a rule, this problem was solved by including the data of empirical models. However, insufficiency of experimental researches and experience of modeling of ionospheric parameters' distributions demonstrate the major limitation of the application of such approach. Obviously, a more natural step in the development of models would be the association of models of the upper atmosphere and ionosphere with those of the middle atmosphere.

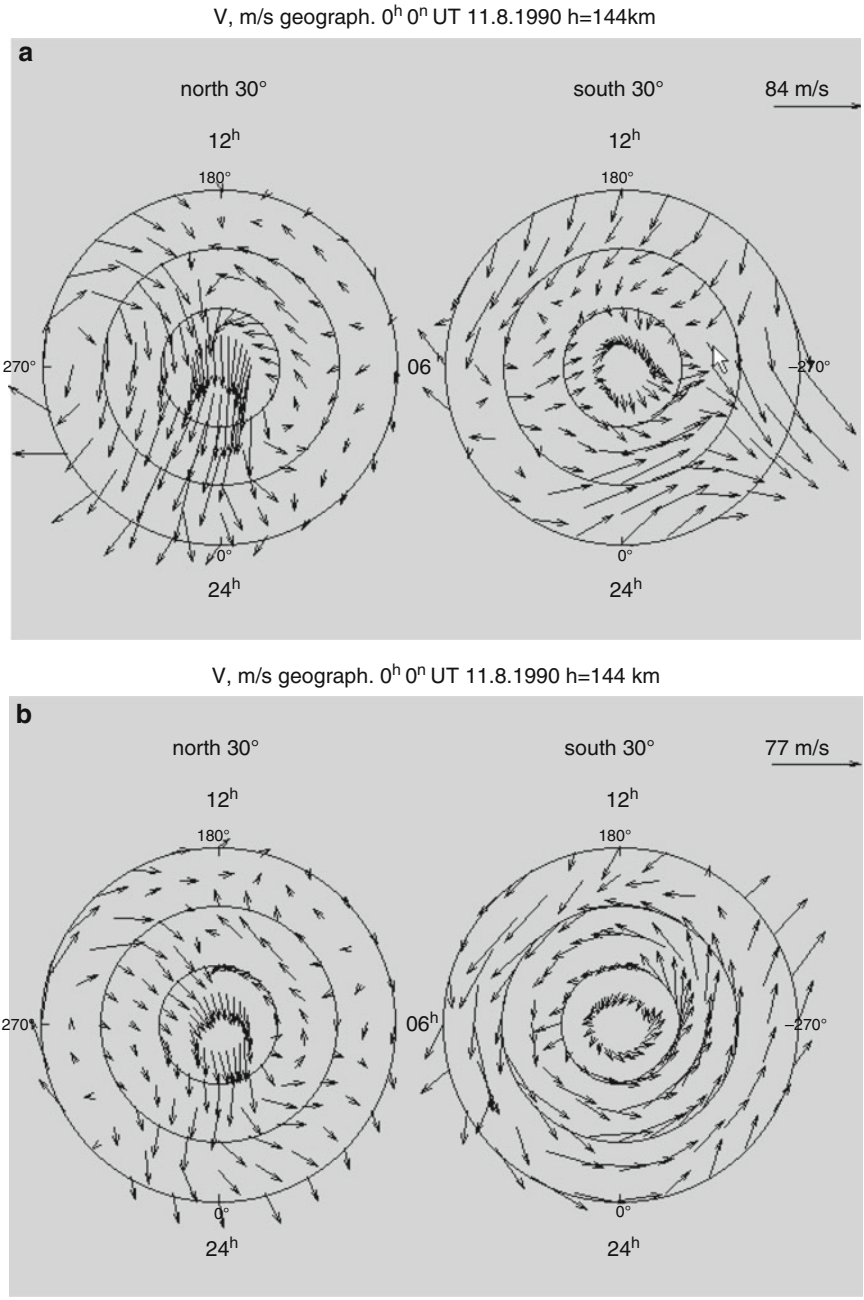

Fig. 5.3 (**a**) Circulation of wind over the polar caps, designed on model [5] with the absence of short-scale IGW in the solar terminator region; (**b**) the same, as on (**a**), with the account of short-scale IGW perturbations in the solar terminator region

5.6 Perfection of the Description of Photochemical Reactions

The trends in the development of the experimental and basic researches are finally directed towards the prognostic system of the condition of the upper atmosphere and ionosphere on the meteorological prognostic systems. From the perspective of the theoretical researches, this may result in the improvement of the numerical models owing to the increase in the technical features of the models (the reduction in the integration equation's time, increase in the spatial and temporal resolution), and thus, may provide more complete description of the sources of the perturbations and channel of the energy of the perturbations transformation in the model equations.

An important aspect in the problem of creation of realistic model of upper atmosphere and ionosphere is the insufficient certainty in describing the complexity of the chemical processes taking place at the height of upper atmosphere and ionosphere. Traditionally, in the model of upper atmosphere, including the most developed model [3, 5, 7, 12, 27], neutral components comprise the basic gas of atmosphere – O, O_2, N_2, and charged components include molecular ions – O_2^+, NO^+, N_2^+ and atomic ions – O^+, H^+, He^+. The description of the photochemical processes in the theoretical model, with the account of chemical composition of the neutral particles and ions considered, includes the processes of photoionization, photodissociation, dissociative recombination, radiative recombination, etc. The contribution of these chemical processes in mass, ionization, and heat balance of the ambience is known as reaction velocity. It is necessary to note that the reaction velocities, along with the sections of absorption and efficiency of heating from chemical reaction, possess the significant uncertainty. In the model study using the theoretical models, detailed researched processes of the formation of the global spatial structure of the neutral gas components and their influence on heat balance thermosphere and ionosphere have been presented [41–44]. On the whole, under quiet geophysical conditions, the applicable schemes including chemical reactions and their influences on heat balance allow for reproducing the particulars of the morphologies of planetary structures' atmospheric parameters, including spatial distribution of neutral and ion components. In disturbed condition, the difference in the model result and experimental data can be more significant. The important reasons for these divergences include the description of the defects of the atmosphere's chemistry. The theoretical researches show that under perturbed condition, the role of small gas components of atmosphere increases, influencing the heat balance of the upper atmosphere and ionization processes [41–47]. The numerical experiments show the possibility of the reproduction of the experimental results by special choice, for instance, the efficiency of heating [41]. On the whole, such situation is indicative of the defect of the description of the chemical processes with the participation of atmospheric gas and uncertainty in the knowledge of the chemical-reaction velocities. Obviously, the basic researches point to the need to include small gas components and account of the chemical-reaction efficiencies with their participation in the schemes of the chemical processes, in the model. Such efficiencies of chemical reactions in the atmosphere can be a change in the chemical-reaction

velocities, as a consequence of turning the particles and participating in the reaction under highly disturbed conditions with the main quantum number n of > 10. The analysis of the experimental data on the observations of electromagnetic radiations from atmosphere [48] points out the need to prove such suggestions and the necessity for theoretical researches to examine processes that influence the upper atmosphere and ionosphere.

Microwave radiations (MWR) are caused by the optical transitions between Rydberg states of the atoms and molecules in the upper atmosphere. For example, the Rydberg-state radiation of atomic oxygen (the basic gas component of upper atmosphere) with a change in the principal quantum number Δnon the unit for $n =$ 10–20 lies in a centimetric range, and in millimetric range for larger changes Δn. Decimeter radiation appears in case of transitions without change in the principal quantum number for $n = 20$–40.

Satellite registration that allows for MWR in the set spectral range along with the measurement of intensity can serve one of the essentially new methods of monitoring and provide a frequency profile of radiation to define the distribution of differential luminosity at different heights. On the basis of the results of the theoretical analysis of *shock* and *radiative* quenching of Rydberg states and those of the subsequent satellite measurements, it is possible to almost replicate the research on the density distribution of the atmosphere from 40 to 100 km, for which, currently, the standard information is practically absent. Owing to the spatial extent of the area of an electronic cloud, Rydberg states are subject to the influence of neutral particles of the environment, which are not weak and should be taken into consideration during the calculation of the corresponding optical characteristics. For their definition, it is necessary to solve a quantum problem on radiation of Rydberg atoms or the molecules that are chaotically located neutral particles in the field. The finding of the resultant intensity and a frequency profile of radiation is impossible without preliminary definition of characteristics of shock suppression that, in turn, demands the information on the potential energy surfaces (PES) for all the fragments of a mix of the gases that make atmosphere (the well-known structure and relative concentration within the specified layer do not depend on height). The method of construction of PES in the case of one revolting center (atom or a molecule) has been developed in detail [49]. To account for the several revolting centers in the general formalism, the theory of repeated dispersion is employed, i.e., the possibility of the analysis of a power spectrum of compound system (quasimolecule) should not cause doubts. The description of shock suppression quasimolecule conditions is usually based on the calculated PES within the limits of the existing dynamic approaches [50]. Calculation of an optical spectrum demands construction of electronic wave function of a system, which is a key problem, because on the whole, the regular method of the decision of this problem is not yet developed. Currently, there is only a scheme of construction of wave function for a case of one revolting center [51].

During the periods of increase in the solar activity, along with ionospheric magnetic storms at the top atmosphere (which stretches from 40 to 100 km and above the surface of the Earth), MWR is formed, whose intensity on some usages

exceeds the background. Over the last 10 years, it has been established that this radiation is caused by the radiating transitions between Rydberg states of atoms and molecules, which are formed by electron flux and thrown out of the ionosphere [52]. Superfluous MWR, practically lost-free, passes through the atmosphere of the Earth and produces an undesirable influence on the biosphere. In fact, its resonant influence on various living organisms, including human beings, has already been directly acknowledged experimentally [53].

Currently, it is not clear whether the maximum intensity of the ultrabackground MWR at greater heights (considerably exceeding 100 km) is small owing to the rarefaction of the atmospheric gas where it is exactly formed, and whether small (lower or about 40 km) superfluous excitation is effectively extinguished at the expense of interaction with the neutral particles of the environment. On the one hand, this fact denotes the absence of reliable information on the character of distribution of density of the atmospheric gas in a strip from 40 to 100 km over the surface of the Earth. The density of the environment, as it is known, essentially influences the speeds of the elementary chemical reactions (dissociation of molecules and recombination of electrons and ions, hemoionization and Penning ionization, shock and radiating suppression of the raised conditions, etc.). On the other hand, there are no uniform mechanisms to form the frequency profile of MWR with respect to density. Construction of an overall picture of the phenomenon demands definition of the dependence of dynamics of *shock* and *radiative* quenching of highly excited states of atoms and molecules from the density of the revolting gas. In the rarefied gas, for the description of a spectrum of radiation, it is possible to be limited to the account of the indignation created by one neutral particle. In denser environment, it is necessary to consider the influence of the final number N of chaotically moving particles in the volume of the raised atom or a molecule, on the optical characteristics of the system (positions and shifts of the levels, wave functions, and corresponding dipole moments). The dependence of N on the principal quantum number n and concentration c of the medium in unit volume is presented in Table 5.1 (a concentration of 10^{17}cm^{-3} in the Earth's atmosphere corresponds to the altitude of ~40 km, and 10^{13}cm^{-3} is attained at ~100 km).

For the low-lying electron-excited states, the existing quantum-chemical methods (e.g., see [54, 55]) allow for calculating the demanded characteristics. In a case with conditions, these methods are hardly suitable, and it is necessary to use the alternative approach [56–58]. The greatest difficulties in describing the shock suppression of the raised conditions include the necessity for correct decision of a dynamic problem of dispersion. The basic processes leading to a fall in the excitation of reagents are the direct exchange of energy (the momentum mechanism) [59] and non-adiabatic transitions (through intermediate valence or ionic configurations) [60, 61]. Their efficiency is defined by the extent of the temperatures of the free

Table 5.1 N as a function of the principal quantum number n and concentration c

c (cm^{-3})	10^{13}		10^{14}		10^{15}		10^{16}		10^{17}	
N	45	60	30	40	20	27	15	18	10	13
N	1	5	1	5	1	5	1	5	1	5

electrons and neutral medium components. For fast collisions (when the relative speed of the facing particles considerably exceeds the root-mean-square speed of the loosely-coupled electron), the momentum mechanism dominates. At lower environmental temperatures (usually found in the upper atmosphere), the second mechanism appears to be more preferable. In this case, consideration demands preliminary construction of PES particles interacting with all the areas of merge and the quasicrossings responsible for non-adiabatic transitions. The following stage is reduced to the calculation of differential and full sections of reaction, which is carried out within the limits of the semiclassical approach using representation of the movement of the representing points on various branches of PES [62].

Development of a method of construction of electronic wave functions of the interacting system for the calculation of the radiation dipole transition moments is necessary. In a case of highly excited states, the integrated device of the theory using a method of functions of Green [49] is considered to be the most convenient. Furthermore, on the basis of the calculated PES and dipole matrix elements, the dynamic problem defining a frequency profile (the line form) radiation spectrum needs to be addressed. For simple "atom-nuclear" of the systems (taking into account the radiating transitions between two low-lying electron states), such procedure has been well developed [63]. Thus, it appears that the presence of extremes in the differences of the considered potential curves leads to the occurrence of "satellites" on the wings of a line of the radiation, which possess high sensitivity to environmental temperature, as well as positions and amplitudes to details of potentials of interaction; that is, they depend on its density and structure [64].

The problem of radiative decaying of the raised conditions at the lower part in the field of several neutral particles is solved in the frameworks of quasi-static approach [65]. During transition to highly excited states, there is a necessity for a set of pseudocrossing PES and the corresponding transformation of the surfaces of the dipole moment optical transitions. This problem has been formulated for the first time.

The fundamental problems of quenching and radiation of highly excited atoms and molecules in the rarefied gas have a direct influence on the applied studies on the structure and dynamics of the upper atmosphere and ionosphere. A number of experimental facts that have not received satisfactory physical interpretation (in particular, sporadic splashes in radio emissions from the ionosphere and their high correlation with the levels of solar and geomagnetic activity, presence of the highly excited atomic oxygen at the upper atmosphere, etc.) till date, can explain the excitation Rydberg states of atmospheric gases.

It is necessary to note that researches on the spectra of electromagnetic radiations from an ionosphere are the basis for the most informative methods of research on environment; for example, a method of non-coherent dispersion. The solution to the problems associated with examining the influence of highly excited particles in the atmosphere on the form of a spectrum provides more exact diagnostics of an environmental condition. The account of such raised conditions of particles should be considered important in the model description of the upper atmosphere and ionosphere. Till date, the most developed theoretical models use rather simplified

description of the photochemical processes taking place in a mix of atmospheric gases [3, 5, 66–68]. The structural blocks of these models describing the chemistry of the upper atmosphere and ionosphere include a complex of chemical reactions with the participation of the basic gas components of the atmosphere:O, O_2, N_2. They also contain the ionized components: molecular ions (O_2^+, NO^+, N_2^+) at the height of the lower ionosphere and atomic ions (He^+, H^+) at the height F – areas of the ionosphere and above. The influence of small gas components (O_3, NO_x) is considered in a parametrical manner in the model of atmosphere and ionosphere under the indignant solar and geomagnetic conditions. In all the above-mentioned models, the speed of the chemical reactions has been observed to depend on the representations of the elastic impacts of the cooperating particles.

The influence of the raised atoms and molecules on the condition of the upper atmosphere and ionosphere can be investigated using methods of mathematical modeling with the application of the global self-consistent model of thermosphere, ionosphere, and plasmosphere (GSM TIP). It is one of the most developed models of the upper atmosphere applied till date for research on the structure and dynamics of the environment. Furthermore, an improved description of the chemical reactions in the framework of the GSM TIP model has also been attempted. The new description of the dissociative-recombination complex of the atmospheric processes can be applied to theoretical investigations of the upper atmosphere and ionosphere, which may expand the possibilities to receive a more complete physical interpretation of the studied phenomena.

Development of the intricate theoretical models of the upper atmosphere is influenced by the necessity to study the dynamic reaction of the atmosphere on external influences. Recently, owing to the fast development of experimental researches, the extent of the problems of modeling of the phenomena and processes in the atmosphere and ionosphere has considerably increased, and thus, the requirement for an accurate physical interpretation has essentially increased. The need for detailed conformity of the theoretical researches to modern requirements demands further perfection of the model description of the environment. Consecutive complication of the schemes of chemical processes and an increase in the accuracy of the description of the elementary chemical processes represent one of the most important directions of development of theoretical models of the upper atmosphere and ionosphere.

5.7 Modeling Ionosphere Precursors of Earthquakes

One of the most important problems of the theoretical researches on upper atmosphere and ionosphere is the development of physically motivated interpretation of the observed phenomena. Obviously, model studies should allow for evaluatin the joint action with many factors simultaneously influencing the condition of the system, executing the main role in the decision of this problem.

The volume of the experimental data on the observations of the atmospheric and ionospheric parameters for the past decennial event has vastly increased. This may be associated with the quick development of the methods of the satellite studies of the atmosphere. Relatively recently, the possibility of the analysis of the planetary distribution of the observed atmospheric parameter appeared. For instance, the incessant observations of the ionosphere parameter TEC (total electron content) allowed for obtaining the planetary distribution with a time resolution of 2 h [69]. Such data helped to carry out the planetary perturbation analysis and increase the physical representations of the mechanism defining the planetary structure variability of the ionosphere. For instance, analysis of the spatial indignations TEC at the geomagnetic storm periods allowed for motivating the suggestion on the generation of high-frequency (a period of less than 12 h) planetary Poincare waves in the upper atmosphere [70], executing important role in the relaxation of atmosphere to quiet condition after perturbations.

The developed systems of the experimental study on the global structure of the atmosphere and ionosphere, in particular, the TEC observations, have allowed for providing exact definition of spatial and temporary efficiencies of the modification of the ionosphere before earthquakes as an ionosphere precursor. Obviously, these problems regarding the explanation of the mechanism shaping these phenomena are very important, and will ultimately help to create the system of the seismic-event forecast. The efficiencies of the ionosphere perturbations during the periods of preparing for the earthquakes have been explained in detail [71–73]. The perturbations are shown in Figs. 5.4–5.6. In Fig. 5.4, the deflection of the critical frequency F-layer of the ionosphere from the average level based on satellite IK-19 is presented. The negative variations of the electronic density existed for 2 days and 1 day before the advent of earthquake on 16.07.1980 in the region of Australia and New Zealand [71].

More extensive morphology of the ionosphere perturbation has been obtained during the last years of TEC observations. The TEC diurnal variations on the middle latitude stations are shown in Fig. 5.5, which were observed in the field of epicenter of the earthquake that occurred on 8.01.2006 [73]. As can be seen from Fig. 5.5, well-marked TEC perturbations, relative to the median values, existed a day before the seismic event.

The spatial maps of the ionosphere perturbations over the epicenter of the earthquake, allowing the establishment of the spatial sizes of the area of perturbations and efficiencies of the manifestation of the ionosphere precursors in different latitude regions are presented in Fig. 5.6. The analysis of the experimental studies has shown that in most cases, the amplitudes of the seismic indignations' ionospheric parameters form $\sim$20% of the median values. The perturbations with such amplitude can be associated with different factors, determined by instability of the geophysical situation. An important problem of the ionosphere's seismic precursors obtained from the ionosphere variations of the other nature is the development of physical interpretation of ionosphere perturbations, determined by seismic activity.

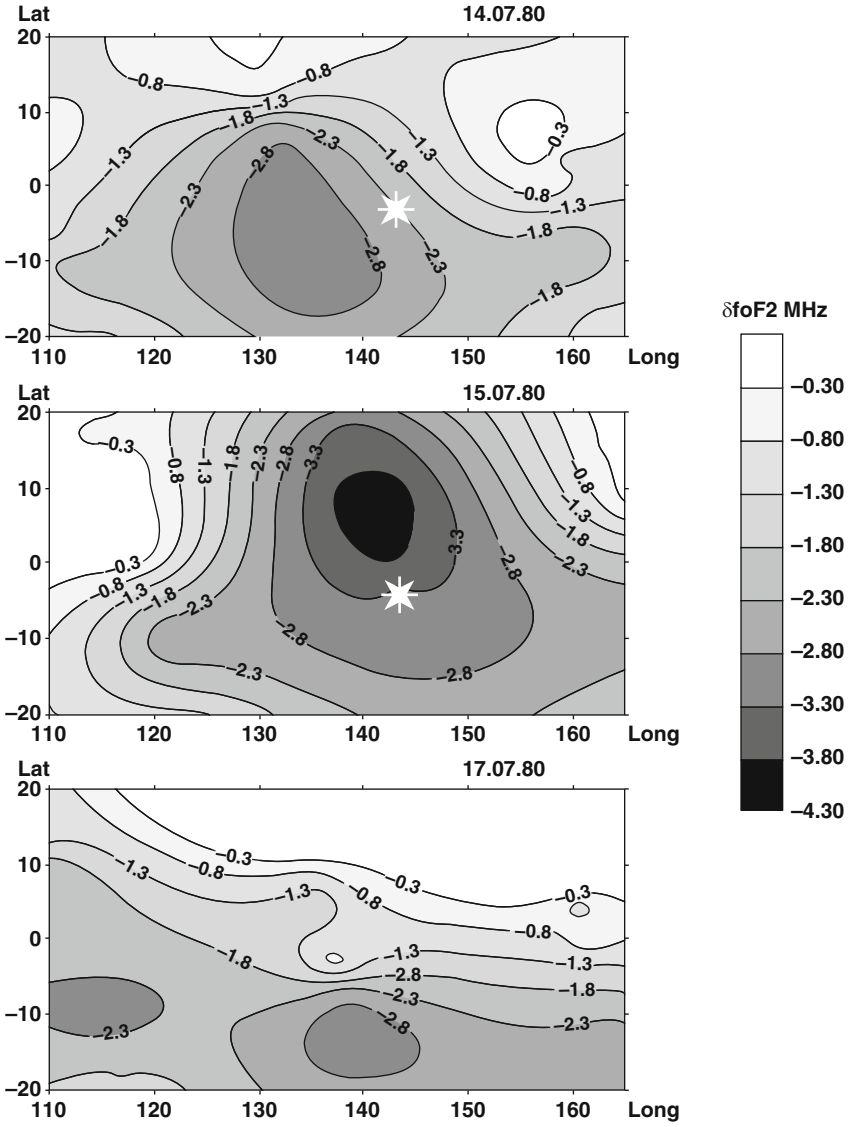

Fig. 5.4 Spatial distribution on the area of earthquake in New Zealand on 16.07.1980 (M7.3) according to satellite IK-19

The basic approaches to interpret ionosphere perturbations are based on the possible increase in the electric fields. Based on such suggestions, it may be possible to try to determine the answer to two important questions:

1. Do electric fields get into the ionosphere?
2. Do the values of these electric fields cause the observed effects in the ionosphere?

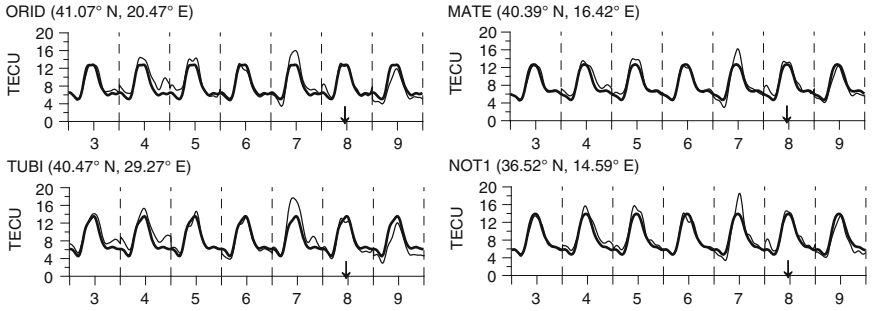

Fig. 5.5 The TEC diurnal variations for station ORID, TUBI, MATE, and NOT1 during January 3–9, 2006 (1 TECU = 1016 el/m2). The *fine line* – current TEC variation, *solid line* – a median. *Arrow* denotes moment earthquakes

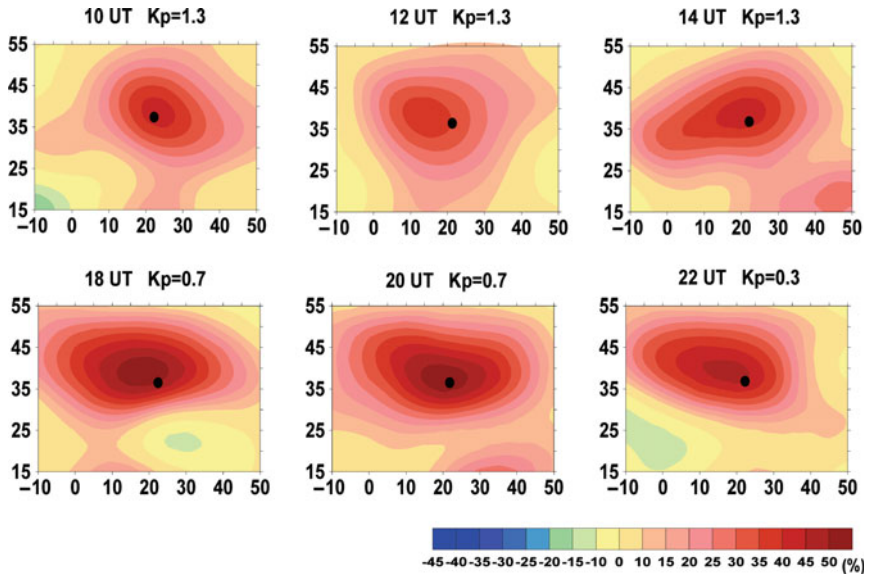

Fig. 5.6 The differential percent TEC maps for European region on January 7, 2006. The points are the specified epicenter of the earthquake

In [72, 73], the qualitative schemes of the electric-field perturbation have been considered, owing to the changes in the atmospheric conductivity over the area of the epicenter. In [74], the results of the study on the influence of the localized perturbations of the electric field on the structure of the ionosphere have been presented. The additional local potential of the electric field has been considered as the source of such field. In this work, it has been demonstrated that the development of such source electric fields with an amplitude of 3–10 mV/m causes perturbations in the ionosphere, which are very cognate with the ionosphere precursors of earthquakes, which appear in TEC observations. Here, a similar space configuration of

the additional potential allows for the reproduction of the known observed particularities of the ionosphere precursors in the middle and low latitudes. In [74], the thrash-out particularities of the change in ionosphere drift cause corresponding perturbations to electronic concentration, as well as demonstrate the importance of the amplitudes of the electric field, which are in agreement with the findings of the other authors [75]. Further studies on the ionosphere precursors of earthquakes need to examine the physical processes and associate local perturbation of electric field with the amplitude observed in [74, 75]. The model realization of any scheme of the penetration seismic-electric field in the upper atmosphere requires the expansion of the area of modeling from the surface of the land up to the upper atmosphere and ionosphere, and data corresponding to the outraging factor. However, there exists an uncertainty in the determination of these outraging factors and the absence corresponding to the experimental data, allowing their quantitative estimation. In such situations, searching for possible mechanism of the propagation of perturbations from landing layers in the upper atmosphere and ionosphere is carried out in the model study. Such studies may be useful to obtain experimental proofs regarding the connections between ionosphere and seismic perturbations. Thus, for instance, in [76], model GSM TIP [5] was applied to examine the possibility of generation of large-scale non-uniformities at the height of the ionosphere, owing to the propagation of IGW with small periods (close to Brent–Vaisala period), localized in the epicenter of the earthquake. The results of such model calculations [76] are presented in Fig. 5.7, which demonstrate the possibilities of such mechanism of ionosphere perturbations excitation and their similarity with the earlier results obtained using more simple model situation [74]. It can be noted that in this study, the source of the generation of the short-scale IGW is not discussed, but the role of such waves in the realization of dynamic connections of atmospheric layers is presented. The possibility of realization of such mechanism of the atmosphere and ionosphere perturbation over the earthquake epicenter can be achieved only by undertaking experimental studies.

5.8 Conclusion

Existing theoretical global models of the upper atmosphere and ionosphere are the powerful tool for studying the physical processes developing in the environment. Prospects of further development of theoretical models depend on the expansion of area of modeling from the surface of the Earth to the magnetosphere. Thus, it is obviously necessary to improve the description of various chemical processes, paying particular attention to the processes including small gas components of the atmosphere and the exited particles. It is also necessary to develop theoretical methods to describe the influence of the final number of neutral particles in the environment (Rydberg atoms and molecules chaotically moving in volume) on the dynamics of the elementary processes with the participation of the basic atmospheric particles. Development of theoretical models in these directions will allow

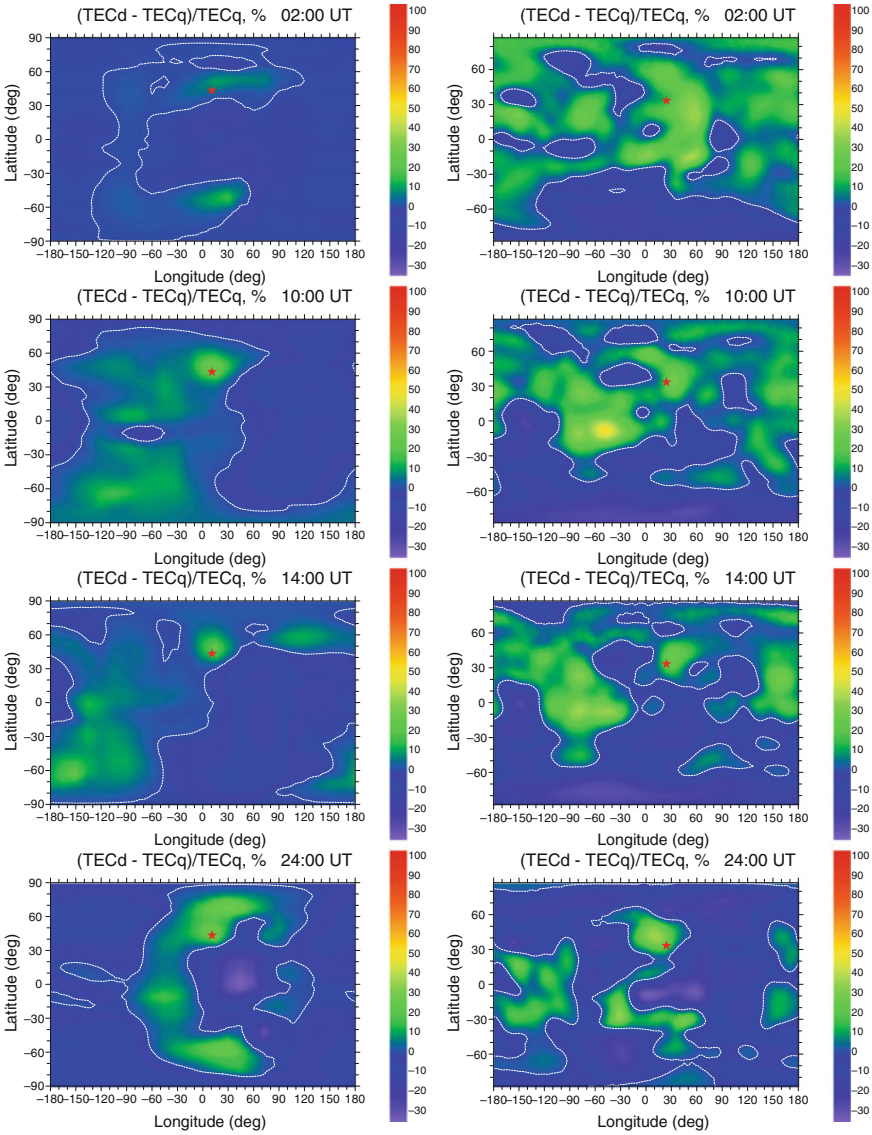

Fig. 5.7 Global maps of deviations of the total electron content in geographic Cartesian coordinate system for the various moments of time, obtained from calculations carried out with and without the IGW parameter generated in the epicenter region (*the left panel*) and calculated according to GPS TEC, obtained 1 day prior to earthquake in Greece, and median values of GPS TEC (*the right panel*). Epicenter of earthquake is marked by *asterisk*

for the improvement of the quality of researches on the physical processes defining the structure and dynamics of the environment. This, in turn, will promote the understanding of the features of the dynamics of the atmosphere and ionosphere

owing to various perturbations, both of geophysical and technologic nature. Furthermore, the obtained results may be helpful to experts in the area of physics and atmosphere chemistry.

References

1. Namgaladze, A.A., Yurik, R.Yu.: Mathematical modeling of Earth upper atmosphere perturbations, RFBR, Earth science, 1998
2. Dickinson, R.E., Ridley, E.C., Roble, R.G.: A three dimensional general circulation model of the thermosphere. J. Geophys. Res. **86**, 1499–1512 (1981)
3. Dickinson, R.E., Ridley, E.C., Roble, R.G.: Thermospheric general circulation with coupled dynamics and composition. J. Atmos. Sci. **41**, 205–219 (1984)
4. Fuller-Rowell, T.J., Rees, D.: A three-dimensional, time dependent global model of the thermosphere. J. Atmos. Sci. **37**, 2545–2567 (1980)
5. Namgaladze, A.A., Korenkov, Yu.N., Klimenko, et.al.: Global model of the thermosphere–ionosphere–protonosphere system. Pure Appl. Geophys. **127**(2/3), 219–254 (1988)
6. Roble, R.G., Ridley, E.C., Richmond, A.D., et al.: A coupled thermosphere and ionosphere general circulation model. Geophys. Res. Lett. **15**, 1325–1328 (1988)
7. Fuller-Rowell, T.J., Rees, D., Moffett, R.J., et.al.: A coupled thermosphere ionosphere model, CTIM. In: Schunk, R.W. (ed.) Paeronomical Models of the Ionosphere STEP Handbook, pp. 217–242 (1996)
8. Fuller Rowell, T.J., Rees, D., Quegan, S., et.al.: Simulations of the seasonal and universal time variations of the high latitude thermosphere and ionosphere using a coupled, three-dimensional model. Pure Appl. Geophys. **127**(2/3), 189–217 (1988)
9. Richmond, A.D., Ridley, E.C., Roble, R.G.: A thermosphere ionosphere general circulation model with coupled electrodynamics. Geophys. Res. Lett. **19**, 601–604 (1992)
10. Roble, R.G., Ridley, E.C.: A thermosphere–ionosphere–mesosphere–electrodynamics general circulation model (TIME-GCM): Equinox solar cycle minimum simulations (30–500 km). Geophys. Res. Lett. **21**, 417–420 (1994)
11. Roble, R.G.: On the feasibility of developing a global atmospheric model extending from the ground to the exosphere. In: "Atmospheric Science Across the Stratopause," Geophysical Monograph 123, American Geophysical Union, pp. 53–67 (2000)
12. Namgaladze, A.A., Martynenko, O.V., Volkov, M.A., et.al.: Highlatitude version of the global numerical model of the Earth's upper atmosphere. Proceedings of the MSTU **1**(2), 23–84 (1998)
13. Namgaladze, A.A., Martynenko, O.V., Volkov, M.A., et.al.: Mathematical modeling of large-scale upper atmosphere perturbations, Modelling of upper polar atmosphere processes. PGI KSC RAS, pp. 167–249 (1998)
14. Fuller-Rowell, T.J.: A two-dimensional, high-resolution nested-grid model of thermosphere 2: response of the thermosphere to narrow and broed electrodynamic features. J. Geophys. Res. **90**(A6), 6567–6568 (1985)
15. Bilitza, D.: International reference ionosphere 2000. Radio Sci. **36**, 261–275 (2001)
16. Hedin, A.E.: MSIS-86 thermospheric model. J. Geophys. Res. **92**, 4649–4973 (1987)
17. Hedin, A. E., Fleming, E.L., Manson, A.H., et.al.: Vial empirical wind model for the upper, middle and lower atmosphere. J. Atmos. Terr. Phys. **58**(13), 1421–1447 (1996)
18. Klimenko, V.V., Korenkov, Yu.N., Bessarab, F.S., et.al.: Model/data comparison of the F2-region parameters for August 11, 1999 Solar eclipse. Adv. Space Res. **31**(4), 995–1000 (2003)
19. Richmond, A.M., Wiltberger, M., Hanli, L.: The upper atmosphere problems in developing realistic models. Geophysical Models at NCAR. A Scoping and Synthesis Workshop, NCAR. Boulder, CO, 13–14 Nov pp. 1–3 (2006)

20. Fuller-Rowell, T.J., Codrescu, M.V., Roble, R.G.: How do the thermosphere and ionosphere react to a geomagnetic storm? Magnetic storm. Geophys. Monogr. AGU **98**, 203–225 (1998)
21. Prölss, G. W.: Ionospheric F-region storms. In: Volland, H. (ed.) Handbook of Atmospheric Electrodynamics, **2**, pp. 195–248. CRC Press, Boca Raton, FL (1995)
22. Kamide, Y.: Interplanetary and magnetospheric electric fields during geomagnetic storms: what is more important – steady-state fields or fluctuating fields? J. Atmos. Sol.-Terr. Phys. **63**(5), 413–420 (2001)
23. Rees, D.: Observations and modeling of ionosphere and thermospheric disturbances during geomagnetic storm: a review. J. Atmos. Terr. Phys. **57**(12), 1433–1457 (1995)
24. Korenkov, Yu.N., Bessarab, F.S., Klimenko, V.V., et.al.: Numerical modeling of the thermosphere–ionosphere coupling during substorm. Adv. Space Res. **18**(1), 41–44 (1996)
25. Fuller-Rowell, T.J., Codrescu, V.C., Wilkinson, P.: Quantitative modeling of the ionospheric response to geomagnetic activity. Ann. Geophys. **18**(7), 766–781 (2000)
26. Codrescu, M.V., Fuller-Rowell, T.J., Foster, J.S.: On the importance of E-field variability for Joule heating in the high-latitude thermosphere. Geophys. Res. Lett. **22**(17), 2393–2396 (1995)
27. Wang, W., Wiltberger, M., Burns, A.G., et.al.: Initial results from the coupled magnetosphere–ionosphere and -thermosphere model: thermosphere-ionosphere responses. J. Atmos. Solar-Terr. Phys. **66**, 1425–1438 (2004). doi:10.1016/j.jastp. 2004. 04. 008
28. Wiltberger, M., Wang, W., Burns, A.G., et.al.: Initial results from the coupled magnetosphere–ionosphere–thermosphere model: magnetospheric and ionospheric responses. J. Atmos. Solar-Terr. Phys. **66**, 1411–1424 (2004). doi:10.1016/j.jastp. 2004. 04. 026
29. Moffett, R.J., Millward, G.H., Quegan, S., et.al.: Results from a coupled model of the thermosphere, ionosphere, and plasmosphere (CTIPM). Adv. Space Res. **18**(3), 33–39 (1996)
30. Salah, J.E., Goncharenko, L.P.: Search for geomagnetic storm effects on lower thermospheric winds at midlatitudes. J. Atmos. Sol.-Terr. Phys. **63**(9), 951–963 (2001)
31. Rees, D., Fuller-Rowell, T.J.: Comparison of empirical and theoretical models of species in the lower thermosphere. Adv. Space Res. **13**(1), 107–129 (1993)
32. Karpov, I.V., Korablinova, N.A.: The migrating tide influence on lower thermosphere circulation at middle latitudes. Geom. Aeron. **38**(2), 112–119 (1998)
33. Fessen, C.G., Roble, R.G., Ridley, E.C.: Thermospheric tides at equinox: Simulation with coupled composition and auroral forcing. 1. Diurnal component. J. Geophys. Res. **96**(A3), 3647–3661 (1991)
34. Fessen, C.G., Roble, R.G., Ridley, E.C.: Thermospheric tides at equinox: Simulation with coupled composition and auroral forcing. 2. Semidiurnal component. J. Geophys. Res. **96**(A3), 3663–3677 (1991)
35. Korenkov, Yu.N., Klimenko, V.V., Bessarab, N.S.: The investigation of boundary conditions influence on thermodynamical balance OH thermosphere at winter solstice. Geom. Aeron. **43**(2), 119–128 (2003)
36. Lashtovicka, J.: Forcing of the ionosphere by waves from below. J. Atmos. Sol.-Terr. Phys. **68**, 479–497 (2006)
37. Altadill, D., Apostolov, E.M.: Time and scale size of planetary wave signatures in the ionosphere F-region. Role of the geomagnetic activity and mesosphere/lower thermosphere winds. J. Geophys. Res. **108**(A11), 1403–1429 (2003)
38. Karpov, I.V., Bessarab, F.S.: Model investigation of solar terminator influence on thermospheric parameters. Geom. Aeron. **48**(2), 217–227 (2008)
39. Frohlich, K., Pogoreltsev, A., Jacobi, Ch: The 48-layer COMMA-LIM model. Rep. Inst. Meteorol. Univ. Leipzig. **30**, 157–185 (2003)
40. Miyahara, S., Miyoshi, Y.: Migrating and nonmigrating atmospheric tides simulated by a middle atmosphere general circulation model. Adv. Space Res. **20**, 1201–1205 (1997)
41. Wells, G.D., Rodger, A.S., Moffett, R.G., et al.: The effects of nitric oxide cooling and photodissociation of molecular oxygen in the thermosphere/ionosphere system over the Argentine islands. Ann. Geophys. **15**, 355–365 (1997)

42. Killeen, T.L., Burns, A.G., Azeem, I.: A theoretical analysis of the energy budget in the lower thermosphere. J. Atmos. Sol-Terr. Phys. **59**, 675–689 (1997)
43. Bessarab, F.S., Korenkov, Yu.N.: The dynamical processes influence on heat balance of upper thermosphere. Geom. Aeron. **33**(5), 120–126 (1993)
44. Bessarab, F.S., Korenkov, Yu.N.: The nitric oxide influence on global distributions of thermosphere and ionosphere parameters. Geom. Aeron. **38**(5), 107–116 (1998)
45. Fuller-Rowell, T.J.: Modeling of solar cycle change in nitric oxide in the thermosphere and upper mesosphere. J. Geophys. Res. **98**, 1559–1570 (1993)
46. Fuller-Rowell, T.J., Rees, D., Rishbeth, H., et al.: Modelling of composition changes during F-region storms – a reassessment. J. Atmos. Terr. Phys. **53**, 541–550 (1991)
47. Fuller-Rowell, T.J., Rees, D., Tinsley, B.A., et.al.: Modeling the response of the thermosphere and ionosphere to geomagnetic storms: Effects of a mid-latitude heat source. Adv. Space Res. **10**(6), 215–222 (1990)
48. Avakyan, S.V.: Physics of solar-terrestrial connections: some results and new approaches. Geom. Aeron. **48**(4), 435–443 (2008)
49. Golubkov, G.V., Ivanov, G.K.: Rydberg atoms and molecules in the medium of neutral particles. Khim. Fiz. **22**(10), 25–86 (2003)
50. Golubkov, G.V., Ivanov, G.K.: Rydberg states of atoms and molecules and elementary processes with their participation. URRS, Moscow (2001)
51. Golubkov, G.V., Golubkov, M.G., Ivanov G.K.: Rydberg atom A^{**} in a field of neutral atom B. In: Gigosos, M.A., Gonzalez, M.A. (eds.) Spectral Line Shapes, Vol. 15; XIX ICSLS, Valladolid, Spain, pp. 140–142. Melville, New York (2008)
52. Golubkov, G.V., Ivanov G.K., Golubkov, M.G., Karpov, I.V.: Rydberg atom microwave radiation the field of the chaotically located neutral particles. Abstracts of 1st International conference "Atmosphere, Ionosphere, Safety" (AIS 2008), pp. 99–101. Kaliningrad (2008)
53. Avakyan, S.V., Voronin, N.A., Serova,. A.E.: The role Rydberg atoms and molecules in the upper atmosphere. Geom. Aeron. **37**(3), 99–106 (1984)
54. Avakyan, S.V.: The microwave radiation from ionosphere as factor of solar flashes and geomagnetic storms influence on biosystems. Opt. J. **72**(8), 41–48 (2005)
55. Szabo, A., Ostlund, N.S.: Modern Quantum Chemistry. Dover, Mineola, New York (1966)
56. Werner, H.-J., Knowles, P.J.: An efficient internally contracted multiconfiguration – reference configuration interaction method. J. Chem. Phys. **89**, 5803–5811 (1988)
57. Golubkov, G.K., Ivanov, G.K., Balashov, E.M.: Interactions of the highly excited atoms and molecules with neutral particles. Features of the potential energy surfaces and the charge exchange processes. Chem. Phys. Rep. **14**(8), 1104–1127 (1995)
58. Golubkov, G.V., Ivanov, G.K., Balashov, E.M., and Golubkov, M.G.: *l* mixing and dissociation of Rydberg molecules accompanying slow collisions with inert-gas atoms, JETP. **87**(1), 56–63 (1998)
59. Matsuzava, M.: Theoretical investigations of Rydberg atom collisions with molecules. In: Stebbings, R., Dunning, F. (eds.) Rydberg States of Atoms and Molecules. Cambridge University Press, Cambridge (1983)
60. Ivanov, G.K., Golubkov, G.V., Balashov, E.M.: Role of non-adiabatic mixing of the vibronic states of highly excited molecules with neutral particles. Dokl. Akad. Nauk SSSR. **323**, 311–315 (1992)
61. Balashov, E.M., Golubkov, G.V., Ivanov, G.K.: Strong irregular excitation-energy dependence of the inelastic transitions and collisional ionization cross-sections of highly excited molecules. JETP **76**(2), 200–209 (1993)
62. Nikitin E.E., Umanskii S.Ya. Theory of Slow Atomic Collisions. Springer-Verlag, Berlin, Heidelberg/New York/Tokyo (1981)
63. Devdariani, A.Z.: Radiation of quasimolecules, Opt. Spectrosc. **86**(6), 954–959 (1999)
64. Zhu, C., Babb, J.F., Dalgarno, A.: Theoretical study of sodium and potassium resonance lines pressure broadened by helium atoms. Phys. Rev. A. **73**, 012506 (2006)
65. Lehner, M., Xu, R., Jungen, M.: The emission spectrum of the Li(2p)He_2. J. Phys. B **38**, 1235–1247 (2005)

66. Namgaladze, A.A., Korenkov, Yu.N., Klimenko, V.V., et.al.: Global model of the Earth thermosphere–ionosphere–protonosphere. Geomagn. Aeron. **30**(4), 612–619 (1990)
67. Namgaladze, A.A., Korenkov Ju.N., Klimenko V.V. et al.: Numerical modelling of the thermosphere-ionosphere-protonosphere system. J. Atmos. Terr. Phys. **53**(11, 12), 1113–1124 (1991)
68. Bessarab, F.S., Korenkov, Yu.N., Karpov, I.V.: Sensitivity of GSM TIP model to the variability of the UV and EUV solar radiation. Phys. Chem. Earth. **25**(5, 6), 543–546 (2000)
69. Afraimovich, E.L., Perevalova, N.P.: GPS-Monitoring of the Earth Upper Atmosphere. SC RRS SB RAMS, Irkutsk, Russia (2006)
70. Karpov, I.V. Shagimuratov, I.I., Yakimova., G.A.: Ionospheric Effects of Poincare Waves. In: Proceedings of International Conference "Fundamental Space Research", pp. 75–77, Sunny Beach, Bulgaria (2008)
71. Liperovskyi, V.A., Pohotelov, O.A., Shalimov, S.A.: The Ionosphere Precursors of Earthquakes. Nauka, Moscow (1992)
72. Pulinets S.A., Boyarchuk K.: Ionospheric Precursors of Earthquakes. Springer, Berlin, Germany 315 p (2004)
73. Zakharenkova, I.E.: The using of GPS signals measurements for finding of earthquake ionosphere precursors.// Cand. Diss., RSU, Kaliningrad 134 p (2007)
74. Namgaladze, A.A., Klimenko, M.V., Klimenko, V.V., and Zakharenkova, I.E.: Physical mechanism and mathematical modeling of earthquake ionospheric precursors registered in total electron content. Geom. Aeron. **49**(2), 252–262 (2009)
75. Sorokin, V. M., Chmyrev, V. M., Yaschenko, A. K.: Theoretical model of DC electric field formation in the ionosphere stimulated by seismic activity. J. Atmos. Sol.-Terr. Phys. **67**, 1259–1268 (2005)
76. Namgaladze, A.A., Klimenko, M.V., Klimenko, V.V., Zakharenkova, I.E.: Physical mechanism and mathematical modeling of earthquake ionosphere precursors registered in total electron content. Geom. Aeron. **49**(2), 267–277 (2009)

Chapter 6
Ball Lightning Investigations

V.L. Bychkov, A.I. Nikitin, and G.C. Dijkhuis

Abstract Ball lightning (BL) researches' review and theoretical models of three different authors are presented. The general review covers investigations from 1838 until the present day, and includes a discussion on observation data, experimental modeling, and theoretical approaches. Section 6.1 is written by Bychkov and Nikitin; authors of the sections 6.2, 6.3 and 6.4 are, respectively, Bychkov, Nikitin and Dijkhuis.

Keywords Ball lightning · Charged eigenstate · Combustion · Concentric gear shells · Condensed melted hot material · Discharges · Dynamic electric capacitor · Electrically charged object · Electron ring · Experiments · Explosion · High energy · Levitation · Observations · Protons · Spherical vortex crystals · Theoretical models · Vacuum cavity

6.1 Modern State on Ball-Lightning Investigations

The historical review of researches on ball lightning (BL) is presented. It is conditionally separated into two stages: first – till 1988, the moment of commencement of the International Committee on BL work, and second – since 1988 till today. Furthermore, researches on gathering and data processing on BL observations, experiments on the reproduction of long-lived shining formations in electric discharges, and BL models, are described. The conclusion that the work on BL observations' data collection has allowed to reliably determine its basic properties has been drawn. Now, there is a necessity for an analysis of its rare properties. Theoretical models need to provide an explanation for BL mechanisms of

V.L. Bychkov (✉)
Physical Electronics Chair, Physical Department, M.V. Lomonosov Moscow State University, Moscow 119992, Russia
e-mail: bychvl@orc.ru

V.L. Bychkov et al. (eds.), *The Atmosphere and Ionosphere,*
Physics of Earth and Space Environments,
DOI 10.1007/978-90-481-3212-6_6,

high-specific energy content and holding of non-compensated electric charge. In the last part of the chapter, detailed descriptions of the three high-energy BL models developed by Bychkov, Nikitin and Dijkhuis, are presented.

6.1.1 Introduction

The Tenth Jubilee International Symposium on Ball Lightning was held in July 2008 in Zelenogradsk city of Kaliningrad region, Russia, on the Baltic seashore. The first symposium on this topic took place exactly 20 years before, from 4th to 6th July 1988, at Waseda University in Tokyo, Japan [1]. The organizers of the first symposium were Professor Dr. Y.-H. Ohtsuki, Professor Dr. N. Kitagawa, and Professor Dr. H. Kikuchi. It was attended by 54 scientists from 8 countries. The first symposium was biannually followed by the second one in Budapest, Hungary (1990), the third in Los Angeles, USA (1992), the fourth in Canterbury, Great Britain (1995), the fifth in Tsugawa-Town, Niigata, Japan (1997), the sixth in Antwerp, Belgium (1999), the seventh in St. Louis, USA (2001), the eighth in Chung-li, Taiwan (2004), and the ninth in Eindhoven, the Netherlands (2006). Usually, the results of scientific activity of the regular symposia were analyzed in reviews of the International Committee on Ball Lightning by President Dr. Stanley Singer [2–5]. Unfortunately, in 2008, Dr. Singer passed away, and hence, the tenth symposium was dedicated to his memory.

Usually, the results of the BL investigators' 2 years' activities were summed up in analytic reports and review articles describing the symposia work [6, 7]. In the present review, we consider reasonable to expand the time in a timetable and describe the most interesting works made before the start of International Symposia constraints and after it, that is, to write something similar to a history of BL investigations.

Traditionally, the following subjects come under discussions at the symposia: (1) data on BL observations; (2) laboratory experiments on BL realization; (3) BL theory; and (4) BL observations video data. Items 1 and 4 are, in essence, devoted to the same subject. In the following review, we will dispose our material in the sequence of subjects 1–3. We will describe the collection and analysis of the observation data, we will consider most interesting works on experimental investigations of laboratory BL analogs, and we will try to present an image of activity in the area of BL theoretical models. Besides works discussed and published in BL Symposia and Conferences transactions, as well as in peer-reviewed journals, Internet, and popular editions, regular information about BL observations and some ideas concerning its physical nature are presented. We have also tried to include such data in our consideration, trying to separate sensation-aimed canards and really reliable reports. Obviously, we might have missed something interesting in this "information sea" distributed over nonspecialized information sources. Therefore, we express our apologies to those authors whose works were left out of our zone of attention.

6.1.2 Collection and Analysis of Ball Lightning Observation Data

6.1.2.1 Data Collected Before 1988

The first meeting of scientists investigating atmospheric electricity with BL was in 1753. Professor George William Richmann was killed by its stroke during a thunderstorm. He was measuring a potential of a metallic bar placed on a roof of his house with a help of an electrometer – a metallic rod that was placed inside the house. The rod was isolated from the ground by a crystal glass and a silk thread was attached to the rod through one of its ends. He judged the value of the rod potential by an angle of a thread deflection. The rod and the electrometer were connected by an iron wire going through an inner porch and a corridor [8]. The event was investigated by Mikhailo Vasil'evich Lomonosov. He established that a fire ball was formed outside the house, which penetrated into a room through either a door or a window. The report of Lomonosov can be considered as the first qualified description of traces left by BL. Besides this event, Lomonosov also knew other cases of BL observations, which have been presented in his article "The word about air phenomena resulting from the electric force" [9]. In this work, he had proposed his explanation of this natural phenomenon as: "combustion of fats, gathered together in air." In fact, this was the first in the world model of BL with a chemical source of energy. Unfortunately, Richmann's death had, for a long time, retarded studies on the atmospheric electricity (including investigations of BL). Leonard Euler stated: "This case has taken away courage from the local naturalists, who were studying the thunderstorm phenomena, and they have interrupted their investigations" [8, P. 7].

We can consider the study by Francois Arago as the next surge of interest in BL. He had collected and published 30 evidences of BL observations and explained this as "lightning energy condensation" [10]. The later BL observation cases and its models were discussed at Paris Academy of Sciences sessions.

An important landmark in BL problem investigation is Walter Brand's book "Ball Lightning" publication in 1923 [11]. This book publication in Germany at that time under conditions of unprecedented inflation was a heroic deed of the scientist. Brand, in his book, had represented 215 BL observation descriptions from 1665 to 1919 as described by eyewitnesses, and indicated 14 main features of BL. As a result of his observation and analysis, nowadays, when we know many other observations, one can make the following conclusions that are based on his first analysis:

1. The thunderstorm in the majority of cases is the cause for BL appearance; however, BL can be observed in fair weather.
2. One can most often observe a single BL; however, there are cases when two or more number of balls were observed simultaneously.
3. BL was observed on a plain, in mountains, and near seas.
4. BL is formed not only during thunderstorms, but also during hurricanes and tornado.
5. The maximum number of BL observations in Central Europe occurs during the summer months – from May to August; this correlates with thunderstorm-appearance frequency. BL is most often observed from 14 to 20 h during day

time, but a period of most thunderstorm activity falls during 12–18 h. It means that BL more often appears at the end of the thunderstorm.

6. In a majority of cases, the form of BL is spherical; sometimes, it is a hollow sphere; and sometimes, it is compared with a soap bubble. Sometimes, one observes deviations from the spherical form: BL has the appearance of an egg, an ellipsoid, a flame tip, a bar, or a pole.
7. The BL contour is usually clearly outlined, but sometimes, it seems to be blurred, surrounded by a glowing gas. During its motion, one can sometimes observe projections on its surface that protrude in different sides. Sometimes, one can see a halo around BL. In a majority of cases, its color is different from those of the ball.
8. Sometimes, one can observe an internal structure of a ball: a decrease in the light intensity from the center to the edge; the ball is dark red in the center and brighter at the edge; or a transparent ball, with a blue flame in the center.
9. Sometimes, sparks, flame bunches, and beams of approximately 50 cm in length fly from the surface of the ball.
10. BL sometimes changes its form: it elongates going through a hole, it is transformed from a "fire snake" to a ball and vice versa; the ball slowly elongates, transforming to thin weakly glowing strip.
11. The average diameter of BL is 20 cm, and its size range is from 1–2 cm to 27 m. During its lifetime, BL size can be constant, increasing, or decreasing.
12. In a number of cases, BL is rotating or rolled over a ground.
13. The major colors of BL are: white, white-blue, dark-blue, yellow-green, yellow-red, and red (the last one appears more often than others). A change in the color of the ball usually takes place before an explosion of the ball: it becomes white from red-yellow; the ball being yellow before an explosion becomes red-blue; the white central part of a ball becomes red before an explosion.
14. There are reports of observations of a black BL, as if consisting of a dense smoke.
15. The light irradiated by BL is characterized in a range from a dim to a dazzling bright light. Observers often state that it was bright but not blinding. The brightness of BL often increases before its disappearance. There are cases when the luminescence brightness of different BL parts was different.
16. Sometimes, BL leaves a smoky trace behind itself or is covered by a smoke or vapor. Observers usually compare the smell of the smoke with those of burning sulfur or burning powder. They generally describe the vapor as the orange gas that can be identified as nitrous oxide (N_2O). In other cases, the smell was identified as the smell of ozone, especially when BL was observed by people belonging to science.
17. In most cases, there are no material traces after a BL explosion.
18. In a vast majority of cases where observers were at a close distance to BL or have touched it, they point out the absence of the feeling of heat from the heat emitted from it. Sometimes, on the contrary, observers report about heat irradiation and even about cases of singing or inflammations of objects by BL. The effects with heat release most often take place during BL explosions. It

is usually difficult to separate the consequences of BL explosions and the effects caused by a stroke of usual linear lightning.

19. An encounter of BL usually leaves an indelible impression in an observer's memory. Most often, it causes a feeling of danger and fear.
20. BL at close contact with an observer's body can cause temporary loss of consciousness, paralysis, or even death. There are many cases of animal deaths during a BL explosion. A "mechanism" of breather affection is similar to the impact of usual linear lightning.
21. There are data about the mechanical work executed by BL: stone spreading, transportation of people and animals in space, and making holes in thick walls, wooden doors, or window glasses. BL is capable of making a deep pit or a trench in the ground, throwing a tile from the roof, or swinging a church bell. It can evaporate wine, oil, and water in earthenware, leaving the vessel safe; tear a shirt to pieces; instantly melt down a piece of ore or gold; and tear away a ring from a finger.
22. BL can impact electrical devices: it can make electrical bells to ring and cause glowing of bulbs; its explosion is accompanied by a melting down of safety fuses and burnout of light bulbs.
23. Sometimes, BL is a sound source. This sound is compared with a whistle of a rising rocket or a shell. Sometimes, a crackling noise accompanies BL motion. St. Elms fires produce a similar set of sounds, but the sound generated by BL is much louder. Probably, one can connect BL sound with electric charge loss.
24. In a large number of cases, the ball dropped out of the sky is observed. Sometimes, BL reaches the earth's surface, but sometimes, BL's fall is stopped at a height of 1–15 m, and BL starts moving horizontally. There are cases when BL, on the contrary, rose up to the cloud from the earth's surface. Sometimes, BL stops and stays motionless in air. BL's path is never straight, but sometimes it falls down from a cloud to earth along the vertical trajectory.
25. BL moves along a complex trajectory in closed premises or near buildings. It can jump aside as an elastic object when it comes into contact with walls or ground.
26. In premises, it often moves round a circle approaching walls and floor not closer than 1 m. BL flying in a room through a window or a door usually moves to an opposite wall. Sometimes, it leaves the room along the same way through which it flew in. This can be caused by electric-field variation in the room or a complicated airflow gas-dynamics in the premises [12] with respect to the location of intake and air vent holes.
27. A sharp change in BL motion direction can be caused by air flows or an impact of electric conductors. However, sometimes, air motion does not visibly impact it, and it may move upwind. The features of BL motion can be explained by its attraction to metallic objects, and its tendency to move through chimneys can be associated with the electrical conductivity of smoke.
28. The path of BL motion, in some cases, remains along the electric conductors: it moves along the telephone, telegraph, and electric cables, wires of lightning rod groundings, drainpipes, and tree trunks.

29. There were marked cases of BL moving along the surfaces of people and animals, leaving skin burns. However, more often it demonstrates a tendency to evade contacts with people, animals, and good conductors.
30. BL can penetrate through keyholes, slits, and cracks. In rare cases, it can penetrate through glasses, leaving it intact; sometimes, it makes a fist-size orifice.
31. During its lifetime, BL can cover a substantial distance of several hundreds of meters.
32. BL moves with a constant velocity only in rare cases; usually, it accelerates and decelerates. BL can be separated into two groups with respect to its motion velocity. The first one consists of BL moving from clouds to earth or between the clouds. On an average, its velocity is of several tens of meters per second. The second group consists of BL observed in premises or outdoors near the earth. Its average velocity is 2 m/s.
33. The duration of existence of BL is from 1 s to 5 min and more. In a majority of cases, one can observe BL with the observation time below 5 s. Short-lived BL is observed inside premises and in the open air, but the long-lived ones were observed only outdoors.
34. A stroke of usual linear lightning often precedes the BL. There are observations of BL originating in the linear lightning channel. However, observers often report nothing about BL appearance associated with usual lightning. In most of the cases, BL had not appeared directly after the linear lightning stroke, but several minutes after and in the absence of linear lightning.
35. BL often disappears silently and does not leave any traces. Its disappearance can take place in the air and also when it comes into contact with some objects, ground, or water. In some cases, BL's disappearance is accompanied by a sizzle and burst of flame tips or sparks. In many cases, BL's life ends with an explosion. Sometimes, an explosive sound is described as a gunshot or rifle shot. The explosion is often accompanied by a bright light flash, lightning, and pieces of matter and sparks flying out of BL.
36. Sometimes, BL divides into several separate balls that either continue their existence or go out. BL division can take place in the air and at a collision with some objects. Balls of a smaller size practically do not differ from the initial ball.
37. There is a description of the case when BL, on the contrary, was composed of smaller-sized balls, which when moving towards a cable or a wire, came nearer and formed a luminescent mass.
38. There are rare cases of BL pairs located one over the other and connected by a "thread" consisting of small luminescent beads.

Besides the conclusions made on the basis of Brand's descriptions, one can formulate additional BL features:

39. BL can lose a part of its matter after an impact with an obstacle, but it does not interrupt its existence as a single whole (Br.14, Br.36, Br.92) (the mark (Br.)

indicates the book [11], and a numeral signifies the number of the report from this book).

40. Natural tissues (cotton, cloth) become fragile or tear to pieces after coming into contact with BL. However, traces of "burns" left on a tissue disappear after washing (Br.3, Br.95).
41. Tinted tissue becomes colorless after coming into contact with BL (Br.95).
42. As a linear lightning, BL can strike a tree and split the tree trunk, and people under the tree can get killed (Br.33, Br.146, Br.149).
43. According to a report, St. Elms fires had appeared at mast tops, 2 min after BL explosion in water at a distance of 2.5 m from the sailing-ship side (Br.47).
44. There is a detailed description of circular holes in a glass produced by BL (Br.95). "Their diameter as a rule 8 cm, the fracture was even, not the star-shaped, smooth on the inner surface and exhibited a small sharp edge on the outer surface. In certain cases, there was a series of concentric wave patterns around the circular hole."
45. An electric discharge had occurred between BL and the grounded electric wire when BL came into contact with it. This caused melting of the wires (Br.136).
46. Sometimes, the disappearance of BL is accompanied by a loud noise; however, sparks do not fly from it (Br.171). This resembles a collapse of evacuated sphere.

Brand finished his review with the summary of 14 items, in which he presented conclusions in a concerted form. We have enumerated them in Items 1–38 mentioned earlier. At the same time, some conclusions made by Brand were represented, which could lead (and unfortunately sometimes lead) to their erroneous interpretation. In this way, in Item 1, he presented BL definition as "rare forms of spherically shaped *electrical discharges*." Usually, the term, an "electrical discharge," is understood as the *process* with the electric current participation and energy delivery to the discharge zone. The presence of such processes does not follow from the observations collected by Brand. In Item 8, he describes a possibility of BL "shoot down to earth" from the lower part of a cloud and its transition to usual streak lightning. However, there is no such case in his list of observations. Hence, it is difficult to determine this phenomenon owing to the incommensurability of linear and BL lightning lifetimes. In Item 10, he describes the existence of two BL types – the freely floating and the stationary ones, which have different characteristics and can transform into one another. However, there are no clear evidences in favor of such BL types among the observation descriptions collected by Brand.

Nevertheless, the indicated inaccuracies do not disparage the great scientific value of the materials collected and analyzed by Brand. It will be shown in the following sections that the main conclusions made by him remain practically unchanged even 85 years after the publication of his book. The massive data collected by Brand increased with the results of new observations, and only a few of them gave "new colors" to a complicated BL picture.

It must be noted that Brand did not make any qualitative estimates of energy contained in BL (or brought by it from external sources) when analyzing cases

executing the mechanical work of BL. This soon became connected with the fact that there were no detailed numerical data about destructions left by BL in the sources used by him. However, 14 years after the publication of the book of Brand, an important event took place, and it forced to fundamentally change the opinion regarding BL as an insignificant formation with small energy.

47. A large, orange-fruit-sized, red-colored BL had fallen in a tub with 18 L of water in Dorstone, a London suburb. The water began to boil and it was boiling for several minutes [13]. A part of the water had evaporated. The BL energy had been evaluated as 10 MJ based on this "natural" experiment and its energy density had been found to be 3×10^{10} J/m^3 [14]. Let us consider that there was no BL explosion in this case, and it had "lived" in the tub gradually giving energy to water (the number at the beginning of this paragraph indicates that we have added a new BL characteristic to the list of features taken from the book of Brand).

In 1965, in the USSR, a popular scientific book of R.A. Leonov, titled "Ball Lightning Enigma," was published and 53,000 printed copies were circulated [8]. In that book, the author described in detail the circumstances of Professor Richmann's death, investigated by Lomonosov. Lomonosov thought that BL could come into the house through an open window of a room adjoining the room where Richmann was. A clock stopped in the room with the opened window and the sand flew from the stove. Further, Leonov described several BL observation cases borrowed from different magazines. These were reports about: a spark that grew to a size of a 10-cm ball in front of the observer [15]; a "golden" ball of 10-cm diameter, which exploded and caused fire on a fur coat and a shed [15]; BL that flew twice around people sitting near a table in a hut, which then flew out of a window. There was also a report about the appearance of a "walnut"-sized bright-red ball from the heated Russian stove. The ball had flown over a bag with surgeon tools, and subsequently flew out of the hut. In a yard, it had transformed into white-colored spindle form and had exploded near a tree, which caught fire. It was determined that metallic tools in the bag became magnetized; however, "their magnetization had disappeared after a day." On the basis of this observation, one can make a supposition about one more feature of BL:

48. BL can magnetize steel objects close to them.

Apparently, this BL feature is presumed to have caused the stopping of the clock, as observed by Lomonosov.

A review of J. Rand McNally appeared in May 1966, which was devoted to the analysis of BL features [16]. The author had distributed a questionnaire about the details of lightning observations among 1,962 OAK Ridge National Laboratory employees. One hundred and ten of the questioned people (5.6%) reported that they saw BL. Subsequently, McNally undertook a wider questioning of all Oak Ridge Union Carbide Nuclear Company employees (15,923) and received 513 positive answers (3.1%). The questions in the questionnaire were about BL's association with a stroke of usual lightning, its life span, its disappearing process, size, form,

sound, traces left by it, its motion type, color, and heat irradiated by it. An analysis of the questionnaire results demonstrated that BL, in majority of the cases, appears after a linear lightning discharge, and the place of its origin can be metallic constructions, transmission facilities, nonmetallic constructions, telephone lines, and free space. It can move along wires, float in air, jump back from earth, rotate and roll, move straightly, or stay motionless. A spherical form is the dominate one. Its sizes can range from 2 cm to 2 m, and the most probable size is 24 cm. The total BL volume shines uniformly in a majority of cases, and rarely, the BL surface shines. The predominant color group is red–orange–yellow (57.5%), with white color observed in 28.8% of the cases, and 13.7% of the cases falls under the color range green to violet. The duration of existence of BL ranges from parts of the second to 2 min; the average time is about 3 s. It usually disappears quickly (often with an explosion).

One can observe that the review of McNally practically add nothing to a list of BL features discovered by Brand. We will also not determine something new in the list of selected witnesses' observations. There are reports about BL appearance over wires of high voltage transmission line at 6 m from a pole and its motion along a wire (Mn.12, Mn.17, Mn.57, Mn.69, Mn.184); vertical descending of BL on a side of a thunderstorm cloud; its jump back when it hits the earth (Mn.49) or water (Mn.64); and BL origination as linear lightning that strikes a tree (Mn.113, Mn.129), electric fence for cattle (Mn.169), or a telephone line (Mn.184) (here, Mn. indicates the reference of [16], and the numeral – the number of the observation). There is an interesting report about BL penetration through a steel mosquito net (Mn.49) and about the production of hissing sound similar to that produced by a red-hot iron when BL came into contact with water (Mn.403). Thus, one can add one more feature to the list of BL features:

49. BL can penetrate metallic net.

A report by a NASA employee, Warren D. Rayle, had been published in 1966, in which the author questioned the NASA Lewis Research Center employees [17]. The questioning consisted of two stages. First, a questionnaire was sent to 4,400 employees with questions about: how often they saw a linear lightning striking a place; bead and BL; do they like to be outdoors during thunderstorms; and do they like an observation of lightning discharges. The author received 1,764 answers, revealing that: 409 people saw a nearby lightning discharge, 180 people saw BL, and 112 people saw a bead lightning. He made a conclusion on the basis of these results that BL is not a rare phenomenon: the ratio of the number of observed BL and the nearby linear lightning discharges was 0.44 (and the ratio of bead-lightning number and the number of nearby linear lightning discharges was also high – 0.27). The second questionnaire was sent to the people who reported that they saw BL, after the analysis of the first questionnaire's results. It comprised the following questions: did the observer see the moment of BL origination, what was its diameter, how often did he come across a BL, in which year it happened, in which month, in which time of the day, where did it happen, was it associated with a thunderstorm, wind, where was BL at the beginning of the observation, what was its distance, what was its form,

diameter, brightness, and color, for how long did the observation last, did its size and brightness change, did the observer hear a sound and smell an odor, did he feel the heat, what was its velocity, did the ball guiding take place, did the ball rotate, how did the ball disappear, and were there any traces after BL disappearance. One can note that the number of these questions is much larger than those in the McNally questionnaire. Rayle received 112 BL-observation descriptions. The main purpose of the investigation was an attempt to find a correlation between different BL characteristics. The analysis of the obtained data demonstrated that the average BL life span was 6 s (whereas McNally obtained 4 s), and a proportion of the balls that remained for more than 30 s was 12% (McNally obtained 8%). The different-diameter BL probability observation lognormal distribution graphs were developed. It was found that the points laid on a straight line (also similar to McNally results) and the slope of the BL square diameter lognormal distribution lines (i.e., the ball surface area) coincided with the slope of the charge (transported by the linear lightning stroke) value frequency lognormal distribution line. The average diameter was found to be 35 cm (McNally obtained a value of 25 cm). The value of the distance from which BL was observed sharply decreased after 30 m, and this was apparently associated with the worsening of its observation conditions. The maximum velocity of BL motion was about 30 m/s, and the minimum velocity was about 2 m/s. BL most often moved horizontally (54% of the cases), and the vertical motion was marked only in 19% of the cases. The brightness was most often characterized as "sufficient to see a ball during the day light," its form was mainly the spherical one, and the sphere shined uniformly. The predominant colors were orange and yellow (while the red color was predominant in McNally analysis). Thirty six per cent of the observers reported rotation of the ball. It was reported that the brightness and sizes of BL did not change during the observation in 85% of the cases, and did not change up to a moment of BL disappearance. A few evidences were obtained in favor of BL's ability to contain high amount of energy, and information about bright flashes and destructions was very rare.

The correlation analysis of the described events' different parameters did not allow the determination of their visible connections. The size, shining brightness, and existence duration proved to be unconnected. The observed weak correlation between BL diameter and its distance to the observer may possibly be associated with the errors in defining the indicated parameters and the difficulty in observing small objects from large distances. Among the 112 observations, one could separate two groups with 12 cases each. In the first group, BL observation after a stroke of linear lightning to the earth was reported. The second group consisted of BL observations first noticed in the open air and remaining there until their disappearance.

Thus, on the basis of Rayle's analysis, one can establish new features of BL:

50. Processes responsible for the size, luminescence brightness, color, and existence duration of BL are practically independent.
51. The value of the BL surface area correlates with a charge value transported by a linear lightning to the earth.

On the basis of BL-characteristics constancy during its lifetime (size and luminescence brightness), Rayle made a conclusion that appears skeptical. For convenience, we call it "Myth No 1" (M1):

> M1. As it is difficult to propose a mechanism of uniform stored energy expenditure, one has to support the idea according to which BL gets energy from the external source.

The argumentation is rather strange, because in nature and technique, there are numerous systems where the stored energy expends uniformly in the long duration (e.g., energy of water from a water reservoir with a dam; benzene energy in an automobile; and energy of a compressed gas released to the atmosphere through a throttle).

A new symbolic event took place in 1971 in USA – the book of Stanley Singer, titled "The Nature of Ball Lightning" [18] was published. After 2 years, its translation into Russian was published in the USSR. The number of copies of the Russian edition was about 10,000, it was typical for that time, and the book price was about a dollar. Owing to this book, the material collected and analyzed by Brand became available to the readers: the book of Brand became the rarest book by that time. Singer added to the data of Brand's new data that appeared during the 30th–60th years of the twentieth century. Thus, the book included a short mention about the 10-MJ BL-energy case in 1936 [13, 14] and BL-observation description near Onega river, published by M.T. Dmitriev in 1967 [19]. For a minute, Dmitriev was observing a flight of a bright yellow-white ball of 8-cm diameter. The ball was surrounded by two shells; the internal – the violet one was of 1–2-cm thickness, and the external – the blue one was of 2-cm thickness. The ball moved with a velocity of 1.5 m/s along the rafts in the river. At the bank, its velocity dropped down to 0.4 m/s, and it hovered above for 30 s. The ball left behind a trace of bluish acrid smoke. Then, the ball began to move to a side of a forest and ejected sparks at each collision with the trees. At the end of the observation, the ball was transformed from white to bright red and disappeared. The noise increased in the transistor receiver during the approach of BL, which transformed into a continuous roar. Dmitriev took four air samples after the ball flight from its trail. In the first and the fourth samples taken at the 55th and 70th seconds after the BL flight, the ozone (O_3) and nitrogen dioxide (NO_2) concentrations proved to be at the level of 0.1 mg/m^3, but in the second and third samples taken during the 60th and 65th seconds, the concentration of these gases proved to be ten times greater. One can formulate two more features of BL on the basis of Dmitriev's observations:

52. BL is a source of radio-radiation at frequencies of 0.3–3 MHz.
53. Ozone and nitrogen dioxide are formed in the BL trail with a delay of about 1 min.

Singer described several cases of BL's encounter with aircrafts. It can fly into a cabin through an open window and fly to the plane's tail. It can explode outside near the aircraft's fuselage or propeller, and can melt a metal and surround the molten place with soot. Furthermore, BL can get into a hermetic cabin of an all-metal

aircraft. It often moves by a straight line along a passage to the tail part of the saloon at a height of about 75 cm over a floor. From this feature of BL behavior in the aircrafts, one can formulate the following:

54. BL can penetrate inside an all-metal aircraft, and usually moves in the center of the saloon at a constant height and velocity of 1–2 m/s in the direction from the cabin to the tail.

Singer devoted a special chapter of his book to the analysis of BL's typical features derived from the observations. He considered that the whole set of BL features contains obvious contradictions: BL can appear both during a thunderstorm and in fair weather; its color can be arbitrary; sometimes it can move and sometimes it can remain motionless; sometimes it can move down a wind and sometimes it can move towards a wind; it can disappear silently and sometimes with an explosion; and sometimes it can move over objects and sometimes without any support. Subsequently, he enumerated 14 BL features defined by Brand and the results of the statistical processing of the questionnaires created by McNally and Rayle. With regard to BL luminescence, Singer compared it with a black body and a plasma-generator torch, whose temperatures remained in the range of 2,000–14,000 K. In addition, in conception of a chemical reaction whose products' outcome depends on the temperature, he considered the ratio of ozone and nitrogen dioxide ($[O_3]/[NO_2]$ ratio) in the air samples found by Dmitriev. The lowest value of $[O_3]/[NO_2]$ ratio proved to be close to 0.8:1, which, according to Singer, indicates that the BL temperature is 4,000 K. Such reasoning has quite a right to life, similar to a hypothesis. However, it does not prove that thermal radiation is a source of BL radiation and that there are some different processes involved. Unfortunately, such an ungrounded opinion of BL radiation cause subsequently became another myth:

M2. BL irradiates energy as heated black body.

Speaking about BL release of extremely high energy, Singer mentioned its falling into a tub with water (its energy was estimated as 6–11 MJ) [13, 14] and a destruction of a cob house at the explosion of BL (with an estimated energy of 400 MJ) [20].

Singer devoted one of the chapters of the book to the analysis of BL photos. A number of these photos are very small owing to the unpredictability of BL and its short life span. BL most often appears in a vision field of a photo camera in an amateur recording of linear lightning discharges. A photographer directs a camera to some section of a sky where thunderstorm discharges occur, and opens an objective for several minutes. Sometimes, in developed films, one can find twisting traces on a background of a landscape, which could be left by moving BL. For example, Singer showed two photos obtained by this method [18, Figs. 14 and 15]. At the same time, he warned against false photos in which a continuous trace could appear as a result of camera motion in the presence of a bright light source in its field of vision; for example, a street light. In the book, one can also find two BL photos made with short exposure. In one of them [18, Fig. 17] (see Fig. 6.1), one can see a big oval form whose large axis is oriented vertically, whose upper and lower parts are somewhat smeared, and the axes lengths' ratio is 1.28:1. It is reported that the ball diameter was

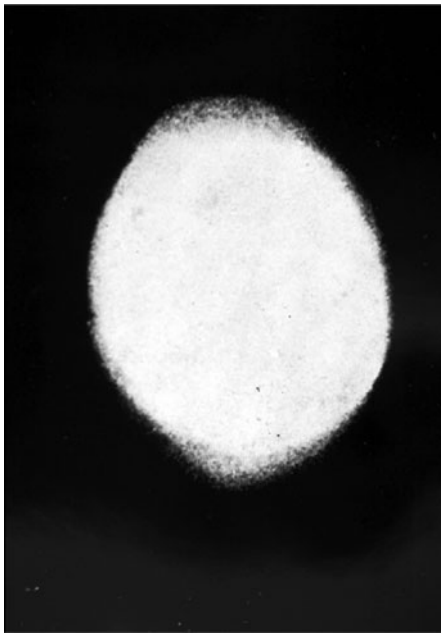

Fig. 6.1 Still photograph taken during a thunderstorm in 1935 by H. Schneidermann [48]

35 cm and the ball during recording was descending to the earth. Let us make our own analysis of this photo. One can find that the length of the large axis of the oval is $35 \times 1.28 = 44.8$ cm, and the difference of the axes lengths is 9.8 cm. This distortion of a ball image could occur if the ball, during the exposition, moved for a distance of 4.9 cm. As the exposure duration is not given in the book, let us consider it to be equal to the average exposure time of a photo camera, that is, 1/30 s. The ball motion velocity in this case is $v_b = 4.9 \times 10^{-2} \times 30 = 1.47$ m/s, and this is a typical velocity of motion for BL. The smaller level of the negative blackening in the upper and the lower parts of the oval form can be easily explained by the vertical motion of the ball. For some reasons, all researchers, including Singer, described an oval but not a ball. In the second photo represented by Singer [18, Fig. 18], one can see a photo of BL with a diameter of 50 cm, which is accompanied by ejection of sparks (this case resembles several descriptions from Brand's book).

A review by W.N. Charman about the BL features was published in 1979 [21]. Charman described the results of statistical investigations of McNally and Rayle, and also presented 14 observation examples collected by him. However, there are no new details with respect to what was known before. Among the new data that appeared in the literature, he mentioned Jennison's evidence when BL flew past him at a distance of 50 cm. Jennison discovered that steel objects in his pockets did not react to BL's presence. From this finding, one can conclude that:

55. BL does not reveal a visible magnetic impact at a distance greater than 0.5 m.

Charman gave special attention to the cases of BL release of extremely large values of energy. He added several cases to those described by Singer with regard to the tub [13, 14] and house destruction [20]. Among them, there was a report about BL, whose size was at 60 cm at the beginning and 8 cm at the end of the observation. It made a trench of 100-m length and 1.2-m depth [22]. A work executed by BL proved to be equal to 10^7 J according to the estimates. In the case when BL descended from a cloud and split a pile of moorage, its minimal energy was estimated as 10^5 J [23, 24]. Thus, according to Charman, BL energy can be in the range from 10^3 to 10^7 J. With regard to the BL photos, Charman described the photos published in Singer's book [18], and concluded that they practically do not add new information to that which follows from visual BL observations. Nevertheless, they serve to confirm this phenomenon's existence, as until now, some scientists doubt about the reality of BL and explain its observation using the physiological effects of the bright object's image on the retina of the eye.

Besides BL photos obtained occasionally, there are rare cases when they were obtained in a course of systematical observations. In the 1960s, a system called Prairie Meteorite Network was effective in the USA for observing meteorites [25]. Sixteen photo cameras were continuously photographing the night sky through objectives that were opened for 25 ms with a period of 75 ms. When a discharge of a linear lightning was in the objective's field of vision, it was recorded during one exposure time (a duration of a stepped leader in an average was about 20 ms, and a duration of a lightning return stroke was about 1 ms). Investigators found that in 2 out of 1.2×10^5 photos of a linear lightning, there were recorded events of some objects going out of the linear lightning trace, which remained for about 3 s. A trace of these objects resembled a dashed line consisting of 40 bright sections. It is quite probable that this trace was left by a moving BL. In another case, when a ball was recorded near a channel of a linear lightning, it remained for about 180 ms. It was observed during the recording of a linear lightning discharge by a high-speed camera [26]. Charman also discussed the question of the possibility of residual radioactivity in the objects that came into contact with BL. It was shown by the thermal luminescence method that there were no traces of radioactivity in stones of the church wall that was hit by BL in 1846 [27, 28].

A book by Igor Pavlovich Stakhanov, titled "Physical Nature of Ball Lightning" [29] was published in 1979 in the USSR, and the number of copies sold was 23,000. After 6 years, in 1985, its second edition was published with a title "On Physical Nature of Ball Lightning", and the number of copies sold was 50,000 [30]. In 1996, 9 years after the death of Stakhanov, the third edition of his book appeared (in this case, only 1,000 copies were sold) [31]. The book was written based on the BL-observation analysis, and the data was collected by I.P. Stakhanov and S.L. Lopatnikov by questioning the readers of the popular-scientific magazine, "Nauka i Zhizn" ("Science and Life"). The readers answered the questions in the questionnaire that was published in the magazine in December 1975. Besides the descriptions collected personally by Stakhanov in these books, he also used the materials of observation analysis published by McNally. A main feature of these books was that they were written by a man who, in the first place, deeply understood

physics, and in the second place, created his own model of BL. On the one hand, this plays a positive role, as the author, besides a statement of one or another BL-feature observation, tried to provide some physical explanation. On the other hand, he started to excessively strictly consider the facts that did not match his own theory. He announced them doubtful, and often "spills out a baby with water." Examples of his selective attitude towards facts can be found in the preface [31], where he wrote: "There a ball lightning is chasing a man mad with fear and plays with him as a cat with a mouse. Here appeared a ball lightning with a diameter of 5, 10, not, even 20 m. There BL destroys a house that is at 50 m from it, another one breaches a huge tunnel in a ground, the third evaporates water in a tub. This is a letter in which a man states that his teeth and hair has gone out and signs of the radiation sickness have appeared after a ball lightning moved by him . . . It is not a ball lightning. It is a myth of a ball lightning." One can expect that the author who follows such reasons can throw away letters describing large-sized BL, BL with large energy, or how BL impacts people's psyche or health. It is doubtful whether impartial investigators, such as Brand, Singer, Charman, and Rayle could venture to take such a step. However, there is a small probability that such "doubtful" data did not disappear, because according to a report by I.G. Stakhanova [31, p. 228], there are about 1,000 unanalyzed observation reports in Stakhanov's data bank from which only 126 descriptions were published in [31]. Expecially, in [29–31] it has no luck the case in which BL got into a tub with water and heated it up to boiling point [13, 14]. Stakhanov considered that "Goodlet's estimate is erroneous. Really there is a possibility that water 'boiling' in the tub was connected not with high temperature of a whole water mass but with gas bubbles formation in places of local heating (i.e., in the places where BL substance has appeared) at low water temperature . . .. But the witness said that water was hot by touch even after several minutes. But these feelings could be exaggerated, and real water temperature was not measured." Ignoring such evident facts seems to be more than strange, as the author of [30] was aware of the book by Imyanitov and Tikhiy [32] (it was marked by number 23 in the literature list [30]). An even more striking case of BL heating 100 L of water to boiling point was described. Furthermore, in this book, attempting to prove that a mistake was made in BL-energy estimation when BL split the pile of moorage [23, 24], Stakhanov executed his own calculations and found that a spent energy of about 100 kJ was involved in the splitting of wood. However, during calculation, he, for some reasons, considered that the pile length was only 0.1 m. Nevertheless, by assuming that the pile was longer, for example, 2 m, one can obtain the energy estimate of 2 MJ.

Disputable from our point of view is the BL problem solution method proposed by Stakhanov. He presumed "that if we try to explain all facts reported about ball lightning then we pose an unsolvable problem for us from very beginning. It is not only the unsolvable but, very likely, a senseless; because at that we will try to explain also mistakes inevitably included to actual facts. Therefore it is quite natural to refuse from an explanation of a number of exotic facts at first steps (for example, as appearance of black ball lightning, ball lightning with a huge energy release of 10 MJ order of magnitude and higher, or ball lightning with a diameter of

several meters) and to direct towards explanation of main observation mass" [29, P. 44]. One could accept the proposed principle of "thoughts economy" as quite reasonable if it was known beforehand that parameters excluded from a consideration (e.g., those enumerated by Stakhanov) were inessential. As this is not evident, the opposite principle can be considered to be more accurate: for the construction of BL theory, one has to use all its features, even those rare ones that are "omitted" during statistical analysis of the observation results.

Description of the massive data collected by Stakhanov confirms the main observation results published by Brand, Singer, and McNally. Again, we have reports of BL of different colors [30, P. 10; 27], absence of heat at close contact with BL [30, P. 10; 22; 72], BL explosions and sooty spots left by it, separation of object parts [30, P. 10; 22; 91; 124; 125], melting and evaporation of metals at BL explosion [30, P. 22; 76; 85], and BL formation near a linear lightning [30, P. 23; 27] and at a lightning stroke to the earth [30, P. 107; 108]. He also discussed the ejection of sparks from BL [30, P. 27; 45; 88; 91], BL reddening before its disappearance [30, P. 27, 127], a form change – transformation of an arrow to a ball [30, P. 75; 121], appearance of holes in glasses or walls [29, P. 79; 90], and kickbacks at hitting objects [30, P. 121]. There are reports about BL propagation through small holes and slits [30, P. 93; 121; 123], barking of trees at BL strokes [30, P. 97; 112], BL's appearance from sockets [30, P. 110; 111], and a case when pellets propagated through BL [30, P. 62].

This last observation, if, of course, a hunter could hit a ball from a distance of 15 m, is a new one and quite interesting. It was reported that the ball after the shot only shook but left safely. Let us consider a pellet radius r_p equal to 1 mm; thus, its mass is $m_\mathrm{pl} = 4\pi r_\mathrm{p}^3 \rho_\mathrm{Pb}/3 = 0.047$ g (here, ρ_Pb is lead density). A pellet momentum moving with a velocity of 100 m/s is $p_\mathrm{p} = 4.7 \times 10^{-3}$ kg m/s. If ten pellets got into the ball and each of them gave it 1/10 of its momentum and the ball obtained a velocity of $v_\mathrm{BL} = 10$ cm/s, then the BL mass would be $M_\mathrm{BL} = p_\mathrm{p}/v_\mathrm{BL} = 47$ g. On the basis of this "experiment," one can conclude that:

56. BL is a material body with a mass of 10–40 g. Propagation of small-sized metallic ungrounded particles through it does not lead to its ruination.

In a similar case, another hunter [33] hit a ball using buckshot from a closer distance. The ball size increased by 1.5 times; after that, it decayed with a bang, and its asymmetric pieces of torn form went out falling. This observation also demonstrates that BL is rather a heavy material body, whose parts are heavier than air, and that the type of its interaction with metallic particles can be changed with respect to their energy and size.

Stakhanov, while making a statistical analysis of 884 cases of BL observations, found that 83% of the observation cases fell on three summer months, and 93% of the observation cases took place during the period from May to September. This coincides with the results of Rayle, indicating that BL appearance correlates with the thunderstorm activity. Stakhanov, by analyzing BL with different lifetimes' observation probability distribution, discovered that there are two groups of BL: "short-lived" (57%) with the average lifetime $\tau_1 = 11$ s and "long-lived" (43%)

with the average lifetime $\tau_2 = 54$ s. Furthermore, he discovered two similar groups by analyzing McNally's data. The BL-diameter probability density distribution in the case of Stakhanov's data practically coincided with the analogous McNally's and Rayle's data distribution. The most probable diameter value proved to be 10–20 cm. It was revealed that about of 50% BL had time to cover a distance of about 50 m during an observation time. About 75% of them moved horizontally and smoothly (about 83%), and the most probable velocity was 0.5–2 m/s. "Guiding" – BL motion along the lengthy conductors – was observed approximately in 20% of the cases. Color in 60% of the observation cases could be attributed to the red edge of the spectrum (red–yellow), and 15–20% belonged to the short-wave edge of the spectrum (green–violet). Stakhanov presumed that "a color of ball lightning is not its typical feature, and in particular say nothing about its temperature and composition." We also agree with this conclusion of Stakhanov. A light flux from BL, on an average, can be compared with that from an incandescent lamp of 100 W. Stakhanov conceded that "ball lightning can emit soft ultra-violet radiation, by absorption of which in surrounding air one can explain the observed blue halo." After making photometric measurements of BL trace in a photographic film, Stakhanov concluded that light freely comes out of the internal part of a ball. It means that BL is transparent for visible light. In the data collected by Stakhanov, an amazing BL feature was confirmed: by radiating light, it radiates almost no heat. Only 8.5% of the witnesses at a distance less than 1 m from the ball reported about feeling the heat (but hardly noticed). This indicates that BL temperature cannot be equal to a thousand or several thousands of degrees. BL, according to the observations, is a source of radiation in radio-range. Stakhanov presumed that the radio-radiation "has essentially non-equilibrium character" (i.e., heated body cannot be its source). A valuable conclusion about BL features was one that "ball lightning substance possesses surface tension." However, he could not indicate a reason for a surface tension existence and proposed to accept it as the fact [30, P. 118]. The presence of surface tension with a value higher than $\sigma = 10^{-6}$ J/cm^2 allows to explain the absence of BL substance diffusion to air during its motion (absence of Rayleigh–Helmholtz instability). Besides, the surface tension also allows saving BL from the convective instability (Rayleigh–Taylor instability). The presence of the surface tension enables "ball lightning substance to create a separate phase in air, different from a gas surrounding it. . . . Most time of its life a ball lightning has sufficiently clearly defined boundary."

Along with the deep conclusions set forth, Stakhanov had great doubts regarding the assumption that BL contains energy greater than 100 kJ. With the same persistence, he did not accept any presumptions that BL can carry high uncompensated charge. However, by trying to explain BL motion, he supposed its presence, but in "homeopathic" doses. Thus, for an explanation of BL rising to a thunderstorm cloud, he considered that it "has to carry a positive charge similar by the sign to those of earth surface" [30, P. 63]. Assuming BL mass to be equal to 2 g and thunderstorm electric-field strength of 10^5–10^6 V/m, with respect to Stakhanov's estimates, one can observe that BL charge should not be lesser than $Q = 2 \times 10^{-8} - 2 \times 10^{-7}$ C for the compensation of gravitation force. The electric capacity C of a ball with a radius

$R = 10$ cm equals to $C = 4\pi\varepsilon_0 R = 1.1 \times 10^{-11}$ F, and the electric energy stored in the capacitor carrying this charge Q is $W_e = Q^2/2C = 2 \times 10^{-5} - 2 \times 10^{-3}$ J. BL – a capacitor with such insignificant energy – cannot express visible electric effects: to melt metallic substance, electric current should strike a breather.

As these effects undoubtedly take place, Stakhanov had to find some explanations for them. The following is the essence of his explanations. He stated that "ball lightning possesses a feature to take off charges from conductors. At that, it has to be a conductor itself and the conductor with low work function of charges" [30, P. 96]. For example, "a tree splitting can take place under an influence of a current pulse that appears at the contact with ball lightning. Energy releasing at 'explosion' in this case does not relate to the energy stored in ball lightning itself. Releasing energy is stored in charged conductors, and the ball lightning is a trigger for release of this energy ..., and the energy can be released also at large distance from the place of ball lightning contact with the conductor." Let us try to understand where the charge can appear from, which BL discharges through itself. Let the lower part of a thunderstorm cloud carry the negative charge of several tens of Coulomb; then, the positive charge of the same value will be gathered on the earth surface under the cloud. An area of such a charged "spot" is approximately equal to the area of the lower part of the cloud ($S = 1{,}000 \times 1{,}000$ m$^2 = 10^6$ m^2), and a distance between the center of the spot and the uncharged area of earth may be about 1 km. Stakhanov, for the estimation of the maximal electric energy store in the "spot," considered its radius as 10 m, and a value of a charge induced in it as 10^{-3}–10^{-2} C [30, P. 104]. Thus, he seemingly considered that an area at 5 m from the "spot" center stays uncharged. Later, he considered the following: BL whose size is 20/0.2 m = 100 times smaller than the "spot" diameter gathers charges by some incomprehensible means from the "spot" and carries them to the uncharged part of the earth. Those of us who "short-circuited" charged capacitors using a piece of wire can clearly understand that if a distance between the condenser clips is 100 times greater than the length of the wire, then it is impossible to discharge the capacitor through this way. Hence, one can consider the process, according to which

> M3. "Ball lightning consists of a conducting substance with low working function which possesses a feature to easily scatter charges at the contact with charged conductors", and "powerful current pulses appearing at that ... are capable to scatter considerable charges induced during a thunderstorm over a large territory – of area ... of tens ... and hundreds of square meters,"

as a type of myth about BL.

Also, another Stakhanov's conclusion about BL is still unproven, which one can consider as another myth.

> M4. "A density of ball lightning is approximately equal to air density".

(See the remark to the feature 56).

A book by Imyanotov and Tikhiy, titled "Beyond Boundary of Science Laws" was published in 1980 in Moscow (the number of copies sold was 50,000) [32].

In that book, a form of a conversation between a scientist and a journalist is presented, along with the analysis results of 500 BL reports collected by Imyanotov. As in fiction, the book starts with a story about the disappearance of a golden bracelet from the hand of a woman during her sleep, the bracelet which she could not remove for several years from her grown plump hand. She was awaked by "a sound of a thunderstorm discharge similar to a shot." When she came to a window, she noticed a hole of about 3-cm diameter in a glass and "suddenly noticed that the bracelet had disappeared from her hand. Only a dark wale was on her wrist. A circular glass with fritted edges was found on a floor." Imyanotov made an estimate of energy value necessary to heat, melt, and evaporate the golden bracelet of 50-g mass, and found that the bracelet heating to a temperature of melting point of gold (1,336 K) needs to spend 6.3 kJ, its melting requires 3.3 kJ, temperature rising to the boiling point (3,239 K) requires 10.5 kJ, and vaporization requires 87 kJ. Finally, the energy spent for bracelet vaporization was found to be 107 kJ [32, P. 94]. As there was no burning of the hand, the process of bracelet disappearance was very quick. If it lasted no longer than 10^{-2} s, then the power realized by BL was not lesser than 10 MW. Brand, in his book, also discussed cases of traceless "vaporization" of golden chains, rings, and other round objects [11, P. 8]. Apparently, these adornments were actually "vaporized", and were not stolen.

Thus, one can formulate one more feature of BL:

57. When passing over ring-type metallic objects with diameters from some millimeters to several centimeters or when exploding near them, BL can instantly vaporize these objects.

Imyanitov's review added some new information to BL maximal energy estimate. It was reported that BL at an explosion separated into two balls, and "the explosion was so strong that it slightly raised a ceiling and slid walls of the house apart" [32, P. 31]. The more interesting was the description of an event that was very much similar to the case in Dorstone [13], which occurred near Perechin city in Western Ukraine. S.S. Mach, a reporter of Imyanitov, wrote the following: "In August of 1962 near 11–12 o'clock p.m. a ball lightning with a size of a tennis ball had fallen into a trough with water for cattle; it was shining by rainbow colors during 10 s. Water from the trough was vaporized almost completely and boiled frogs were on a bottom. Sizes of the trough were 0.3 × 2.5 m. Depth of a water layer was 15 cm. Boiled frogs were also found in two other troughs." A calculation of energy spent by BL for heating and vaporization of water led to a result of 270 MJ, and the energy density (if we accept the radius of the ball as 3 cm) was 2.4×10^{12} J/m^3. Based on this "natural experiment," one can formulate two more features of BL:

58. BL can release an energy value of 270 MJ, and that its average energy density can be 2.4×10^{12} J/m^3.
59. BL energy absorbed by water can be transported through a dielectric wall (in this case, through wood).

In this case, it must be noted that there were no doubts about water heating to boiling temperature, and it did not lead to bubbling. The frogs that gave their lives for the science were the indicators of temperature rise.

In the book by Imyanitov, there is one more report exhibiting the magnetic features of BL [32, P. 72]: "It was physics exam for 7-th grade. A thunderstorm was approaching. Magnets of different forms and other devices were on a table. Suddenly ... a small cloud flew in through the open ventilator window ... its color was bluish–violet, it approached the table where aids were lying, it immediately rose and again flew out through the ventilator window without breaking the window. When the cloud rose from the table, all of us saw that the magnets rose and flew through the ventilator window as if they had life in them. One horseshoe-shaped magnet made a hole in the iron tank and the other one fell down ... and deeply went into earth." On the basis of this description, one can define three additional features of BL:

60. In the presence of magnetized objects, BL can also become a magnet and be attracted to the magnet.
61. The magnetic features of BL can unexpectedly disappear even in the presence of the magnetized object.
62. BL is capable to hold objects with a mass of about 1 kg near itself and raise them in air.

One can estimate a height H, to which BL could raise two magnets. Let us suppose that a projectile of a mass of $m_s = 50$ g moving with a velocity of $v_s = 100$ m/s can make a hole in a wall of the iron tank. Let us consider that a kinetic energy of the falling magnet of a mass $m_m = 0.5$ kg is equal to the energy of the projectile. Then, the height from which the magnet could fall down is $H = m_s v_s^2/2m_m g = 50$ m (here, g is gravitational acceleration).

In other cases, BL features derived from the observations collected by Imyanitov agree well with the data observed by other investigators. Also, cases of roar at BL explosion, production of the smell of sulfur, noises in electric net at BL moving by, its appearance from radio-sockets, creation of round holes in windows, motion of BL along the wires, melting of metallic objects at BL explosion, and the mass deaths of four-legged animals when BL gets discharged to the earth, have been reported. Surprisingly, during the two centuries of BL observation, nobody reported about the death of poultry, that is, biped beings. This may be owing to the pace voltage striking factor when BL strikes the earth; it releases strong currents that spread in the earth. However, Imyanitov, similar to other investigators of his time, accepted the obvious for the real: he considered that a fact of free soaring of a ball could be explained only by the equality of the Archimedean raising force and the ball weight [31, P. 96].

In the Journal of Technical Physics in 1981, an article in which a case when BL of $D = 150$ cm hit the earth during a thunderstorm observed by several people was described, which then raised up [34]. A layer of caked earth with a volume of 0.4 m^3 was formed in the soil in the place of BL touching the earth. The authors of [34] modeled the formation of an earth layer impacting the soil by different means, and

came to the conclusion that most close structures realized in nature appear at a high frequency radiation zone of the earth. From their estimate for caking of a piece of earth of indicated volume, it was found that one requires an energy of $W = 10^9$ J. Let us consider that BL spent only a part of its energy to the indicated action, and in this case, a density of spent energy $\rho_W = 6W/\pi D^3 = 5.7 \times 10^8$ J/m^3 proved to be high. Certainly, there are no direct evidences to show that BL impacted earth through electromagnetic radiation, and thus, other mechanisms of energy transfer are possible. However, in any case, one can consider that a level of energy value was estimated correctly.

A book by James Dale Barry, titled, "Ball Lightning and Bead Lightning" was published in 1980 in the USA [35], and in 1983, its translation into Russian was published (with 6,000 copies being sold). Unlike previous monographs on BL, where the authors used the data that they have personally collected, Barry did not present a review of reports about BL observations and information from a vast literature list consisting of 1,979 references compiled by him. Instead, he dedicated a substantial part of the book to BL photos and processes that accompany it, and to the analysis of the experimental attempts to realize BL in a laboratory. Based on the works of previous investigators, he gave a short review of BL characteristics: its form and size, color, structure, motion, sound, and smell. He discussed the traces of destruction and heating left by BL, its lifetime, processes of decay and connection with linear lightning, and its tendency to get into the closed premises. With regard to BL density, he again repeated an old idea that it is close to those of air. Barry represented data of different authors on the estimation of energy density of BL that got into the tub water [13, 14], which proved to be in the range from 2.5×10^9 to 1.9×10^{10} J/m^3. With respect to the case of splitting of the pile [23, 24], he found the energy value of 1.5×10^5 J and the energy density of 8.5×10^7 J/m^3. He also analyzed other cases where it was possible to determine BL energy. Their BL-energy density proved to be in the range from 4×10^5 to 1.7×10^9 J/m^3. With the help of his energy-estimates results, Barry built a graph of BL-observation probability lognormal distribution with definite values of energy density. The experimental points were located on a straight line. From this fact, he concluded that there is only one type of BL in nature. Unfortunately, this conclusion has not yet been comprehended by BL investigators. For example, O.A. Sinkevich again wrote about BL as a physical object "which realization mechanisms ... can have different nature" in the afterword to the third edition the book by Stakhanov [31], published 16 years after the printing of Barry's book [35].

In contrast to Stakhanov's conclusion, Barry considered that BL color "can be connected with the radiation characteristics of the absolute black body." Thus, the red BL should have a temperature of 4,600 K and the white one – higher than 10,000 K. However, Barry also allowed another possibility: "that application of color temperature to a phenomenon of ball lightning ... might be unacceptable" [35, P. 78]. With regard to the reason for the church bell swinging deceleration, he made a supposition that one had to blame BL magnetic field with the induction of 1.5×10^{-2} T [35, P. 81].

Barry represented a large number of BL traces photos, many of which could be faulty owing to a camera motion during a photographic survey. Unfortunately, with rare exception, they do not bring something essential for the formation of BL database.

6.1.2.2 Discussion of Ball Lightning Observation Results During the First Symposium on Ball Lightning in 1988

The above-mentioned 62 features of BL can be considered as "a scientific store" that was available to investigators gathered at the First International Symposium on BL in Japan, in July 1988 [1].

Stanley Singer made a report "Ball lightning – The continuing challenge" at the Symposium [1, P. 1–18]. He described the BL phenomenon investigation history, starting from the first publication of F. Arago. The BL problem has passed a period of negation, reducing it to optic illusions, and a skepticism period rose on behalf of an outstanding scientist, M. Faraday. "In view of the skepticism which has diminished but not disappeared in recent consideration, it is necessary to assess the significance of the phenomenon. Certainly, the repeated observation in nature of a striking occurrence which has not been clearly explained demands a serious interest."

Unfortunately, this phenomenon, owing to its unpredictability, is impossible to study with the help of devices. The only data left was the information from unprepared observers, who could report nothing but the size, velocity, color, and the life span of an object. Observations indicate a connection of BL with thunderstorms and a very small probability of their observation, which was about 3×10^{-11} km^{-2}s^{-1} (for usual lightning, it was 3×10^{-8} km^{-2}s^{-1}). A ball usually has a red or orange color, its diameter is 30 cm, and its average velocity is 2 m/s. The estimates of its energy density gave values from 5×10^{-5} to 10^{5} J/cm^{3}.

In spite of the appearance of about five articles a year devoted to the new theoretical models, neither of them could explain all the features of natural BL. Successful experimental attempts to reproduce BL were also quite limited. Plasma formations (plasmoids) were obtained in electrical discharges, including a magnetic plasma confinement in installations of spheromak types. Fire balls were observed at ignition of lean mixtures of flammable gases with air, and at explosion of metallic wires during the transmission of high currents. "Our understanding of the ball lightning phenomenon has progressed significantly since the ... investigations in the early 1800s, yet we lack knowledge of the mechanism of formation and the structure."

George Egely (Hungary) made two reports: "Hungarian Ball Lightning Observations in 1987" and "Physical Problems and Physical Properties of Ball Lightning". Egely, in the first report [1, P. 19–30], described nine cases of BL observations; its energy in three of them was determined as exceeding 10 kJ. Grey BL in the first of them had a diameter of 2 m, which exploded in an attic floor of a house. The explosion slightly raised the roof with a 35×15 m^{2} and threw

it down to a field of a neighbor (man). After that, according to the observation of the neighbor (woman), a reddish ball had flown from the destroyed house and began moving horizontally over the field. The mass of the 1 m^2 of the roof was 20 kg. If one considers that the roof was raised for about 1 m, then a work executed by BL is about 100 kJ. It must be noted that BL continued its existence after that. In the second case, an explosion of a yellow ball of 20-cm diameter was reported. As a result of the explosion, aluminum wires of a concealed wiring in the walls melted, their total length was estimated to be about 100 m, and the diameter was 2.5 mm. Starting from this, a minimal BL-energy density was estimated as 350 J/cm^3. Other reports described similar destructions occurring at BL explosions in closed premises: wires melting, electrical bulbs exploding, brick walls moving, and sooty spots appearing. There were also reported cases of spontaneous BL formation without a stroke of usual lightning. BL in one of them unexpectedly turned up from a lake; in another, five balls of diameter of 10 cm each had unexpectedly appeared on a bank, and then gathered to form a ball of 25–30-cm diameter. In the third case, glowing balls of 20-cm diameter appeared one after another in a garden near the earth, and they unexpectedly disappeared and again silently appeared at a height of 20 m.

Egely, in the second report [1, P. 81–87], grouped the main BL features and demonstrated the difficulties in their theoretical explanation. Thus, according to him, models that considered the presence of surface tension cannot explain the existence of BL in a form of a pear or ellipsoid [36]. Models in which BL represented ring currents [37] or rotating dipoles [38] cannot explain the reason for the decrease in BL size when it penetrates through small holes. The color of BL does not change even at its interaction with metallic objects or at substantial energy losses. This lowers the belief on models in which BL color is connected with its high temperature as well as the chemical and plasma processes. BL-energy density can be of 0.6 kJ/cm^3 and even 34 kJ/cm^3, when the maximal energy density for chemical and plasma models is only 0.2 kJ/cm^3. Even holes in glasses and walls left by BL cannot be reproduced in laboratory conditions. We cannot understand the reason for the electric effects realized by BL. If one considers that electric-field strength on the surface of BL of 20-cm diameter does not exceed the breakdown value of 2.5×10^6 V/m, then the BL charge can be considered to be equal to 3×10^{-6} C, and its electric energy may only be 0.8 J. At the same time, it is known that a current conditioned by BL charge can cause the melting of 100 m of aluminum wire of 1.5-mm diameter. If this effect was caused by the current with a duration of about 1 s, then the charge of about of 80 C would have been transported through the wire.

Ohtsuki and Ofuruton (Japan) [1, P. 31–57] reported about BL observations in Japan. The Japanese Information Center of the Ball Lightning (Fire Ball) started its work in July 1986, and has collected 2,060 evidences of witnesses from all over the islands of Japan. It turned out that 89.7% of BL in Japan were observed in fair or cloudy weather without rain, in contrast to those of Europe and America where the substantial BL part appeared during thunderstorms. Nevertheless, thunderstorms' probability and BL observations over a month's distribution strictly correlate, and their maximum falls on July–August as in Europe. The authors found that high air

humidity in Japan – the humidity in summer rises to 80% even in fair weather may be the reason; however, the higher humidity in the Continent occurs only during thunderstorms. Other BL characteristics – size, color, form, and lifetime – turned out to be the same as in Europe and America.

Alexander Keul (Austria) made a report, "Phenomenological and Physiological Analysis of 150 Austrian Ball Lightning Reports" [1, P. 58–80]. Austrian BL, similar to others, demonstrated some unusual features along with typical, often repeated ones: there are cases of one ball division into several ones; BL motion as "a rubber ball"; destruction of walls, and creation of holes in them. Keul undertook a computer analysis of 150 selected reports using nine parameters concerning observation conditions and the main BL features. Subsequently, he developed the following conditions: (1) If the diameter of the observed BL turned to be larger, the distance to it was longer and (2) If the feeling of fear when seeing a BL was lesser, then the BL was farther. Both these effects have a physiological basis under them: the larger object – the more attention it attracts at large distances, and small objects can leave unnoticed. BL observations in Austria correlate with the frequency of lightning and the density of population. BL was observed both in the plains and on high land in the country. BL investigations are based on the analysis of observations and not on laboratory experiments; thus, a specialist in plasma physics may be as helpless as a specialist in psychology and vice-versa. Besides, there is an additional difficulty: there is no clear definition regarding what is BL.

An article by A.I. Grigorjev, I.D. Grigorjeva, and S.O. Shiryaeva, titled, "Statistical Analysis of the Ball Lightning Properties" [1, P. 88–134], was presented at the Symposium. The authors of the article have collected 2,082 descriptions of BL in Russia; they have executed a statistical analysis of materials by the method proposed by Stakhanov. They had an opportunity to make a sampling of observations where BL was observed: (1) from a moment of its origination till its death, (2) sometime after linear lightning discharge, and (3) when it went out of a field of vision. They found that one can represent a decay probability dependence in a chosen group of BL as a combination of three exponents (but not two, as in Stakhanov's analysis) with typical times $\tau_1 = 3$ s, $\tau_2 = 29$ s, and $\tau_3 = 213$ s. A predominant BL form was a sphere (91.2% of the cases out of 2,013). There were cases of a ball transformation to a tape (18.66% of the cases out of 134) and vice versa, from the tape to the ball (11.19%). A total of 119 witnesses reported that BL had a tail. In 266 reports, information that it had a coat (shell) of 3-cm thickness was observed. It was reported in 143 cases (6.9%) that BL had an internal structure: bright, luminescent points chaotically moving inside the coat, or beams of bright filaments (threads). A form of diameters probability distribution dependences coincided with those found by McNally, Rayle, and Stakhanov. However, the distribution maximum moved from 20 to 7.5 cm. There were cases of BL separation into several parts (3.5%), and that it bounced back from the obstacles like a rubber ball. BL in 83% of the 319 cases did not emit heat, and in other (17%) cases, witnesses indicated a feeling of heat. In three cases, BL caused burns, similar to those of ultraviolet radiation. The authors came to a conclusion that BL appearance is closely connected with thunderstorm activity. Cases of

BL observations in fair weather can include errors: (1) Observers considered a weather to be "fair" always when the sun shines; (2) Thunder can be heard from a distance up to 10 km; however, overvoltage waves can be propagated over high-voltage (power) lines (BL origination on a conductor took place in 68.53% of the 286 cases); and (3) Witnesses can forget weather conditions because of event remoteness.

We found that by 1988, the investigators' team from different countries has made a large work on collection and analysis of BL observation data. It was revealed that the data from different investigation groups practically completely coincided. This favorably testifies that a subject of investigations was a unique natural phenomenon. However, a search of correlations between different characteristics of BL gave an ambiguous result: only evident connections of BL with other events were determined, such as with thunderstorms, connection of an observed object with a distance to it, and a feeling of fear with respect to the distance to BL. At the same time, there are no clear correlations between properties such as size, life span, energy, color, and radiation intensity. Besides, there is no clear definition of an object that is understood as "ball lightning," as it was truly noted by Keul in his report. In a majority of cases, we could distinguish BL from St. Elmo's fires, corona discharge, meteorites, electric arc, swamp lights, etc. However, in our opinion, undefined boundaries are left, in which an object can be attributed to BL. For example, if the average diameter of BL is 20 cm, then what one can say about a spherical object with a diameter of 20 or 100 m? Is it a BL or something else? or How to call an object that is not observed during 10 s but during 1 h?

Here, we encroach upon an area of unknown flying objects (UFO) observations. An important part of UFO is the optic illusion, as it was shown by Menzel [39] (remember that BL was also for a long time considered as optic illusion by scientists). However, some of the UFO observations are reliable, and it is striking that the main UFO characteristics coincide with those of BL. Thus, the following dilemma appears: either to include observations of UFO into the data bank on BL or to ignore these results. The first step in the positive side has been made during the First Symposium on BL – participants listened to the report by Y.S. Zou on UFO observation in China [1, P. 273–287].

On March 18, 1988, at 21 h 35 min, the Beijing pilots and passengers of aircraft TU-154 during the night flight at height of 11,000 m over a mountain region saw a strange fire ball to the right of the aircraft and somewhat higher than it. The ball emitted a bright beam of white color resembling a beam of a searchlight. People considered that UFO was flying towards the aircraft, which could be seen better and better. Till that time, all aircraft electronic devices and radio were working normally. The flying object turned to the left after 3 min and began to move from the aircraft. After several minutes, it separated into two parts; a ball was created from above, and under it, there was a part in the form of a kidney bean. One of the objects was rotating with a high speed and was surrounded by a green ring. After that, both the bodies associated into one, and the green ring surrounding them left safe. Then, the flying object began to become smaller and smaller. At 21.48, it disappeared among the stars. Thus, the object was observed for 13 min. The air velocity at a height of

11,000 m was 27.8 m/s, and it blew towards the aircraft and approximately perpendicularly to the flight direction of the flying object. The air temperature was −50°C.

P.A.M. Koloc, in his report [1, P. 289–309], devoted to explain his own BL model as a magneto-plasma configuration in which there are relativistic electrons, had cited a report on a case that took place in Venezuela in 1886 [40]. He stated that in that case, the symptoms of radiation sickness were observed in a group of inhabitants after their contact with BL: vomiting occurred and lips swelled. "The next morning the swellings had subsided, leaving upon the face and body large blotches. No special pain was felt until the ninth day, when the skin peeled off, and the blotches were transformed into virulent raw sores. The hair of the head fell off upon a side which happened to be underneath when the phenomenon occurred, the same side of the body being, in all nine cases, the more seriously injured."

On the basis of this description, one can suppose that

63. BL can cause radiation-sickness symptoms in humans.

6.1.2.3 Results of Ball Lightning Observations Published After 1988

Now, let us consider the new traits in the BL "portrait," which brought observations made after the First Symposium.

In Yaroslavl city (USSR) in 1990, Professor A.I. Grigorjev published, on his own account, a small book, titled, "Fiery Killers" (of 7,000 copies) [41]. Having a databank consisting of 6,000 cases of BL observations, the author represented descriptions of frequently repeated and rarely encountered features of BL. The book included information about the death of people and animals caused by the electric current (Gr.1; 3; 5; 10) (here Gr. means the book [41], and the numeral is the number of the report from this book). There is written information about the appearance of burns after contacts with BL (Gr.7; 8; 9; 35) and about the severe destructions at BL explosions (Gr.2; 3; 6; 8; 13; 60). In Grigorjev's collection, there are about 50 reports mentioning that BL penetrated window glasses without causing any damage (Gr.30; 31; 32; 33; 35). He represented many descriptions on how BL went out of electric sockets or electrical devices (Gr.11; 20; 24; 25; 26; 30; 43; 47; 49; 50; 54), or rolled up as a ball after initially being a tape (Gr.19; 21; 22; 61). This character of rolling is complicated: BL thread rolls up the coil or hanks; hence, the character of the tape transformation in the ball is different from the opposite process. There are reports that BL ejected sparks or small BL (Gr.17; 46; 53; 54; 57); however, there is no case in the collection with regard to the confluencing of BL pieces. All this information has allowed Grigorjev to add new features to the list developed by Brand:

64. BL can possess high electric potential and electric charge.
65. At the explosion, it can cause the appearance of a very large induction electromotive force in the surrounding wires.
66. During the process of its existence, BL can emit electromagnetic waves in the radio range.

67. It can be a source of hard ultraviolet and soft X-ray radiations.
68. BL can appear on wires at electrical overloads.

In Grigorjev's opinion, BL "represents . . . a charged plasma – a highly ionized gas with domination of unipolarly charged ions" [41, P. 27]. Grigorjev considered that BL's ability to store high energy is its very important feature: "in the football-sized BL can be stored the amount of energy that is released at the explosion of some ten kilograms of trinitrotoluene."

At the beginning of the 1990s, Grigorjev wrote a new book – the monograph "Ball Lightning." However, because of events that took place in Russia during those years, it was published only in 2006, with a modest copy number of 200 [42]. Concerning the creation of a theoretical model, Grigorjev considered that it is unproductive to create "averaged BL portraits." In his opinion, "the ideal situation for the investigator's entry to the BL problem is such when he makes himself a list of its features basing on a sufficiently large data of detailed descriptions of ball lightning's behavior in natural conditions, the features that later will be lain down in the basis of the future model." Following this, Grigorjev represented in his book "a set of ball lightning behavior descriptions in natural conditions concentrating attention on its features that are not in a scope of standard averaged portraits."

In the first chapter of the book, Grigorjev described the general, often repeating BL features. He considered that the BL portrait created by Brand [11] is "the most compact, complete, detailed list of ball lightning properties that is not distorted by false constructions of the author." However, Grigorjev stated that the list of Brand is not precise. "Thus, apparently BL that is attached to or is sitting on a conductor does not exist"; sooner, this was found to be St. Elmo's fires. Furthermore, BL's size and form are not always constant (Grg.1; 2; 5; 9–11), and its color can be changed (Grg.2) (here Grg. means the book [42], and the numeral is the observation number from this book).

An analysis of BL origination and disappearance as well as the description of facts represented in the second chapter can give very important information about BL's nature. Among 5,315 descriptions collected by Grigorjev, witnesses in 1,138 cases saw the birth of BL lightning. In 8% of the cases, it appeared from a channel of linear lightning, and in 8% of the cases, it appeared in the place where the linear lightning hit the earth, while in 4% of the cases – in clouds and in 66% of the cases – on metallic conductors. Grigorjev considered that BL can originate at the linear lightning channel decay through an intermediate state – bead lightning type, or can throw itself out of the incomplete branch of the lightning channel (Grg.21; 23; 24–27). However, in the predominant number of cases, BL origination was marked on electrical wires, radiator's tubes, loudspeakers, radio sockets, and electric sockets (Grg.44–67). "This can occur at sharp rise of the conductor's potential when the overvoltage wave that has appeared in it (e.g., at nearby discharge of a linear lightning) comes to an end of a long wire." BL at explosion can scatter sparks (Grg.74–80), can soundlessly thaw in air (Grg.81–91), or go into earth or a conductor (Grg.88–91). BL carries some uncompensated electrical charge and is a "material object, sooner consisting of some variety of plasmas." Therefore "an

ability to pass through windowpanes not leaving holes in them" is very intriguing attributed to it. This BL feature was for the first time marked by Brand, and among the 5,315 descriptions collected by Grigorjev, there are 42 such cases (Grg.100–115). The only material objects capable of penetrating through a glass are electric and magnetic fields, radiowaves, and visible light. This, by some means, can decrease a number of BL-energy carriers. In the list of observations collected by Grigorjev, there are 26 events reporting that BL left holes in glasses (Grg.117–132). Disks that fell out of glasses have "sharp edges and do not carry any traces of melting." There is still no answer to the question "about a physical mechanism of ball lightning penetration glasses without their damage ... a possibility of the answer to it is closely connected with a clarification of a substance nature of which it is composed." The data obtained from witnesses who saw BL nearby are very valuable. In the descriptions collected by Grigorjev, there is a report about a "ball with a core of 30 cm diameter ... Something was rotating inside the core leaving streaks of white threads after itself" (Grg.133). A ball in another case has penetrated a metallic net against mosquitoes: "it resembled a tangle of golden-orange threads or dots, to be more exact" (Grg.134). There was an observation of two balls with clear boundaries, "a flame was boiling filling a whole volume behind their transparent covers. . . . The whole mass was in continuous motion" (Grg.135). There is a report of an observer, who at a distance of 5–7 m "at a height of two meters over earth" saw "something resembling a sheaf consisting of a multitude of balls as if of melted metal. Each yellow with redness ball was separated from another one, and slightly trembling and moving in the 'sheaf' it did not connect to others, but to the contrary it, as if, slightly pushed them away. 'The sheaf' had a form of irregular oval of two-three meters size. ... All the balls were absolutely identical" (Grg.136). There were balls resembling "a tangle of bright threads" (Grg.138) or "consisting of stirring small white-red sparks" (Grg.139). Grigorjev stated that BL can be separated into sparks or balls at collisions with obstacles; this makes one to suppose that they are "elementary bricks of which a ball lightning is composed .... A small ball can be considered as a small ball lightning."

With regard to BL radiation detection, Grigorjev informed that only 1.5% of the witnesses who saw BL from the distance lesser than a meter (35%) reported about the presence of a thermal flow from it. Fires and burns to people owing to BL occurred only at its explosion. A more interesting BL feature is "its ability to emit electromagnetic waves in a microwave and radio-wave ranges." Thus, a ball moving by a room antenna of a TV set "has caused strong interferences: streaks began moving over a screen, an image was distorted, and one could hear crackling" (Grg.141). It was told that the hairs of girls rose when the ball of 8–14 cm diameter was passing over their heads. Their hairs dropped down when the ball flew away. "An incandescent hair in a bulb began to glow reddish color when a ball was passing by a lamp, though a switch was shut downed ... When the ball has flown away then the incandescent filament went out" (Grg.143). There is an interesting report about BL formation process. "A trolleybus's bow has come off. It several times hit wires causing short-time shorting, crackles have sounded, and sparks began to fall. Suddenly a bright, round ball of 12–20 cm in a diameter has separated

from a total mass of sparks. ... The ball crossed a roadway ... and began to move along the trolleybus wires. ... The wires were fixed to poles with lighting lamps. Lamps in turn flashed as the ball moved under the lamps. The ball in this moved by 3–4 lamps" (Grg.145). There are evidences in favor of BL having a hard component in its radiation: injured persons got skin burns typical for the burns under action of ultraviolet radiation (Grg.148–152). Grigorjev presented cases of injury of persons and animal by BL (Grg.153–167): on touching it answers "either by an electric discharge or by an explosion". The lifetime of BL explosion by Grigorjev's estimates does not exceed a millisecond, and hence, a shock wave cannot extraordinarily harm a human. "Apparently a man loses consciousness only for a time of shock wave propagation." "Release of a large charge at ball lightning disappearance" can cause more serious effects. There is a report about BL explosion near an electrical supply distributional box in Kiev studio of feature films (Grg.168). "All the lamps began to shine" at the moment of the explosion. Then it "turned to be that all the incandescent lamps of different power were burned out, independently of the fact were they switched on or no."

Among Grigorjev's observations, there are evidences that BL changes its size during an observation (4%) or changes its form (6.5% of the cases). In one of them, a transformation "of a burning needle of about ten centimeter length and about of a half of a centimeter thickness into a ball of 5–6 cm in a diameter" after hitting a door (Grg.176) is described. "Burning yellow-red color tape" in another case "has been assembled into a football sized ball near a threshold of 1–2 cm height" (Grg.177). In the third case: "A thin yellow-white line-thread has flown through a glass. ... It hit a brick and has transformed into a ball of about ten centimeters diameter" (Grg.178). "A yellow-red tape of a meter length with a diameter of 3 cm stopped having flown to a threshold, then it started to rotate on the spot winding into a football sized ball" (Grg.180). A transformation of a ball into a tape is also possible: the ball slowly during 5 s "has elongated into a long tape, and the whole tape immediately went through a ventilator window to a street when one of its ends has reached the ventilator window, then it leaped up" (Grg.184). BL can move over the water, leaping back from its surface (Grg.193–198), but can descend into the water. It was reported that "there was no explosion, a hissing has sounded, and ripples began to move as from a thrown stone from the place where the ball has hid in the water. For several seconds there was nothing, but then bubbles have appeared in the place of the ball lightning fall and a water column of two-three meters height has gushed"(Grg.199).

During an analysis of his data, Grigorjev tried to find correlation dependences between different characteristics of BL, but similar to other investigators, he found practically a complete absence of connection between BL diameter and its luminescence brightness. There were weak signs that large BL is more often red; and red BL has a somewhat shorter life than the yellow ones. The only parameter that one succeeded to connect is BL lifetime t_L and its diameter D, which can be described by a relation $t_L = t_0 \exp(-D_0/D)$ ($t_0 = 75$ s, $D_0 = 7$ cm). One can see that t_L limits to $t_0 = 75$ s at $D \gg D_0$, but more long-lived BL were observed in nature.

As investigator, Grigorjev was confident regarding the opinion that for the creation of BL theory, it is necessary to know all its features in detail. He thought that even 6,000 descriptions collected by him were still "insufficient for serious investigation of ball lightning." New information is necessary about rare and poorly investigated BL features; for example, how it propagates through glasses [41, P. 32].

In 1989, in "Pravda (Truth)" (Moscow) newspaper, a news story under the title: "Visit of Fiery Lady" appeared. It was reported in it that a "curious case" has occurred in Khabarovsk city. "There ball lightning has flown into a cauldron with about of 7,000 L of water. The water has started to boil immediately. Lightning was bathing in water for about of ten minutes, and then it went out" [43]. To heat 7 t of water from 20 to 100°C, one needs an energy of 2.35×10^9 J. There was no indication about BL size in the news story, and hence, one can only expect that it was smaller than the sizes of the cauldron. If one considers that its form was close to a spherical one, then its diameter would be 2.4 m. Let us assume that BL diameter was by two times smaller, that is, 1.2 m. Subsequently, its volume would be 0.9 m^3 and the energy density contained in it would be 2.6×10^9 J/m^3. Based on this observation, let us add one more feature to BL properties:

69. BL can release an energy of 2.3×10^9 J.

In 1993, Egely published BL observations data bank in Hungary [44]. He published in four Hungarian newspapers articles about BL and asked the readers who saw BL to send him a detailed description of their observations. Egely's method is comparably more informative, as it allows getting data about a physical nature of a phenomenon without the loss of important details, which can disappear at statistical or questionnaire analysis. Data collection was started in April 1986 and was finished in September of the same year. At the end, Egely collected 300 BL-observation descriptions.

According to the received reports, "Hungarian" BL did not differ from BL observed in other countries. In some of them, an internal structure (luminescent grains) and a cover (sharp projections were sometimes observed on it) were noticed (Eg. 54; 63; 64; 112; 125; 183) (here Eg. means Collection [42], and a numeral – a serial number of an observation from this Collection). There were marked cases when BL took the form of a long tape, which then coiled into a ring or a ball (Eg. 54; 57; 76; 177; 248), went out of sockets or keyholes, and then returned to them (Eg. 12; 26b; 31). They often moved over wires, cables, or railroad rails (Eg. 32; 36; 67; 68; 69; 136). A case when the ball was accompanying a carriage moving along a fence (seemingly metallic) and left behind it, when the fence ended (Eg. 56a), or "felt" a motion of a man in a room (Eg. 56c) was also reported. There are cases when BL, for a long time, was flying nearby an automobile or a running man, keeping up with him (Eg. 101; 223). The most striking case of such an accompany is described in (Eg. 178a, b). A driver and doctors of an ambulance carrying a patient at night saw a spherical luminescent object of about 4-m diameter. It was surrounded by a halo, and three "flame tips" were gushing from it. This ball was flying nearby the automobile moving with a velocity of 40 km/h during 15 min. After that, it descended to the earth and disappeared. On the way back, they met a second BL.

It was of the same size as the first one, but already had 6–7 "flame tips." Moving at a height of 10–15 m, it moved parallel to the automobile with a velocity of 60 km/h. The velocity of the ball decreased to 5–10 km/h when the car stopped. The automobile again went with the velocity of 70 km/h and BL again flew besides it. After this, it disappeared in the same place where the first BL disappeared. The weather on that day was cloudy, but without rain and thunderstorm. Both BLs were moving with constant velocities; however, their motion was visibly accelerated when they moved near villages. The halo thickness around the ball was approximately equal to its diameter and the "flame tips" or "tails" went out, and then flashed again.

Electric bells and electronic alarm clocks began to ring, and electric lamps start to flash when BL appeared in premises (Eg. 146; 197; 247; 248). There are reports about cases of injuries and death of people when BL touched them (Eg. 39–41; 56b; 100). On a victim's body, burns in the form of lines branching as roots of trees were found. However, in one case, BL exploded near a patient lying in a resuscitation department with electrocardiograph suction caps on his chest, and it had completely cured him from arrhythmia (Eg. 179). There are marked multiple cases of animal deaths caused by BL (Eg. 55; 97). There is also a case when cows escaped from BL when they put their front legs in a trough. However, they did not give milk for several days after this (Eg. 166). There has been a report of BL flying into a room, which then jumped from nail to nail, throwing down pictures hanging on them, and then flew out after a silver spoon hit a window (Eg. 99b). In another case, it moved along a railroad platform passing round the benches with steel feet (Eg. 102). One witness noticed that a ball jumped up and went down at the moment when a linear lightning struck (Eg. 13). In Egely's opinion, BL jump had occurred owing to the action of the external electromagnetic field.

There has been a report where a witness described in details the whole process starting with the formation and ending with the death of BL (Eg. 69). First, he, for 3 s, saw weakly glowing ball of 4-m diameter with diffuse edges. Then, gradually growing bright, "small islands" appeared on its surface (this lasted for about 3 s). In the center of the ball, there was an area with a diameter of 0.8 m, free of "islands." Suddenly, a ball of 50-cm diameter flew out of this area with a high velocity in a direction of a high-voltage line. The color of the ball was orange-red, and it had a clear black contour to the left. The ball existed for 1 s. The ball's diameter decreased to 10 cm during the next moment, the luminosity of its surface sharply increased, and its color became blue. The ball in this state remained for 5–8 s. On approaching high-voltage line, the ball "floated" over the wires and exploded after covering 10 m. It produced a dazzlingly shining white ball of 8-cm diameter. Red jets were ejected from the ball surface, and their length was 30 cm. This lasted for 0.5–1.5 s, and everything disappeared.

BL sometimes appeared in groups (Eg. 184). There is a report that first in a witness field of vision, BL of 3-cm diameter appeared flying over the earth at a height of 2.5–3 m. Then, after sometime, two balls of the same size appeared approximately at the same height, which were moving parallel to the earth at a distance of 10 cm from each other in the same direction as of the first BL. Several seconds after this, three small balls appeared at the same height, which were located

in the corners of an isosceles triangle: two of them were at a distance of 15–20 cm from each other and the third one was at a distance of 30 cm from them.

There are case descriptions when BL demonstrated its ability to carry heavy objects. Thus, it can attract a fork (Eg. 53) or through from itself, a black stone with a smooth surface of 10-cm diameter (Eg. 60).

There is a report that a red-brown spot of burned ground appeared after an explosion of BL of 100-cm diameter (Eg. 220b). The witness discovered that a magnet was attracted to this absolutely smooth section of earth. At the same time, the magnet was not attracted to the earth around the spot that the BL did not touch. The witness supposed that the red-brown color of earth could be explained by the presence of iron in it.

Egely represented a description of an "immersion" case of a witness inside a glowing sphere (this case resembled a similar event described by Singer [18, Case 12]). A young man with a bicycle before a thunderstorm was inside a yellow cloud for 1–2 min, feeling himself being enclosed in a yellow glass sphere. After that, the spherical cover was torn and disappeared without traces. Being inside the ball, the young man did not see anything outside, and it was also invisible for an observer outside.

In Egely's data bank, there are several cases that allow estimating the energy store of BL. He reported about melting of wires at BL explosion (Eg. 10; 173; 174), and the formation of holes in glasses, walls, metallic plates, and stones (Eg. 4; 56b; 58; 71). There is a case (Eg. 272) about BL that made a hole of 30-cm diameter in an adobe wall of a house, and went away from a room through a window without damaging the glass. However, a metallic handle of a frame disappeared somewhere. There is a report that a potato-shaped BL flew over a ditch and left a brown mass of fluidized sand of 70-cm length, 10-cm width, and of several centimeters thickness (the case resembled the one described in [34], where it was possible to estimate BL-energy store). The volume of the fluidized mass of sand was $V_{pt} = 0.7 \times 0.1 \times (0.02–0.04)$ m $= (1.4–2.8) \times 10^{-3}$ m^3. By assuming the density of the sand to be $\rho_s = 2 \times 10^3$ kg/m^3, heat capacity $C_s = 0.84$ kJ/kg K, and a melting temperature of the silica gel $T = 1{,}570$ K, one can find that the energy that was spent for melting was $W = C_s \rho_s V_{pt} \Delta T = 3–6$ MJ. Note that BL did not perish from the indicated impact, but continued its existence (as in the case [34]).

We would finish Egely's book description with the case (Eg. 222) of its energy measurement, with a help of "water calorimeter," which is very much similar to the case of BL falling into a tub [13] or trough with water [32]. On a hot July day, a yellow BL of 25-cm diameter rolled over a glass light of a workshop's roof and then with a deafening crash, fell down into a pit near the corner of a building. This was observed by a multiple group of workers who went into a yard during lunch hour. The sizes of the pit were $0.6 \times 0.6 \times 0.5$ m, and 2/3 of it was filled with water. All 120 L of water evaporated; the vapor from the pit was appearing for half an hour after the ball fell. An examination of the event place showed that water was evaporated, but was not spilled out. Burnt leaves and grass stems were lying around the hole. Egely estimated the energy of this BL as 2.8×10^8 J, and its energy density as 3.4×10^{10} J/m^3.

Summing up, from the data analysis collected and analyzed by Egely and Grigorjev, one can say that their method of complete events description texts representation turned out to be very useful.

Along with the observations of BL "standard" properties that can be statistically analyzed, rare cases gradually came out (that allow them not to be neglected at statistical analysis), which were also considered to demonstrate important BL features: its large energy store, the respond to variations of external electric field, its internal charge, capability to transmit energy "at distance," and features of its motion. Their rare events were summed up and allowed to formulate new features of BL:

70. BL has a cover inside which one can observe a motion of smaller parts.
71. BL can change its form: it can transform its form from a tape to a ball and from a ball to a tape.
72. BL "feels" variations of external electric field; it is sensitive to motions of the objects (people and automobiles).
73. One can observe an interaction of separate elements in a group of BL: two BLs move at a definite distance from each other, and three BLs create an isosceles triangle.
74. BL can carry a heavy object, for example, a stone or a steel fork.
75. At explosion, BL can reduce iron oxides to metal.
76. BL can transmit energy at a distance, most probably in a form of electromagnetic radiation. This causes electric devices (bells and lamps) reaction or can lead to melting of wires, sand, or glasses.
77. BL is capable of making holes or deepenings in walls, metallic plates, and glasses.
78. BL can penetrate a glass and leave it unharmed.

Unfortunately, we are not aware of any investigations of glasses through which BL has penetrated, and hence, we do not know if BL could change their properties.

79. By getting into a tank with water, BL can heat water to boiling point and evaporate it. BL-energy density estimated in this case equals to 3.4×10^{10} J/m^3.

In 1994, in Moscow, a Collection of works, titled, "Ball Lightning in a Laboratory" [45] was published. In the introduction, signed by all editors of the Collection, there are words that "the most important feature of natural ball lightning is its capability to carry high uncompensated electric charge as large as some Coulombs." Stating this, the authors have addressed Stakhanov's works or talks, which, in our view, has been misunderstood. We have mentioned earlier that Stakhanov gave quite a decorative role to BL charge, and considered that a reason for strong electric effects was some hypothetical BL capability to transport charges accumulated in the conductors. It is interesting that at that time, there was no uncompensated charge in the BL models developed by the editors and authors of the collection.

Some cases in [45] confirmed that BL can have a substantial uncompensated electric charge. During the Second World War, a girl who was on a wooden watchtower of 20-m height was killed by BL [45, P. 222]. There was "a halo of white fluff" around her body, which "turned out to be of underwear and soldier's puttees comminuted in the fluff. At that a soldier's blouse and a skirt were safe, and there were no traces of burns on the body. Only a round burn was noticed on a place where there was a ring before, but the ring itself has disappeared." There is also a description of another case when BL came at 1 m from a man and a woman sitting on the hay [45, P. 222]. The woman's hair "stood on end (like a fan), and hairs of the man began to stir under a service cap." When they came back to their senses after BL went away, the observers discovered that "rings have disappeared from women's fingers," and from the man, "the penknife chain, a metal tip from a mechanical pen and metal rims from the boots, fixing edges of holes for laces have disappeared."

On the basis of these reports, one can consider that

80. BL can possess a substantial uncompensated electric charge.
81. BL can be a source of powerful electromagnetic radiation causing resonance of currents in the ring conductors with diameters from 1 to 2 cm.

The case that occurred on July 10, 2006 in Jürmala (Latvia) can be a confirmation of this conclusion. When the resident of Yelgava city, Oleg Andrejev, went from the sea to the coast, "the yellow-orange bright ball about a tennis ball in size has flown" nearby him and "the strong roar has appeared. Oleg has fallen face downwards the sand. He did not lose consciousness, but he was very sluggish with a disseminated consciousness. When Oleg was turned, his face was in a smoke black (salts of gold?). People bathing at this time in a gulf have felt an appreciable current blow . . . The golden chain on Oleg's neck has evaporated (see Fig. 6.2), having left an appreciable burn round his neck in the form of a dotted line. On his stomach and on his heels also there was a trace of a lightning (the current channel)" [46]. Apparently, the BL has blown up at the level of Oleg's waist and the current of

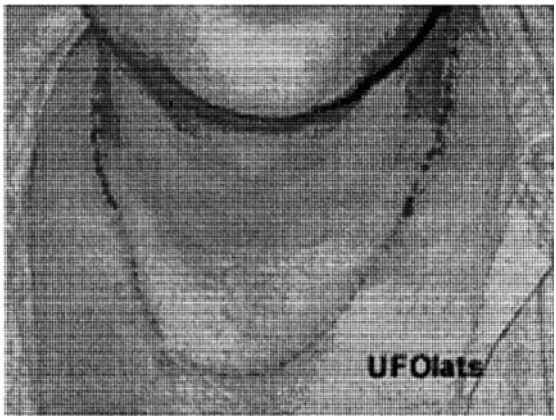

Fig. 6.2 Still photograph of a man's neck hit by ball lightning (BL) [46]

its discharge has gone to earth through the lower part of the man's body, not having touched the heart area. At the moment of explosion, there was a generation of high-frequency radiation pulse with a basic frequency, resonant with the absorption frequency of golden chain links (with the size of 3–4 mm). Having accepted a chain weight of $m = 17$ g, we can find that the energy $Q_1 = c_1 m\,(T_m - T_0)$ that has been spent for its heating to a fusion temperature $T_m = 1{,}063°C$ was $Q_1 = 2.46$ kJ. Energy $Q_2 = c_2 m\,(T_b - T_m) = 4.96$ kJ has been spent on the heating of a melt to boiling temperature $T_b = 2{,}887°C$. And, finally, the energy spent on chain evaporation was $Q_3 = c_3 m = 28.56$ kJ (here, $T_0 = 30°C$ is air temperature, c_1 is the specific thermal capacity of solid gold, $c_1 = 140$ kJ/(kg·K), c_2 is the specific heat capacity of liquid gold, $c_2 = 160$ kJ/(kg·K), and c_3 is the specific heat of gold evaporation, $c_3 = 1{,}680$ kJ/(kg·K) [47]). Thus, the total energy spent for the chain evaporation is $Q = Q_1 + Q_2 + Q_3 = 36$ kJ. If the explosion took place during 10^{-2} s, then a power of BL radiowave radiation would be about 3.6 MW.

There is an interesting description in [45, P. 223] about BL movement over a narrow-gauge railway rails at a height of 3 m. When it came nearer to the observers, they "were shined with a narrow bright beam, outside of which it was dark, and behind them the beam sharply broke that does not happen at the illumination by searchlights or headlights." Therefore, it is possible to consider that in rare cases

82. BL visible radiation can have a form of a narrow beam.

In 1999, Mark Stenhoff's monograph, "Ball Lightning" [48] was published. Unlike the books about BL written by the experts having their own ideas on how it is arranged, and consequently and subconsciously choosing the "most authentic" among the facts, the book by Stenhoff was written by the impartial researcher. However, another extreme is peculiar to Stenhoff's approach: its excessive skepticism is shown in aspiration to reduce many power effects caused by BL on the action of usual linear lightning discharge. The temptation of it is great, as the energy of an ordinary linear lightning (2×10^8 J) greatly exceeds the energy of an "English" BL (10^7 J), known to Stenhoff [13, 14]. However, here, he again questioned the reliability of the classic example of energy estimate. Hence, by reproducing the calculations of a sphere energy content made by Goodlet [48, P. 194], he considered only the lower estimation of energy (3.1 MJ) as correct, when water heated up only to 60°C. With the assumption that water was heated up to 100°C and its part had boiled away, he speculated that "it was not in event descriptions of Mr. Morris and in additional inquiries of Sir Charles Boys." He was more inclined to consider that water heating could be caused by a stroke of a linear lightning, and as a proof, presented an opinion of V.M. Uman who suggested that "lightning caused the arc from nearby electric power lines." Such an attitude to the event description appears strange enough, as Mr. Morris "in the clear" stated that "the water *boiled* for some minutes," and near a tub with water, there was no power electric line, but "telephone wires" [48, P. 7]. According to Stenhoff, the reason of observable destructions comprised "close association between CG (cloud – ground) lightning and a ball lightning. Ball often precedes a CG lightning flash to the immediate vicinity, which coincides with the apparent decay of the ball" [48, P. 196] (note that, here, Stenhoff

departs from the principle of impartiality as among the observations collected by him, and in the observations collected by other researchers, the specified time correlation cannot be found). Stenhoff also cautiously considered the assumption that BL can bear in itself a considerable electric charge. For "it seems quite implausible that ball lightning could contain within its small volume sufficient charge per unit volume or sufficient electrical potential energy to deliver such large currents. It is much more credible that an ordinary CG flash was responsible." Thus, in the approach regarding BL-energy store and its charge, Stenhoff appeared to stick to a myth that

> M5. BL is some sort of a "trigger" switching on a linear lightning. ". . . ball lightning may not in itself represent a hazard, . . . it may be a precursor of an impending lightning flash" [48, P. 196].

Basically, Stenhoff "has walked over already plough up field" of data about BL observations, and his book practically does not contain new data that could add to the full list of BL properties made by us. An exception is the analysis of BL behavior in the planes, undertaken by Stenhoff. There is a story as once "a dim yellowish light appeared ahead of the aircraft's nose . . . This light expanded in circumference . . . When the light was close to the windscreen, it was possible to hear a swishing noise. At the same time the light seemed to be rotating rapidly . . . There was a loud report followed by a strong smell of ozone . . . But it was accompanied by . . . a blinding flash . . . They saw a ball of fire come out of the flight deck and roll down the aisle. It was about the sizes of a football . . . It continued to the rear of the aircraft and disappeared . . . On arrival . . . we examined the airframe . . . and found a burn mark on the radome about the size of a half-crown" [48, P. 112–113].

In another case, "the aircraft was evidently struck by lightning (observers saw a bright flash of light and heard a loud bang) and some seconds later, a perfectly symmetrical glowing sphere of diameter 22 ± 2 cm emerged from the pilot's cabin and traveled at constant height and speed (75 cm above the floor at $\approx 1.5 \pm 0.5$ m/s relative to the aircraft) and in an undeviating path down the central aisle of the aircraft . . . The blue-white sphere had no structure, and was somewhat limb-darkened and optically, hence appearing almost solid. It did not seem to radiate heat, and appeared to have an optical power of about 5 to 10 W . . . It disappeared into the toilet compartment at the rear of the aircraft" [48, P. 114].

"A DC6 aircraft was flying north over Alps in heavy turbulence when a luminous ball with fuzzy edges, about 10 in. (25 cm) in diameter, was seen traveling rapidly along the floor on the central aisle. There was no integral damage, but on landing blackness holes were found in the nose and tail of the aircraft, 3 to 4 in. and 10 to 12 in. (8–10 and 25–30 cm) in diameter, respectively" [48, P. 115].

During the flight of Ilyushin-18 aircraft "at an altitude of 1,200 m, a ball of fire 10 cm in diameter appeared on the fuselage in front of the cockpit. It disappeared with a deafening noise, but re-emerged several seconds later in the passenger's lounge, after piercing in an uncanny way through the air-tight metal wall. The fireball slowly flew above the heads of the stunned passengers. In the tail section of

the airliner it divided into two glowing crescents which then joined together again and left the plane almost noiselessly ... The radar and several other instruments were damaged, so the aircraft returned to the airport. Two holes were found in the fuselage – one in the nose section and one in the tail plane. There were no traces inside the aircraft, and none of the passengers was hurt" [48, P. 115].

Thus, one can assert that

83. BL can get in the all-metal plane through cabin glass, aerial fairings, or through apertures in a fuselage. Having got into the plane salon, it, as a rule, slowly moves between the rows of seats in a direction from a plane nose to a tail. It can leave a plane tail silently or with an explosion, leaving a hole.

Besides BL considered by us, objects that have obtained the name of "the Unknown Flying Objects" (UFO) are often observed in the nature. They, along with BL, represent shining spheres, ellipsoids, disks, or cylinders, moving in air sometimes smoothly and sometimes very quickly. They can throw out sparks and substance streams from themselves, and can leave circles of the burnt earth. Therefore, in our opinion, the distinct border that could be placed between BL and UFO does not exist. If the distinction of these objects is made, it is possible to say that it does not have a basic, but "ideological" character. The BL's nature is not yet well understood, and we fairly declare it, whereas with regard to UFO, there appears a steady myth that they are the ships of newcomers from other planets.

The complete report about UFO observations can be found in Chernobrov's book [49]. After reading this book, it is difficult to get off the thought that in an overwhelming number of cases reported, there is a description about BL that is familiar to us. The specificity of UFO observation is revealed only in the fact that all messages concern objects out of premises, and great attention is focused on the emotional condition of the observer – to a stream of his/her imagination caused by the influence of a shining object. As it was mentioned earlier, an encounter with BL for any strange reason "is imprinted" forever in the observer's memory; that you will not tell about other, not smaller impressions of dramatic events of a life. Another feature of UFO observation reports comprised the fact that sometimes objects of large sizes (up to 100 m), existing for hundreds of minutes, have been reported. However, this can hardly serve as a criterion for the differentiation of BL and UFO. If one looks at the dependence graphs of BL observations probability of the size and its lifespan (e.g., see [48, P. 14; 15]), it is possible to notice that at the growth of the size and time, they come near an abscises axis smoothly, thereby supposing the possibility of BL existence with large sizes (>10 m) and large life span (>10 min). Hence, Stenhoff, without any doubts, considered BL as a sphere of 6 m in diameter [48, P. 173]. On the other hand, Chernobrov named all shining yellow-red spheres from 30 cm to 4 m in diameter as UFO [49, P. 26; 33; 38; 85; 89; 92; 95; 126; 252; 391; 414]. Thus, having added the data from the data banks of UFO to BL data banks, and supposing that they describe objects of similar nature, we can make those BL properties more authentic, which were considered earlier as rare. Thus, it is possible to assert that in an upper atmosphere, the existence of

spherical, disk, and cylindrical form of BL with sizes up to 100 m is probable. These objects may exist for several hours.

The most interesting feature of these objects (of both small and large sizes) is that they can emit narrow beams. Sometimes, it is simply an emission of "flame tips," and sometimes, narrow rays of light similar to the laser beams are emitted [49, P. 20; 44; 83; 88; 97; 100; 102; 109; 113; 114–117; 122; 152; 187; 404]. It must be noted that among the above-mentioned BL observations, there was only one case when light emitted by it looked like a projector beam [45, P. 218]. In one of the descriptions [49, P. 83], a light going from a sphere, which decayed to ring zones of violet, yellow, and pale yellow color, was described. This report wonderfully agrees with the observation description of shining object from a plane board in an article that appeared in 1985 in the Soviet newspaper "Trud (Labor)" [50]. In this article, a long-time observation of an object of 20 m in size at a height of 10,000 m was described. It emitted narrow light beams. When the beam slipped on a plane cabin, the pilots saw "the dazzling white point surrounded with concentric color circles."

There is a report about an orange-red disk of 20 m in diameter, which dived on the parking of tourists [49, P. 42]. The fire occurred because of it, the tents were broken, the frozen water became warm, and all clocks stopped. This, as we remember, is very similar to BL action which can heat up water and even bake a soil section. UFO can move with a plane speed [49, P. 88; 113] and make sharp turns, by not reducing the speed [49, P. 153]. We found similar properties in the descriptions of BL behavior [48, P. 110; 111]. The UFO as well as BL generates noise in radio receivers: when the object flew by a car at a height of 100 m over it, "the receiver as if has blown up" produced a strong whistle [49, P. 164].

If one recognizes an identity (or likeness) of UFO and BL, then it is possible to consider a typical specificity of pairs, and especially, three fireballs' interaction. As discussed earlier, in one of Egely's reports, the property of BL groups to create a structure in the form of an isosceles triangle, was described (Eg. 184). According to the book by Chernobrov, such a tendency to self-organize is one of the important properties of UFO: observers everywhere saw "three-star structures" in the sky [49, P. 23; 39; 43; 200; 238; 246; 248; 269; 297; 382]. It is marked that close location of UFO leads to "a paralyzing action" on a person; it causes spasms, catalepsy, hallucinations, and loss of consciousness [49, P. 21; 44; 111; 290]. It is quite probably that these objects (including BL) impact not only the basic senses of the person (sight, hearing and sense of smell), but also the brain.

So far, we have considered the information on BL properties, "concentrated" on monographs and reviews, covering an observation material from the beginning of a "history" till the end of the first decade after the International Symposia on Ball Lightning. Now, we will shortly analyze what has changed in this area during the last 10 years. During this period, results of the researches devoted to BL were published in journal articles as well as in the proceedings of the International Symposia on Ball Lightning and the Russian Conferences on Ball Lightning.

At the Fifth International Symposium on Ball Lightning in Japan, from August 26 to 29, 1997, statistical data about BL properties observed in Japan [51] have been

presented. Again, as in the report presented 10 years ago, 89% of BL in Japan was observed in fair weather, and other characteristics of the Japanese BL did not differ from the worldwide.

In the report by Keul [52], a collision case of a BL of 50 cm in diameter with a car was reported. At the moment of the collision, the driver – the school teacher (female) – felt as if the car has run into an obstacle. Everything that was to the right of her became bright green – the cowl, windshield, instrument panel, and even upholstery. Having flown around the car from above, the sphere had landed on a highway. Thus, the Faraday cage – the metal car – could protect the driver.

Stakhanova (Russia) [53] presented some BL photos from the archive of I.P. Stakhanov at the Symposium. The pictures were taken in September 1985 near Undugun lake 100 km from the city of Chita. Amirov and Bychkov (Russia) [54] reported about the results of the statistical analysis of SKB data bank: 1,503 cases of the observations collected by Stakhanov, 150 supervision collected by Keul, and 100 events collected by Bychkov. The increase in BL lifetime with the growth of its size was revealed, and the most probable diameter of BL was defined as 10–20 cm.

On August 23–25, 1999, in Antwerp (Belgium), the Sixth International Symposium on Ball Lightning took place.

In the report by Stakhanova [55], a connection between BL observable characteristics and weather conditions has been described. An analysis of 1,086 cases of observations where the weather condition was specified, demonstrated that BL characteristics, such as form, diameter, brightness, and color, appeared to be the same as in the cases where information on weather conditions was not provided. However, BL of larger sizes, greater brightness, and longer lifetime were more often observed in fine weather, which can be connected with improvement in the observation conditions.

The Japanese researchers, H. Ofuruton and M. Kamogava, informed about the continuation of BL researches in Japan [56]. Two years after the fifth symposium, they had collected 500 additional observations. Their analysis demonstrated that unlike Europe where the overwhelming number of BLs is observed in summer, in Japan, there are more chances to observe them during other seasons. With regard to the color of the BL, they assumed a possibility of radiation of infrared and ultraviolet light by it. For BLs of the small size ($<$30 cm), two peaks of average lifetime were found: 10 and 60 s. The first peak can be explained by the fact that people do not always see BL from the moment of its formation. Therefore, the actual lifetime of BL may be close to 60 s.

Keul (Austria) [57] reported about the attempt of BL detection by means of linear lightning detecting system. In Austria, since 1992, ALDIS – Austrian Lightning Detection and Information System of eight field stations has been operating, with the help of which, the place of lightning stroke is determined with an error of less than 1 km, and polarity of discharge and amplitude of a current are defined. The system can distinguish intercloud discharges from discharges between clouds and earth. Keul chose nine cases of BL observations after May 1992 from his data bank, and compared them with the results of the linear lightning strokes registration obtained by means of the ALDIS system. Coincidence between the data when the

linear lightning has struck at the same time and in the same area and those of observed BL has occurred only in two cases.

Bychkov [58] stated that for all the cases of BL observations, the increase in lifetime with the diameter was evident. Definition of this dependence is important for the development of BL theory. Hence, the lifetime in plasma models should not depend on diameter, and in theories based on vortical structures, the lifetime should be proportional to the square of the diameter. Bychkov found that BL's life span increases approximately linearly with its diameter in the case of small-sized (<10 cm) BL. In [59], Amirov and Bychkov analyzed the interaction of luminous objects with airplanes. Having compared the statistics of intercloud discharges and BL occurrence, they came to a conclusion that only in 18 cases of the 73 observations known to them (from and in the planes) with BL sizes smaller than 5 m, BL's occurrence was evident. In one case of plane crash, BL's impact could be observed. It occurred in February when the plane flew over a powerful radio-transmitting station. The BL has appeared on a control panel, and then struck the pilot's chest. He was injured and catapulted, and traces typical for electric current blow were found on his body.

Toselli and Fedele [60] reported about the project of the Ball Lightning Italian Observations Database (BLITA). The beginning of this database took place with the analysis of 12,000 UFO observations collected by the Italian Center for UFO Studies. From this database, 40 cases similar to BL observations were selected.

In July 2001, in the St. Louis (USA), the Seventh International Symposium on Ball Lightning took place. Unfortunately, the proceedings of this symposium were not published. Three reports devoted to BL observations and analysis were presented. In the report by I.G. Stakhanova, read by D. Turner, the data about the electric effects made by BL was presented. P. Handel read the report of A.G. Keul and O. Stummer about the gathering of the new BL observations in Austria. The statistics of the results of BL observations appeared invariable on time and space of all Central Europe. According to Bychkov, the old question of "Whether ball lightning exists?" needs to be replaced with the new one "Whether highly energetic ball lightning exists?" As a positive answer to the second question, he presented examples of 17 observations known to him, comprising reports on BL with huge energy content. Moreover, he asserted that the analysis of descriptions leads to a conclusion that BL's surface is hot in 25–30% of cases [33].

Subsequently, the Eighth International Symposium on Ball Lightning took place on August 3–6, 2004, in Chung-li, Taiwan, and four reports were devoted to the BL observation analysis. The first report [61] described how the sparks fell down to the earth from a support of a high-voltage line after a lightning stroke. One of them changed the flight direction horizontally at 1 m from the earth. Its diameter was equal to 2 cm, and it was lightly yellow and fluffy. The length of the "hairs" was 2–10 cm and on the tip of each of them, small droplets were visible. In another case, the witness (a female) within 1 s could observe a shining sphere with a boiling surface. "It consisted of randomly located 'hillocks' with strongly pronounced peaks and deepening between them." The streams were ejected in all directions from the sphere. The diameter of the sphere was 35 cm and the distance between the

peaks was 3 cm. The streams had the form of cylinders of 5 mm in diameter and 15–20 cm in length These hillocks were similar to the fountain streams in a gravitational field: the long ones, having reached the maximum height, "abruptly changed a direction and in the form of drops fell downwards, on a sphere surface."

Earlier, we had presented Egely's conclusion of the presence of a shell over BL. However, the case analysis required further investigation [62], and it was found that the BL that blow on the earth could break up to pieces of a shell – a form that is small and could melt (going out) – which are similar to pomegranate grains. Thus, the destruction is viscous as rolled clod of snow. The observation [63] also affirmed that the BL has a cellular, granular structure. Along with the observations of streams beating from a surface of a BL and falling back to the form of drops [33, 61], such BL descriptions lead to the conclusion that

84. BL cover represents a complicated system comprising solid internal layer and liquid outside layer.

There is a report about the explosion of BL (BL hit it) nearby an electric lamp. The lamp glass appeared with holes of small apertures of 0.1–0.2 mm in diameter. At explosion of BL near to an iron oven in a tent of a Nenets family the aluminum table ware standing about the stove has fused and has turned to a metal ingot, and grains of small shot in cartridges was alloyed into a uniform piece of lead. Other cases reported about how BL went out of radio transmitter plugs, the electric socket, a phone tube, or power cable; in the latter case, during the strong thunderstorm.

Arora (India) [64] reported about BL mass occurrence case in India in the dry long summer of 2002 when the day temperature of air was +42°C and the night temperature was +28°C. There was no thunderstorm activity during that time, and BL could appear because of the currents flowing in the earth generated by power stations. In the report by Keul [65], the analysis of shining object video-recording was reported. The shining object came out of the next house roof, had risen upwards, and through 2.24 s, disappeared into the clouds. Its color was yellow-orange, and at flashes, the object became white. Kavano (Japan) [66], in a substantiation of his version, stated that BL is an undeveloped channel of a linear lightning, had demonstrated a drawing of BL with a tail on an ancient Japanese engraving.

The Ninth International Symposium on Ball Lightning took place on August 16–18, 2006, in Eindhoven, the Netherlands. In the report "About observation properties of a ball lightning" [67], Bychkov brought the result of 10 years' work on the statistical analysis of BL properties. The definition of the average characteristics of this phenomenon was the result of this work. It was found that the diameter, life span, and radiating ability of BL depend on where it is observed – indoors or in the open air. The distribution of colors in the BLs does not depend on their site. The statistical analysis demonstrated that the increase in the humidity of air and the intensity of the atmospheric electric field led to a reduction of BL's life span. The estimated levels of BL-energy density based on observations are in the range from 10^2 to 3×10^6 MJ/m^3. According to Bychkov, cases of occurrence of burns on the bodies of people injured by a BL show that "the part of BLs possesses a very hot surface."

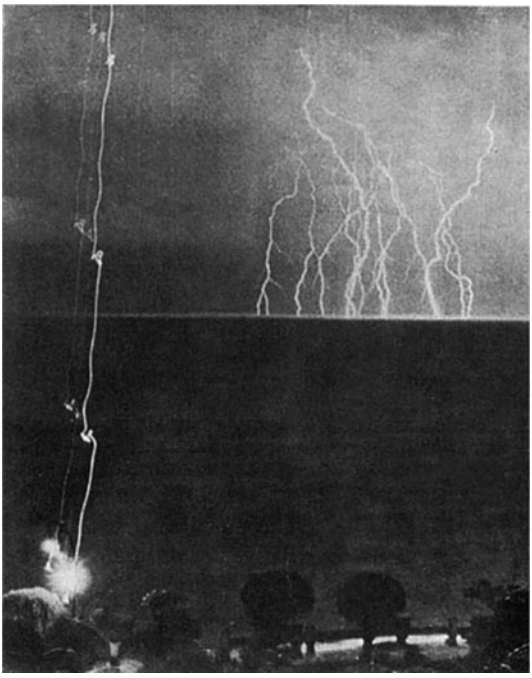

Fig. 6.3 Still photograph taken during a thunderstorm in1960 by I. Shagin [48]

Keul [68] presented the results of BL properties that were compared with the two German data banks: Hentschel Data Bank (200 events) and Central European Data Bank Germany (CEBLD) (132 events) with data from CEBLD Austria (150 messages). The key parameters on which comparison was made were: time of observation, weather condition, observation time duration, distance to the object, its diameter, surface kind, color, brightness, features of movement, and event details. A comparison of data demonstrated that the properties of BL are common across Central Europe.

In the report by Nikitin, Velichko, Vnukov, and Nikitina [69], an analysis of the photo taken in 1960 in Sochi city in the USSR (see Fig. 6.3) was carried out. One can observe the trace of a bright object, which fell down, with short-term stops. In the comment to the first publication of a picture in the USSR magazine "Ogonyok (Small light)," this trace was identified with BL trace, and image doubling was explained using light reflection from the lenses of a camera objective. However, Stenhoff was skeptical about this photo [48, P. 137] because of the plurality of the traces. Modeling of the photographing process of bright light sources demonstrated that the cause of double images is the reflection of light from lenses, and not the camera movement at shooting. It has been defined that the BL descended with a constant speed of about 25 m/s, and its stops were caused by the action of linear lightning discharging an oscillating electric field. Thus, it was concluded that the

BL had a positive electric charge of nearly 10^{-4} C, a weight of nearly 1 g, and a diameter of nearly 3 cm.

In the illustrations in the report by Papaelias [70], in which he considered that BL is an antimatter display, he presented an interesting photo, which can be interpreted as a trace of BL leaving a bend of linear lightning channel. Tar [71] told about his observation how BL was formed after a linear lightning struck the earth. Within 2 s after the blow, at the distance of 2.5 m from the blow place at a height of 1.2 m over the earth, there was a bright sphere of 30–40 cm in diameter, rotating counter-clockwise round a horizontal axis. To the right of the blow place at the same distance (2.5 m), there was a bush whose branches were bent under the pressure of the wind which started from the place of a lightning stroke. The fireball had one or two reddish tails. After the third of the second tail was drawn into the sphere, it continued its slow movement to the left. In 3 s, the sphere instantly disappeared. Based on his observation, the author proposed a model of BL formation: (1) After a lightning struck, the vortical toroidal ring was formed. It was cold and consequently remained invisible. (2) Having come across a bush, a ring was broken off, and the figure resembling a sickle of moon was formed. (3) The broken-off ring was pulled together in the sphere. (4) Because of strong electrification, the gas molecules were excited and the sphere became visible.

On 7–12 July 2008, in Zelenogradsk, the Kaliningrad area of Russia, the Tenth International Symposium on Ball Lightning took place. New reports on BL observation were discussed during this event.

In the report by [72] Bychkov and Nikitin, the likeness of BL and UFO phenomena was underlined and it was concluded that the part of these objects can represent the result of geological and geophysical processes, during the shift of the Earth and rock layers.

Keul [73] compared the results collected from six BL European national data banks: 200 observations of Hentschel in Germany, 132 observations of Keul in Austria, and 249 reports from France, collected by Hubert. From two Italian databases (Toselli, Carbognani), 201 reports were collected. Egely provided descriptions of 281 BL-observation cases in Hungary. Two Russian data banks contained 3,104 documents. Europe is an ideal place for doing research on lightning, including BL, unlike America with its "hot" storm areas like Florida and Paraguay, where moderate storm activity with an annual frequency of lightning strokes from 8–10 km^{-2} (Italy, Spain) to 1–2 km^{-2} (Southern Scandinavia) could be observed. A comparison of the European cards of storm activity and the "density" of BL observations showed the absence of correlation among these parameters. There is no wonder that lightning is recorded immediately by means of tools, and that data on BL observations pass through some social filters such as population density type, association between public and thunderstorms observation, educational level, and critical attitude to reports. The observation period for all banks was 1900–2000, and a maximum number of observations were recorded during the 1950s and 1960s. Furthermore, the maximum number of BL observations were reported during summer months. The more observations occurred during the afternoon hours (from 12 to 18 h); in Italy, the peak of observation shifted to

18–21 h. In 80% of the cases, BL observation was connected with thunderstorms. In the rest of the data banks, one can trace the usual characteristics of BL observed in former researches. A comparison of the European databases with those of the American and Japanese ones was carried out. A distinction was observed only with regard to Japanese data, where 2.6% of the observation cases were connected only with a thunderstorm; however, BL-observation frequency distribution during the months of the year (a maximum of 26% in August, and 16% in July) in Japan was similar to those observed all over the world.

VanDevender (USA) [74], in his report, described the results of field researches on the event that occurred on August 6, 1868 in County Donegal, Ireland [75]. The witness, Michael Fitzgerald, during a walk, noticed a red fiery sphere of about 60 cm in diameter, slowly moving in air. "After passing the crown of the ridge . . . it descended gradually into the valley, keeping all the way about the same distance from the surface of the land, until it reached the stream" (coast) in 300 yards (90 m) from a place where an observer was standing. "It then struck the land and reappeared in about a minute, drifted along the surface for about 200 yards (60 m) and again disappeared into the boggy soil, reappearing about 20 perches (100 m) further down the stream; again it moved along the surface, and again sunk, this time into the brow of the stream, which it flew across and finally lodged in the opposite brow, leaving a hole in the peat bank, where it buried itself . . . I . . . found a hole about 20 feet square (6 m), where it first touched the land, with the only pure peat turned out on the lea as if it had been cut out with a huge knife. This was one minute work . . . It next made a drain about 20 perches (100 m) in length and 4 feet (1.2 m) deep, afterwards ploughing up the surface about 1 foot (30 cm) deep, and again tearing away the bank of the stream about 5 perches (25 m) in length and 5 feet (1.5 m) deep, and then hurling the immense mass into the bed of the stream, it flew into the opposite peaty brink. From its first appearance till it buried itself could not have been more than 20 minutes . . . It appeared at first to be a bright red globular ball of fire, about 2 feet in diameter (60 cm), but its bulk became rapidly less, particularly after each dip in the soil, so that it appeared not more than 3 inches (8 cm) in diameter when it finally disappeared." A brigade of researchers found out that even 137 years after the incident on earth, traces of the ditches made by BL could still be observed. In [74], the authors estimated the work spent by BL as 4×10^7 J and considered that the ditch has been pressed through the earth by a microscopic black hole with a weight from 2×10^4 to 10^6 kg, which "magnetically levitated by a large electromagnetic field."

In another report [76], studies on glass-disk characteristics were presented. The glass disk was of 8 cm in diameter, cut out of a window by a BL. The disk had a cone edge with expansion in the direction of the room where it dropped out of a hole in a windowpane. The analysis demonstrated that the hole formation most likely occurred because of local heating of glass, and glass heating occurred from the room side that is from the side opposite to those to which the BL touched. It specified that BL energy passed in any form through the glass. If it was electromagnetic radiation, then its frequency should be no more than 10^{10} Hz [77]. The disk from the inside of the glass had a sharp edge that torn off from the edge of an

aperture; its thickness was about 50 μm. By means of X-ray spectrometer, it was revealed that in the direction from the center of the disk to the edge, the element structure of glass on an edge surface varied: its silicon content (from 26% to 18%) decreased and the oxygen content (from 59% to 69%) increased.

Apart from the above-stated BL-observation reports that have entered into the books and in the proceedings of the symposia, articles reporting new BL features continue to appear in the current literature. Earlier, we mentioned about cases when the BL had lifted air magnets weighing about 1 kg [32, P. 72] or stones weighing about 1.3 kg (Eg. 60). Some researchers doubt the validity of these observations as these actions by light BL violate the law of momentum conservation. However, if we consider that the BL has a charge and acts as a hook on a rope of the elevating crane, "it is suspended on a power electric line" to a cloud, then this contradiction disappears. In [78], even more surprising BL properties are described – its ability to lift objects weighing up to 100 kg. It is reported that "flying by over a tractor station, BL has crushed a framework welded of metal rods, and other framework . . . at first it has dragged over the ground. When BL has overtaken it, the framework has been lifted, carried for 300 m and softly descended. The framework weight was not less than 100 kg." In the same book, it is reported that "flying by over an apartment house covered with slate, BL has torn off nails together with the slate from a house roof (from a surface of some hundreds square meters order) and, having raised all this slate in air, has entailed it behind itself, scattering over all village." Furthermore, photos of the carried steel framework and the house with the damaged roof have also been presented.

We have already discussed the case of BL birth by means of "technical mean" – trolley-bus bars (Grg.145). It appears that this is not the only case. A witness of the same event in 1997 was Professor R.N. Kuzmin [33]. On a road hollow, the trolley-bus bar came off the wires. "The spark discharge between a boot of a bar of a trolley bus and current carrying wire has generated a white ball which has come off the birthplace, and has grown up a little." Subsequently, the sphere of blue color with a yellowish shade, 10–12 cm in diameter, smoothly passed through a handrail of the bridge and "has blown up practically without noise in one and a half or two meters from an earth surface, scattering a sheaf of sparks. Before the explosion BL has decreased in size, has reddened, and there was a blackout inside it."

Prospects of Future Work on Collection of Ball Lightning Observation Data

Now, let us draw a result. In the present review, we have tried to make a representation of the ways of accumulation and processing of data on properties of an unusual short-term natural phenomenon – BL. It seems that the hope that the statistical processing of data files can help to get into its physical nature was not successful. It did not reveal any, except trivial, correlations between its key parameters: size, life span, brightness, and color. This may be owing to the fact that they really do not depend on each other. Work on data gathering and their averaging, in our opinion, "came to saturation" and does not give practically any new results

useful for the construction of BL theory. In this connection, the change in the "paradigm" is more reasonable: a transition from operating by the processed data to the analysis of detailed descriptions of real events. The supporters of such approach are G. Egely and A.I. Grigorjev. Certainly, it will require granting open access to a full set of data on the occurred events of observations to the researchers. However, whether it will be possible to achieve this during our period of the Internet and permanent world crisis remains an open question. Nevertheless, it is possible to hope that, as in the past, enthusiasts will continue collecting BL data with their own expenses, time, and health. Perhaps, a time will come when people will start showing interest in this topic.

At data gathering, however, it is not necessary to forget the limitation of means by which BL data are extracted: about the limitation regarding the range of human senses. In fact, through vision, we cannot define whether the fireball radiates in infrared and ultraviolet areas of a spectrum, whether its light is polarized, whether it consists of narrow spectral lines or has a continuous spectrum, and is radiated in the form of short impulses or is continuous. Unfortunately, cameras and video-cameras cannot help in the search of answering these questions, as the range of their perception coincides with the human vision possibilities' range. We do not feel the presence of weak and average magnetic and electric fields, radiowaves, we cannot define all the shades of a strong smell, and we do not hear ultrasonic and infrasonic sounds that BL can generate. Certainly, all these can be defined by means of devices, but where is this universal portable device that could be supplied to all potential observers of BL?

6.1.3 Experimental Modeling of Ball Lightning

For many years, BL studies included repeated attempts to reproduce this phenomenon in the laboratory. These experiments can be divided into two groups. The first one is an experimental verification of the definite conclusions of BL models. The second one comprises attempts to "invent" the new form of the electric discharge in which conditions of "a fiery sphere", similar to that realized in the nature would be generated automatically. This division is conditional to a large extent, as in both the approaches, there is the general aspiration to imitate nature and in any way to deduce a "technology" that can be used for the creation of BL.

Long before it was confirmed through statistical analysis of observations, researchers intuitively felt that BL's birth is somehow connected with the discharge of a linear lightning. Therefore, it was natural to consider that it can be obtained by means of the electric discharge in the air or in other natural environment. According to Ford [79, P. 211], BL's occurrence in the discharge can promote: the presence of water vapor in air, dust, or soot; presence of nonhomogeneities in current conductors of bends and waists type; very slow increase in electric-field intensity to breakdown potential; and the presence of a shock or sound wave, for example, a thunder.

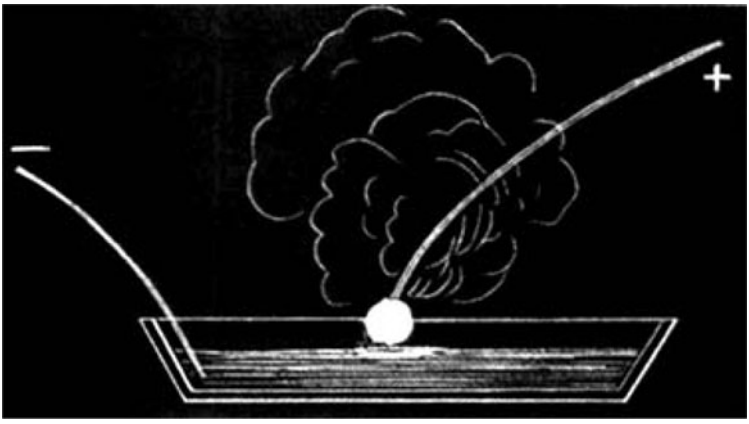

Fig. 6.4 A scheme of G. Plante's experiment [35]

6.1.3.1 Experiments on Ball Lightning Modeling Made Before 1988

Experiences on the generation of shining spheres during electric discharge began from the time of creation of the first electric devices (influence machine), first electric capacitors (Leyden jar), and first chemical sources of current (galvanic batteries and accumulators). The description of the experiments on the generation of shining balls (see Fig. 6.4) at the application of the direct current (Plante [80], N.A. Gezekus) or alternating current can be found in some earlier books [8, 18, 32, 35, 48]; therefore, it is senseless to repeat them here. Instead, we will mention some experiments that have left an appreciable trace in the history of BL experimental researches.

The very first experiment, in which the ball with the properties of a BL was casually formed, was carried out in 1757 by the natural philosopher, Arden, in the presence of Wm. Constable, Esq. [79, P. 216–221]. In the experiments, he used the Leyden jar, made from crown glass, of 4 gal (18 L) in volume, which was connected to the high-voltage generator through the brass core located in the glass isolating tube. After the researcher made "nearby 100 or 150 turns" by rotating the handle of the electric machine's wheel, in the bottom part of the jar, he "perceived a ball of fire, much resembling a red-hot iron bullet, and full three quarters of an inch in diameter, turning round upon its axis, and ascending up the glass tube that contained the brass wire." The researcher continued to rotate the wheel handle. The fiery ball "continued turning upon its axis, and ascending up the glass tube till it got quite upon the top of the prime conductor. There it turned upon its axis some little time, and then gradually descended, turning upon its axis as it had done in its ascent," on the bottom of the jar. "But soon after this, a very bright flash was seen; a large explosion was heard, and a strong smell of sulfur was perceived all over the room; a round aperture was cut through the side of the jar, as fine as it had been cut with a diamond, rather more than three quarters of an inch (2 cm) in diameter, and

between two and three inches (5–7.6 cm) below the top of the coating." Though researchers have replaced the punched Leyden jar, the effect was not reproduced.

A very large resonance was caused by cases of fiery sphere formations in the American submarines [81]. Spheres appeared at disconnection of the relay silver contacts at the passage of a strong current through it. The green fiery spheres separated from the contacts, which "floated" indoors for some seconds. "In 1947 in Philadelphia experiments onboard a submarine 'Catles' have been made. The sphere has been created in an engine room at voltage of a direct current 260 V and a current strength of 156 kA, the peak value of power was thus equal 40 MW. As time of disconnection for breakers of mechanical type is equal to 0.1–0.01 s then energy of plasmoid formation is of an order 0.4–4.0 MJ. The diameter of the sphere has appeared equal to 10–15 cm." In the 1980s, G.C. Dijkhuis undertook experiments on the reproduction of the processes described by Silberg [82]. For this purpose, he used the complete set of submarine accumulators with the power of 30 MW developed at short circuit. At a current higher than 150 kA, orange fiery spheres of 10 cm in diameter with a lifetime of 1 s were obtained, which scattered from the place of the relay contacts' disconnection over the parabolic trajectories.

The approach to BL modeling goes in two directions: development of conceptions about it as an independent object and as an electric discharge in air. The most impressing experiences on the generation of high-frequency discharges in air were realized in 1941 by G.I. Babat in blockade Leningrad [8]. Babat used the generator with a frequency of 60 MHz and a power of 20 kW. The energy of the generator was delivered to a glass cylinder of 5 L in capacity through its walls in the form of an alternate magnetic field. At first, the cylinder was pumped out to a pressure of 0.1–5 Torr. After switching on the high-frequency generator in a cylinder, a shining red ring appeared. After that, the cock was opened and air filled the cylinder. The ring began to pull together in a lump and turned to a fiery sphere. In the process of pressure increase, its color at first became violet, then green, and at last, became dazzling white. Fiery tips were pulled out from the sphere's surface, and it was possible to distinguish concentric zones of different colors and different intensities of luminescence. At the shutdown of the generator, the sphere went out, and dull, green shining fog remained in the cylinder.

6.1.3.2 Experiments on Ball Lightning Modeling Discussed During the First Symposium on Ball Lightning

During the symposium, two works devoted to experimental modeling of BL were presented. Ofuruton and Ohtsuki (Japan) [1, P. 310–324] repeated the experiments of Barry [35] on the inflammation of strongly diluted mixtures of flammable gases with air. They used methane, ethane, and an aerosol in the form of cotton fibers as fuels. The electric spark was applied to initiate the reaction in a gap with a length of 3 mm between the copper electrodes. The mixture of gases filled a glass vessel of 73 $\times$ 37 $\times$ 43 cm in size. During the inflammation of 2% methane–air mixture, a flame

of the spherical form of 3–6 cm in diameter appeared. At first, it had green color because of the presence of copper atoms (from electrodes), and then it took the color of a usual flame. In the experiments with the mixtures containing 2% ethane, spheres of about 4 cm in diameter, in the beginning were greenish, and then turned red. The lifetime of fiery spheres was nearly 0.3 s. Also, experiments were carried out when in a vessel that contained about 100 cm^3 of cotton fibers that were broken into small bits. The fibers were distributed over the volume of the vessel by a stream of compressed air. During the inflammation of this mixture, a shining white sphere of 3 cm in diameter was formed. After that, its size decreased and it disappeared 0.8 s after the discharge initiation. In the experiments, two shining objects appeared after the discharge pulse near electrodes, in the presence of a mixture of 2.7% ethane, 100 cm^3 of cotton fibers, and air in the vessel. The first of them (5 cm in diameter) disappeared after 2 s, and the second (1 cm in diameter) moved upwards and downwards and vanished after 1 s.

G.C. Dijkhuis (Netherlands) [1, P. 325–337] reported about the creation of installation to verify his BL model. According to this model, in the nature, long life span and huge energy of BL are the result of superconductivity and nuclear reactions as well as the presence of fusion reactions in strongly turbulent plasma of BL. He considered that BL is formed in the atmosphere by means of free-electron gas-phase transition. Electrons, owing to exchange interaction, unite in Cooper pairs, and collapse in a collective basic state in particles satisfying Bose–Einstein statistics. The "bosonizing" threshold exceeds the value of electric-field strength arising before a linear lightning breakdown development only by four times. On the basis of the nonrelativistic theory of the charged superconductors, microscopic bosonic vortex is represented as a core of self-captured Cooper electron pairs, around which positive ions rotate on circular orbits owing to Coulomb's force. If the radius of their orbit is close to Bohr radius, then the speed of the ions reaches a level at which reactions of nuclear fusion are possible.

An experimental installation for research on the possibility of "bosonic" BL existence has been created. Laval nozzles were used for cooling a gas mixture to the temperatures necessary to start the process of bosonization. A small amount of deuterium was introduced into a nitrogen stream. High-voltage electric capacitors were used for the charge accumulation, whose value can be compared with the charge of the thunderstorm clouds. In the space between the electrodes, the discharges were initiated, whose currents were comparable with those of usual lightning. Two capacitor batteries in the capacity of some microfarads were used, and were charged up to a voltage of 240 kV. Thus, a full charge of the battery was nearly 1 C. The voltage of each capacitor's battery was put to opposite located electrodes. Full inductance of the batteries was equal to 124 μH, and the period of current oscillations was about 50 μs. The experiment was undertaken as follows. Batteries of capacitors were charged, a gas was delivered to a pipeline with a supersonic nozzle, and two dischargers were simultaneously short-circuited. The voltage on the electrodes on the nozzle side increased, and at last, breakdown took place. After the breakdown, the voltage on the electrodes decreased and experienced strong oscillations. The highest value of the voltage appeared to be equal to 94 kV.

This value was smaller than those necessary according to the calculations to start the process of electron bosonization (143–157 kV). The number of neutrons measured with the help of the activation analysis did not exceed 3×10^{11}, which was smaller than expected. By means of a high-speed video camera, the place of an exit of the gas from a nozzle into the air was recorded. No long-lived fiery spheres were discovered; however, the gas luminescence proceeded approximately ten times longer than the duration of the electric discharge.

6.1.3.3 Experimental Investigation of Ball Lightning After 1988

As stated earlier, there are simultaneously two approaches to the conception of BL entity. BL, according to the first, is considered as a special discharge form in air, which gets energy from an external source. According to the second, BL is an independent body with an internal energy source. There are two branches of experimental investigations with respect to these conceptions.

High-Frequency Discharge in Air

We have described the experiments of Babat with high-frequency discharge in air. However, he did not connect them with BL. A hypothesis according to which BL is fed by radio-frequency radiation energy of thunderstorms was proposed by Kapitsa [83] in 1955. He was also one of the few scientists who have verified their ideas in practice. Kapitsa, along with other research workers, managed to realize the high-frequency constricted discharge in the atmosphere of helium, argon, carbon dioxide, and air at a pressure from 10 Torr to several atmospheres [84]. The discharge was lighted in the spherical cavity resonator working on H_{011} wave type, the wavelength of radio emission was equal to 19 cm, and power introduced into the resonator ranged from 0.6 to 6.4 kW. At low powers, the discharge had an oval form with dim borders; however, with an increase in power, it took the form of a cord, came up to the top wall of the resonator, and soared at some distance from it. The discharge became steadier when there was a gas rotation, and the temperature of its central part was about 6,000 K. In spite of such a high temperature, heat exchange of hot area with a wall appeared insignificant because of the occurrence of a double layer of charges on its border. The plasma formations obtained by Kapitsa had a faint resemblance to BL. However, the discharge in the air was supported only in the presence of a continuous supply of a considerable radio-radiation power to it. With the shutdown of the radio-frequency generator, the discharge died away.

The shining spheres, similar to plasmoids investigated by Kapitsa, was also obtained by the Japanese scientists [85]. Spheres in air at atmospheric pressure appeared inside the cylindrical cavity resonator of 16.1 cm in diameter and 37 cm in length, with a supply of a continuous flux of radiation power of 5 kW at a frequency of 2.45 GHz ($\lambda = 12.24$ cm). Four types of plasma spheres were observed. Spheres of the first type were steady and only sometimes showed the tendency to be divided

into two spheres. Formation of plasma spheres of the second type began with bright flash with 0.2-s duration. After that, the sphere was divided into two spheres, and these spheres started to move in the resonator in different directions. The discharge of the third type had the form of a flame and was located in a place of the connection with the waveguide bringing the radiation to the resonator. Sometimes, this flame was drawn into the waveguide. If the ceramic plate of 3-mm thickness was located between a waveguide and the resonator, then the plasma formation passed through a plate, neither destroying nor melting it. The fourth type of plasma formations had the form of the flame flowing from the resonator in free space through a hole in an aluminum foil, which was burnt by the flame, closing the resonator's end face. This "plasma fire" continued to exist during 1–2 s after the shutdown of the magnetron. The shining plasma formations, similar to the plasmoids obtained by Kapitsa and plasma spheres obtained by Ofuruton and Ohtsuki, have been observed by the authors of another study [86].

Later, Ofuruton along with his coworkers, received plasma fiery spheres not in a waveguide but in free space [87, 88]. In their experiments, a magnetron continuously radiating power up to 5 kW at a frequency of 2.45 GHz was used. The radio-frequency radiation went to air through an open waveguide. Two copper electrodes of 3 mm in diameter were placed near the waveguide; the gap between them was 3 mm. The distance from a spark gap to a waveguide cut varied from 0 to 9 cm. The capacitor with the capacity from 0.2 to 10 μF, charged to 8–10 kV, was discharged through the electrodes. When the magnetron was switched on, fiery balls appeared in air after the discharge; they were of spherical or ellipsoidal forms. At distances from a spark gap to the waveguide, lesser than 3 cm, the plasma sphere usually moved horizontally and was drawn in the waveguide. At the distances greater than 5 cm, it moved upwards. The color of the sphere changed from red to white. After the discharge initiation, the sphere, gradually decreasing in sizes, disappeared after 0.5 s. The spheres appeared with 100% probability at the large discharge power and/or the large power of the microwave radiation.

As can be seen, if it was possible to find the processes providing continuous delivery of some kilowatt of high-frequency power in some allocated area of space, then "Kapitsa's BL" would become the real fact in nature. Regarding the continuity factor, it seems to be an intractable problem. However, the second part of a problem – concentration of energy in a definite place – can be solved with an interference of radiowaves. In this connection, "Anderson localization" is an intensively investigated problem, which is a possibility of local increase in high-frequency field intensity owing to the summation of amplitudes of the waves reflected from subjects located in a random way [89].

Tanaka and Tanaka [90] presumed that "Anderson localization" in air conditions of a fireball formation in the form of the plasma spheres obtained by Ohtsuki and Ofuruton can be created. The authors [91] made numerical calculations of electric-field strength with a frequency of 2.45 GHz in a rectangular waveguide for a case in which a row of ceramic plates of 2.25 mm in thickness was located in it. Two kinds of one-dimensional disordered systems of an arrangement of plates were investigated: a quasi-periodic system of some Fibonacci series type and a fractal system

of the Cantor lattice type. In both the cases, from the calculations of the authors, the intensity of a high-frequency field was found to increase more than 100 times in the limited areas of waveguide. Further work of the Japanese scientists was devoted to experimental verification of the obtained results [92–96]. When ceramic plates of 2.25 mm in thickness were used, whose sizes were equal to those of a waveguide (109 × 55 mm), the passing and reflected power was measured at a power of 1–2 kW of the microwave radiation. The plates were placed according to Fibonacci series from first to sixth generation (22 plates in the latter case were used). At transition from fourth to fifth and from fifth to sixth generation, it was possible to hear a sound of breakdown of air in the waveguide; however, the plasma discharge did not appear.

As it is improbable that in the nature there can be conditions when a high-frequency field strength of external sources exceeds the breakdown value of air (>3 × 10^6 V/m) or there may be a local-pressure decrease promoting ignition of the discharge, researches on the discharge ignition processes by means of passive initiators has gained interest. Metal needles, multi-needle metal whisks, metallic-dielectric plates, flame, and aerosol can serve as initiators. Using the initiator made of a wire of 1 mm in diameter, the authors [45, P. 119–136] obtained the low-threshold spherical high-frequency discharge at the frequency of 7 GHz, which existed at energy fluxes of 10–100 mW/cm^2 in an air pressure range from 3 to 110 Torr. The maximum diameter of a sphere was equal to a wavelength of radiation, and the minimum was equal to the quarter of the wavelength. With the increase in pressure, the discharge took the form of a torch, and the intensity of its luminescence sharply increased. At atmospheric pressure, the discharge was supported by the power of some hundreds watt. In [45, P. 136–159], for discharge ignition, the short pulse of powerful high-frequency radiation was used, and plasma maintenance was carried out by the second pulse of small amplitude, which was incapable to independently cause a breakdown of the gas.

Chukanov [97] obtained shining spheres in a quartz flask of 10 cm in diameter, placed inside an industrial microwave of 2.2 kW. The flask could be pumped out by the forevacuum pump and could be filled with various gases. It had two tungsten electrodes, brought to its internal wall. The alternating voltage (60 Hz) of 1,500 V at a current of 10 A could be delivered to the electrodes. Besides, the electron beam could be injected into the flask in a radial direction (from the periphery to the center). At first, the flask was pumped out. When the microwave was switched on, the discharge was lighted. A gas was delivered to the flask, and brightness of the luminescence increased. The limiting pressure of the gas was 1 atm. When the electron gun was switched on, the gas luminescence became very bright. The alternating current was given to the electrodes – the plasma started to shine, similar to a lamp of 12-kW power. The discharge burned easily in air, oxygen, nitrogen, and carbon dioxide. In hydrogen, helium, and water vapor, the discharge did not burn.

The special group of experiments comprised tests that investigated the burning processes in a high-frequency field. Golka obtained plasmoids by placing a 5-cm burning candle in a household microwave. During the time while it was switched

on, fiery spheres [98] were flying. In [45, P. 154–155], the interaction of the high-frequency discharge with a candle flame was investigated. It was found that a diffusion-type electrodeless discharge appeared in a zone of a burning candle because of the formation of a cavity with the lowered density of the gas.

In [99], the technique of realization of fiery spheres from hot points of the fused substance was described. The rectangular waveguide with a length of 20 cm and section of 8.6×4.3 cm^2 was used, whose open end was blocked by a mirror made of vanes under cutoff, and in the other end, power of 0.6 kW was delivered from a magnetron working at a frequency of 2.45 GHz. In the center of the wide side of a waveguide at a distance of 5 cm from its open edge, the hole, into which the metal drill reaching an internal surface of the bottom side of a waveguide could be inserted, was drilled. This configuration was termed "a microwave drill" [99]. In the bottom part of the waveguide, the substrate of silicon, glasses, germanium, alumina, or basalt, in the form of plate, bulk, or powder could be placed. At first, the drill resulted in contact with a substrate, thereby concentrating the release of microwave power in a contact point. There appeared a hot point, and approximately after 1 s, there was substance melting. "After that the microwave drill bit was pulled out and detached from the molten spot while dragging a condensed, nearly vaporized drop out of the substrate. A stream of fire is ejected then from the molten hot spot forming a fire column . . . Shortly after, this fire column rises, detaches from the hot spot, and forms a fireball in the air. The confined fireball flies up to the metallic ceiling, where it is slightly squeezed to a form of a Gaussian-like shape. The floating fireball looks like a dense heavy vapor, almost a liquid, glowing in yellow red . . . It becomes buoyant in the air and quivers elastically as a jellyfish. The floating fireball ($\sim$15 cm^3 in volume) may remain stable as long as microwave power is on, and it continues to glow for another 30–40 ms after the microwave energy is turned off." It was possible to observe kickbacks of a fiery sphere at collisions with walls, rotation of a fiery column, and sphere movement in the waveguide in a direction towards the power source. At the contact of a teflon partition, the sphere left burn traces on it, and its contact to a glass plate of 2-mm thickness resulted in its melting, cracking, and destruction of the fiery sphere.

In [100], to obtain shining spheres, streamer discharges created by high-frequency Tesla generator at a frequency of 67 kHz, with an average power of 3.2 kW submitted to a high-voltage electrode were used. The authors stated that they used reconstructed N. Tesla installation with reduced size. It has been experimentally established that during the development of discharges, a large number of carbon particles and particles of the evaporated metal from the electrode in small near-electrode area were formed. In the same area, there may be strong electric fields (with a strength of up to 10–20 kV/cm), and thus, the formed particles were quickly heated up. The spheres appeared near the high-voltage electrode as if they appeared "from nowhere," because they were not observed on the previous frame that was video-recorded, i.e., their time of formation was $\tau_{cr} < 40$ ms. The spheres had different colors, including red, yellow, blue, and white, their lifetime reached 2 s, and their diameter was 1–5 cm. Often, at the end of existence, they blew up with a loud bang that indicated the energy store $E \sim 5/2 \cdot kT \cdot N > 0.2$ J/cm^3

(where $5/2 \cdot kT \cdot N$ – equilibrium energy content of air at room temperature). The best results were obtained in those experiments in which the high-voltage electrode was covered by wax or charred wood.

Plasmoids

In 1999, at the Sixth Symposium on Ball Lightning, P. Koloc reported about the experiments regarding the installation of "Plasmak"; he had stated its theory at the First Symposium in 1988 [101, 102]. The scheme of its installation in [101] is not represented; however, through indirect signs, it is possible to conclude that it is the coil of a thin copper wire, which blows up when a strong current pulse passes through it. Energy from 20 J to 5 kJ was put into the discharge. Koloc managed to realize plasma formations of approximately spherical form with smeared borders. The plasma spheres had the sizes from 2 to 18 cm, radiated white light during 5–50 ms, and usually emerged upwards. Emission of a substance from sphere poles (along an axis of a plasma torus) was sometimes observed. Energy measurements of plasmoids were not undertaken. The small lifetime of the plasma formations testifies to fast attenuation of currents in a "mantle" of the plasmoid, which indicates the absence of superconductivity in it.

Since 1971, in the Vladimir State University (Russia), experiments on obtaining electric discharges with possibly large current strength have been undertaken [103]. The last variant of power installation is the system with the inductive storage of energy [104]. The electromagnet with the opened U-shaped core of a transformer steel of 22 t in weight serves as energy accumulator. Fifteen coils of several parallel bundles of a copper wire are reeled up on the core with the total section of 4,000 mm^2. The inductance of the storage is 6.5×10^{-4} H. At a feeding current of 30 kA, an energy of about 500 kJ is stored in it. The current pulse duration at removal of energy of the storage can be changed from 70 to 120 ms. This installation works as follows. The storage inductance is connected with the block of rectifiers through the switch. After accumulation of magnetic energy, the storage by means of the second switch is connected with a load, and 70 ms after that, the first switch is disconnected. Extra current of disconnection is generated in a working chain. This current passes through a round metal diaphragm of 56 μm in thickness. One electrode is connected with a peripheral part of the diaphragm, and the second, with its center. As a result, the current flows over the disk radii. At the moment of diaphragm explosion, the currents flowing in it and lead wires create a toroidal magnetic field. Ions appear to be "frozen in" this field. Convection electric currents appear in electrically neutral plasma. These currents take the form of a torus, and then the form of a sphere [105–107]. A transformation of a torus in a sphere occurs at 0.25 s, whereas the magnetic field fades at 0.4 s. The generated shining object has the form of a spheroid with a sharp border. After that, diffuse decay of electromagnetic energy occurs from thermal to optical ones, and the object slowly dies away. Sometimes, at local destruction of a sphere surface, "energy flash decay, including a beam with characteristics close to those of a laser beam" occurs. It is revealed that

radiation is polarized by 1.5–5.5% and the polarization plane is parallel to the plane of a diaphragm [108]. The authors [109] considered that it is possible to explain these phenomena by accumulation of electromagnetic radiation energy in the internal area of plasma formation, which occurs owing to light reflection from internal walls of the toroid caused by increase in free-electron concentration in the direction of a vortex radius.

Some authors [110, 111] obtained plasmoids in the form of heated air spheres kept from expansion by atmospheric air pressure. They came to a conclusion that heating of a gas in a volume of some cubic centimeters by the powerful spark discharge leads to pressure increase in it to several thousand atmospheres, which causes fast destruction of the sphere by a supersonic shock wave. As a result, the lifetime of the heated sphere does not exceed 1 ms. In this connection, they have chosen a mode of slow heating of a gas volume. They used six high-voltage transformers (60 Hz, 120 V/15 kV, 60 mA), whose secondary windings were switched in parallel through the spark gaps exciting small volume of air. The transformers were periodically switched on for 0.5 s, and then were switched off for 0.5 s. The shining formations rose upwards from the discharge zone existing from 0.25 to 0.5 s.

Erosive Discharge

In the early 1990s, the pulse electric discharge in the channel with evaporating walls (the erosive discharge) attracted the interest of researchers. The plasma stream that is ejected out of the channel has the density close to air density, and at low temperature, the intensity of radiation is small, the density of energy is high, and the concentration of the charged particles is high. This stream burns holes in the metal plates, but leaves a paper intact, and seeks to keep the integrity at an encounter with an obstacle. According to some authors [45, P. 15–66; 112], this set of properties is typical for BL. Owing to this fact an erosive plasma stream was called a laboratory analog of BL. This analogy looks adequately artificial (and should cause the active protest in those who saw a real BL), as a stream of flying plasma, neither by the form nor by the motion character, remind of BL in any way. Nevertheless, analogy declared in [112] has been unconditionally accepted by other researchers.

In typical installation for generation of erosive plasma streams, capacitors from 630 μF to 2.5 mF charged to a voltage of 450 V are used. Capacitors are discharged through the channel of 1 mm in diameter and 5 mm in length drilled into a plate of an insulator (organic glass is used more often). For the maintenance of the laminar flow of the evaporated substance from the channel, it is necessary that the increase in the speed of the current does not exceed 10^5 A/s; at higher speeds, the stream becomes turbulent. For the creation of the required form of a current pulse, an inductance is included into a discharge circuit. The typical length of the stream at atmospheric pressure is about 10–40 cm, and speed of its motion is 60–100 m/s. The stream consists of a thin central part (core) of 1–2 mm in diameter and a cover of

6–10 mm in diameter. The continuous spectrum of radiation of the stream is caused by a luminescence of soot particles, and lines of atomic radiation of hydrogen, carbon, copper, sodium and calcium, and molecular bands of C_2 and CN are also observed. On the whole, the plasma formation turns out to be electrically neutral; the excess negative charge in the core does not exceed 10^{-3} from the charge value that has passed through the discharge channel. The maximum floating potential of plasma is 12 V. The radiation power of the plasma formation in wavelengths ranging from 0.2 to 10 μm appeared to be about of 30 W, and thus, no more than 1% of the energy stored in it (50 J) leaves during its existence. The temperature of a neutral gas in the stream appeared to be equal to 1,000–6,000 K [113], and the temperature of ions was defined as 6.5×10^3 K. The plasma stream is capable to pass through a hole in a textolite plate. If the diameter of the hole is small, then only the core passes through it, and the cover "is taken off." It was revealed that at the direction of the plasma stream in a ditch with liquid nitrogen in it, bright spherical plasmoids up to 5 cm in diameter, whose color during a lifetime (20–40 s) changed from white to violet, and dark spheres from 1 to 2 cm in diameter existing for 1–2 s were formed. The energy stored in bright plasmoids reached 100–200 J. Some authors [45, P. 72–78] considered that plasmoids consist of Rydberg substance – an ensemble of highly excited atoms.

Investigation of the material objects that are taken out by a stream from the discharge channel also attracted considerable interest. To increase the weight of the evaporated substance, the wall of the channel was covered with wax, and the length of the channel was increased to 5 cm [45, P. 66–72; 114]. In the head part of the stream, an ellipsoidal "shaggy" plasmoid consisting of a set of branching shining filaments from 2 to 6 cm in the length, created by such a generator was formed. After plasmoid extinction, the polymeric threads of 1–10 μm in diameter and 1 cm in length stayed in its place. According to some authors [114], in the course of plasmoid material condensation, a formation of mosaic, such as a charged fractal polymeric structure, capable of saving electric energy up to 100 J, was observed.

For obtaining the fractal charged objects, the authors [45, P. 87–95] placed the activated coal or lumps of cotton wool in the discharge chamber. At the discharge from the channel, parts of 5 mm in size were flown out, which were shining for about 6 s with red light. Under a microscope, it was possible to see white porous structure with short fibers on the surface of the parts; their density was about 5×10^{-2} g/cm^3. The authors of [115] placed metal particles of 50–100 μm in size in the channel of the plasma generator made of organic glass. Thus, on an exit from the plasma generator at a distance of 30–100 cm from an injector, there was an explosive formation of bright areas of 10–30 cm in size, shining for about 0.1 s. At the interaction of a plasma stream with a tin wire, there were yellow-red balls of 3–5 mm in diameter. Falling on a plastic surface, they jumped aside, leaving traces of burns on it. The cooled down surface of the balls appeared covered with threads of tin oxide of 50 μm in length. Besides the balls, there were fractal structures up to 3 cm in length and of some millimeters in width, with fractal dimension $D > 1.8 \pm 0.2$. Within several minutes, they became highly elastic, and then became fragile and quickly got destroyed.

The authors of [115] carried out an experiment whose conditions were close to those which can be realized when a lightning strikes the earth. The electric discharge occurred in a thin tube of an insulator with thick walls. The products of the discharge consisting of steams of a material of a tube and electrodes, and also of ionized air, having broken through a tube wall, went outside. The lifetime of similar formations reached 5–7 s. Having hit an obstacle, they blew up. Their remains reminded shells of the oxidized metal. It was one of the few experiments in which an explosion of luminescent formation was observed. In [116, 117], the stream of erosive plasma with energy of about 200 J passed over a dish with melted paraffin or wax. After the stream passage through a cloud of steams over the dish, there were emerging formations of spherical or mushroom forms of 10–20 cm in size. They were shining for 0.5 s. With the use of the plasma generator with a capillary of 1–2 mm in diameter, drilled in a composite material of a mixture of paraffin, rosin and wood sawdust of size $1 \times 0.3 \times 0.3$ mm shining objects of 1–2 cm in size with a lifetime of 1–2 s were obtained. They left the channel approximately 30 ms after the start of the plasma stream. Their residuals represented particles of black color of 1–2 mm in size with polymeric fractal-porous structure of the surface.

In [118], the interaction of the erosive discharge stream tip with an oncoming supersonic stream of air was investigated. It was revealed that the shock wave is not formed in front of the plasmoid owing to the fact that a drag force falls by 20%. The plasmoid is a source of radiowaves with a wavelength of 0.5–2 cm and it amplifies laser radiation at wavelengths of 0.63 and 10.6 μm. In [119–121], it is shown that a cluster plasmoid obtained in the erosive discharge bears a positive charge on itself. The floating potential of the plasmoid was equal to 100 V. This value is 100 times greater than the expected potential of decaying plasma with an electron temperature of 10^4 K.

In the nature, the configuration similar to the device of laboratory plasma generator can appear when a lightning strikes the earth. As is known, fulgurites thus appear, which are tree-like formations from caked sand and soil. Abrahamson and Dinnis [122] assumed that at high temperature, sand (SiO_2) and organic substances of soil can react resulting in the formation of silicon:

$$SiO_2 + 2\,C \rightarrow Si + 2\,CO.$$

Silicon vapors are thrown out to the atmosphere, where their condensation takes place and nano-size silicon balls are formed. Under the influence of electric fields, balls gather in aggregates that start to shine because of warming up owing to the reaction of silicon oxidation, $Si + O_2 \rightarrow SiO_2$. Abrahamson undertook experiments to imitate conditions when lightning strikes the earth [123]. He passed a discharge current of capacity of 204 μF, charged to a voltage of 20 kV, through a layer of humidified soil of 3-mm thickness. The soil filled the bottom electrode – a graphite substrate; as the top electrode, the graphite rod of 15-mm diameter was used, located at a distance of 22–36 mm from the surface of the earth layer. The energy released at the discharge was 110 kJ, and a charge of 1.3–3.4 C was transferred

through the soil. In experiments with the highest power, the negative potential was applied to the top electrode. The reaction products were sucked away by the pump and deposited on the filter of quartz fibers and the lattice of nickel. Fiber threads of 100 nm in diameter and 7 μm in length were found on the filter, by means of a scanning electron microscope. Sometimes, spheres of 2 μm in diameter were deposited on the fibers. Chains from 25 to 120 nm in length consisting of balls with an average size of 25 nm were found on the surface of the nickel lattice. It was not possible to define the elemental structure of the threads and chains. Spheres of 2 μm in diameter basically consisted of silicon, and impurities in them included Al, Mg, Ca, Na, and Fe (components of minerals of soil). The author of [123] did not manage to observe the formation of aerogel-isolated spheres. He explained that it was because of a strong shock wave, and accordingly, a strong gas disturbance near the discharge area. Therefore, he considered that in the nature, vapors from a cavity made by a lightning come out after the discharge is terminated. The ring whirlwind is formed of charged nanoparticles.

The authors of [124] repeated the experiments of Abrahamson, by replacing a layer of soil with a silicon plate of 5 cm in diameter and a thickness of 350 ± 50 μm. This plate was placed on the steel base of 10×10 cm in size and 5 mm in thickness, serving as an earthed electrode. The rod of tungsten or graphite of 4 mm in diameter and 30 cm in length was used as the second electrode whose movement could be operated manually. The alternating voltage of 20–25 V (50 Hz) was applied to the electrodes, and the current could be varied from 100 to 140 A. The rod was lowered, and when it came into contact with the silicon plate, current appeared. After that, the electrode was raised to 1–2 mm, and an electric arc appeared between the electrode and the plate. At this time, shining fragments extensively flew out from the arc. At the further lifting of the electrode, the arc went out. This cycle took 1–2 s. Shining formations appeared, on an average, once in 30 attempts. However, with the replacement of the silicon plate with an aluminum or copper foil, addition of some salt water, or dry or humid microspheres of SiO_2, or humid wood, it was impossible to get shining spheres. The spheres that appeared in the experiments with a silicon plate had a diameter from 1 to 4 cm and existed for 8 s, whereas their fragments went out at 1 s. When hitting a floor, they jumped aside and were scattered into small parts. There were observed cases when the shining sphere passed through a crack under a plank or left behind a spiral smoky trace. Examination of the surface of a silicon plate using a scanning electron microscope demonstrated that after the discharge, there were deepenings of about 5 μm in size and aggregates of particle chains of micron sizes on the surface of the originally smooth plate. The obtained shining formations had some properties coinciding with the properties of natural BL; however, freely levitating sphere was never observed.

Electric Discharge in Water

For the purpose of reproducing the conditions in submarines, which produced fiery spheres [81], Golka carried out experiments using a transformer of 150 kW power,

with 60-Hz frequency, a current of 10 kA, and voltage of 15 V [98]. At short circuit of a copper cable of 2.5 cm in thickness and an aluminum plate of 3–6 mm in thickness, under water, fiery balls of 6 mm in diameter appeared on the water surface. Hissing, they slid on a surface. Sometimes, fiery spheres of the irregular form rose in the air, leaving spiral smoky traces. Such fiery spheres could also be obtained without water; however, in this case, they scattered with much larger speeds, and it was difficult to watch them. These fiery spheres were shining with a bright white light, which may be due to the slow burning of aluminum. At contact with iron electrodes, yellow fiery spheres appeared. Their luminescence lasted for 2–5 s, and at the end of their life, their size decreased. The cooled-down spheres represented metal spheres of about 2 mm in diameter covered with oxides in the form of small hairs.

In 2000, in Gatchina near St. Petersburg (Russia), the new type of electric discharge named "the Gatchina discharge" was achieved by its inventors [125–135]. They consider the erosive discharge ("Avramenko stream") as a prototype of this discharge, but unlike the last one, they could increase the size and life span of the shining formation by two orders of magnitude [126, 127]. The basis of installation for discharge realization is the condensers battery with a capacity of 0.6 mF, charged to a voltage of 5.5–6.0 kV. The plastic cylindrical vessel with water was used. The earthened anode represented a ring made of a wire, lying at the bottom of the vessel. The thickness of the water layer was usually equal to 15 cm. As the cathode, the graphite electrode of 6 mm in diameter protruding over a water surface at a height of 2–3 mm was used. The lateral surface of an electrode was isolated from water by a quartz tube. By means of a manual discharger, the capacity's voltage was given to the cathode. The sliding discharge was developed on a water surface, and from the electrode protruding over water, the stream was thrown out upwards. The discharger was disconnected at the 80th ms (at that time, the residual voltage of the battery was 3 kV), and the stream, separating from the electrode was transformed into shining formation. From 60th to 100th ms, it had the form of jelly-like body, and sometimes, took the form of an ideal sphere (see Fig. 6.5). The object rose upwards and decayed. The decay started at 200th ms, and the decay itself lasted about 400 ms.

By means of electric probes, the authors of [127–130, 132, 134, 135] found that the object bore non-compensated negative charge on itself in the size of 2×10^{-7} C on its cover. The cover potential exceeded 10 kV. The plasmoid did not influence dielectrics, but melted off thin wires. Hence, when entering inside the plasmoid with a nichrome wire of 0.08 mm in diameter on its tip, the ball of 0.2 mm in diameter [128] was formed. In [135], it was reported that at melting of a wire of 0.1 mm in thickness, the ball of 0.5 mm in diameter was formed. The authors considered that "the basic energy of ball lightning is stored in the form of the electric field created by electron sphere, and this energy has the potential character" [131]. We can estimate the energy of "Gatchina Plasmoid." Let the diameter of the charged sphere be $D = 13$ cm, and its charge be $Q = 2 \times 10^{-7}$ C. The potential of the sphere is $U = Q/2\pi\varepsilon_0 D$, and energy of electric field is $W_e = Q^2/4\pi\varepsilon_0 D$. For accepted values of D and Q, one can obtain $U = 27.7$ kV

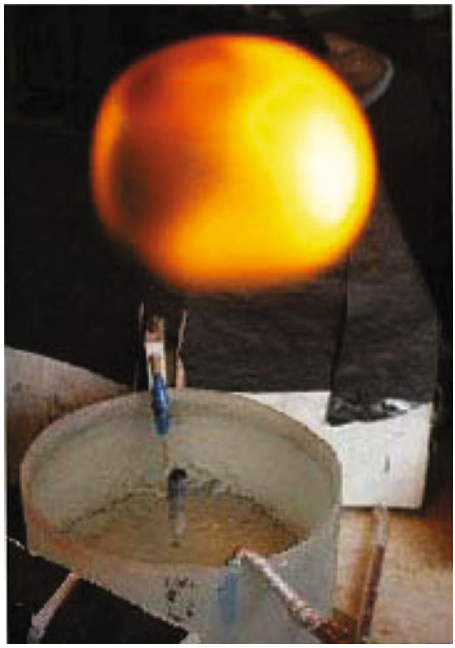

Fig. 6.5 A photo of Gatchina discharge [135]

and $W_e = 2.8 \times 10^{-3}$ J. Now, we will define the energy necessary for the melting of the nichrome wire. A specific heat capacity of the nichrome is $C_p = 0.46$ kJ/kg·K, its density is $\rho_N = 8.4 \times 10^3$ kg/m^3, and temperature of melting is $T_m = 1{,}390$°C [47]. For the formation of the melted ball with a diameter d, energy $W_m = \pi d^3 \rho_N C_p \Delta T/6$ is required (here, ΔT is the difference between the melting and room temperature). For the formation of a ball of 0.2 mm in diameter, energy of 2.2×10^{-2} J is required, and the ball of 0.5 mm in diameter can be formed at an energy expense of 3.5×10^{-1} J. This energy is 10–100 times greater than those of plasmoid electric energy. However, in [132], the authors reported that right after the discharge termination, the plasmoid charge was $Q_0 = 4 \times 10^{-6}$ C, and accordingly, we found that the energy of its electric field was equal to 1.1 J. At the same time, according to the authors' observation, in the initial stage of existence (during $\tau = 100$–200 ms), the plasmoid intensively lost its charge because of the corona discharge. Apparently, these can explain that at the moment of its lifting to height where the probe is located (when a wire melts), the plasmoid charge decreases by 99%. From here, an average current of the corona discharge is $I_c = Q_0/\tau = 20$–40 μA. For a sphere having a charge Q, a current defined by air conductivity λ_a is $I_a = \lambda_a Q/\varepsilon_0$ [136]. Hence, $I_a = 1.6 \times 10^{-2}$ μA at $\lambda_a = 3.5 \times 10^{-14}$ Ω/m (a conductivity of dry air) [137] and $Q = 4 \times 10^{-6}$ C. For a "Gatchina" BL, current I_c exceeds I_a by 2,000 times. Apparently, this can be explained by high conductivity of the channel ("leader") connecting the emerging shining formation with the cathode of the installation.

Inconsistency of the results of the measurement of the laboratory BL energy obtained from the results of melting conductors and its electric energy estimation testify that there should be other energy sources in it.

The authors of [127, 138] considered that "Gatchina" shining formations appear "because of structurally-energy self-organizing of a metastable substance on a basis of coulomb and polarizing nonideality of a plasma containing the smallest particles of metal and dielectric. The existence of this nonideality is maintained by catalytic energy liberation in the electric discharge at a decay of chemically active plasma. The majority of large particles concentrates near the external border, forming 'a cold cover', and small particles form 'a hot core.'" "The object luminescence has the chemical nature and, besides elementary reactions of chemiluminescence, is supported by the energy accumulated by particles of an aerosol in the form of vibrational and electronic excitation. It occurs thanks to burning and catalytic reactions on surfaces of particles. To one of channels of liberation of excess electronic excitation serves ejection as dust particles of electrons, ions, excited molecules and atoms by dusty particles."

In [125–135], to obtain shining formations, the electric charge was located on a cover surface. Therefore, it cannot cause the force creating a surface tension. This force could appear, if the charge has been located in the volume limited by the cover [136, 139, 140]. Therefore, the sharp plasmoid's border, most likely, appears because of the vortical movement of heated gas volume rising upwards.

Creators of a new kind of discharge [130] reported that in case the capacity discharge is broken off before the 80th ms when there is a voltage greater than 3 kV on the battery of the capacitors, the second sphere takes off from a copper electrode of the bar closing and disconnecting a circuit of the discharge. The color of both the spheres is approximately identical. On the basis of it, the authors [130] concluded that water in installation only plays a role of variable resistance. This conclusion has found experimental confirmation [141]. It has been shown that the current falls down faster than the voltage of the discharge and the voltage on the water surface at a point located 1 cm from the cathode starts to decrease 50 ms earlier than at a point at 7 cm from the cathode . Besides, it has been found that the shining formations, similar to those observed at a standard "water" configuration of the discharge, appear at short-term short circuit and disconnection of electrodes made of coal, steel, copper, and aluminum or at passing of a current pulse through a glass with metallic sputtering [142, 143].

In 2007, "the Gatchina discharge" was investigated by the German scientists [144, 145]. Their installation was made under the scheme of [125]. The cylindrical vessel of glass or plastic of 25 cm in diameter and height, filled with tap water or distilled water with the salt additive (NaCl or $CaCl_2$), was used. At the bottom of a vessel, the copper ring (anode) was placed, and the central electrode (cathode) acted at some millimeters over the water surface. The battery of the capacitors of 1-mF capacity charged to a voltage of 4.8 kV was connected to the anode through a discharger that produced a current of the discharge from 10 to 100 A. After 100–150 ms, the current was broken off. At the 30th ms after the current interruption, the spherical object with accurate border was formed. In a photograph taken

with large exposure, it looked as a bright homogeneously shining sphere; however, at small exposure in a picture, drop-shaped bright core whose size was two times smaller than the diameter of the sphere, surrounded by a weakly luminescent cover, was observed. Usually, energy about 8 kJ was put in the discharge. Calorimetry demonstrated that the energy spent for heating and water evaporation was about 5 kJ, and the other 3 kJ was spent for the formation of a plasma sphere. About 0.7 kJ (23%) of plasmoid energy went to radiation. The temperature at $t = 235$ ms from the beginning of the discharge appeared equal to 900 K, and at $t = 260$ ms, $T = 600$ K. At $t = 200$ ms, the thermocouple detected a temperature greater than 1,300 K. By means of a probe, the floating potential of a rising plasma sphere was measured, which appeared positive. From the 200th to 300th ms, it was equal to about 0.5 V, and at the 650th ms, it decreased to 0.05 V. This indicates the presence of positive charges in the sphere, also proving the presence of radiation lines of Ca (II) and Mg(II) ions in the spectrum. The radiation spectrum consisted of lines of elements with a small energy of excitation, whereas the lines with energy greater than 5 eV were absent. Therefore, the electronic temperature in a sphere hardly exceeded 1 eV. On the basis of Stark broadening value measurement of hydrogen, Li(I), and Cu(I) lines, it was found that the electron density was about 10^{20}–10^{22} m^{-3} in the initial stage (from $t = 0$ to $t = 75$ ms); however, in the generated plasmoid, it has decreased to 10^{14}–10^{15} m^{-3}. The electron temperature after initial fast falling from 5,000 to 4,000 K smoothly decreased to 2,000 K during the subsequent plasmoid's life. The molecular band of CaOH was a prevailing source of visible radiation. Thus, it is possible to consider that the energy reservoir of radiation is the chemical energy stored in water-dissociation products. Measurements of the laser beam deviation angles at the passage through the sphere volume showed that the average density of the particles in it is approximately eight times smaller than the air density, which follows that the temperature of the sphere substance is $T = 8 \times 273\ K = 2{,}200$ K [145]. It can be observed that the conclusions of [144, 145] are somewhat differ from those of "the Gatchina discharge" study: the sphere temperature appeared greater than that assumed earlier; the sphere charge appeared smaller, and the chemical energy seemed to be the energy source and not the electric one. In this connection, the burning of the sphere with a combustible substance was already considered in [146].

Explosion of Metallic Wires

The authors of [147, 148] got shining formations at the explosion of wires of 0.5 mm in diameter of copper, tungsten, iron, titan, and nickel in small plastic ditch that was filled with mixture of organic material with water. In the ditch, there was a hole through which explosion products could go out to the atmosphere. At passing of a current of 5–20 A through the wire, the wire evaporated, and from the gas that moved through the hole, the shining sphere of 5–6 cm in diameter was formed. The sphere was shining for 2–3 s. Then, the sphere was flattened and gradually turned to a nonshining toroidal ring. It rose upwards – at first quickly, and then slowly – and

its size increased from 5 to 50 cm. According to the authors, the sphere luminescence could not be supported by charges recombination, as the characteristic time of this process was very short. Most likely, the reason for luminescence was the burning of the disperse wire material in the air.

A.N. Vlasov considered that BL represents toroidal current layer induced inside a vortical gaseous ring [149–152]. The toroidal vortex can be formed at the blow of a linear lightning in the earth. For modeling this process, Vlasov undertook experiments on the induction of a strong toroidal magnetic field at the passing of a current pulse through the long wire coil rolled in the torus [153–155]. The winded coil was made of a copper wire of 0.5 mm in diameter. Through it, by means of an electronic key, the capacitors' battery with a capacity of 45 mF charged up to a voltage of 300 V, was discharged. Subsequently, an electric explosion of the coil took place. From the explosion place, the shapeless or pear-shaped body of 15–20 cm in size rose up quickly, and was shining for about 0.3 s. Before decay, the plasmoids took the toroidal form. At explosion of the spiral wire that had not been rolled in torus, long-lived plasmoids with large sizes did not appear.

Microscopic Ball Lightning

In [156], the results of a relaxation of the expanding plasma formed at the high-voltage discharge in water were described. For obtaining the discharge with a duration of 2 μs, Marx's generator with a voltage of 60 kV and an energy of 30 J that has been accumulated in the capacitors was used. The discharge chamber, filled with water, had a volume of 1.5 dm^3. Observation of the discharge was carried out through the windows located on an axis of the chamber. Under the impact of the discharge in water, the pulsating cavity up to 2.5 cm in diameter was formed. It was revealed that sometimes the plasma in the cavity did not disappear, and decayed to separate shining objects from 0.1 to 1 mm in the size. Their number in different experiments ranged from several units to several tens. Some objects went through the cavity walls into a liquid and existed in it for about of 0.5 ms. Research on the formations' luminescence spectrum showed that at the change of wavelength from 550 to 750 nm, the increase in the intensity of luminescence was observed, and the dependence course approximately coincided with a kind of a short-wave wing of a black body spectrum at $T = 2{,}850$ K. However, in the area of wavelengths from 750 to 900 nm, the intensity of radiation sharply fell. In the radiation spectrum, there were no lines and bands of atoms and molecules. The authors considered that the luminescence cannot be caused by the radiation of heated solid particles, as photometric measurements of images demonstrated that shining objects are optically transparent. Subsequently, researchers included a device into the installation, which allowed to throw out products of water plasma decomposition into the air [157, 158]. At the discharge of objects from water, their size increased by three to five times (from 1 to 5 mm), and the luminescence time reached 0.1 s. Sometimes, it was possible to observe how spherical objects are formed during approximately 300 μs from the shining cloud, consisting of water plasma decomposition products.

These objects were destroyed at passing through a zone of hot air ($T = 800$–$1{,}000$ °C), and on the contrary, condensation of objects on the surface of the plate cooled to a temperature of liquid nitrogen was observed. Sometimes, objects blew up, and the scattering parts' speed was greater than 50 km/s. On the basis of the observation over the behavior of these objects, the authors of [158] assumed that they can be the porous friable bodies whose "skeleton" consists of unusual metastable compositions of hydrogen and oxygen. At a transition from metastable to basic state, energy release takes place.

T. Matsumoto [159–161] carried out researches on the spark discharge in tap water and solutions of electrolytes. In one modification of his installation, the wire was used as an electrode; it was made of lead, cadmium, iron, or gold, with a diameter of 1 mm. Its one end was dipped into a solution of KOH (1.5 mol/L) or a carbonate of cesium, Cs_2CO_3 (0.6 mol/L), to a depth of 3 mm. As the other electrode, a box of 25 × 25 × 25 mm in size, made of polished copper plates, was used. The box with the wire into it stood at the bottom of the Petri cup, in which there was a layer of electrolyte of 8-mm thickness. Between the electrodes, pulses of an alternating current with a voltage of 120 V (50 Hz) and a duration of 20 ms were introduced, and the time between the pulses was 20–30 s. Traces of the round form from 20 to 200 μm in diameter were found on the copper plates. The same traces appeared in films with nuclear photoemulsion, which were located around the discharge zone. Matsumoto considered that microscopic BL left these traces. In his opinion, they represent clusters of strongly compressed hydrogen atoms. Binding of atoms in such a cluster is ensured by exchange forces of degenerate electrons' attraction. These clusters are capable to pass through plates made of dielectric, over thin copper wires, jump aside from obstacles, and blow up at the end of its life.

In [162], the results of investigations of electric explosion of metallic foils of 50-μm thickness and 1 × 5 cm size located in the hermetic tank filled with water were presented. Eight tanks were used, in which the discharge energy of 50 kJ at a pulse duration of 60–150 μs was maintained. The spheres of 10–15 cm in diameter appeared over the tanks at the discharge, and they were lighted for 5 ms. In the photos of frame-to-frame shooting of the process, it was possible to see that the originally diffuse luminescence of spheres changed to radiation of the bright particles filling their volume. This can explain the process of condensation of metal vapors' plasma, which penetrated into the atmosphere through the destroyed vacuum sealing of the tank.

In [163], "strange tracks" of the shining particles created by the pulsed erosive plasma generator in external electric field were observed. The size of the particles was 10–100 μm, they moved with a speed of 20–200 km/s, possessed an electric charge, and at impact with a target, emitted soft X-ray radiation directed forward. The characteristic time of these particles' luminescence (∼1 s) considerably exceeded the luminescence time of the cluster plasmas when it was discharged from the plasma generator (∼10 ms). The shining particles flew off the capillary dielectric channel of 1–2 mm in diameter with the walls made of organic glass, paraffin, or wax. They could be collected in a ditch with liquid nitrogen. The analysis demonstrated that they consist of pyrolitic graphite. In another experiment,

in a stream leaving the channel, the aluminum powder with the grains of size 10–100 μm was admixed. When they were discharged from the nozzle, these particles burned. They appeared negatively charged and sometimes blew up because of Coulomb's forces. In a spectrum of burning aluminum particles along with the lines of Al and AlO, the lines of Na, Li, and K were observed, and the last ones appeared with a delay greater than 10 ms. Radiation in quasi continuum in the spectra amplified approximately during the same time, corresponded to the equilibrium radiation of heated solid-state particles.

Experiments on Modeling of Ball Lightning Features

Along with the above-described attempts to obtain an artificial BL in laboratory, experiments on modeling its separate properties by means of known scientific and technical processes have been increasing. Among these properties accessible to experimental verification, there were cases of its interaction with windowpanes and features of its movement over the conductors.

There are many reports on the ability of BL to cut out round holes of 5–8 cm in diameter in glasses, and sometimes, there are no cracks both in the cut-out disk and in the glass that remained in a frame [11, 18, 32, 42, 76, 164, 165].

In [166], the case when the BL, in the presence of a group of schoolboys during a lesson, heated up a window glass, forming hole was presented. On the basis of this observation, the author of [166] undertook experiments to obtain holes in the glasses through their local heating with the help of a beam of laser on carbon dioxide, with a power of 500 W, or with a flame of a gas torch. The glass was heated up to the fusion of an aperture in it. After that, the heating source was switched off, glass was cooled, and a round crack covering a zone of fused glass in it appeared. The diameter of the crack exceeded the diameter of a heated-up zone approximately by 1.4 times. To heat the glass to fusion, it was necessary to spend energy of about 20 kJ. In these experiments, it was important to heat the glass area to a softening that removed the stress of compression from other parts of the glass. At smaller power of heating, the glass sprung. The results obtained in [166] do not absolutely correspond to those of BL's influence on glass, because in the latter case, burning-off of a disk is not observed and there is no aperture in it.

This finding stimulated the authors of [167–169] to carry out experiments to study the heating influence on windowpanes. Glass of 3.7-mm thickness was heated up by a flat spiral of a nichrome wire of 0.7-mm thickness. The external diameter of a spiral was equal to 40 mm, which contained 3–5 coils. The spiral was heated up using an alternating current (50 Hz) to red or yellow heat. At values of the energy from 12 to 24 kJ spent in heating the spiral, the glass got destroyed with the formation of radial cracks, and at the heated place, there was a round or oval piece of glass. It had the form of the truncated cone, and the cone base was turned towards the surface that was heated up by the spiral. However, in one of the experiments, both a round disk and other part of the glass practically remained intact. In this case, on the brink of the glass, there was occasional crack nucleus.

After 11 s following glass heating by a spiral fed with power of 260 W, the crack from edge extended to a heating zone. After 5 min of heating, the current was switched off, and the glass started to cool. During the course of cooling of the glass, there appeared a ring crack whose diameter (50 mm) exceeded the diameter of an external coil of the spiral by 1.25 times. Simultaneously, in an external part of the glass, the second crack with its edge going tangentially towards a ring crack was formed. Similar kind of cracks could be observed in some pictures of the glasses that were affected by BL [32, 42, 164]. However, full identity of results when without cracks remained both a disk, and the glass with a hole, it was not possible to achieve in experiments.

The important property of BL, which can serve as a criterion for an artificial and natural BL identity is its ability to move in a horizontal direction over a conductor surface. In [136, 139, 140], the hypothesis that it is possible to explain such BL behavior through the interaction of alternating magnetic fields generated by currents flowing in a substance of BL with magnetic fields of eddy electric currents induced in conductors, was stated. The results of the experimental verification of this hypothesis were described in [170, 171]. The value of the force that pushed away the coil fed by an alternating current with a frequency of 440 kHz from a copper plate was measured. The coil from three densely laid loops of a copper tube of 3 mm in diameter with an external diameter of $D = 52$ mm was used. The water stream that passed in the tube cooled it. The coil was connected to the high-frequency generator with a limiting power of 10 kW. The tubes connecting the coil with the generator simultaneously played the role of a spring, which at displacement of the coil along an axis to 10 mm, had no residual deformation. The coil was located at some distance l from the copper plate of 24 × 14 cm size and 2-mm thickness. The plane of loops of the coil was parallel to the plate's plane. It was found that the force F that pushes away the coil from the plate appeared proportional to the square of the value of the current flowing through the coil ($F \sim I^2$), and was inversely proportional to the seventh degree of distance l (mm) from the center of the coil to the plate's plane ($F = K/(b + l)^7$, where the current was $I = 26$ A and the coefficient was $K = 3.7 \times 10^7$ mN mm^7, and $b = 4.5$ mm). Because of the sharp dependence of the force F on the distance l, it appears to be appreciable only at $l \ll D$; however, it sharply decreased at $l = D$. Therefore, the mechanism of the interaction of currents cannot explain the cases of BL levitation over a conductor at the distances equal to its several diameters.

In this connection, in [170, 171], the assumption has been made that the presence of the corona discharge on BL surface might be the reason for its levitation. This discharge appears because of continuous leakage of a part of BL charge to the atmosphere. At the corona discharge in the restricted area of space near an electrode (in an ionization zone), there exists neutral plasma in which ionization and excitation of a gas by electron avalanches occur. From the ionization zone, the flux of charge carriers whose sign coincides with a charge sign of the corona-forming electrode moves to an external zone. The space charge formed as a result of it decelerates the further development of the ionization processes, weakening the field near the ionizing electrode. It leads to localization of the ionization zone near the

electrode. Thus, the corona-forming sphere appears surrounded by a "fur coat" of charges whose sign coincides with the sphere sign. If the sphere is at a large distance from the conductors, then this "fur coat" envelops it uniformly. However, when the sphere approaches a conductor, the cloud of the space charge moves to the area between the sphere and the conductor. As a result, the "pillow" weakening the attraction of the sphere charge to a charge of an opposite sign, induced in a conductor, is created.

The experiment of George S. Piggott confirmed the subjects' levitation possibility owing to corona discharge, as described in [79, P. 192–195]. Piggott observed a levitation of a silver ball weighing 1.3 g in an electric field of a sphere of 10 cm in diameter, charged up to a voltage of 500 kV. The distance from the center of the sphere to the floor was about 50 cm, and the ball was hanging half of this height. In [172], experiments on levitation observation of corona-forming spheres in the field of the flat condenser were described. The sphere of 12-cm diameter was made of a steel microwire of 20-μm thickness, the weight of the sphere was 0.03 g. Vertically directed electric field was created between two parallel metal disks of 120-cm diameter, being at the distance of 100 cm from each other. Negative voltage of 20–160 kV was put to the top electrode, and the bottom electrode was grounded. At voltages above 60 kV, the corona appeared on the sphere surface and it made fluctuations in a vertical direction, not touching the electrodes, or hung at some height between the electrodes. At distortion of the field uniformity, one could observe the sphere aspiration to be drawn into an area of stronger field. On entering several (two or three) spheres into the condenser, they were lined along one vertical axis, and connected through the common ion current, made group flight in a horizontal plane.

In [173], measurements of the weakening force of the flat capacitor plates' attraction in the presence of the corona discharge in space between them were carried out. The electric capacitor consisting of two duralumin disks of 12 cm in diameter was used. The top plate was hung on the shoulder of the scale's balancing arm. To other shoulder, the steel rod, which could be drawn in the solenoid was hung. By measuring the current at which the rod was drawn in the solenoid, it was possible to define an attraction force of plates of the capacitor. In the top plate, there were compressed sewing needles (90 or 420 units) coming out of it at a height of 5 or 8 mm. The surface of the plate with needles was faced inside the capacitor. The distance between the plates varied from 4 to 7 cm, and a voltage on the top plate changed from 0 to 30 kV. At values of $U < 15$ kV, the attraction force F of the capacitor plates increased proportionally to a square of the voltage U^2. However, after reaching the corona discharge ignition conditions (at $U = 15$ kV), this force became smaller than those defined by the law $F \sim U^2$. Also, it was revealed that the attraction force of plates started to increase quickly at $U = 25$ kV. The ion wind creating rarefaction under the top plate of the condenser might be the reason for this. However, after 88 holes were drilled in the plate, this effect was gone (Fig. 6.6). On the basis of these experiments, the force ΔF decreasing the attraction of the plates owing to the presence of the corona discharge $\Delta F = zU^2$ ($z = 4 \times 10^{-12}$ N/V^2) was found. It was assumed that if this dependence remained at potentials $U \gg 30$ kV;

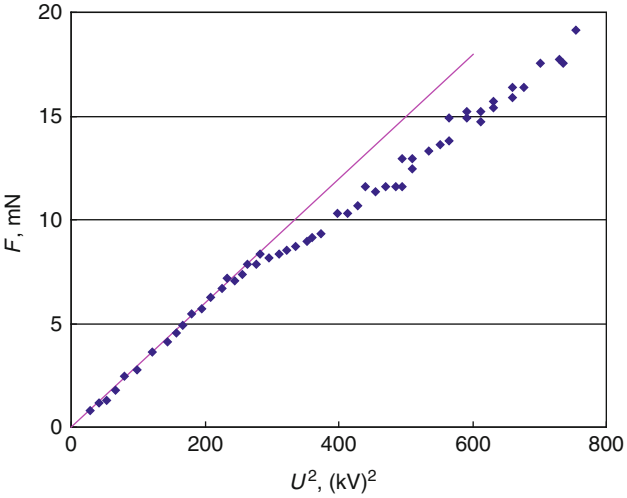

Fig. 6.6 The dependence of the attraction force F (mN) on a voltage square U^2 (kV^2) for the plate with 90 needles and 88 orifices [173]

the results of the experiments allowed to provide an explanation for BL levitation over a conductor surface at the heights exceeding a value of its several diameters.

In the first part of the review, we discussed a case when BL with a "boiling" surface from which substance fountains were thrown out was observed [63, 174]. Thus, it could be assumed that the BL surface can possess properties of a liquid, and dynamics of its surface can be defined by the electric field of a unipolar charge of BL. For studying the behavior of the surface of the liquids in the electric field, the authors of [175] have carried out experiments on corona-discharge influence on tap water, double distilled water, ethyl alcohol, glycerin, kerosene, and a mixture of alcohol with water and glycerin. The liquid was poured into the flat vessels of the rectangular or cylindrical form made of a dielectric or steel. More often, the positive voltage from the rectifier (3–50 kV) was brought through the resistor of 100–300 MΩ to a liquid through an electrode sealed in a wall of a vessel, and the negative electrode (cathode) was placed over a liquid surface at a height of 5–15 mm and was inclined to it by 40°. The diameter of the cathode was 3 mm, which sharpened under a corner of 30°, and the radius of its rounding tip was 0.4 mm. For a more exact definition of the moment of breakdown between the electrodes, the capacitor with a capacity of 500 pF was included. The breakdown moment was detected by the occurrence of a spark between the cathode and liquid surface, as well as by a sharp reduction of voltage on the capacitor.

At the ignition of the corona discharge on the surface, there was a funnel of a rotating liquid, which may be due to the ion wind. When the negative corona voltage increased, streams started to be thrown out from the funnel edges (see Fig. 6.7). These streams sometimes turned to the liquid columns whose tips were shining with a violet light. At the voltage above 15–25 kV, the liquid surface started

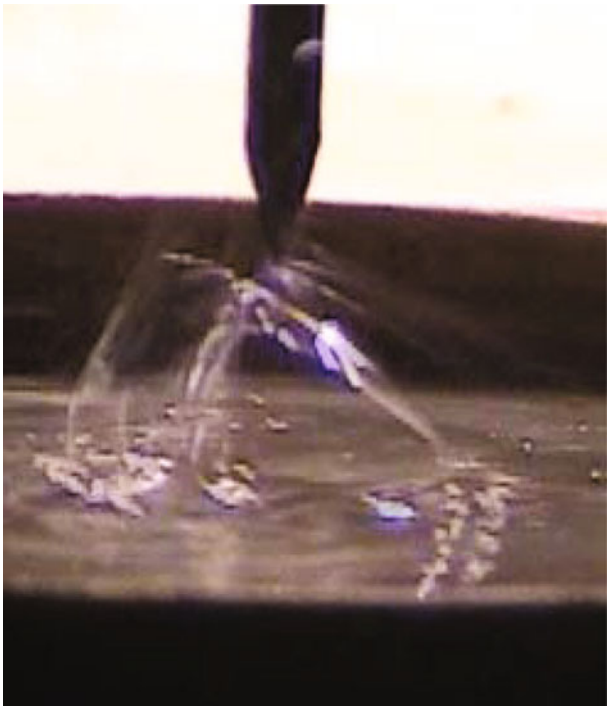

Fig. 6.7 Appearance of bursting streams over a surface of alcohol under a corona discharge [175]

to shake, and there was a breakdown in the formation of the plasma channel (Fig. 6.7). The authors of [175] explained the occurrence of streams and disturbances of a liquid by developing Tonks–Frenkel instability of the charged surface. A field strength, at which there is instability, is greater for liquids with greater densities and forces of surface tension; therefore, instability easily develops on an alcohol surface than on a water and glycerin surface. The bursting of streams observed in the experiments is connected with the development of charged drops' instability. Thus, if the BL surface represents the unipolarly charged liquid, then one can observe streams, columns, and bursting of streams because of the development of hydrodynamic instabilities on it.

Intermediate Conclusions and Perspectives of Future Experiments

Apparently, within the last decades, many qualified researchers worked hard to create laboratory analogs of BL. It has led to the finding of new properties at known electric discharges and creation of new types of discharges. However, in no case it was possible to obtain shining object with the properties of natural BL. We presume that in future work, it is necessary to consider two circumstances. The first – it is

necessary to search and experimentally model only systems that *basically* consider the possibility of considerable quantities of energy concentration in small volumes. It will allow to considerably narrow a circle of searches and to concentrate efforts to studying and creation of systems with high density of energy. The second – it is necessary to shift from creation of equilibrium systems (or close to equilibrium) to essentially nonequilibrium systems capable of self-organizing. Therefore, with the generation of objects with properties of BL, it is necessary to not only provide sufficient energy store in them, but also conditions of their ordering (entropy decrease).

It is necessary to thoroughly analyze cases when objects with properties of BL appeared as a result of "extraordinary" work of electric installations with certain parameters. In the first part of our review, we have mentioned two cases of formation of BL at short-term distortion of contact of a pantograph bar of a trolley-bus with a contact wire [42, 176]. Trolley-buses use a direct current of about 200 A at a voltage from 500 to 750 V, and a current collection is carried out by carbonic-graphite brushes [177]. Reproduction of discharges with the specified range of voltage and currents is not difficult in laboratories. Moreover, the specified cases indicate that the threshold value of the current necessary for the creation of BL is much lower than 156 kA, required to start the process of "bosonization" of electrons [82]. It is interesting to carry out the analysis, and probably, reproduce the experimental conditions when the plasma bunch that has got into a vacuumed plasma gun, initiated an origination of a fireball [178]. It is also interesting to define the physical nature of "microscopic fireballs," appearing in the discharges in water [156–161]. It is necessary to continue research and modeling of traces of BL's impact on material objects, in particular, on glasses. It is interesting to understand how holes are formed with the separation of thin edge on the edge of the hole, and what is the reason for the change of element structure of the glass coming into contact with BL [76].

6.1.4 Development of Ball Lightning Theory

Usually, development of scientific idea goes under the following scheme: an idea → a theoretical model → an experimental check of the idea, etc. With respect to BL, the first part of this chain − formation of an idea, which in this definite case, was shown as data gathering about the characteristics of the observable phenomenon − has developed more or less safely (see Section 6.1.2). Numerous researchers have worked in this area and are still working. The data obtained by them have been rechecked, and most importantly, are not lost, but are constantly replenished. In some measures, it concerns the last link: experiments on realization of "fire balls" (which is unrelated to BL) are repeated regularly and checked. The middle link of this chain drops out of an overall picture and stands independently. In most cases, each new model of BL does not arise as criticism or development of existing models, but as though from nothing. This, in turn, remains almost unnoticed (neither critics nor potential followers) and dies along with its author. Besides,

each model is capable to explain only a limited number of BL properties. Authors, as a rule, also do not try to cover all the BL properties, leaving the final "finishing" of the model to the descendants. And, at last, there is another extreme: aspiration to reduce BL problem to even more difficult unresolved problems (to dark energy, black holes, an antimatter, etc.), transforming it into a certain place where all unclear concepts are "merged."

We will try as much as possible to understand the reasons for such a state, and to realize whether there is "light in the end of a tunnel," leading to the creation of BL theory. Following our scheme, along with other two directions – data gathering of observations and experiments – let us take a look at the history. We should remember that because of the above-mentioned continuity absence, the concept of historicity concerning BL theory works is relative to a considerable extent. Following our scheme, we will first speak about the theoretical works executed before 1988 (year of the First Symposium on Ball Lightning). Then, we will get acquainted with the reports on the theory made on this symposium. After that, we will look at what has occurred in this area during the next 20 years. Basically, the time boundary dividing works on the BL theory might not be 1988, but 52 years earlier, in 1936, when for the first time, an extremely large energy content of this natural formation was found out experimentally. However, up to 1998, this observation either remained unnoticed or was announced doubtful [29, 30, 48].

6.1.4.1 Ball Lightning Models Created Before 1988

The review of early theoretical approaches to the BL problem solution can be found in monographs of Brand [11], Singer [18], and Stenhoff [48]. It is natural that till "fatal" 1936, BL model suited everything that could explain the existence of the spherical object radiating light during tens of seconds. Stenhoff [48, P. 179–180] gave a rather uncomplimentary appraisal to research approaches to create the BL theory. He considered that prior to the beginning of the work of BL Symposia, "theoretical proposals were initiated by publication of quite brief and tentative papers stimulating an occasional letter by way of debate. Some of these papers could better be described as light-hearted musings rather than disciplined contributions to discussion." The majority of the theories contain essentially weak positions. "The most serious ... is that many theories do not correlate with observational evidence. Some theories predict overt behavior by ball lightning that is simply not reported by eyewitnesses. Equally other theories fail to predict frequently reported observational characteristics of the natural phenomenon." Despite the demonstrated severity, Stenhoff [48], for the first time in BL studies' history, gave the fullest review of works on search of approaches for the creation of its theory. Owing to space constraint, we will present only a short abstract of his analysis.

Similar to Brand, Stenhoff divided BL theories based on the characteristic of whether they have an internal energy source or get energy from an external source. The simplest BL model with an internal energy store is a sphere of heated air. For the sake of justice, it is necessary to remind that comparison of a fireball with

club of air heated by the energy of nuclear explosion has been made by Kapitsa [83] in 1955. He came to a conclusion that a sphere of air of 20 cm in diameter, originally heated to a temperature of 10,000 K, should be cooled to a temperature below 6,000 K during the time of about 10^{-2} s. On the basis of this, he concluded that the existence of BL with an internal energy source is impossible, and it can live only owing to an energy supply from the outside. From the logic point of view, this conclusion is incorrect: there was a thesis substitution in it, and a particular aspect was replaced by the general one. Kapitsa *only* proved that independent existence of BL in the form of heated air sphere is impossible.

Uman and Lowke returned to the idea of BL in the form of heated air area, in 1968 [179], and calculated that cooling speed of heated spheres decreases during the process of their temperature fall. Thus, cooling of a sphere of 20-cm diameter, originally heated to $T = 10{,}000$ K, in a range of temperatures from 3,000 to 2,000 K should occur in 4 s. Thus, the radiating ability of a hot body is proportional to T^4. However, the considered model cannot be connected with BL, not only due to a fast reduction of its luminosity, but because the cloud of hot gas should necessarily float in air and cannot have a distinct border.

Bostick [180, 181] experimentally obtained plasma structures (plasmoids) that were kept by their own magnetic field for a short time (some ms). It served the beginning of BL plasma model creation, which was appreciably supported by the development of works on magnetic confinement of hot plasma for thermonuclear fusion of light elements. V.D. Shafranov theoretically considered the balance conditions of magneto-plasma structures and demonstrated that spherical plasmoid, defined as the self-limited clot of electromagnetic energy, cannot exist without the compressing force directed to its center, for example, gravitation [182, 183]. If the atmospheric pressure is such a force, then the energy of the plasmoid of 10-cm diameter cannot exceed several hundreds of joules [184, 185], and according to the virial theorem [186], this means limiting of the plasmoid energy density by $\rho_E = 2.5 \times 10^5$ J/m^3.

Attempts to find a force, which along with atmospheric pressure would promote confinement of the plasmoid in the limited area of space, have been undertaken. Wooding [187] assumed that BL can be a vortical plasma ring in which centrifugal force is counterbalanced by pressure force of the captured magnetic field. Bergström [188] stated that plasmoids from expansion, except magnetic forces, can keep short-range forces of dielectrics' attraction to diamagnetics.

Another mechanism that can promote the creation of forces keeping from the scattering system of charges is the quantum mechanical exchange forces. Neugebauer [189, 190] demonstrated that such forces can arise in neutral plasma if the density of the electrons in it is high (not less than $n_e = 2.7 \times 10^{25}$ m^{-3}), and its temperature T_{ex} is low (not above 600 K). Considering that for electron separation from an atom, it is necessary to spend about of 14 eV energy, Neugebauer found that in such a disordered system, the density of the internal energy will be equal to $\rho_E = 6.7 \times 10^7$ J/m^3. Neugebauer's model was developed by G.C. Dijkhuis, who replaced it with the ordered system of vortical tubes of quantum mechanically connected electron pairs,

around which positive ions rotate [82, 191, 192] (we will discuss the Dijkhuis model in more detail later).

The search for the conditions promoting the preservation of the plasma formation's spherical form and restraint of its expansion, as well as the fact that BL was often seen rotating, has guided some researchers to a thought that it can be a whirlwind of the spherical form (a whirlwind of Hill [193]). This whirlwind of ionized air can arise because of a gas stream in the channel of a linear lightning if there are opposite-directed channels [37, 194] or the channels have a sharp bend [195]. Some models where the fireball was considered as "a bubble filled with radiation" – a cover of highly ionized gas, in which strong superficial current flows were proposed. This cover keeps in itself the powerful resonant high-frequency radiation reflected from walls of a cover [196]. The pressure of radiation upon a cover wall is counterbalanced by the atmospheric pressure; thus, the energy of radiation for a sphere of 10 cm in radius does not exceed 400 J ($\rho_E = 10^5$ J/m^3). Endean [38], independent of Dawson's finding [196], proposed a model according to which BL consists of electromagnetic field enclosed in a vacuum spherical cavity, separated from the atmosphere by a cover of the ionized gas. According to him, the stability of the cover is provided by the quickly rotating magnetic field.

Unlike the above-mentioned models, where it is assumed that BL in the course of its life only spends the energy obtained by it at the moment of formation, in other models, it is supposed that it obtains the energy continuously from chemical reaction. As mentioned earlier, the first who admitted that such energy source existence is possible in BL, was Lomonosov [9]. In 1838, Arago published an article [10] in which the BL-energy source was considered to be the burning of the substances that appeared in air under the influence of the linear lightning discharge. Later, some power-intensive compounds were proposed: nitrogen oxide (NO) [197], ozone (O_3) [198], and a mixture of hydrogen with oxygen [199–202] or with nitrogen oxides [203]. It was also considered that organic substances and gases, which are constantly present in air – as the products of rotting of the vegetative remnants and methane coming out of the earth [35, 204, 205] – could be the fuel delivering BL energy. It was supposed that condensation of the charged particles of dust, droplets, and aerosols can result in BL formation [206–209].

Estimations show that none of the above-mentioned models could explain the origin of high specific energy content of "Dorstone" BL [13, 14] ($\rho_E = 10^{10}$ J/m^3). Alternatively, models with a nuclear energy source, which could explain such high density of energy were proposed. An assumption was made that under the influence of strong electric fields in the channel of a linear lightning, there can be an acceleration of the charged particles and formation of neutrons. Neutrons, reacting with nitrogen nuclei ^{14}N, can form nuclei of radioactive carbon ^{14}C with a half-life decay period of $T_{1/2} = 5{,}570$ years [210]. Fast protons (1 MeV), facing oxygen nuclei ^{16}O or nitrogen ^{14}N, can form radioactive isotopes ^{17}F ($T_{1/2} = 66$ s) and oxygen ^{15}O ($T_{1/2} = 124$ s), which decay with the emission of positrons [22]. The model of BL with a nuclear energy source, basically, is capable to explain its high energy content and comprehensible lifetime, but is ineffective to explain something about the

electric effects caused by it and about the features of its movement. Besides, such fireball should be a source of high radiation that took place only in several cases [40].

The authors of other models (also low energy ones) considered that BL energy is reserved in electric field of the separated charges. For the first time, an idea that BL is the natural electric capacitor (Leyden jar) was stated by Tessan [211]. Other researchers considered BL as the sphere filled with positively and negatively charged droplets of water, separated by an insulator – water steam [212]. In some models, molecular ions were considered as carriers of charges, and BL was considered to be similar to "a tiny storm cloud" [213, 214]. Stakhanov assumed that recombination of ions of a different sign can be suppressed, if ions are surrounded by covers of water molecules [29–31, 215].

For models with an external energy source, there are no difficulties connected with the virial theorem (which are caused by necessity to constantly store the large amount of energy in BL). Such BL should have the source located outside, from which they obtain energy for the maintenance of their luminescence. However, these models experience difficulties in explaining the cases of allocation of considerable quantities of energy at BL explosions, the electric effects, and trivial properties such as fireball movement (especially – in a vertical direction) and its occurrence in the closed premises.

The energy supply to BL from an external source can occur in the form of constant or alternating current. In the model developed by Finkelstein and Rubinstein [184], it was supposed that BL is the localized glow discharge fed by the currents flowing in the atmosphere. According to this model [185], BL appears as the rest of a linear lightning discharge or St. Elmo's fire. If the intensity of the electric field near the channel after the termination of the lightning discharge exceeds the value of 100 kV/m in the area of ionized gas, then the Tawnsend process of reproduction of charges of a different sign will occur, which, under the influence of a field, will flow down from a sphere in the opposite direction. Because of the electrons' higher mobility, the sphere will be charged positively. After that, the cloud of the positive space charge, which flows down from the sphere, will start to contain electrons in it from the space area, which is much larger than the sizes of the cloud. This model describes the fireball passage through the glass as follows. As electric field lines of a cloud charge penetrate the glass, the charges of a different sign gather on the opposite side of the glass. In the BL approach, the glass is heated up, becomes a conductor, and is broken down. The current passes through the glass, and a sphere, having separated off the glass, is formed indoors.

Kapitsa [83] proposed the BL concept as high-frequency electric discharge in air, which arises in the field of a standing electromagnetic wave. Based on Kapitsa's estimations, BL diameter D and a wavelength λ of radio-frequency radiation feeding it are connected by the relation $\lambda = 3.65 \cdot D$, and the discharge appears in a loop of a standing wave. Starting from a range of a typical BL size of (D = 10–50 cm), an area of radio frequencies f can be defined as f = 160–820 MHz. Later, it was shown that BL, having arisen in a loop of wave, should move to wave knot under the action of pondermotive forces, where it is maintained owing to the balance of radiating and atmospheric pressures [216, 217]. The basic difficulty

for a substantiation of Kapitsa's theory is the absence of any appreciable continuous radio-frequency radiation in the indicated wavelength's range (from 37 to 183 cm), and investigations have given a negative result.

All the above-mentioned models has appeared that scientific reserve in development of BL theory by the beginning of the First International Symposium on a Ball Lightning in 1988. Now, we will describe the works on BL theory discussed at this symposium.

6.1.4.2 Works on Ball Lightning Theory Represented at the First Symposium on Ball Lightning

Earlier, we presented reports in which the results of BL observation were discussed and we observed large consistency and reproducibility of the obtained data. On this background, works on the theoretical research on a BL problem looked inadequate at the symposium. Apparently, as stated in the previous section, instead of the allocation of key BL properties and work on "quality" increase (deep elaboration of models), the activity, basically, has poured out in "quantitative" increase in a number of models describing only separate features of the phenomenon. Some researchers employed a combination of different models. A typical example of such association is the report by K. Nickel (Germany) at the First Symposium [1, P. 177–191]. He considered that BL represents a sphere of rotating air, gas, or plasma, which is kept by the hydrodynamic forces operating in Hill's whirlwind or in a smoke ring of the smoker. Its luminescence and heat allocation is made by burning chemical process of the gases captured by a sphere. BL creation is initiated by the blow of a usual lightning, which transfers the moment, kinetic energy, and electric charge to BL. Nickel's model is presented in traditional for BL theory developers manner – at the level of declarations that have not been confirmed even with simple estimations after completely ignoring the properties of the real BL obtained by the analysis of thousands of observations. Hence, with regard to BL charge, he estimated its potential U as 10^6 V and more, without explaining how this potential was retained by this system. It is known that the electric capacity C of a sphere $D = 0.2$ m in diameter is $C = 2\ \pi\varepsilon_0 D = 10^{-11}$ F, and its charge is $Q = C{\cdot}U = 10^{-5}$ C. The energy of the sphere's electric field is $W_E = CU^2/2 = 5$ J, which is obviously insufficient to cause appreciable actions – fusion of wires or other destructions. An extremely unpersuasive reasoning is that BL, for maintenance of burning in itself, can collect fuel from car exhaust gases.

B.M. Smirnov (USSR) [1, P. 192–228] considered that the BL problem "cannot be solved on the basis of successful idea" … "Because of complexity of this multilateral phenomenon in order to become successful, it is necessary to divide a problem into separate elements and to investigate each of these elements." The main BL problems, in his opinion, are the structure of BL substance; processes of storage and energy transformation; chemical, thermal, gas-dynamic, electric processes, and radiation mechanism. As an example of such an approach to a problem, he considered BL phenomenological model with substance comprising separate threads or,

more precisely, fractal clusters. The waves of the chemical reaction propagate along the threads, accompanied by a luminescence of hot zones. These waves can be transferred to the subsequent threads. This chemically active substance is similar to a pyrotechnic mixture. BL possesses the firm framework similar to the aerogel; the specific density of this framework is approximately equal to the specific density of air. The active combustible substance is located in the pores of this framework. Owing to the active substance's chemical reaction, there is a release of heat and heating of air in BL to a temperature of some thousands of degrees. As a result, the BL shines as a black body, and its color is defined by impurities, giving color to the burning of pyrotechnic mixture. The framework bears an electric charge on itself, which is about 10^{-6} C, which provides its strength, and vibrations of the ends of the charged threads are a radio-radiation source.

There is nothing reprehensible in the represented approach: everyone has the right to propose an idea and to build the BL model on the basis of this idea. However, it is necessary that conclusions of this model coincide with the properties of a real BL. Unfortunately, it is impossible to imply this on fractal BL model. Its charge is very small to be dangerous to the person, whereas there are many cases when the opposite was observed. The energy stored in such BL is chemical energy of several grams of solid fuel; therefore, it cannot cause the destructions left by BL and is substantially less than 20 kJ, which are allowed for an "average" BL.

A detailed description of Smirnov's idea has been represented in the book [146]. In an explanation of the nature of BL's electric action, he is in agreement with Stakhanov's explanation. He considered that "in these cases electric energy is taken from an external source (a cloud or a dust cloud), and BL is a conducting body which creates initial ionization of air and transfers energy of the external source" [218]. From our point of view, it is impossible to imagine that the ephemeral object with a charge of 8×10^{-7} C and energy which "is possible to provide approximately by 10 matches" is capable to impact the linear lightning, transferring a charge of tens of Coulomb and energy of thousands of megajoules.

H. Jamamoto's report [1, P. 229–241] at the symposium is a fresh sight at BL problem of the person working in another area of physics which has gotten acquainted with the discussed problem only recently. He had an impression that based on the observation, it is possible to draw a conclusion that there are many types of fireball. Therefore, in his opinion, "it is impossible to explain all properties of BL within the limits of one model." He also considered that a statistical analysis of observation results could lead to an exclusion of the important information of consideration. Therefore, he considered that it is much more useful to publish original reports of witnesses, and leave the right to make conclusions to the readers. Personally, he proposed a BL model in the form of a combination of a ring electron current and electrons, moving on a surface of the torus whose axis is the above-named ring. He considered that the full charge of the system is equal to zero, indicating that there are also positive charges besides electrons. However, how they move, how collisions of particles with air are eliminated, and how

recombination charges of a different sign is prevented, have not been discussed in the article.

G.P. Gladyshev (USSR) [1, P. 242–253] considered that high-temperature physical and chemical processes serve as BL-energy source in thunderstorm atmosphere. Under the influence of lightning discharges in it, combustible components, such as nitrogen oxide and ozone, are formed, which can react with the oxygen of air with heat release. BL is formed as follows. Under the influence of the lightning discharge in some part of space, the concentration of ions increases and the temperature raises, indicating that conditions for a flame ignition are created. This flame takes the form of a sphere and continues to be supported by the direct currents flowing in the atmospheric air. Necessity of their presence is caused by the fact that heat of oxidation reaction of strongly diluted combustible gases does not suffice for the maintenance of temperature of a zone of reaction even at a level of 600–700 K. Thus, it appears impossible to create a purely "chemical" model of the phenomenon without the presence of an external energy source. External currents heat up a sphere to temperatures at which burning and synthesis of nitrogen oxide (NO) begins. Heat of the reaction is transferred to an environment, and inside BL, a quasi-stationary distribution of temperatures is established. The author considered that "reduction of atmospheric currents force leads to going out of BL, and, on the contrary, at critical values of the discharge (during a thunderstorm), there can be an explosion or the discharge of a linear lightning (spark, arc) to huge release of energy. It is obvious that though the BL has a rather small store of internal energy, it can initiate high-energy discharges in atmosphere." Again, for some reason, without any substantiation, properties are imposed to the nature, which it never shows! The author recognized that the part of the concepts, which have been employed in its model, was proposed earlier by other researchers. However, nobody had proposed any physical and chemical mechanism of ion formation and maintenance of the level of charge concentration in BL.

In 1955, Kapitsa proposed a model of BL fed by radio-frequency radiation of a linear lightning discharge [83]. As discussed earlier, the basic problem of this model is the search of the energy source supporting BL during the time between the two lightning strokes. However, P. Handel (USA) [1, P. 254–259] found this source. In his opinion, under the influence of the strong electric-field short pulse generated by the linear lightning discharge, a population inversion between the pairs of rotation energy levels of water molecules takes place. It leads to the formation of an atmospheric maser with a huge volume of active medium – 10^2–10^9 m^3. Owing to the maser radiation under a cloud near the earth's surface, the standing electromagnetic wave is formed. If at some point, there is a coincidence of local plasma frequency of ions and the maser frequency, then it will cause local increase in the intensity of electric field. It, in turn, will create pondermotive forces, which will "pump out" ions from the area with a strong electromagnetic field, thus creating a cavity in the plasma. It will result in the formation of the so-called "caviton" – a practically empty sphere containing only a resonant electromagnetic field and ions. Thus, "the caviton is a stable quasi-spherical configuration of the captured electromagnetic field surrounded with plasma. It moves horizontally

at a loop level of a standing wave and manifests, as BL." Handel represented the equations describing the process of population inversion creation in the two-level system under the influence of resonant high-frequency radiation pulse; however, for some reason, there are no terms in them, which are considered to be responsible for the relaxation of excited water molecules at collisions with the molecules of air. The equations describing the caviton formation in the atmosphere were also represented.

According to H. Kikuchi (Japan): [1, P. 288], now the theory of a lightning and electric discharges is at an initial stage and requires development. For its development, the following are necessary: (1) Definition of more exact laws of electrostatics and electromagnetism; (2) Working out of the new theory of plasma in which the dominating role is played by collisions; and (3) Creation of a new scientific area – of electro-magneto-hydrodynamics (EMHD), which combines the physics of plasma and meteorology. According to this approach, for the solution of a BL problem, it meaningful sense to bring three new concepts into the theory of the electric discharge: (1) process of reconnection of the electric field lines, similar to the phenomenon of reconnection of the magnetic field lines, leading to solar flashes; (2) the theory of critical speed for gases, in which the dominating role is played by the processes of collisions, similar to Alfven critical speed; and (3) the account for pondermotive forces.

P.M. Koloc (USA) [1, P. 289–309] considered that BL represents the steady plasma configuration, which he termed as the "Plasmak". "Plasmak" grows out of evolutionary development of hot plasma magnetic confinement systems, and Tokamak was the first to be developed [219, 220]. In the Tokamak, the toroidal chamber, filled with plasma, represents a secondary winding of the transformer. Under the influence of a vortical electric field on an axis of the toroid chamber, the current flows through the chamber, which creates a "poloidal" magnetic field (in which field line flows are similar to that wound on the torus generatrix). For plasma confinement on a toroid axis in Tokamak, the "toroidal"magnetic field created by a current through a wire wound on the toroidal vacuum chamber is used. Lines of this magnetic field go on an axis of the torus that remains along the current lines in plasma. As a result, the configuration of "magnetic fields, free from forces" appears. It is possible to replace the toroidal metal chamber with the spherical one for the creation of the magnetic field, and by keeping the charges on an axis of the toroidal area of plasma, it is possible to use the vortical currents flowing in the walls of the chamber. Such a configuration has been named as "Spheromak" [221]. In the "Plasmak" of Koloc, the metal spherical chamber is replaced with a cover of plasma [222]. According to Koloc, BL consists of a core (Kernel) – a toroidal ring of hot magnetized plasma and a cover (Mantle) – a shell in the form of a plasma layer with high conductivity. It is considered that the current in a shell is supported by relativistic electrons. Magnetic lines of the field, created by the current flowing on a ring axis, go to infinity on a ring axis. Therefore, on the shell's "poles," hot electrons can leave the system, and it should have ledges on the poles. To confirming his conclusion, Koloc used a photo of the elliptic BL (see Fig. 6.1). As mentioned earlier, elongation of the image in a photo, most likely, has been caused

by BL movement at shooting. The typical form of BL, according to a overwhelming number of supervisions, is the ideal sphere. Estimating the energy that BL can contain in the form of "Plasmak", Koloc addressed the case of "lightning in a tub" [13] and came to the conclusion that his model can explain it if its energy release did not exceed 1 MJ and its diameter was about 80 cm (however, it is not clear how BL of 80 cm in diameter and volume of 270 dm^3 could get into the tub of nearby 20 dm^3 in volume).

6.1.4.3 Ball Lightning Theory Development After 1988

Now, we will discuss what has changed in the field of work on the creation of the BL theory in 20 years, after the first symposium. For the purpose of analysis, we will use the material of the theoretical articles presented at the subsequent symposia and also the reviews on BL models [223–226].

Ball Lightning Models with External Source of Energy

During the considered 20 years, Kapitsa's idea was developed according to which BL is the discharge in air, which obtains energy from an external source. Lowke [227] assumed that the electric field of the currents spreading in the earth from a place where a linear lightning struck can be this source. It can explain the observation cases of horizontal BL movement along the earth's surface, but, unfortunately, can explain nothing about the reasons for the other types of BL motion.

Handel [228–230] worked on the development of the concept of atmospheric maser on water molecules (see [1, P. 254–259]). The existence of maser radiation in the nature, in principle, could solve the problem of maintenance of discharge burning in the air during the interval between two lightning strokes. According to Handel, water molecules serve as the keepers of energy during the period between lightning discharges. In the system of close rotation levels of water molecules, the inversion of population occurs under the influence of the electric-field pulse. As the radiative transition between these levels is forbidden, a lifetime of a molecule at the excited level can reach several tens of seconds. "In absence of the high sharpened conductors equipotential surfaces are flat and the population inversion can be formed in a volume of many cubic kilometers. When the electric field increases to a value of 10^4 V/m, some of the forbidden transitions become weakly allowed and start to feed a huge atmospheric maser which volume exceeds the critical. The volume is considered big enough if the number of photons, created in unit of time due to the induced radiation, is greater than a speed of their losses which is mainly caused by the absence of the resonator [1, P. 254–259]." According to Handel, the population inversion in a system of two singled-out rotation levels of the water molecule W_1 and W_2 is realized owing to the action of electromagnetic radiation pulse at the transition frequency $\omega_{12} = (W_2 - W_1)/\hbar$. This method of pulse pumping is usually used in quantum

paramagnetic amplifiers [231, 232]. Under the influence of a high-frequency field, the population of rotation levels periodically change with a frequency [233, 234]:

$$2\Omega = [(\omega - \omega_{21})^2 + (\mu_{21}E_0/\hbar)^2]^{1/2}. \tag{6.1}$$

Here, ω is a circular frequency of a high-frequency field, E_0 is the amplitude of electric-field strength, and μ_{12} is a matrix element of a transition between the levels W_1 and W_2. At $\omega = \omega_{21,}$ population densities of the levels oscillate with the Rabi frequency:

$$\Omega_0 = \mu_{21}E_0/(2\hbar). \tag{6.2}$$

If one impacts a medium by a pulse of resonant high-frequency radiation of duration $\Delta t_\pi = \pi/\Omega_0$ (by so-called π-pulse), the population densities of the upper and lower energy levels exchange places. As in the conditions of thermal balance, the population of the lower level is greater than those of the upper level by $\exp(\hbar\omega_{21}/k_BT)$ times, and in the system of levels, the population inversion arises, that is, the number of molecules capable to radiate energy will be greater than the number of molecules capable to absorb it (here, k_B is Boltzmann constant). However, this process is possible only in the case when the pulse action time Δt_π is much smaller than the relaxation time of the upper level (or, in other words, the time of thermal balance establishment in the system of considered levels). Under the conditions of terrestrial atmosphere, a main factor of such balance establishment is the collisions of water molecules with air molecules. It is known that the rotational relaxation occurs quickly enough, with the probability close to unity during one to ten collisions [235]. At atmospheric pressure and room temperature, the average free path of water molecule is 6×10^{-6} cm, and the average speed is $v = 6 \times 10^4$ cm/s. Thus, the molecule will make 10^{10} collisions during a second. If 100 collisions are necessary for the rotational relaxation realization, then the time of balance establishment will be $t_{eq} = 10^{-8}$ s. This time is much smaller than those of a linear lightning discharge of $t_{ltn} = 10^{-4}$ s [236], during which radiation, resonant with the frequency of the transition ω_{21} between the rotational levels, can be generated. Moreover, even if it is possible to create the population inversion by a large duration pulse ($\Delta t_{n\pi} = n\pi/\Omega_0$), it will be destroyed in time t_{eq} [231]. Thus, in terrestrial atmosphere, the idea of energy accumulation in the form of molecules' rotation energy cannot be realized in spite of even large rotational transitions' radiating lifetime.

As demonstrated by Wieder [237], maser existence on water molecules at atmospheric pressure and BL feeding by it are also impossible owing to other reasons. Among the rotational transitions in water molecule, transitions with the frequencies being in the area of "Kapitsa's radiation" from 429 to 857 MHz have not been found. The longest wave transition found in the radiation of space masers on water molecules was the rotational transition $6_{16} \rightarrow 5_{23}$ with a wavelength of $\lambda_M = 1.35$ cm ($f = 22.235$ GHz) [238]. According to Kapitsa's criterion, powerful high-frequency radiation with such a wavelength can form a plasma bunch in the

size $D = \lambda_M/3.65 = 3.7$ mm. However, this turned out to be much smaller than the observed BL. Nevertheless, though there are lines with wavelengths from 35 to 70 cm in a rotational spectrum of water molecule, the width of these lines will be about 7,000 MHz, because of collisions of water molecules with air molecules, that is, it will be greater than the distance between the hypothetical energy levels (400–900 MHz). In this case, both levels become indistinguishable.

Maser of Handel, has no a resonator with the walls effectively reflecting a radio-wave radiation. Hence, it had to radiate isotropically [239]. Therefore, it is not clear what could have caused the radiation focusing in a small area of space. The statement of Handel that the functioning of atmospheric maser and, hence, BL formation is impossible in the conditions of a mountainous terrain, is also not clear [229]. Actually, in the literature, there are reports that fireballs were repeatedly observed in mountains [18, P. 108].

Despite criticism, Handel continued to work to provide an explanation to BL properties on the basis of his model. In the reports presented at the Eighth International Symposium on BL, Handel gave an explanation of two features of BL movement based on his model. In [240], he tried to find the reason for why a sphere of air heated by the discharge did not rise upwards owing to convection and remained at place. Handel explained this stating that maser does not continuously radiate energy, but in the form of often repeating pulses (spikes). Because of this, the discharge often dies away and again lights up within a second at the same place. Handel explained the movement of BL along the earth surface using the difference in the frequencies of two running waves feeding BL [241]. As a result, the focus place of a resultant standing wave slowly moves, which is perceived by the observer as BL movement. At the Ninth Symposium on BL, Handel proposed another reason for BL movement: phase shift of the waves feeding the discharge [242]. This shift can arise because of an asymmetrical distribution in the space of inversion density of water molecules population levels. As the inversion density experiences chaotic variations, BL movement can also be chaotic.

It can be seen that for Handel's model, a major difficulty not only represents the explanation of the reasons for the continuous feeding of the discharge, but also a trivial BL property such as its movement. Nevertheless, his idea of "caviton" (an area with the lowered pressure of the gas, surrounded by plasma cover) formation in the air under the influence of high-frequency radiation can appear useful in explaining "material" BL passage processes through the glass.

Stakhanov considered the models of BL in the form of electric discharge obtaining feeding from an external source, as contradicting the reality [29–31]. He absolutely and fairly wrote that Kapitsa's and Finkelstein's models [83, 184] cannot provide answer to the simple questions connected with BL behavior. Hence, the mechanism of BL moving in space (more precisely, places where there is an allocation of energy of an external source) is not clear. Furthermore, it is not clear, why BL appears single, instead of many plasma bunches in the neighboring loops of standing electromagnetic wave. The intensity of the radio-radiation generated at the linear lightning discharge is, by many orders of magnitude, smaller than those which are required for discharge maintenance in the air, and the basic frequency of

this radio-radiation (~50 kHz) is by 10^4 times smaller than the frequency of radiation that presumably feeds BL (500 MHz). It is not clear how it manages to remain in the conditions of strong convection, which takes heat away from it released at the high-frequency discharge.

Nevertheless, researches on BL model with the external energy supply continue, and an authority of P.L. Kapitsa, the Nobel Prize winner, has played a great role in this field.

Ball Lightning Models Without Feeding from External Energy Source

Certain complicated questions stand in front of models with an internal energy store. Hence, according to Stakhanov, BL cannot be a plasmoid, that is, the high-temperature plasma held by its own magnetic field [31, P. 175]. In fact, the systems held by their own magnetic field can be steady only in the presence of additional compressing forces (external pressure or gravitation) [182, 183]. If the atmospheric pressure plays a role of constraining force, then according to the virial theorem [184], energy of the plasmoid W_{pl} cannot exceed a value $3P_aV$ (where P_a – atmospheric pressure, $P_a = 10^5$ Pa, and V – a volume of the plasmoid). For $V = 10^{-3}$ m^3, energy is $W_{pl} \leq 300$ J, which is much smaller than the values of BL energy found on the basis of its action on various objects (water heating, pile splitting, etc.). Hot plasma will quickly lose its energy because of electrons braking radiation. Somehow, to reduce the speed of this loss, the plasma temperature should be below 10^7 K [184]. BL cannot exist in the form of a low-temperature plasma volume at atmospheric pressure, as the atomic ions transform to molecular ions during 10^{-8} s, which, in turn, recombine for a thousand part of a second [31, P. 177; 146, P. 47].

The properties of BL cannot be explained by the model based on the assumption that it represents a mixture of neutral molecules capable to react with each other chemically [31, P. 181]. First, it is impossible to explain the maintenance of the spherical form of BL, if the presence of large uncompensated charge of BL substance should be excluded. Second, BL with a chemical store of energy cannot provide energy storage of some tens kilojoules in a liter. And, third, the chemical model of BL (even supposing the presence of a small charge of 10^{-7} C in it) is incapable to explain the electric effects connected with it.

In addition, the system consisting of charged dust particles [31, P. 184] cannot provide a comprehensible energy store. According to estimations, the energy density, stored by such system, cannot exceed 1 J/m^3. The substance of BL cannot contain free electrons. Owing to small mass, the acceleration of an electron is 10^5 times greater than those of an ion, and the radiated power by it is greater by 10^{10} times. This has led to the conclusion that the radiation power of BL of 20 cm in diameter will be equal to 10 MW, which will release its energy for 10^{-3} s [31, P. 188]. BL cannot exist during adequately large time, in which energy is stored in atoms or molecules excited to metastable electronic levels. In spite of the fact that the lifetime with respect to radiation of such atoms and molecules can reach

hundreds of seconds, the time of their relaxation in collisions with air molecules is only 10^{-8}–10^{-2} s [31, P. 49].

However, the energy of BL cannot be stored for a long time in the form of the ions surrounded with covers of polarized water molecules (this assumption considers the basic idea of Stakhanov model [31]). As shown in [146, P. 47], for recombination processes of unlike charged ions in air, the parameter $\varepsilon\tau$, representing the product of density of the stored energy and the characteristic time of a process, shifts from 10^{-12} to 10^{-11} (J/cm^3) s. If we assume that charges are located on aerosol particles, it is possible to admit that the speed of the aerosol particles approaching, caused by their Coulomb attraction, will be slowed down by forces of friction in the gas. Therefore, the parameter $\varepsilon\tau \sim 10^{-7}\ r_o/q^2$ for aerosol plasma, where r_o is the average radius of an aerosol particle (in a μm) and q is its charge in terms of an electron charge. Having put $r_o = 1$ μ and $q = 1$, we can observe that $\varepsilon\tau \sim 10^{-7}$ (J/cm^3) s [146, P. 47]. Thus, the time of aerosol plasma existence with the energy density of 5 J/cm^3 will be only $\tau \sim 2 \times 10^{-8}$ s.

On the basis of this not very comforting analysis made by Stakhanov and Smirnov, we can conclude that the overwhelming majority of hypotheses of BL structure proposed in 90th years of 20th century cannot accurately describe its properties. In this connection, within the last 20 years, attempts to eliminate the contradiction in the "traditional" models of BL, were undertaken.

Models with Chemical Source of Internal Energy

Experiments with the burning of methane–air mixtures have shown that at a concentration of methane of about 1.5%, sometimes balls with the diffuse borders, bearing a faint resemblance to the BL form, were observed [35, P. 166]. In the nature, such processes, in principle, could take place with the release of significant amounts of methane from bogs or earth-crust breaks. However, the natural maintenance of methane in the air does not exceed 10^{-4}%, which explains that burning of BL by methane is improbable.

The assumption that energy-containing reagents are labile substances, created in the course of storm activity (ozone, nitrogen oxides), is more natural [243, 244]. According to Smirnov [244], the concentration of ozone in BL volume can be about of 1%; this can provide it with an energy of 100 J. This energy can support its luminescence within 5 s. However, in [243], an attempt was made to estimate the value of the force connecting BL together, which showed that the interaction of particles inside it (dipoles and charges) cannot create surface tension, sufficient for the maintenance of BL spherical form.

Eventually, Smirnov's model evolved, and BL was considered to be the light aerosol framework containing a fuel (coal, stearin, and ozone) and a small amount of charges of one polarity in its pores [146, 218]. The structure described in [218] is similar to the aerosol model of BL proposed in [208], according to which, it consists of "the volumetric threadlike structures suspended in air". The authors of [208] considered that the particles with which BL is formed are gathered by the electric field from a large volume in the small one. "If . . . particles possess excess internal

energy it means . . . an increase of such energy density in the volume." Nevertheless, the density of chemical energy in an aerosol BL appears very small (about 1 J/cm^3). This allowed Smirnov to figuratively compare its energy with the energy of ten matches [218].

Absence of electric charge presence necessity in chemical BL model (or its auxiliary role – only for stabilization of its skeleton [218]) reduces a merit of this model. In fact, electric manifestations of BL interaction with various objects are one of its basic features. Therefore, one can understand the aspirations of some authors to connect together chemistry and its electric properties.

For example, B.B. Kadomtsev considered BL as the self-organized mixture of chemically active dust particles with plasma ions – a certain isotropic accumulator of electric energy [245]. The authors of [246, 247] considered that in the volume of BL consisting of an aerosol and dust, chemical reactions take place in which the charged particles (electrons and ions) are formed. If there is an electric field, then the originated electrons will move in it, colliding with the polarized extended particles of the dust. These dusty particles will try to be oriented so that their dipole moment is directed along the lines of a field. At collision of an electron with the end of the particle charged negatively, it will bend around a particle, and, on the contrary, if the particle's end is charged positively, it will collide with it. Therefore, the impact cross-section of an electron with the particle is different in these cases. In the space between the cathode and anode, the particles try to be guided, so that their negatively charged end is turned to the anode. Therefore, the electrons, moving from the anode to the cathode (in the direction opposite to the direction of a conductivity current), will less often encounter with the dusty particles, than the electrons moving from the cathode to the anode. Owing to this, in space between the electrodes, the current from the cathode to the anode will flow, charging the electrodes and increasing the field strength between them. The energy for current maintenance is drawn from the kinetic energy of the electrons, which, in turn, obtain it from the energy of the chemical reaction. Owing to the described process of "negative conductivity," electric-field strength can increase to $E_{ch} = 6 \times 10^5$ V/m. However, the electric energy density in the volume of such "chemical" BL appears equal to $\rho_{ch} = \varepsilon_o E_{ch}^2/2 = 1.6$ J/m^3, and it is obviously not enough for an explanation of conductors' fusion processes and other manifestations of electric charges present in BL.

Summing up, it is necessary to agree with Stakhanov's opinion that BL with the chemical energy source, having a density equal to the air density, can neither explain its source of high-specific energy content nor the reasons for the electric phenomena caused by it [31].

Cluster Model of Ball Lightning

This model was proposed by Stakhanov [29, 31, 248]. According to this model, the substance of BL represents the nonideal plasma, consisting of positive and negative ions with the big covers of polar neutral molecules. In hydrated ions or hydrates, a cluster cover, from three to five molecules of water, has a binding energy of about

4 eV, and it should not be destroyed by collisions at temperatures below 1,000 K. Such a cover can prevent recombination. However, cases when hydrated ions' recombination speed decreases to the values necessary for the explanation of BL's long existence, have not been revealed.

In the model developed by Stakhanov [29, 31], the question on the mechanism of the origination of the surface tension interfering with the mixing of a cluster ion cloud with air was left open. Turner [249] tried to find the answer this question. He considered that BL consists of the central area filled with plasma, which is surrounded by three concentric spherical zones. In the hot central area, there is a formation of ions and metastable molecules, which, leaving this zone, go to the external layers saturated with cold humid air. Here, they become covered with a fur coat of water molecules, and heat release takes place. Strongly hydrated ions move outside and a cluster recombination reaction takes place in an external layer. The most probable cluster types are the clusters formed by the hydrated proton H_3O^+ and ion NO_2^-. Nitric acid is formed at their recombination:

$$H_3O^+ \cdot nH_2O + NO_2^- \cdot nH_2O = HNO_2 + (2n + 1)H_2O. \tag{6.3}$$

Reaction (6.3) is endothermic and should lead to cooling of an adjoining layer of air that according to [249], will cause the appearance of an air stream directed inside the BL. This stream will create the pressure compressing an area where there are chemical reactions, and simultaneously deliver reagents for their feeding, that is, BL will work as the thermo-chemical thermal pump.

Turner's model, to some extent, is a development of Stakhanov's idea: it allows finding the reasons of the occurrence of surface tension and spatial separation of areas of clusters formation and recombination. However, together with this, it shows a number of difficult compatible requirements for the considered system (a chemical reactor). First, the model assumes the presence of the substance's constant movement from the center to the periphery. Then, to fill in the substance losses in the center, it is necessary that there are gas streams moving in an opposite direction – from the periphery to the center. It should break the central symmetry of the system. Second, the generation and maintenance of high-temperature plasma mechanism in the central zone is not clear. Turner assumed that the formation of metastable molecules with the subsequent spontaneous ionization of the latter can be the underlying mechanism that, however, does not remove the question on an energy source necessary for this process. Third, for the creation of the force compressing Turner's chemical reactor, it is necessary that not only temperature but also pressure has to be decreased in the external layer. As to the latter, the answer remains undetermined, because in the course of the chemical reaction (6.3), there is a growth in particle number, and hence, pressure. And, fourth, for an explanation of BL passage through the intact glass cases, Turner supposed that cluster molecules and ions can generate electromagnetic radiation, which can be absorbed by similar types of molecules on the glass' opposite side; however, he did not describe the mechanism of this radiation occurrence.

In [250], an attempt to create a BL model by combining the models of various authors, was undertaken. This model known as condensational, includes Stakhanov's ideas about the cluster nature of BL [29], Smirnov's idea that these clusters form fractal structures [146], Bychkov's idea that BL structure includes polymeric threads [251], and Stepanov's, who proposed the mechanism of electric-field generation in chemical reactions [246, 247]. According to the condensational model, BL is formed owing to a nonequilibrium condensation of the overcooled steam leaving a supersonic nozzle. The basic energy source of BL is the energy of the clusters, excited to metastable high-lying energy levels. Besides, the authors of the model considered an oxidation process of BL substance as an additional energy source.

Thus, the hypothesis that BL consists of charged clusters has aroused interest among researchers in this poorly investigated area of electrochemistry. However, restriction of limiting energy density, which the system of these clusters is capable to store with a value of 5×10^5 J/m^3 [31] forces to recognize that the specified processes have nothing to do with BL.

Ball Lightning Model on the Basis of "Rydberg" Substance

It is possible to avoid the difficulties connected with fast recombination of charges if BL substance consists of neutral particles. In this case, energy can be stored, for example, in the form of electronic excitation of atoms and molecules. At excitation of atoms to states with high principal quantum number n ($n = 10$), the system is capable to get new properties. We will consider, for example, the gas consisting of hydrogen atoms. The radius of a Bohr orbit of hydrogen atom at $n = 1$ is equal to $a_0 = 0.529 \times 10^{-8}$ cm. At the growth of n, the orbit radius increases as $r_n = a_0 n^2$; thus, for $n = 10$, it is 0.529×10^{-6} cm. The average distance between the atoms is $l_{\text{atm}} = 0.33 \times 10^{-6}$ cm at atmospheric pressure, which is comparable with the size of highly excited "Rydberg" atom. As a result, there can be an overlapping of electron shells of the neighboring excited atoms, which can result in "collectivization" of electrons. Exchange and correlation effects lead to electron attraction among each other. The authors of [252–255] considered that BL consists of "Rydberg" substance with the density close to that of air. The energy density stored in BL substance lies from 1 to 10 J/cm^3, and the surface tension, caused by the electron attraction, is close to 10^{-6} J/cm^2 (for comparison – the surface tension coefficient of water at 20°C is equal to 7.3×10^{-6} J/cm^2). As the density of electrons is small, the plasma frequency appears to be much smaller than the frequency of visible radiation. In this connection, BL, consisting of "Rydberg" substance, should seem transparent. This can be observed due to the radiation caused by the recombination of the charges. It can conduct an electric current and possess a small electric charge.

The idea that BL substance is a nonideal plasma in which the potential energy of particles' interaction is comparable with their kinetic energy [256], has also been expressed. In [257–259], it was shown that a hypothesis according to which the substance of BL represents the overcooled metastable non-ideal plasma, and a hypothesis about "Rydberg" BL substance, supplement each other and can be combined into a general hypothesis.

Unfortunately, the model on the basis of the "Rydberg" substance cannot explain the reason for the high energy content of BL. The limiting values of energy density, which can store such substance lie in the range from 10^6 to 10^7 J/m^3 [254].

Ball Lightning Models with Energy Accumulation in Electromagnetic Field

For the first time, the idea that BL energy can be stored in the form of the electric capacity energy was stated by de Tessan in 1859 [211]. In the process of perfection of work techniques with electric fields, the authors of new BL models repeatedly addressed this issue. Hence, according to Mesenjashin, BL is the charged bubble whose shell consists of water molecules oriented in the electric field [260, 261]. The thickness of the bubble shell ranges from 0.01 to 100 μm, and charges of an opposite sign settle down on the bubble poles. The bubble formed at inflating of a water drop with an impurity of dust is charged in the electric field of a thunderstorm cloud, thus, the dipole moments of water molecules are guided along the force lines of the electric field. Owing to this, the bubble gets a mechanical durability. The main component of free energy of a bubble is the energy of the molecules' orientation. For a bubble of 10-cm radius with a shell with a thickness of 10 μm, this energy is 11 kJ (thus, the energy density in regard to the bubble volume is 3×10^6 J/m^3). Mesenjashin's bubbles shine by reflected light, and their color can vary because of an interference of beams in a thin film of a bubble.

The model of unipolarly charged BL, representing a vacuum bubble in atmosphere, was proposed in 1975 [36]. The balance in this system was provided with the equality of atmospheric pressure force and the force of Coulomb charges' repulsion at the border of the vacuum cavity. The authors found that the limiting value of energy density was 4×10^5 J/m^3 in their model, which is in full agreement with an estimation that can be obtained on the basis of the virial theorem.

The model of BL in the form of the charged water bubble was also described [262]. Furthermore, in [36], the bubble with a shell bearing charges of one polarity was considered. In this model, it was assumed that the pressure of electric field $\varepsilon_o E^2/2$ was counterbalanced by the pressure of the bubble shell, proportional to a gradient of electric-field strength. For a bubble of 7 cm in radius, this pressure was 2.3×10^8 N/m^2 at a field strength of $E = 5.5 \times 10^9$ V/m on its surface. The basic contribution to energy was given by the energy of the external electric field, which for the specified conditions, was equal to 5.8×10^5 J. Having divided this value of energy by the volume of a sphere of 7 cm in radius, we found an energy density of $\rho_E = 4 \times 10^8$ J/m^3.

R. Fedele stated that the behavior of electromagnetic radiation bundles and bunches of the charged particles can be described by the equations, which resemble Schrödinger's equation. The solution of these equations leads to the description of the processes of self-modulation, self-capture, and self-channeling of bunches with the formation of solitons [263]. He considered that these processes can be related to a BL. It can be formed in the atmosphere as follows: (1) under the influence of intensive electromagnetic radiation in the field of space with the raised level of ionization, radiation self-capture takes place; (2) owing to the pondermotive force,

electrons are pushed outside and form a spherical layer, and heavier ions remain in the sphere; (3) the spherical capacity is formed, in which electric-field energy is stored; and (4) as the formed system is unstable, an ionic core starts to extend and eventually reaches an electronic shell, returning the stored energy. The time during which the proposed system exists depends on the competition of the processes of core inertial compression and Coulomb ion repulsion.

As it can be seen, in Fedele's model, BL energy is stored in the form of electric-field energy $W_e = CU^2/2$ (where C is the condenser capacity and U is the potential difference between an ionic kernel and electronic sphere). This energy is not large owing to the small capacity value.

A serious obstacle on the way of accumulation of energy in the electric field is a rather small value of breakdown electric-field strength in the air, $E_{bra} = 3 \times 10^6$ V/m. Therefore, it seems that the problem can be facilitated if energy is stored in a magnetic field. The energy density of a magnetic field in vacuum is $\rho_M = B^2/2\mu_0$ (where B is a field induction and μ_0 is a magnetic constant). For obtaining "Goodlet" energy density $\rho_{BL} = 10^{10}$ J/m^3, it is necessary for BL to have a magnetic field with an induction of $B = 158$ T (we noticed that in the case of accumulation of such energy density in electric field, its intensity should be 4.7×10^{10} V/m, which is 10^4 times greater than the breakdown strength of air). Magnetic fields with energy density up to 10^{12} J/m^3 could be obtained at a conductor with a current produced by the compression energy of explosion, and the pressure of the explosive counteracting the pressure of a magnetic field exceeded the atmospheric pressure by 10^7 times [264].

The holding requirements of an area with a strong magnetic field somewhat softened when the magnetic-field configurations free from forces were considered (Force Free Field) [265]. The basic idea of such magnetic-field configuration is to direct a current $\mathbf{j}$, creating the second magnetic field along the force lines of the first magnetic field $\mathbf{H}$. This condition is described by the equations:

$$\begin{aligned} \mathbf{j} &= \text{rot } \mathbf{H} = \alpha \mathbf{H}, \\ \text{div } \mathbf{H} &= 0. \end{aligned} \tag{6.4}$$

Having taken advantage of this idea, the authors of [266, 267] proposed a BL model in the form of a free from forces bundle of magnetic field lines. According to their model, in BL of 30 cm in diameter, only a small area of 2×10^{-2} cm^3 in volume heated up to a temperature of 18,000 K, emitting light. This area represented a streamer with fast movement consisting of several knots. The streamer had a diameter of about 100 μm and a length of some meters. At the magnetic-field induction of $B = 3$ T, the energy stored in the field was 24 kJ. The described kind of BL in the form of a ball of magnetic force lines faced sharp criticism from Jennison who had seen the real BL [268]. In his opinion, the "magnetic" BL has nothing in common with the natural one. Besides, the question connected with fast light emission of such high-temperature BL remains unexplained [31].

One should also remember that the constant magnetic field can be supported only by currents. In usual conductors, these currents tend to fade because of ohmic losses, and in this connection, the time of magnetic-field existence is limited. Callebaut [269] demonstrated that a characteristic time of attenuation for magnetic field, free from forces, is

$$\tau_{\mathrm{dp}} = \left(\alpha^2 \eta\right)^{-1}. \tag{6.5}$$

Here, α is the proportionality factor in the formula (6.4), which has a dimension of m^{-1}, and η is the specific resistance of a medium in which the current flows, $\eta = (\mu\sigma)^{-1}$ (μ is the magnetic permeability and σ is the specific conductivity). For plasma, it is possible to accept $\eta = 1\ \mathrm{m}^2/\mathrm{s}$. Starting from the BL size of $d_{\mathrm{BL}} = 0.1$ m, the parameter α can be estimated as $\alpha = {d_{\mathrm{BL}}}^{-1} = 10\ \mathrm{m}^{-1}$. By substituting these figures in the formula (6.5), we can obtain the magnetic-field existence time $\tau_{\mathrm{dp}} = 10^{-2}$ s.

If superconductivity conditions are somehow provided, the time τ_{dp} can be increased. Superconductivity can create runaway electrons. They can appear in special conditions, for example, owing to acceleration in an initial phase of the strong solitary wave initiated by the discharge of a linear lightning [270].

Many researchers proposed a BL model in the form of the cavity resonator for high-frequency radiation with walls of plasma. One of the early examples of such model is "a bubble filled with radiation" [196]. It is considered that in a dielectric plasma sphere, there is the high-frequency radiation whose resonant frequency considerably exceeds the frequency of electron collisions with the molecules. The existence of plasma in a sphere is supported by high-frequency radiation, and conducting plasma walls of the cavity resonator are formed owing to the currents flowing on an internal surface of its walls. The radiation pressure upon the resonator walls is counterbalanced by the atmospheric pressure; therefore, the energy density of a high-frequency field appears to be low – approximately $10^5\ \mathrm{J/m}^3$. The authors considered collisions of electrons with molecules as the main channel of energy losses; however, they did not consider the attenuation of radiation because of ohmic losses in the resonator walls. In fact, even at a very high quality factor of the resonator (e.g., $Q = 10^6$), oscillations with a frequency of $\nu = 2.6 \times 10^9$ Hz will attenuate during

$$Q/\nu = 4 \times 10^{-4}\ \mathrm{s}.$$

The authors of [271–273] believed that it is possible to find conditions when energy of the radiation, "locked" in a cavity with reflecting walls, whose separation displacement is restrained by atmospheric pressure, can considerably exceed the limit allowed by the virial theorem ($\rho_{\mathrm{E}} = 3 \times 10^5\ \mathrm{J/m}^3$). However, the analysis of such configuration [225] has shown that the virial theorem acts in this case with all its restrictions.

The authors of [105, 106] found out that at an explosion of round metal diaphragms, at the impact of a powerful current pulse, shining spheres that existed for some seconds, were formed. They considered that it is the analog of BL representing a potential hole for captured electromagnetic radiation.

Models Capable to Explain Specific Ball Lightning Energy Content Greater than 10^9 J/m^3

As observed earlier, the force creating a surface tension in the ensemble of "Rydberg" atoms arises owing to the exchange interaction of electrons. The idea about the important role of this interaction with reference to BL was proposed for the first time by Neugebauer in 1937 [189]. In a case when plasma is almost completely ionized and the density of the charges is high enough, force of their mutual attraction can appear, because of the exchange interaction of electrons exceeding their Coulomb repulsion force. At electron density $n_e = 2.7 \times 10^{19}$ cm^{-3}, this condition is reached if the temperature of the ionized gas is not higher than 600 K.

Neugebauer's idea was developed in Dijkhuis's works. Unlike Neugebauer, who considered a homogeneous sphere of plasma, and electrons as fermions, Dijkhuis considered that at the large density of electrons, formation of vortical tubes of coupled electrons, satisfying the Boze–Einstein statistics, is possible [191]. The "Bozonized" electrons in the tubes are attracted to each other not owing to the exchange forces, as considered by Neugebauer. These forces are too weak for maintenance of high-energy BL existence. Thus, the necessary binding energy is provided by the nonuniformity of "Bozon" charge-density distribution.

Condensation of electrons and formation of vortices can occur at the lightning discharge at critical values of temperature of 1,844 K, pressure of 6.04 MPa, and an electron density of 1.28×10^{27} m^{-3} [82, 274]. Nonuniform distribution of electronic vortices density ρ over the sphere volume (that occurs because of the temperature difference between the central and peripheral areas of a sphere at constant pressure) should lead to the occurrence of the force directed to the center of a sphere whose value is proportional to $\nabla^2\rho^{1/2}/\rho^{1/2}$ [275]. Dijkhuis considered that the virial theorem in the traditional form is inapplicable to two-component plasma considered by him [276].

According to Dijkhuis, the radius of vortical electronic tubes is equal to 53×10^{-12} m (Bohr radius), and around these tubes, positive ions rotate at a distance of about 10^{-7} m. At the extension of coaxial electron-ion tubes, there is an acceleration of ions to a limiting energy of 511 keV (energy of electron–positron pairs production). Dijkhuis considered that this restriction is artificially limited to nonrelativistic consideration of processes. At the extension of tubes, new bends appear that allows them pack up in limited volume. BL formation occurs at displacement of the channel of a linear lightning. If BL can accumulate in itself a full charge of typical linear lightning $Q = 6$ C (in the form of the sum of positive and negative charges, equal in value) the full kinetic energy of ions will be about 3 MJ, which is comparable with the energy value of "Goodlet" BL that entered a tub with water (10 MJ) [13, 14]. In Dijkhuis's model, new lines of the approach to the BL problem

solution appeared. The BL substance can be conditionally called highly ordered plasma. Along with the usual plasma, it consists of unlike charges; however, they do not recombine as they are spaced. Another important property of Dijkhuis's model is that the main BL energy is stored in the form of kinetic energy of ions. Basically, the capacity of this reservoir is boundless. According to the virial theorem, movement of particles demands the presence of the force compensating the centrifugal force of ions. According to Dijkhuis, the nature of this force is the quantum-mechanical mutual attraction of electrons, and the electrostatic force keeps the ions on an orbit near the electronic vortical tube.

Dijkhuis considered the reaction of nuclear fusion of deuterium nuclei in water vapor in atmospheric air as the energy source of BL. The kinetic energy of the ions rotating around the vortical electronic tubes is quite sufficient for the realization of such reaction [192].

The problem of dense packing of rotating tubes, such that they do not brake each other in places of contacts, has spilled over into an interesting mathematical problem. To obtain a solution to this problem, Dijkhuis devoted a number of studies [277–282].

Thermonuclear reaction of deuterium nuclei fusion also serves as BL-energy source in the model proposed by A.N. Vlasov. He considered that BL looks like a toroidal vortical air ring [149–152]. In this ring, the toroidal current circulates, creates a magnetic field, and is directed along a toroid axis. The toroid layer is formed by a cover of positive ions, around which relativistic electrons move, and are collected in a layer of one electron in thickness. The vortex with a system of moving charges is formed at a stroke of a linear lightning in earth. Thus, the mode of continuous electron acceleration is formed and they get the speed close to a velocity of light. Owing to an exchange of photons and interaction with positive ions, a Bose-condensation of electrons takes place, and the electronic monolayer becomes superconducting. Electrons in the monolayer remain practically motionless with respect to each other; in this connection, their temperature is near to absolute zero. Vlasov assumed that ions, for example, deuterium nuclei in a monolayer of electrons, are screened by the last ones. Approaching of the nuclei at distances of about 10^{-12} cm, may result in a possible nuclear synthesis reaction. The analog of this process is muonic catalysis. According to Vlasov's estimations, in a volume of BL of 30 cm in diameter, a power of 1.7 kW owing to nuclear reaction can be realized. As neutrons are formed in the course of nuclear synthesis, such BL will represent danger to the observer.

It is known that with the reaction of one deuterium nucleus, energy of 1.6 MeV $= 2.9 \times 10^{-13}$ J is released [283, P. 6]. One liter of air at a temperature 20°C and absolute humidity contains 1.8×10^{17} deuterium atoms. At a full expenditure of these atoms in the reaction of thermonuclear synthesis, energy $W_{nc} = 2.9 \times 10^{-13} \times 1.8 \times 10^{17}$ J $= 52$ kJ can be released, which corresponds to the energy density $\rho_{nc} = 5.2 \times 10^{7}$ J/m^3. This value is more than two orders smaller than the energy density of "Goodlet" BL [13, 14]. Therefore, in the specified case, thermonuclear energy cannot be the basic supplier of BL energy.

In 1994, V.L. Bychkov published an article [251] with the description of a model of a polymeric BL. His "theory is a development of theories [31, 146] in application to polymeric structures. Fractality is a natural property of a polymeric BL. The model is electric, as [31], and chemical as [146], and includes all achievements of [146] in case of polymeric materials." Bychkov found that in the summer "plants throw out hundred million tons of organic molecules and macromolecules; and there is a process of destruction of vegetation of type of leaves and a grass. The characteristic sizes of such hydrocarbon structures are 10^{-5}–10^{-3} cm. In presence of electric fields of a thunderstorm or the electric equipment these macromolecules gather in the easy connected porous structures of the macroscopic sizes." Association of globules occurs as follows: "electric field induces the electric moments on globules, and interaction of these dipole moments at some spatial configurations leads to an attraction of globules." In storm conditions "at growth of fractal polymeric formations there is a process of their charging by ions and electrons. Polymeric units can accumulate a considerable quantity of charges because of existence of traps – emptiness inside or between macromolecular chains or subchains." The size "of an ionic current on the unit is the sum of diffusion and hydrodynamic currents in a direction to a surface. Charging can be carried out by simultaneously positive and negative ions, and because of various speeds of drift of ions generally the polymeric structure should not be electrically neutral. Thanks to dielectric properties of polymer structure the recombination of captured positive and negative charges occurs extremely slowly, therefore the object can accumulate considerable quantities of electric energy. The charged structure can cause occurrence of discharge near its surface. Presence of electron current to a surface of BL in the field of the discharge leads to heating of a polymeric material. This heating causes acceleration of processes charges recombination in polymer and to corresponding additional heating of structure therefore the structure collapses." Having accepted that the intensity of breakdown electric field for polymers is equal to $E_{\mathrm{brp}} = 10^9$ V/m, Bychkov found that for an object with a radius of 10 cm, its fractal polymeric structure at an uncompensated charge of $Q = 10^{-3}$ C can store electric energy of up to 10^6 J.

Let us make a simple estimation of a polymeric BL-energy content. Bychkov considered BL substance consisting of islets of charges of a different polarities, that is, from small electric capacitors. We will accept that all the volume of a sphere is filled by such capacitors, and that the electric-field strength between their facings is equal to $E_{\mathrm{brp}} = 10^9$ V/m. The energy density of the electric field is $\rho_{\mathrm{E}} = \varepsilon\varepsilon_0 {E_{\mathrm{brp}}}^2/2$. Having put a value of dielectric permeability of polymer $\varepsilon = 2.5$, we found that $\rho_{\mathrm{E}} = 1.11 \times 10^7$ J/m^3. In a sphere of radius $R = 10$ cm, energy $W_{\mathrm{ei}} = 4.65 \times 10^4$ J can be stored. Now, we will image that this sphere also possesses the unipolar electric charge created on its surface electric-field strength of $E_{\mathrm{brp}} = 10^9$ V/m. A charge of this sphere is $Q = 4\pi\varepsilon_0 R^2 E_{\mathrm{brp}} = 1.11 \times 10^{-3}$ C, and the energy of the external electric field is $W_{\mathrm{ee}} = 2\pi\varepsilon_0 {E_{\mathrm{brp}}}^2 R^3 = 5.56 \times 10^4$ J. The sum of the internal and external field energy is 10^5 J, and the density of the stored electric energy is 2.4×10^7 J/m^3. Bychkov, at the charge of 10^{-3} C, found that the energy of the sphere was close to 10^6 J, which is by ten times greater than what we found. However, the

estimation made showed that even in the considered extreme case, when the electric-field strength on a sphere surface exceeds the value of the breakdown field strength of the air by 33 times ($E_{bra} = 3 \times 10^6$ V/m), BL-energy store of 10–100 MJ could not be reduced to the energy of its electric field. We noticed that though Bychkov considered himself as a follower of Stakhanov and Smirnov, he brought elements in the BL model, which were rejected by his predecessors: the large electric charge (as well as the one connected with it) and the possibility of increase in its weight. In fact, in the presence of a charge in atmospheric electric fields, objects can levitate not only with a mass of 3 g but also with a weight of 1–10 kg.

In [284], by supplementing calculations and earlier estimations [251], Bychkov found that because of the recombination charges in the polymeric structure, its surface can heat up to temperature of 550 K, that is, to a temperature of ignition of a majority of polymeric materials (500–600 K). In [285], Bychkov informed that breakdown electric fields in thin polymeric threads can reach 10^{10} V/m, and the value of the limiting density of energy of a polymeric fireball can be raised to 4.5×10^8 J/m^3.

In 2004, Bychkov completely changed the approach to a structure and an energy source of a polymeric BL [286]. Thus, according to his ideas, the BL does not arise because of aggregation of the small parts weighed in air, but "as the result of unipolar stroke of a linear lightning in any material at which there is its heating and fusion. Thus occurs formation of the loose unipolarly charged structure – BL." It can be "the ball of threads, fused sphere or a bubble." Thus, the electric field on the BL surface will be of the order $E \sim 3 \times 10^6$–10^8 V/m and will be defined by the density of the charge that has passed from the charge of a linear lightning to an area of melt. "On BL surface the discharge is developed (during 1–10^2 s), it heats up the surface to ignition temperature, and the object collapses. The size of a charge of such BL is defined by conditions of its levitation in the field of a storm cloud." It also "leads to development of electrostatic instabilities on a surface of BL ... with formation of threads and drops on it. ... Limits of ignition of drops and threads in air are much lower, than for a massive material." Ignition and burning of BL material leads to energy storing whose density can reach 10^9 J/m^3. In [287, 288], Bychkov considered conditions of explosion of BL at heating of its surface, occurrence of burns when a hot BL comes into contact with people, and features of its passing through holes.

In 1998, Nikitin published an article [139, 140] with the new concept of BL. A year later, he described the model at the Sixth International Symposium on Ball Lightning [289]. Similar to other authors of modern models, he had a predecessor – de Tessan, who proposed, in 1859, a BL model in the form of the spherical electric capacitor [211]. As we have shown, even at the replacement of air by an insulator with an electric-field strength $E_{brp} = 10^9$ V/m, the energy stored in the capacity is insufficient for the explanation of high-specific energy density of BL. However, strong dependence of energy density on the electric field ($\rho_E \sim E^2$) makes the use of this electric capacitor as the keeper of energy an attractive option. Besides, in the nature, there is an ideal insulator – vacuum. The complexity consists in that in real

electric capacitors the field pulls out the electrons at super-strong electric fields from metal electrodes, and there is an electric breakdown even at the use of a vacuum as insulator. Therefore, for capacitor "designing," it is necessary to refuse application of solid-state electrodes (as the nature hardly has them during BL creation). Therefore, it is necessary to search for a configuration whose existence would be supported by the separated electric charges of different polarity. It is clear that such charges cannot remain motionless. During this reasoning, the author developed the "design" termed as "the dynamic electric capacitor." In the capacitor, electrons are located in the center, moving in a ring orbit, and positive ions rotate around them (the lightest of them – protons) under the action of the electric field created by electrons charge. The current created by the movement of protons generates a magnetic field inside their orbits, whose vector, in the location of an electronic ring, is perpendicular to a vector of electric-field strength. In these "crossed" fields, electrons move over a cycloid (as electrons in a magnetron do). It appeared that at equality of total charges of protons and electrons (i.e., at an electric neutrality of the system), a value of the magnetic field strength, created by the movement of protons, is not sufficient to make electrons move in the closed orbit. Thus, the system turned out to be positively charged, which added difficulties in the maintenance of system stability: a force of Coulomb repulsion of the like charges was added to the obviously unstable combination of two coaxial rings of rotating charges of different polarities. Besides, for the maintenance of vacuum in the capacity, the developed "design" should have a shell, isolating it from the atmosphere. Fortunately, it appeared that this shell can exactly provide stability to the system. If it is made of the dielectric (e.g., water) in nonuniform electric field of the charged core (system of moving protons and electrons), then there will be a polarization of a shell substance, and it will begin to be shrunk along the radius, interfering with the core expansion. The shell has to be positively charged so that the core is reflected inside the sphere at the contact of an internal surface of a shell with external "proton facing" the condenser. It can obtain a charge owing to the fact that the core gradually loses a charge despite the presence of a vacuum. This charge, "having filtered" through a cover, flows down into the atmosphere. Estimations have shown that the main energy in such capacitor is stored not in the form of electric and magnetic fields, but in the form of kinetic energy of protons. The density of this energy can reach the limiting values, which have been found out in high-energy BL ($\rho_W = 10^{11}$ J/m^3). The electric charge of BL plays a double role. On the one hand, its presence causes expansion of the system because of Coulomb repulsion of charges, and on the other hand, it creates the force that draws up the shell. Therefore, at certain values of BL energy and a thickness of its shell, its existence is possible both at small and large values of the charge [136, 290, 291]. The nature, apparently, chooses the first variant. Estimations show that the energy density stored in the dynamic electric capacitor increases with the reduction of its size (connected with increase in orbital speed of protons). Therefore, it is "energetically favorable" to BL to include elements of small size (tiny BL with own core and shell), placed in the common shell of large size. In the considered system, electrons are relativistic; therefore, they are a source of synchrotron radiation.

Fast decay of electrons emission is hindered because they are many in number and are homogeneously distributed in the orbit. Such BL can be formed at a course of a strong current pulse in the conductor bend (e.g., in a bend of the linear lightning channel) [136, 291–293]. Thus, in air, for short time, the vacuum cavity is formed in which separation and acceleration of charges take place under the action of a magnetic field of a lightning current and eddy electric field.

In this collection, the ideas of Bychkov, Nikitin, and Dijkhuis – authors of three high-energy BL models (with respect to their mathematical complexity) – about BL construction are detailed.

Hence, one can consider that comprehension of the importance of BL's basic properties, such as the ability to accumulate large amount of energy, was a push to working out the full BL theory. From the modern point of view, the BL is considered as a strongly nonequilibrium high-energy open system capable of self-organizing. The considered three models, each in their own way, reflect the general principles of existence of this system. Undoubtedly, a definitive conclusion about the advantages and disadvantages of these models can be made only after its experimental verification.

6.1.5 Conclusion

The Tenth jubilee Symposium served as an occasion to make the review of BL researches' history, and in particular, the analysis of work carried out in the last 20 years – an activity time of the International Committee on Ball Lightning (ICBL). It is possible to state that the Committee managed to fulfill its primary goal: to give the chance to the scientists working in the field of BL researches, to meet and discuss the results of their researches periodically (once in 2 years). It can be seen from the above-stated facts that the last 20 years witnessed active researches on BL problem. Data banks of BL observations were collected and replenished, experiments on long-lived shining formations were carried out, and studies on the creation and verification of BL models were conducted. Unfortunately, these activities have not yet brought notable results. The reason for failure, apparently, is owing to the fact that we could not choose "the main link" in the properties of BL, and as a result, have incorrectly chosen the ways of its experimental modeling. Also, the hope that a dialog of researchers on these symposia and conferences will help to somehow smooth these disadvantages, cannot be justified. For some reason, practically there is no reaction to criticism, and corrections are not made to the developed models. Constantly, new models of BL are appearing, not as a result of criticism or the development of existing models, but as though "from nowhere." As a rule, authors of new models should explain only separate characteristics of BL and should not pretend to explain all its properties. At the heart of many experiments, no accurate plan and theoretical base exist. It leads to the fact that researchers give primary attention to reproduction of only certain properties of BL: the spherical form of an object, presence of luminescence, and a lifetime of

about 1 s. Thus, the basic properties of BL, such as high density of energy, the presence of uncompensated electric charge, the complex nature of its structure, the nonthermal mechanism of radiation, and the features of its movement, have been neglected.

In the field of BL-observation data collection, there was the same situation: new data practically added nothing to a "portrait" of an average BL, which for some reason, has not yet helped to create an adequate model of this phenomenon. Similarly, the time has come to shift to the publication of full descriptions of BL observations. Quite probably, they may contain data that can become the "key," opening its secrets. The time has come to seriously consider the data file of UFO observations, more than half of those objects possess properties of BL. This, however, will require an explanation on the rare characteristics of BL and UFO, as objects of some tens of meters in size, existing for tens of minutes, moving with high speeds and accelerations, and also their ability to emit out narrow beams of light.

The history of scientific development shows that as a rule, it is difficult to interpret the consequences of a particular discovery. In the nineteenth century, no one would have guessed that the opening of an electromagnetic induction by Faraday could become the basis of the electric power industry in the future. In the beginning of the twentieth century, only science-fiction writers expected technical revolution, which took place in the second half of the century, with the creation of lasers, development of an atomic energy, and a flight in the cosmic space. In the same way, now, it is impossible to predict what advantage mankind will gain after the secret of BL will be solved. For now, it has not occurred, and BL researches will proceed as before – with the efforts of the small group of enthusiasts aspiring "to satisfy their curiosity." It is necessary to realize that BL science is the interdisciplinary science requiring the participation of experts working in various areas of physics, chemistry, power, synergetics, biology, and psychology. Let us hope that the International Committee on Ball Lightning can help to organize a teamwork of experts from these areas of science.

6.2 Ball Lightning as an Object of Condensed Substance

A BL model has been considered in this subchapter. According to it, BL appears as the result of linear lightning impacting different materials. At this impact, an heated unipolarly charged condensed substance area is created, from which some mass is thrown out. This mass is transformed into a sphere. The sphere's surface cools down leading to the creation of a quasi-solid-vitrified cover. The field in the charged substance of BL is distributed, such that its greater value is situated in the thin layer under the surfaces. As BL substance is created in natural conditions, there are pores with captured air and other defects in it. Hence, the favorable conditions for the creation of discharges exist in this layer. Discharges begin to heat captured air and surface. At some temperature of heating, the surface reaches the temperature of melting (some structures such as jets and waves appear on the object surface), and

then, the temperature of ignition. The BL disappears either owing to explosion or combustion. It releases a chemical energy of combusted material. Its ability to levitate is defined by the high value of electrical charge on its surface.

6.2.1 Introduction

One of the theoretical directions of BL description comprises models of BL with a solid framework (e.g., see [294–300]). They are constructed based on the assumption that these objects at storm activity are formed of different sorts of inorganic [294–296, 298–300] or organic [297] particles, specks of dust, products of various materials' destruction and soil, arising at a lightning stroke, or at the interaction of charged water clusters [295]. They can have aerosol, drop, or a bubble-like structure.

BL, whose models are described in [294–296, 298–300], have low values of energy density – 30–100 MJ/m^3. These models are not capable of explaining the cases of BL observation with energy density in the range of 10^3–10^6 MJ/m^3, described by observers (e.g., see [301]). In [297], to explain the nature of BL with its organic origin, an attempt was made with the polymeric threads in the form of a ball formation that accumulates electric charges on the surface of the threads. Thus, the density of the polymeric threads in the ball influenced the ability to store energy. In the case of unipolar charging, it could store energy up to 300 MJ/m^3, which is obviously smaller than those given out by most of the interesting observations. To develop a theory [302, 303], experiments with the application of organic and inorganic materials to create long-lived shining objects (LSO), were conducted.

It was possible to create LSO with a lifetime of 5–7 s and size of up to 1 cm at an insertion of cotton wool or charred wood particles in the channel of erosive plasma generator with walls of organic glass [302], and LSO with a lifetime of up to 2 s and size of up to 2 cm in a plasma generator with walls of a mixture of wax, rosin, and small particles of wood [303]. During the experiments, LSO was observed in which fused metal particles and pieces of metallic electrodes were found in its base. The existence time of such objects was defined by their combustion. In case of metal particles' oxidation, bang sounds have been detected. These experiments showed that the composite particles consisting of metal and organic particles can be BL analogs.

In [298], successful experiments on LSO reproduction were carried out at discharge blow in soil. The authors started from an idea that BL is born in fulgurites area – in the place of a linear lightning blow where there is a soil fusion, and the tangle of silicon nanodimensional chains takes off – and the life span of such an object is basically defined by the time of reduction and oxidation reactions in the air. Experiments carried out in [304, 305] were the ideological continuation of an earlier work [298]. Under the influence of an electric arc or MW discharges, subjects of SiO_2 were heated, they turned into the fused shining objects, and perished as a result of high-temperature oxidation–reduction processes; the upper time of arc discharge excited doped silicon wafers combustion processes [305] was about 8 s and the sizes of the objects reached several centimeters.

The results of these works show the perspectives of models where BL exists in the form of the composite condensed substance created at the impact of a linear lightning on various materials.

The collection and analysis of BL observations and successful experiments on the creation of BL analogs have allowed to single out the following BL features that should be explained using BL theory: a high BL-energy density of up to 10^5–10^6 MJ/m^3, BL's unipolar charge and own electric field, long lifetime – about tens of seconds, an ability to levitate, an ability to ignite subjects, an ability to blow up, an ability to be transformed from sphere to tape, an ability to penetrate through holes, an ability to decay not only in balls but in pieces, its manifestation in the form of a subject with liquid surface with jets ejecting from it, and a condensed object that, at jumping, can sound like a solid sphere. This theory has to take into account BL's appearance in the summer period when thunderstorms occur, and the interaction of linear lightning with different materials leads to BL's appearance in accordance with the observations. This object can have a hot surface, and hence, the developed theory has to include the possibility of different materials for BL framework.

The model presented here includes some features of [306–308] BL-melted unipolarly charged object and has developed it further.

6.2.2 General Model

Let us consider the following scenario of BL's origination and life. The possibility of BL's existence follows from the fact that linear lightning leader and the return stroke are unipolarly charged objects, and they can transfer energy directly and inductively to the substances. In the simplest case of analysis, which we take as the starting point, the linear lightning impacts the earth (with soil consisting of inorganic and organic components). At this impact, heated unipolarly charged area is created. Some mass of melted–charged substance is thrown out from it. This mass is transformed into a sphere mainly under Coulomb force of charges in this substance and the counteraction of surface tension force. The sphere's surface cools down leading to the creation of quasi-solid-vitrified cover. Convective air flows create a convective boundary layer over the surface, and hence, observers do not experience heat from this object. The electric field in the charged substance of BL is distributed, so that its greater value is situated in the thin layer under the surfaces. As BL substance is created in natural conditions, there may be pores with captured air and other defects in it. Hence, favorable conditions for the creation of discharges exist in this layer. Discharges begin to heat captured air and surface. At some temperature of heating, the surface reaches the temperature of melting (some structures such as jets and waves appear on the object surface), and it can be separated into two balls. Then, at the rising of temperature, the BL surface reaches ignition temperature. As a result, the BL disappears either owing to explosion or combustion (with extinction).

6.2.3 Ball Lightning Energy

The main feature of BL presenting scientific and applied interest is its high-energy density. As we consider the combustion of BL substance, we have to account for two main parameters playing their roles at the release of BL energy. The first one is the mass m_{sph} of BL material, and the second is the combustion energy ΔU_{comb} release of BL substance. They allow estimation possible at the upper levels of BL-energy density. For this, let us consider the natural material at that was impacted by linear lightning. Its density ρ can be widely ranged due to its different conditions of impact from porous to condensed one so $\rho \sim (0.1-10)\cdot 10^3 \text{kg/m}^3$. The combustion-energy release of the substances changes in a wide range with respect to the properties of definite substance, $\Delta U_{\text{comb}} \sim (2\text{–}20) \times 10^7$ J/kg [309]. Hence, it is possible to estimate energy W and energy density W_{spec} of BL released at the combustion of these materials:

$$W = m_{\text{sph}} \cdot \Delta U_{\text{comb}}, \tag{6.6}$$

$$W_{\text{spec}} = m_{\text{sph}} \cdot \Delta U_{\text{comb}} / (4\pi R_{\text{sph}}^3/3) = \rho \cdot \Delta U_{\text{comb}}, \tag{6.7}$$

$$\rho = m_{\text{sph}} / (4\pi R_{\text{sph}}^3/3), \tag{6.8}$$

where R_{sph} is the radius of the sphere. By inserting values of density and combustion-energy release of materials, one can obtain the following range of energy density possible to be released at combustion of BL material, $W_{\text{spec}} = 2 \times 10^2$ to 2×10^6 MJ/m^3. These values lie in the range of observed BL-energy densities. Hence, appearing under linear lightning impact, combusting material can produce the energy necessary to explain high-energy BL events, and the combustion of material excited by linear lightning can be the reason for its high energy.

As BL has to levitate, its mass has to be dependent on a value of the electric force allowing it to levitate. Hence, the force has to be dependent on BL charge value q_{surf} and the external electric field E_{ext}. At a definite charge on BL's surface and high thunderstorm electric field (including electric fields of the Earth and the cloud, or their combination), BL would levitate. This follows from the fact that high thunderstorm electric fields of $\sim 3 \times 10^3$ V/m were detected [310]. The second fact confirming this is that: usually soil consists of 50% of SiO_2 [298], and samples of SiO_2 can accumulate high values of electrical charge [311] (with the creation of electric fields of $\sim 10^7$ V/m and higher over them). Hence, at multiple strokes of linear lightning at some region on earth, there is a possibility of realization of extremely high electric fields over it, owing to the accumulation of charges from these strokes. If we consider BL to be a charged sphere, then the electric charge value on the surface of it is proportional to the electric field on the surface. However, one has to remember that the electric field E_{surf} on the surface of BL can be very high up to inter-atomic fields that are about 5×10^{11} V/m.

Let us write down the known equation [312, 313] describing BL levitation over the conducting surface corresponding to this model (in SI units system):

$$q_{\text{surf}}E_{\text{ext}} = m_{\text{sph}} \cdot g + \frac{q_{\text{surf}}^2}{16\pi x^2 \varepsilon\varepsilon_0}, \tag{6.9}$$

where g is the gravitation constant, $\varepsilon = 1$ is the dielectric permeability of the air, ε_0 is the vacuum constant, x is the BL height over the earth (here, we consider that BL and earth surface have an electric charge of same polarity). Furthermore, q_{surf} and electric field E_{surf} are connected by Coulomb law in the form of

$$q_{\text{surf}} = 4\pi\varepsilon\varepsilon_0 E_{\text{surf}} \cdot R_{\text{sph}}^2. \tag{6.10}$$

Using these equations, it is easy to obtain the following equation connecting the density of BL material with BL charge, q_{surf}, external electric field, E_{ext}, and the electric field, E_{surf}, on the surface of BL:

$$\rho = \frac{3\varepsilon\varepsilon_0 E_{\text{surf}} E_{\text{ext}}}{gR_{\text{sph}}}\left(1 - \frac{E_{\text{surf}}}{E_{\text{ext}}}\frac{R_{\text{sph}}^2}{4x^2}\right) = \frac{W_{\text{spec}}}{\Delta U_{\text{comb}}}. \tag{6.11a}$$

This equation allows estimation of the parameters of BL and its height over the earth with respect to atmospheric thunderstorm conditions.

For example, BL with $R_{\text{sph}} = 0.1$ m, density $\rho = 3.8 \times 10^3$ kg/m^3, and the electric field on its surface $E_{\text{surf}} = 1.44 \times 10^9$ V/m, can levitate at a height $x = 2$ m in a thunderstorm atmosphere with the field $E_{\text{ext}} = 1.0 \times 10^6$ V/m, and its energy density can be in the range $W_{\text{spec}} = (1.6\text{–}4) \times 10^5$ MJ/m^3. It can be observed that the obtained values are about those observed for high-energy BL [301] and are only by an order of factor 5–7 smaller than those of the extreme cases (1.1–2.5) $\times$ 10^6 J/m^3 [301].

Similarly, BL with $R_{\text{sph}} = 1$ m, density $\rho = 3.8 \times 10^3$ kg/m^3, and electric field on its surface $E_{\text{surf}} = 1.44 \times 10^8$ V/m, can levitate at height $x = 2$ m in a thunderstorm atmosphere with the field $E_{\text{ext}} = 1.0 \times 10^6$ V/m, and its energy density can be in the range $W_{\text{spec}} = 1.6 \times 10^3$–$4 \times 10^3$ MJ/m^3.

If $1 \gg E_{\text{surf}}/E_{\text{ext}} \cdot R_{\text{sph}}^2/(4x^2)$, then one has the most interesting case when

$$W_{\text{spec}} = \frac{3\varepsilon\varepsilon_0 E_{\text{surf}} E_{\text{ext}} \Delta U_{\text{comb}}}{gR_{\text{sph}}}, \tag{6.11b}$$

and

$$\rho = \frac{3\varepsilon\varepsilon_0 E_{\text{surf}} E_{\text{ext}}}{gR_{\text{sph}}} = \frac{W_{\text{spec}}}{\Delta U_{\text{comb}}}. \tag{6.11c}$$

Let us use the formulas (6.11b and 6.11c) for the analysis of different situations. Let us consider an organic charged sphere with a typical density of organic material $\rho \approx 2.0 \times 10^3$ kg/m^3, $\Delta U_{\text{comb}} \sim 5 \times 10^7$ J/kg, and $W_{\text{spec}} \approx 10^{11}$ J/m^3. This means

that the electric field strength on the surface of this BL has to be $E_{surf} \sim 2.5 \times 10^{11} R$ V/m (R is in m) at $\varepsilon \sim 3$ and $E_{ext} \sim 10^3$ V/m.

Let us consider some natural mineral-type material with $\rho \approx 2.5 \times 10^3$ kg/m^3, $\Delta U_{comb} \sim 10^8$ J/kg, and $W_{spec} \approx 2.5 \times 10^{11}$ J/m^3, and it corresponds to $E_{surf} \sim 2.0 \times 10^{11} \cdot R$ V/m at $\varepsilon \sim 5$ and $E_{ext} \sim 10^3$ V/m.

We can observe that the obtained values are about those observed for high-energy BL [301] and are only by an order of magnitude smaller than those of the extreme cases of (1.1–2.5) $\times 10^{12}$ J/m^3 (see Section 6.1.2). Electric fields on BL's surface in these cases are of inter-atomic values. In such anomalous conditions, where the BL consists of excited atomic components, ΔU_{comb} can be much higher.

According to [314], BL components in the form of a powder or little particles, will be more effective from the point of view of combustion. In this case, (6.11c) can be changed to

$$\rho_1 = \frac{3\varepsilon\varepsilon_0 E_{surf} E_{ext}}{g R_{sph}} \left(1 - \frac{E_{surf}}{E_{ext}} \frac{R_{sph}^2}{4x^2}\right) \left(1 + n \cdot r_i^2 / R_{sph}^2\right) = \frac{W_{spec1}}{\Delta U_{comb}}. \qquad (6.11d)$$

Here, n is the number of particles of radius r_i inside the sphere R_{sph}. For simplicity, we consider that small particles are identical and that the electric-field strength E_{surf} on the surface of the large sphere and on the internal spheres is the same. These formulas also show that large energy effects can be realized in anomalous conditions at large E_{surf} and ΔU_{comb}. At $n \gg 1$ formula (6.2.6d) limits to the result of (6.2.6c), but it shows that almost all the chemical energy in this case is located in small particles. Hence, the process of heating and destruction of the BL surface can lead to an inflammation of small particles resulting in their ignition or explosion in the air.

Estimates also show that the electric energy of the considered objects is much smaller than their chemical energy. BL, of course, can exist at the violation of (6.11b); in this case, they will not exhibit such a unique property as levitation.

From the point of view of the presented theory, the objects obtained in experimental works with ignition and combustion of materials in a plasma represented variants of BL, such as burning objects of condensed melted material, and they were analogous to the natural BL.

6.2.4 Electric-Field Parameters

The question of BL charge and electric-field distribution is important for BL, since it determines the behavior of BL. There are no questions when the electric-field strength on the BL surface E_0 is below the air breakdown value $E_{br} \sim 3 \times 10^6$ V/m, and the electric-field strength distribution over the radial direction is $E(r) = E_0 (R_{sph}/r)^2 (r \geq R_{sph})$. Usually, in models [295, 296], the authors accepted fields on BL's surface below the breakdown value.

According to the previous section, electric fields on BL's surface can be much higher. In this case, the appearance of plasma has to be realized over the BL's surface as a result of ionization, attachment, recombination, and other processes [315]. This plasma is characterized by electron temperature T_e in the range of 3–10 eV and concentrations of electrons $N_e \sim 10^{13}$–10^{16} cm^{-3}. According to [316], electrons and ions of plasma will create a layer in the region between E_0 and E_{br} directed oppositely to the electric field of the sphere, and essentially, decrease the initial field of the sphere. After that, the plasma decays and the initial electric field is restored, and the whole process is repeated. The distance at which the field decreases is the Debye radius [315, 316] $r_D = (\varepsilon\varepsilon_0 T_e/(2e^2 N_e))^{1/2}$; it ranges within the limits $r_D \sim 4.0 \times 10^{-4}$–$2.0 \times 10^{-5}$ cm. Furthermore, the time of switching off of the initial field is approximately equal to the time of electron drift over this distance: $\tau \sim r_D/w_{dr}$, where electron drift velocity is $w_{dr} \sim 10^7$–10^8 cm/s, or the corresponding frequency $\nu \sim 3 \times 10^{10}$–$5 \times 10^{12}$ s^{-1} ionization times and creation of electrons may be even smaller. Hence, the frequency of field pulses will be of $\sim \nu$.

The presence of pulsed electric field and appearance of the plasma-change processes are connected with the attraction to the image of charged objects [317]. Hence, the appearance of plasma can substantially decrease the influence of charge image and rise the electric-field strength on the BL surface.

The presence of such pulsed field can cause luminescence of lamps with cut wires (see below). At the introduction of easily ionized particles in this area, change in the electric field near their surfaces and breakdown can occur. This can explain the appearance of large luminescent clouds that surround BL.

A distribution of electric field inside the sphere depends on the distribution of charges in it and the thickness of the cover. For example, in the case of a uniformly charged sphere with charge Q, its internal field distribution is well known [312, 313]

$$E_{int}(r) = Q \cdot r/(4\pi\varepsilon\varepsilon_0 R_{sph}^3),$$

In particular, this formula shows that the maximum values of electric-field strength in the case of the charged sphere are realized near its surface. In the presence of pores or defects in such a sphere, the breakdowns of air inside them will occur, as it usually takes place in real-charged dielectric substances at an applied voltage to their surface [318], and this can explain the luminescence of BL and heating of its surface.

6.2.5 *Ball Lightning Surface*

Evidently, the surface of BL will be cooled owing to radiation and thermal conductivity, whose durations are of minutes for their typical sizes of 0.1–1 m. Also, there is a process of convection that may be connected with BL cooling.

A convective boundary layer creation takes place over its surface. At the typical temperature of melted material of BL, which is 400–600 K for organic and 1,200–1,500 K for inorganic substances, a thin boundary layer owing to convection is created near a spherical body. The thickness of this layer can be estimated as [319]

$$L \sim 2R_{\text{sph}}/\sqrt{Re} = 2R_{\text{sph}}/\sqrt{u \cdot 2R_{\text{sph}}/v_{\text{d}}},$$

here Re is the Reynolds number, u is the air velocity, and v_{d} is the dynamic viscosity ($v_{\text{d}} = 0.15$ cm^2/s for air at room temperature). Considering BL with a radius in the range $R_{\text{sph}} = 0.5-25$ cm, and air velocity (typical for air flows in quiet room conditions) in the range $u = 1$–10 m/s, one can obtain that the width of BL boundary is $L \sim 0.1$–0.3 cm. This means that the drop of the gas temperature from the BL's wall temperature to the ambient gas temperature takes place in this region, and observers will not feel BL's surface temperature.

A very important mechanism of modification of BL surface was considered in [320]. It was shown that in the case of charges inside a sphere with water cover, a polarization of molecules in the cover appeared, which realizes a strong force that subtends the molecules to the center. Thus, for the charge value of $Q \sim 10^{-2}$ C (corresponding electric-field strength on the surface $E \sim 10^{10}$ V/m) of a sphere of 6-cm radius, the force was about $F \sim 6 \times 10^8$ N. Evidently, this force can be realized in our case that created a solid cover over BL.

Quick processes of cooling and compression of the surface can not only lead to the creation of a solid surface, but also a vitrified surface [321, 322] whose temperature of vitrification is 200–300 K smaller than those of melting.

In the case of BL with a heated surface, when it represents the charged liquid, the instability phenomena of charged liquid surfaces can be realized [308]. The instability of the charged melted sphere with the formation of structures on its surface (corrugation), according to [300], was developed with the following condition for the electric field on the surface:

$$E_{\text{surf}} > \frac{2}{\sqrt{\varepsilon\varepsilon_0}} \left(\alpha_{\text{t}} \cdot P_{\text{atm}}/R_{\text{sph}}\right)^{1/4},$$

where α_{t} is the surface tension coefficient of the melted material and P_{atm} is the atmospheric pressure. This formula gives fields of $E_{\text{surf}} = 9 \times 10^6$ V/m in the case of paraffin at $R_{\text{sph}} = 0.1$ m and $E_{\text{surf}} = 1.2 \times 10^7$ V/m in the case of glass at the same R_{sph}.

Another instability leading to the separation of particles [299] from the charged sphere (the electrostatic instability) realizes at

$$E_{\text{surf}} > \frac{2}{\sqrt{\varepsilon\varepsilon_0}} \left(\alpha_{\text{t}}/R_{\text{sph}}\right)^{1/2}.$$

For example, it realizes at $E_{surf} = 3 \times 10^5$ V/m for the sphere of paraffin with $R_{sph} = 0.1$ m and at $E_{surf} = 1.3 \times 10^7$ V/m of glass at the same R_{sph}.

Development of these instabilities leads to the destruction of the surface and its separation into pieces.

Let us discuss the question about the type of BL form. First, let us consider BL with continuous material. As we consider BL consisting of liquid, melted material, Laplace surface tension, pressure of charges, and atmospheric pressure can impact BL. In this case, an equation to balance the forces acting on charged BL sphere in the air has the form [300]

$$\frac{kQ^2}{8\pi R_{sph}^4} = P_{atm} + \frac{2\alpha_t}{R_{sph}}, \tag{6.12}$$

where $k = 1/(4\pi \cdot \varepsilon\varepsilon_0)$. Using the fact that $P_{atm} \gg 2\alpha_t/R_{sph}$ for materials like silicon, alumina and paraffin, by which we can model BL substance at typical sizes, one can obtain the following formula connecting the main parameters

$$R_{sph} = \left(\frac{kQ^2}{8 \cdot \pi \cdot P_{atm}}\right)^{1/4}. \tag{6.13}$$

From this formula, it can be observed that a sphere of radius $R_{sph} = 0.1$ m can be formed at $Q = 1.8 \times 10^{-4}$ C and of radius $R_{sph} = 1$ m at $Q = 1.7 \times 10^{-2}$ C. One can see from this equation that the radius decreases with the loss of electric charge by BL, for example, in the result of streamers or charge runoff, and hence, the collapse of the object takes place.

Second, let us consider BL as a bubble with a charged liquid surface. In equilibrium, the following equation is valid [300]:

$$P_{vap} + P_{gas} + \frac{kQ^2}{8 \cdot \pi \cdot R_{sph}^4} = P_{atm} + \frac{4\alpha_t}{R_{sph}}, \tag{6.14}$$

where P_{vap}, P_{gas} describe vapor and gas pressure inside a cavity of the bubble, respectively, which depend on the conditions of bubble formation. Their sum can be either higher than the atmospheric pressure or smaller than that with respect to the conditions of formation.

If the BL's surface is heated, then P_{vap}, and P_{gas} values can rise and lead to a variation of the BL's radius. In the case of molecular gas in the cavity, one can show

$$P_{vap} + P_{gas} = P_{int\,0} \cdot (T/T_0) \cdot (R_0/R_{sph})^3, \tag{6.15}$$

where $P_{int\,0}$, T_0, R_0 are the initial pressure inside a sphere, initial temperature, and initial radius of the bubble, respectively.

Let us consider different situations using the fact that $P_{atm} \gg 4\alpha_t/R_{sph}$ for materials like silicon, alumina, paraffin. If the ball was created so that $P_{vap} + P_{gas} \ll P_{atm}$, then its radius is determined using (6.13).

Table 6.1 Ball lightning (BL) radius (m) for different materials (6.16b) at electric field E_{surf} (V/m) on BL surface

E_{surf}	Si	Glass	Paraffin
10^6	0.8	0.12	0.04
3×10^6	0.09	0.013	0.004
10^7	0.008	0.0012	0.00045

If the ball was created so that the initial pressure in it was close (by its value) to the external pressure value (e.g., blowing out of BL) $P_{vap} + P_{gas} \approx P_{atm}$, then its initial radius is determined by the equation

$$R_{sph} \approx \left(\frac{kQ^2}{32 \cdot \pi \cdot \alpha_t}\right)^{1/3} = \frac{32 \cdot \pi \alpha_t \cdot k}{E_{surf}^2}. \tag{6.16a}$$

It must be noted that usually $\alpha_t = \alpha_0 \cdot (T_0/T)^{\beta}$; where α_0 and T_0 are the initial values of surface tension coefficient and a temperature of a liquid, respectively, and $\beta > 0$, then

$$R_{sph} \approx \left(\frac{kQ^2 \cdot (T/T_0)^{\beta}}{32 \cdot \pi \cdot \alpha_0}\right)^{1/3}. \tag{6.16b}$$

In Table 6.1, one can observe the values of BL radii obtained by (6.16b) at different electric-field values on BL surface. These values reasonably agree with the observed radii of BL.

Now, let us consider BL explosion possibility, for example, when the surface of BL is heated as the result of gas-discharge development over it, so that it can be ignited. Thus, in (6.15), we consider that the temperature inside BL and on its surface rises as $T \sim T_0 \cdot \exp\left(t/\tau_{ign}\right)$, where τ_{ign} is an ignition time. Thus, from (6.15) and (6.16b), one can obtain the following equation:

$$P_{int\,0} \cdot \exp\left(t/t_{ign}\right) \cdot \left(R_0/R_{sph}\right)^3 \approx 4\frac{\alpha}{R_0}\left(\frac{R_0}{R_{sph}}\right).$$

Or

$$R_{sph} \sim \exp\left(t/\left(2 \cdot \tau_{ign}\right)\right), \tag{6.17}$$

BL's radius rises sharply in time, and this leads to BL's destruction.

The appearance of small melted particles due to the electrostatic instabilities of the BL's surface facilitates ignition and accelerates the combustion of disperse material on the BL's surface and also leads to its explosion.

6.2.6 Ball Lightning Lifetime

Let us estimate the maximal life span of BL. As this model is represented by a unipolarly charged sphere, charges from air in a form of oppositely to sphere charged ions will move to its surface. Hence, the time of the sphere's discharging is connected with the recombination of atmospheric ions with charges of the sphere. Let us write down an equation describing the process of decrease in the charge Q on the sphere, to which ions come through an area $4\pi R^2$:

$$\begin{aligned}\frac{\mathrm{d}Q}{\mathrm{d}t} &= -4\pi R^2 w N_i e = -4\pi R^2 b_i E \cdot N_i e \\ &= -4\pi R^2 b_i \cdot N_i e Q/(4\pi R^2 \varepsilon\varepsilon_0) = -b_i \cdot N_i e Q/\varepsilon\varepsilon_0,\end{aligned} \tag{6.18}$$

where w is the drift velocity of ions, e is the elementary charge, b_i is the mobility of ions, and N_i is their concentration. Solution of (6.18) gives the typical time of the charge decrease τ:

$$\tau = \varepsilon\,\varepsilon_0/(b_i\, e\, N_i). \tag{6.19}$$

Assuming that in atmospheric air, charged particles are mainly produced by background ionization with a rate S and disappear through ion-ion recombination with a rate constant α_{ii} one obtains that a average number of ions in air is

$$N_i \approx \sqrt{S/\alpha_{ii}}. \tag{6.20}$$

By inserting (6.20) into (6.19), one obtains the following formulae for a typical time of charge decrease in the sphere (maximal value of its lifetime)

$$\tau = \varepsilon\varepsilon_0/b_i \cdot \sqrt{\alpha_{ii}/S}. \tag{6.21}$$

The average value of ion mobility is $b_i = 2.8 \times 10^{-4}$ m^2/(V s) [296, 315], ion-ion recombination coefficient at room temperature in air $\alpha_{ii} = 2 \cdot 10^{-6}$ cm^3/s [296, 315], and $S = 4$ cm^{-3} s^{-1} (S changes with respect to location on earth) [312]. By inserting these values in (6.13), one obtains the maximal BL lifetime $\tau \approx 1.4 \times 10^2$ s.

As noted in the previous paragraph, at the surface of BL in pores and defects, an electric field with a high strength is realized and there is an ionization of air and plasma formation in a thin layer at the surface. The time of life of BL is defined by the time of a warming up of a thin layer of the BL's surface. It is either the heating temperature of a dielectric material to a temperature of destruction of solid BL cover at which electrostatic instabilities or temperature of ignition of a dielectric material occur ($T_\mathrm{ign} - T_0 \sim 300$ K, T_ign – temperature of air corresponding to temperature of ignition of BL material). It is supposed that the time of destruction or burning of this material is much smaller than the time of BL surface warming.

The simplest equation describing the heating of a surface layer has the form:

$$C_p \frac{\partial T}{\partial t} = \mathrm{div}(\chi \ \mathrm{grad}\ T), \tag{6.22}$$

where χ is the thermal conductivity coefficient, C_p is the heat capacity of air, T is the temperature in the layer of air, and t is the time. In a spherical case, (6.22) has the form [323]:

$$\frac{\partial T(r,t)}{\partial t} = \frac{\chi}{C_p}\left(\frac{\partial^2 T(r,t)}{\partial r^2} + \frac{2}{r}\frac{\partial T(r,t)}{\partial r}\right), \tag{6.23}$$

with the following initial conditions

$$t > 0, \quad 0 < r < R_{\mathrm{sph}},$$

$$\frac{\partial T(r,t)}{\partial r} - \frac{q_{\mathrm{ef}}}{\chi} = 0, \quad \frac{\partial T(0,t)}{\partial r} = 0, \quad T(0,t) \neq \infty.$$

Heating of the surface of the sphere is determined by a flux of heat q_{ef} to the surface. If it has a gas discharge origination, then it is connected with the parameters of a discharge:

$$q_{\mathrm{ef}} = N_{\mathrm{e}} \cdot w \cdot \varepsilon_{\mathrm{e}}, \tag{6.24}$$

where N_{e} is the electron concentration in the area of the plasma, w is their mobility, and ε_{e} is their mean energy. For estimations, we supposed uniformity of parameters for all the surface. At $q_{\mathrm{ef}} \approx 100$ W/m^2, typical for air plasmas, the parameters were $N_{\mathrm{e}} \approx 10^{9}$–$10^{10}$ cm^{-3}, $w \approx 10^{7}$ cm/s, and $\varepsilon_{\mathrm{e}} \approx$ 3–4 eV. In principle, q_{ef} can vary in wide limits with respect to external conditions, and for comparison, we also considered $q_{\mathrm{ef}} \approx 1{,}000$ W/m^2.

There is an analytical solution for (6.23) [323]:

$$T(r,t) - T_0 = \frac{q_{\mathrm{ef}} R_{\mathrm{sph}}}{\chi} \cdot F(r,t), \tag{6.25}$$

where $F(r, t)$ is some function depending on radius and time. Calculations in [324] were carried out for a condition of a flux to the surface $r = R_{\mathrm{sph}}$. The results of the calculations are represented in Fig. 6.8.

Lines **a** and **b** correspond to heating of the surface layer for $T_{\mathrm{ign}} - T_0 = 300$ K, **a** at $q_{\mathrm{ef}} \approx 100$ W/m^2; and **b** at $q_{\mathrm{ef}} \approx 1{,}000$ W/m^2.

The obtained values allowed comparing them with the observed data on BL's life span; solid line corresponds to decaying BL, dashed lines indicate to exploding BL, and the dashed-point line corresponds to going out (with extinction). As one

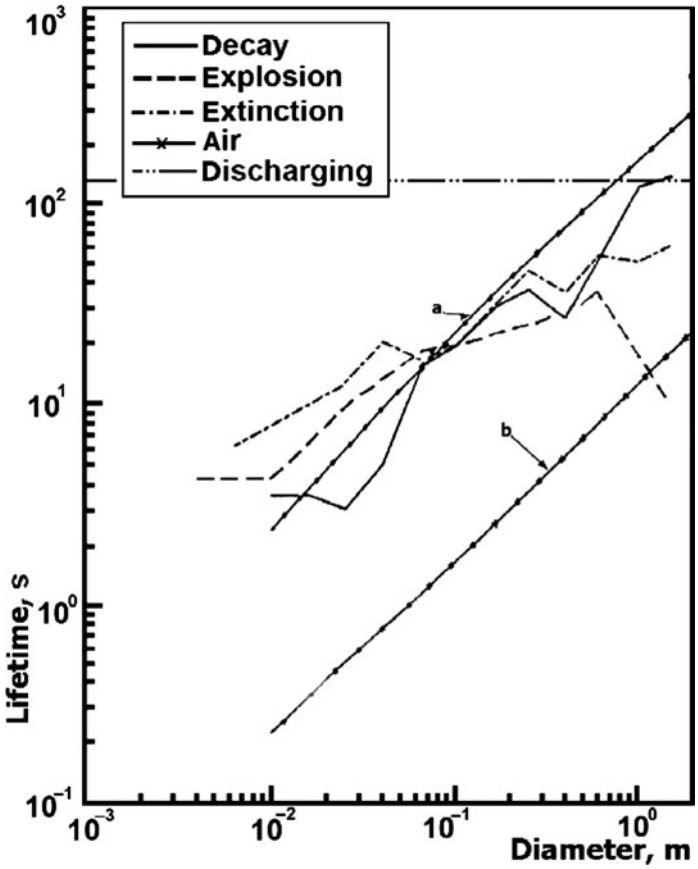

Fig. 6.8 Ball lightning (BL) lifetime – radius dependence with respect to different ways of elimination. (**a**, **b**) – BL surface heating by discharges with a power of 100 and 1,000 W/m^2, respectively; *solid line* – decay of real BL; *dashed line* – explosion of real BL; *dashed-point line* – extinction of real BL; *two-point – dashed line* – discharging of BL

can see that the addition of $q_{ef} \approx 100$ W/m^2 to the surface can, in general, explain the destruction of BL, the corresponding curve is not far from the set of observed BL curves. It also explains the tendency of BL's life span, which increases with size. However, the values of heating of the BL's surface at a delivered additional heat flux of $q_{ef} \approx 1{,}000$ W/m^2, are very small. But, they can explain quick BL destructions at getting into stoves.

From (6.25) at small BL radii (<5 cm), one obtains

$$t \sim \frac{(T_{max} - T_0)}{T_0 \cdot q_{ef}} R_{sph}. \tag{6.26}$$

In other words, BL's life span is directly proportional to a temperature interval of heating, the size of BL, and is inversely proportional to the power released near its surface. This result can explain the lifetime-diameter dependence for BL observed during thunderstorms [325].

This section shows that the considered mechanisms that determine BL's life span limit its lifetime by the value of $\sim 10^2$ s and that the life span increases with its size.

6.2.7 Examples

Let us consider examples of the presented model application.

The first one is connected with BL observation in Novosibirsk in 1996 [326]. BL had appeared on a pine-tree at a height of about 12 m. Then, it descended down, almost directly. At that, it created a furrow, whose width was about 5 mm at the top and 50 mm near the ground. Then, it moved and covered about 62 m and exploded in the end. Subsequently, its total observation time was about 8–9 s (we represent only the necessary data for our analysis).

Before our analysis, we have to mention that a theory of vapor explosion created by linear lightning and BL was delivered in [327]. According to it, the electric field of the lightning creates electric current in water, Joule heating takes place, it heats water to vaporization, and vapor pressure breaks the tree surface.

We also consider this reason for BL's bark destruction. We accept [328] that water in trees moves upward exactly under the bark, and hence, there should be destructions. Also, one has to note that water in trees is purified due to its transportation through the molecular membranes of a root system [328]. Hence, its electrical conductivity is close to those of distilled water.

Let us determine the amplitude value of pulsed electric field strength on the surface of BL, at which evaporation of water takes place under the bark and causes vapor explosion.

$$W_{\mathrm{v}} \approx \lambda_{\mathrm{v}} \cdot \rho \cdot V, \tag{6.27}$$

where λ_{v} is the specific water vaporization heat, $\lambda_{\mathrm{v}} \approx 2.26 \cdot 10^6$ J/kg, ρ is the water density, and V is the volume occupied by water.

The electrical energy spent for water vaporization is:

$$W_{\mathrm{e}} \approx \sigma \cdot E^2 \cdot V \cdot \tau, \tag{6.28}$$

where E is the pulsed electric field strength on BL's surface, σ is the water electrical conductivity, $\sigma \approx 5 \times 10^{-4}$ S/m (S is siemens) is the average value of distilled water conductivity, and τ is the time of BL interaction with water in the layer under

a bark. For estimates, we took $\tau \approx 1.5$ s, proportionally to the covered distance. Combining (6.27) and (6.28), one has:

$$E \approx \sqrt{\frac{\lambda_v \cdot \rho}{\sigma \cdot \tau}}. \tag{6.29}$$

By inserting necessary data into (6.29) one obtains $E \sim 1.7 \times 10^6$ V/m.

This result shows that electrical-field strength was about air breakdown field strength; it impacted water under the bark and led to the explosion of vapors there.

Let us consider a second example. There are well-known cases of BL passing by the lines of lighting, where there was damage of wires connecting lamps, and the moment when BL was near them, the lamps began to shine.

We can explain this through the well-known effect of a capacity in a circuit of alternating current [329]. In this case, the amplitude value of voltage U_0 on the capacity C, current i_0, circular frequency of the current ω, and capacity are connected by the equation

$$U_0 = i_0/(\omega \cdot C). \tag{6.30}$$

By inserting the circular frequency of pulsed electric field $\omega = 2 \times 10^{11}$–$2 \times 10^{12}$ s^{-1}, a small capacity of the electric lamp of an order $C \sim 10^{-12}$ F, and a current $i_0 \sim 10$ A necessary to ignite the lamp, from (6.30), one can conclude that a voltage applied to the lamp has to be $U_0 \sim$ 5–50 V, which can be realized by BL. Considering a distance at which this voltage has to be applied, $L \sim 10$ cm, one can conclude that BL has created a pulsed electric field with the amplitude value of $E \sim$ 50–500 V/m, which can be realized by BL or a radius of 0.1 m at a distance of 2 m if the electric field on the BL's surface remains in the range $E_0 \sim 2 \times 10^4$–2×10^5 V/m.

Let us consider the third example – BL blowing out of a socket. For this purpose, we consider the simplest case – BL as a bubble with a charged liquid surface. Its radius via charge dependence is described by (6.16b).

In Fig. 6.9, we represent the consequence accounting for the processes taking place with a bubble created inside the socket (see Fig. 6.9a), which we obtained on the basis of the equations (6.14)–(6.16). The appearance of a bubble takes place in the socket at an overloading voltage in the electrical circuit: melting and charging of some material piece (wire, solder material and the composite material of a socket) takes place inside the socket, a charged liquid drop occurs, then at motion, as a result of cavitation, it transforms into the charged bubble [307]. It is covered with a plasma layer, and hence, there is no direct contact with the walls of the socket.

If the internal bubble volume is greater than those of the cavity inside the socket, then it begins to propagate outside through the holes in the socket (Fig. 6.9b).

Charges in the melted, conductive material are concentrated at the edges of the structure [329], and hence, in (6.15), (6.16), conditions for the outside local bubbles' appearance on these edges appear (Fig. 6.9c). The electric-field conditions

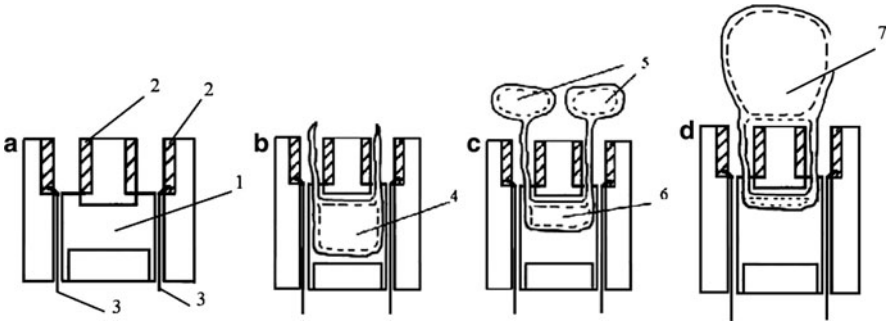

Fig. 6.9 Ball lightning (BL) blowing out process

creating plasma in the cavities of the surface are improved on the surface of the outside bubbles, their temperature rises owing to joule heating of plasma layer (see above), and the conductivity rises. Charges begin to flow to these outside bubbles from the internal bubble, and hence, the size of the internal bubble decreases.

The processes of plasma joule heating in the surface of the outside bubbles continue to rise their temperature and sizes (6.16b) (Fig. 6.9d). Being melted, the large, liquid bubbles outside coalesce at touching, producing a single large outside sphere. As the temperature of the sphere is the highest, all the charges penetrate to it, and the internal bubble disappears and its connecting part closes. This description coincides with the pictures represented in [330].

6.2.8 Conclusions

The development of a unipolarly charged melted structure BL theory has been made. In the present model, in most interesting cases, BL is a heavy condensed object with a high storage of chemical energy, and the electric fields in this object are extremely high. In the frames of the presented model, one can explain BL's lifetime, explosion and its impact on some materials (wood).

Being quasi-solid, it can be separated into parts, jump, and make the sound of a solid body, and when it consists of small particles, it can resemble a container of caviar. As it is made of vitrified materials, it can be transparent and semi-transparent. When its surface is heated up to melting temperature, BL has an ability to penetrate through holes, and manifest its liquid surface in the form of jets. Such BL appearance is most probable in the summer period when thunderstorms take place and an interaction of linear lightning with different materials leads to BL's appearance.

We believe that this work is only the beginning of investigations of such unusual material object developed by the presented hypothesis.

Estimates of BL's energy have been made using equilibrium data on energy released at combustion. These values can be different in the case of excited material.

For a sequential analysis of the electrical characteristics of charged BL, it is necessary to solve a problem on plasma characteristics in a strong nonstationary electric field of BL.

In the analysis of condensed melted substance, we could not find data on its hardening and vitrification. Hence, there are questions about the plasma layer near the BL surface, because we do not know exactly what type of surface the BL has.

There are also questions on the combustion and explosion of BL substance; however, the experimental results of [298, 302, 304, 305] showed that combustion and explosion take place with condensed melted materials leading to their disappearance during several seconds.

At this stage of investigations, we did not consider penetration of such BL through windows in this work. The explanation of rare BL properties for penetration through window panes without visible destruction requires an additional analysis of observation reports, properties of melted glasses, and the formulation of new experiments. The last part of the work was started only recently. The same can be said about the disappearance of golden adornments from the bodies of people.

6.3 Electrodynamical Model of Ball Lightning

A BL model, as a dynamic electric capacitor, has been presented. According to this model, the core of BL is formed of a great number of elements, defined as "dynamic electric capacitors". In the center of this capacitor, an electrons' ring is located, and protons rotate around this ring. Because of protons' movement, a magnetic field is generated; this field provides a circular motion of electrons. To make this field sufficiently strong, it is necessary that the number of protons exceeds the number of electrons, so that this system has an excess of positive charge. The charges' movement takes place in vacuum, which can exist owing to the presence of a shell separating the vacuum cavity from atmosphere. In a nonuniform electric field of the unipolarly charged core, a force that tends to shrink the shell appears. The core, in its turn, tends to expand because of Coulomb repulsion of charges and the centrifugal force of rotating protons. The balance of the oppositely directed forces maintains the stable existence of this system.

6.3.1 Introduction

A key to solving the BL problem is in an explanation of the cases showing its extremely high energy content. There are some cases when BL had fallen into vessels with water. On the basis of these events, through water heating, its limit energy density was estimated to be in the region from 10^{10} to 10^{12} J/m^3 [331–335]. For the autonomous BL, which does not receive energy from the outside, such high

values of energy density cannot be explained either by the chemical energy of gaseous reagents or by the electric energy of ionized gas. The most probable form of BL energy is the kinetic energy of its particles. However, in this case, for the holding of moving particles in the restricted volume, there has to exist some container, preventing the expansion of the power core of BL.

Among the numerous BL models, only these that possess a potential ability to explain its high energy content deserve attention. It is the author's opinion that there are three such models [336–338]. The first one is the BL composed of the closely stowed nanotubes. On the axis of this nanotube, an electron thread, compressed by quantum exchange forces, is located, and the surface of the tube comprises ions, rotating around the electron thread [339–341]. The second one is the model of BL in the form of a charged bubble with hard walls (of polymer, metal, or silicon), in which the energy is produced owing to the combustion of solid shell [342, 343]. And, lastly, the third one is the author's model, named as the electrodynamical model of BL [344–347]. According to this model, the core of BL is formed of a great number of elements, defined as "dynamic electric capacitors". In the center of this capacitor, an electrons' ring is located, and protons rotate around this ring. Because of protons' movement, a magnetic field is generated, and this field provides a circular motion of electrons. To make this field sufficiently strong, it is necessary that the number of protons exceeds the number of electrons; hence, this system must have an excess of positive charge. The charges' movement must take place in vacuum, which can exist owing to the presence of a shell, separating vacuum cavity from the atmosphere. In a nonuniform electric field of unipolarly charged core, a force appears, which tends to shrink the shell. The core, in its turn, tends to expand because of Coulomb repulsion of charges and the centrifugal force of rotating protons. The balance of the oppositely directed forces maintains the stable existence of this system.

6.3.2 Dynamic Electric Capacitor

The considered system may be schematically represented by two concentric flat rings, the inner one (of radius r) comprises the electrons, and the outer (of radius R) comprises the protons (see Fig.6.10).

Electrons, located in the radial electric field E, with a magnetic field H orthogonal to it, drift with a velocity v_d [348, 349]:

$$v_d = E/\mu_0 H, \tag{6.31}$$

where μ_0 is the magnetic constant, $\mu_0 = 1.2566 \times 10^6$ V s/A m. The condition must be fulfilled in the order in which the electrons move in a round orbit [350, P. 75]:

$$H/E \geqslant (\varepsilon_0/\mu_0)^{1/2}, \tag{6.32}$$

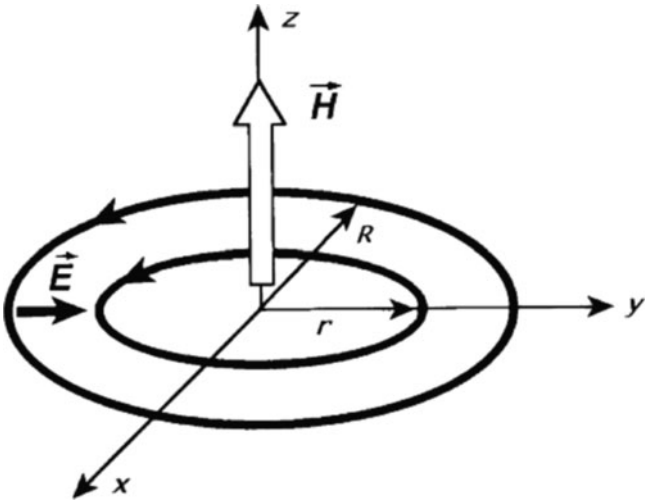

Fig. 6.10 Diagram of charges movement in dynamic electric capacitor. The inner rings includes electrons, the outer ring comprises protons

where ε_0 is an electric constant, $\varepsilon_0 = 8.8542 \times 10^{-12}$ F/m. By substituting $H = (\varepsilon_0/\mu_0)^{1/2}E$ in (6.31), we obtain that electrons must move with a speed near the light velocity:

$$v_\mathrm{d} \leq (\varepsilon_0\mu_0)^{-1/2} = c. \tag{6.33}$$

While moving in a closed orbit, the electrons execute oscillations along the direction of the electric field with amplitude [351]:

$$b = (2mE)/\left(e\mu_0{}^2H^2\right), \tag{6.34}$$

where m and e are mass and charge of electron, respectively. The value b must be less than the gap $R - r$ between the orbits of electrons and protons. By substituting the expression $H^2 = \varepsilon_0E^2/\mu_0$ from (6.32) in (6.34), we obtain:

$$b \leq 2m/(e\mu_0\varepsilon_0E). \tag{6.35}$$

To validate the possibility of existence of the discussed system, let us make some estimates. For the convenience of calculations, let us replace our system, composed of negatively charged electron ring and positively charged spherical shell of rotating protons, with a cylindrical electric capacitor with external positive electrode of radius R, negative inner electrode of radius r, and cylinder height h. The capacitance of this condenser is $C = 2\pi\varepsilon_0h/\ln(R/r)$ [352]. Let the total charge of the electrons be Q_e. In this case, a potential difference on its electrodes is

$U = Q_e/C = Q_e \ln(R/r)/2\pi\varepsilon_0 h$, and an average electric field in the space between electrodes is

$$E = \frac{U}{(R-r)} = \frac{Q_e \ln(R/r)}{2\pi\varepsilon_0 h(R-r)}. \tag{6.36}$$

Let us assume that protons are retained in the orbit because of the action of electric field E. By equating centripetal force $F_e = eE$ to centrifugal force $F_c = (m_p v_p{}^2)/R$ (m_p is a proton's mass, and v_p is a proton's velocity), we find:

$$v_p = \left(\frac{eER}{m_p}\right)^{1/2}. \tag{6.37}$$

The frequency of the proton rotation in an orbit is

$$f_p = \frac{v_p}{2\pi R} = \left(\frac{eE}{4\pi^2 m_p R}\right)^{1/2}. \tag{6.38}$$

Let the total charge of protons be Q_p, then a current, produced by their motion, is

$$I_p = Q_p \cdot f_p = \left(\frac{Q_p^2 eE}{4\pi^2 m_p R}\right)^{1/2}. \tag{6.39}$$

The protons' movement generates a magnetic field in the center of orbit

$$H_p = \frac{I_p}{2R} = \left(\frac{Q_p^2 eE}{16\pi^2 m_p R^3}\right)^{1/2}. \tag{6.40}$$

Taking into account (6.32), we obtain:

$$\frac{Q_e}{Q_p^2} \le \frac{e\mu_0}{8\pi m_p} \cdot \frac{h(R-r)}{R^3 \ln(R/r)} = 4.7889 \cdot \frac{h(R-r)}{R^3 \ln(R/r)}. \tag{6.41}$$

For the performance of numerical estimates, let us set specific relationships between the dimensions of the capacitor. Let $h = R$ and $r = 0.7R$. In this case, (6.41) may be rewritten as

$$Q_p^2 \ge 0.2483 R Q_e. \tag{6.42}$$

The velocity of proton is (see (6.36) and (6.37)):

$$v_{\mathrm{p}} = \left[\frac{eR}{m_{\mathrm{p}}} \cdot \frac{Q \ln(R/r)}{2\pi\varepsilon_0 h(R-r)}\right]^{1/2}. \tag{6.43}$$

For the accepted dimensions of the condenser

$$v_{\mathrm{p}} = \left(2.0469 \times 10^{18} Q_{\mathrm{e}}/R\right)^{1/2}. \tag{6.44}$$

The kinetic energy of proton is

$$w_{\mathrm{p}} = \frac{m_{\mathrm{p}} v_{\mathrm{p}}^2}{2} = \frac{eRQ_{\mathrm{e}}}{2} \cdot \frac{\ln(R/r)}{2\pi\varepsilon_0 h(R-r)}. \tag{6.45}$$

The total number of protons is $N_{\mathrm{p}} = Q_{\mathrm{p}}/e$, and hence, the kinetic energy of N_{p} protons is

$$W_{\mathrm{p}} = N_{\mathrm{p}} \cdot w_{\mathrm{p}} = \frac{RQ_{\mathrm{p}}Q_{\mathrm{e}}}{2} \cdot \frac{\ln(R/r)}{2\pi\varepsilon_0 h(R-r)}. \tag{6.46}$$

At $h = R$ and $r = 0.7R$

$$W_{\mathrm{p}} = 1.0686 \times 10^{10} Q_{\mathrm{p}}Q_{\mathrm{e}}/R. \tag{6.47}$$

Expressing Q_{p} from Q_{e} and R (see (6.42)), we can obtain:

$$W_{\mathrm{p}} = 5.3248 \times 10^{9} {Q_{\mathrm{e}}}^{3/2}/R^{1/2}. \tag{6.48}$$

By assuming the volume of dynamic capacitor as $V_{\mathrm{c}} = 4\pi R^3/3$, one can find an average density of protons' kinetic energy:

$$\rho_{\mathrm{W}} = \frac{W_{\mathrm{p}}}{V_{\mathrm{c}}} = \frac{3Q_{\mathrm{p}}Q_{\mathrm{e}}}{16\pi^2 R^2} \cdot \frac{\ln(R/r)}{\varepsilon_0 h(R-r)}. \tag{6.49}$$

For the accepted dimensions of the capacitor

$$\rho_{\mathrm{W}} = 2.551 \times 10^{9} Q_{\mathrm{p}}Q_{\mathrm{e}}/R^4. \tag{6.50}$$

Using (6.42), we can obtain:

$$\rho_{\mathrm{W}} = 1.271 \times 10^{9} {Q_{\mathrm{e}}}^{3/2}/R^{7/2}. \tag{6.51}$$

In Table 6.2, values of the total protons' charge Q_{p}, uncompensated positive charge of the system $Q_{\mathrm{p}} - Q_{\mathrm{e}}$, proton's velocity v_{p}, total kinetic energy of protons W_{p}, and density of protons' kinetic energy ρ_{W} for values of the total electrons' charge from $Q_{\mathrm{e}} = 10^{-12}$ to $Q_{\mathrm{e}} = 10^{-3}$ C and for values of condenser radius from $R = 10^{-10}$ to $R = 10^{-1}$ m, are presented. Only these cases were considered when

Table 6.2 Dynamic electric capacitor parameters with respect to its dimensions $R = h$, $r = 0.7R$ at different values of electrons' charge and protons' charge

R (m)	Q_p (C)	$Q_p - Q_e$ (C)	v_p (m/s)	W_p (J)	ρ_W (J/m^3)
$Q_e = 10^{-12}$ (C)					
10^{-1}	1.58×10^{-7}	1.58×10^{-7}	4.52×10^{3}	1.68×10^{-8}	4.02×10^{-6}
10^{-2}	4.98×10^{-8}	4.98×10^{-8}	1.43×10^{4}	5.32×10^{-8}	1.27×10^{-2}
10^{-3}	1.58×10^{-8}	1.58×10^{-8}	4.52×10^{4}	1.68×10^{-7}	4.02×10^{1}
10^{-4}	4.98×10^{-9}	4.98×10^{-9}	1.43×10^{5}	5.32×10^{-7}	1.27×10^{5}
10^{-5}	1.58×10^{-9}	1.58×10^{-9}	4.52×10^{5}	1.68×10^{-6}	4.02×10^{8}
10^{-6}	4.98×10^{-10}	4.97×10^{-10}	1.43×10^{6}	5.32×10^{-6}	1.27×10^{12}
10^{-7}	1.58×10^{-10}	1.57×10^{-10}	4.52×10^{6}	1.68×10^{-5}	4.02×10^{15}
10^{-8}	4.98×10^{-11}	4.88×10^{-11}	1.43×10^{7}	5.32×10^{-5}	1.27×10^{19}
10^{-9}	1.58×10^{-11}	1.48×10^{-11}	4.52×10^{7}	1.68×10^{-4}	4.02×10^{22}
10^{-10}	4.98×10^{-12}	3.98×10^{-12}	1.43×10^{8}	5.32×10^{-4}	1.27×10^{26}
$Q_e = 10^{-11}$ (C)					
10^{-1}	4.98×10^{-7}	4.98×10^{-7}	1.43×10^{4}	5.32×10^{-7}	1.27×10^{-4}
10^{-2}	1.58×10^{-7}	$1.58 \cdot \times 10^{-7}$	4.52×10^{4}	1.68×10^{-6}	4.02×10^{-1}
10^{-3}	4.98×10^{-8}	$4.98 \cdot \times 10^{-8}$	1.43×10^{5}	5.32×10^{-6}	1.27×10^{3}
10^{-4}	1.58×10^{-8}	$1.58 \cdot \times 10^{-8}$	4.52×10^{5}	1.68×10^{-5}	4.02×10^{6}
10^{-5}	4.98×10^{-9}	$4.97 \cdot \times 10^{-9}$	1.43×10^{6}	5.32×10^{-5}	1.27×10^{10}
10^{-6}	1.58×10^{-9}	$1.57 \cdot \times 10^{-9}$	4.52×10^{6}	1.68×10^{-4}	4.02×10^{13}
10^{-7}	4.98×10^{-10}	$4.88 \cdot \times 10^{-10}$	1.43×10^{7}	5.32×10^{-4}	1.27×10^{17}
10^{-8}	1.58×10^{-10}	$1.48 \cdot \times 10^{-10}$	4.52×10^{7}	1.68×10^{-3}	4.02×10^{20}
10^{-9}	4.98×10^{-11}	$3.98 \cdot \times 10^{-11}$	1.43×10^{8}	5.32×10^{-3}	1.27×10^{24}
$Q_e = 10^{-10}$ (C)					
10^{-1}	1.58×10^{-6}	$1.58 \cdot \times 10^{-6}$	4.52×10^{4}	1.68×10^{-5}	4.02×10^{-3}
10^{-2}	4.98×10^{-7}	$4.98 \cdot \times 10^{-7}$	1.43×10^{5}	5.32×10^{-5}	1.27×10^{-1}
10^{-3}	1.58×10^{-7}	$1.58 \cdot \times 10^{-7}$	4.52×10^{5}	1.68×10^{-4}	4.02×10^{4}
10^{-4}	4.98×10^{-8}	$4.97 \cdot \times 10^{-8}$	1.43×10^{6}	5.32×10^{-4}	1.27×10^{8}
10^{-5}	1.58×10^{-8}	$1.57 \cdot \times 10^{-8}$	4.52×10^{6}	1.68×10^{-3}	4.02×10^{11}
10^{-6}	4.98×10^{-9}	$4.88 \cdot \times 10^{-9}$	1.43×10^{7}	5.32×10^{-3}	1.27×10^{15}
10^{-7}	1.58×10^{-9}	$1.48 \cdot \times 10^{-9}$	4.52×10^{7}	1.68×10^{-2}	4.02×10^{18}
10^{-8}	4.98×10^{-10}	$3.98 \cdot \times 10^{-10}$	1.43×10^{8}	5.32×10^{-2}	1.27×10^{22}
$Q_e = 10^{-9}$ (C)					
10^{-1}	4.98×10^{-6}	4.98×10^{-6}	1.43×10^{5}	5.32×10^{-4}	1.27×10^{-1}
10^{-2}	1.58×10^{-6}	1.58×10^{-6}	4.52×10^{5}	1.68×10^{-3}	4.02×10^{2}
10^{-3}	4.98×10^{-7}	4.97×10^{-7}	1.43×10^{6}	5.32×10^{-3}	1.27×10^{6}
10^{-4}	1.58×10^{-7}	1.57×10^{-7}	4.52×10^{6}	1.68×10^{-2}	4.02×10^{9}
10^{-5}	4.98×10^{-8}	4.88×10^{-8}	1.43×10^{7}	5.32×10^{-2}	1.27×10^{13}
10^{-6}	1.58×10^{-8}	1.48×10^{-8}	4.52×10^{7}	1.68×10^{-1}	4.02×10^{16}
10^{-7}	4.98×10^{-9}	3.98×10^{-9}	1.43×10^{8}	5.32×10^{-1}	1.27×10^{20}
$Q_e = 10^{-8}$ (C)					
10^{-1}	1.58×10^{-5}	1.58×10^{-5}	4.52×10^{5}	1.68×10^{-2}	4.02
10^{-2}	4.98×10^{-6}	4.97×10^{-6}	1.43×10^{6}	5.32×10^{-2}	1.27×10^{4}
10^{-3}	1.58×10^{-6}	1.57×10^{-6}	4.52×10^{6}	1.68×10^{-1}	4.02×10^{7}
10^{-4}	4.98×10^{-7}	4.88×10^{-7}	1.43×10^{7}	5.32×10^{-1}	1.27×10^{11}
10^{-5}	1.58×10^{-7}	1.48×10^{-7}	4.52×10^{7}	1.68	4.02×10^{14}
10^{-6}	4.98×10^{-8}	3.98×10^{-8}	1.43×10^{8}	5.33	1.27×10^{18}
$Q_e = 10^{-7}$ (C)					
10^{-1}	4.98×10^{-5}	4.97×10^{-5}	1.43×10^{6}	5.32×10^{-1}	1.27×10^{2}
10^{-2}	1.58×10^{-5}	1.57×10^{-5}	4.52×10^{6}	1.68	4.02×10^{5}

(*continued*)

Table 6.2 (continued)

R (m)	Q_p (C)	$Q_p - Q_e$ (C)	v_p (m/s)	W_p (J)	ρ_W (J/m^3)
10^{-3}	4.98×10^{-6}	4.88×10^{-6}	1.43×10^{7}	5.32	1.27×10^{9}
10^{-4}	1.58×10^{-6}	1.48×10^{-6}	4.52×10^{7}	16.8	4.02×10^{12}
10^{-5}	4.98×10^{-7}	3.98×10^{-7}	1.43×10^{8}	53.2	1.27×10^{16}
$Q_e = 10^{-6}$ (C)					
10^{-1}	1.58×10^{-4}	1.57×10^{-4}	4.52×10^{6}	16.8	4.02×10^{3}
10^{-2}	4.98×10^{-5}	4.88×10^{-5}	1.43×10^{7}	53.2	1.27×10^{7}
10^{-3}	1.58×10^{-5}	1.48×10^{-5}	4.52×10^{7}	168.0	4.02×10^{10}
10^{-4}	4.98×10^{-6}	3.98×10^{-6}	1.43×10^{8}	532.0	1.27×10^{14}
$Q_e = 10^{-5}$ (C)					
10^{-1}	4.98×10^{-4}	4.88×10^{-4}	1.43×10^{7}	5.32×10^{2}	1.27×10^{5}
10^{-2}	1.58×10^{-4}	1.48×10^{-4}	4.52×10^{7}	1.68×10^{3}	4.02×10^{8}
10^{-3}	4.98×10^{-5}	3.98×10^{-5}	1.43×10^{8}	5.32×10^{3}	1.27×10^{12}
$Q_e = 10^{-4}$ (C)					
10^{-1}	1.58×10^{-3}	1.48×10^{-3}	4.52×10^{7}	1.68×10^{4}	4.02×10^{6}
10^{-2}	4.98×10^{-4}	3.98×10^{-4}	1.43×10^{8}	5.32×10^{4}	1.27×10^{10}
$Q_e = 10^{-3}$ (C)					
10^{-1}	4.98×10^{-3}	3.98×10^{-3}	1.43×10^{8}	5.32×10^{5}	1.27×10^{8}

the protons' charge exceeded the electrons' charge, and proton's velocity was less than the light velocity. The second restriction was a limit of the number of electrons in the orbit because of quantum mechanics laws.

According to the uncertainty principle, distance Δx between the electrons cannot be less than $\hbar/2p$ (where $\hbar$ is the Planck's constant, $\hbar = 1.05457 \times 10^{-34}$ J·s, and p is the electron's pulse). For relativistic electrons, $p = w_e/c$ (where w_e is the electron's energy and c is the light velocity), hence

$$\Delta x \geqslant \hbar c/2w_e. \tag{6.52}$$

Let us assume that electrons may occupy a space inside a ring tube with a cross-section b^2 (see (6.35)) and a length $2\pi r$. The volume of this tube is

$$V_{tb} = 2\pi r b^2 = \frac{8\pi m^2}{e^2\mu_0^2\varepsilon_0^2} \cdot \frac{r}{E^2} = 6.564 \times 10^{-12} \frac{r}{E^2}. \tag{6.53}$$

By expressing E in the charge of electron ring (see (6.36)), we have

$$V_{tb} = \frac{32\pi^3 m^2}{e^2\mu_0^2\varepsilon_0^2 Q_e^2} \cdot \frac{rh^2(R-r)^2}{[\ln(R/r)]^2}. \tag{6.54}$$

By assuming $h = R$, $r = 0.7R$, we find

$$V_{tb} = 1.006 \times 10^{-8} R^5/Q_e^2. \tag{6.55}$$

Let the volume that an electron may occupy in space be

$$v_e = (\Delta x)^3 = (\hbar c/2w_e)^3. \tag{6.56}$$

Then, the limit number of electrons inside the ring tube is $N_{max} = V_{tb} \cdot v_e$ and the limit charge of these electrons is

$$(Q_e)_m = eN_{max} = \frac{8.048 \times 10^{-8} eR^5 w_e^3}{\hbar^3 c^3 Q_e^2}. \tag{6.57}$$

From (6.57), a ratio of maximum electron charge to real electron charge can be obtained as

$$(Q_e)_m/Q_e = 4.08 \times 10^{50} R^5 w_e^3/Q_e^3. \tag{6.58}$$

Let $w_e = 1$ MeV $= 1.6 \times 10^{-13}$ J. Then, $(Q_e)_m/Q_e = 1.677 \times 10^{12}\, R^5/{Q_e}^3$. In the Table 6.2, only those combinations of R and Q_e are allowed when $(Q_e)_m/Q_e = 1$. The analysis showed that the most severe criterion is the requirement that the proton's velocity should be less than light velocity, rather than an electron's density in the ring should be less than its limit value.

One can see from Table 6.2 that the energy, stored in the dynamic capacitor increases with decreasing radius R. This is explained by the corresponding increase in the proton's velocity, and hence, its kinetic energy. The second conclusion based on the table is that the greatest possible energy may be stored in the system consisting of a great number of small-sized condensers. Let us estimate the amount of energy contained in the system of dynamic condensers with a total proton's charge $Q_\Sigma = 10^{-1}$ C. If the proton's charge of the unit condenser is Q_p, then the number of such condensers is $N_c = Q_\Sigma / Q_p$ and these total energy is (see (6.47)):

$$W_\Sigma = W_p \cdot N_c = W_p Q_\Sigma / Q_p = 1.0686 \times 10^{10} Q_e Q_\Sigma / R. \tag{6.59}$$

For the lower lines of Table 6.2 at different Q_e, relation $Q_e/R = 10^{-2}$ C/m. At $Q_\Sigma = 10^{-1}$ C, $W_\Sigma = 10.689 \times 10^6$ J. Thus, it can be observed that this system is able to store about 10 MJ of energy in the form of the kinetic energy of protons.

6.3.3 *Features of Ball Lightning, Following from Electrodynamical Model*

6.3.3.1 Energy of Ball Lightning

The main goal of the performed estimates was to demonstrate the capability of the discussed system to store energy, comparable with the energy that may be contained in the natural BL. However, we did not take into account forces

expanding the proton's orbits owing to their Coulomb repulsion, as well as the possibility of the fact that their orbital (or "quasi-orbital") motion, besides attraction to central negative charge, may be maintained by their reflection from the walls of some container. Now, let us turn our attention to the discussion of properties of this container – a shell of BL.

Let us consider that inside the spherical shell of some dielectric (e.g., water), a power core (one or some dynamical capacitors) with uncompensated charge Q is located. This charge generates electric field in the place, where the shell is located, $E_{sh} = Q/4\pi\varepsilon_0 R_{sh}^2$ (R_{sh} is the inner radius of the shell). In such field, polarization of the shell will take place: on its inner surface, negative charges will appear, and on the outer surface, positive ones will occur. Under the total polarization of the shell's material in a strong electric field, the surface density of the charges σ may be assumed to be equal to N_s , which is the number of water molecules on the unit of the shell surface. The distance γ between the water molecules in ice crystal is $\gamma = 3 \times 10^{-10}$ m, and hence, $N_s = (\gamma)^{-2} = 10^{19}$ m^{-2} and the surface density of charges is $\sigma = N_s \cdot e = 1.6$ C/m^2. The dipole moment of a surface unit of thickness a is $D = \sigma a = 1.6a$ C/m. Therefore, the force P_{cp}, attracting a unit of surface towards the charge Q, is equal to

$$P_{cp} = D \cdot \text{grad}\, E = -2DQ/4\pi\varepsilon_0 R^3 = -2DE/R. \tag{6.60}$$

By multiplying P_{cp} by an area of the inner surface of the shell $S = 4\pi R^2$, we can find a force shrinking the shell towards the center:

$$F_{cp} = P_{cp} \cdot 4\pi R^2 = 2\sigma a Q/\varepsilon_0 R. \tag{6.61}$$

As in the above-discussed numerical example, let the uncompensated charge (whose value is near the total charge of the protons) be $Q = 10^{-1}$ C, and the inner radius of the shell be $R_{sh} = 10^{-1}$ m. In this case, $F_{cp} = 3.614 \times 10^{11} a$ (N). A centrifugal force of protons with a total mass M_p, possessing the energy W_p, is

$$F_{cf} = \frac{2M_p v_p^2}{2R} = \frac{2W_p}{R}. \tag{6.62}$$

$F_{cf} = 2 \times 10^8$ N at $W_p = 10^7$ J. By equating F_{cp} to F_{cf}, we can find that for the compensation of centrifugal force, the shell thickness must be equal to $a = 0.55$ mm. For the shell to reflect positively charged core at impact, it must also be positively charged. It can acquire this charge from a continuous loss of charge of the energic core. This charge, passing through the shell's wall, leaks to the atmosphere from its outer surface.

Besides the centrifugal force F_{cf}, the shell is stretched by the force F_{el}, produced by Coulomb repulsion of charges and by magnetic field, generated by protons' current. This force [353, P. 46] is:

$$F_{\mathrm{el}} = \frac{kQ^2}{8\pi\varepsilon_0 R^2}. \tag{6.63}$$

where k is a coefficient, depending on the proton's velocity and parameters of cross-section of the current's layer, $k \approx 2$. Thus, two forces shrink the shell: a "gradient" electric force (see (6.61))

$$F_{\mathrm{cp}} = \frac{4\sigma a Q}{\varepsilon_0(2R + a)}, \tag{6.64}$$

(where R is replaced by $R + a/2$), and a force of atmospheric pressure P_{a}:

$$F_{\mathrm{a}} = P_{\mathrm{a}} \cdot 4\pi R^2. \tag{6.65}$$

The condition of shell equilibrium is a balance of all forces acting on it:

$$F = F_{\mathrm{cf}} + F_{\mathrm{el}} + F_{\mathrm{cp}} + F_{\mathrm{a}} = \frac{2W_{\mathrm{p}}}{R} + \frac{kQ^2}{8\pi\varepsilon_0 R^2} - \frac{4\sigma a Q}{\varepsilon_0(2R + a)} - 4\pi P_{\mathrm{a}} R^2 = 0. \tag{6.66}$$

Taking the derivative $\mathrm{d}F/\mathrm{d}R$ and accounting the constancy of shell's volume as well as the fact that the increase in the shell's radius takes place because of the work of forces expanding the energic core, one can show that at any values of k, Q, a, and R derivative $\mathrm{d}F/\mathrm{d}R < 0$. This means that the equilibrium of the shell is stable [354].

In Fig. 6.11, the dependencies of the shell thickness a on the energic core charge Q, constructed by (6.66) for inner radius $R = 3$ cm, $k = 2$, and kinetic energy of protons W_{p} from 1 to 10^7 J are shown. One can see that when the energy exceeds 16.9646 J, the curves of dependence $a = f(Q)$ have a minimum value. From the condition $\mathrm{d}a/\mathrm{d}Q = 0$ from (6.66), one can find values of minimum wall thickness a_{m} and the corresponding values of charge Q_{m}:

$$Q_{\mathrm{m}} = \left[\frac{16\pi\varepsilon_0 R}{k} \cdot \left(W_{\mathrm{p}} - 2\pi P_{\mathrm{a}} R^3\right)\right]^{1/2}, \tag{6.67}$$

$$a_{\mathrm{m}} = \frac{2R\varphi}{1 - \varphi}, \tag{6.68}$$

where

$$\varphi = \left[\frac{k\varepsilon_0\left(W_{\mathrm{p}} - 2\pi P_{\mathrm{a}} R^3\right)}{16\pi\sigma^2 R^3}\right]^{1/2}.$$

By rewriting (6.66) in the form:

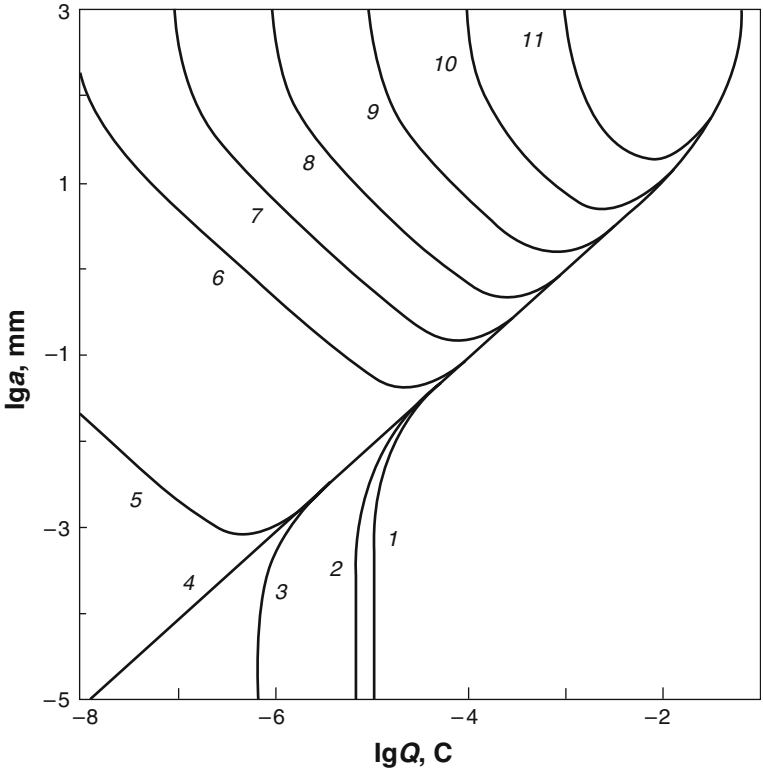

Fig. 6.11 The dependence of shell thickness a for the ball lightning (BL) with inner shell's radius $R = 3$ cm on the charge Q of power core for values of kinetic energy of protons W_p equal to 1 J (curve 1), 10 J (curve 2), 16.9 J (curve 3), 16.9646 J (curve 4), 17 J (curve 5), 10^2 J (curve 6), 10^3 J (curve 7), 10^4 J (curve 8), 10^5 J (curve 9), 10^6 J (curve 10), and 10^7 J (curve 11)

$$W_p = 2\pi P_a R^3 + \frac{2\sigma a R Q}{\varepsilon_0 (2R + a)} - \frac{kQ^2}{16\pi\varepsilon_0 R}, \tag{6.69}$$

we can find a relation between energy W_p and radius R. By substituting a value Q_m in (6.69) (see (6.67)), we can obtain:

$$\left(W_p - 2\pi P_a R^3\right)^2 \left[\frac{\varepsilon_0 (2R + a)}{\sigma a R}\right]^2 = \frac{16\pi\varepsilon_0 R}{k}\left(W_p - 2\pi P_a R^3\right). \tag{6.70}$$

The apparent solution of this equation is $(W_p)_1 = 2\pi P_a R^3$. At this value of W_p, according to (6.66) and (6.67), $Q_m = 0$ and $a_m = 0$, and thus, the equilibrium is sustained by the atmospheric pressure without the participation of electric forces. The second solution of (6.70) is

$$\left(W_{\mathrm{p}}\right)_2 = 2\ \pi P_{\mathrm{a}} R^3 + \frac{16\pi\sigma^2 a^2 R^3}{k\varepsilon_0 (2R+a)^2}. \tag{6.71}$$

The first term in the right part reflects the contribution to energy of the atmospheric-pressure force, and the second one reflects the contribution to energy of electric forces. The ratio of these terms is

$$\eta = \frac{k\varepsilon_0 P_{\mathrm{a}}(2R+a)}{8\sigma^2 a^2}. \tag{6.72}$$

If $R \rightarrow 0$, then $\eta \rightarrow 0$, and if $R \rightarrow \infty$, then $\eta \rightarrow \infty$. This means that at small radii of the shell, the core's energy is sustained predominantly by electric forces, while at large values of radius, the atmospheric force becomes a determining factor. When $a = 10^{-2}$ m, the action of both the forces becomes equal ($\eta = 1$) at $R = 17$ m; on the other hand, when $a = 10^{-3}$ m, $\eta = 1$ at $R = 1.7$ m.

There are some cases described in the literature, when the energy of BL that fell in a vessel with water was measured. The range of the measured energy values was from 10 to 4,000 MJ. The considered model allows explaining the observed cases of extremely high energy content of BL.

In Fig. 6.12, the plots of dependencies of outer radius $R + a$, the shell wall volume V_{en}, and power core charge Q on the protons' energy W_{p} are shown. The graphs are constructed based on (6.66) [347, 354]. Adjacent to the straight line of dependence $R + a$ (the observable parameter), points of measured values of BL energy are plotted. One can see that the experimental data fit the calculated line reasonably well. It is self-evident that the model, which is able to explain a mechanism of energy storage for highly-energetic BL, can also explain the reasons for the energy content for usual BL with energy from 10 to 1,000 J.

6.3.3.2 Radiation of Ball Lightning

The model, trying to approach fact as closely as possible, must be able to explain not only the nature of its energy content, but also its other characteristics: long life span, peculiarities of its radiation and movement, and demonstration of its electric features. According to the considered model, every element of the core of BL – dynamic capacitor – has electrons, moving in a circular orbit of radius r with a velocity near to light velocity (see (6.33)). Such electrons are the source of synchrotron radiation. It is directed at a tangent to the electron's orbit and is gathered in a narrow conical beam with an angle of divergence (in radians) [357, P. 97]:

$$\delta\Psi = \left(1-\beta^2\right)^{1/2} = mc^2/w_{\mathrm{e}}, \tag{6.73}$$

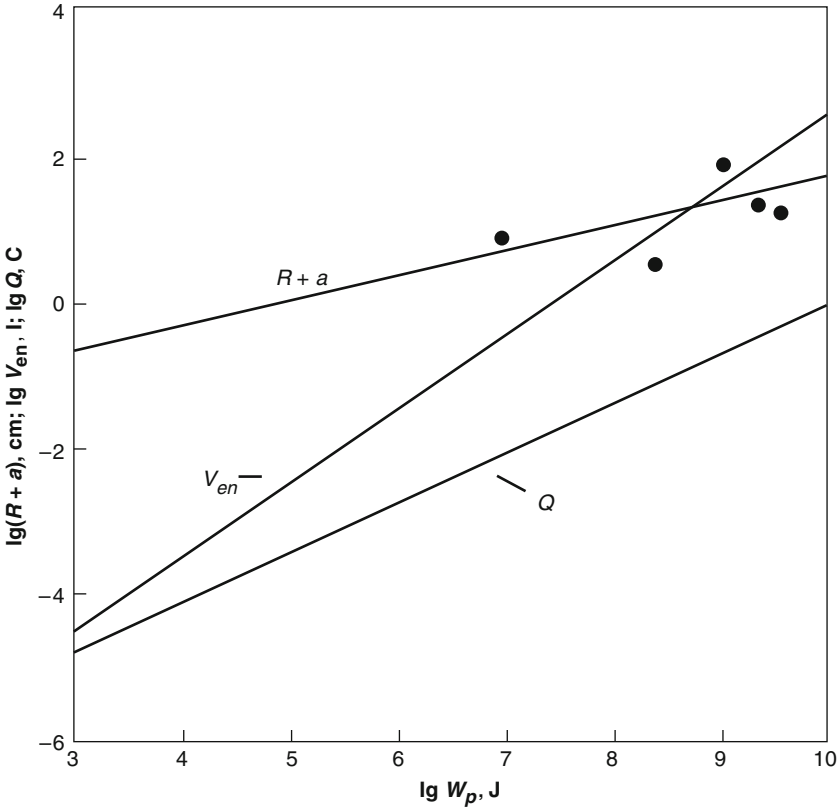

Fig. 6.12 Dependence of outer radius of ball lightning (BL) $R + a$, the shell's wall volume V_{en}, and power core charge Q for minimum value of V_{en} on the kinetic energy of protons W_p. Points are values of the external radius of the observed BL with energy (from left to right): 10 MJ (Goodlet, B.L. [14]), 260 MJ (Imianitov, I., Tikhii, D. [32]), 1,000 MJ (Dmitriev, M.T., Bakhtin, B.I., Martynov, V.I. [355]), 2,300 MJ (Batygin,A., Mosin, I. [43]), and 4,000 MJ (Balyberdin, V.V. [20, 356])

where β is the ratio of electron's velocity v to the light velocity c, $\beta = v/c$, m is the rest mass of the electron, and w_e is the electron energy. For the synchrotron radiation, the number n_{max} of the harmonic of basic frequency of orbital movement of electron $v = c/2\pi r$, corresponding to a maximum of intensity, is defined by the expression [357, P. 115]:

$$n_{\max} = \frac{3}{2}\left(\frac{w_e}{mc^2}\right)^3 = \frac{3}{2}\left(1-\beta^2\right)^{-3/2}. \tag{6.74}$$

For example, let us consider an electron rotating in the orbit of radius $r = 10^{-5}$ m (see Table 6.2). The frequency of its rotation is $v = 4.775 \times 10^{12}$ s^{-1}. Frequency, corresponding to a middle of visible radiation spectrum ($\lambda = 500$ nm), is $f = c/\lambda$

$= 6 \times 10^{14}$ Hz. For this frequency, number $n_{max} = f/v = 126$. From (6.74), we can find $w_e = 1.1941 \times 10^{-13}$ J $= 0.7453 \times 10^6$ eV. For the condenser with a radius of electron orbit $r = 10^{-4}$ m for wavelength $\lambda = 500$ nm, $n_{max} = 1256$, for which $w_e = 2.5726 \times 10^{-13}$ J $= 1.6057 \times 10^6$ eV. For $r = 10^{-3}$ m, $n_{max} = 12{,}565$ and $w_e = 5.5424 \times 10^{-13}$ J $= 3.4593 \times 10^6$ eV. The ratios β of the electron's velocity to the light velocity for three considered values of radius r are equal: for $r = 10^{-5}$ m, $\beta = 0.72794$; for $r = 10^{-4}$ m, $\beta = 0.94801$, and for $r = 10^{-3}$ m, $\beta = 0.98903$.

Power of synchrotron radiation (W) [357, P. 95] is

$$P_e(W) = 5.99 \times 10^9 \cdot \frac{ce^2\beta^4}{r^2(1-\beta^2)^2}. \tag{6.75}$$

By substituting values of β for different radii r in this formula, we can find that at $r = 10^{-5}$ m, $P_e = 5.86 \times 10^{-10}$ W, at $r = 10^{-4}$ m, $P_e = 3.63 \times 10^{-10}$ W, and at $r = 10^{-3}$ m, $P_e = 0.93 \times 10^{-10}$ W. If the total charge of the electrons is $Q_e = 10^{-8}$ C (see Table 6.2), their number $N_e = Q_e/e = 6.24 \times 10^{10}$, and the power emitted by them will be in the range from 5.8 W (for $r = 10^{-3}$ m) to 36.6 W (for $r = 10^{-5}$ m). With regard to Table 6.2, we can see that for radius $R = 10^{-3}$ m, a store of protons' kinetic energy W_p is 0.168 J, for $R = 10^{-4}$ m, $W_p = 0.532$ J, and for $R = 10^{-5}$ m, $W_p = 1.684$ J. Supposing that some effective mechanism of transferring of protons' kinetic energy to energy of electrons exists, this store will be exhausted: for $r = 10^{-5}$ m at 4.6×10^{-2} s, for $r = 10^{-4}$ m at 2.3×10^{-2} s, and for $r = 10^{-3}$ m at 2.8×10^{-2} s. The obtained result is at variance with the observation data, according to which, glowing of BL may last from 1 to 100 s, which is 10^2–10^4 times longer. The reason for the inconsistency lies in the fact that (6.75) describes the emission of a single electron or a bunch of electrons. If the electrons are uniformly distributed in the orbit, the power of their collective emission intensity may become considerably lower [358]. With the absolutely uniform distribution of electrons, the power of electrons' ring emission may become equal to zero (it is known that the coil with a constant current does not radiate any electromagnetic energy).

The spectrum of synchrotron radiation consists of a set of electron's orbital rotation harmonics nv. It extends from value vn_{max} of the critical frequency, corresponding to the maximum of radiation intensity, towards long waves (up to $\lambda = 2\pi r/c$), which is also observed with regard to the short waves. Decrease in the harmonics intensity with the lowering of the frequency proceeds rather slowly – as $(nv)^{1/3}$, for frequencies above the critical value, the emission power falls exponentially with the harmonic number. At some n, it becomes equal to zero [357, P. 115]. The minimum wavelength λ_{min} relates to the maximum intensity wavelength λ_{max} as $\lambda_{min} = 0.42\lambda_{max}$ [357, P. 212]. For $\lambda_{max} = 350$ nm, $\lambda_{min} = 147$ nm.

If the main reason of BL radiation is, indeed, a synchrotron emission of electrons, one can predict some basic characteristics of its glowing. Radiation of BL is not monochromatic, but is a set of frequencies, whose intensity slowly decreases in the region of low frequencies and sharply falls in the region of high frequencies. The frequency of emission, corresponding to the maximum

intensity, depends on the electron's energy. As it decreases (e.g., before decay of BL), the BL color must become red. Furthermore, the existence of BL emitting only in the infrared region is possible ("black BL"). The ultraviolet part of the emission spectrum, penetrating through the shell of BL, may cause ionization and excitation of air molecules. This may show up in darkness as a halo around the BL. In the case of transparency of the shell's wall and of ordering of the electrons' orbits, a BL emission may have the form of a conical beam with a partly polarized light. Synchrotron emission in a range of infrared and millimeter waves may resonantly interact with the metallic objects of small size (rings and chains), heating them. As it was discussed earlier, the radiation intensity of BL must sharply depend on the degree of ordering of the emitting electrons in the orbits. With the destruction of uniformity of the electrons' distribution in the orbit (owing to external action or before its death), the radiation intensity (in the whole range of waves) may increase by some orders.

6.3.3.3 Motion of Ball Lightning

The character of movement of BL is determined by the availability of noncompensated electrical charge. At fine weather near the earth's surface, an electric field E_{fw} presents with vector directed upward (the earth is charged negatively) and the field intensity is $E_{fw} = 130$ V/m [359, 360]. In this field, BL with positive charge Q will be caused by the force $F_{fw} = QE_{fw}$ to fall from the sky to earth. During a thunderstorm, the intensity of the electric field near the earth under a cloud may increase to $E_{cl} = 10^4$–10^5 V/m, and the direction of vector $\mathbf{E_{cl}}$ is opposite to that of vector $\mathbf{E_{fw}}$. In this field, BL will experience a lifting force $F_{cl} = QE_{cl}$. At charge $Q > 10^{-3}$ C, $F_{cl} = 10$–100 N. This force is able to lift an object with a mass of 1 – 10 kg. Just as the direction of the electric field vector, its intensity near the earth's surface may vary over a wide range. These variations are caused by relief of the country, the presence of electro-transmission lines and buildings, as well as the currents flowing in earth. External electric fields may "sag" inside buildings through windows. Because of this BL moving along electric field lines, can enter inside the shielded facilities. Electric fields in the near-earth layer are inconstant in time. Because of this, often the movement of BL is irregular. On the basis of the described mechanism of charge motion, it has become possible to explain the behavior of the falling BL in the photo [361, 362].

With the approach of charged BL to earth (or to other conductor), on its surface charges of opposite polarity are induced. Hence, the force, attracting BL, must increase at $F_{at} = Q^2/4\pi\varepsilon_0(2l)^2$ (Here l is the distance between BL and the earth's surface). However, the observations show that often BL does not fall on conductor, but hovers over it at a distance of some of its diameters. One of the hypothesis explaining such behavior of BL, is an assumption that BL is repelled from the conductor because of the interaction of eddy currents induced in the conductor, with currents flowing in it [344, 347]. However, the experimental testing of this hypothesis had shown that forces, generated by these currents, rapidly diminish when

moving away from the conductor surface (as l^{-7}) [363]. The hypothesis, according to which the reason for the decrease in the attraction of charged BL to a conductor is the creation of space charge between BL and conductor, is closer to reality. The polarity of this charge coincides with that of the charge of BL. This charge may appear due to corona discharge on the surface of BL [364].

When approaching the dielectric, for instance, glass, BL can be attracted to it because of gradient forces arising due to the dielectric's polarization. In the electric field created by the charge of BL, on the glass surface a discharge appears. This discharge is fed by the energy flow from BL. As a rule, this discharge takes place on the side of glass, opposite to the side, where BL is located [365]. Local heating and subsequent cooling results in the creation of a ring hole in glass [366–368]. BL is able to pass through chinks or small holes even when their dimensions are less than BL diameter. These evidences are in favor of the assumption that BL's core consists of small-size elements (10^{-4}–10^{-3} m, see Table 6.2), which are able to change mutual position under the action of external force. Because of the oppositely directed forces of Coulomb repulsion and magnetic attraction present in this system, the possibility of the indicated rearrangement of the core seems quite possible. As the shell's form is determined mainly by the pressure of the power core, its rearrangement may be accompanied by the rearrangement of the shell.

It is a considerable challenge for explanation (for all models of autonomous BL) of the cases of BL passing through glass without its destruction [333, P. 173; 369, P. 77–85]. In the context of the proposed model, it is assumed that this process consists of the following steps: (1) BL adhered to the glass fires discharge at the opposite side of the glass. (2) In the nonuniform electric field of this discharge, charges are pushed away from the center to the periphery, carrying with them neutral particles; near the glass surface, a vacuum cavity is created. (3) The dying "mother" BL transfers its energy to the "daughter" BL in the form of a pulse of high-frequency radiation. The low-frequency envelope curve of this pulse favors formation of its power core (this process is described below). (4) From particles (water, dust) evaporated from the inner surface of glass, the vacuum shell is formed. A circumstantial evidence of the described scenario's possibility is the fact that BL that had passed through the intact glass, as a rule, had the small energy content [369].

6.3.3.4 Electric Effects Caused by Ball Lightning

By shooting out of the vacuum gap between the shell and power core, the discharge current may melt conductors, heat water in capillaries of trees, or injure people or animals. In the last case, the consequences of the impact of BL differ from the analogous consequences of impact of usual linear lightning. Let the electrical capacitance of BL be equal to the capacitance of a sphere with a radius $R = 10^{-1}$ m: $C_{\text{bl}} = 4\pi\varepsilon_0 R = 10^{-11}$ F. At the resistance of human body, $R_{\text{b}} = 10^3$ Ω, the

duration of the current pulse passing through the body at a discharge of BL is $\tau_{bl} = R_b C_{bl} = 10^{-8}$ s. The depth δ of skin layer for the current's pulse of duration τ is [344]:

$$\delta = 0.5(\rho\tau)^{1/2}(\text{m}), \tag{6.76}$$

where ρ is the resistivity of the conductor. By substituting $\tau_{bl} = 10^{-8}$ s and resistivity of body $\rho_b = 10\,\Omega\,\text{mm}^2/\text{m}$ in (6.76), we obtain $\delta = 0.16$ mm. This means that at the impact of BL, the great part of current will flow at the body's surface, not getting to the heart area. In contrast, the pulse duration of linear lightning is much larger – up to 10^{-5} s. In this case, according (6.76), $\delta = 0.5$ cm. This makes the discharge of linear lightning more dangerous than that of BL.

The microwave part of BL radiation, whose intensity may be noticeably increased due to external disturbance of BL, may cause skin burn at close contact with it. As fast particles (protons and electrons) enter into the composition of the power core, they may have been thrown out through the torn shell in the form of streams during the death of BL that did not completely exhaust its energy [332, P. 106; 40, P. 65]. These streams may cause radiation injury to the breathers, who occasionally found themselves near the exploding BL [333, 370].

According to the observations, the magnetic field of a majority of BL is very weak. It was reported that BL did not produce any influence on iron nails passing over them [371, P. 120], and did not cause any movement of steel objects lying in the pocket of a passenger of aircraft, when it had passed near him at a distance of 50 cm [333]. However, a case is known when BL had lifted a permanent magnet with a mass of about 0.5 kg [334, P. 72]. In the context of the discussed model, one can explain the magnetic features of BL with the fact that its core consists of many elements, and each of them is a magnet [372]. In a normal state, all elementary magnets are closed to each other, and the external magnetic field of BL is absent. However, under the influence of the external magnetic field, some parts of the magnets may change their orientation, and as a result, a magnetic field will appear outside of BL.

As discussed earlier, BL is a complex ordered system. Therefore, it is reasonable to suggest that it may be created in nature only as a sequence of certain events. As a result of these events, there must be: (1) the creation of vacuum cavity in air; (2) producing of ions and electrons; (3) separation of positive and negative charges in space; (4) acceleration of protons and electrons; (5) formation of the highly ordered energy core with excess of positive charges; and (6) creation of a shell, separation of vacuum cavity from the atmosphere and preventing expansion of the energy core. It would appear reasonable that the source of BL energy and entropy is a discharge of linear lightning. The energy of the average lightning is about 5×10^9 J [333, 360, 373, 374]. This is a sufficient value even for the generation of BL with an extremely high energy content. Besides, the creation of a low-entropy, highly ordered object such as BL is possible only in the system with low entropy. The linear lightning, undoubtedly, is such a system.

6.3.4 Creating of Ball Lightning in Nature

A germ of BL – a vacuum cavity in the air may appear due to the vortical motion of the air near the channel bend of linear lightning [347, 375, 376]. The estimates show that the lifetime of the spindle-like vortex may be about 40 ms. Let us consider that a new lightning discharge passes along the coil bend of the channel surrounding the vortex, after a time of vortex formation. The ultraviolet light of this discharge will cause the creation of electrons and ions in the wall of the cavity. Besides, the current of this discharge will produce a pulse of magnetic field inside the vacuum cavity, directed perpendicular to the plane of the current coil. Let the radius of this coil be $R_{\mathrm{cl}} = 0.2$ m. Consider that the lightning current I increases linearly up to $I_{\max} = 4 \times 10^5$ A in a period $\Delta t_1 = 10$ μs, and after that, it falls to zero in a time $\Delta t_2 = 50$ μs [373]. The magnetic field strength at the coil center is $H = I/2R_{\mathrm{cl}}$, at $t = 10$ μs, and it reaches a maximum value $H_{\max} = I_{\max}/2R_{\mathrm{cl}} = 10^6$ A/m. In the period Δt_1 of increase in the magnetic field inside the coil, an eddy electric field is induced. The vector $\mathbf{E}_{\mathrm{ed}}$ of this field lies in a plane of the current coil and is directed along the tangent to a circle of radius r. The intensity of this field is

$$E_{\mathrm{ed}} = -\frac{\pi r^2 \mu_0}{2\pi r} \cdot \frac{\mathrm{d}H}{\mathrm{d}t} = -\frac{r\mu_0}{2} \cdot \frac{H_{\max}}{\Delta t_1}. \tag{6.77}$$

During the period $\Delta t_1 = 10$ μs at $r = 0.2$ m, $E_{\mathrm{ed}} = 1.26 \times 10^4$ V/m. Let us consider the behavior of charges placed in a small volume of gas in the vortex's wall, adjusted to the vacuum cavity. Let us direct the magnetic field vector $\mathbf{H}$ along the negative values of the vortex's axis Z, and vector $\mathbf{E}_{\mathrm{ed}}$ in the direction of positive values of X-axis. In the system of coordinates rotating with an angular velocity equal to vortex's rotation velocity, the motion of electrons may be described with an equation [377]:

$$m(\mathrm{d}v/\mathrm{d}t) = -(\mathbf{E}_{\mathrm{ed}} + \mathbf{E}) - e\mu_0[\mathbf{vH}] - m\mathbf{v}\nu_{\mathrm{m}}, \tag{6.78}$$

where $\mathbf{v}$, m, and e are velocity, mass, and charge of electron, respectively, ν_{m} is the rate of electron collisions with molecules of gas, $\mathbf{E}_{\mathrm{ed}}$ and $\mathbf{E}$ are the x- and y-components of the vector of the electric field, respectively, and $\mathbf{H}$ is the z-component of the magnetic field vector. Equation (6.78), being written in coordinates X and Y, can be split into two equations:

$$m(\mathrm{d}v_x/\mathrm{d}t) = -eE_{\mathrm{ed}} + e\mu_0 v_y H - mv_x\nu_{\mathrm{m}}, \tag{6.79}$$

$$m\big(\mathrm{d}v_y/\mathrm{d}t\big) = -eE - e\mu_0 v_x H - mv_y\nu_{\mathrm{m}}. \tag{6.80}$$

(Here, a condition $H < 0$ is taken into account). Equating the derivative $d\mathbf{v}/dt$ to zero, we can find the velocity components of the settled motion of electrons from (6.79) and (6.80):

$$v_x = \frac{e^2\mu_0 EH + emE_{ed}v_m}{(mv_m)^2 + (e\mu_0 H)^2}, \tag{6.81}$$

$$v_y = \frac{e^2\mu_0 E_{ed}H - emEv_m}{(mv_m)^2 + (e\mu_0 H)^2}. \tag{6.82}$$

At the beginning of the process, $E = 0$ and the velocity of electrons' movement along the Y-axis to the center of vortex is

$$(v_y)_0 = \frac{e^2\mu_0 E_{ed}H}{(mv_m)^2 + (e\mu_0 H)^2}. \tag{6.83}$$

Using the relation $v_m\,(s^{-1}) = 2 \times 10^9 P$ (Torr) [377], for $E_{ed} = 1.26 \times 10^4$ V/m, $H = 10^5$ A/m ($H = 0.1\,H_{max}$), and $P = 10$ Torr (1.33×10^3 Pa), we can find that $(v_y)_0 = 5.51 \times 10^4$ m/s. Let the thickness of the vortex wall from which the electrons' emission takes place be 2 cm [347, 375]. To pass this way, electron needs time $t_{pn} = 2 \times 10^{-2}$ m/5.51×10^4 m/s $= 0.36 \times 10^{-6}$ s. Finding themselves in the vacuum region, electrons will drift to the vortex's axis with a velocity $v_{dr} = E_{ed}/\mu_0 H = 10^5$ m/s. Moving with this velocity, they can reach the system's axis at a time $\tau_{dr} = R/v_{dr} = 2 \times 10^{-6}$ s.

The motion of positive ions (we shall consider only the lightest of them – protons) is described by (6.51) and (6.52), where one must change the polarity of the terms involving the charge of the particle to the opposite, change the mass of the electron m to mass of the proton m_p, and replace v_m by $v_{m,p}$ – the rate of protons' collisions with air particles. By assuming the equality of electrons' and protons' temperatures and the equality of cross-sections of their collisions with the gas particles, we can find that $v_{m,p}$ is in $(m_p/m)^{1/2} = 40$ times less than v_m. Because of this, one can assume $v_{m,p}\,(s^{-1}) = 5 \times 10^7\,P$ (Torr). At $E = 0$, $E_{ed} = 1.26 \times 10^4$ V/m, $H = 10^5$ A/m, and $P = 10$ Torr, we can find from (6.53) that $(v_p)_y = 58$ m/s. This value is 0.95×10^3 times lower than the drift velocity of electrons. At time $\Delta t_1 = 10^{-5}$ s, protons can shift only by a distance $(v_p)_y\,\Delta t_1 = 0.6$ mm; thus, they have no chance to come out to the vacuum cavity from the dense layers of rotating gas. Hence, because of great difference of drift velocities of electrons and protons at the first study of process, the separation of charges will take place and the electric field $\mathbf{E}$, directed along the axis Y, will appear. As the strength of E is increasing, the drift velocity v_y of the electrons is lowered, until according to (6.82), it becomes equal to zero at

$$E_{max} = (e\mu_0 E_{ed}H)/(mv_m). \tag{6.84}$$

By assuming $P = 5 \times 10^{-3}$ Torr (0.67 Pa), $E_{ed} = 1.26 \times 10^4$ V/m, and $H_{max} = 10^6$ A/m, we can obtain $E_{max} = 2.8 \times 10^8$ V/m.

The increase in the radial electric field **E** must produce protons' drift along the *Y*-axis. According to (6.82), the velocity of this drift at $E_{ed} = 1.26 \times 10^4$ V/m, $H = 10^6$ A/m, $E_{max} = 2.8 \times 10^8$ V/m, and $v_{m,p} = 5 \times 10^8\ s^{-1}$ is $(v_p)_y = eE/m_p v_{m,p} = 5.36 \times 10^7$ m/s. As a result of this, a part of protons will pass through dense layers of gas and will come to the vacuum cavity. After reaching the vacuum cavity, the protons will stop their motion in the direction of **E**. Under the action of the axial magnetic field **H,** vector $\mathbf{v_p}$ will be turned and the protons will drive in the direction perpendicular to the vectors **E** and **H**. Moving in the field **E**, protons gain energy, at the same time, field $\mathbf{E}_{ed}$, directed opposite to proton's velocity, brakes their motion.

At the stage $\Delta t_2 = 50$ μs of decreasing magnetic field *H,* the eddy electric field vector $\mathbf{E}_{ed}$ changes its direction to the opposite. This will favor the acceleration of protons. At this period, the emission of charges into vacuum cavity will be absent. As a result of the discussed processes inside the vacuum cavity, separation of charges and protons' acceleration will occur. The electrons will be gathered in the center, and the protons will rotate around the negative center.

An axial magnetic field has a marked effect on the charges' motion in the plane *XY*, but it essentially does not prevent their motion in the direction of axis *Z*. In principle, owing to their high mobility, electrons at the period of lightning stroke are able to move away from the coil axis to larger distances than protons. During their travel, the electrons may come across positive charges (e.g., in cover of streamer of lightning [374]) and recombine with them. As a result, the system will lose a part of negative charge and will acquire excess positive charge.

Because of the described processes inside the vacuum cavity, a double flat ring of moving charges will be formed: the outer ring of protons (at the excess of one) and the inner ring of electrons (see Fig. 6.10). Owing to the deformation type of twisting to eight, this double ring may fall to many small rings. From these rings, dynamical electric capacitors will be formed. The shell of BL may be gathered from water containing in the vortex's wall.

6.4 Ball Lightning as the Thermodynamic Limit of the Periodic System

In the lightning discharge plasma, we find a regime for negative dielectric response from microwave transmission through tenuous wire grids. From photonic response in vortex plasma, we treat BL as a charged eigenstate fully defined by its central potential, and evolving without change in the radius and brightness. Helical plasmon waves in spherical vortex crystals enhance self-confinement by interfering like worm gears packed with octahedral symmetry. The thermodynamic limit packs taped tori in concentric gear shells at energies beyond those of electron shells in the natural elements.

By Madelung's method for Coulomb interaction in ionic crystals, we derived the potential energy in periodic arrays of line sources with logarithmic interaction potentials. For straight rows, our gauge choice ensured convergence to finite and scale-free lattice sums with lowest energy expressed as Wallis product. For vortex streets, we obtained a smooth energy surface via the complex plane, extendable to 3D lattices via quaternion space. We presented a matrix formulation of quaternion inversion that maps vortex flow in a wedge on potential flow driven by an equatorial vortex row on the surface of a sphere.

We obtain 3D potential fields and flows from quaternion functions satisfying six local and six global conditions for a smooth closure. For quaternion matrices and Jacobians, we found real eigenvalues, orthogonal eigenvectors, nonzero determinants, and inverses by transposition. Group structure includes 8D octavian space resolving into three quaternion sub-spaces, in turn, resolving into three complex sub-planes.

Our matrix method plots equipotential surfaces in parametric form, orthogonal to streamlines as an intersection of two complementary sets of stream surfaces. By quaternion inversion, we calculated the atmospheric circulation patterns as belts, lattices, and Von Karman vortex streets mapped on the unit sphere. The quaternion sine function bends the atmospheric electricity into elliptic coordinates for triggered lightning near the ground level or for spark gaps in high-voltage test facilities.

6.4.1 Introduction

Maxwell's equations endow materials combining negative permittivity and permeability with surprising properties, including reversal of refraction angles, Doppler shifts, and Cherenkov radiation [378]. Such photonic response is not found in natural substances, but various designs predicted this behavior for periodic microstructures made from dielectric or metallic materials, as shown in Fig. 6.13 [379, 380].

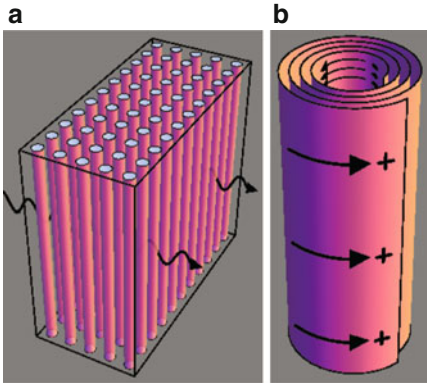

Fig. 6.13 Two photonic microstructures. (**a**) Square array of cylinders in microwave beam. (**b**) Capacitive 'Swiss roll' design enhances negative magnetic response

Meanwhile, several classes of artificial structures called "photonic crystals" have conclusively demonstrated their negative electromagnetic constitution, ranging from microwave to optical frequencies [381]. Ionospheric plasma provides a natural example of negative permittivity causing reflection of radiowaves with long enough wavelength. Here, we will argue for a crucial role of photonics in the electromagnetic constitution of BL.

Despite two centuries of scientific investigation covered in Singer's inspirational monograph, the true nature of BL remains undecided [382]. Smirnov's comprehensive review combines BL physics with electrochemistry on fractal skeletons [383]. The leading database now stores several thousand eyewitness reports collected in the Stakhanov–Keul–Bychkov data bank [384, 385]. Their statistical analysis has fostered consistency and consensus regarding the mean properties of the global BL population. At the same time, laboratory efforts are still far removed from reproducing the full range of its observed characteristics [386, 388–390]. Two BL events reported by professional scientists highlight the features challenging the conventional plasma theory.

In 1964, an all-metal airliner carrying British radio-astronomer, R.C. Jennison, encountered an electrical storm on a late night flight from New York to Washington [391]. Some seconds after a bright and loud discharge, a glowing sphere emerged from the pilot's cabin, passing the observer at an arm's length in steady motion along the aisle. The blue-white ball measured 22 cm with perfect 3D symmetry, free of any polar or toroidal structure. Its surface had a solid appearance with some limb darkening, radiating light at 5–10 W, but not heat. Three years later, the Russian plasma chemist, Dmitriev, standing on the Onega River bank, witnessed a BL with a lifetime of over 1 min, following an intense flash of ordinary lightning [382, 392]. The yellow-white core with 6–8 cm diameter of this slightly elongated ball was covered in violet and blue envelopes measuring 1–2 and 2 cm, respectively. A transistor receiver recorded its radio emission as a continuous rumble with maximum loudness even at 65 m from the ball. As it passed overhead, the observer heard a noise emission with some crackling, and smelled the acrid odor of its bluish mist trail from high-energy radiation in air. On his gamma scintillation radiometer, Dmitriev read 1.2 Mrad/h as the dose rate at 2 m from the source, but a photo film in a holder remained practically unexposed.

Nowadays, carefully screened scintillation counters have established energetic gamma radiation as a common feature of natural or triggered lightning in Florida, USA [393]. Previously, BF_3 counters had already detected neutron generation by lightning bolts in the Himalayan foothills much above the background levels from cosmic rays [394]. For particle acceleration by turbulent vortex dynamics, our helix string model details a planar version for the lightning channel and a spherical version for BL [395, 396]. For both the geometries, we included generic formulas from microwave photonics rescaled to vortex lattices in atmospheric discharge plasma. Through reversed Coulomb forces, we connected the central concentration of charge with evolutionary tracks of BL resembling stellar evolution driven by gravity. Negative dielectrics enable standard balls to consume their energy content without a visible change at the surface as in Jennison's case, or explode into sparks

when disturbed prematurely. And in exceptional cases such as Dmitriev's event, circulation velocities make fusion reactions of light nuclei as inevitable as in main sequence starsi such as our Sun [397].

Tenuous metallic wire grids, as used in fast-particle detectors, demonstrate plasma behavior in microwave propagation analysis and tests reported by Pendry et al. [398]. Their micron-size wires downscale the plasma threshold for wave reflection or transmission from optical to gigahertz frequencies. Transmission data and Maxwell theory agree on photonic band gaps within 5% and *negative* dielectric constant as a robust feature of 3D wire arrays, as shown in Fig. 6.14.

Transverse modes incident on wires excite the surface waves turning into massive plasmons through the Higgs mechanism for the mass of elementary particles. These would range down to the DC level with wires made loss-free by superconductivity.

Pre-Higgs models link high-energy storage in BL with plasmons mediating dielectric attraction between *like* charges, similar to pions in atomic nuclei [382, 399, 400]. Bergström's electromagnetic model freezes bare nuclei into a uniform atmospheric cloud by an immediate dielectric reaction effect [399]. In [400], long lifetime and high energy storage arise from the bosonic nature of microscopic vortex filaments in turbulent BL plasma. Early support for high-energy processes in the air came from lightning-triggered neutron counts recorded over a 3-year period in the Himalayan foothills [394]. New evidence for such intriguing processes

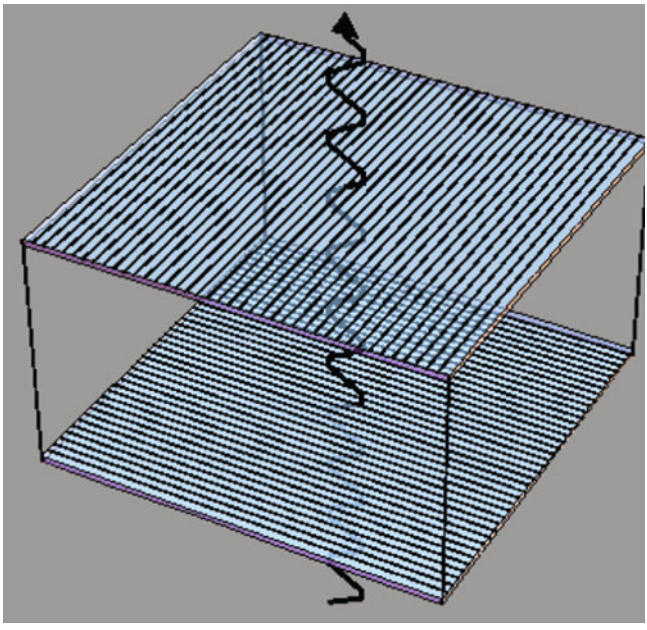

Fig. 6.14 Cubic thin-wire grid with photonic response to microwave transmission

is provided by energetic radiation from rocket-triggered lightning and high-energy gamma rays emitted by thunderclouds [393, 401]. Recent BL data reviewed by Bychkov revealed significant thermal and electric impact causing fires (body) burns, melts, and water heating in a quarter of the reviewed events [402]. Nikitin et al. concluded that the Sochi 1960 photo tracks a charged BL descending towards a lamppost while hovering during repeated field reversals by a nearby lightning discharge [403]. Advanced statistical analysis by Keul revealed a time-constant and space-invariant set of BL phenomena recorded over several centuries in Central Europe [385].

Comparison of Pendry's wire grid with vortex plasmas modeling BL and its laboratory analogs showed common ranges for their critical parameters. An early ruby laser facility at Philips Research Laboratories in Eindhoven, the Netherlands, regularly produced such analogs from an open induction coil upon discharge of a capacitor bank. Data on wire gauges, mesh size, source voltage, and pulse duration supplied by the operator comply with Plasmon-regime parameters [404]. More recently, lightning impact formed a bright ball at a tall lamp post supporting traffic lights and power lines at a T-crossing for trams in Rijswijk, the Netherlands. A Saturday shopping crowd watched this event for about 1 min, and two of them recorded the static ball on their digital cameras. Our site investigation revealed erosive damage on several nearby support wires [405]. Again, estimates for wire gauges and mesh sizes in the complex wiring structure locate this event inside the regime for plasmon waves, as shown in Fig. 6.15.

A Japanese test facility for the study of BL generates gigahertz microwaves at much higher power levels than that generated in Pendry's transmission tests [386, 398]. Instead of thin wires, ceramic plates cause local field amplification approaching breakdown levels in the air by photonic interference [406]. Current Russian experiments achieve reproducible fireball formation by erosive discharges, water surfaces, thin films, and exploding wire rings, with afterglow durations approaching 1 s [388–390, 407, 408].

Function theory of complex variables provides electrodynamics and aerodynamics with a powerful tool for the calculation of planar potential fields [409–411]. Two Cauchy–Riemann relations keep fields and flows irrotational, and the complex function, smooth. The level curves of their real and imaginary parts draw equipotential lines and field- and stream-lines at right angles. By swapping these results, a complementary field pattern with line charges turned into currents, and vice versa could be obtained. The conformal property preserves the angles in maps by regular complex functions. A large class of such functions is expressible as polynomials and power series with real coefficients. In Hamilton's 4D quaternion space [412], an earlier study [396] presented smoothness conditions for 3D potential field and flow solutions, through such functions. By quaternion inversion and exponentials, another study [413] obtained spherical fields and flows, and cast in real matrix format for the three division algebras [414]. Underneath, we applied this format for modeling global atmospheric circulation and pre-stroke potential field calculation for rocket-triggered lightning.

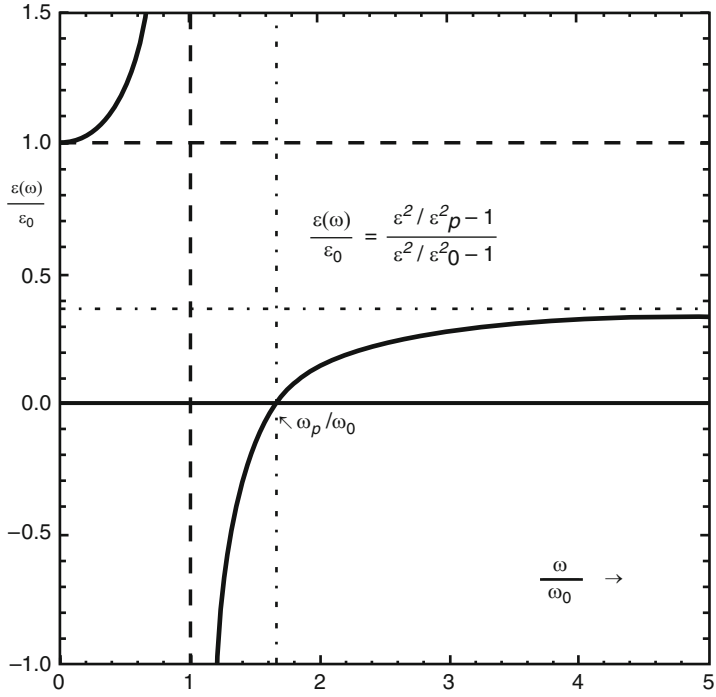

Fig. 6.15 Generic formula for dielectric response turns negative in the shaded frequency range. Replacing ε by μ gives the equivalent formula for magnetic response

6.4.2 Photonic Response

Our bosonic model treats BL as cool, dense plasma threaded by microscopic vortex filaments in coherent rotation at the quantum limit for electron circulation. Its conduction electrons primarily interact by exchange forces as in alkali metals. Ambient vorticity merges them into a superfluid ground state around hollow vortex cores also seen in cavitation of normal fluids. Coulomb forces dress electronic cores in a co-rotating ion mantle restoring overall charge neutrality around vortex loops. This core-mantle structure confines electromagnetic fields between conducting cylinders as in coaxial waveguides. Their elastic stretching, bending, and torsion extend *reversible* energy storage to the relativistic regime [397]. Here, we show that local contraction of their cross-section nicely fits tapered vortex rings into a spherical potential solution for BL.

Let a threshold electric field E_{th} as in (6.85a) dissociate air molecules into equal numbers of electrons, ions, and neutral particles in the cavitation regime of vortex plasma [397]. With uniform current I in the lightning channel, the field lines of magnetic induction B encircle discharge plasma by Ampère's law, as in (6.85b). Screening by electrons in loss-free layers restricts magnetic fields to the London penetration depth λ_{L}, as in (6.85c). Let us consider the cavitation thread quantum

units of flux as hollow tori through the plasma. Inertial mass of vortex rings comes mainly from entrainment of ambient fluid, resulting in migration times as in (6.85d). Together, these relations constitute our vortex plasma through:

$$E_{\text{th}} = \frac{ne^2}{80\pi\varepsilon_0^2 V_{\text{i}}} \approx 23 \text{ MV/m}, \tag{6.85a}$$

$$B = \frac{\mu_0 I}{2\pi R} \approx 0.4 \text{ T}, \tag{6.85b}$$

$$\lambda_{\text{L}} = \sqrt{\frac{m}{\mu_0 ne^2}} \approx 1.1 \text{ μm}, \tag{6.85c}$$

$$\tau = \frac{4\pi e E_{\text{th}} R^2}{\rho\kappa^3} \approx 230 \text{ μs}, \tag{6.85d}$$

with fundamental constants $e \approx 1.6 \times 10^{-19}$ C, electron mass $m \approx 9.11 \times 10^{-31}$ kg, $\varepsilon_0 \approx 8.85$ pF/m, $\mu_0 = 400\pi$ nH/m, and $\kappa = 7.3 \times 10^{-4}$ m^2/s as quantum unit for electron circulation. As material parameters, we used mass density $\rho \approx 1.3$ kg/m^3 of air and ionization potential $V_{\text{i}} \approx 14$ V of nitrogen. At 50% ionization, our electron concentration reached $n \approx 2.5 \times 10^{25}$ m^{-3}, with peak current $I = 10^5$ A and channel radius $R = 0.05$ m as discharge parameters. As the length and timescales for field gradients, λ and τ in (6.85c) and (6.85d) are set as conditions for photonic response to electromagnetic waves in our vortex plasma.

Microwave transmission through Pendry's cubic wire grid demonstrates negative dielectric response at gigahertz frequencies [380]. His micron-sized wires reduce mean electron concentration by a factor of 10^6 relative to solid metal, and raise the canonical electron mass to baryon values. Thus, his grid cuts off microwave propagation below the plasma frequency at 8.2 GHz, where dielectric response turns *negative*. By generic formulas for dielectric response, loss-free waves still propagate along wire surfaces in between resonance at ω_0 and plasma frequency ω_{p}, as shown in Fig. 6.15. More refined microstructures in Fig. 6.13 show negative *magnetic* response for microwaves, confirming Veselago's prediction of refraction at reversed angles from Snell's law [378, 381].

6.4.3 Charged Eigenstates

Superconducting wires in Pendry's grid will extend negative dielectric response down to the static limit, where plasmon wavelength merges with London penetration depth. Their longitudinal and transverse modes share dispersion relations with elementary particle models creating Higgs bosons in a vacuum [380]. By an *attractive* dielectric reaction between *like* charges, Coulomb forces cause self-confinement of nuclei and

BL in Bergstrom's electromagnetic theory of strong interaction [399]. For spherical charge distributions, we derived smooth potential profiles via conformal mapping in quaternion space [396]. Fixed radius and net charge serve as boundary conditions recasting these profiles into charged eigenstates of BL with the central potential as an evolutionary parameter. As the conserved and observable surface field strength, the threshold electric field in (6.85a) sets reference values for other electric-state variables.

Most lightning strokes carry negative charge down to earth, but positive strokes are more powerful on the average. The 4D quaternion space inverts a uniform pre-stroke field into a spherical potential function $\Phi \sim w/(w^2 + r^2)$, parametrized by w for its evolution [396, 400]. Equation (6.86a) shifts its zero from infinity to $r = R$ at the surface, with central potential Φ_C as the reference value. From standard vector relations, the profiles for electric field E and charge density ρ with their reference values E_S and ρ_C are as follows:

$$\frac{\Phi}{\Phi_C} = -\frac{w^2}{R^2}\frac{R^2 - r^2}{w^2 + r^2}, \quad \frac{E}{E_S} = -\frac{r}{R}\left(\frac{w^2 + R^2}{w^2 + r^2}\right)^2, \quad \frac{\rho}{\rho_C} = -\frac{w^4}{3}\frac{3w^2 - r^2}{(w^2 + r^2)^3}, \tag{6.86a}$$

$$\Phi_C = \frac{1}{2}E_S R\left(1 + \frac{R^2}{w^2}\right)\mathrm{V}, \quad E_S = \frac{ne^2}{80\pi\varepsilon_0^2 V_i} \approx 2.3\frac{\mathrm{MV}}{\mathrm{m}}, \quad \rho_C = \frac{3\varepsilon_0 E_S}{R}\left(1 + \frac{R^2}{w^2}\right)^2 \frac{\mathrm{C}}{\mathrm{m}^3}, \tag{6.86b}$$

with minus signs denoting a *negative* well potential and *inward* field directions from *negative* charge density balanced by *positive* surface charge. In (6.86b), the central potential and charge density evolve via w without change in the surface potential and field strength. Figure 6.16a and b plot successive curves meeting in $\Phi(R) = 0$ for potentials, and with a common beginning and end for the electric

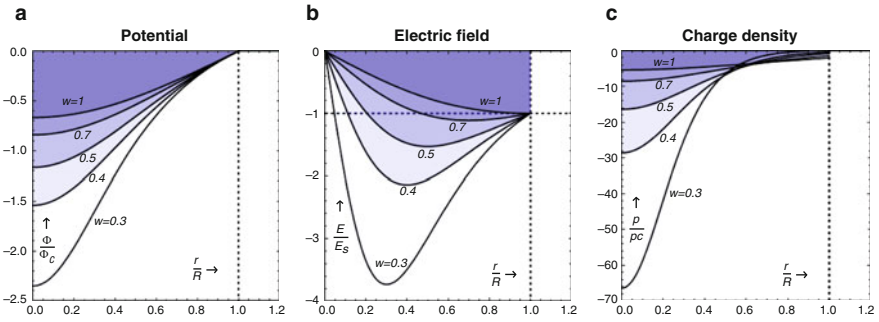

Fig. 6.16 Electric profiles in ball lightning (BL) plasma evolve without change in radius and net charge. (**a**) Potential curves decay smoothly towards ground level. (**b**) Photonic vortex plasma requires field strength below the dashed line. (**c**) Flattening charge density curves release energy for radiative output

field. Each charge density curve plotted in Fig. 6.16c integrates to the same net charge by volume, but they lack a common point.

Steep initial profiles shown in Fig. 6.16 gradually flatten as BL evolution increases w from an initial value below 1. Small w values concentrate space charge near the center of a deep potential well, much like what the nucleus does in the atoms, but with opposite polarity. A proportional rise in electric-field strength will increase the initial ionization levels above single ionization as used in (6.85a). The top curve in Fig. 6.16b defines our final stage of BL, where photonic response just vanishes. The bottom curve defines an initial stage with a compact core region dressed in a wide photonic envelope. Successive curves show that its thickness and peak field diminish towards the surface. Chemical reactions or atomic Rydberg states can increase the life span by releasing additional energy [387, 401–403], and likewise, for light nuclei when central voltages in (6.86b) enter the regime for their fusion reactions [395, 397].

6.4.4 Coherent Rotation

For dynamic effects in vortex plasma, we need much stronger photonic response than tenuous wire grids shown in microwave transmission experiments. Hence, we seek compact vortex structures with constructive interference of their photonic plasmon waves. These structures will serve as a unit cell for periodic vortex lattices extending to infinity in the thermodynamic limit. By the inversion method used for electric profiles in (6.86), we can map various lattice structures onto a spherical vortex state conserving their photonic response. These inversion maps straighten tube lattices into tapered vortex loops packed in concentric shells with geometries resembling electron orbitals in the periodic system of elements. Nature allows stable atoms with at most 92 electron orbitals, but the loop count provides a free parameter for energy storage in such spherical vortex crystals.

We used coherent rotation of various gear wheel combinations as visualization for constructive interference of photonic plasmon waves on vortex tubes. With gear wheels packed on spheres, as in Fig. 6.17, coherent rotation visualizes constructive interference of plasmon waves propagating along their outer edges.

On each sphere, units of four or six connect wheels in even numbers are required for coherent rotation. Spherical combinations connecting gear wheels in odd numbers must remain static. Clearly, the same distinction between static and dynamic grip applies to planar gear-wheel combinations.

The Euclidean plane packs identical gear wheels most densely in triangular unit cells, but coherent rotation requires square-based or hexagonal lattices. Spherical surfaces admit just one fully regular co-rotation pattern, packing eight wheels in units of four in Cartesian octants, as shown in Fig.6.17a. Vertices of the other four Platonic solids have threefold or fivefold symmetries that block co-rotation. Out of 13 Archimedean solids, 3 trace out semi-regular co-rotation patterns. The truncated octahedron, shown in Fig.6.17a, copies the partition of its Platonic parent. Figure

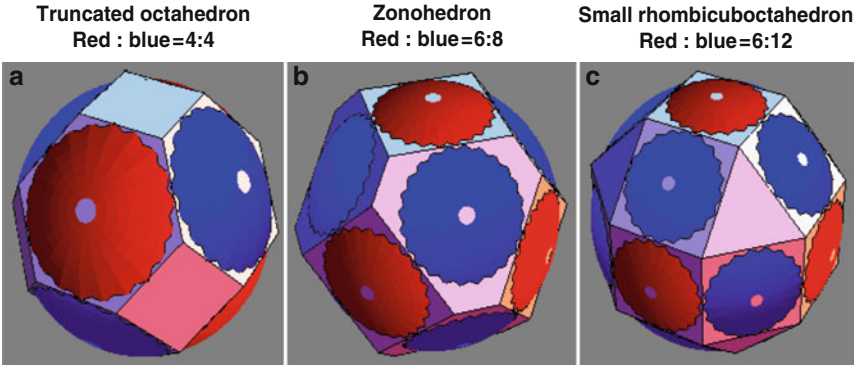

Fig. 6.17 Some (semi-) regular solids and some zonohedra partition of a spherical surface for coherent rotation. (**a**) Octahedral symmetries connect eight gear wheels in six loops of four with balanced 4:4 ratio of spin sense; wheel centers define the edges of a cube. (**b**) Unbalanced 6:8 spin ratio results from octahedral symmetries connecting 14 gear wheels in 12 loops of 4; the wheel centers define a rhombic dodecahedron. (**c**) Unbalanced 6:12 spin ratio results from octahedral symmetries connecting 18 gear wheels in eight loops of 6; a 45° twist of the top section restores spin balance by changing the Archimedean partition into the Miller solid

6.5c packs 18 wheels in 8 units of 6. As a third Archimedean solid, the snub cube partitions spherical surfaces for co-rotation of 32 wheels in 6 units of 12. The wheel count sequence 8, 18, 32 obeys the $2n^2$ formula counting electron orbitals in successive shells of noble gas atoms. The $l = 3, m = 2$ spherical harmonic solution of Schrödinger's wave equation traces out the octant partition in Fig. 6.17a by its zero lines, but the other two have no such connection. While atomic physics gives most electron states a non-zero orbital angular momentum, vortex tubes have none in the static co-rotation patterns of Fig. 6.17.

Remarkably, the 18 gear wheels on the Archimedean solid in Fig. 6.17c show a 2:1 spin imbalance absent from the Miller solid produced by a 45° twist of its top section. At a slightly lower zonohedral level of symmetry, co-rotation with a 4:3 spin imbalance appears with 14 wheels packed in 12 rhombic units of 4, as shown in Fig. 6.17b. In the periodic system, 14 is the number of *M*-shell electrons in iron atoms, distinguished by their magnetism, nuclear binding energy, and complicated optical spectrum.

6.4.5 Vortex Crystals

On vortex tubes in 3D Euclidean space, we visualized photonic plasmon waves by rotating worm wheels, as shown in Fig. 6.18. We constructed regular gear units with cell faces at right angles to worm-wheel axes. Axis directions of a twin worm pair have two bisectors that define the complementary values for pitch angles with opposite sign, as shown in Fig. 6.18.

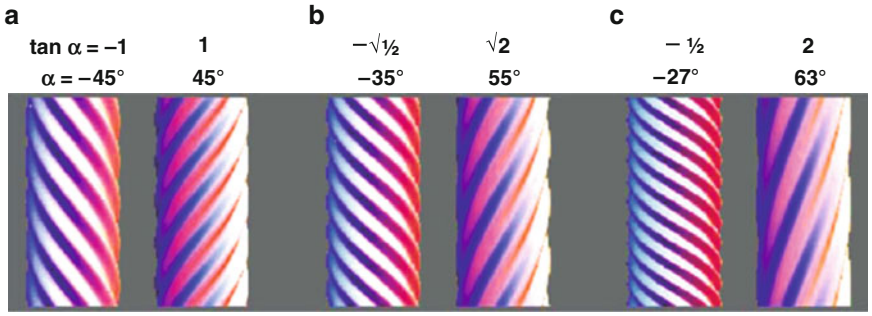

Fig. 6.18 Helical plasmon waves on vortex tubes look like the surface of rotating worm wheels. Dihedral angles |2α| in (**a**) cubic, (**b**) octahedral, and (**c**) dodecahedral cells determine the screw pitch tanα

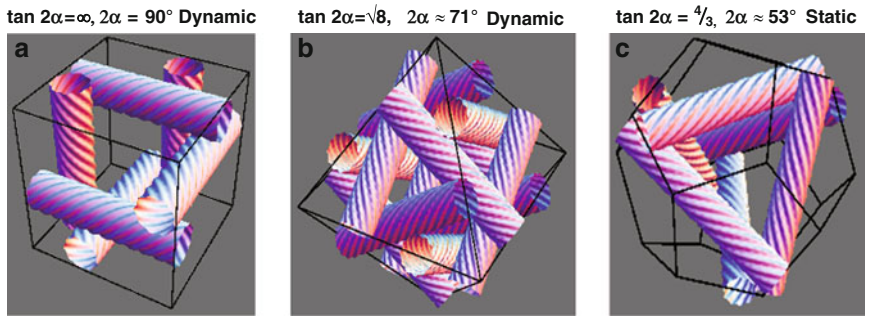

Fig. 6.19 Three Platonic solids stack gripping worm wheels normal to cell faces at dihedral angles 2α. Symmetry admits co-rotation in (**a**) cubic and (**b**) octahedral lattices, but not in (**c**) dodecahedral cells

For strong photonic response by constructive interference between plasmon waves, we produced a coherent rotation of worm gear units, extendable to an infinite lattice in the thermodynamic limit.

From their face and vertex symmetries, we labeled the cubic cells by {4, 3}, octahedral cells by {3, 4}, and dodecahedral cells by {5, 3}, as in Schläfli's {p,q} symbol [415]. Figure 6.19a shows the *left*-handed worm wheels packed in *right*-handed triplet units centered on a body diagonal to the cubic unit. This *left–right* combination allows co-rotation, because its triplet units have continuous normal velocities in all three tangent points, and likewise, for *right–left* triplets. Conversion to either *right–right* or *left–left* triplets blocks co-rotation in the unit cell and throughout the vortex lattice. Compactness doubles when helicities are packed alternately in a filled-up static version.

The octahedral {3,4} cell shown in Fig. 6.19b packs worm wheels in triplet units by face symmetry and in quartet units by vertex symmetry. Twelve *large*-pitch and *left*-handed worm wheels are packed in *right*-handed triplet units and *left*-handed

quartets, resulting in overall co-rotation. This dynamic grip will survive inversion to *right*-handed worm wheels packed in *left*-handed triplets and *right*-handed quartets. Other conversions give static grip at best. In the dodecahedral {5,3} cell shown in Fig. 6.19c, vertex symmetry suffices to pack worm wheels at equal angles in large and small triplet units. Here, *large* pitch allows co-rotation in *large* triplets, but blocks co-rotation in *small* triplets, reducing the unit to static grip. The same holds for the same cell packing thinner wheels in quintets by face symmetry in addition to triplets by vertex symmetry.

6.4.6 Tapered Torus Shells

The 4D inversion map used for our charged eigenstates in (6.86) also bends cylinders into toroidal tubes with variable cross-section. At infinite cylinder length, the torus end points converge to the center of inversion, where cross-sections shrink to zero. In general, any torus mapped from an unbounded vortex lattice converges on this center as a tapered vortex ring. Conversely, cylinder sections nearest to the center of inversion end up farthest and largest on image tori. Tubes at equal distance from the center of inversion define a circumsphere by their outermost image points. A smaller concentric circumsphere for end points of tube images encloses a vortex-free core region. Together, these circumspheres enclose a photonic plasma envelope threaded by toroidal vortex tubes, as shown in Fig. 6.20.

The octahedral unit of Fig. 6.19b packs 12 worm wheels with midpoints at equal distances from its center. Their inversion to a spherical gear packs 12 tapered worm

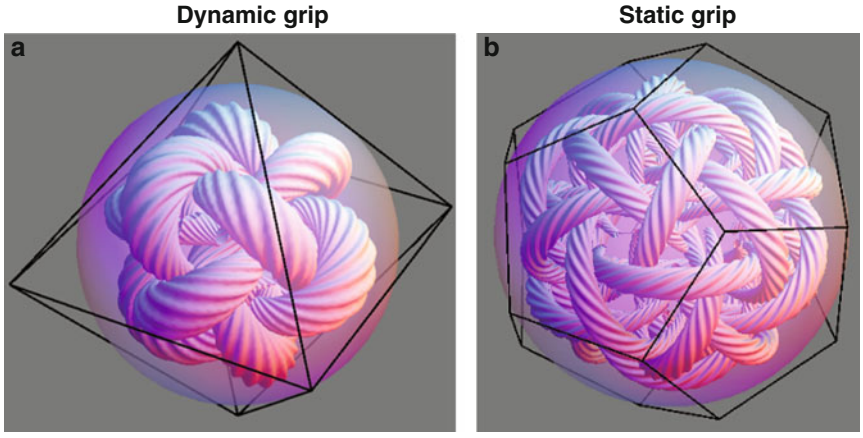

Fig. 6.20 Tapered toroidal tubes retain symmetry, helicity, and grip of worm gear units. (**a**) Octahedral {3, 4} grip enhances photonic response of plasmon waves in gear sphere. (**b**) Dodecahedral {5, 3} grip weakens photonic plasma response of 30 toroidal tubes

tori, as shown in Fig. 6.20a. Clearly, this inversion preserves {3, 4} face and vertex symmetries. As an improper map, it also reverses pitch angles and packing helicities, preserving dynamic grip of gear wheels and photonic response in vortex lattices. Likewise, for dodecahedral units, packing six worm wheels as shown in Fig. 6.19c, will preserve their static grip upon inversion onto tapered tori. Static grip also survives for 30 worm wheels packed in a dodecahedral cell, with {5, 3} face and vertex symmetries clearly visible in the image sphere of Fig. 6.20b.

Periodic vortex lattices pack the central unit in copies weaving successive tube layers around it. In cubic lattices shown in Fig. 6.19a, parallel tubes spin with alternating sense in three square-based grids. More compact octahedral lattices, shown in Fig. 6.19b, align vortex tubes in four triangular grids. Successive tube layers invert to concentric torus shells *inside* the circum-sphere of Fig. 6.20a. As cross-sections at end points approach zero near the center, their circulation speeds up for the conservation of angular momentum. By this vortex acceleration, ions gain more kinetic energy than electrons in proportion to their masses. Circulation in the lowest Bohr orbit gives light nuclei enough energy for fusion reactions [397].

6.4.7 Thermodynamic Limit

The thermodynamic limit of Pendry's wire grid fills space with identical cubic cells extending to infinity in all directions. Its wire directions are either parallel or cross at right angles by alignment with cube edges. Such unbounded straight wires interact by logarithmic potentials for electric or magnetic forces. Hence, their interaction energy diverges to infinity when moving two parallel wires apart without bound. Grid response with negative epsilon follows Maxwell theory given in [398] gauged for noninteracting wire currents. Here, we included (Coulomb) interactions between (charged) vortex tubes, as Madelung sums do for spheres packed in ionic crystals.

The logarithmic potentials also hold for hydrodynamic interaction between straight and parallel vortex lines in potential flows. These arise as twin vortex–anti-vortex pairs shed by thin wires moving through fluid at Reynolds numbers near transition from laminar to turbulent flow [395]. Von Karman vortex streets arrange such wake flows of source–sink pairs into rows with alternating polarity, as shown in Fig. 6.21.

Planar vortex lattices also form in liquid helium by rotation of its container, and in one-component electron plasmas inside magnetic traps [396]. Coherent 3D forms of vortex lattices arise in tenuous Bose–Einstein condensates of ultra-cold atoms. For straight-line sources [397], 3D vortex crystals with symmetries and topologies for minimal dissipation of their circulation patterns, were constructed.

For a stable equilibrium, all systems must settle into states with minimum energy. In ionic crystals, Coulomb's law arranges ions as hard spheres in rows with alternating polarity. Their inverse-square interaction profile ensures convergence to finite row energies by the Leibniz criterion for alternating series. Such

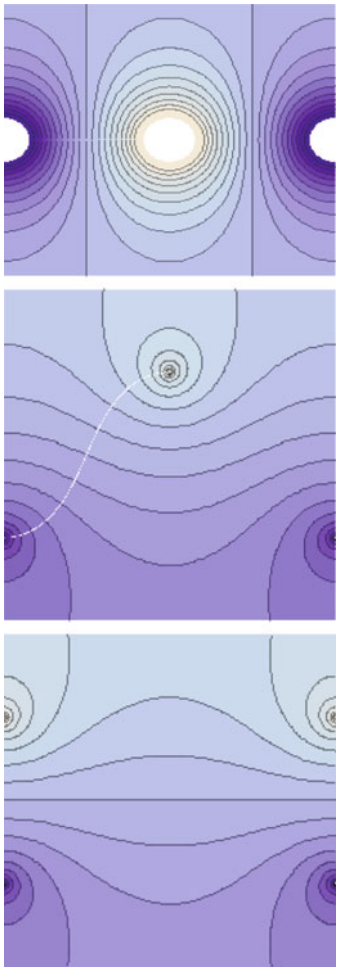

Fig. 6.21 Von Karman vortex streets align alternating source polarities in straight, staggered, or symmetric rows

series converge to finite sums when absolute values of their terms decrease monotonously to zero. Underneath, we derived corresponding energy sums for logarithmic potential profiles, showing their convergence to finite-row energies. Our dimensionless form scales potential sums relative to nearest-neighbor interaction as a Madelung lattice constant for wire grids and vortex lattices.

6.4.8 Wallis Product

Let a reference distance d separate adjacent vortices with opposite circulation in an unbounded straight row, as shown in Fig. 6.13. Each vortex finds itself halfway between identical vortex pairs at successive distances d, $2d$, $3d$, $4d$, ... exerting

potentials $2\ln(d)$, $-2\ln(2d)$, $2\ln(3d)$, $-2\ln(4d)$, ... Combining successive logarithms readily gives a scale-free potential series $2\ln(1/2), 2\ln(3/4), 2\ln(5/6), \ldots$ with terms that converge monotonously to zero without alternating signs. However, the closely related alternating series $\ln(1/2), \ln(3/2), \ln(3/4), \ln(5/4), \ldots$ does meet both Leibniz' conditions for convergence. Hence, we secured finite potential sums for alternating line rows by defining their Madelung constant α through:

$$\alpha \equiv 2\sum_{n=1}^{\infty}(-1)^{n+1}\ln(nd) - \ln(d) \equiv \Phi_{\infty} - \ln(d), \tag{6.87}$$

where $-\ln(d)$ shifts the row potential Φ_{∞} by a gauge transformation without the consequence for classical electromagnetic fields [410]. This achieves a convergent and scale-free potential sum for the straight vortex row, expressed in the classical Wallis product through:

$$\Phi_{\infty} - \ln(d) = \ln(1d) - 2\ln(2d) + 2\ln(3d) - 2\ln(4d) + \cdots \tag{6.88a}$$

$$\alpha = \ln\left(\frac{1\times 3}{2\times 2}\cdot\frac{3\times 5}{4\times 4}\cdot\frac{5\times 7}{6\times 6}\cdot\frac{7\times 9}{8\times 8}\cdot\cdots\right) = \ln\left(\frac{2}{\pi}\right) \tag{6.88b}$$

showing sign alternation in (6.88a), and monotonous decrease to zero for absolute values $|\ln(1/2)|$, $|\ln(3/2)|$, $|\ln(3/4)|$, . . . in (6.88b). Thus, we can find a *finite* Madelung constant for the straight vortex row, much like corresponding ion rows summing to 2ln(2) via the alternating harmonic series 1, −1/2, + 1/3, −1/4, . . ., also named as Brouncker series.

Inside the unit cells, we may shift the positive (or negative) vortices horizontally without affecting the convergence of their potential sums. For a row with period 2, two complementary distances a and $2 - a$ give the potentials $\ln(1 - a/2)$, $\ln(1 + a/2), \ln(1 - a/4), \ln(1 + a/4), \ldots,$ which for $0 < a < 1$, continue to meet the Leibniz conditions. Likewise, for rows with period $2d$, complementary distances ad en $(2 - a)d$ between (next-)nearest neighbors rearrange and sum to a Madelung *formula*:

$$\begin{aligned}\alpha &= \ln\left(\frac{(2-a)(2+a)}{2\times 2}\cdot\frac{(4-a)(4+a)}{4\times 4}\cdot\frac{(6-a)(6+a)}{6\times 6}\cdot\cdots\right)\\ &= \ln\left(\frac{\sin(a\pi/2)}{a\ \pi/2}\right), \qquad 0\leqslant a\leqslant 1\end{aligned} \tag{6.89}$$

which is easily seen to reproduce the Wallis product in (6.88b) by the substitution of $a = 1$. Moreover, when vortices and anti-vortices coincide and cancel, the limit $a \to 0$ reduces α in (6.89) to zero by the standard limit $\sin(x)/x \to 1$ for $x \to 0$. Thus, (6.89) ensures a smooth transition from zero energy in fluid at rest to negative energies when vortex–anti-vortex separation increases from 0 to 1 for the straight

row in Fig. 6.21. This contrasts with ionic crystals, where ions cannot neutralize their charges by merging, zero energy requires infinite separation between all ions, and bound states have negative energy relative to infinity.

6.4.9 Vortex Streets

What remains to be done is translations in other than horizontal directions, as shown in Fig. 6.21. This can be done by expressing potential flow patterns around line vortices in complex coordinates and functions, scaled to agree with the previous section. Accordingly, stream function and potential around a line vortex at the origin follow as real and imaginary parts of a logarithmic complex potential $\zeta(z) = \ln((x + \mathrm{I}y)\pi/2)$. Likewise, a compound potential function $\ln(\sin(z))$ creates a periodic row of identical vortices along the x-axis with period 2. By sign reversal, the potential $-\ln(\sin(z-p))$ creates a complementary row of anti-vortices, shifted over $p = (a + \mathrm{I}b)\pi/2$ in arbitrary directions and distances. In this way, setting $a = 1$ and $b = 0$ recovers the straight row, with lowest Madelung sum as given in (6.88a). For general Von Karman vortex streets, we combine the vortex and anti-vortex rows in a single complex potential ζ as:

$$\varsigma = \ln\left(\frac{\sin(z)}{\sin(z-p)}\right), \quad \alpha = \ln\left|\frac{\sin(p)}{p}\right| \qquad (6.90a, b)$$

Periodic units of their streamline patterns are plotted in Fig. 6.10a–c as level curves of the real part from (6.90a). The straight row pattern in Fig. 6.22a stands out by the near absence of open streamlines.

For Madelung sums at complex vortex–anti-vortex separation, we rely on sum limits returned by our *Mathematica* program. For the symmetric Von Karman street shown in Fig. 6.22a, an imaginary separation vector Ib replaces a in (6.89). Writing $\sin(\mathrm{I}b) = \mathrm{I}\sinh(b)$ gives $\ln(2\sinh(\pi/2)/\pi) \approx 0.382$ as *positive* Madelung sum for the symmetric row with $b = 1$, shown in Fig. 6.22b. As stated earlier, merging vortices reproduce the zero level of Madelung energy, now by the limit $\sinh(x)/x \to 1$ for $x \to 0$. For the staggered vortex street in Fig. 6.22 with complex p, the lattice sum re-arranges into a Madelung *formula* given in (6.90b) with $\alpha = \ln(2/\pi)) \approx -0.452$ as the lowest value for vortex–anti-vortex separation $p = \pi/2$. When compared with (6.90a), the general potential sum of (6.90b) differs only by its modulus bars that make sure that α is real for any complex vector p.

The Madelung surface, shown in Fig. 6.23, illustrates a saddle point on the left, uniting two separatrix lines that trace out the zero energy level of fluid at rest.

Our lattice sum for α converges for separation vectors in a vertical strip between $a = 0$ (solid line) and $a = 1$ (dashed line) in Fig. 6.23. In this domain, the straight row, shown in Fig. 6.22, serves as an attractor for other configurations. Instead of neutralization by vortex–anti-vortex recombination, gradients of our Madelung

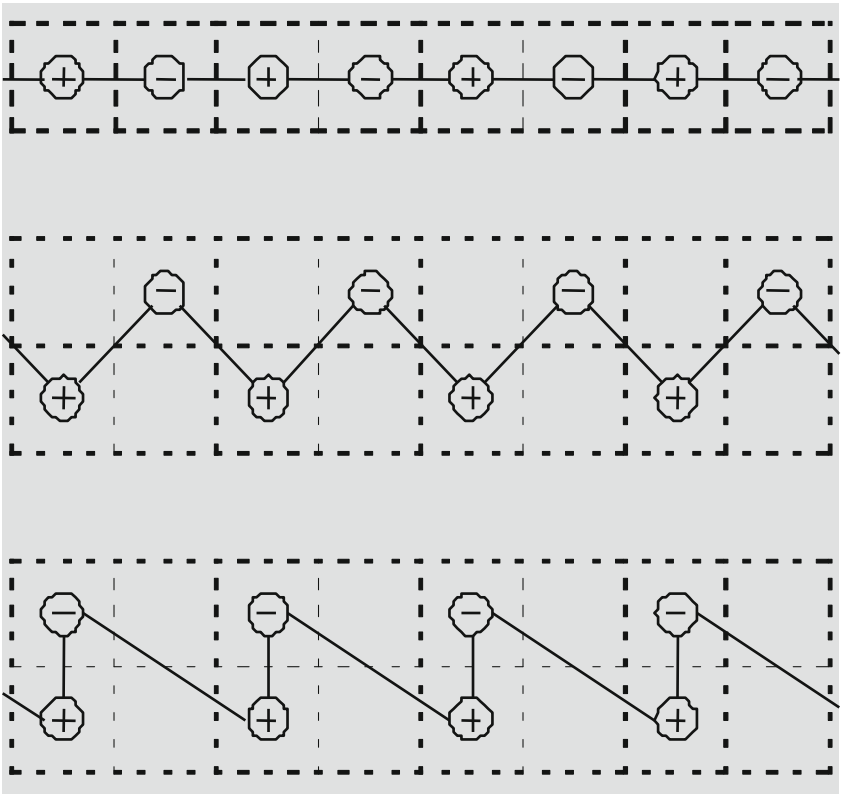

Fig. 6.22 Streamlines for straight, staggered, and symmetric vortex streets from Eq. (6.90a)

surface, shown in Fig. 6.23, favors evolution of turbulent systems towards a bound state resembling a vortex crystal.

The staggered row, shown in Fig. 6.22b, enables construction of an unbounded square-based vortex lattice by periodic vertical translations, and similar oblique translations do the same for the two other rows. Now, the resulting flow pattern is periodic in two directions, and elliptic functions will replace sine functions in the complex potential of (6.88). Thus, the same replacement in (6.89) suggests an expression for the corresponding Madelung formula.

6.4.10 3D-Lattice Sums

For corresponding 3D-lattice sums, we can preserve the great convenience of complex coordinates via Hamilton's 4D quaternions [412]. By his definition, quaternions q combine a scalar real part w with a vector imaginary part $\mathrm{I}r = \mathrm{i}x + \mathrm{j}y + \mathrm{k}z$, with four real variables r, x, y, z, and four imaginary units I, i, j, k connected by:

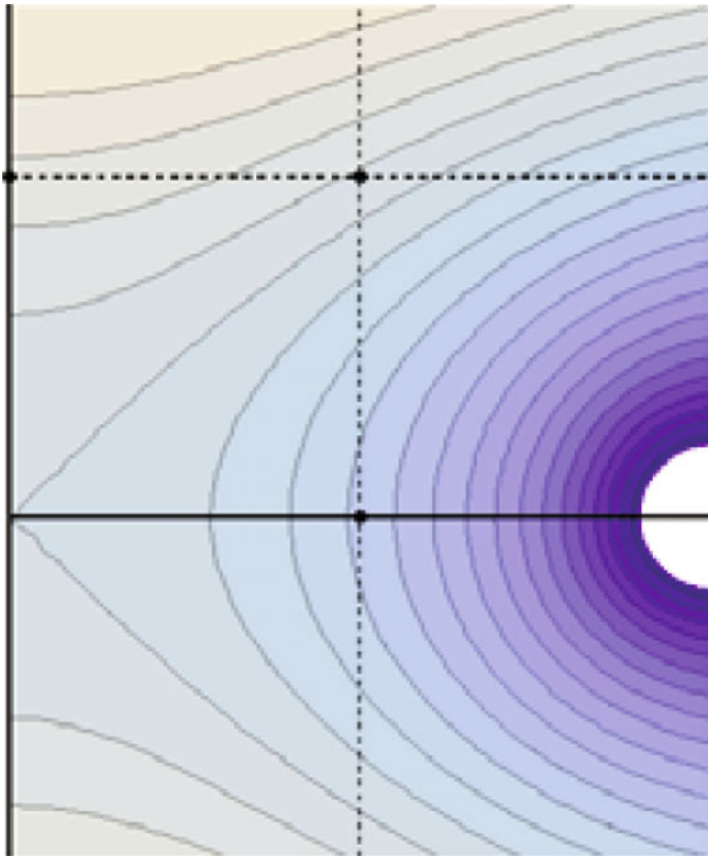

Fig. 6.23 Level curves for Madelung energy surface of vortex streets

$$q = w + \mathrm{i}x + \mathrm{j}y + \mathrm{k}z, \quad i^2{=}j^2{=}k^2{=}-1, \quad ijk = -1 \tag{6.91a}$$

$$q = w + \mathrm{I}r, \quad \mathrm{I} = (ix + jy + kz)/r, \quad r = \sqrt{x^2 + y^2 + z^2} \tag{6.91b}$$

with r as norm of the imaginary part $ix + jy + kz$ for short. The i, j, k units readily follows $i = jk$, etc., as in outer products of Cartesian unit vectors. For this quaternion algebra, we give an equivalent matrix formulation, which is more convenient for the calculation of potential flows with *Mathematica*.

Construction of polynomial and other standard functions in quaternion space only requires addition and multiplication formulas valid for complex functions. Thus, Von Karman vortex street potentials as given in (6.91a) separate into real and imaginary parts for their sine and logarithmic functions as:

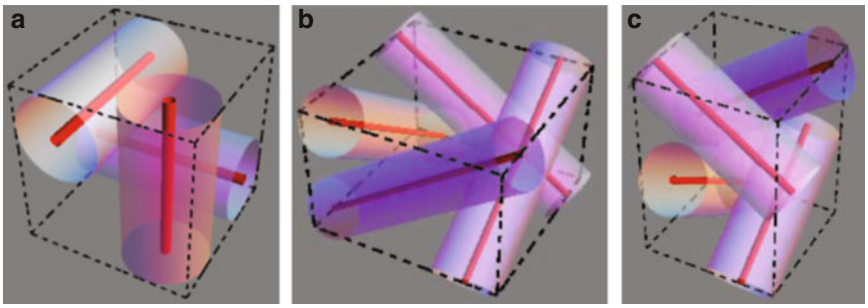

Fig. 6.24 Three unit cells stack identical cylinders with axes at equal angles and distances; (**a**) left-handed vortex trio at normal angles; (**b**) right-handed quartet at tetrahedral angles; (**c**) quartet with mixed helicities

$$\sin(q) = \sin(w + \mathrm{I}r) = \sin(w)\cosh(r) + \mathrm{I}\cos(w)\sinh(r) \tag{6.92a}$$

$$\ln(q) = \ln(w + \mathrm{I}r) = \ln(\mu) + \mathrm{I}\theta, \quad \theta = \arctan(r/w), \quad \mu = \sqrt{w^2 + r^2} \tag{6.92b}$$

with μ as the norm of the full quaternion $w + \mathrm{I}r$ and angle θ for its argument. Hereby, the potential flows and Madelung formulas for our vortex streets acquire 4D freedom in quaternion space. For 3D lattices, an earlier study [398] developed a cubic unit cell with three orthogonal line sources, as shown in Fig. 6.24a. The unit cells shown in Fig. 6.24b, c stack four line sources at equal angles, like diagonals inside a cube or valences of carbon atoms. Reference [411] classified symmetries, topology, and compactness of their respective lattices.

6.4.11 Regular Quaternions

Parametric plots of potential flows need explicit formulas for $z \equiv x + \mathrm{I}y$ in terms of complex potentials $\zeta \equiv \Phi + \mathrm{I}\Psi$, with potential Φ and stream function Ψ as parameters. A single vortex–anti-vortex pair with complex potential $\zeta = \ln((z + 1)/(z - 1))$ turns into a circular row of four pairs upon substitution of z^4 for z. In this way, we obtain the complex potential for vortex circulation confined by a wedge, and its inverse function as:

$$\zeta \equiv \Phi + \mathrm{I}\Psi \equiv \ln\left(\frac{z^4 + 1}{z^4 - 1}\right), \quad z \equiv x + \mathrm{I}y = \left(\frac{1 + \exp(\Phi + \mathrm{I}\Psi)}{1 - \exp(\Phi + \mathrm{I}\Psi)}\right)^{1/4} \tag{6.93a, b}$$

The planar part of Fig. 6.25 shows one of the eight sectors in the circular vortex row with flow pattern as parametric plot of the inverse complex potential in (6.93b).

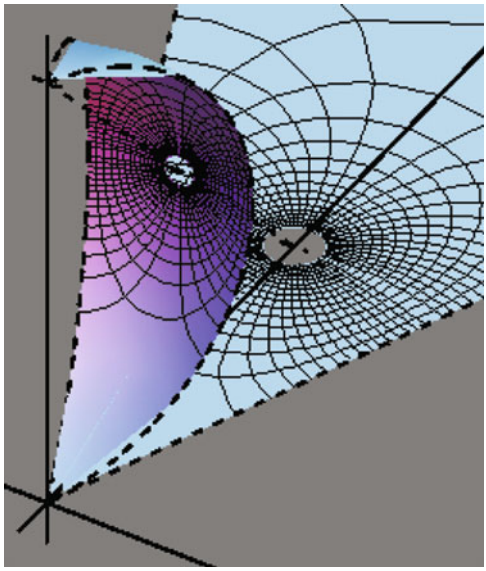

Fig. 6.25 Vortex flow pattern inside π/4 wedge mapped on sphere by quaternion inversion

In 4D quaternion space, an earlier study [416] connected position vectors $q = w + ix + jy + kz$ with square matrices Q having q as leading column, as written in (6.94a, b). Matrix products of Q with four vectors copy the results of quaternion algebra. Q's determinant $(w^2 + x^2 + y^2 + z^2)^2$ ensures inverse matrices for all nonzero matrices Q, similar to what q's norm $(w^2 + x^2 + y^2 + z^2)$ does for the vectors. Quaternion space splits functions $f(q) = W + iX + jY + kZ$ into four real functions W, X, Y, Z of four real coordinates w, x, y, z. Their 16 partial derivatives $W_w, W_x, \ldots, Z_z$ enter the Jacobian matrix J with quaternion derivative $\mathbf{d}f/\mathbf{d}q$ as leading column through:

$$q \equiv \begin{pmatrix} w \\ x \\ y \\ z \end{pmatrix}, \qquad Q \equiv \begin{pmatrix} w & -x & -y & -z \\ x & w & -z & y \\ y & z & w & -x \\ z & -y & x & w \end{pmatrix},$$

$$f(q) \equiv \begin{pmatrix} W(w,x,y,z) \\ X(w,x,y,z) \\ Y(w,x,y,z) \\ Z(w,x,y,z) \end{pmatrix}, \qquad J \equiv \begin{pmatrix} W_w & W_x & W_y & W_z \\ X_w & X_x & X_y & X_z \\ Y_w & Y_x & Y_y & Y_z \\ Z_w & Z_x & Z_y & Z_z \end{pmatrix}, \quad \frac{\mathrm{d}f}{\mathrm{d}q} \equiv \begin{pmatrix} W_w \\ X_w \\ Y_w \\ Z_w \end{pmatrix}. \tag{6.94}$$

By selective removal of rows and columns from matrix Q, we can recover the corresponding matrix pairs for three different complex planes with axes (w, x), (w, y), and (w, z). Each plane has a 2×2 J-matrix imposing one off-diagonal Cauchy-Riemann-condition, collected in the gradient column of (6.95a). Plane-wise, the second Cauchy–Riemann condition emerges from the eigenvalues column in (6.95). Determinant and transpose of Q together yield its inverse matrix. Q's eigenvalues are quaternion vector q and its conjugate, both twice. The moment equation is indispensable for inductive proofs of all 12 conditions in (6.95c) covering quaternion polynomials and power series with real coefficients:

$$\begin{matrix}\text{Gradient} \\ \begin{pmatrix} X_w \\ Y_w \\ Z_w \end{pmatrix} = \begin{pmatrix} -W_x \\ -W_y \\ -W_z \end{pmatrix},\end{matrix} \quad \begin{matrix}\text{Rotation} \\ \begin{pmatrix} Y_z \\ Z_x \\ X_y \end{pmatrix} = \begin{pmatrix} Z_y \\ X_z \\ Y_x \end{pmatrix},\end{matrix}$$

$$\begin{matrix}\text{Moment} \\ \begin{pmatrix} yZ \\ zX \\ xY \end{pmatrix} = \begin{pmatrix} zY \\ xZ \\ yX \end{pmatrix},\end{matrix} \quad \begin{matrix}\text{Eigenvalues} \\ \begin{pmatrix} X_x & X_y & X_z \\ Y_x & Y_y & Y_z \\ Z_x & Z_y & Z_z \end{pmatrix} \begin{pmatrix} x \\ y \\ z \end{pmatrix} = W_w \begin{pmatrix} x \\ y \\ z \end{pmatrix}.\end{matrix} \tag{6.95a, b, c, d}$$

We find explicit coordinate dependence in six *global* conditions, and six *local* conditions without it. For smooth closure in quaternion space, they leave $16-12 = 4$ partial derivatives needed for uniqueness of quaternion derivative given by (6.94). Gradient entries anti-symmetrize the leading row and column of matrix J, and rotation entries symmetrize the remaining sub-matrix S, linking their determinants as follows:

$$\mathrm{Det}(J) = \frac{W_w^2 + X_w^2 + Y_w^2 + Z_w^2}{W_w} \mathrm{Det}(S), \quad \{W, X, Y, Z\} = \frac{\{w, -x, -y, -z\}}{w^2 + x^2 + y^2 + z^2}. \tag{6.96a, b}$$

The vector expression (6.96b) for quaternion inversion $f(q) = 1/q$ satisfies all smoothness conditions (6.95). It enables conformal maps of planar potential solutions on spherical potential solutions by stereographic projection as shown in Fig. 6.25 for wedge flow.

6.4.12 Matrices for Quaternion Maps

For 3D potential solution by quaternion calculus in real matrix form, we defined three elementary matrices that reproduce the algebra of Hamilton's imaginary triple i, j, k in (6.91). We obtained a unit matrix E_0 and three elementary matrices E_1, E_2, E_3 as partial derivatives of quaternion matrix Q with respect to w, x, y, and z as:

$$\frac{\partial Q}{\partial w} \equiv \begin{pmatrix} 1 & 0 & 0 & 0 \\ 0 & 1 & 0 & 0 \\ 0 & 0 & 1 & 0 \\ 0 & 0 & 0 & 1 \end{pmatrix} \equiv E_0, \quad \frac{\partial Q}{\partial x} = \begin{pmatrix} 0 & -1 & 0 & 0 \\ 1 & 0 & 0 & 0 \\ 0 & 0 & 0 & -1 \\ 0 & 0 & 1 & 0 \end{pmatrix} \equiv E_1,$$

$$\frac{\partial Q}{\partial y} = \begin{pmatrix} 0 & 0 & -1 & 0 \\ 0 & 0 & 0 & 1 \\ 1 & 0 & 0 & 0 \\ 0 & -1 & 0 & 0 \end{pmatrix} \equiv E_2, \quad \frac{\partial Q}{\partial z} = \begin{pmatrix} 0 & 0 & 0 & -1 \\ 0 & 0 & -1 & 0 \\ 0 & 1 & 0 & 0 \\ 1 & 0 & 0 & 0 \end{pmatrix} \equiv E_3. \tag{6.97a–d}$$

The elementary E's in (6.97a–d) and identity matrix E_0 copy all product –rules ${E_1}^2 = -E_0, E_1E_2 = E_3 > -E_2E_1$, etc. of Hamilton's imaginary triple i, j, k in (6.91). Using these real matrices simplifies linear algebra for 3D potential solutions and programming for their plots.

6.4.13 Atmospheric Circulation

Geometrical inversion maps circles on circles and spheres on spheres. Lines and planes turn into circles and spheres passing through the center of inversion. Stereographic projection, as shown in Fig. 6.25, maps planar patterns conformally on a spherical surface, or vice versa in cartographic applications. We reproduce this map as parametric plot of the inverse quaternion function $f(q) = 1/q$ defined in (6.96b). Let a potential Φ and a stream function ψ serve as independent variables. Substitute the wedge flow functions $f(\Phi, \psi) \equiv x_2$ and $g(\Phi, \psi) \equiv y_2$ from Eq. (6.93a) in (6.96a, b) for x and y, and remove the z-component. Let parameter w take its place by cyclic permutation of remaining 3D coordinate axes (w, x, y). Our inverse quaternion map on a unit sphere now reads:

$$w = 1, \quad x = f(\phi, \psi), \quad y = g(\phi, \psi), \quad z = 0, \tag{6.98a}$$

$$(X, Y, Z) \equiv \frac{(x, y, w)}{w^2 + x^2 + y^2 + z^2}, \quad 0 \leqslant \psi \leqslant 2, \quad 0 \leqslant \phi \leqslant 4, \tag{6.98b}$$

with flow parameters Φ and ψ in domains as for vortex circulation inside the wedge shown in Fig. 6.25. An eightfold rotation about the z-axis completes the spherical flow pattern shown in Fig. 6. 26b as an equatorial vortex–anti-vortex belt.

Inversion maps by (6.98a); (6.98b) apply to arbitrary planar flows. Multiple source or vortex combinations add up as in linear vector spaces. Parametric plots of a complex potential (Φ, ψ) use its inverse function as coordinates (x, y) in (6.98b). Thus, confined wedge flow of source–sink doublets maps into spherical versions of

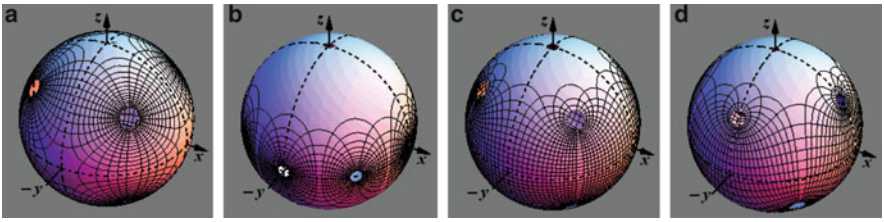

Fig. 6. 26 (**a**) Streamlines close locally in octahedral vortex lattice. (**b**) An equatorial vortex row closes its stream-lines locally. (**c**) Symmetric vortex street sends equatorial circulation around the globe. (**d**) Staggered vortex street gives 'wavy' equatorial circulation

some classical planar potential flows. Equation 6.98 maps the regular octahedral vortex lattice in Fig. 6.26a from a vortex–anti-vortex doublet inside a π/2 wedge. Polarities alternate between neighbors, and each streamline encloses just one singularity, as in the vortex belt in Fig. 6.26b. Opposite polarities in the upper and lower hemispheres of Fig. 6.26c, d send equatorial flows around the globe. They have planar equivalents in the symmetrical and the staggered Von Karman vortex street, respectively.

6.4.14 Triggered Lightning

Reference [393] reported about lightning discharges triggered by grounded copper wires carried into overhead thunderclouds by rockets launched from a platform in Florida, USA. Nearby scintillation counters consistently recorded energetic emissions that challenged conventional models for breakdown in air by lightning. With high voltage along the vertical wires above the ground level, their electric field matched the standard spark gap configurations as used in high-voltage technology. Currently, scintillation counters also record similar energetic radiations from atmospheric spark discharges in controlled laboratory conditions.

Parametric plots of complex sine functions draw field patterns for planar spark gaps in elliptic coordinates. For 3D parametric plots, we can rewrite the quaternion sine function in (6.92a) with potential and field parameters Φ, ρ, σ, τ rescaled for convenient notation and computation as:

$$\begin{pmatrix} W \\ X \\ Y \\ Z \end{pmatrix} = \begin{pmatrix} \sin(w)\cosh(r) \\ x\cos(w)\sinh(r)/r \\ y\cos(w)\sinh(r)/r \\ z\cos(w)\sinh(r)/r \end{pmatrix}, \quad \begin{pmatrix} w \\ x \\ y \\ z \end{pmatrix} = \begin{pmatrix} \phi\pi/15 \\ \rho/2 \\ \sigma/2 \\ \tau/2 \end{pmatrix}. \qquad (6.99a, b)$$

From 4D quaternion space in (6.99a); (6.99b) we remove the stream function τ and its rescaled substitute z. A 3D coordinate frame (X, Y, W) serves for parametric

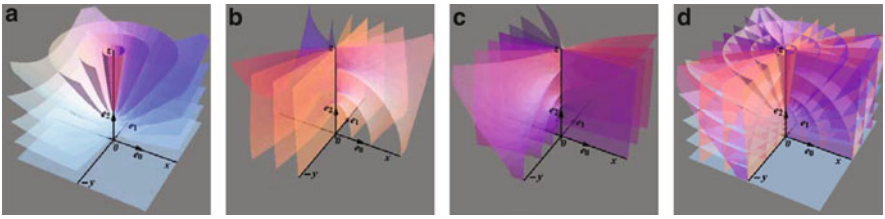

Fig. 6.27 (**a**) Quaternion sine plots hyperbolic equipotential surfaces around spark gap. (**b**) Field surfaces are orthogonal to equipotential surfaces in (**a**). (**c**) Complementary field surfaces branch at the gap electrode, as in (6.99b). (**d**) Combination of potential and field surfaces around a vertical spark gap

plots of the potential function Φ and two remaining stream functions ρ and σ. Substitution of $\Phi = 0$ gives $W = 0$ for the surface of zero potential shown in Fig. 6.27a as XY-plane for a vertical spark gap scaled to unit length at unit vector e_2. The real function $\cosh(r)$ has no zeroes and increases monotonously from unity in the first quadrant, and likewise, for $\sinh(r)/r$ [409, 417]. The range between zero and $\pi/2$ for parameter w allows seven unit steps for the rescaled potential Φ. Starting from zero, the unit steps separate equipotential surfaces drawn by field parameters (ρ, σ) on a square domain given in (6.100a). They dress the spark gap in seven equipotential surfaces, shown in Fig. 6.27a, as confocal hyperboloids of revolution.

Obvious rotation and reflection symmetries map these potential surfaces from the first to any other octant.

$$\text{Potential: } \phi = \{0, 1, ..., 8\}, \quad 0 \leqslant \rho \leqslant 6, \quad 0 \leqslant \sigma \leqslant 6, \quad \tau = 0, \tag{6.100a}$$

$$\text{Field: } 0 \leqslant \phi \leqslant 8, \quad \rho = \{0,\ 1,\ 2,\ 3\}, \quad 0 \leqslant \sigma \leqslant 6, \quad \tau = 0, \tag{6.100b}$$

$$\text{Surfaces: } 0 \leqslant \phi \leqslant 8, \quad 0 \leqslant \rho \leqslant 6, \quad \sigma = \{0, 1, 2, 3\}, \quad \tau = 0. \tag{6.100c}$$

Equations (6.100b, c) define the parameter ranges for complementary sets of field surfaces on square domains shown in Fig. 6.27b and c. One side of their open octant shows streamlines along confocal ellipses. The same holds for interior field lines traced by field surfaces that are not orthogonal. A common branch line above the electrode gap unites all field surfaces, securing their uniqueness, which is also needed for inverse sine potentials in the complex plane.

Figure 6.27d combines the potential and field surfaces of the quaternion sine function in a 3D mesh for spark gap configurations. The conjugate solution will dress a charged bar in confocal ellipsoids of revolution as equipotential surfaces. In [413], our matrix format derives a spherical potential distribution from exponential quaternion functions.

6.4.15 Conclusions

We have connected plasma conditions in lightning channels and BL using the following scenario:

- Electric field threshold initiates cavitation by exchange forces in cool, dense discharge plasma.
- Quantum limit for plasma circulation sets length and time-scales for its photonic response.
- Condensation of photonic plasmon waves suddenly accumulates free charge in central regions.
- A charged eigenstate ensures compactness and coherent circulation by octahedral symmetry.
- Steady radiative loss at fixed radius slowly flattens the radial electric profiles until extinction.

For wire grids or charged vortex lattices interacting by logarithmic potentials, we derived the following:

- A gauge condition securing finite lattice sums by the Leibniz condition for convergence
- A smooth Madelung curve with a finite minimum expressed by the Wallis product
- Extension of complex functions to 4D quaternion space for 3D lattices sums
- Smoothness conditions on quaternion functions enabling 3D potential field calculations
- Quaternion inversion maps on tapered tori with nuclear potential in the thermodynamic limit

Our matrix format for quaternion functions and their Jacobians:

- Ensures nonzero determinants, real eigenvalues, and orthogonal eigenvectors.
- Maps planar flow patterns on the unit sphere by stereographic projection.
- Maps lightning potential distributions near ground level in elliptic coordinates.
- Extends corresponding smoothness conditions to 8D octavian space.

As touchstones for the validation of our BL model by laboratory reproduction, we put forward:

- Preservation of net charge content, radius, and luminosity throughout its life span
- Increased life span resulting from chemical reactions and atomic processes in outer layers
- A steady state resulting from ignition of fusion reactions between light nuclei in the core region

Acknowledgement The author wishes to thank J. de Graaf for the helpful and stimulating discussions on field theory.

References

1. Ohtsuki, Y.-H. (ed.): Science of Ball Lightning (Fire Ball). World Science, Singapore (1989)
2. Singer, S.: The first decade of International Symposia on Ball Lightning. In: Proceedings of the 5th International Symposium on Ball Lightning (ISBL97), Tsugawa-Town, Niigata, Japan, pp. 1–5 (1997)
3. Singer, S.: Direction in recent research and miscellaneous activities in ball lightning. In: Proceedings of the 6th International Symposium on Ball Lightning (ISBL99), Antwerp, Belgium, pp. 1–2 (1999)
4. Singer, S.: Consideration of selected ball lightning models. In: Proceedings of the 8th International Symposium on Ball Lightning (ISBL04), Chung-li, Taiwan, pp. 1–5 (2004)
5. Singer, S.: Progress toward a solution of ball lightning. In: Proceedings of the 9th International Symposium on Ball Lightning (ISBL06), Eindhoven, The Netherlands, pp. 1–2 (2006)
6. Bychkov, V.L., Golubkov, G.V., Nikitin, A.I.: Contemporary state of investigations of ball lightning. Khim. Fiz. **25**(3), 3–6 (2006)
7. Nikitin, A.I., Bychkov, V.L.: 2nd International Symposium on Unconventional Plasmas (ISUP06) and 9th International Symposium on Ball Lightning (ISBL06). Khim. Fiz. **27**(2), 87–96 (2008)
8. Leonov, R.A.: Ball Lightning Enigma. Nauka, Moscow (1965)
9. Lomonosov, M.V.: Selected Works on Chemistry and Physics, pp. 220–256. AS USSR Publishers, Moscow (1961)
10. Arago, F.: Sur le Tonnerre. Annuare au Roi par le Bureau des Longitudes, Notices Scient. p. 221 (1838)
11. Brand, W.: Der Kugelblitz. Verlag von H. Grand, Hamburg (1923)
12. Baturin, V.V., Khanzhonkov, V.I.: Air circulation in premises with respect to location of intake and air vent holes. Heating and Ventilation (4–5), 29–33 (1939)
13. Morris, W.: A thunderstorm mystery. *Daily Mail (London)*. November 5 (1936)
14. Goodlet, B.L.: Lightning. J. IEE, London **81,** 1 (1937)
15. Chirvinsky, P.N.: Ball lightning. Priroda (6), 14–20 (1949)
16. McNally, J.R., Jr.: Preliminary Report on the Ball Lightning. Oak-Ridge National Laboratory, Report N. ORNL3938 (1966)
17. Rayle, W.D.: Ball Lightning Characteristics. NASA Technical NOTE-D- 3188 (1966)
18. Singer, S.: The Nature of Ball Lightning. Plenum, New York (1971)
19. Dmitriev, M.T.: Ball lightning nature. Priroda (6), 98 (1967)
20. Balyberdin, V.V.: Determination of ball lightning energy. Samoletostroenie i Tehnika Vozdushnogo Flota. KhGU Publishers, Kharkov N.3, 102–104 (1965)
21. Charman, W.N.: Ball lightning. Phys. Rep. **54**(4), 261–306 (1979)
22. Altschuler, M.D., Houste, L.L., Hildner, E.: Is ball Lightning a nuclear phenomenon? Nature **228**, 545–547 (1970)
23. Covington, A.E.: Ball lightning. Nature **226**, 252 (1970)
24. Zimmerman, P.D.: Energy content of Covington's lightning ball. Nature **228**, 853 (1970)
25. Tompkins, D.R., Rodney, P.F., Gooding, R.: Photographic observations of ball lightning. Bull. Am. Phys. Soc. **20**, 659 (1975)
26. Eriksson, A.J.: Videotape recording of a possible ball lightning event. Nature **268**, 35 (1977)
27. Mills, A.A.: Ball lightning and thermoluminescence. Nature **233**, 131 (1971)
28. Fleming, S.J., Aitken, M.J.: Radiation dosage associated with ball lightning. Nature **252**, 220 (1975)
29. Stakhanov, I.P.: Physical Nature of Ball Lightning. Atomizdat, Moscow (1979)
30. Stakhanov, I.P.: On Physical Nature of Ball Lightning. Energoatomizdat, Moscow (1985)
31. Stakhanov, I.P.: On Physical Nature of Ball Lightning. Nauchny Mir, Moscow (1996)
32. Imyanitov, I., Tikhiy, D.: Beyond Boundary of Science Laws. Atomizdat, Moscow (1980)
33. Bychkov, V.L.: On observation features of ball lightning. Khim. Fiz. **25**(3), 7–17 (2006)

34. Dmitriev, M.T., Bakhtin, B.I., Martynov, B.I.: Thermal factor of ball lightning. Zhur. Tech. Fiz. **51**(12), 2567–2572 (1981)
35. Barry, J.D.: Ball Lightning and Bead Lightning. Plenum, New York (1980)
36. Brovetto, P., Maxia, V., Bussetti, G.: On the nature of ball lightning. J. Atmos. Terr. Phys. **38,** 921–934 (1976)
37. Moigno, F.: Le Cosmos. 14, 672 (1859)
38. Endean, V.G.: Ball lightning as electromagnetic radiation. Nature **263**, 753 (1976)
39. Menzel, D.H.: Flying Saucers. Harvard University Press, Harvard (1965)
40. Cowgill, W.: Curious phenomenon in Venezuela. Sci. Am. **55**, 389 (1886)
41. Grigorjev, A.I.: Fiery Killers. Mysteries and Secret of Ball Lightning. Debiut, Yaroslavl (1990)
42. Grigorjev, A.I.: Ball Lightning. YarGU Publishers, Yaroslavl (2006)
43. Batygin, A., Mosin, I.: Visit of "fiery lady". Pravda (Moscow). 220 (25938), August, 8 (1989)
44. Egely, G.: Analysis of Hungarian ball lightning observations. In: Keul, A.G. (ed.) Progress in Ball Lightning Research. Proceedings of the VIZOTUM, Salzburg, Austria (1993)
45. Avramenko, R.F., Bychkov, V.L., Klimov, A.I., Sinkevich, O.A. (eds.): Ball Lightning in a Laboratory. Khimiya, Moscow (1994)
46. Novosti UFOLATS http://www.ufo.lv/index. php? id= 13323112072006125332
47. Grigorjev, I.S., Meilikhov, E.Z. (eds.): Physical Values. Reference Book. Enrgoatomizdat, Moscow (1991)
48. Stenhoff, M.: Ball Lightning. An Unsolved Problem in Atmospheric Physics. Kluwer, New York (1999)
49. Chernobrov, V.A.: Chronicle of UFO Visits. Drofa, Moscow (2003)
50. Vostrukhin, D.: At 4.10 sharp. Trud (Moscow), January, 30 (1985)
51. Ofuruton, H., Ohtsuki, Y.-H., Kondo, N., Kamogawa, M., Kato, M., Takahashi, T.: Nature of ball lightning in Japan. In: Proceedings of the 5th International Symposium on Ball Lightning (ISBL97), Tsugawa-Town, Niigata, Japan, pp. 17–19 (1997)
52. Keul, A.G.: The Southern Bavaria ball lightning car collision. In: Proceedings of the 5th International Symposium on Ball Lightning (ISBL97), Tsugawa-Town, Niigata, Japan, pp. 27–34 (1997)
53. Stakhanova, I.G.: Ball lightning pictures from the I.P. Stakhanov's archive and their interpretation. In: Proceedings of the 5th International Symposium on Ball Lightning (ISBL97), Tsugawa-Town, Niigata, Japan, pp. 35–41 (1997)
54. Amirov, A.Kh., Bychkov, V.L.: Observational and computer assisted analysis of data from SKB data base. In: Proceedings of the 5th International Symposium on Ball Lightning (ISBL97), Tsugawa-Town, Niigata, Japan, pp. 42–46 (1997)
55. Stakhanova, I.G.: Observed properties of the ball lightning depending on weather conditions. In: Proceedings of the 6th International Symposium on Ball Lightning (ISBL99), Antwerp, Belgium, pp. 3–9 (1999)
56. Ofuruton, H., Ohtsuki, Y.-H., Kondo, N., Kamogawa, M., Kato, M., Takahashi, T., Sato, S., Shintani, K.: Nature of ball lightning in Japan (Part 2). In: Proceedings of the 6th International Symposium on Ball Lightning (ISBL99), Antwerp, Belgium, pp. 10–12 (1999)
57. Keul, A.G.: Attempted ball lightning tracking with a Lightning Detection System. In: Proceedings of the 6th International Symposium on Ball Lightning (ISBL99), Antwerp, Belgium, pp. 13–18 (1999)
58. Amirov, A.Kh., Bychkov, A.V., Bychkov, V.L.: Ball lightning nature in respect to dependence lifetime diameter. In: Proceedings of the 6th International Symposium on Ball Lightning (ISBL99), Antwerp, Belgium, pp. 19–26 (1999)
59. Amirov, A.Kh., Bychkov, V.L.: On the ball lightning interaction with airplanes. In: Proceedings of the 6th International Symposium on Ball Lightning (ISBL99), Antwerp, Belgium, pp. 34–37 (1999)

60. Toselli, P., Fedele, R.: Project for a database of ball lightning observations in Italy. In: Proceedings of the 6th International Symposium on Ball Lightning (ISBL99), Antwerp, Belgium, pp. 27–33 (1999)
61. Timoshuk, A.S.: Observations of two consequently formed and decayed ball lightning. In: Smirnov, B.M. (ed.) Sharovaya Molniya, vol. 1, p. 9. Institute for High Temperature AS USSR, Moscow (1990)
62. Bychkov, V.L.: Observations of ball lightning. In: Materials of 13-th Russian Conference on Cold Nuclei Transmutation of Chemical Elements and Ball lightning, 2005. Dagomys, city of Sochi, pp. 237–245. NITs FTP "Ersion", Moscow (2006)
63. Bychkov, V.L., Bychkov, D.V., Sedov, Y.B.: Some new ball lightning observation data. In: Proceedings of the 8th International Symposium on Ball Lightning (ISBL04), Chung-li, Taiwan, pp. 6–10 (2004)
64. Arora, R.: Ball lightning without lightning strike. In: Proceedings of the 8th International Symposium on Ball Lightning (ISBL04), Chung-li, Taiwan, pp. 11–15 (2004)
65. Keul, A.G., Schrattenecker, R., Baumegger, S.: The Zwoenitz, Germany, ball lightning webcam record. In: Proceedings of the 8th International Symposium on Ball Lightning (ISBL04), Chung-li, Taiwan, pp. 44–50 (2004)
66. Kawano, S.: Is a spatial stem a ball lightning? In: Proceedings of the 8th International Symposium on Ball Lightning (ISBL04), Chung-li, Taiwan, pp. 79–82 (2004)
67. Bychkov, V.L.: On observation properties of ball lightning. In: Proceedings of the 9th International Symposium on Ball Lightning (ISBL06), Eindhoven, The Netherlands, pp. 18–25 (2006)
68. Keul, A.G., Hentschel, K.H., Stummer, O.: German ball lightning data banks results. In: Proceedings of the 9th International Symposium on Ball Lightning (ISBL06), Eindhoven, the Netherlands, pp. 96–105 (2006)
69. Nikitin, A.I., Velichko, A.M., Vnukov, A.V., Nikitina, T.F.: Estimation of ball lightning characteristics based on the analysis of its photo. In: Proceedings of the 9th International Symposium on Ball Lightning (ISBL06), Eindhoven, The Netherlands, pp. 148–156 (2006)
70. Papaelias, Ph.M.: Photographs of ball lightning support evidence of antimatter. In: Proceedings of the 9th International Symposium on Ball Lightning (ISBL06), Eindhoven, the Netherlands, pp. 167–171 (2006)
71. Tar, D.: Observation of lightning ball – a new phenomenological description of the phenomenon. In: Proceedings of the 9th International Symposium on Ball Lightning (ISBL06), Eindhoven, The Netherlands, pp. 222–225 (2006)
72. Bychkov, V.L., Nikitin, A.I.: Recent ball lightning investigations: short review. In: Proceedings of the 10th International Symposium on Ball Lightning (ISBL08) and 3rd International Symposium on Unconventional Plasmas (ISUP08), Kaliningrad, Russia, pp. 36–38 (2008)
73. Keul, A.G.: European ball lightning statistics. In: Proceedings of the 10th International Symposium on Ball Lightning (ISBL08) and 3rd International Symposium on Unconventional Plasmas (ISUP08), Kaliningrad, Russia, pp. 66–71 (2008)
74. VanDevender, J.P., VanDevender, A.P., Wilson, P., VanDoorn, P., McGinley, N.: Extreme ball lightning event of August 6, 1868 in County Donegal, Ireland. In: Proceedings of the 10th International Symposium on Ball Lightning (ISBL08) and 3rd International Symposium on Unconventional Plasmas (ISUP08), Kaliningrad, Russia, pp. 142–148 (2008)
75. Fitzgerald, M. Notes on the occurrence of globular lightning and of waterspouts in County Donegal, Ireland. Quarterly Journal of the Meteorological Society. First Quarter of 1878. Quarterly Proceeding at the March 20, 1878, Proceedings at the Meeting of the Society, pp. 160–161 (1878)
76. Shelkunov, G.P., Nikitin, A.I., Bychkov, V.L., Nikitina, T.F., Velichko, A.M., Vasiliev, A. L.: Examination of a window pane exposed to ball lightning. In: Proceedings of the 10th International Symposium on Ball Lightning (ISBL08) and 3rd International Symposium on Unconventional Plasmas (ISUP08), Kaliningrad, Russia, pp. 127–134 (2008)

77. Mashkovich, M.D.: Electric Properties of Inorganic Dielectrics in MW Range. Soviet Radio, Moscow (1969)
78. Nikolayev, G.V.: Mysteries of Electromagnetism. "Znamya mira", Tomsk (1999)
79. Ford, R.A.: Homemade Lightning. McGraw-Hill, New York (2002)
80. Planté, G.: Electrical Phenomena in Atmosphere. Paris (1891)
81. Silberg, P.A.: A review of ball lightning. In: Coroniti S.C. (ed.) Problems of Atmospheric and Space Electricity, pp. 436–466. Proceedings of the 3rd International Conference on Atmosphere and Space Electricity, 1963, Montreux, Switzerland. Elsevier, Amsterdam (1965)
82. Dijkhuis, G.C.: Threshold current for fireball generation. J. Appl. Phys. **53**(5), 3516–3519 (1982)
83. Kapitsa, P.L.: On nature of ball lightning. Doklady AN SSSR **101**, 245–248 (1955)
84. Kapitsa, P.L.: Free plasma filament in high frequency field at high pressure. Zhur. Experim. i Teoretich. Fiziki. **57,** N. 6(12), 1801–1866 (1969)
85. Ohtsuki, Y.-H., Ofuruton, H.: Plasma fireballs formed by microwave interference in air. Nature **350**, 139–141 (1991)
86. Zhiltsov, V.A., Leitner, J.F., Manykin, E.A., Petrenko, E.A., Skovoroda, A.A., Handel, P.: Spatially-localized discharge in the atmosphere. Zhur. Experim. i Teoretich. Fiziki. **108**. N. 6 (12), 1966–1985 (1995)
87. Ofuruton, H., Kondo, N., Kamogawa, M., Aoki, M., Ohtsuki, Y.-H.: Experimental condition of artificial ball lightning by using microwave and discharge. In: Proceedings of the 5th International Symposium on Ball Lightning (ISBL97), Tsugawa-Town, Japan, pp. 215–217 (1997)
88. Ofuruton, H., Kondo, N. Kamogawa, M., Aoki, M., Ohtsuki, Y.-H.: Experimental condition for ball lightning creation by using air gap discharge embedded in microwave field. J. Geoph. Res. **106.** N. D12. 12367–12369 (2001)
89. Anderson, R.W.: Absence of diffusion in creation random lattices. Phys. Rev. **109**(5). 1492–1505 (1958)
90. Tanaka, K., Tanaka, M.: Is ball lightning "Anderson localization"? In: Proceedings of the 5th International Symposium on Ball Lightning (ISBL97), Tsugawa-Town, Japan, pp. 137–141 (1997)
91. Kamogawa, M., Tanaka, H., Ofuruton, H., Ohtsuki, Y.-H.: Possibility of microwave localization to produce an experimental plasma fireball. Proc. Jap. Acad. **75**(10) Ser. B, pp. 275–280 (1999)
92. Ofuruton, H., Kamogawa, M., Tanaka, H., Ohtsuki, Y.-H.: Experiment of the localization of the electromagnetic wave in the waveguide. In: Proceedings of the 6th International Symposium on Ball Lightning (ISBL99), Antwerp, Belgium, pp. 207–211 (1999)
93. Kamogawa, M., Ofuruton, H., Liu, J.Y., Tanaka, H., Ohtsuki, Y.-H.: Study of microwave localization mode for appearance of plasma fireballs. In: Proceedings of the 8th International Symposium on Ball Lightning (ISBL04), Chung-li, Taiwan, pp. 118–119 (2004)
94. Ofuruton, H., Kamogawa, M., Tanaka, H., Ohtsuki, Y.-H.: Experiments on microwave localization for ball lightning research. In: Proceedings of the 8th International Symposium on Ball Lightning (ISBL04), Chung-li, Taiwan, pp. 120–122 (2004)
95. Ofuruton, H., Kamogawa, M., Ohtsuki, Y.-H.: Experiments on ball lightning by using microwave localization. In: Proceedings of the 9th International Symposium on Ball Lightning (ISBL06), Eindhoven, The Netherlands, pp. 157–158 (2006)
96. Ofuruton, H., Kamogawa, M., Ohtsuki, Y.-H.: Experiments for artificial ball lightning by using microwave localization. In: Proceedings of the 10th International Symposium on Ball Lightning (ISBL08) and 3rd International Symposium on Unconventional Plasmas (ISUP08), Kaliningrad, Russia, pp. 99–100 (2008)
97. Chukanov, K.B.: Ball Lightning – source of free energy. In: Proceedings of the 10th International Symposium on Ball Lightning (ISBL08) and 3rd International Symposium on Unconventional Plasmas (ISUP08), Kaliningrad, Russia, pp. 22–26 (2008)

98. Golka, R.K., Jr.: Laboratory-produced ball lightning. J. Geophys. Res. **99**, N. D 5, 10679–10681 (1994)
99. Dikhtyar, V., Jerby, E.: Fireball ejection from a molten hot spot to air by localized microwaves. Phys. Rev. Lett. **96**, 045002-1–045002-4 (2006)
100. Corum, K.L., Corum, J.F.: Tesla's production of electric fireballs. Tesla Coil Builder's Association News **8**(3), 13–18 (1989)
101. Koloc, P.M.: Formed PLASMAK artificial ball lightning results. In: Proceedings of the 6th International Symposium on Ball Lightning (ISBL99), Antwerp, Belgium, pp. 219–226 (1999)
102. Koloc, P.M.: Comparison between PLASMAK BL model and formed PMKs. In: Proceedings of the 6th International Symposium on Ball Lightning (ISBL99), Antwerp, Belgium, pp. 227–232 (1999)
103. Kunin, V.N.: Research experiments on method of ball lightning laboratory model obtaining. Khim. Fiz. **25**(3), 94–95 (2006)
104. Kunin, V.N., Pleshivtsev, V.S., Furov, L.V.: A method of obtaining of independent long-lived plasma formations in free atmosphere. Khim. Fiz. **25**(3), 96–100 (2006)
105. Kunin, V.N., Furov, L.V.: Investigations of plasma toroidal vortices appearing at electric explosion of diaphragms in air. Izvestiya VUZov. Fizika **33**(6), 119 (1990)
106. Kunin, V.N., Pleshivtsev, V.S., Furov, L.V.: Experimental laboratory research of the ball lightning nature. In: Proceedings of the 5th International Symposium on Ball Lightning (ISBL97), Tsugawa-Town, Japan, pp. 225–229 (1997)
107. Kunin, V.N., Pleshivtsev, V.S.: On the possible mechanism of transformation of toroidal plasma vortex into the laboratory analog of ball lightning. In: Proceedings of the 6th International Symposium on Ball Lightning (ISBL99), Antwerp, Belgium, pp. 233–235 (1999)
108. Kunin, V.N., Kondakov, V.P., Pleshivtsev, V.S., Furov, L.V.: Experimental results of anomalous decay of independent long-lived plasma formation in free atmosphere. Khim. Fiz. **25**(3), 101–103 (2006)
109. Kunin, V.N., Furov, L.V.: On refractional mechanism of energy accumulation in a volume of long-lived plasma formation. In: Materials of 13-th Russian Conference on Cold Nuclei Transmutation of Chemical Elements and Ball Lightning, 2005. Dagomys, city of Sochi, pp. 284–289. NITs FTP "Ersion", Moscow (2006)
110. Alexeff, I., Parameswaran, S.M., Thiayagarajan, M., Grace, M.: An experimental study of ball lightning. IEEE Trans. Plasma Sci. **32**(3), 1378–1382 (2004)
111. Alexeff, I., Parameswaran, S.M., Thiayagarajan, M., Grace, M.: An observation of synthetic ball lightning. IEEE Trans. Plasma Sci. **33**(2), 498–499 (2005)
112. Avramenko, R.F., Bakhtin, B.I., Nikolayeva, V.I., Poskachheva, L.P., Shirokov, N.N.: Investigation of plasma formations initiated by erosive discharge. Zhur. Tekhnich. Fiziki. **60**(12), 57–64 (1990)
113. Ershov, A.P., Rozanov, V.A., Sysoev, N.N., Timofeev, I.B., Chuvashev, S.N., Shibkov, V. M.: Subsonic plasma jets flowing into atmosphere created by capillary. Physical faculty of M.V. Lomonosov MSU. Physical Hydrodynamics. N. 4. Preprint N. 8 (1994)
114. Bychkov, V.L., Gridin, A.Y., Klimov, A.I.: On nature of artificial ball lightning. Teplofiz. Vysok. Temper. **32**(2), 190–194 (1994)
115. Emelin, S.E., Semenov, V.S., Bychkov, V.L., Belisheva, N.K., Kovshik, A.P.: Some objects formed in the interaction of electrical discharges with metals and polymers. Tech. Phys. **42** (3), 269–277 (1997)
116. Bychkov, A.V., Bychkov, V.L., Timofeev, I.B.: Experimental modeling of long-lived luminescent formations in air on a basis of polymeric organic materials. In: Materials of 10-th Russian Conference on Cold Nuclei Transmutation of Chemical Elements and Ball Lightning, 2002. Dagomys, city of Sochi, pp. 125–148. NITs FTP "Ersion", Moscow (2003)
117. Bychkov, A.V., Bychkov, V.L., Timofeev, I.B.: Experimental modeling of long-lived shining formations in air on a basis of polymeric organic materials. Zhur. Tekhnich. Fiziki. **74**(1), 128–133 (2004)

118. Klimov, A.I.: Plasmoid generation in airflow and its physical properties. In: Materials of 10-th Russian Conference on Cold Nuclei Transmutation of Chemical Elements and Ball Lightning, 2002. Dagomys, City of Sochi, pp. 229–235. NITs FTP "Ersion", Moscow (2003)
119. Klimov, A., Moralev, I., Zhirnov, K., Kutalaliev, V.: Investigation of physical properties of plasmoids in air and airflow. In: Materials of 13-th Russian Conference on Cold Nuclei Transmutation of Chemical Elements and Ball Lightning, 2005. Dagomys, City of Sochi, pp. 298–306. NITs FTP "Ersion", Moscow (2006)
120. Klimov, A.I.: Investigation of physical properties of plasmoids in air and air flow. Khim. Fiz. **25**(3), 104–109 (2006)
121. Klimov, A., Moralev, I., Zhirnov, K., Kutalaliev, V.: Investigation of physical properties of plasmoids in air and airflow. In: Proceedings of the 9th International Symposium on Ball Lightning (ISBL06), Eindhoven, The Netherlands, pp. 112–121 (2006)
122. Abrahamson, J., Dinnis, J.: Ball lightning caused by oxidation of nanoparticle networks from normal lightning strikes on soil. Nature **403**, 519–521 (2000)
123. Abrahamson, J.: Ball lightning from atmospheric discharges via metal nanosphere oxidation: from soils, wood or metals. Phil. Trans. Roy. Soc. Lond. **360**(1790), 61–88 (2002)
124. Piva, G.S., Pavão, A.C., de Vasconcelos, E.A., Mendes Jr., O., Da Silva Jr., E.F.: Production of ball-lightning-like luminous balls by electrical discharge in silicon. Phys. Rev. Lett. **98**, 048501-1–048501-4 (2007)
125. Shabanov, G.D.: Optical properties of long-lived luminescent formations. Pis'ma v Zhur. Tekhnich. Fiziki. **28**(4), 81–86 (2002)
126. Shabanov, G.D., Zherebtsov, O.M.: Experimental modeling of ball lightning analog. In: Materials of 10-th Russian Conference on Cold Nuclei Transmutation of Chemical Elements and Ball Lightning, 2002. Dagomys, City of Sochi. pp. 285–301. NITs FTP "Ersion", Moscow: (2003)
127. Emelin, S.E., Pirozerskyi, A.L., Egorov, A.I., Stepanov, S.I., Shabanov, G.D., Bychkov, V. L.: Modeling of ball lightning with a help of electric discharge through a surface of weak water solution. In: Materials of 9-th Russian Conference on Cold Nuclei Transmutation of Chemical Elements and Ball Lightning, 2001. Dagomys, City of Sochi, pp. 240–248. NITs FTP "Ersion", Moscow (2002)
128. Shabanov, G.D., Zherebtsov, O.M.: Electric properties of independent luminous formations. In: Materials of 11-th Russian Conference on Cold Nuclei Transmutation of Chemical Elements and Ball Lightning, 2003. Dagomys, City of Sochi, pp. 279–290. NITs FTP "Ersion", Moscow (2004)
129. Shabanov, G.D., Zherebtsov, O.M.: Electric discharge to air half-space. Optich. Zhurl. **71**(1), 6–8 (2004)
130. Shabanov, G.D., Sokolovskyi, B.Y.: Macroscopic separation of charges in the pulsed electric field. Fizika Plasmy **31**(6), 560–566 (2005)
131. Shabanov, G.D., Zherebtsov, O.M., Sokolovskyi, B.Yu.: Experimental modeling with a help of pulsed electric discharge to air half-space of linear lightning leader and ball lightning. In: Materials of 13-th Russian Conference on Cold Nuclei Transmutation of Chemical Elements and Ball Lightning, 2005. Dagomys, City of Sochi. pp. 246–265. NITs FTP "Ersion", Moscow (2006)
132. Shabanov, G.D., Krivshich, A.G., Sokolovsky, B.Yu., Zherebtsov, O.M.: Ball lightning nature. In: Materials of 14-th Russian Conference on Cold Nuclei Transmutation of Chemical Elements and Ball Lightning, 2006. Dagomys, City of Sochi, pp. 243–254. NITs FTP "Ersion", Moscow (2008)
133. Shabanov, G.D., Krivshich, A.G, Sokolovsky, B.Yu.: In: Materials of 14-th Russian Conference on Cold Nuclei Transmutation of Chemical Elements and Ball Lightning, 2006. Dagomys, City of Sochi, pp. 255–266. NITs FTP "Ersion", Moscow (2008)
134. Shabanov, G.D., Krivshich, A.G., Sokolovsky, B.Yu., Zherebtsov, O.M.: Performance of the laboratory ball lightning. In: Proceedings of the 9th International Symposium on Ball Lightning (ISBL06), Eindhoven, The Netherlands, pp. 202–209 (2006)

135. Shabanov, G.D., Zherebtsov, O.M., Sokolovskyi, B.Y.: Independent long-lived luminescent formations in open air. Experimental check of ball lightning formation by the linear lightning leader hypothesis. Khim. Fiz. **25**(4), 74–88 (2006)
136. Nikitin, A.I.: Electrodynamic model of ball lightning. Khim. Fiz. **25**(3), 38–62 (2006)
137. Chalmers, J.A.: Atmospheric Electricity. Clarendon, Oxford (1949)
138. Emelin, S.E., Pirozersky, A.L., Vassiliev, N.N.: The dust-gas fireball as a special form of the electric erosive discharge afterglow. In: Proceedings of the 9th International Symposium on Ball Lightning (ISBL06), Eindhoven, The Netherlands, pp. 51–61 (2006)
139. Nikitin, A.I.: Electric capacitor as element of energy core of ball lightning. Elektrichestvo. (11), 14–23 (1998)
140. Nikitin, A.I.: Electrical capacitor as the element of the power core of ball lightning. Electr. Technol. Russ. (4), 70–85 (1998)
141. Emelin, S.E., Astafiev, A.M., Pirozerski, A.L.: Investigation of space-time structure of the discharge with an electrolyte anode and face-type, air half-space directed cathode (Gatchina's discharge). In: Proceedings of the 10th International Symposium on Ball Lightning (ISBL08) and 3rd International Symposium on Unconventional Plasmas (ISUP08), Kaliningrad, Russia, pp. 42–45 (2008)
142. Emelin, S.E., Pirozerski, A.L.: Some questions of power-consuming plasma-chemical ball lightning. Khim. Fiz. **25**(3), 83–89 (2006)
143. Pirozerski, A.L., Emelin, S.E.: Long-living plasmoids generation by high-voltage discharge through thin conducting layers. In: Proceedings of the 9th International Symposium on Ball Lightning (ISBL06). Eindhoven, The Netherlands, pp. 180–190 (2006)
144. Juettner, B., Noak, S., Versteegh, A., Fussmann, G.: Long-living plasmoids from a water discharge at atmospheric pressure. In: Proceedings of the 28th International Conference on Phenomena in Ionized Gases, Prague, Czech Republic, pp. 2229–2234 (2007)
145. Versteegh, A., Behringer, K., Fantz, U., Fussmann, G., Jüttner, B., Noak, S.: Long-living plasmoids from an atmospheric water discharge. Plasma Sour. Sci. Technol. **17**(2), 02414–02421 (2008)
146. Smirnov, B.M.: Problem of Ball Lightning. Nauka, Moscow (1988)
147. Kuz'min, R.N., Miskinova, N.A., Shvilkin, B.N.: Laboratory model of ball lightning. In: Materials of 10-th Russian Conference on Cold Nuclei Transmutation of Chemical Elements and Ball Lightning, 2002. Dagomys, City of Sochi, pp. 236–242. NITs FTP "Ersion", Moscow (2003)
148. Kuz'min, R.N., Miskinova, N.A., Shvilkin, B.N.: Laboratory model of ball lightning. Khim. Fiz. **25**(3), 90–93 (2006)
149. Vlasov, A.N.: A ball lightning is a natural nuclear reactor? In: Proceedings of the 5th International Symposium on Ball Lightning (ISBL97), Tsugawa-Town, Japan, pp. 75–79 (1997)
150. Vlasov, A.N.: Bose-Einsten condensed electron catalyzed fusion as a possible mechanism of the ball lightning energy supply. In: Proceedings of the 6th International Symposium on Ball Lightning (ISBL99), Antwerp, Belgium, pp. 133–138 (1999)
151. Vlasov, A.N.: Ball lightning as the current layer induced in a vortex. In: Proceedings of the 9th International Symposium on Ball Lightning (ISBL06), Eindhoven, The Netherlands, pp. 243–249 (2006)
152. Vlasov, A.N.: Magnetohydrodynamical model of plasma object capable to be generated at impact of ordinary lightning. In: Proceedings of the 10th International Symposium on Ball Lightning (ISBL08) and 3rd International Symposium on Unconventional Plasmas (ISUP08), Kaliningrad, Russia, pp. 149–150 (2008)
153. Vlasov, A.N. Experimental modeling of ball lightning on a basis of electric explosion of a wirespiral rolled in torus. In: Materials of 13-th Russian Conference on Cold Nuclei Transmutation of Chemical Elements and Ball Lightning, 2005. Dagomys, City of Sochi, pp. 290–297. NITs FTP "Ersion", Moscow (2006)
154. Vlasov, A.N., Kolesnikov, S.A.: Calculations of an installation parameters for obtaining of plasmoids at electric explosions of wire spirals rolled in torus. In: Materials of 14-th Russian

Conference on Cold Nuclei Transmutation of Chemical Elements and Ball Lightning, 2006. Dagomys, City of Sochi, pp. 162–179. NITs FTP "Ersion", Moscow (2008)
155. Vlassov, A., Vlassov, A.: Getting a fireball by means of electric explosion of wire spiral twisted into a ring. In: Proceedings of the 9th International Symposium on Ball Lightning (ISBL06). Eindhoven, The Netherlands, pp. 234–242 (2006)
156. Golubnichiy, P.I., Gromenko, V.M., Krutov, V.M.: Formation of long-lived luminescent objects at decay of dense low temperature water plasma. Zhur. Tekh. Fiziki. **60**(1), 283–186 (1990)
157. Golubnichiy, P.I., Gromenko, V.M., Krutov, V.M., Nikitin, E.V.: Plasma of electric discharge in water as a raw material for laboratory analogue of a ball lightning. In: Proceedings of the 9th International Symposium on Ball Lightning (ISBL06), Eindhoven, The Netherlands, pp. 62–66 (2006)
158. Golubnichiy, P.I., Krutov, V.M., Nikitin, E.V.: Long-living luminous objects, formed from the products of disintegration of water plasma. In: Proceedings of the 9th International Symposium on Ball Lightning (ISBL06), Eindhoven, The Netherlands, pp. 67–73 (2006)
159. Matsumoto, T.: Ball lightning during underwater spark discharges and the Matsumae earthquakes. In: Proceedings of the 5th International Symposium on Ball Lightning (ISBL97), Tsugawa-Town, Japan, pp. 193–201 (1997)
160. Matsumoto, T.: Micro ball lightning during underwater spark discharges. In: Proceedings of the 6th International Symposium on Ball Lightning (ISBL99), Antwerp, Belgium, pp. 249–254 (1999)
161. Matsumoto, T.: Transport of micro ball lightning. In: Proceedings of the 6th International Symposium on Ball Lightning (ISBL99), Antwerp, Belgium, pp. 255–262 (1999)
162. Urutskoev, L.I., Liksonov, V.I., Tsinoev, V.G.: Experimental discovery of "strange" radiation and transformation of chemical elements. Prikl. Fiz. **4**, 83–100 (2000)
163. Klimov, A., Baranov, D., Kutlaliev, V., Moralev, I., Zhirnov, K., Tolkunov, B.: Study of anomalous "traces" of moving bright particles created by erosive pulsed plasma generator. In: Materials of 14-th Russian Conference on Cold Nuclei Transmutation of Chemical Elements and Ball Lightning, 2006. Dagomys, city of Sochi, pp. 199–208. NITs FTP "Ersion", Moscow (2008)
164. Turner, D.J.: The investigation of ball lightning with glass window panes. J. Meteorol. **22** (216), 52–64 (1997)
165. Shelkunov, G.: Ball lightning: observations and analysis of traces. Nauka i Zhizn. (10), 52–53 (2001)
166. Kolosovsky, O.A.: Investigations of ball lightning trace on a window pane. Zhur. Tekh. Fiz. **51**(4), 856–858 (1981)
167. Nikitin, A.I., Bychkov, V.L., Nikitina, T.F., Velichko, A.M.: Modeling of ball lightning interaction with window panes. In: Materials of 11-th Russian Conference on Cold Nuclei Transmutation of Chemical Elements and Ball Lightning, 2003. Dagomys, City of Sochi, pp. 254–268. NITs FTP "Ersion", Moscow (2004)
168. Nikitin, A.I., Bychkov, V.L., Nikitina, T.F., Velichko, A.M.: Modeling of ball lightning interaction with window panes. In: Proceedings of the 8th International Symposium on Ball Lightning (ISBL04), Chung-li,Taiwan, pp. 23–31 (2004)
169. Nikitin, A.I., Bychkov, V.L., Nikitina, T.F., Velichko, A.M.: Modeling of ball lightning interaction with window panes. Khim. Fiz. **25**(4), 98–105 (2006)
170. Nikitin, A.I., Leipunsky, I.O., Nikitina, T.F.: A search for the reasons explaining hovering of ball lightning over conductor surface. In: Materials of 13-th Russian Conference on Cold Nuclei Transmutation of Chemical Elements and Ball Lightning, 2005. Dagomys, City of Sochi, pp. 307–319. NITs FTP "Ersion", Moscow (2006)
171. Nikitin, A.I., Leipunsky, I.O., Nikitina, T.F.: A search for the reasons explaining hovering of ball lightning over conductor surface. In: Proceedings of the 9th International Symposium on Ball Lightning (ISBL06), Eindhoven, The Netherlands, pp. 139–146 (2006)

172. Aleksandrov, V.Y., Podmoshenskyi, I.V., Sall, S.A.: Experiments on electric field impact on gas discharge model of ball lightning. Zhur. Tekh. Fiz. **60**(1), 73–76 (1990)
173. Nikitin, A.I., Nikitina, T.F., Velichko, A.M.: Corona discharge as a means to levitation of ball lightning. In: Proceedings of the 10th International Symposium on Ball Lightning (ISBL08) and 3rd International Symposium on Unconventional Plasmas (ISUP08), Kaliningrad, Russia, pp. 89–98 (2008)
174. Bychkov, V.L., Bychkov, A.V., Bychkov, D.V.: Some new observations of ball lightning. In: Materials of 10-th Russian Conference on Cold Nuclei Transmutation of Chemical Elements and Ball Lightning, 2002. Dagomys, City of Sochi, pp. 109–124. NITs FTP "Ersion", Moscow (2003)
175. Bychkov, V.L., Ershov, A.P., Chernikov, V.A.: Corona discharge modeling of some ball lightning features. In: Proceedings of the 10th International Symposium on Ball Lightning (ISBL08) and 3rd International Symposium on Unconventional Plasmas (ISUP08), Kaliningrad, Russia, pp. 7–11 (2008)
176. Kuz'min, R.N.: On physical and chemical nature of ball lightning. In: Materials of 9-th Russian Conference on Cold Nuclei Transmutation of Chemical Elements and Ball Lightning, 2001. Dagomys, City of Sochi, pp. 235–239. NITs FTP "Ersion", Moscow (2002)
177. Vvedenskyi, B.L. (ed.): The Big Soviet Encyclopedia, vol. 43, pp. 280–281. BSE Publishers, Moscow (1956)
178. Bychkov, V.L., Nikitin, A.I.: Observations of ball lightning. In: Materials of 12-th Russian Conference on Cold Nuclei Transmutation of Chemical Elements and Ball Lightning, 2004. Dagomys, City of Sochi, pp. 165–169. NITs FTP "Ersion", Moscow (2005)
179. Uman, M.A.: Decaying lightning channels, bead lightning and ball lightning. In: Coroniti, S. C., Hughes, J. (eds.) Planetary Electrodynamics, vol. 2, p. 199. Gordon and Breach, New York (1968)
180. Bostick, W.H.: Experimental study of ionized matter projected across magnetic field. Phys. Rev. **104**(2), 242–299 (1956)
181. Bostick, W.H.: Experimental study of plasmoids. Phys. Rev. **106**(3), 404–412 (1957)
182. Shafranov, V.D.: On equilibrium magneto-hydrodynamic configurations. Zhur. Exper. i Teor. Fiz. **33**(3(9)), 710–722 (1957)
183. Shafranov, V.D.: On magnetohydrodynamical equilibrium configurations. Sov. Phys. JETP. **6**, 545 (1957)
184. Finkelstein, D., Rubinstein, J.: Ball lightning. Phys. Rev. **135**(2A), A390–A396 (1964)
185. Powell, J.R., Finkelstein, D.: Ball lightning. Am. Scientist. **58**, 262 (1970)
186. Endean, V.G.: Electromagnetic field energy models – some recent developments. In: Stenhoff, M. (ed.) Proceedings of the 4th TORRO Conference: Ball lightning, Tornado and Storm Research Organization (TORRO), pp. 75. Oxford Brooks University, Oxford (1992)
187. Wooding, E.R.: Ball lightning. Nature **199**, 272 (1963)
188. Bergström, A.: Electromagnetic theory of strong interaction. Phys. Rev. **D3**, 4394 (1973)
189. Neugebauer, Th.: Zu dem Problem des Kugelblitzes. Zeit. für Phys, **106**(7), 8.474–8.484 (1937)
190. Neugebauer, Th: Zu der Quanten-mechanischen Theorie des Kugelblitz. Acta Physica **42**(1), 29 (1977)
191. Dijkhuis, G.C.: A model for ball lightning. Nature **248**, 150–151 (1980)
192. Dijkhuis, G.C.: Scaling law for fusion power from ball lightning. In: Janiszewski, J., Moron, W., Sega, W. (eds.) Proceedings of the of International Wroclaw Symposium on Electromagnetic Compatibility, Wroclaw, Poland, pp. 21–25 (1988)
193. Hill, E.: Globular lightning. Nature **56**, 293 (1897)
194. Coulvier-Gravier. Recherches sur les meteors et sur les lois qui les regissent, p. 185. Paris (1859)
195. Meissner, A.: Über Kugelblitze. Meteorol. Zeit. **47**, 17–20 (1930)
196. Dawson, G.A., Jones, R.C.: Ball lightning as a radiation bubble. Pure Appl. Geophys. **75**, 247–262 (1969)

197. Besnou, M.: De l'état de l'iode dans l'atmosphere, et de la possibilité de la formation de l'iodide d'azote dans les orages. Mem. Soc. Sci. Nat. Cherbourg. **1**, 103 (1852)
198. Thornton, W.M.: On thunderbolts. Fortsch. Phys. **67**(3), 342 (1911)
199. De la Rive, A.: Traite de l'electricité theoretique et appliqué. Paris. **3**, 197 (1858)
200. Hildebrandsson, H.H.: Kugelblitz. Fortsch. Phys. **39**, H. 3518 (1883)
201. Schonland, B.F.J.: The Flight of Thunderbolts. Oxford University Press, Oxford (1950)
202. Benedicks, C.: Theory of lightning balls and its application to the atmospheric phenomenon called 'flying saucers'. Ark. Geof. **2**(1), 1 (1951)
203. Chirvinsky, P.N.: Materials on ball lightning observations, collected by V.K. Cherkas. Klimat i Pogoda. N. 5, 49 (1936)
204. Barry, J.D.: Ball lightning. J. Atmos. Terr. Phys. **29**, 1095 (1967)
205. Barry, J.D.: Fireball, ball lightning and St. Elmo's fire. Weather **23**, 180 (1968)
206. De Tastes, M.: L'orage du 1-er fevrier 1884, a Torus. Météorologie **32**, 105 (1884)
207. Frenkel, Y.I.: On nature of a ball lightning. Zhur. Exper. i Teor. Fiz. **10**, 1424–1426 (1940)
208. Aleksandrov, V.Y., Golubev, E.M., Podmoshensky, I.V.: Aerosol nature of ball lightning. Zhur. Exper. i Teor. Fiz. **52**(10), 1987–1992 (1982)
209. Mukharev, L.A.: The nature of ball lightning. Sov. J. Commun. Technol. Electron. **30**(9), 77 (1986)
210. Dauviller, A.: Foudre globulaire et reactions thernonucleaires. Comp. Rendu Hebd. Séances Acad. Sci. **245**, 2155 (1957)
211. De Tessan, M.: Sur la foudre en boule. Comp, Rendu Hebd. Séances Acad. Sci. **49**, 189–191 (1859)
212. Püringer, A.: Comments. In: Coroniti, S.C. (ed.) Problems of Atmospheric and Space Electricity, pp. 460. Elsevier, Amsterdam (1965)
213. Hill, E.L.: Ball lightning. Am. Scientist. **58**, 479 (1970)
214. Crew, E.W.: Ball lightning. New Scientist **56**, 764 (1972)
215. Stakhanov, I.P.: On the nature of ball lightning. JETP Lett. **18**, 114 (1974)
216. Watson, W.K.R.: A theory of ball lightning formation. Nature **185**, 449–450 (1960)
217. Tonks, L.: Electromagnetic standing waves and ball lightning. Nature **187**, 1013–1014 (1960)
218. Smirnov, B.M.: Physics of ball lightning. Uspekhi Fiz. Nauk. **160**(4), 1–45 (1990)
219. Tamm, I.E.: Theory of magnetic thermonuclear reactor. In: Physics of plasma and problem of controlled thermonuclear reactions, vol. 1, pp. 3–19; 31–41. Izdatelstvo AN SSSR, Moscow (1958)
220. Sakharov, A.D.: Theory of magnetic thermonuclear reactor. In; Physics of plasma and problem of controlled thermonuclear reactions, vol. 1**,** pp. 20–30. Izdatelstvo AN SSSR, Moscow (1958)
221. Rosenbluth, M.N., Bussac, N.N.: MHD stability of Spheromak. Nucl. Fusion **19**(4), 489 (1979)
222. Koloc, P.M.: "PLASMAK" star power for energy intensive space applications. Fusion Technol. **15**(3), 1136–1141 (1989)
223. Nikitin, A.I.: The requirements for elaboration of theory of ball lightning. In: Proceedings of the 8th International Symposium on Ball Lightning (ISBL04), Chung-li, Taiwan, pp. 16–22 (2004)
224. Nikitin, A.I.: Analysis of the models of highly energetic ball lightning. In: Proceedings of the 8th International Symposium on Ball Lightning (ISBL04), Chung-li, Taiwan, pp. 57–63 (2004)
225. Nikitin, A.I.: The principles of developing the ball lightning theory. J. Rus. Laser Res. **25**(2), 169–191 (2004)
226. Nikitin, A.I.: Will ball lightning problem be resolved in 21-st century? Khim. Fiz. **25**(3), 18–37 (2006)
227. Lowke, J.J.: A theory of ball lightning as an electric discharge. J. Phys. D. (Appl. Phys.) **29** (5), 1237–1244 (1996)

228. Handel, P.H.: Maser theory of ball lightning. Bull. Am. Phys. Soc. Ser. II. **20**(1), 26BF8 (1975)
229. Handel, P.H., Leitner, J.F.: Theory of the stationary nonlinear ball lightning system of fireball and atmospheric maser. In: Proceedings of the 5th International Symposium on Ball Lightning (ISBL97), Tsugawa-Town, Japan, pp. 114–119 (1997)
230. Handel, P.H., Leitner, J.F.: Development of the maser-caviton ball lightning theory. J. Geophys. Res. **99**, 10689–10691 (1994)
231. Singer, J.R.: Masers. Wiley, New York (1959)
232. Vuylsteke, A.A.: Elements of maser theory. D. Van Nostrand, New York (1960)
233. Oraevsky, A.N.: Radiation echo. Uspekhi Fiz. Nauk. **91**(2), 181–191 (1967)
234. Akulin, V.M., Karlov, N.V.: Intense Resonant Interactions in Quantum Electronics. Nauka, Moscow (1987)
235. Gordiets, B.F., Osipov, A.I., Shelepin, L.A.: Kinetic processes in gases and molecular lasers. Nauka, Moscow (1980)
236. Meek, J.M., Craggs, J.D.: Electrical Breakdown of Gases. Clarendon, Oxford (1953)
237. Wieder I.: On the absence of water maser at atmospheric pressure. In: Proceedings of the 9th Intern. Symp. on Ball Lightning (ISBL06), Eindhoven, The Netherlands. pp. 250–255 (2006)
238. Cheung, A.C., Rank, D.M., Townes, C.H., Thornton, D.D., Welch, W.J.: Detection of water in interstellar regions by its microwave radiation. Nature **221**, 626–628 (1969)
239. Letokhov, V.S.: Astrophysical masers. Kvantovaya elektronika **32**(12), 1065–1079 (2002)
240. Handel, P.H. Carlson, G.A., Grace, M., Leitner, J.F.: Electric ponderomotive forces cause explosive ball lightning damages. In: Proceedings of the 8th International Symposium on Ball Lightning (ISBL04), Chung-li, Taiwan, pp. 95–100 (2004)
241. Handel, P.H., Carlson, G.A., Grace, M., Leitner, J.F.: Motion of a BL discharge fed by an atmospheric maser. In: Proceedings of the 8th International Symposium on Ball Lightning (ISBL04), Chung-li, Taiwan, pp. 89–94 (2004)
242. Handel, P.H., Carlson, G.A.: Rise time of maser-caviton ball lightning energy spikes. In: Proceedings of the 9th International Symposium on Ball Lightning (ISBL06), Eindhoven, The Netherlands, pp. 74–80 (2006)
243. Smirnov, B.M.: On analysis of ball lightning nature. Uspekhi Fiz. Nauk. **116**(4), 731–739 (1975)
244. Smirnov, B.M.: Origination of ball lightning. Doklady AN SSSR **226**(4), 806–808 (1976)
245. Kadomtsev, B.B.: Ball lightning as a phenomenon of self-organization. J. Moscow Phys. Soc. **1**(4), 335–340 (1991)
246. Stepanov, S.I., Sall, S.A., Arutjunan, A.V.: Electric machine in ball lightning. In: Proceedings of the 5th International Symposium on Ball Lightning (ISBL97), Tsugawa-Town, Japan, pp. 183–187 (1997)
247. Stepanov, S.I.: Further development of electrochemical model of ball lightning. In: Proceedings of the 6th International Symposium on Ball Lightning (ISBL99), Antwerp, Belgium, pp. 96–101 (1999)
248. Stakhanov, I.P.: To a question of ball lightning nature. Zhur. Tekh. Fiz. **57**(8), 1575–1582 (1987)
249. Turner, D.J.: Ball lightning and other meteorological phenomena. Phys. Rep. **293**(1), 1–60 (1998)
250. Igolkin, S.I., Savelyev, S.K.: Condensation model of the ball lightning. In: Proceedings of the 5th International Symposium on Ball Lightning (ISBL97), Tsugawa-Town, Japan, pp. 80–86 (1997)
251. Bychkov, V.L.: Polymer ball lightning model. Physica Scripta. **50**, 591–599 (1994)
252. Manykin, E.A., Ozhovan, M.I., Poluektov, P.P.: On collective electronic state in a system of strongly-excited atoms. Doklady AN SSSR **260**, 1096–1098 (1981)
253. Manykin, E.A., Ozhovan, M.I., Poluektov, P.P.: Theory of the condensed state in the system of excited atoms. ZhETF **84**(2), 442–453 (1983)
254. Manykin, E.A., Ozhovan, M.I., Poluektov, P.P.: To the question of ball lightning nature. ZhTF **52**(7), 1474–1476 (1982)

255. Manykin, E.A., Ojovan, M.I., Poluektov, P.P.: Rydberg matter and ball lightning. In: Proceedings of the 6th International Symposium on Ball Lightning (ISBL99), Antwerp, Belgium, pp. 114–119 (1999)
256. Biberman, L.M., Norman, G.E.: On existence possibility of overcooled dense plasma. Teplofiz. Vysok. Temper. **7**(5), 822–831 (1969)
257. Norman, G.E.: Ball lightning as overcooled non-ideal plasma. Khim. Fiz. **18**(7), 78–86 (1999)
258. Norman, G.E.: Ball lightning as a supercooled nonideal plasma. Chem. Phys. Rep. **18**(7), 1335–1352 (2000)
259. Manykin, E.A., Norman, G.E.: Ball lightning as supercooled plasma condensed phase. In: Proceedings of the 6th International Symposium on Ball Lightning (ISBL99), Antwerp, Belgium, pp. 120–125 (1999)
260. Mesenyashin, A.I.: Electrostatic and bubble nature of ball lightning. Appl. Phys. Lett. **58** (23), 2713–2715 (1991)
261. Mesenyashin, A.I.: Spherical formations in the atmosphere as a physical phenomenon. J. Electrostatics **38**, 139–150 (1995)
262. Zaitsev, I.V., Zaitsev, S.V.: Electrostatic model of ball lightning. Pisma v ZhTF. **17**(7), 34–37 (1991)
263. Fedele, R.: A possible quantum-like approach to non-conventional plasmas. In: Proceedings of the 6th International Symposium on Ball Lightning (ISBL99), Antwerp, Belgium, pp. 126–132 (1999)
264. Pavlovsky, A.I., Dolotenko, M.I.: Pisma v ZhTF **38**(9), 473 (1983)
265. Marsh, G.: Force free magnetic fields: solutions, topology and applications. World Scientific, Singapore (1996)
266. Rañada, A.F., Trueba, J.L.: Ball lightning as an electromagnetic knot? Nature **383**, 32 (1996)
267. Rañada, A.F., Soler, M., Trueba, J.L.: Ball lightnings and force-free magnetic knots. In: Proceedings of the 6th International Symposium on Ball Lightning (ISBL99), Antwerp, Belgium, pp. 102–107 (1999)
268. Jennison, R.C.: Ball lightning. A general critique. In: Proceedings of the 5th International Symposium on Ball Lightning (ISBL97), Tsugawa-Town, Japan, pp. 6–11 (1997)
269. Callebaut, D.K.: Energy storage by force-free magnetic field in the initial phase of ball lightning. In: Proceedings of the 8th International Symposium on Ball Lightning (ISBL04), Chung-li, Taiwan, pp. 32–37 (2004)
270. Callebaut, D.K., Karugila, G.K., Khater, A.H.: Ball lightning with force-free magnetic fields and runaway current. In: Proceedings of the 9th International Symposium on Ball Lightning (ISBL06), Eindhoven, The Netherlands, pp. 33–38 (2006)
271. Shakirzjanov, F.N.: Electromagnetic model of ball lightning. Elektrichestvo. N. 10, 74–77 (1999)
272. Arnhoff, G.H.: On the spheric radiation. In: Proceedings of the 5th International Symposium on Ball Lightning (ISBL97), Tsugawa-Town, Japan, pp. 101–107 (1997)
273. Arnhoff, G.H.: On the spheric radiation. In: Proceedings of the 6th International Symposium on Ball Lightning (ISBL99), Antwerp, Belgium, pp. 160–165 (1999)
274. Dijkhuis, G.C.: State equation and phase diagram for fractal growth in ball lightning. In: Kikuchi, H. (ed.) Environmental and Space Electromagnetics, pp. 535–546. Springer, Tokyo (1991)
275. Feynman, R.F., Leighton, R.B., Sands, M.: The Feynmann Lectures on Physics. **9,** p. 246. Mir, Moscow (1967)
276. Dijkhuis, G.C.: Plasmoid confinement by the charged particles micro-fields. Nature **290**, 166 (1981)
277. Dijkhuis, G.C.: Verhulst dynamics and fractal stretching of transition layer vorticity. In: Kikuchi, H. (ed.) Dusty and Dirty Plasmas, Noise, and Chaos in Space and in the Laboratory, pp. 163–176. Plenum, New York (1994)

278. Dijkhuis, G.C.: Random walk and fractal deformation of transition layer vorticity. In: Proceedings of the 1st International Symposium on Heat and Mass Transfer under Plasma Conditions, Çesme, Turkey, pp. 611–621 (1994)
279. Dijkhuis, G.C.: Constructions for scale-invariant and kink-free vortex stretching. Physica B. Condensed Matter **228**, 144–152 (1996)
280. Dijkhuis, G.C.: Helix string field in ball lightning. In: Proceedings of the 5th International Symposium on Ball Lightning (ISBL97), Tsugawa-Town, Japan, pp. 144–151 (1997)
281. Dijkhuis, G.C.: Exponential particle acceleration by recursive stretching of vortex filaments in turbulent discharge plasma. In: Proceedings of the 8th International Symposium on Ball Lightning (ISBL04), Chung-li, Taiwan, pp. 70–75 (2004)
282. Dijkhuis, G.C.: On Madelung sums for bound states in a plasma vortex system. In: Proceedings of the 10th International Symposium on Ball Lightning (ISBL08) and 3rd International Symposium on Unconventional Plasmas (ISUP08), Kaliningrad, Russia, pp. 27–33 (2008)
283. Artsimovich, L.A.: Controlled Thermonuclear Reactions. GIFML, Moscow (1961)
284. Bychkov, V.L., Bychkov, A.V., Stadnik, S.A.: Polymer fire balls in discharge plasma. Phys. Scripta **53**, 749–759 (1996)
285. Amirov, A.K., Bobkov, S.E., Bychkov, V.L., Emelin, S.E., Klimov, A.I., Semenov, V.S.: Modern theoretical and experimental approaches to the problem of ball lightning. In: Proceedings of the 5th International Symposium on Ball Lightning (ISBL97), Tsugawa-Town, Japan, pp. 52–60 (1997)
286. Bychkov, V.L.: Unipolar ball lightning model. In: Proceedings of the 8th International Symposium on Ball Lightning (ISBL04), Chung-li, Taiwan, pp. 64–69 (2004)
287. Bychkov, V.L., Bychkov, D.V.: Ball lightning as unipolarly charged object with hot surface. In: Proceedings of the 9th International Symposium on Ball Lightning (ISBL06), Eindhoven, The Netherlands, pp. 26–32 (2006)
288. Bychkov, V.L.: Unipolarly charged ball lightning. Khim. Fiz. **25**(3), 63–71 (2006)
289. Nikitin, A.I.: The dynamic capacitor model of ball lightning. In: Proceedings of the 6th International Symposium on Ball Lightning (ISBL99), Antwerp, Belgium, pp. 81–84 (1999)
290. Nikitin, A.I.: Stability and limiting energy content of autonomous ball lightning. Elektrichestvo. **3**, 29–36 (2004)
291. Nikitin, A.I.: Substance of ball lightning as a certain form of unconventional plasma. Int. J. Unconven. Electromag. Plasmas. **1**(1–2), 101–108 (2008)
292. Nikitin, A.I.: How ball lightning can be created in nature. In: Proceedings of the 6th International Symposium on Ball Lightning (ISBL99), Antwerp, Belgium, pp. 85–90 (1999)
293. Nikitin, A.I.: Origination of a ball lightning at development of a linear lightning. Elektrichestvo. (3), 16–23 (2000)
294. Aleksandrov, V.Y., Golubev, E.M., Podmoshensky, I.V.: Aerosol nature of ball lightning. Zhur. Tech. Fizi. **52**(10), 1987–1992 (1982)
295. Stakhanov, I.P.: On Physical Nature of Ball Lightning. Energoatomizdat, Moscow (1985)
296. Smirnov, B.M.: Problem of Ball Lightning. Nauka, Moscow (1988)
297. Bychkov, V.L.: Polymer ball lightning model. Physica Scripta. **50**, 591–599 (1994)
298. Abrahamson, J., Dinniss, J.: Ball lightning caused by oxidation of nanoparticle networks from normal lightning strikes on soil. Nature **403**, 519–521 (2000)
299. Grigoriev, A.I., Shiryaeva, S.O., Grigorieva, I.D., et al.: On possibility of one ball lightning division in two. Z. Tekh. Fiz. **61**, 25–31 (1991)
300. Saranin, V.A.: Equilibrium of Liquids and its Stability. Institute of Computer Investigations, Moscow (2002)
301. Bychkov, A.V., Bychkov, V.L., Abrahamson, J.: On the energy characteristics of ball lightning. Phil. Trans. Roy. Soc. Lon. **360**(1790), 97–106 (2002)
302. Emelin, S.E., Semenov, V.S., Bychkov, V.L., Belisheva, N.K., Kovshyk, A.P.: Some objects formed in the interaction of electrical discharges with metals and polymers. Tech. Phys. **42** (3), 269–277 (1997)

303. Bychkov, A.V., Bychkov, V.L., Timofeev, I.B.: Experimental modeling of long-lived shining formations in air on a basis of polymeric organic materials. Z. Tekh. Fiz. **74**(1), 128–133 (2004)
304. Piva, G.S., Pavão, A.C., de Vasconcelos, E.A., Mendes Jr., O., Da Silva Jr., E.F.: Production of ball-lightning-like luminous balls by electrical discharge in silicon. Phys. Rev. Letts. **98**, 048501-1–048501-4 (2007)
305. Dikhtyar, V., Jerby, E.: Fireball ejection from a molten hot spot to air by localized microwaves. Phys. Rev. Lett. **96**, 2–4 (2006)
306. Bychkov, V.L.: Unipolar ball lightning model. In: Proceedings of the 8th International Symposium on Ball Lightning (ISBL04), Chung-li, Taiwan, pp. 64–69 (2004)
307. Bychkov,V.L., Bychkov, D. V.: Ball lightning as unipolarly charged object with hot surface. In: Proceedings of the 9th International Symposium on Ball Lightning (ISBL06), Eindhoven, the Netherlands, pp. 26–32 (2006)
308. Bychkov, V.L.: Unipolarly charged ball lightning. Khim. Fiz. **25**(3), 63–71 (2006)
309. Drysdale, D.: An Introduction to Fire Dynamics. Wiley, Chichasler/New York/Brisbane/Toronto/Singapore (1985)
310. Anderson, F.J., Freier, G.D.: Relation of electric fields to thunderstorm days. J. Geophys. Res. **78**(27), 6359–6363 (1973)
311. Sessler, G.M. (ed.): Electrets. Springer-Verlag, New York (1980)
312. Terletskyi, Y.P., Rybakov, Y.P.: Electrodynamics. Vysschaya Schkola, Moscow (1980)
313. Panofsky, W.K.H., Phillips, M.: Classical Electricity and Magnetism. Addison-Wesley, Cambridge, MA (1962)
314. Merzbacher, C.I.: Materials that emit light by chemical reaction. Phil. Trans. Roy. Soc. Lon. **360**(1790), 89–96 (2002)
315. Raizer, Y.P.: Physics of gaseous discharge. Nauka, Moscow (1992)
316. Aleksandrov, A.F., Bogdankevich, L.S., Rukhadze, A.A.: Basics of Plasma Electrodynamics. Vyschaya Schkola, Moscow (1988)
317. Nikitin, A.I., Nikitina, T.F., Velichko, A.M.: Corona discharge as a means to levitation of ball lightning. In: Proceedings of the 10th International Symposium on Ball Lightning (ISBL08) and 3rd International Symposium on Unconventional Plasmas (ISUP08), Kaliningrad, Russia, pp. 89–98 (2008)
318. Blythe, T., Bloor, D.: Electrical Properties of Polymers. Cambridge University Press, Cambridge (2005)
319. Abramovich, G.N.: Applied gas dynamics. Nauka, Moscow (1986)
320. Nikitin, A.I.: Electrodynamic model of ball lightning. Khim. Fiz. **25**(3), 38–62 (2006)
321. Rawson, H.: Inorganic Glass-Forming Systems. Academic, London/New York (1967)
322. Bartenev, G.M.: Structure and Mechanical Properties of Inorganic Glasses. Publishers of Building Literature, Moscow (1966)
323. Lykov, A.V.: Theory of Thermal Conductivity. Vysschaya Schkola, Moscow (1967)
324. Amirov, A.Kh., Bychkov, V.L., Bobkov, S.E.: On the dependence lifetime- diameter for ball lightnings. Physica Scripta. **54**, 13–14 (1998)
325. Amirov, A.K., Bychkov, A.V., Bychkov, V.L.: Ball lightning in respect to dependence lifetime diameter. In: Proceedings of the 6th International Symposium on Ball Lightning, 23–25 August, Antwerp, Belgium, pp. 19–26 (1999)
326. Pudovkin, A.K.: Ball lightning in Novosibirsk Akademgorodok. Uspekhi Fiz. Nauk. **166** (11), 1253–1254 (1996)
327. Saranin, V.A.: The theory of electrothermal explosion produced by lightning. Teplofiz. Vysok. Temper. **37**(1), 31–36 (1999)
328. Mineev, A.: About high trees. In: Tikhomirova,V.A., Chernoutsan, A.I. (eds.) Physics and Biology. Bureau Quantum, Moscow (2001)
329. Kalashnikov, S.G.: Electricity. Nauka, Moscow (1964)
330. Likhosherstnykh, G.U.: 138 approaches to a mystery of nature. Tekhnika Molodezhi. (3), 38–43 (1983)

331. Goodlet, B.L.: Ball Lightning. J. Inst. Elect. Eng. **81**, 1 (1937)
332. Barry, J.D.: Ball Lightning and Bead Lightning. Extreme Forms of Atmospheric Electricity. Plenum, New York (1980)
333. Stenhoff, M.: Ball Lightning. An Unsolved Problem in Atmospheric Physics. Kluwer/ Plenum, New York (1999)
334. Imianitov, I., Tikhii, D.: Beyond the Laws of Science. Atomizdat, Moscow (1980)
335. Batygin, A., Mosin, I.: Visit of "Fairy Lady". Pravda (Moscow), N. 220 (25938), pp. 6 (1989)
336. Nikitin, A.I.: The principles for developing of ball lightning theory. J. Russian Laser Res. **25** (2), 169–191 (2004)
337. Nikitin, A.I.: The requirements for elaboration of theory of ball lightning. In: Proceedings of the 8th International Symposium on Ball Lightning, Chung-li, Taiwan, pp. 16–22 (2004)
338. Nikitin, A.I.: Analysis of the models of highly energetic ball lightning. In: Proceedings of the 8th International Symposium on Ball Lightning, Chung-li, Taiwan, pp. 57–63 (2004)
339. Dijkhuis, G.C.: A model for ball lightning. Nature **248**, 150–151 (1980)
340. Dijkhuis, G.C.: Plasmoid confinement by the charged particles microfields. Nature **290**, 166 (1981)
341. Dijkhuis, G.C.: Helix string model for turbulent vorticity and cavitation in shearing arc plasma. Ann. NY Acad. Sci. **891**, 259–272 (1999)
342. Bychkov, V.L.: Polymer ball lightning model. Physica Scripta **50**, 591–599 (1994)
343. Bychkov, V.L.: Ball lightning as unipolarly charged object with hot surface. In: Proceedings of the 9th International Symposium on Ball Lightning, Eindhoven, The Netherlands. pp. 26–38 (2006)
344. Nikitin, A.I.: An electrical capacitor as the element of the power core of ball lightning. Electri. Technol. Russia (4), 70–85 (1998)
345. Nikitin, A.I.: The dynamic capacitor model of ball lightning. In: Proceedings of the 6th International Symposium on Ball Lightning, Antwerp, Belgium, pp. 91–95 (1999)
346. Nikitin, A.I.: Substance of ball lightning as a certain form of unconventional plasma. Int. J. Unconven. Electromag. Plasmas. **1**(1–2), 101–108 (2008)
347. Nikitin, A.I.: Electrodynamical model of ball lightning. Khim. Fiz. **25**(3), 38–62 (2006)
348. Artsimovich, L.A.: The Elementary Physics of Plasma. Atomizdat, Moscow (1969)
349. Frank-Kamenetskii, D.A.: Lectures on Plasma Physics. Atomizdat, Moscow (1968)
350. Landau, L.D., Lifshits, E.M.: Field Theory. GIFML, Moscow (1961)
351. Artsimovich, L.A.: Controlled Thermonuclear Reactions. GIFML, Moscow (1961)
352. Kalashnikov, S.G.: Electricity. Nauka, Moscow (1985)
353. Sarantsev, V.P., Perel'shtein, E.A.: Collective Acceleration of Ions by Electron Rings. Atomizdat, Moscow (1979)
354. Nikitin, A.I.: Stability and limit energy content of an autonomous ball lightning. Elektrichestvo. (3), 29–36 (2004)
355. Dmitriev, M.T., Bakhtin, B.I., Martynov, V.I.: Investigation of a thermal factor of ball lightning. J. Tech. Phys. **51**(12), 2567–2572 (1981)
356. Balyberdin, V.V.: Estimate of the inner energy of ball lightning. In: Samolyotostroenie i Tekhnika Vozdushnogo Flota, vol. 3, pp. 102–104. Publishing of Kharkov State University, Kharkov (1965)
357. Ternov, I.M., Mikhailin, V.V., Khalilov, V.R.: Synchrotron Radiation and Its Applications. Publishing of Moscow State University, Moscow (1980)
358. Artsimovich, L.A., Lukianov, S.Y.: Motion of Charged Particles in the Electric and Magnetic Fields. Nauka, Moscow (1978)
359. Frenkel', Y.I.: Theory of the Phenomenon of Atmospheric Electricity. GITTL, Leningrad-Moscow (1949)
360. Uman, M.A.: Lightning. McGraw-Hill, New York (1969)
361. Nikitin, A.I.,Velichko, A.M., Vnukov, A.V, Nikitina, T.F.: Estimation of ball lightning characteristics based on the analysis of its photo. In: Proceedings of the 9th International Symposium on Ball Lightning, Eindhoven, the Netherlands, pp. 148–156 (2006)

362. Nikitin, A.I., Velichko, A.M., Vnukov, A.V., Nikitina, T.F.: Estimate of the ball lightning parameters on the base of analysis of its photo. Khim. Fiz. **26**(8), 80–89 (2007)
363. Nikitin, A.I., Leipunsky, I.O., Nikitina, T.F.: A search for the reasons explaining hovering of ball lightning over conductor surface. In: Proceedings of the 9th International Symposium on Ball Lightning, Eindhoven, The Netherlands, pp. 139–147 (2006)
364. Nikitin, A.I., Nikitina, T.F., Velichko, A.M.: Corona discharge as a means to levitation of ball lightning. In: Proceedings of the 10th International Symposium on Ball Lightning and 3rd International Symposium on Unconventional Plasmas, Kaliningrad, Russia, pp. 89–98 (2008)
365. Schelkunov, G.P., Nikitin, A.I., Bychkov, V.L., Nikitina, T.F., Velichko, A.M., Vasiliev, A. L.: Examination of a Window Pane Exposed to Ball Lightning. In: Proceedings of the 10th International Symposium on Ball Lightning and 3rd International Symposium on Unconventional Plasmas, Kaliningrad, Russia, pp. 127–134 (2008)
366. Turner, D.J.: The interaction of ball lightning with glasses window panes. J. Meteorol. **22** (216), 52–64 (1997)
367. Nikitin, A.I., Bychkov, V.L., Nikitina, T.F., Velichko, A.M.: Modeling of ball lightning interaction with window panes. In: Proceedings of the 8th International Symposium on Ball Lightning. Chung-li, Taiwan, pp. 23–31 (2004)
368. Nikitin, A.I., Bychkov, V.L., Nikitina, T.F., Velichko, A.M.: Modeling of interaction of ball lightning with window panes. Khim. Fiz. **25**(4), 98–105 (2006)
369. Grigor'ev, A.I.: Ball Lightning. Publishing of Yaroslavl' State University, Yaroslavl' (2006)
370. Singer, S.: The Nature of Ball Lightning. Plenum, New York (1971)
371. Stakhanov, I.P.: On a Physical Nature of Ball Lightning. Nauchny Mir, Moscow (1996)
372. Nikitin, A.I., Velichko, A.M., Nikitina, T.F.: Principles for search of conditions of ordered plasma structures creation. Izvestia Akademii Nauk, Energetics. N.2. pp. 115–132 (2008)
373. Meek, J.M., Craggs, J.D.: Electrical Breakdown in Gases. Clarendon, Oxford (1953)
374. Bazelian, E.M., Raizer, YuP: Physics of Lightning and of Protection Against Lightning. Nauka, Moscow (2001)
375. Nikitin, A.I.: Creation of ball lightning at developing of linear lightning. Elektrichestvo. (3), 16–23 (2000)
376. Nikitin, A.I.: How ball lightning can be created in nature. In: Proceedings of the 6th International Symposium on Ball Lightning, Antwerp, Belgium, pp. 85–90 (1999)
377. Raizer, YuP: Physics of Gas Discharge. Nauka, Moscow (1987)
378. Veselago, V.G.: The electrodynamics of substances with simultaneously negative values of ε and μ. Sov. Phys. Uspekhi. **10**, 509–514 (1968)
379. Yablonovitch, E., et al.: Photonic band structure: the face-centred cubic case employing non-spherical atoms. Phys. Rev. Lett. **67**, 2295–2298 (1991)
380. Pendry, J.B., et al.: Magnetism from conductors and enhanced nonlinear phenomena. IEEE Trans. Microwave Theor. Tech. **47**, 2075–2084 (1999)
381. Shelby, R.A., et al.: Experimental verification of a negative index of refraction. Science **292**, 77–79 (2001)
382. Singer, S.: The Nature of Ball Lightning. Plenum, New York (1978)
383. Smirnov, B.M.: Physics of ball lightning. Phys. Rep. **224**, 151–236 (1993)
384. Amirov, A.K.h., Bychkov, V.L.: Ball lightning diameter-lifetime statistical analysis of the SKB data bank. Physica Scripta. **50**, 413–416 (1994)
385. Keul, A.G., et al.: German ball lightning data bank results. In: Proceedings of the 9th International Symposium on Ball Lightning, Eindhoven, The Netherlands. pp. 96–105 (2006)
386. Ofuruton, H. et al.: Experimental conditions for ball lightning creation by using air gap discharge embedded in a microwave field. J. Geophys. Res. **106**, 12,367–12,369 (2001)
387. Golubkov, G.V., et al.: Collision of Rydberg atom A** with ground-state atom B. JETP Lett. **75**, 314–316 (2002)
388. Klimov, A. et al.: Investigation of physical properties of plasmoids in air and airflow. In: Proceedings of the 9th International Symposium on Ball Lightning. Eindhoven, The Netherlands. pp. 112–121 (2006)

389. Shabanov, G.D.: Performance of the laboratory of ball lightning. In: Proceedings of the 9th International Symposium on Ball Lightning. Eindhoven, The Netherlands. pp. 202–209 (2006)
390. Vlassov, A.: Getting a fireball by means of electric explosion of a wire spiral. In: Proceedings of the 9th International Symposium on Ball Lightning, Eindhoven, The Netherlands. pp. 233–241 (2006)
391. Jennison, R.C.: Ball lightning. Nature **224**, 895 (1969)
392. Dmitriev, M.T.: Stabilility mechanism for ball lightning. Sov. Phys. Tech. Phys. **14**, 284–289 (1969)
393. Dwyer, J.R., et al.: Energetic radiation produced during rocket-triggered lightning. Science **299**, 4 (2003)
394. Shah, G.N., et al.: Neutron generation in lightning bolts. Nature **313**, 773–775 (1985)
395. Dijkhuis, G.C.: Helix string model for turbulent vorticity and cavitation in shearing arc plasma. Ann. NY Acad. Sci. **891**, 259–272 (1999)
396. Dijkhuis, G.C.: Exponential particle acceleration by recursive stretching of vortex filaments in turbulent discharge plasma. In: Proceedings of the 8th International Symposium on Ball Lightning, Taiwan, Chung-li, pp. 70–76 (2004)
397. Dijkhuis, G.C.: Scaling law for fusion power from ball lightning. In: Janiszewski, J., Moron, W., Sega, W. (eds.). Proceedings of the International Wroclaw Symposium on Electromagnetic Compatibility, pp. 21–25 (1988)
398. Pendry, J.B., et al.: Low frequency plasmons in thin-wire structures. J. Phys. Condens. Matter. **10**, 4785–4809 (1998)
399. Bergström, A.: Electromagnetic theory of strong interaction. Phys. Rev.D. **8**, 4394–4402 (1978)
400. Dijkhuis, G.C.: A model of ball lightning. Nature **284**, 150–151 (1980)
401. Tsuchiya, H. et al.: Detection of high-energy gamma rays from winter thunderclouds. Phys. Rev. Lett., **99**, 4165002, 4 (2007)
402. Bychkov, V.L.: On observation properties of ball lightning. In: Proceedings of the 9th International Symposium on Ball Lightning. Eindhoven, The Netherlands. pp 39–42 (2006)
403. Nikitin, A.I. et al.: Estimation of ball lightning characteristics based on the analysis of its photo. In: Proceedings of the 9th International Symposium on Ball Lightning, Eindhoven, The Netherlands, pp. 148–156 (2006)
404. Noten, L.C.: Private communication supported by his original laboratory journal. (1995)
405. Dijkhuis, G.C.: Site report and evaluation of Dutch ball lightning event. In: Proceedings of the 9th International Symposium on Ball Lightning, Eindhoven, The Netherlands, pp. 39–42 (2006)
406. Ofuruton, H., Kamogawa, M., Ohtsuki, Y.-H.: Experiments on ball lightning by using microwave localization. In: Proceedings of the 9th International Symposium on Ball Lightning (ISBL06), Eindhoven, The Netherlands, pp. 157–158 (2006)
407. Emelin, S.E., et al.: The dust-gas fireball as a special form of the electric erosive discharge afterglow. In: Proceedings of the 9th International Symposium on Ball Lightning, Eindhoven, The Netherlands, pp. 51–61 (2006)
408. Pirozerski, A.L., et al.: Long-living plasmoids generation by high-voltage discharge. In: Proceedings of the 9th International Symposium on Ball Lightning, Eindhoven, The Netherlands, pp. 180–190 (2006).
409. Spiegel, M.R.: Theory and Problems of Complex Variables. McGraw-Hill, New York (1964)
410. Panofsky, W.K.H., Phillips, M.: Classical Electricity and Magnetism. Addison-Wesley, Cambridge, MA (1962)
411. Dijkhuis, G.C.: Crystal lattices for 3D vortex systems with uniform curvature and torsion at minimal dissi-pation. In: Doerffer, P. (ed.) Internals Flows. IFFM Publishers. Gdansk, Poland, pp. 661–668 (2001)
412. Hamilton, W.R.: On a New Species of Imaginary Quantities Connected with the Theory of Quaternions. Proc. Roy. Irish Acad. **2**, 424–434 (1844)

413. Dijkhuis, G.C.: On potential flow solutions from the division algebras. In: Proceedings of the 6th European Symposium on Aerothermod. for Space Vehicles, ESA SP-659 (2009)
414. Conway, J.H., Smith, D.A.: On Quaternions and Octonions. A.K. Peters, Natick, MA (2003)
415. Coxeter, H.S.M.: Regular Polytopes, 3rd ed. Dover, New York (1973)
416. Kuipers, J.B.: Quaternions and Rotation Sequences. Princeton University Press, New York (1999)
417. Abramowitz, M., Stegun, I.A.: Handbook of Mathematical Functions. Dover, New York (1968)

Index